PHYSICAL REVIEW

VOLUME 85

MARCH 1, 1952

Published by the

AMERICAN PHYSICAL SOCIETY

THE PHYSICAL REVIEW

A journal of experimental and theoretical physics established by E. L. Nichols in 1893

Published by the American Institute of Physics
for the
AMERICAN PHYSICAL SOCIETY

Officers

President

J. H. VAN VLECK
Harvard University
Cambridge, Massachusetts

Vice-President

ENRICO FERMI
Institute for Nuclear Studies
University of Chicago
Chicago 37, Illinois

Secretary

K. K. DARROW
Bell Telephone Laboratories
Office:
Columbia University
New York 27, New York

Treasurer

G. B. PEGRAM
Columbia University
New York 27, New York

Local Secretary
for the Pacific Coast

J. KAPLAN
University of California at Los Angeles
Los Angeles, California

Managing Editor

S. A. GOUDSMIT
Brookhaven National Laboratory
Upton, Long Island
New York

BOARD OF EDITORS

Editor

S. A. GOUDSMIT

Assistant Editor

S. PASTERNACK

Associate Editors

HARVEY BROOKS
R. F. CHRISTY
C. L. CRITCHFIELD
M. DEUTSCH
T. H. JOHNSON
BRUNO ROSSI
M. GOLDHABER
R. HOFSTADTER
A. W. LAWSON
A. PAIS
R. SERBER
C. H. TOWNES
W. P. ALLIS
F. G. BEECKWITH
W. B. FRETTER
CONYERS HERRING
H. W. LEVERENZ
ARNOLD NORDSIECK

Manuscripts for publication should be submitted to S. A. Goudsmit, Brookhaven National Laboratory, Upton, Long Island, New York. The authors' institutions are requested to pay a publication charge of $8 per page which, if honored, entitles them to 100 free reprints. Instructions will be sent with galley proofs.

Proof and all correspondence concerning papers in the process of publication should be addressed to the Publication Manager, American Institute of Physics, 57 East 55 Street, New York 22, New York.

Subscription Price

United States and Canada $25.00
Elsewhere $27.00

Back Numbers[1]

Yearly back number rate when complete year is available:
Prior to 1949: $20.00
Thereafter: $27.00
Single copies: $2.00 each, prior to July, 1929;
$1.00 each, July, 1929–December, 1941;
$2.00 each, January, 1942–December, 1946;
$1.00 each, January, 1947–December, 1948;
$1.25 each, thereafter.
General Index, 1893–1930: $4.00.

Subscriptions, renewals, and orders for back numbers should be addressed to the American Institute of Physics, 57 East 55 Street, New York 22, New York.

Changes of address in the case of members of the American Physical Society should be addressed to the Treasurer; in the case of other subscribers to the American Institute of Physics.

[1] For Series I (Physical Review) Department, Cornell University, Ithaca, New York.

The Physical Review is published semi-monthly at Prince and Lemon Streets, Lancaster, Pennsylvania.

Entered as second-class matter March 6, 1917, at the Post Office at Lancaster, Pennsylvania, under the Act of March 3, 1879.

Acceptance for mailing at special rate of postage provided for in paragraph (d-2), section 34.40, P. L. & R. of 1948, authorized January 27, 1925.

THE
PHYSICAL REVIEW

A journal of experimental and theoretical physics established by E. L. Nichols in 1893

SECOND SERIES, VOL. 85, NO. 5 MARCH 1, 1952

Radial Distribution Function of a Gas of Hard Spheres and the Superposition Approximation*

B. R. A. NIJBOER
Institute for Theoretical Physics, University of Utrecht, Utrecht, Holland

AND

L. VAN HOVE†
University of Brussels, Brussels, Belgium

(Received November 8, 1951)

The term $g_2(r)$ proportional to the square of the density in the expansion of the radial distribution function $g(r)$ of an imperfect gas in powers of the density is calculated exactly in the case of a gas consisting of hard spheres. The result is checked by means of Boltzmann's value of the 4th virial coefficient of such a gas. The integral equation for $g(r)$, obtained on applying the superposition approximation introduced by Kirkwood and by Born and Green, can also be solved by an expansion in powers of the density. For the case of hard spheres the approximate $g_2'(r)$ found in this way is compared with the exact $g_2(r)$. As a further application of our result on $g_2(r)$ a certain integral is discussed, which is of interest in the treatment of interference effects in neutron scattering problems.

I. INTRODUCTION

As has been shown by Yvon, Kirkwood, de Boer and others,[1] the radial distribution function of a compressed gas may be expanded in powers of the density

$$g(r)=\exp\{-V(r)/kT\}\cdot\{1+\rho g_1(r)+\rho^2 g_2(r)+\cdots\}. \quad \text{(I.1)}$$

The distance between molecules has been denoted by r, the intermolecular potential by $V(r)$ and by ρ the number of molecules per unit volume. The function $g(r)$ is normalized to the value 1 for large distances. As is known, $g_1(r)$, $g_2(r)$, $\cdots$ can be expressed by cluster integrals in which the position of two particles is kept fixed. In classical statistical mechanics, and on the assumption of additivity of intermolecular forces, one has[2]

$$g_1(r_{12})=\int f(r_{13})f(r_{23})d\mathbf{r}_3, \quad \text{(I.2)}$$

$$g_2(r_{12})=\tfrac{1}{2}\{g_1(r_{12})\}^2+\varphi(r_{12})+2\psi(r_{12})+\tfrac{1}{2}\chi(r_{12}), \quad \text{(I.3)}$$

where r_{ik} is the distance $|\mathbf{r}_i-\mathbf{r}_k|$ between particles i and k, where the function $f(r)$ is related to the intermolecular potential by

$$f(r)=\exp\{-V(r)/kT\}-1 \quad \text{(I.4)}$$

and

$$\varphi(r_{12})=\int f(r_{13})f(r_{24})f(r_{34})d\mathbf{r}_3 d\mathbf{r}_4, \quad \text{(I.5)}$$

$$\psi(r_{12})=\int f(r_{13})f(r_{23})f(r_{24})f(r_{34})d\mathbf{r}_3 d\mathbf{r}_4, \quad \text{(I.6)}$$

$$\chi(r_{12})=\int f(r_{13})f(r_{23})f(r_{14})f(r_{24})f(r_{34})d\mathbf{r}_3 d\mathbf{r}_4. \quad \text{(I.7)}$$

* Part of this work was done at the Institute for Advanced Study, Princeton, New Jersey. The authors are indebted to the Institute for grants which made their stay possible, and to ONR for making available computational help.

† Associé du Fonds National de la Recherche Scientifique (Belgium).

[1] For a survey we refer to J. de Boer, "Reports on Progress in Physics," Phys. Soc. (London) **12**, p. 305 (1949).

[2] J. de Boer and A. Michels, Physica **6**, 97 (1939).

Kirkwood was the first to evaluate $g_1(r)$ in the simple case of hard spheres without attractive forces, for which, if the diameter of the spheres is taken as unit of length,

$$V(r)=\begin{cases}\infty & \text{for } 0\leqslant r<1\\ 0 & \text{for } r\geqslant 1\end{cases}, \quad f(r)=\begin{cases}-1 & \text{for } 0\leqslant r<1\\ 0 & \text{for } r\geqslant 1\end{cases}. \tag{I.8}$$

He found[3]

$$g_1(r)=\begin{cases}\frac{3}{2}\pi(2-\frac{3}{2}r+\frac{1}{8}r^3) & \text{for } r\leqslant 2\\ 0 & \text{for } r\geqslant 2\end{cases}. \tag{I.9}$$

The function $g_1(r)$ was also calculated by numerical integration by de Boer and Michels[2] for the case of a Lennard-Jones potential.

For the simple case of hard spheres again we give in this work the calculation of the ρ^2-term $g_2(r)$, in the expansion (I.1). Our result enables us to test, at least for small densities, the validity of the so-called "superposition approximation" proposed by Kirkwood in the theory of liquids.[1] This test includes as a special case the recent work of Hart, Wallis, and Pode[4] as well as that of Rushbrooke and Scoins[5] who compared the exact value of the 4th virial coefficient in the case of hard spheres with the value obtained from the superposition assumption.

The superposition assumption, when applied as proposed[1] by Born and Green,[6] leads for the $g(r)$-function to the approximate integral equation

$$kT\partial \ln(r_{12})/\partial \mathbf{r}_1=-\partial V(r_{12})/\partial \mathbf{r}_1$$
$$-\rho\int[\partial V(r_{13})/\partial \mathbf{r}_1]g(r_{13})g(r_{23})d\mathbf{r}_3, \tag{I.10}$$

the solution of which from now on we will call $g'(r)$, in distinction from the exact $g(r)$. The function $g'(r)$ can also be expanded in powers of the density

$$g'(r)=\exp\{-V(r)/kT\}\cdot\{1+\rho g_1'(r)+\rho^2 g_2'(r)+\cdots\}. \tag{I.11}$$

As will be shown in Sec. IV, $g_1'(r)$ is identical with the corresponding $g_1(r)$-function of the exact expansion (I.1), whereas $g_2'(r)$ is different from $g_2(r)$. The calculation of $g_2'(r)$ and its comparison with the exact $g_2(r)$ will provide the test of the superposition approximation mentioned above. A short account of the results was published elsewhere.[7]

As a second application of the exact expression of $g_2(r)$, we use it to determine for small densities the value of the following integral

$$K=\int_0^\infty\{1-g(r)\}dr,$$

which is of interest in the discussion of interference effects in neutron scattering problems and has been discussed from quite a different standpoint in the region of large densities.[8]

II. CALCULATION OF $g_2(r)$

For the calculation of φ defined by (I.5) it turns out to be convenient first to calculate

$$\frac{d\varphi(r_{12})}{dr_{12}}=\int\frac{df(r_{13})}{dr_{13}}\frac{\mathbf{r}_{12}\cdot\mathbf{r}_{13}}{r_{12}r_{13}}f(r_{24})f(r_{34})d\mathbf{r}_3d\mathbf{r}_4$$
$$=\int\frac{df(r_{13})}{dr_{13}}\frac{\mathbf{r}_{12}\cdot\mathbf{r}_{13}}{r_{12}r_{13}}g_1(r_{23})d\mathbf{r}_3.$$

In the case of hard spheres, df/dr is the δ-function $\delta(r-1)$, and, when applying (I.9) and noting that φ vanishes for $r\geqslant 3$, we find

$$\varphi(r)=\begin{cases}\pi^2[-r^6/1260+r^4/20-r^3/6-r^2/4\\ \quad+(9/5)r-9/4+(27/70)(1/r)] & \text{for } 1\leqslant r\leqslant 3,\\ 0 & \text{for } r\geqslant 3.\end{cases} \tag{II.1}$$

The function $\psi(r)$ defined in (I.6) is calculated in the same simple way, with the result

$$\psi(r)=\begin{cases}\pi^2[r^6/1260-r^4/20+r^3/6+r^2/4-(97/60)r\\ \quad+16/9-(9/35)(1/r)] & \text{for } 1\leqslant r\leqslant 2,\\ 0 & \text{for } r\geqslant 2.\end{cases} \tag{II.2}$$

Now as to $\chi(r)$ given by (I.7), we may remark first that $\chi(r)=0$ for $r\geqslant 2$. Further, in the region $\sqrt{3}\leqslant r\leqslant 2$, the factor $f(r_{34})$ in (I.7) is -1 and hence in this region $\chi(r)$ reduces to $-\{g_1(r)\}^2$. The evaluation of $\chi(r)$ in the remaining region $1\leqslant r\leqslant\sqrt{3}$, proves to be much more complicated. We could perform it by applying the following somewhat indirect procedure, making use of the theory of Fourier transforms.

Let us introduce

$$F(h)=\int f(r)\exp(2\pi i\mathbf{h}\cdot\mathbf{r})d\mathbf{r}=-h^{-\frac{1}{2}}J_{\frac{3}{2}}(2\pi h), \tag{II.3}$$

where $J_{\frac{3}{2}}$ is the Bessel function of order $\frac{3}{2}$, and

$$G(\mathbf{h})=\int f(r_{13})f(r_{23})\exp\{2\pi i\mathbf{h}\cdot[\mathbf{r}_3-\tfrac{1}{2}(\mathbf{r}_1+\mathbf{r}_2)]\}d\mathbf{r}_3.$$

[3] J. G. Kirkwood, J. Chem. Phys. **3**, 300 (1935).
[4] Hart, Wallis, and Pode, J. Chem. Phys. **19**, 139 (1951).
[5] G. S. Rushbrooke and H. I. Scoins, Nature **167**, 366 (1951); Phil. Mag. **42**, 582 (1951).
[6] M. Born and H. S. Green, Proc. Roy. Soc. (London) **A188**, 10 (1946).
[7] B. R. A. Nijboer et L. Van Hove, Proc. Koninkl. Nederlandse Akad. Wetenschappen **B54**, 256 (1951). The relation for the compressibility integral [Eq. (III.3) in the present paper] was quoted incorrectly here.
[8] Placzek, Nijboer and Van Hove, Phys. Rev. **82**, 392 (1951).

We make use of cylindrical coordinates z, ρ, φ with the axis passing through the points 1 and 2, and the origin midway between these points. We denote accordingly by h_z and h_ρ the components of $\mathbf{h}$ respectively parallel and perpendicular to the axis. The integration with respect to φ gives

$$G(\mathbf{h})=4\pi\int_0^{1-\frac{1}{2}r_{12}}\cos(2\pi h_z z)dz \times\int_0^{\{1-(\frac{1}{2}r_{12}+z)^2\}^{\frac{1}{2}}} J_0(2\pi h_\rho\rho)\rho d\rho \tag{II.4}$$

$$=2h_\rho^{-1}\int_0^{1-\frac{1}{2}r_{12}}\cos(2\pi h_z z)\{1-(\tfrac{1}{2}r_{12}+z)^2\}^{\frac{1}{2}} \times J_1\{2\pi h_\rho[1-(\tfrac{1}{2}r_{12}+z)^2]^{\frac{1}{2}}\}dz.$$

Known properties of the Fourier transformation give

$$\chi(r_{12})=\int F(h)\{G(\mathbf{h})\}^2 d\mathbf{h}. \tag{II.5}$$

Introducing (II.3) and (II.4) into (II.5) and noticing that

$$2\cos(2\pi h_z z)\cos(2\pi h_z z')=\cos\{2\pi h_z(z+z')\}+\cos\{2\pi h_z(z-z')\}$$

and that[9] (for $|z\pm z'|\leqslant 1$)

$$\int_{-\infty}^{+\infty}(h_\rho^2+h_z^2)^{-1}J_1\{2\pi(h_\rho^2+h_z^2)^{\frac{1}{2}}\}\cos\{2\pi h_z(z\pm z')\}dh_z =h_\rho^{-1}\{1-(z\pm z')^2\}^{\frac{1}{2}}J_1\{2\pi h_\rho[1-(z\pm z')^2]^{\frac{1}{2}}\},$$

we find ($r=r_{12}$)

$$\chi(r)=-4\pi\int_0^{1-\frac{1}{2}r}dz\{1-(\tfrac{1}{2}r+z)^2\}^{\frac{1}{2}} \times\int_0^{1-\frac{1}{2}r}dz'\{1-(\tfrac{1}{2}r+z')^2\}^{\frac{1}{2}} \times\int_0^{\infty}J_1\{2\pi h_\rho[1-(\tfrac{1}{2}r+z)^2]^{\frac{1}{2}}\} \times J_1\{2\pi h_\rho[1-(\tfrac{1}{2}r+z')^2]^{\frac{1}{2}}\}\cdot[\{1-(z+z')^2\}^{\frac{1}{2}} \times J_1\{2\pi h_\rho[1-(z+z')^2]^{\frac{1}{2}}\}+\{1-(z-z')^2\}^{\frac{1}{2}} \times J_1\{2\pi h_\rho[1-(z-z')^2]^{\frac{1}{2}}\}]h_\rho^{-2}dh_\rho. \tag{II.6}$$

Thus we are led to the calculation of an integral having the form

$$I=\int_0^\infty J_1(\alpha x)J_1(\beta x)J_1(\gamma x)x^{-2}dx.$$

[9] See W. Magnus und F. Oberhettinger, *Formeln und Sätze für die speziellen Funktionen der mathematischen Physik* (Julius Springer, Berlin, 1943), p. 119.

Integrating by parts and using the relation

$$(d/dx)J_1(\alpha x)=x^{-1}J_1(\alpha x)-\alpha J_2(\alpha x),$$

we obtain

$$I=\tfrac{1}{2}\alpha\int_0^\infty J_2(\alpha x)J_1(\beta x)J_1(\gamma x)x^{-1}dx +\tfrac{1}{2}\beta\int_0^\infty J_1(\alpha x)J_2(\beta x)J_1(\gamma x)x^{-1}dx +\tfrac{1}{2}\gamma\int_0^\infty J_1(\alpha x)J_1(\beta x)J_2(\gamma x)x^{-1}dx.$$

This expression reduces to elementary functions when we apply the formula due to Sonine and Dougall (see reference 9, p. 37),

$$\int_0^\infty J_2(\alpha x)J_1(\beta x)J_1(\gamma x)x^{-1}dx=(4\pi\alpha^2)^{-1}\beta\gamma(2A-\sin 2A),$$

where

$$A=\begin{cases}0 & \text{for } \alpha^2<(\beta-\gamma)^2\\ \arccos\{(2\beta\gamma)^{-1}(\beta^2+\gamma^2-\alpha^2)\} & \text{for } (\beta-\gamma)^2<\alpha^2<(\beta+\gamma)^2\\ \pi & \text{for } (\beta+\gamma)^2<\alpha^2.\end{cases}$$

Hence according to (II.6) the calculation of $\chi(r)$ is now reduced to the evaluation of a double integral. This turns out to be a straightforward though very lengthy process. The result is finally given by

$$\begin{aligned}\chi(r)=&-\{g_1(r)\}^2+\pi\{-(3/280)r^4+(41/420)r^2\}(3-r^2)^{\frac{1}{2}}\\ &+\pi\{-(23/15)r+(36/35)(1/r)\}\\ &\times\arccos\{r[3(4-r^2)]^{-\frac{1}{2}}\}\\ &+\pi\{(3/560)r^6-(1/15)r^4+\tfrac{1}{2}r^2+(2/15)r\\ &-(9/35)(1/r)\}\arccos\{(r^2+r-3)\\ &\times[3(4-r^2)]^{-\frac{1}{2}}\}+\pi\{(3/560)r^6-(1/15)r^4\\ &+\tfrac{1}{2}r^2-(2/15)r+(9/35)(1/r)\}\\ &\times\arccos\{(-r^2+r+3)[3(4-r^2)]^{-\frac{1}{2}}\}\\ &\text{for } 1\leqslant r\leqslant\sqrt{3},\end{aligned} \tag{II.7}$$

$$\chi(r)=-\{g_1(r)\}^2 \quad \text{for } \sqrt{3}\leqslant r\leqslant 2,$$

$$\chi(r)=0 \quad \text{for } r\geqslant 2.$$

It is seen that $\chi(r)$ as well as $\varphi(r)$ and $\psi(r)$ can be expressed in terms of elementary functions.

III. NUMERICAL RESULTS AND CHECKS

The expressions occurring in (II.1), (II.2), and (II.7) have been computed numerically in the relevant interval $1\leqslant r\leqslant 3$ for the values of r indicated in the first column of Table I. Then from (I.3) the function $g_2(r)$ could be computed; the result is given in the second column of Table I. $g_2(r)$ is represented graphically in Fig. 1, a plot of $g_1(r)$ may be found in de Boer's article.[1]

TABLE I. Numerical values of the term proportional to ρ^3 in the expansion of the radial distribution function of a gas of hard spheres in powers of the density ρ. $g_2(r)$ represents this term when calculated exactly, $g_2'(r)$ when the superposition approximation of Kirkwood and $g_2''(r)$ when another approximation mentioned in IV is used.

r	$g_2(r)$	$g_2'(r)$	$g_2''(r)$
1.00	1.258702	0.987940	1.096623
1.08	0.823710	0.575533	0.723392
1.16	0.453089	0.234207	0.394808
1.24	0.143406	−0.042523	0.112278
1.32	−0.108740	−0.260480	−0.123544
1.40	−0.307092	−0.425349	−0.313051
1.48	−0.455149	−0.542248	−0.456999
1.56	−0.556369	−0.615922	−0.556722
1.64	−0.613934	−0.650636	−0.613956
1.72	−0.630774	−0.650097	−0.630776
1.80	−0.608749	−0.617356	−0.608749
1.88	−0.552826	−0.554682	−0.552826
1.96	−0.463399	−0.463475	−0.463399
2.04	−0.350613	−0.350613	−0.350613
2.12	−0.254150	−0.254150	−0.254150
2.20	−0.178107	−0.178107	−0.178107
2.28	−0.119833	−0.119833	−0.119833
2.36	−0.076678	−0.076678	−0.076678
2.44	−0.046047	−0.046047	−0.046047
2.52	−0.025451	−0.025451	−0.025451
2.60	−0.012563	−0.012563	−0.012563
2.68	−0.005265	−0.005265	−0.005265
2.76	−0.001704	−0.001704	−0.001704
2.84	−0.000344	−0.000344	−0.000344
2.92	−0.000022	−0.000022	−0.000022
3.00	−0.000000	−0.000000	−0.000000

The result obtained for $g_2(r)$ may be checked in two ways by means of the known value of the fourth virial coefficient B_4 for a gas of hard spheres. First, as a consequence of the virial theorem we have generally (see e.g., reference 1, p. 327)

$$B_4=-2\pi(3kT)^{-1}\int_0^\infty \exp\{-V(r)/kT\} \times[dV(r)/dr]g_2(r)r^3dr.$$

In the case of hard spheres this becomes

$$B_4=\tfrac{2}{3}\pi\int_0^\infty \delta(r-1)g_2(r)r^3dr=\tfrac{2}{3}\pi g_2(1). \quad \text{(III.1)}$$

On substituting $r=1$ into our result for $g_2(r)$ we find an expression for B_4 which is analytically identical with the one obtained by Boltzmann.[10] Its numerical value is

$$B_4=0.2869b^3, \quad \text{(III.2)}$$

where according to the customary notation $\frac{1}{4}b$ is the volume of each particle.

An additional check which includes the values of $g_2(r)$ for all r can be based upon the well-known relation, due to Ornstein and Zernike, that connects the relative compressibility with the radial distribution function (see reference 1, p. 365)

$$kT(\partial\rho/\partial p)_T=1+4\pi\rho\int_0^\infty\{g(r)-1\}r^2dr. \quad \text{(III.3)}$$

Expanding both members of this relation into powers of ρ and equating the coefficients of equal powers, we are led to the following equality holding for hard spheres

$$B_4=-\tfrac{1}{8}b^3-\pi\int_1^\infty g_2(r)r^2dr. \quad \text{(III.4)}$$

Numerical integration of the function $g_2(r)$ gave again the result (III.2) for B_4.

IV. THE SUPERPOSITION APPROXIMATION

As has been mentioned in the introduction, the superposition assumption of Kirkwood when applied in the form as discussed by Born and Green leads to the integral Eq. (I.10) for the approximate radial distribution $g'(r)$. If we now substitute

$$g'(r)=v(r)\exp\{-V(r)/kT\},$$

then $v(r)$ obeys the integral equation

$$\frac{\partial v(r_{12})}{\partial \mathbf{r}_1}=-\frac{\rho v(r_{12})}{kT}\int v(r_{13})v(r_{23})\frac{\partial V(r_{13})}{\partial \mathbf{r}_1} \times\exp\left\{-\frac{V(r_{13})}{kT}-\frac{V(r_{23})}{kT}\right\}d\mathbf{r}_3. \quad \text{(IV.1)}$$

In accordance with the expansion (I.11) we try to solve this equation by the expansion

$$v(r)=1+\rho g_1'(r)+\rho^2 g_2'(r)+\ldots.$$

Introducing this expansion into (IV.1) and equating

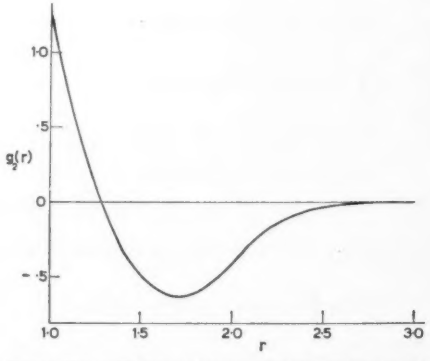

FIG. 1. The coefficient $g_2(r)$ of the term proportional to ρ^2 in the expansion of the radial distribution function for a gas of hard spheres into powers of the density ρ.

[10] L. Boltzmann, Verslag. Gewone Vergadering Afd. Natuurk. Nederlandse Akad. Wetensch. **7**, 484 (1899), see also H. Happel, Ann. Physik **21**, 342 (1906); R. Majumdar, Bull. Calcutta Math. Soc. **21**, 107 (1929).

the coefficients of ρ on both sides we find, making use of the fact that $g_1'(r)\to 0$ as $r\to\infty$

$$g_1'(r)=\int f(r_{13})f(r_{23})d\mathbf{r}_3. \qquad \text{(IV.2)}$$

Comparison of (IV.2) with (I.2) shows that

$$g_1'(r)=g_1(r), \qquad \text{(IV.3)}$$

so that the approximate $g'(r)$ is exact to first order in ρ.

In a similar way it is found that

$$g_2'(r)=\tfrac{1}{2}\{g_1(r)\}^2+\varphi(r)+2\psi(r)+\tfrac{1}{2}\chi'(r), \qquad \text{(IV.4)}$$

so $g_2'(r)$ is identical with the exact $g_2(r)$ given by (I.3) except that $\chi(r)$ must be replaced by $\chi'(r)$ where

$$\partial\chi'(r_{12})/\partial\mathbf{r}_1=-2\int f(r_{13})f(r_{23})f(r_{34})[\partial f(r_{14})/\partial\mathbf{r}_1]d\mathbf{r}_3d\mathbf{r}_4,$$

or also

$$\frac{d\chi'(r_{12})}{dr_{12}}=-2\int f(r_{13})f(r_{23})\frac{\mathbf{r}_{12}\cdot\mathbf{r}_{13}}{r_{12}r_{13}}\frac{dg_1(r_{13})}{dr_{13}}d\mathbf{r}_3. \qquad \text{(IV.5)}$$

Thus it is seen that on the assumption of superposition $g_2(r)$ is given incorrectly. An analogous result was derived by Rushbrooke and Scoins for the 4th virial coefficient.[5] For the special case of hard spheres $\chi'(r)$ can be evaluated easily with the help of (I.9). One finds[11]

$$\chi'(r)=\begin{cases}\pi^2[-r^6/630+r^4/10-(19/72)r^3-r^2/2 \\ \quad +(12/5)r-22/9+(18/35)(1/r)] \\ \qquad\qquad\qquad\qquad \text{for } 1\leqslant r\leqslant 2, \\ 0 \text{ for } r\geqslant 2.\end{cases} \qquad \text{(IV.6)}$$

Numerical values for the approximate function $g_2'(r)$ in the case of hard spheres are given in the third column of Table I. The difference $g_2(r)-g_2'(r)$ is plotted as a function of r in Fig. 2 (full curve). It is seen that for $r=1$ the Kirkwood approximation $g_2'(r)$ deviates considerably (by more than 20 percent) from the exact $g_2(r)$; for larger values of r the deviation decreases quickly and for $r\geqslant 2$ $g_2'(r)$ is equal to $g_2(r)$.

It is now very easy to calculate an approximate value for the 4th virial coefficient B_4 on the assumption of superposition. Formula (III.1), derived from the virial theorem, gives

$$B_4'=0.2252b^3, \qquad \text{(IV.7)}$$

a value that was found recently in a different way by Hart, Wallis and Pode[4] as well as by Rushbrooke and Scoins.[5] However, B_4' may also be calculated from (III.4), that is from the relation of Ornstein and Zernike. Then one obtains

$$B_4'=0.3424b^3. \qquad \text{(IV.8)}$$

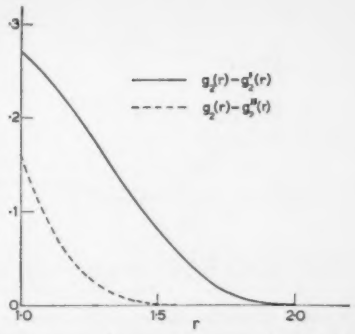

FIG. 2. Difference of the exact function $g_2(r)$ for hard spheres and the approximate functions $g_2'(r)$ (superposition approximation) and $g_2''(r)$.

We notice that the superposition approximation destroys the consistency between the equation of state as derived from $g(r)$ through the virial theorem and the equation of state resulting from the compressibility integral. This consistency requires some special analytical property of the exact $g(r)$, which is not compatible with the superposition assumption. In view of this fact one may think it questionable whether one is entitled to attach any physical meaning to analytical peculiarities exhibited by the approximate $g(r)$-function obtained under the superposition assumption. In particular conclusions drawn from Kirkwood's integral equation about a kind of condensation phenomenon for a fluid consisting of hard spheres should be accepted only with caution.[12,13]

It may be worth while to remark here that a better and simpler approximation for $g_2(r)$ is obtained in the case of hard spheres when in formula (I.7) for $\chi(r_{12})$ the factor $f(r_{34})$ in the integrand is replaced by -1, so that $\chi(r_{12})$ becomes $-\{g_1(r_{12})\}^2$. Then $g_2(r_{12})$ becomes simply [see Eq. (I.3)]

$$g_2''(r_{12})=\varphi(r_{12})+2\psi(r_{12}). \qquad \text{(IV.9)}$$

The numerical values of $g_2''(r)$ are given in the fourth column of Table I; the difference $g_2(r)-g_2''(r)$ is plotted as a dotted line in Fig. 2. The values for the 4th virial coefficient derived in this approximation from the virial theorem and from the relative compressibility integral are now respectively

$$B_4''=0.2500b^3 \quad \text{and} \quad B_4''=0.2969b^3.$$

This simple approximation is therefore much more satisfactory than that of Kirkwood, at least for the term $g_2(r)$ dealt with here. However, until now we have not

[11] This result can of course also be easily obtained directly from the integral equation (IV.1), after it has been reduced to the particularly simple form valid for hard spheres. Starting from that one could also easily calculate higher terms in the expansion of $g'(r)$ in powers of the density.

[12] Kirkwood, Maun, and Alder, J. Chem. Phys. **18**, 1040 (1950).

[13] See also R. J. Riddell, thesis (Ann Arbor, 1951).

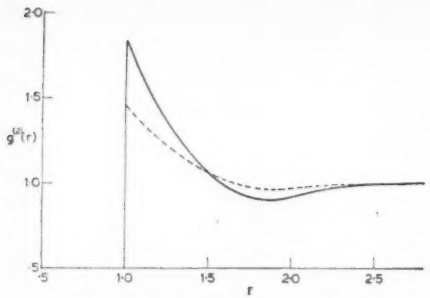

FIG. 3. Radial distribution function $g^{(2)}(r)$ (expansion into powers of the density ρ up to the term with ρ^2) for hard spheres as a function of r for values of $\rho=0.442$ (full line) and 0.275 (dotted line).

been able to extend it into a more general scheme superior to the superposition assumption.

Up to now we have discussed only the term $g_2(r)$ in the expansion (I.1) of the radial distribution function $g(r)$ into powers of the density. Evaluation of this term for hard spheres both exactly and on application of the superposition approximation made the deficiencies of the latter appear clearly. Let us consider now for a moment the radial distribution function $g(r)$ itself. Only for small densities does the part of the expansion up to the ρ^2-term, which we will call $g^{(2)}(r)$

$$g^{(2)}(r)=\exp\{-V(r)/kT\}\cdot\{1+\rho g_1(r)+\rho^2 g_2(r)\} \quad \text{(IV.10)}$$

give an adequate approximation for the function $g(r)$, because for larger densities the neglected terms would give an appreciable contribution. $g^{(2)}(r)$ has been plotted for the case of hard spheres in Fig. 3 for two values of the density: $\rho=0.442$ (full line) and $\rho=0.275$ (dotted line). It is for these densities and a few higher ones that Kirkwood, Maun, and Alder[12] recently calculated the total $g'(r)$-function for hard spheres by numerical integration of the integral Eq. (I.10). It is interesting to compare our graphs of $g^{(2)}(r)$ with the corresponding ones given by these authors for $g'(r)$; for these relatively low densities the deviations are only small. To obtain some insight in the behavior of the total $g'(r)$-function for the higher densities, one might reason as follows.[14]

From (IV.10) in combination with (I.9), (III.1), and (III.2) we have

$$g^{(2)}(1)=1+1.851\gamma+2.517\gamma^2, \quad \text{(IV.11)}$$

where $\gamma=2^{-1}\rho$ is the ratio of the density ρ to the density for close packing of the hard spheres. If in analogy with (IV.10) the function $g^{(2)\prime}(r)$ is defined by

$$g^{(2)\prime}(r)=\exp\{-V(r)/kT\}\cdot\{1+\rho g_1(r)+\rho^2 g_2'(r)\}, \quad \text{(IV.12)}$$

we find from (III.1) and (IV.7)

$$g^{(2)\prime}(1)=1+1.851\gamma+1.976\gamma^2. \quad \text{(IV.13)}$$

Table II compares, for various values of γ, the quantities $g^{(2)}(1)$ and $g^{(2)\prime}(1)$ with $g'(1)$ as obtained numerically by Kirkwood, Maun, and Alder.[12] We see that not only is

$$g'(1)<g^{(2)}(1), \quad \text{(IV.14)}$$

but also, for the higher densities

$$g'(1)<g^{(2)\prime}(1). \quad \text{(IV.15)}$$

From (IV.15) it follows that some of the virial coefficients obtained in the superposition approximation from the virial theorem are negative. It would seem extremely likely, however, that for hard spheres all virial coefficients are positive, though, as far as we are aware, this has not yet been proved in a rigorous way. Accepting this conjecture, one would conclude from (IV.14) that the pressure obtained in the superposition approximation from the virial theorem is too low, and for the higher densities, very much too low.

TABLE II. Values of the approximate radial distribution functions $g^{(2)}(r)$, $g^{(2)\prime}(r)$, and $g'(r)$ in the point $r=1$ for various densities in the case of hard spheres.

γ	$g^{(2)}(1)$	$g^{(2)\prime}(1)$	$g'(1)$
0.1942	1.455	1.434	1.45
0.3125	1.825	1.772	1.80
0.476	2.45	2.23	2.36
0.578	2.91	2.73	2.66
0.654	3.29	3.06	2.85
0.676	3.40	3.15	2.90

V. THE INTEGRAL $\int_0^\infty\{1-g(r)\}dr$

In a previous paper[8] it was shown that, when interference is taken into account, the total cross section for scattering of neutrons by a system of heavy nuclei is given asymptotically in the region of small wavelength by

$$(\sigma_{\text{tot}})_{\text{As}}=1-\rho\lambda^2/2\pi\int_0^\infty\{1-g(r)\}dr. \quad \text{(V.1)}$$

Here the total cross section of an isolated particle is taken as the unit of cross section and the radial distribution function $g(r)$ which has the same meaning as above, is obtained from the possibly angle dependent pair distribution function $g(\mathbf{r})$ by averaging over all directions. The value of the integral was investigated extensively for dense systems of particles in reference 8.

For the special case of hard spheres without attractive forces (we will take the diameter of the spheres as unit of length as we did in the foregoing) it was shown that in the region of high density the coefficient

$$K=\int_0^\infty\{1-g(r)\}dr \quad \text{(V.2)}$$

[14] The following argument was kindly pointed out to us by Dr. G. Placzek.

can approximately be represented by

$$K \approx 0.643\gamma^{-\frac{1}{2}}, \qquad (V.3)$$

where γ again is the ratio of the density ρ to the density for close packing of the spheres. Actually (V.3) does represent an upper bound, but the deviations of the true K from (V.3) may for high densities be expected to be small. On the other hand our calculation of the term $g_2(r)$ in the expansion (I.1) now enables us to evaluate K in the region of small densities. Indeed, the introduction of (I.1) into (V.2) gives

$$K = 1 - \sqrt{2}\gamma \int_1^\infty g_1(r)dr - 2\gamma^2 \int_1^\infty g_2(r)dr - \cdots. \qquad (V.4)$$

Computation of the integrals, the first from (I.9) and the second numerically from Table I, leads to

$$K = 1 - 0.648\gamma + 0.537\gamma^2 - \cdots. \qquad (V.5)$$

It may be noted that, if we had replaced the exact $g_2(r)$ in (V.4) by $g_2'(r)$ (superposition approximation) or by $g_2''(r)$, the coefficient of γ^2 in (V.5) would have been 0.741 or 0.583, respectively.

It is rather remarkable that the integral K appears to be now pretty well known for all densities, because the two representations (V.3) and (V.5) valid for high and for small densities respectively join very nicely in the intermediate region. Both approximations namely yield for $\gamma = 0.5$ the same value $K = 0.810$ (which is of course accidental) and the slopes of the two $K(\gamma)$-curves are not too different at this junction. This fact is illustrated in Fig. 4, where the function $K(\gamma)$ is plotted using Eq. (V.5) for $0 \leqslant \gamma \leqslant 0.5$ and Eq. (V.3) for $0.5 \leqslant \gamma \leqslant 1$.

For comparison we have calculated values of K for the approximate functions $g'(r)$, mentioned already in IV, which were obtained by Kirkwood, Maun, and Alder by numerical integration of the integral equation (I.10).[12] Actually in their work to every solution $g'(r)$, characterized by the value of a certain parameter λ, belong two different values of the quantity γ, depending on whether the Born-Green or the slightly different Kirkwood version of the theory is used. By a rough numerical integration of their results for the $g'(r)$-functions we find the values of K, given in Table III.[15] In this table we have also given the respective values for $I = 4 \cdot 2^{1/6}\gamma^{1/3}K$, because it was this quantity that, at least for high densities, was discussed extensively in an earlier paper.[8] The results for K are included in Fig. 4. The circles correspond to the γ-values according to Born and Green, the crosses to those according to Kirkwood. It is seen that in particular the circles (densities according to Born and Green) appear to lie rather closely on a curve joining smoothly the low and high density parts of our $K(\gamma)$-curve. In the opinion of the authors, however, the values of K do not readily lend themselves to a discussion of the validity of the superposition approximation; without a more precise investigation of accuracy the fact, that the K-values resulting from the superposition assumption lie in the neighborhood of our approximate $K(\gamma)$-curve, would hardly seem significant. As to the question of the validity (of the Born-Green form) of the superposition assumption we must rather refer to IV. In the light of the investigation in reference 8 one could only state that the values of I (and hence also of K) resulting from the Kirkwood form of the superposition assumption are definitely too high for the higher densities.

TABLE III. Values of the integrals $K = \int_0^\infty \{1 - g(r)\}dr$ and $I = 4.2^{1/6}\gamma^{1/3}K$ for various values of γ computed for the approximate radial distribution functions for hard spheres given by Kirkwood *et al.* (reference 12).

λ	K	γ(K.)	I(K.)	γ(B.G.)	I(B.G.)
5	0.89	0.211	2.38	0.194	2.31
10	0.84	0.353	2.67	0.313	2.56
20	0.78	0.562	2.91	0.476	2.75
33	0.72	0.775	2.98	0.654	2.81

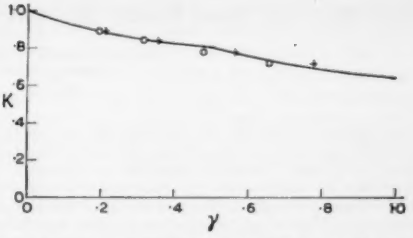

FIG. 4. The integral $K = \int_0^\infty \{1 - g(r)\}dr$ for hard spheres as a function of the ratio γ of density to density for close packing. Values obtained from integration of the numerical solutions by Kirkwood *et al.* (reference 12) of the integral equation (I.10) are indicated by circles when the Born-Green, by crosses when the Kirkwood version of the theory is adopted.

In conclusion the authors wish to thank Dr. G. Placzek of the Institute for Advanced Study, Princeton, New Jersey, who suggested the present investigation, for his stimulating interest.

[15] The values of K for the higher densities had also been computed by Kirkwood some time ago (private communication).

The Molecular Beam Electric Resonance Method Study of Thallium Monochloride*†

R. O. Carlson,‡ C. A. Lee, and B. P. Fabricand
Columbia University, New York, New York

(Received November 12, 1951)

The hyperfine structure of the first rotational state of $TlCl^{35}$ and $TlCl^{37}$ was studied by the molecular beam electric resonance method. Two types of molecular transitions were observed: the conventional m_j transition in very weak and in strong Stark fields, the type previously studied in several alkali fluorides; the ΔJ transition ($J=0\rightarrow J=1$), a molecular transition observed for the first time by molecular beam methods in this experiment.

Using the m_j type transition, the electric quadrupole interactions involving the chlorine nuclei were determined for the $J=1$, $v=0$ state. The values were $eqQ(TlCl^{35})=-(15.795\pm0.004)$ Mc/sec, $eqQ(TlCl^{37})=-(12.446\pm0.003)$ Mc/sec. The ratio of quadrupole interactions, 1.2691 ± 0.0004, is in good agreement with the ratio found for other chlorine molecules and for the chlorine atoms. The quadrupole interaction increased in absolute value by $\frac{1}{2}$ percent from one vibrational state to the next higher one. The spin-rotation ($\mathbf{I}\cdot\mathbf{J}$) interaction constants in TlCl were $+(73\pm2)$ kc for Tl, $+(1.2\pm0.2)$ kc for Cl^{35}, and $+(1.0\pm0.2)$ kc for Cl^{37}. These quadrupole interaction constants and the spin-rotation interaction constants for chlorine agree with the values given by the molecular beam magnetic resonance method.

From the rotational transition data and the strong Stark field m_j transition data, the following molecular constants were evaluated for $Tl^{205}Cl^{35}$: the rotational constant $B_e=(2620.1\pm2.5)$ Mc/sec; moment of inertia $A_e=(320.2\pm0.4)\times10^{-40}$ g-cm^2, internuclear distance $r_e=(2.541\pm0.002)$A, and dipole moment for the zeroth vibrational state $\mu_0=(4.444\pm0.014)$ Debye. The internuclear distance is in very good agreement with the electron diffraction value, (2.55 ± 0.03)A, in contrast to the case of KCl and CsCl where discrepancies of 3 to 5 percent exist between electric resonance method values and the electron diffraction experiment values. Within the experimental error, the vibration-rotation interaction constant, (13 ± 1) Mc/sec, agrees with the theoretical value predicted assuming a Morse potential for this molecule.

I. INTRODUCTION

THE molecular beam electric resonance method[1] has been used to study the molecular structure of $TlCl^{35}$ and $TlCl^{37}$. This method was previously used to investigate the radiofrequency spectra of the polar diatomic molecules CsF,[2] RbF,[3] and KF.[4] Both the thallium chlorides and the alkali fluorides were studied in the $^1\Sigma$ ground states of these molecules. The thallium compounds, however, represent a somewhat different type of molecule because the thallium atom exists in a P ground state while the alkali atoms in the alkali fluorides are in S ground states.

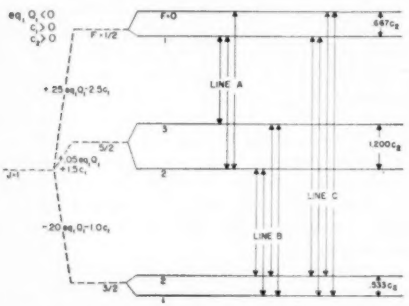

FIG. 1. The energy levels of the first rotational state of a diatomic molecule with one quadrupole moment. Observed m_j transitions are "lines A, B, and C." Arbitrary energy units. The c_2 spin-rotation splitting is greatly exaggerated in the figure relative to the quadrupole interaction splitting.

From observation of the hyperfine structure of the first rotational state of thallium chloride, it was possible to determine the electric quadrupole interactions arising from the quadrupole moments of the chlorine nuclei, and the spin-rotation ($\mathbf{I}\cdot\mathbf{J}$) interactions between the molecular angular momentum J and the chlorine or thallum nuclear spin. Other quadrupole interactions involving the chlorine nuclei have been measured in the atoms and in molecules by molecular beam magnetic resonance and microwave absorption methods.

The molecular transitions which were observed for thallium monochloride were of two types. One type of transition was between two states with the same rotational quantum number J but different values of the electric quantum number m_j, the projection of $\mathbf{J}$ in the direction of the applied electric field. This m_j transition has been used to study the $J=1$ and $J=2$ states of the alkali fluorides. A description of the apparatus and the techniques used to obtain a refocused beam in these states is given in the papers on the fluorides. The specific transition which was observed in TlCl by similar techniques was the $(1,0)-(1,\pm1)$ transition.

The second type of transition observed for $Tl^{205}Cl^{35}$ was between two energy levels in different rotational states. Such molecular transitions have been observed by microwave absorption methods for many molecules. An absorption method, however, is very difficult to use for most diatomic molecules because of the high temperatures required to form a vapor of these molecules and the consequent difficulty of keeping the absorbing wave guide hot enough to prevent excessive condensation on its walls. Neither thallium nor alkali halide molecules have as yet been studied by absorption methods.

This experiment marks the first time that a rotational

* This research has been supported in part by the ONR.

† Submitted by Richard O. Carlson in partial fulfillment of the requirements for the degree of Doctor of Philosophy in the Faculty of Pure Science, Columbia University.

‡ A.E.C. Predoctoral Fellow.

[1] H. K. Hughes, Phys. Rev. **72**, 614 (1947).

[2] J. W. Trischka, Phys. Rev. **74**, 718 (1948).

[3] V. Hughes and L. Grabner, Phys. Rev. **79**, 314 (1950).

[4] L. Grabner and V. Hughes, Phys. Rev. **79**, 819 (1950).

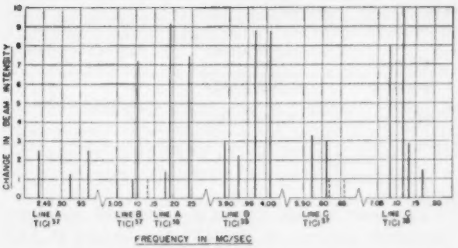

FIG. 2. Schematic plot of very weak field spectrum of $TlCl^{35}$ and $TlCl^{37}$. Zero vibrational state lines only. Dotted lines indicate predicted lines not distinguishable because of overlap with higher vibrational state lines.

transition in a molecule has been observed by a molecular beam method.[5] The entire group of alkali and thallium halides is now open to systematic study by this rotational transition method for the determination of such molecular data as the moment of inertia, internuclear distance, dipole moment, and quadrupole interactions.

Since for the rotational transition the observed energy level differences will have a dependence on the moment of inertia and hence reduced mass of the molecule, the spectral patterns for isotopic molecules will be separated from one another. In addition, because of the vibration-rotation interaction, the transition frequency which corresponds to a certain energy level separation will be appreciably different for molecules in different vibrational states.

II. THEORY AND DATA

1. The m_j Transition

The m_j transition ($\Delta J=0$) in a diatomic molecule is strictly forbidden in the absence of a static electric field. An applied Stark field superimposed on the radio-frequency C-field makes the transitions possible but splits the energy levels of the molecule and complicates the spectrum. To obtain the hyperfine structure pattern of the $J=1$ state of TlCl, the Stark field was made as small as possible consistent with observability of the transition so that the field corrections would be small. It was found possible to observe all the lines at fields of less than 5 v/cm. Corrections of less than 2 kc were then necessary to find the zero field spectrum.

The energy levels and selection rules for m_j transitions in the alkali fluorides are discussed in detail in an earlier paper.[6] This description of the energy levels is directly applicable to thallium chloride. The thallium nucleus takes the place of the fluorine nucleus since both nuclei have a spin of $\frac{1}{2}$ and hence no quadrupole moment. The chlorine nucleus has a spin of $\frac{3}{2}$ and replaces the alkali nucleus which has a quadrupole moment. The subscript 1 in this paper will apply to the chlorine nucleus and subscript 2 to the thallium nucleus.

The zero field energy levels and observable frequency pattern for a diatomic molecule in the first rotational state and with $I_1=\frac{3}{2}$, $I_2=\frac{1}{2}$, eq_1Q_1 negative, c_1 and c_2 positive, is shown in Fig. 1. The chlorine spin I_1 is coupled to J through the quadrupole interaction and the chlorine spin-rotation interaction and splits the $J=1$ rotational level into three F_1 levels where $\mathbf{F}_1=\mathbf{I}_1+\mathbf{J}$. Further splitting of the F_1 levels, caused by the coupling of the thallium spin and J through the thallium spin-rotation interaction, gives rise to the $\mathbf{F}=\mathbf{F}_1+\mathbf{I}_2$ levels. The latter splitting is much smaller than the quadrupole splitting. To show the splitting clearly in Fig. 1, however, the F levels are drawn much further apart than they would be if the figure were to scale. In the case of TlCl, the quadrupole splitting is of the order of several megacycles while the thallium spin-rotation splitting is less than 100 kc.

Transitions are observed between F states subject to various selection rules and the observability criterion.[6] The latter criterion requires that m_j change by unity in the C-field region for a transition to be observable as a defocusing of the molecular beam. Figure 2 is a schematic plot of the spectrum of $TlCl^{35}$ and $TlCl^{37}$ observed under very weak field conditions. These transitions were for zeroth vibrational state molecules only. Molecules in higher vibrational states have a spectrum slightly shifted from the frequency positions shown because of the dependence of quadrupole interaction on vibration.

The resolution[2] of the observed pattern at very weak fields is determined by the line width arising from the uncertainty relation $\Delta\nu\Delta t\sim 1$, where Δt is the time during which a transition can occur, that is, the time a molecule spends in the 4 cm wide C-field region. The oven source for a TlCl beam is at approximately 600°K. This means that the average velocity of a molecule in the beam is 2.5×10^4 cm/sec. $\Delta\nu$ is then about 6 kc. The full width at half-maximum of the observed lines was 5 to 6 kc for the narrowest lines.

When the Stark field is made very large, the field splitting becomes much larger than the quadrupole interaction splitting and the predicted pattern of observable lines becomes a known function of dipole

TABLE I. Internal interactions in TlCl for the observed line groups; $J=1$, $v=0$ state.

Molecule	Line group	$+C_2/h$ kc	$-eqQ/h$ Mc/sec Before C_1 correction	$-eqQ/h$ Mc/sec After C_1 correction
$TlCl^{35}$	A	74±1	15.7697	15.7937±0.015
	B	71±2	15.8021	15.7901±0.010
	C	74±3	15.7939	15.7979±0.005
$TlCl^{37}$	A	73±2	12.4272	12.4474±0.015
	B	75±5	12.4596	12.4496±0.010
	C	73±3	12.4401	12.4434±0.005

[5] A complete description of the apparatus and the techniques used for the rotational transition data will be given in a forthcoming paper by us on potassium chloride.

[6] V. Hughes and L. Grabner, Phys. Rev. 79, 829 (1950).

TABLE II. Internal interactions in TlCl; $J=1$, $v=0$ state.

Molecule	$+C_1^a/h$ kc	H_1^a gauss	Average $+C_2^b/h$ kc	H_2^b gauss	$-eqQ/h$ Mc/sec weighted average	Ratio of quadrupole interactions
$Tl^{205}Cl^{35}$	1.2±0.2	2.9±0.5	73±2	29.6±0.9	15.7950±0.004	1.2691±0.0004
$Tl^{205}Cl^{37}$	1.0±0.2	2.9±0.6	73±2	29.6±0.9	12.4458±0.003	

[a] Subscript 1 = Cl.
[b] Subscript 2 = Tl.

moment μ, moment of inertia A, and the static field E.[7] A plot of the energy levels of a diatomic molecule *vs* the square of the applied electric field is given in the KF paper[4] as Fig. 2(a). The pattern of observable lines consists of seven lines separated by known fractions of the quadrupole interaction. Line 1, the lowest frequency line of the pattern, was observed in $Tl^{205}Cl^{35}$ for Stark fields between 600 and 800 v/cm. The line 1 frequencies were in the range 100 to 200 Mc/sec. Only zeroth vibrational state lines were resolved since higher vibrational state lines overlap other lines in the pattern.

Under strong field conditions, the line width is principally determined by the nonuniformity of the C-field gap.[2] For the field values used in these experiments the line widths were more than 100 kc so that the spin-rotation interaction splittings could be neglected. To find the position of the unperturbed Stark line, that is, the position in the absence of quadrupole interaction splitting, corrections were made to the observed line 1 frequencies for both the diagonal and off-diagonal matrix elements of the quadrupole operator in the suitable strong field representation.[6] The effect of mixing of J states by the applied static field was also taken into account in the calculations.

2. The Rotational Transition

The rotational energy levels of a vibrating rotator model diatomic molecule in zero field, exclusive of hyperfine structure, are given by[8] $W=B_e J(J+1) - \alpha_e(v+\frac{1}{2})J(J+1)+\cdots$ where $B_e=\hbar^2/2A$ is the rotational constant of the molecule and α_e is the vibration-rotation interaction constant. The rotational transition, in contrast to the m_j transitions, can be observed at zero Stark field, and all runs in TlCl were made under this condition.

The spectrum of the $J=0$ to $J=1$ transition will consist of a series of lines, with a spacing of $2\alpha_e$ between adjacent vibrational state lines. Since the zeroth rotational state has negligible hyperfine structure, the transition pattern for a given vibrational state will be further split only by the hyperfine structure of the $J=1$ state. The spectral patterns for $Tl^{205}Cl^{35}$ and $Tl^{205}Cl^{35}$ do not coincide in frequency for the rotational transition whereas they do for the very weak field m_j transition because their quadrupole interactions are identical.

[7] H. K. Hughes, Phys. Rev. **76**, 1675 (1949).
[8] G. Herzberg, *Molecular Spectra and Molecular Structure, I. Diatomic Molecules* (D. Van Nostrand Company, Inc., New York, 1950), second edition, p. 106 ff.

The most intense line of the observed rotational transition spectrum of $Tl^{205}Cl^{35}$ was located at 5228 Mc/sec. The hyperfine structure of this $v=0$ line was only partially resolved because excessive power from a 2K43 klystron was fed into the C-field region. Several other lines were observed so that a definite assignment of this line to one of the four isotopic species of TlCl could be made. The peak of a power-broadened line corresponding to the $v=2$ state line of $Tl^{205}Cl^{35}$ was located at 5176 Mc/sec, and from the difference in frequency of this vibrational state line and the zeroth vibrational state line, the value of α_e was computed.

III. RESULTS

From the splitting of line groups A, B, and C into three or four components (see Fig. 2), we could calculate the value of c_2 and the positions of the F_1 levels after small corrections were made to account for the dipole-dipole interaction, the second-order $\mathbf{I}_2\cdot\mathbf{J}$ interaction, and the second-order quadrupole interaction coupling the $J=1$ and $J=3$ states. The quadrupole interaction constants were then computed for the three line groups as tabulated in Table I. Finally the value of c_1 was chosen which gave best agreement for the eq_1Q_1 values of a given isotope.

The averaged values of c_1, c_2, and eq_1Q_1 are listed in Table II, together with the ratio of the eq_1Q_1's for the two chlorine isotopes. H_1 and H_2 are the magnetic fields per unit rotational quantum number at the chlorine and thallium nuclei produced by the molecular rotation as computed from the equation $H=hc/\mu_N g$. The errors listed for each quantity in the table take account of the estimated accuracy of measurement of frequency and the line position centers.

In Table III are listed the molecular constants for $Tl^{205}Cl^{35}$ as determined from a combination of the rotational transition data and the strong field m_j transition data. Only the $\mu_0^2A_0$ product was used from the latter set of data although the moment of inertia and dipole moment were also calculated from this data. The values were $A_0=(331\pm16)\times10^{-40}$ g-cm^2 and $\mu_0=(4.38\pm0.15)\times10^{-18}$ esu. The $\mu_0^2A_0$ product can be determined from the m_j transition data to a much higher precision than either A_0 or μ_0 separately. The coefficient of the quadratic term in the expression[7] for the dependence of frequency of the m_j transition on electric field contains $\mu_0^2A_0$. The A_0 and μ_0 are calculable

only by observing the departure of the frequency from an E^2 field dependence.

IV. DISCUSSION

The quadrupole interactions in thallium chloride are about forty times those for an alkali chloride[9] and one-seventh that found for the chlorine atoms.[10] The negative signs of both quadrupole interactions, as determined by the observability criterion for the m_j transitions, is the same as that given for eqQ in all chlorine molecules previously investigated by microwave absorption methods.[11] The ratio of the eqQ's in $TlCl^{35}$ and $TlCl^{37}$ is in excellent agreement with other recent measurements on chlorine compounds.[10,12]

Higher vibrational state lines in the very weak Stark field m_j transition spectrum were found to be displaced to slightly higher frequencies than the corresponding $v=0$ lines. To account for this pattern, the absolute value of quadrupole interaction constant must increase by about $\frac{1}{2}$ percent for an increase of unity in the vibrational quantum number. This shift is in the opposite direction to the case of the alkali fluorides[3,4] where a decrease of about 1 percent in eqQ was observed on going to the next higher vibrational state.

A study of thallium chloride has been made simultaneously with this investigation by Zeiger and Bolef[13] using the molecular beam magnetic resonance method. The quadrupole interaction constants and the c_1 constant can be determined from their zero magnetic field spectrum. Their numerical values are in agreement with the electric resonance method results listed in Table II. This agreement provides a strong check on the validity of the analysis of the observed spectra in the two methods.

The value of the spin-rotation interaction constant, c_2, is much larger than any spin-rotation interaction constants previously reported.[2,3] Both the sign and magnitude of c_2 are definitely established by the close fit of observed and theoretical spectral patterns. The positive sign of c_2 is predicted by Foley's theory and model of the spin-rotation interaction,[14] and is the same sign as that reported for all other molecules in which this type of interaction has been observed.

It is of interest to note[15] that the ratio of the spin-rotation interactions for the thallium and chlorine nuclei, $c_2/c_1(Cl^{35})$, is equal to $73/1.2=61$, which is approximately the same as the ratio of the hyperfine structure splittings,

$$\Delta\nu(Tl)/\Delta\nu(Cl^{35})=21300^{16}/410^{10}=52.$$

[9] Lee, Carlson, Fabricand, and Rabi, Bull. Am. Phys. Soc. **27**, No. 1, 32 (1952).
[10] V. Jaccarino and J. G. King, Phys. Rev. **83**, 471 (1951).
[11] C. H. Townes and B. P. Dailey, J. Chem. Phys. **17**, 782 (1949).
[12] R. Livingston, Phys. Rev. **82**, 289 (1951).
[13] H. Zeiger and D. Bolef, Phys. Rev. **85**, 788 (1952).
[14] H. M. Foley, Phys. Rev. **72**, 504 (1947).
[15] This relationship was pointed out to us by Mr. R. A. Frosch.
[16] Berman, Kusch, and Mann, Phys. Rev. **77**, 140 (1950).

TABLE III. Molecular constants of $Tl^{205}Cl^{35}$.

Quantity	Value	Units
A_e	320.2±0.4	10^{-40} g-cm²
B_e	2620.1±2.5	Mc/sec
	874.0±0.8	10^{-4} cm^{-1}
r_e	2.541±0.002	10^{-8} cm
μ_0	4.444±0.014	10^{-18} esu
$\mu_0^2 A_0$	63.4±0.3	10^{-74} g-cm²-esu
α_e	13±1	Mc/sec

The internuclear distance, r_e which is tabulated in Table III, is in very good agreement with less accurate results obtained by two other methods.[17] An electron diffraction experiment gave a value of (2.55±0.03)A, while band spectroscopy gave a value of 2.53A. This excellent agreement of the present experimental value and the electron diffraction value for TlCl is in marked contrast to the case of KCl[9] and CsCl.[18] In KCl, the electric resonance rotational transition value was about 3 percent less than the electron diffraction value,[19] while for CsCl the electric resonance m_j transition value was about 5 percent less than the electron diffraction value.[19]

If the percent of ionic character be defined as the ratio of the dipole moment to the product of internuclear distance and electronic charge, then the value for TlCl is 37 percent.

Within its rather large experimental error, the vibration-rotation interaction constant, α_e, which is (13±1) Mc/sec, agrees with the theoretical value[20] of 13.2 Mc/sec computed from the assumption of a Morse potential for the TlCl molecule. Thallium chloride, in this respect, is radically different from the case of potassium chloride[9] where the experimental value of α_e and the Morse potential calculated value differ by about 30 percent.

We wish to express our thanks to Professor I. I. Rabi for his valuable suggestions on experimental techniques and his continued aid in the interpretation of observed spectral patterns. We have benefited from discussions with Professor H. M. Foley concerning the spin-rotation interactions. Professor Foley suggested the use of the term spin-rotation interaction rather than the previously used term spin-orbit interaction for the $\mathbf{I}\cdot\mathbf{J}$ interaction in a molecule. The apparatus on which the rotational transition was observed was constructed by Dr. V. W. Hughes.

[17] W. Grether, Ann. Physik **26**, 1 (1936).
[18] R. G. Luce and J. W. Trischka, Phys. Rev. **83**, 851 (1951).
[19] Maxwell, Hendricks, and Mosley, Phys. Rev. **52**, 968 (1937).
[20] See reference 8, p. 108.

Molecular Beam Magnetic Resonance Spectra of $TlCl^{35}$ and $TlCl^{37}$ at Zero Field*

H. J. Zeiger† and D. I. Bolef
Columbia University, New York, New York

(Received October 17, 1951)

The molecular beam magnetic resonance method has been used to investigate the spectra of $TlCl^{35}$ and $TlCl^{37}$ at zero field. A splitting of the quadrupole line for both isotopes is observed and is attributed to a cosine coupling of the form $c_a\mathbf{I}\cdot\mathbf{J}$, between the chlorine spin $\mathbf{I}_a$ and the rotational angular momentum of the molecule $\mathbf{J}$.

It is assumed that the gradient of the electric field at the position of the chlorine nucleus q is a function of the internuclear distance R of the form

$$q(R)=q^{(0)}+q^{(1)}[(R-R_e)/R_e]+q^{(2)}[(R-R_e)/R_e]^2+\cdots$$

where R_e is the equilibrium value of R in the zeroth vibrational and rotational state ($v=0$, $J=0$). The average of $q(R)$ over the vibration and rotation of the molecule is shown to lead to a v and J dependence of the quadrupole coupling eqQ of the form

$$eqQ=e\bar{q}Q+eq^{(J)}QJ(J+1)+eq^{(v)}Qv.$$

The variation of eqQ with v and J explains the asymmetry observed in the TlCl line shapes.

The energy levels and transition frequencies are calculated for TlCl, a heteronuclear diatomic molecule with one nucleus having a quadrupole coupling with v and J dependence, and a cosine coupling with $\mathbf{J}$; and the second nucleus having a cosine coupling with $\mathbf{J}$. A detailed analysis of the line shape is presented.

The results for Cl^{35} in $TlCl^{35}$ are: $|e\bar{q}Q|/h=15.788\pm0.02$ Mc, $|eq^{(v)}Q|/h=96$ kc, $|eq^{(J)}Q|/h=18.4$ cps, $|c_a|/h=1.4\pm0.1$ kc. The results for Cl^{37} in $TlCl^{37}$ are: $|e\bar{q}Q|/h=12.425\pm0.02$ Mc, $|eq^{(v)}Q|/h=76$ kc, $|eq^{(J)}Q|/h=16.4$ cps, $|c_a|/h=1.1\pm0.1$ kc. $eq^{(v)}Q$ and $eq^{(J)}Q$ are shown to have the same sign as $e\bar{q}Q$ for both $TlCl^{35}$ and $TlCl^{37}$.

The zero field lines for Na^{23} in $Na^{23}F$ and $Na^{23}Cl$ are also discussed and are analyzed using the same theory. The results for Na^{23} in $Na^{23}Cl$ are: $|e\bar{q}Q|/h=5.608\pm0.02$ Mc, $|eq^{(v)}Q|/h\sim88$ kc, $|eq^{(J)}Q|/h\sim24$ cps, $|c_a|/h\sim1$ kc. The results for Na^{23} in $Na^{23}F$ are: $|e\bar{q}Q|/h=8.40\pm0.02$ Mc, $|eq^{(v)}Q|/h\sim80$ kc, $|eq^{(J)}Q|/h\sim32$ cps, $|c_a|/h\sim1$ kc. The signs of $eq^{(v)}Q$ and $eq^{(J)}Q$ are shown to be opposite to the sign of $e\bar{q}Q$ for both $Na^{23}Cl$ and $Na^{23}F$.

I. INTRODUCTION

THE molecular beam magnetic resonance method[1-3] has been used extensively in the investigation of nuclear and molecular properties of diatomic molecules. In determining the quadrupole interaction constants of diatomic molecules, the method of "zero field" has been found of particular value. In this method, the homogeneous magnetic field in which transitions occur is reduced to zero. The zero field technique has been applied successfully by Nierenberg and Ramsey[4] in the determination of the quadrupole interaction constants of NaBr, NaCl, and NaI. The positions of the lines at zero field agreed with those predicted from the high field spectrum, in agreement with the theory of Feld and Lamb.[5] However, the lines were unexpectedly broad (150–200 kc half-width), and showed a marked asymmetry in shape.

Nierenberg and Ramsey attributed the line broadening to a cosine coupling, $c\mathbf{I}\cdot\mathbf{J}$, between the nuclear spin of sodium $\mathbf{I}$ and the rotational angular momentum of the molecule $\mathbf{J}$. It will be shown in the discussion to follow that the addition of this term to the Hamiltonian should cause a splitting of the zero field quadrupole line. That the splitting was not observed in the case of the sodium halides, Nierenberg and Ramsey attributed to a dependence of the quadrupole coupling eqQ on the vibrational quantum number v and rotational quantum number, J. As shown in Appendix III, this dependence is expected to be of the form $eqQ=e\bar{q}Q+eq^{(J)}QJ(J+1)+eq^{(v)}Qv$, where $q^{(J)}$ and $q^{(v)}$ are very much smaller than $\bar{q}$, and all three are independent of $\mathbf{J}$ and v. The spectrum observed is due to transitions between the quadrupole hyperfine structure components within a given state characterized by v and J. The transition frequencies then have a slight v and J dependence which, in the case of the sodium halides, masks the $\mathbf{I}\cdot\mathbf{J}$ splitting and causes a line asymmetry. In the case of TlCl, the v and J dependence leads to an asymmetry in the shape of the line which has been split by the $\mathbf{I}\cdot\mathbf{J}$ interaction.

In this investigation, the method of zero field has been applied not only to the determination of the quadrupole interaction constant, but also to the determination of the constants c, $eq^{(J)}Q$, and $eq^{(v)}Q$ for Cl in the molecules $TlCl^{35}$, $TlCl^{37}$; and for Na^{23} in the molecules $Na^{23}F$ and $Na^{23}Cl$. The signs of $eq^{(J)}Q$ and $eq^{(v)}Q$ are determined relative to the sign of $e\bar{q}Q$. Because the transition frequencies have only a slight v and J dependence through $eq^{(J)}QJ(J+1)$ and $eq^{(v)}Qv$, it is necessary to analyze statistically the envelope of a large number of unresolved lines in order to obtain the desired values of these nuclear and molecular constants.

These finer molecular effects on the quadrupole hyperfine structure are of interest for their contribution to the understanding of the internal interactions in a diatomic molecule. They are also of value in increasing the precision with which the quadrupole interaction constant can be measured.

* This research has been supported in part by the ONR.

† Submitted by H. J. Zeiger in partial fulfillment of the requirements for the degree of Doctor of Philosophy in Physics at Columbia University.

[1] Rabi, Millman, Kusch, and Zacharias, Phys. Rev. **55**, 526 (1939).

[2] Kellogg, Rabi, Ramsey, and Zacharias, Phys. Rev. **56**, 728 (1939).

[3] J. M. B. Kellogg and S. Millman, Revs. Modern Phys. **57**, 677 (1940).

[4] W. A. Nierenberg and N. Ramsey, Jr., Phys. Rev. **72**, 1075 (1947).

[5] B. T. Feld and W. E. Lamb, Jr., Phys. Rev. **67**, 15 (1945).

II. APPARATUS AND METHOD

The apparatus is essentially one built by Kusch and Millman[1] and used later by Nierenberg and Ramsey in their experiments on the sodium halides. Data on construction, strength of deflecting fields, and other details may be found in references 1 and 4. For the substances used in this experiment, a beam of molecules is obtained at an elevated temperature (~1000°K) in the hot oven source. At this temperature, a large number of rotational states are excited. For example, the most probable value of J for TlCl is 55.

To generate the large radiofrequency currents needed for the oscillating field, a modified form of the Hartley oscillator was used. By the use of interchangeable tank components, it was found possible to maintain oscillations with rf output currents up to 20 amperes in the frequency range from 5 to 3000 kc. Above 3000 kc, another similar oscillator designed for higher frequencies was used.

The rf current from the generator passed through the homogeneous C-field region in water-cooled twin copper sheets 1.9 cm wide, 7 cm long, and $\frac{1}{16}$ in. thick, separated by Lavite spacers so as to leave a gap $\frac{1}{16}$ in. wide down the center of the C-field. Lavite spacers were also used to prevent the hairpin (as the rf magnetic field assembly is often called) from shorting to the pole faces of the C-field. A current of 1 ampere through the hairpin gave rise to a field of 1.7 gauss in a direction perpendicular to the C-field and to the direction of the beam.

Frequency measurements at low frequency were made on a General Radio precision wavemeter, type 724B. Intermediate and high frequency measurements were made on a General Radio heterodyne meter, type 620A, with which frequency can be measured to better than 0.005 percent. Both instruments, within the range in which they were used, provide a degree of precision higher than the limits imposed by other factors which determine line positions.

Since all the data were taken at zero field, it was not necessary to measure the value of the magnetic C-field. It was, however, necessary to develop a procedure for obtaining zero field. The demagnetization procedure adopted was applied before an experimental run was made, and the fact that the results of several runs on the same resonance minima agreed so closely was taken to be adequate proof of the consistency of the demagnetization procedure. The value of the field after demagnetization was estimated as less than 4 gauss. The application of a very small dc field, less than 10 gauss, was found, as is to be expected from the Feld-Lamb theory, to have negligible effect on both the position and intensity of the resonance lines. The broadening of the zero field line by a small dc field is also predicted by the theory, but the broadening in this experiment is less than that due to the oscillating field.

By line intensity we mean the change in total beam produced by the application of the oscillating field.

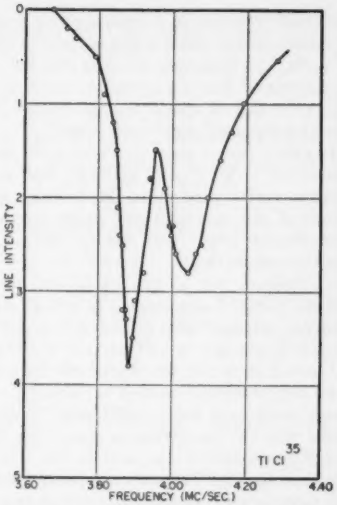

FIG. 1. Zero field spectrum of Cl^{35} in $TlCl^{35}$. Line intensity (decrease of beam at the detector) is expressed in cm deflection on a galvanometer scale. Peak intensity corresponds to a 0.5 percent decrease in total beam. Radiofrequency current was 12 amperes. The width of the line at half-intensity of each component is ~100 kc, considerably greater than the 3 kc resolution half-width of the apparatus for this molecule.

Because of the v and J dependence of the transition frequency, only a small number of states take part in the transition at a particular frequency. For this reason, the line intensity observed was small (about 1 percent of the total beam). In practice, values of the rf current were used which gave maximum line intensity without obscuring the details of the spectrum. Lowering the rf in most cases resulted in a decrease in line intensity without any observable decrease of line half-width or increase of resolution of two neighboring lines.

Due to sharply varying magnetic fields in the C-field region, nonadiabatic transitions[6] may occur between the A and B fields when the C-field is zero. Under these circumstances, the line intensity decreases because of a decrease in the number of space quantized molecules available for transition. To test whether the apparatus used in these experiments was free of such difficulties, the refocused beam intensity under normal high field conditions was compared with the beam intensity when the C-field was reversed with respect to the A and B fields. The loss in beam intensity was only a few percent, indicating a negligible loss in beam due to nonadiabatic transitions.

III. EXPERIMENTAL DATA

Neglecting all internal magnetic interactions and the variation of eqQ with v and J, one expects to see, for

[6] E. Majorana, Nuovo cimento 9 (1932).

the zero field spectrum of a heteronuclear molecule, a single resonance line whose width is given by rf broadening alone. The frequency at which this line appears would correspond to the quadrupole transition energy, which, in the case of spin $\frac{3}{2}$, is given by $\Delta W = eqQ/4$, where eqQ is the usual quadrupole coupling.[7]

It is evident from Figs. 1–4, showing the zero field spectra of Cl^{35} in $TlCl^{35}$, Cl^{37} in $TlCl^{37}$, Na^{23} in $Na^{23}F$, and Na^{23} in $Na^{23}Cl$, that other effects enter to change the shape of the curves. These effects have already been mentioned briefly and will be discussed more fully in the next section.

Since thallium has a spin of $\frac{1}{2}$, and hence no quadrupole moment, one expects to see, at zero field, quadrupole resonance lines corresponding only to the quadrupole interaction of Cl^{35} and Cl^{37} in TlCl. From Figs. 1 and 2, it can be seen that both lines are split into two components of marked asymmetry, the high frequency component being considerably broadened as compared with the low frequency component. The low frequency component is also seen to rise much more sharply than the high frequency component, the latter, indeed, tapering off very gradually to high frequencies. The width at half intensity of either component, of the order of 100 kc, is much greater than the resolution half-width of the apparatus, which is of the order of 3 kc for TlCl. Broadening due to the large rf currents, approximately 10 kc, is also too small to explain the large half-widths of the components. The ratio of the intensities of the Cl^{35} and Cl^{37} resonances is explained on the basis of relative abundance, and the difference in throwout power due to the difference in values of the nuclear g-factors. For both isotopes of chlorine, the ratio of the intensities of the split peaks is, on the average, equal to 1.7, while the ratio of the half-widths is 0.72. The splitting for the case of Cl^{35} is 156 kc; for Cl^{37}, 105 kc.

The values of these constants for both Cl isotopes in TlCl are obtained from a weighted average of data from a number of curves taken under varying experimental conditions. It was found necessary to take a large volume of data primarily because the line intensity never exceed a value of 0.5 percent of the total beam.

The general features exhibited by the resonance curves in Figs. 3 and 4 (Na^{23} in $Na^{23}F$ and $Na^{23}Cl$, respectively) are the same as those of the resonance curves in Figs. 1 and 2, although in the case of Na the splitting is not as prominent, the components being barely resolved in the case of NaCl. For the Na resonances, the high frequency approach to the resonance minimum is sharp, while the low frequency end trails off very gradually, which is opposite to the case of TlCl. In the case of NaF, the ratio of the peak intensities is 1.2; in the case of NaCl it is 1.4. The separation between peaks for NaF is 60 kc; for NaCl it is 88 kc. The ratio of the half-width of the composite line to the splitting is 2.4 in the case of NaF; in the case of NaCl it is 2.0.

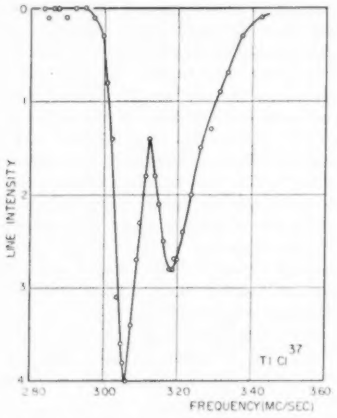

FIG. 2. Zero field spectrum of Cl^{37} in $TlCl^{37}$. Peak intensity corresponds to a 0.3 percent decrease in the total beam. The ratio of the half-widths of the split lines and the ratio of the intensities of the two wings are approximately the same as those of Fig. 1. Radiofrequency current was 15 amperes.

[7] J. Bardeen and C. H. Townes, Phys. Rev. **73**, 97 (1948).

IV. THEORY

A. Hamiltonian and Transition Energies

The Hamiltonian operator which best explains the observed magnetic resonance spectra of $TlCl^{35}$ and $TlCl^{37}$ at zero field is:

$$\mathcal{H} = \frac{-eq(R)Q}{2I_a(2I_a-1)(2J+3)(2J-1)} \times\{3(\mathbf{I}_a\cdot\mathbf{J})^2+\tfrac{3}{2}(\mathbf{I}_a\cdot\mathbf{J})-I_a(I_a+1)J(J+1)\} +c_a(\mathbf{I}_a\cdot\mathbf{J})+c_b(\mathbf{I}_b\cdot\mathbf{J}). \quad (1)$$

The first term is the electric quadrupole interaction between the chlorine nucleus and the molecular charge external to the chlorine nucleus.[7,8] Q is the electric quadrupole moment of the chlorine nucleus, and $q(R)$ is the gradient, at the position of the chlorine nucleus, of the electric field along the internuclear axis, due to all the molecular charge external to the chlorine nucleus. $q(R)$ is assumed to be a function of internuclear distance R and will be discussed further under Sec. B and in Appendix III. The second term is a cosine coupling between the spin $\mathbf{I}_a$ of the chlorine nucleus and the rotational angular momentum of the molecule.[9] The third term is a cosine coupling between the spin $\mathbf{I}_b$ of the thallium nucleus and $\mathbf{J}$. This last term is necessary to explain the electric resonance spectra of $TlCl^{35}$ and

[8] H. B. G. Casimir, Teyler's Tweede Genootschap, 1936.

[9] H. M. Foley, Phys. Rev. **72**, 504 (1947); G. C. Wick, Phys. Rev. **73**, 51 (1948).

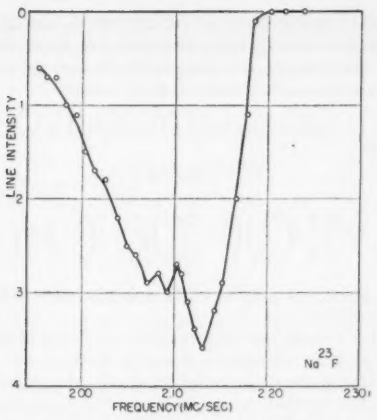

FIG. 3. Zero field spectrum of Na^{23} in Na^{23}F. Peak intensity corresponds to a 3-percent decrease in total beam. Radiofrequency current was 20 amperes.

TlCl^{37}, but will be shown in Appendix II to have a negligible effect on the spectra observed in this experiment. The effects of matrix elements of the quadrupole operator off-diagonal in J are also considered in Appendix II and are shown to be small.

Since the quadrupole coupling of $\mathbf{I}_a$ to $\mathbf{J}$ is much stronger than the cosine coupling of $\mathbf{I}_b$ to $\mathbf{J}$, the appropriate representation in which to discuss the energy levels due to (1) is the $(J, I_a, F_1, I_b, F, M_F)$ representation.[10] In this representation, $\mathbf{I}_a$ and $\mathbf{J}$ couple to give $\mathbf{F}_1$, and $\mathbf{F}_1$ couples with $\mathbf{I}_b$ to give $\mathbf{F}$. M_F is the component of $\mathbf{F}$ on the field direction.

The Hamiltonian can be written as the sum of a large part, $\mathcal{H}_0$, which is diagonal in this representation, and a small part, $\mathcal{H}_1$, which is not diagonal, as follows:

$$\mathcal{H}_0=\frac{-eq(R)Q}{2I_a(2I_a-1)(2J+3)(2J-1)}\times\{3(\mathbf{I}_a\cdot\mathbf{J})^2+\tfrac{3}{2}(\mathbf{I}_a\cdot\mathbf{J})-I_a(I_a+1)J(J+1)\}+c_a(\mathbf{I}_a\cdot\mathbf{J})+c_b(\mathbf{I}_b\cdot\mathbf{F}_1) \quad (2)$$

$$\mathcal{H}_1=-c_b(\mathbf{I}_b\cdot\mathbf{I}_a).$$

$\mathcal{H}_0$ gives energy levels nondegenerate in F_1 and F, but degenerate in M_F. However, because $(\mathbf{I}_b\cdot\mathbf{I}_a)$ does not connect states of different M_F, nondegenerate perturbation theory may be used to obtain the contribution of $\mathcal{H}_1$ to the energy levels.[11] The energy levels obtained when $I_a=\frac{3}{2}$, $I_b=\frac{1}{2}$ (the case for TlCl^{35} and TlCl^{37}) are given in Appendix I.

Transitions are produced by an oscillating magnetic field at right angles to the direction of motion of the beam, as in the usual molecular beam magnetic resonance experiments.[1-3] The selection rules for the spectra observed in this experiment are: $\Delta F=+1$, $\Delta F_1=+1$, $\Delta M_F=\pm1$; or $\Delta F=-1$, $\Delta F_1=-1$, $\Delta M_F=\pm1$. These correspond to a reorientation of spin $\mathbf{I}_a$ with respect to $\mathbf{J}$, and no reorientation of spin $\mathbf{I}_b$; they are then essentially the same as the zero field selection rules $\Delta F=\pm1$, $\Delta M_F=\pm1$ for the case of a single nuclear spin $\mathbf{I}$ coupled to $\mathbf{J}$ to give the resultant $\mathbf{F}$.

Application of these selection rules leads to the transition energies for the case $I_a=\frac{3}{2}$, $I_b=\frac{1}{2}$,

$$W(F_1=J+\tfrac{3}{2}\leftrightarrow F_1=J+\tfrac{1}{2})=-\frac{eq(R)Q}{4}+c_a(J+\tfrac{3}{2})+\frac{3c_b}{4J}-\frac{3[1\mp1]c_b^2}{eq(R)Q} \quad (3a)$$

$$W(F_1=J+\tfrac{1}{2}\leftrightarrow F_1=J-\tfrac{1}{2})=-\frac{3}{4}\frac{eq(R)Q(2J+1)}{(2J+3)(2J-1)}+c_a(J+\tfrac{1}{2})+\frac{c_b}{J}[\pm1-\tfrac{3}{4}] \quad (3b)$$

$$W(F_1=J-\tfrac{1}{2}\leftrightarrow F_1=J-\tfrac{3}{2})=\frac{eq(R)Q}{4}+c_a(J-\tfrac{1}{2})+\frac{c_b}{J}[\mp1+\tfrac{3}{4}]+\frac{3[1\mp1]c_b^2}{eq(R)Q}, \quad (3c)$$

where $W(F_1+1\leftrightarrow F_1)=E(F_1+1)-E(F_1)$, $F=F_1+i_b$, and $(\pm)$ refer to $i_b=\pm\frac{1}{2}$.

Since $c_b\sim73$ kc,[12] $eqQ\sim15$ Mc, and the most probable $J=55$ (see Sec. II), the contribution of the second

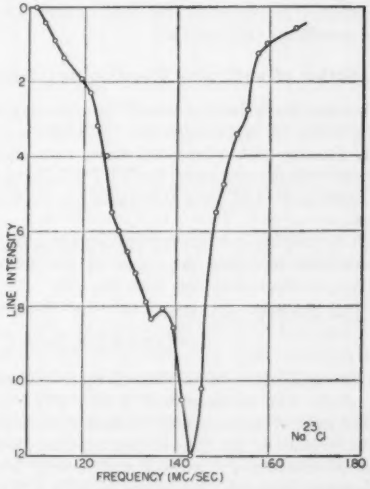

FIG. 4. Zero field spectrum of Na^{23} in Na^{23}Cl. Peak intensity corresponds to a 0.8-percent decrease in total beam. Radiofrequency current was 10 amperes.

[10] E. U. Condon and G. Shortley, *Theory of Atomic Spectra* (Cambridge University Press, London, 1935), Chapter III.

[11] See reference 10, Chapter II.

[12] Carlson, Lee, and Fabricand, Phys. Rev. **85**, 784 (1952).

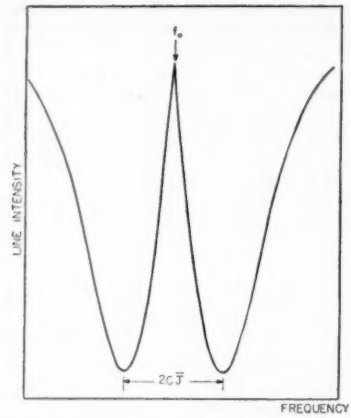

FIG. 5. The effect of the cJ term on a zero field line, assuming no other v or J dependence. f_0 marks the frequency at which the single resonance line would fall if there were no $\mathbf{I}\cdot\mathbf{J}$ interaction. The frequencies of the peaks of the wings are given by $f_1=f_0+c\bar{J}$, $f_2=f_0-c\bar{J}$, where $\bar{J}$ is the most probable J in the oven source. The splitting, neglecting all other effects, is then given by $2c\bar{J}$. This figure is a graphical representation of step 2 in the line shape analysis of Sec. C.

nucleus to the transition energies is negligibly small for most molecules in the beam. The effect of the second nucleus is considered in Appendix II.

For large J, the J dependence in (3b) gives a low frequency transition which is not observed in this experiment. The observed zero field spectra are due to the transitions (3a) and (3c).

B. Variation of eqQ with Vibration and Rotation

It has previously been observed[13] in molecular beam electric resonance experiments that eqQ varies approximately linearly with vibrational state, with about a 1 percent variation per state. For $TlCl^{35}$, Carlson, Lee, and Fabricand[12] find that this variation is (0.5 ± 1) percent.

Such a variation can be explained by assuming that q varies with R during the course of the molecular vibration, as assumed in Sec. A above, with

$$q(R)=q^{(0)}+q^{(1)}[(R-R_e)/R_e]+q^{(2)}[(R-R_e)/R_e]^2+\cdots. \quad (4)$$

R_e is the equilibrium internuclear distance in the state $v=0$, $J=0$. The coefficients $q^{(0)}$, $q^{(1)}$, $q^{(2)}$, $\cdots$ are assumed to be of the same order of magnitude to ensure the convergence of (4). It is interesting that the theoretical calculations of Nordsieck and Newell[14] for q in the deterium molecule give values of $q^{(0)}=1.15\times10^{15}$, $q^{(1)}=-5.50\times10^{15}$, and $q^{(2)}=13.0\times10^{15}$, in esu all the same order of magnitude. It is shown in Appendix III that the average value of expansion (4) over the molecular rotation and vibration is of the form:

$$q=q^{(0)}+q^{(J)}J(J+1)+q^{(v)}(v+\tfrac{1}{2}) \quad (5)$$

where

$$q^{(J)}=(2B_e/\omega_e)^2q^{(1)},$$

and

$$q^{(v)}=\left[3\left(\frac{B_e}{\omega_e}\right)\left(1+\frac{\alpha_e\omega_e}{6B_e^2}\right)q^{(1)}+2\left(\frac{B_e}{\omega_e}\right)q^{(2)}\right]$$

and B_e, ω_e, α_e, are the usual molecular constants[15] in units of cm^{-1}.

This average not only describes the linear variation of eqQ with vibrational quantum number, but also predicts a quadratic variation of eqQ with rotational quantum number. As will be seen in Sec. V, an analysis of the zero field line shape of $TlCl^{35}$ and $TlCl^{37}$, assuming a rotational and vibrational variation, can be made to explain the observed spectra rather well. The values of $eq^{(0)}Q$, $eq^{(1)}Q$, and $eq^{(2)}Q$ obtained will be consistent with the assumption that $q^{(0)}$, $q^{(1)}$, $q^{(2)}$ are all of the same order of magnitude. While $q^{(J)}$ and $q^{(v)}$ have a slight dependence on isotope through the rotational and vibrational constants, $q^{(0)}$, $q^{(1)}$, and $q^{(2)}$ are the same for different isotopes in the same molecule.

C. Line Shape

If we neglect the terms due to c_b, and replace $q(R)$ in (3a) and (3c) by q of (5), we obtain for the observed transition frequencies:

$$f_1=f_0+Pv+gJ^2-CJ, \quad f_2=f_0+Pv+gJ^2+CJ \quad (6)$$

where

$$f_0=(eq^{(0)}+\tfrac{1}{2}eq^{(v)})Q/4h\equiv e\bar{q}Q/4h, \quad P=eq^{(v)}Q/4h,$$
$$g=eq^{(J)}Q/4h, \quad c=c_a/h.$$

In (6) we have neglected small v and J independent terms of order $|c_a|/h$, since $|c_a|/h$ is only about 1 kilocycle; and we have neglected gJ compared to cJ, since $g\ll c$. Also, $e\bar{q}Q$ has been assumed positive for convenience. We cannot deduce the sign of $e\bar{q}Q$ from our observations, though Carlson, Lee, and Fabricand[12] are able to determine the sign. The v and J independent part of (6) is not $eq^{(0)}Q$, but $e\bar{q}Q$, which is only very slightly different.

For convenient analysis of the zero field line shape, we neglect rf line broadening and other small effects, and reconstruct the line by the following steps:

1. With no v or J dependence, we have two superposed resonance curves, whose half-widths are determined by the resolution properties of the apparatus.

[13] L. Grabner and V. Hughes, Phys. Rev. **79**, 819 (1950).
[14] A. Nordsieck, Phys. Rev. **58**, 310 (1940); G. F. Newell, Phys. Rev. **78**, 711 (1950).
[15] G. Herzberg, *Spectra of Diatomic Molecules* (D. Van Nostrand Company, Inc., New York, 1950), second edition.

2. The cJ terms cause a linear displacement of f_1 and f_2 with J. Because of the close spacing of the levels for successive values of J, the transitions for individual J values will not be separately resolved, and a pair of structures will result, one for f_1 and one for f_2. The distribution of J states in the beam is given approximately by:

$$N(J)dJ \sim (2J+1)\exp[-\tfrac{1}{2}\alpha^2 J(J+1)] \sim J\exp(-\tfrac{1}{2}\alpha^2 J^2) \text{ for large } J, \quad (7)$$

where

$$\alpha^2 = 2B_e hc/kT = 1/\bar{J}^2.$$

$\bar{J}$ is the most probable J of the beam, and B_e is the rotational constant of the molecule.[15] The wings corresponding to f_1 and f_2 are symmetric about f_0, with a shape function given by the rotational distribution $N(J)$ (Fig. 5). Since the rotational distribution has its maximum at $J=\bar{J}$, the splitting between the wings is $2c\bar{J}$. If the sign of c were reversed, the roles of f_1 and f_2 would be reversed, and there would be no change in the observed spectrum.

3. The effect of gJ^2 will be to spread the wing where c and g are of the same sign (the additive wing) still further, and to narrow the wing where they are of opposite sign (the subtractive wing). This will give an observable asymmetry in the two wings, even though $g \ll c$, because g appears as gJ^2 while c appears as cJ. For large enough J, for the subtractive wing, gJ^2 will overcome the effect of cJ, and the wing will fold back on itself (Fig. 6). If $q^{(0)}$ and $q^{(J)}$ are of opposite sign, the subtractive wing will fall at higher frequencies; if $q^{(0)}$ and $q^{(J)}$ are of the same sign, the subtractive wing will fall at lower frequencies.

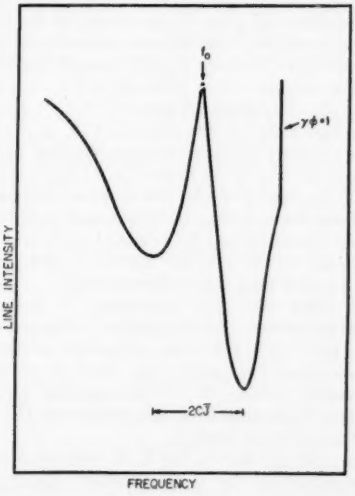

FIG. 6. The effect of the gJ^2 term on the curve of Fig. 5, as discussed in step 3 of Sec. C. The additive wing in this instance is the low frequency wing. For large J, the subtractive wing will fold back on itself, as is indicated here by the high frequency cutoff, at $\gamma\phi=1$.

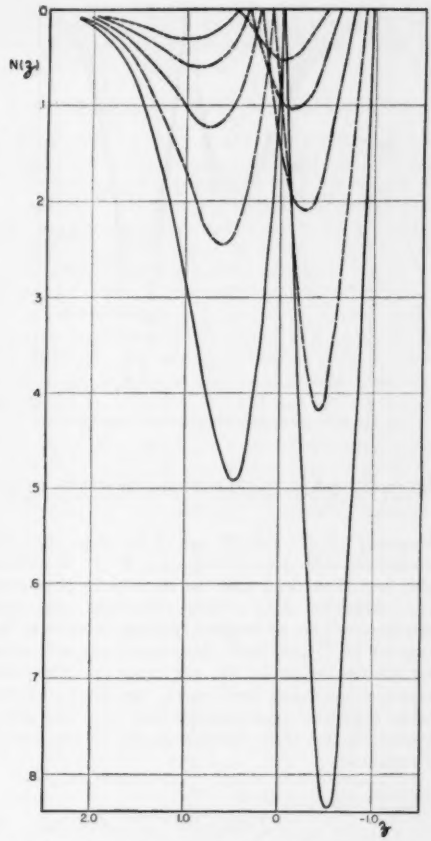

FIG. 7. The effect of the term Pv in Eq. (6), corresponding to step 4 in the line shape analysis. A series of curves of the form of Fig. 6 is found, each shifted in frequency by an amount Pv. The curves shown here are for $\gamma=0.30$. Their envelope, given in Fig. 9, gives best agreement with the experimentally observed resonance curves of TlCl^{35} and TlCl^{37}, shown in Figs. 1 and 2. $N(z)=\phi\exp(-\frac{1}{2}\phi^3)/|1\mp\gamma\phi|$, where $z=\pm\phi+\frac{1}{2}\gamma\phi^2=h(f-f_0)/c_\omega\bar{J}$.

4. The ratio of populations of successive vibrational states for a diatomic molecule is $\exp(-hc\omega_e/kT)$, where ω_e is the vibrational constant of the molecule.[15] The term Pv in (6) thus gives a series of pairs of wings, as in (3), of relative intensity $\exp(-hc\omega_e/kT)$, each shifted in frequency by an amount Pv (Fig. 7). If $q^{(0)}$ and $q^{(v)}$ are of opposite sign, the vibrational shift is down in

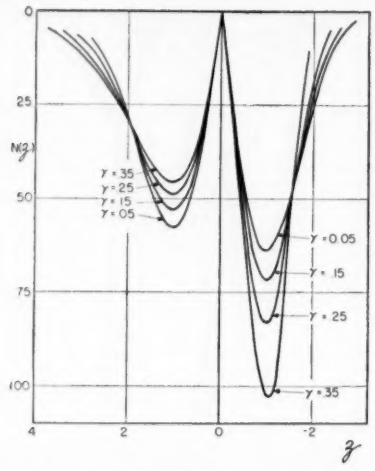

FIG. 8. $N(z)$ *vs* z for various values of the parameter γ, where $\gamma=(\bar{J}/2c_a)eq^{(J)}Q$, $z=h(f-f_0)/c_a\bar{J}$. (See definitions (9).)

frequency; if $q^{(0)}$ and $q^{(v)}$ are of the same sign, the vibrational shift is up in frequency. If $|P|$ is appreciably less than $|c|J$, and the decrease in population per vibrational state is large, then the vibrational structure will not be resolved. This turns out to be the case for $TlCl^{35}$ and $TlCl^{37}$. We obtain a shape function for the frequencies of (6), neglecting the vibrational superposition due to the term Pv. The latter effect has to be considered separately for each case. The distribution function (7) is transformed from J variables to f variables:

$$N(f)df=N(J)|dJ/df|df$$
$$=J\exp(-\tfrac{1}{2}\alpha^2J^2)df/|\pm c+2gJ|, \quad (8)$$

where the (+) and (−) refer to f_1 and f_2, respectively. We introduce the parameters:

$$\phi=\alpha J=J/\bar{J} \quad (9)$$
$$z=\alpha(f-f_0)/c=(f-f_0)/c\bar{J}=\pm\phi+(g/c\alpha)\phi^2, \quad \text{from (6)}$$
$$g/c\alpha=\gamma/2$$

(8) then gives

$$N(z)\sim\phi\exp(-\tfrac{1}{2}\phi^2)/|1\mp\gamma\phi| \quad (10)$$

where $z=\pm\phi+\frac{1}{2}\gamma\phi^2$.

$N(z)$ *versus* z is plotted in Fig. 8 for several values of the parameter γ. A small value of g is enough to produce a considerable asymmetry. For example, when $\gamma=0.25$, the ratio of the peak intensities of the wings is 1.7:1. If J is about 40, this corresponds to g/c of 6×10^{-8}. Because of the large value of $\bar{J}$, c and g can be determined fairly accurately, since the line splitting is about $2c\bar{J}$, and γ is proportional to $\bar{J}$.

The subtractive wing shows a discontinuity at $\gamma\phi=1$. The density function goes to infinity at this point, but for $\gamma\lesssim0.4$, the integrated area at the discontinuity is so small that the line is not affected appreciably.

V. ANALYSIS OF $TlCl^{35}$ AND $TlCl^{37}$ CURVES

The spectra of $TlCl^{35}$ and $TlCl^{37}$ are analyzed, using the theory of the previous section. The value of $\gamma=2g/c\alpha$, in the notation of the previous section, is selected so that, when used in conjunction with a known value of $eq^{(v)}Q$,[12] the composite curve resulting from a graph of $N(z)$ *versus* z for several vibrational states will agree as closely as possible with the experimental curve. In the case of $TlCl^{35}$ and $TlCl^{37}$, a value of $\gamma=0.25$ was found to give the best fit. The reason the same value of γ serves for both isotopes is that

$$\frac{\gamma^{35}}{\gamma^{37}}\sim\left(\frac{g}{c}\right)^{35}\Big/\left(\frac{g}{c}\right)^{37}\sim\left(\frac{Q}{\mu}\right)^{35}\Big/\left(\frac{Q}{\mu}\right)^{37}$$

(μ is the nuclear magnetic dipole moment), and this ratio is very close to one. There are two isotopes of Tl, Tl^{203}, and Tl^{205}, but both have spin $\frac{1}{2}$ and almost identical masses, so that the spectra of Cl for these two isotopes of Tl are the same.

The factor for the decrease in line intensity for successive vibrational states is 0.50. With a value of $eq^{(v)}Q$ equal to $0.006e\bar{q}\bar{Q}$, which is close to the value of $(0.005\pm0.001)e\bar{q}\bar{Q}$ given by the results of the electric resonance method,[12] the curves corresponding to the states $v=0$, 1, 2, 3, and 4 are plotted in Fig. 7. The envelope of these curves is shown in Fig. 9, together with a set of experimental points for $TlCl^{37}$. The ratio of the half-widths of the wings is 1.75, as compared with an average of 1.8 for the experimentally observed minima; the ratio of the intensities is 0.62 as compared with an average of 0.7 for the observed minima. The difference between the calculated and experimental ratio of intensities may be explained by rf broadening effects, and by the difficulty inherent in observing the peak intensity for a narrow resonance line.

The value of $|c_a|/h$ is obtained by noting the separation between the split peaks of the zeroth vibrational line. $|e\bar{q}\bar{Q}|/h$ is then determined as the mean between these two peaks. The value of $eq^{(J)}Q/h$ is obtained by solving for g in the equation $g=c\alpha\gamma/h$. The results obtained from this analysis of $TlCl^{35}$ and $TlCl^{37}$ are given in Table I.

The splitting due to the $\mathbf{I}_a\cdot\mathbf{J}$ interaction can be expressed as that due to an equivalent magnetic field at the chlorine nucleus due to the rotation of the molecule as a whole. The magnitude of the magnetic field per rotational quantum number H_a is given by $H_a=|c_a/g_I\mu_N|$. The value of c_a for $Cl^{35}=1.4$ kc,

equivalent to $H_a=3.4$ gauss; the value of c_a for Cl^{37} is 1.1 kc, equivalent to $H_a=3.2$ gauss.

The sign of eqQ has been found to be negative, the sign of c_a to be positive.[12] Since the resonance curve tapers off gradually at high frequencies, $eq^{(v)}Q$ has the same sign as eqQ. Since the high frequency wing is broadened by the effect of the rotational variation, as discussed in Sec. IV C, $eq^{(J)}Q$ has the same sign as eqQ. In other molecules in which results are available (CsF,[16] RbF,[17] KF[18]), $eq^{(v)}Q$ and eqQ have opposite signs.

The criteria for the validity of the expansion of $q(R)$ given in Eq. (4) are given in Eq. (20) of Appendix III as:

$$\begin{aligned}&(\Delta R/R_e)_{\text{rot}}=(2B_e/\omega_e)^2\bar{J}(\bar{J}+1)\ll 1\\&(\Delta R/R_e)_{\text{vib}}=(B_e/\omega_e)^{\frac{1}{2}}\ll 1 \quad \text{for } J=\bar{J}, \text{ and } v=0.\end{aligned} \tag{11}$$

For TlCl^{35}, $B_e\sim 0.0873$ cm^{-1}, $\omega_e=287.47$ cm^{-1}, $\alpha_e=4.3\times 10^{-4}$ cm^{-1},[18] $\bar{J}=55$. Substituting in Eqs. (11), we obtain:

$$\begin{aligned}&(\Delta R/R_e)_{\text{rot}}=11.4\times 10^{-4},\\&(\Delta R/R_e)_{\text{vib}}=1.74\times 10^{-2},\end{aligned} \tag{12}$$

TABLE I. Experimental values for molecular constants in the molecules TlCl^{35}, TlCl^{37}, Na^{23}F, and Na^{23}Cl.[a]

Molecule	eqQ/h Mc	c_a/h kc	H_a gauss	$eq^{(v)}Q/h$ kc	$eq^{(J)}Q/h$ cycles/sec
TlCl^{35}	(−)15.788 ±0.02	(+)1.4 ±0.1	3.4 ±0.3	−96	−18.4
TlCl^{37}	(−)12.425 ±0.02	(+)1.1 ±0.1	3.2 ±0.3	−76	−16.4
Na^{23}F	8.40 ±0.02	~1	~1	+80	+32
Na^{23}Cl	5.61 ±0.02	~1	~1	+88	+24

[a] Signs for eqQ/h for TlCl^{35} and TlCl^{37} are from reference 12. Signs for c_a/h for TlCl^{37} and TlCl^{35} are from reference 18.

from which we infer that for TlCl^{35} the expansion of $q(R)$ given in Eq. (4) is valid. For TlCl^{35} the experimental values which are used to obtain $eq^{(0)}Q$, $eq^{(1)}Q$, and $eq^{(2)}Q$ are:

$$\begin{aligned}eqQ/h&=-15.788\times 10^6 \text{ cycles/sec},\\eq^{(v)}Q/h&=-96\times 10^3 \text{ cycles/sec},\\eq^{(J)}Q/h&=-18.4 \text{ cycles/sec}.\end{aligned}$$

From the relationships of (5) and the definition of $\bar{q}$ in (6), we obtain:

$$\begin{aligned}eq^{(0)}Q/h&=-15.740\times 10^6 \text{ cycles/sec},\\eq^{(1)}Q/h&=-49.6\times 10^6 \text{ cycles/sec},\\eq^{(2)}Q/h&=+100\times 10^6 \text{ cycles/sec}.\end{aligned}$$

In the case of TlCl^{35}, then, the assumption that $|q^{(0)}|\sim|q^{(1)}|\sim q^{(2)}|$ is justified.

[16] J. W. Trischka, Phys. Rev. **74**, 718 (1948).
[17] V. Hughes and L. Grabner, Phys. Rev. **79**, 314 (1950).
[18] Carlson, Lee, and Fabricand, private communication.

The results for TlCl^{37} are obtained in a similar manner, and the constants for both TlCl^{35} and TlCl^{37} are given in Table I.

VI. ANALYSIS OF Na^{23}Cl AND Na^{23}F CURVES

An analysis similar to that of the spectrum of TlCl is performed for the observed zero field lines of Na^{23}Cl and Na^{23}F. Since the splitting in the latter cases is not as prominent, less sensitive criteria are used to guide the choice of constants in constructing the line shapes. Thus the ratio of intensities of the two wings, and the ratio of the half-width of the composite line to the splitting are used in the selection of values of γ and of $eq^{(v)}Q$ which lead to a line shape similar to that experimentally observed. The value of ω_e is not known for Na^{23}F, but an empirical estimate gives $\omega_e=530$, so that the decrease in line intensity with vibrational state is 0.53. Values of $\gamma=0.25$ and $eq^{(v)}Q=0.01eqQ$ are found to give the best fit. The line, constructed as described in Sec. IV C, then has for the ratio of intensities 1.22, as compared with 1.25 actually observed for Na^{23}F; and for the ratio of half-width of composite line to splitting 2.1, compared with 2.4 actually observed.

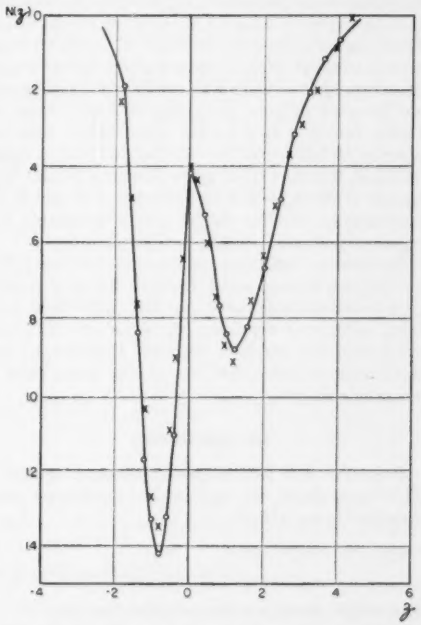

FIG. 9. Envelope of the curves of the first five vibrational states for TlCl given in Fig. 7. γ was taken to be 0.30 for best agreement with the experimental resonance curves for TlCl^{35} and TlCl^{37}. For purposes of comparison, the experimental points of the TlCl^{37} resonance in Fig. 2 are indicated here by crosses.

The values of the constants obtained are listed in Table I. The zero field value of eqQ for Na in $Na^{23}F$, 8.40 Mc, is to be compared with the high field value of 8.12 Mc, obtained by Logan and Coté.[19] The 3 1/2 percentage discrepancy between these results is consistent with similar discrepancies found in the other sodium halides.[4] This effect in the sodium halides will be discussed more fully in the following section.

In the case of Na^{23} in $Na^{23}Cl$, the decrease of line intensity with vibrational state is 0.58, and the values of γ and $eq^{(v)}Q$ which give the best fit are again $\gamma=0.25$ and $eq^{(v)}Q=0.01eqQ$. The ratio of intensities of the wings is 1.36, as compared with the experimentally observed ratio of 1.43; while the ratio of the half-width of the composite line to the splitting, 1.9, is to be compared with the experimentally observed ratio of 2.0. The constants obtained from an analysis of the $Na^{23}Cl$ line are listed in Table I. The signs of $eq^{(v)}Q$ and $eq^{(J)}Q$ are found to be opposite to the sign of eqQ for both $Na^{23}F$ and $Na^{23}Cl$.

In the analysis of the line shape of $Na^{23}F$ we have neglected the effect of an $\mathbf{I}_b\cdot\mathbf{J}$ interaction for fluorine; and in the case of $Na^{23}Cl$, we have neglected both the quadrupole interaction and $\mathbf{I}_b\cdot\mathbf{J}$ interaction of chlorine. As indicated in Appendix II, eqQ for Cl in $Na^{23}Cl$ would have to be greater than 3.2 Mc to affect the line shape. The values of c_b for F in $Na^{23}F$ and Cl in $Na^{23}Cl$ would have to be about 100 kc or more to affect the line shapes. However, eqQ for Cl in KCl is 420 kc,[19] which should not be much different from eqQ for NaCl; while the known values of $\mathbf{I}_b\cdot\mathbf{J}$ for the alkali halides observed experimentally[17] are of the order of 10 kc. It is highly probable, therefore, that these constants are not large enough to affect the sodium spectra in NaF and NaCl. Furthermore, the line shapes can be reasonably well explained without assuming their presence.

Because the molecular constants of NaCl and NaF are not well known, and because of the large possible error in determining $eq^{(v)}Q$ and $eq^{(J)}Q$ for these molecules, we cannot determine the constants $eq^{(1)}Q$ and $eq^{(2)}Q$ with any degree of precision. However, an estimate indicates that they are of the same order of magnitude as $eq^{(0)}Q$.

VII. DISCUSSION

From the zero field magnetic resonance spectra of $TlCl^{35}$ and $TlCl^{37}$, the ratio of the quadrupole interactions is found to be:

$$|eqQ(Cl^{35})|/|eqQ(Cl^{37})| = 15.788/12.425 = 1.270\pm0.005.$$

The electric resonance method gives the result:

$$|eqQ(Cl^{35})|/|eqQ(Cl^{37})| = 1.2691\pm0.0005.$$

These results and the results of recent atomic beam[20] and microwave[21] measurements of the chlorine-quadrupole-moment-ratios all agree within limits of experimental error.

It is interesting to note that the quantity eq, which normally enters into the experimentally measured quadrupole coupling, is not the same for two isotopes in the same molecule because of different zero point vibration for the two isotopes. A simple calculation shows that the error introduced by this effect into the quadrupole moment ratio is about 1 in 14,000 for TlCl, negligible for these experiments. The ratio of the magnitude of c_a for $TlCl^{35}$ to c_a for $TlCl^{37}$ is:

$$|c_a(Cl^{35})|/|c_a(Cl^{37})| = 1.4/1.1 = 1.25\pm0.10.$$

The Foley and Wick[9] theories of the $\mathbf{I}\cdot\mathbf{J}$ interaction explain the effect as due to the coupling of the nuclear magnetic moment with the internal magnetic fields of the molecule. On this model, or, in fact, on any reasonable model, the constant c_a would be expected to be proportional to the nuclear magnetic moment for isotopes in the same molecule. The ratio of the magnetic moments of Cl^{35} and Cl^{37} is $\mu(Cl^{35})/\mu(Cl^{37})=1.21$,[22] in good agreement with the ratio of $|c_a(Cl^{35})|/|c_a(Cl^{37})|$. This gives further support for assuming that the split line in TlCl is actually due to an $\mathbf{I}\cdot\mathbf{J}$ interaction.

Nierenberg and Ramsey[4] point out that there exists a 5-percent discrepancy between the values of the quadrupole coupling obtained at zero field and at high field. They are able to explain about $\frac{1}{5}$ of this discrepancy by a refinement of the analysis of the high field line, taking into account resolution and the distribution of J states in the beam. Another small fraction of the discrepancy may be explained by the fact that they took the position of the zero field quadrupole resonance to be at the position of the highest peak. The actual zero field quadrupole resonance corresponds more nearly to the midpoint between the highest peak, for the subtractive wing, and the lower secondary peak for the additive wing (which, in the case of the sodium halides is barely resolved). After these effects have been considered, there still remains a small discrepancy between the zero and high field values, which can perhaps be explained by considering the effect of the rotational and vibrational variations of eqQ on the high field spectrum.

We are grateful to Professor I. I. Rabi for suggesting this problem, and for his guidance throughout the course of the experiment. We are greatly indebted to Professor T. Y. Wu for his help and encouragement during the early stages of the experiment. We also wish to thank the members of the molecular beams laboratories, and Professors C. H. Townes and H. M. Foley for several helpful suggestions.

[19] Logan, Coté, and Kusch, private communication.
[20] V. Jaccarino and J. G. King, Phys. Rev. **83**, 471 (1951).
[21] R. Livingston, Phys. Rev. **82**, 289 (1951).
[22] F. Bitter, Phys. Rev. **75**, 1326 (1949); H. Taub and P. Kusch, Phys. Rev. **75**, 1481 (1949).

APPENDIX I. ZERO FIELD ENERGY LEVELS FOR $I_a=\frac{1}{2}$, $I_b=\frac{1}{2}$

The matrix elements of $(\mathbf{I}_a\cdot\mathbf{I}_b)$ are calculated in the $(F, F_1, J, I_a, I_b, M_F)$ representation as:

$$\langle I_A JF_1 I_b FM_F|\mathbf{I}_a\cdot\mathbf{I}_b|I_A JF_1 I_b FM_F\rangle=\frac{1}{2}\left\{\frac{I_a(I_a+1)-J(J+1)+F_1(F_1+1)}{2F_1(F_1+1)}\right\}\{F(F+1)-F_1(F_1+1)-I_b(I_b+1)\}$$

$$\langle I_a JF_1-1I_b FM_F|\mathbf{I}_a\cdot\mathbf{I}_b|I_a JF_1 I_b FM_F\rangle=\frac{[(F_1-I_a+J)(F_1+I_a-J+1)(F_1+I_a+J+1)(I_a+J+1-F_1)]^{\frac{1}{2}}\cdot[(F+F_1-I_b)(F+I_b-F_1+1)(F+I_b+F_1+1)(F_1+I_b-F)]^{\frac{1}{2}}}{4F_1[4F_1^2-1]^{\frac{1}{2}}} \quad (13)$$

$$\langle I_a JF_1+1I_b FM_F|\mathbf{I}_a\cdot\mathbf{I}_b|I_a JF_1 I_b FM_F\rangle=\frac{[(F_1-I_a+J+1)(F_1+I_a-J+1)(F_1+I_a+J+2)(I_a+J-F_1)]^{\frac{1}{2}}\cdot[(F+F_1-I_b+1)(F+I_b-F_1)(F+I_b+F_1+2)(F_1+I_b-F+1)]^{\frac{1}{2}}}{4(F_1+1)[4(F_1+1)^2-1]^{\frac{1}{2}}}.$$

The perturbation H_1 is $[-c_b(\mathbf{I}_a\cdot\mathbf{I}_b)]$. From (13), the first-order perturbation $E^{(1)}$ is of order $|c_b|$. The energy denominator appearing in the second-order perturbation energy $E^{(2)}$ is

$$E(F_1, F)-E(F_1+1, F)\sim\frac{3}{8}\frac{eqQ(2J+2i_a+2)}{I_a(2I_a-1)(2J+3)(2J-1)}[(4i_a+2)J+2i_a(i_a+2)-2I_a(I_a+1)+3]-c_aJ+c_bJ, \quad (14)$$

for large J.

From (14), we see that, for large J, the second-order perturbation energy $E^{(2)}$ is of order $|c_b|^2/|eqQ|$ for $i_a\neq-\frac{1}{2}$; in the case when $i_a=-\frac{1}{2}$, $E^{(2)}\sim|c_b|^2/|c_b|J$.

Note, the perturbation calculation may diverge for $i_a=-\frac{1}{2}$ when (14) is zero. However, if this does occur at all, it occurs for fairly low J, and (14) remains small only for a few J states, so that the effect on the line shape should be small.

The energy levels for large J, up to order $E^{(2)}$, are:

$$E(F_1=J+\tfrac{3}{2})=\frac{-eqQ}{8(2J+3)(2J-1)}\{9J^2+3J-5J(J+1)\}+\frac{3c_aJ}{2}+\frac{c_b}{2}\left\{\pm J\pm\frac{1}{2}-\frac{1}{2}\mp\frac{3}{4J}+\frac{3}{4J}\right\}-\frac{3[\frac{1}{2}\mp\frac{1}{2}]c_b^2}{eqQ}$$

$$E(F_1=J+\tfrac{1}{2})=\frac{-eqQ}{8(2J+3)(2J-1)}\{J^2-5J+6-5J(J+1)\}+\frac{c_a}{2}(J-3)+\frac{c_b}{2}\left\{\pm J\pm\frac{1}{2}-\frac{1}{2}\mp\frac{3}{4J}-\frac{3}{4J}\right\}+\frac{3[\frac{1}{2}\mp\frac{1}{2}]c_b^2}{eqQ}$$

$$E(F_1=J-\tfrac{1}{2})=\frac{-eqQ}{8(2J+3)(2J-1)}\{J^2+7J+12-5J(J+1)\}$$
$$+c_a(-J-4)+\frac{c_b}{2}\left\{\pm J\pm\frac{1}{2}-\frac{1}{2}\mp\frac{11}{4J}+\frac{3}{4J}\right\}+\frac{3[\frac{1}{2}\mp\frac{1}{2}]c_b^2}{eqQ} \quad (15)$$

$$E(F_1=J-\tfrac{3}{2})=\frac{-eqQ}{8(2J+3)(2J-1)}\{9J^2+15J+6-5J(J+1)\}$$
$$+\frac{c_a}{2}(-3J-3)+\frac{c_b}{2}\left\{\pm J\pm\frac{1}{2}-\frac{1}{2}\mp\frac{3}{4J}-\frac{3}{4J}\right\}-\frac{3[\frac{1}{2}\mp\frac{1}{2}]c_b^2}{eqQ}$$

where the $(\pm)$ refer to $i_b=\pm\frac{1}{2}$.

These energy levels give the transition energies of (3).

APPENDIX II. EFFECT OF SMALL PERTURBATIONS ON THE LINE SHAPE

To test whether a perturbation term of the form K_nJ^n affects the line shape, we will calculate the shape function neglecting the terms gJ^2 and Pv. The frequencies f_1 and f_2 of (6) then become:

$$f_1=f_0-cJ+K_nJ^n, \quad f_2=f_0+cJ+K_nJ^n \quad (16)$$

where K_n is assumed to have the same sign in f_1 and f_2 to produce the maximum possible line asymmetry. By a series of steps analogous to those of Eqs. (8)–(10), we obtain:

$$N(z)\sim\phi\exp(-\tfrac{1}{2}\phi^2)/|1\mp\gamma^n\phi^{n-1}|, \quad (17)$$

where

$$z=\pm\phi+(\gamma/n)\phi^n=(f-f_0)/cJ, \text{ and } \gamma_n=|nK_n/c\alpha^{n-1}|.$$

This reduces to Eq. (10) for $n=2$.

For a small value of K_n, the position and magnitude of the two peaks will not be much different from those

produced by cJ alone. Then, the peaks will occur when $\phi=1$, and the ratio of the two peaks will be:

$$R=(1-\gamma_n)/(1+\gamma_n). \tag{18}$$

We take as the condition for the neglect of a perturbation, that $(1-R)$ be less than 0.1. This gives as the condition for neglect,

$$|nK_n/c\alpha^{n-1}|<0.05. \tag{19}$$

The perturbations of interest will be of the form $K_{-1}J^{-1}$ and $K_{-2}J^{-2}$. These diverge for small values of J, giving rise to apparent discontinuities in the shape function. However, the perturbations are obtained in these cases, assuming J fairly large, while the discontinuities occur for low J. In addition, the density of states is low for small values of J. We will then take (19) as the criterion for neglect of a term, even for $n=-1$ and -2.

The perturbations we consider are:

(1) The perturbations of order $\sim c_b/J$ in Eq. (3). The largest term of this form is $7c_b/4J$.

(2) The perturbation terms due to the off-diagonal matrix elements of the quadrupole operator. These are of order $|eqQ|^2/hcB_eJ$.

(3) Perturbations (in the case of NaCl) due to a quadrupole coupling eq_bQ_b of the second nucleus. These terms can be shown to contribute to the transition energies in order $\sim|eq_bQ_b|/J^2$.

For TlCl, $c_b\sim75$ kc,[12] $eqQ\sim15$ Mc, $B_e\sim0.087$ cm^{-1}, $c_a\sim1$ kc, $J=55$. For perturbation (1), TlCl gives $\gamma_{(1)}=|7c_b/c_a4J^2|\sim0.043$. The exact evaluation of perturbation (2) requires a rather lengthy calculation. However, the fact that the zero field electric resonance spectrum of TlCl can be well explained without considering these terms indicates that the terms are at most a few kc. Assuming perturbation (2) to be about 10 kc/sec/J, $\gamma_{(2)}=|10$ kc/sec/$c_aJ^2|\sim0.003$. For NaCl, $c_a\sim1$ kc, $J\sim40$. There are no data available on the quadrupole coupling of chlorine, eq_bQ_b, in NaCl. However, from (19), the effect of the chlorine on the spectrum of sodium in NaCl is negligible if $|eqQ|<3.2$ Mc.

APPENDIX III. ROTATIONAL AND VIBRATIONAL VARIATION OF q

As in Eq. (4), we take $q(R)$ to be a function of the form:

$$q(R)=q^{(0)}+q^{(1)}[(R-R_e)/R_e]+q^{(2)}[(R-R_e)/R_e]^2+\cdots.$$

For this expansion to converge rapidly, the coefficients $q^{(0)}$, $q^{(1)}$, $q^{(2)}$, $\cdots$ must be of the same order of magnitude, and the change in R during the course of the molecular vibration and rotation must be much less than R_e. A semiclassical argument gives

$$(\Delta R/R_e)_{\text{rot}}=(2B_e/\omega_e)^2J(J+1),$$
$$(\Delta R/R_e)_{\text{vib}}=(2B_e/\omega_e)^{\frac{1}{2}}(v+\tfrac{1}{2})^{\frac{1}{2}},$$

so that the criteria for the validity of the expansion are:

$$(2B_e/\omega_e)^2J(J+1)\ll1, \quad (2B_e/\omega_e)^{\frac{1}{2}}(v+\tfrac{1}{2})^{\frac{1}{2}}\ll1. \tag{20}$$

To average $q(R)$ over vibration and rotation, we must use appropriate vibrator-rotator wave functions. A general molecular vibrator potential is assumed of the form,

$$V(R)=K_2[(R-R_e)/R_e]^2+K_3[(R-R_e)/R_e]^3 +K_4[(R-R_e)/R_e]^4+\cdots. \tag{21}$$

The wave functions for this potential are obtained, solving a harmonic oscillator problem, with $K_3[(R-R_e)/R_e]^3+K_4[(R-R_e)/R_e]^4+\cdots$ as perturbations. The average of $q(R)$ then becomes,

$$q=q^{(0)}+(2B_e/\omega_e)^2q^{(1)}J(J+1)+[-3q^{(1)}(B_e/\omega_e)(K_3/K_2) +2q^{(2)}(B_e/\omega_e)](v+\tfrac{1}{2}). \tag{22}$$

To evaluate (K_3/K_2), a perturbation calculation of the energy for the potential of (21) is performed. Identifying the coefficient of the $(v+\frac{1}{2})J(J+1)$ term in the energy, as $(-\alpha_e hc)$,

$$\alpha_e=-\tfrac{3}{2}\omega_e(2B_e/\omega_e)^2[1+(K_3/K_2)]. \tag{23}$$

Substituting for (K_3/K_2) into (22),

$$q=q^{(0)}+(2B_e/\omega_e)^2q^{(1)}J(J+1)+[3q^{(1)}(B_e/\omega_e) \times(1+\alpha_e\omega_e/6B_e^2)+2q^{(2)}(B_e/\omega_e)]. \tag{24}$$

The relations (5) then follow from this.

Molecular Beam Magnetic Resonance Spectra of $Rb^{87}F$ and $Rb^{87}Cl$ at Zero Field*

D. I. Bolef† and H. J. Zeiger
Columbia University, New York, New York
(Received October 17, 1951)

The radiofrequency spectra of $Rb^{87}F$ and $Rb^{87}Cl$ were investigated by the zero field molecular beam magnetic resonance method. The quadrupole line was found to be split into a series of component lines. The separations between the lines, as well as the shapes of the lines, are explained by taking into account the effects of (1) a cosine coupling of the form $c_a\mathbf{I}\cdot\mathbf{J}$ between the spin of Rb^{87}, $\mathbf{I}_a$, and the rotational angular momentum of the molecule $\mathbf{J}$; and (2) the dependence of the quadrupole interaction constant eqQ on vibrational quantum number v and rotational quantum number J of the form:

$$eqQ=eQQ+eq^{(J)}QJ(J+1)+eq^{(v)}Qv.$$

The results for Rb^{87} in $Rb^{87}F$ are: $|eQQ|/h=33.96\pm0.02$ Mc, $|eq^{(v)}Q|/h=410\pm40$ kc, $|eq^{(J)}Q|/h=26\pm4$ cycles/sec, $|c_a|/h=1.1\pm0.1$ kc. $eq^{(v)}Q$ and $eq^{(J)}Q$ are shown to have signs opposite to that of eQQ.
The results for Rb^{87} in $Rb^{87}Cl$ are: $|eQQ|/h=25.37\pm0.04$ Mc, $|eq^{(v)}Q|/h=230\pm50$ kc, $|eq^{(J)}Q|/h=12\pm2$ cycles/sec, $|c_a|/h=1.0\pm0.1$ kc. $eq^{(v)}Q$ and $eq^{(J)}Q$ are shown to have signs opposite to that of eQQ.

I. INTRODUCTION

THE radiofrequency spectra of $Rb^{87}F$ and $Rb^{87}Cl$ have been observed at zero field by the molecular beam magnetic resonance method.[1-3] The observed resonance lines, corresponding to the quadrupole interaction constant of the molecule, eqQ, are found to exhibit characteristic structure which may be attributed to the effects of (1) a cosine coupling, $c_a\mathbf{I}\cdot\mathbf{J}$, between the nuclear spin of rubidium, $\mathbf{I}_a$, and the rotational angular momentum of the molecule, $\mathbf{J}$; and (2) the dependence of eqQ on the vibration and rotation of the molecule, of the form:

$$eqQ=eQQ+eq^{(J)}QJ(J+1)+eq^{(v)}Qv.$$

The analyses of the observed lines are performed following the theory and procedure outlined in detail by Zeiger and Bolef.[4]

In the investigation of $Rb^{87}F$ by the electric resonance method,[5] an unusually large quadrupole interaction constant, $eqQ/h=34.00$ Mc, was observed. In addition, the absolute value of the interaction constant was found to decrease about 1.1 percent (410 kc) from one vibrational state to the next higher state for the first three vibrational states. As discussed in I, the individual lines which correspond to the vibrational states of the molecule will be resolved under zero field conditions if $|eq^{(v)}Q|$ is greater than $|c_a\bar{J}|$, where $\bar{J}$ is the most probable J in the molecular beam source. For $Rb^{87}F$, $\bar{J}=46$, while $|c_a/h|$ for the alkali halides is of the order of 1 kc. For the spectrum of $Rb^{87}F$ at zero field, therefore, a series of closely spaced "vibrational lines," each split by an $\mathbf{I}\cdot\mathbf{J}$ interaction, is predicted. Such structure was indeed observed for $Rb^{87}F$. Similar structure was observed in the spectrum of $Rb^{87}Cl$.

No spectrum for Rb^{85} in RbF and RbCl was observed. On the basis of factors contributing to the line intensity, a line intensity considerably lower than that for Rb^{87} in these molecules is predicted. These factors are discussed further in Sec. IV.

II. APPARATUS AND METHOD

The apparatus used in these investigations was the same as that described in I. The method of taking data was to vary the frequency of the oscillating field in small steps, while the homogeneous C-field was maintained at zero, and to record changes in beam intensity at the detector. The change in beam intensity at a particular value of the frequency is defined as the line intensity at that frequency. The beam intensity is expressed in centimeters deflection on a galvanometer scale.

A major difficulty in investigating the types of resonance minima observed in this experiment, broadened by the variation of eqQ with rotational and vibrational state, is the low line intensities observed. In the case of $Rb^{87}Cl$, for instance, a series of resonance minima six centimeters in depth was investigated out of a total of 2000 centimeters of refocused beam. The difference between an adjacent maximum and minimum in the pectrum was of the order of one centimeter out of a total beam of 2000 centimeters.

The conventional method of observation is that in which the detector is so placed that the reoriented molecules miss the detector. In several runs, the beam steadiness was such that the conventional method could not be used. In such instances, an alternative technique, which utilizes a detector off-set so that only a small background beam and the reoriented molecules reach the detector, was used. In this method, the detector is displaced to such a position that a maximum increase,

* This research has been supported in part by the ONR.
† Submitted by D. I. Bolef in partial fulfillment of the requirements for the degree of Doctor of Philosophy in Physics at Columbia University.
[1] Rabi, Millman, Kusch, and Zacharias, Phys. Rev. **55**, 526 (1939).
[2] J. M. B. Kellogg and S. Millman, Revs. Modern Phys. **57**, 677 (1940).
[3] W. A. Nierenberg and N. F. Ramsey, Phys. Rev. **72**, 1075 (1947).
[4] H. J. Zeiger and D. I. Bolef, Phys. Rev. **85**, 788 (1951). For brevity, this paper will henceforth be referred to as I.
[5] V. Hughes and L. Grabner, Phys. Rev. **79**, 314 (1950).

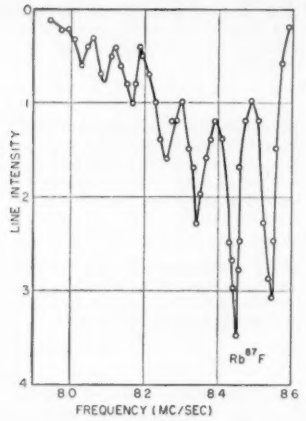

FIG. 1. Zero field spectrum of Rb^{87} in $Rb^{87}F$. Line intensity is expressed in centimeters deflection on a galvanometer scale. Peak intensity corresponds to a 0.2 percent change in the total beam. Radiofrequency current was 15 amperes. The widths of the lines at half-intensity are considerably greater than the 6 kc resolution half-widths expected for this molecule.

rather than a decrease, of beam intensity is observed at resonance. Thus, the resonance lines appear as peaks of beam intensity. If the deflection of the reoriented molecules at the position of the detector is not large, this method is not feasible, since in that case the detector cannot be moved far enough from the original line-up position to decrease the background appreciably. Since a large value of g_I results in a large deflection, the method works most efficiently for nuclei, such as Rb^{87} ($g_I=1.822$), with large g_I.

Measurements taken by use of both techniques during a single run indicated that the resonance curves did not differ from each other in any way but in intensity. No significant change in the position or shape of the lines was observed.

III. EXPERIMENTAL DATA

The spectrum of $Rb^{87}F$ at zero field (see Fig. 1) differs from other zero field spectra heretofore observed[3,4] in that a large number of closely spaced lines are resolved. In the case of TlCl, discussed in I, the zero field spectrum consisted of two components, one considerably broader than the other. The shape of the spectrum was explained as that arising from a superposition of the spectra corresponding to the several vibrational states of the molecules in the beam. The resolved lines in the $Rb^{87}F$ spectrum are relatively narrow, with half-widths of the order of 45 to 100 kc. These, however, are larger than the half-widths ($\sim$30 kc) to be expected from the values of the rf magnetic fields which induced the transitions. The separations between the component lines range from approximately 70 to 100 kc. Beginning with the most intense peak, there is an exponential decrease in intensity of the peaks toward lower frequency. The line intensity is reduced to a sufficiently low value between successive peaks to give a clear separation of the peaks.

The zero field spectrum of Rb^{87} in $Rb^{87}Cl$ is shown in Fig. 2. The similarity between Figs. 1 and 2 is evident, and, as will be seen in Sec. V, the two spectra can be explained by similar analyses. In the case of RbCl more peaks are resolved than in the case of RbF, even though the degree of resolution is better for RbF. The rate of decrease of intensity to lower frequency from the most intense peak is less for $Rb^{87}Cl$ than for $Rb^{87}F$. The widths at half-intensity are of the order of magnitude of 80 kc. Except for the separation between the first two peaks, which is 35 kc, the separation between peaks is approximately constant and of the order of 55 kc.

IV. THEORY

The energy levels of the diatomic molecules discussed here are adequately described by the Hamiltonian,

$$\mathcal{H}=\frac{-eqQ}{2I_a(2I_a-1)(2J-1)(2J+3)}\{3(\mathbf{I}_a\cdot\mathbf{J})^2+\tfrac{3}{2}(\mathbf{I}_a\cdot\mathbf{J}) -I_a(I_a+1)J(J+1)\}+c_a\mathbf{I}_a\cdot\mathbf{J}+c_b\mathbf{I}_b\cdot\mathbf{J}, \quad (1)$$

where the notation is that of I. In the present case, I_a is the spin of Rb, I_b that of the accompanying halogen nucleus, and J, the rotational quantum number of the molecule. The first term is the electric quadrupole interaction between the Rb nucleus and the molecular charge external to the Rb nucleus. Q is the electric quadrupole moment of the Rb nucleus, and q is the gradient, at the position of the Rb nucleus, of the

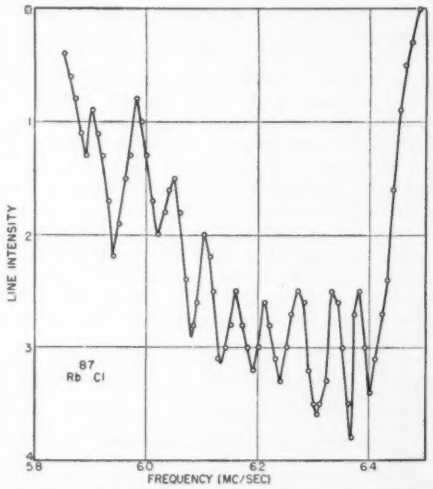

FIG. 2. Zero field spectrum of Rb^{87} in $Rb^{87}Cl$. Peak intensity corresponds to a 0.2 percent change in the total beam. Radiofrequency current was 15 amperes. Comparing this spectrum with that of $Rb^{87}F$ (Fig. 1) it is seen that although more peaks are resolved, the resolution between adjacent peaks is not as good.

electric field along the internuclear axis, due to all charges external to the Rb nucleus. The second and third terms are cosine-coupling terms, the former between the spin of Rb and **J**, the latter between the spin of the halogen nucleus and **J**. The third term will be shown to have negligible effect on the observed spectra of RbF and RbCl. Similarly, in the case of RbCl, the contribution of the quadrupole moment of the Cl nucleus to the energy will be shown to be negligible. This term has been omitted from the Hamiltonian (1).

The transition energies of interest, for the case $I_a=\frac{3}{2}$, $I_b=\frac{1}{2}$, and for $J\gg1$, are then given by,

$$W(J+\tfrac{3}{2}\leftrightarrow J+\tfrac{1}{2})=-\tfrac{1}{4}eqQ+c_a(J+\tfrac{3}{2}), \quad (2a)$$

$$W(J+\tfrac{1}{2}\leftrightarrow J-\tfrac{1}{2})=\tfrac{3}{4}eqQ(2J+1)/[(2J+3)(2J-1)]+c_a(J+\tfrac{1}{2}), \quad (2b)$$

$$W(J-\tfrac{1}{2}\leftrightarrow J-\tfrac{3}{2})=\tfrac{1}{4}eqQ+c_a(J-\tfrac{1}{2}), \quad (2c)$$

where (a) and (c) are the transitions which give rise to the lines observed in this experiment. The quadrupole portions of both (2a) and (2c) are seen to be J-independent.

For the case $I_a=5/2$, $I_b=\frac{1}{2}$, and for $J\gg1$, the transition energies are:

$$W(J+5/2\leftrightarrow J+\tfrac{3}{2})=(3/20)eqQ(2J+5)/(2J+3)+c_a(J+5/2), \quad (3a)$$

$$W(J+\tfrac{3}{2}\leftrightarrow J+\tfrac{1}{2})=(3/20)eqQ(J-3)/(2J-1)+c_a(J+\tfrac{1}{2}), \quad (3b)$$

$$W(J+\tfrac{1}{2}\leftrightarrow J-\tfrac{1}{2})=-(3/20)eqQ[4(2J+1)/(2J-1)(2J+3)]+c_a(J+\tfrac{1}{2}), \quad (3c)$$

$$W(J-\tfrac{1}{2}\leftrightarrow J-\tfrac{3}{2})=-(3/20)eqQ(J+4)/(2J+3)+c_a(J-\tfrac{1}{2}), \quad (3d)$$

$$W(J-\tfrac{3}{2}\leftrightarrow J-\tfrac{5}{2})=-(3/20)eqQ(2J-3)/(2J-1)+c_a(J-\tfrac{3}{2}). \quad (3e)$$

In this case the quadrupole portions of the energies are J dependent: $(dW/dJ)/dW\sim1/J^2$ for (3a), (b), (d), (e), and $(dW/dJ)/dW\sim1/J$ for (3c). Due to this J dependence, a broadening of the resonance minima in the spectrum of a molecule, such as $Rb^{85}F$, in which one nucleus has a spin $I=5/2$, is predicted. In general, for any value of I except $\frac{3}{2}$, the spectrum of a diatomic molecule at zero field will show a $1/J^2$ dependence. This factor, together with the effects of decreased throwout power for Rb^{85} ($g_I=0.536$ as compared with $g_I=1.822$ for Rb^{87}), and the presence of a larger number of m_I states, results in a decrease of line intensity for Rb^{85} to approximately one-sixth that observed for Rb^{87}. As a result, the spectrum of Rb^{85} in RbF and RbCl was not observed.

In the case of $Rb^{87}F$, the presence of fluorine, with spin $I=\frac{1}{2}$, will contribute an energy of the order of c_b/J to the transition energies (2a) and (2c). Since the most probable value of J is of the order of 46, and $c_b=14$ kc,[5] this term can be neglected.

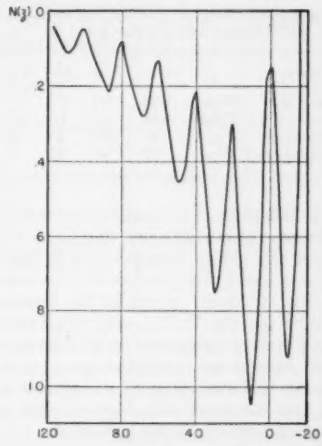

FIG. 3. Envelope of the curves corresponding to the first six vibrational states of $Rb^{87}F$, obtained by selecting $\gamma=0.30$ and following the analytical procedure described in detail in I. The first peak is the subtractive wing for the $v=0$ state. (See I, Sec. IV C, and Fig. 6.) The second peak is due to the superposition of the additive wing of the $v=0$ state and the subtractive wing of the $v=1$ state. In a similar manner, the peaks of lower intensity are obtained from a superposition of the additive and subtractive wings of higher vibrational states. This theoretical curve is to be compared with Fig. 1, the observed zero field spectrum of $Rb^{87}F$. The notation is that given in I. $N(z)=\phi\exp(-\frac{1}{2}\phi^2)/|1\mp\gamma\phi|$, where $z=\pm\phi+\frac{1}{2}\gamma\phi^2=h(f-f^0)/c_a\bar{J}$.

In the case of $Rb^{87}Cl$, c_b is not known. However, the largest known value of c_b for an alkali halide is 16 kc for CsF.[5] Assuming that c_b for $Rb^{87}Cl$ is of the same order of magnitude, and since $\bar{J}=64$ for RbCl, the term of the order of c_b/J can be neglected. As in the case of NaCl (see I), the perturbation due to a quadrupole coupling eq_bQ_b of the chlorine nucleus can be shown to contribute an energy of order $|eq_bQ_b|/J^2$ to the transition energies. From Eq. (19) of I we have the criterion, $|2eq_bQ_b/c_aJ^2|<0.05$, that this perturbation be negligible. Thus the effect of Cl on the spectrum of Rb^{87} in $Rb^{87}Cl$ is negligible if $|eq_bQ_b|\lesssim6.5$ Mc. From the value of eqQ for Cl^{35} in KCl[35] (~420 kc),[6] it seems probable that the above criterion is easily satisfied for $Rb^{87}Cl$.

V. ANALYSES OF $Rb^{87}F$ AND $Rb^{87}Cl$ SPECTRA

The analysis of the spectrum of $Rb^{87}F$ is made in accordance with the procedure given in I. As in the case of TlCl, the reconstruction of the experimental curve is considerably facilitated by a knowledge of the value of $eq^{(v)}Q$. From reference 5, $eq^{(v)}Q$ for $Rb^{87}F$ is taken to be 410 kc (0.012 eqQ). The ratio of intensities of the lines corresponding to successive vibrational states is given by 0.61. A value of $\gamma=0.30$ ($\gamma=2g/c\alpha$, where $\alpha=1/\bar{J}$, $g=eq^{(J)}Q/4h$, and $c=c_a/h$) was found to give

[6] Logan, Coté, and Kusch, to be published.

TABLE I. Comparison of experimental and theoretical curves of $Rb^{87}F$ at zero field (see Figs. 1 and 3).

Peaks		1–2	2–3	3–4	4–5	5–6
Ratio of line intensities	Exper.	0.88	1.5	1.4	1.6	1.25
	Theor.	0.88	1.4	1.6	1.7	1.3
Separation between successive peaks (kc)	Exper.	95	104	79	92	73
	Theor.	98	100	96	98	90

the best fit. This value of γ, the above values for $eq^{(v)}Q$, and the decrease of intensity per vibrational state are used to plot the curves corresponding to the states $v=0$, 1, 2, 3, 4, and 5. The envelope of these curves, as shown in Fig. 3, closely resembles the experimental curve of $Rb^{87}F$ (see Fig. 1). The ratios of successive line intensities, as well as the separations between successive component peaks of the theoretical spectrum as compared to those of the experimental spectrum, are given in Table I. The theoretical and observed widths at half-intensity are found to be in fair agreement.

The discrepancy between the theoretical and experimental curves may be attributed to: (1) lack of precision of ω_e ($\sim 340\pm 68$ cm^{-1}) as given in reference 5, and (2) the difficulty inherent in locating the peak intensities of narrow resonance lines.

The results of the analysis are:

$$|e\bar{q}Q|/h=(33.96\pm 0.02)\text{ Mc},$$
$$|c_a|/h=1.1\pm 0.1\text{ kc},$$
$$|eq^{(J)}Q|/h=26\pm 4\text{ cycles/sec}.$$

The magnitude of the magnetic field per rotational quantum number, H_a, given by $H_a=|hc_a/g_I\mu_N|$, has the value 1.4 gauss for Rb^{87} in $Rb^{87}F$. Since the low frequency component of the curve corresponding to each vibrational state is broadened by the effect of the rotational variation, $eq^{(J)}Q$ has the sign opposite to that of $e\bar{q}Q$ (see I). Also, since the resonance curve tapers off gradually to low frequencies, $eq^{(v)}Q$ has the sign opposite to that of $e\bar{q}Q$. The fact that the signs of $eq^{(J)}Q$ and $eq^{(v)}Q$ are opposite to that of $e\bar{q}Q$ is in agreement with the results for all the other alkali halides investigated by the molecular beam method.[4,5]

The results for $Rb^{87}Cl$ are obtained by a similar analysis. The results are:

$$|e\bar{q}Q|/h=25.37\pm 0.04\text{ mc},$$
$$|c_a|/h=1.0\pm 0.1\text{ kc},$$
$$|eq^{(J)}Q|/h=12\pm 2\text{ cycles/sec},$$
$$|eq^{(v)}Q|/h=230\pm 50\text{ kc}.$$

H_a for $Rb^{87}Cl$ is 1.3 ± 0.1 gauss. The signs of $eq^{(J)}Q$ and $eq^{(v)}Q$ are both opposite to that of $e\bar{q}Q$.

The results in the case of $Rb^{87}Cl$ are less precise than those for $Rb^{87}F$, primarily because of the lower line intensity and greater unsteadiness of the RbCl beam. Also, the individual peaks in the case of $Rb^{87}Cl$ were not as well resolved as were those of $Rb^{87}F$.

TABLE II. Values of the coefficients $eq^{(0)}Q$, $eq^{(1)}Q$, and $eq^{(2)}Q$, in the expansion

$$eq(R)Q=eq^{(0)}Q+eq^{(1)}Q[(R-R_e)/R_e]+eq^{(2)}Q[(R-R_e)/R_e]^2+\cdots$$

for molecules investigated by the molecular beam magnetic resonance method at zero field. Since the sign of $eq^{(0)}Q$ for $Rb^{87}Cl$ is not known, the signs of the coefficients for $Rb^{87}Cl$ are given under the assumption that $eq^{(0)}Q$ is negative.

Molecule	$eq^{(0)}Q/h$ (MC)	$eq^{(1)}Q/h$ (Mc)	$eq^{(2)}Q/h$ (Mc)
$Tl^{35}Cl$	−15.740	−49.6	100
NaCl	−5.61[a]	24	−5.5
NaF	−8.4[a]	9.1	20
$Rb^{87}Cl$	(−)25.4	30.3	225
$Rb^{87}F$	−33.96	19.9	−21

[a] See reference 6.

VI. DISCUSSION

As is discussed in detail in I, Sec. IV B, the fact that q is a function of internuclear distance R can be expressed by the expansion

$$q(R)=q^{(0)}+q^{(1)}[(R-R_e)/R_e]+q^{(2)}[(R-R_e)/R_e]^2+\cdots, \quad (4)$$

where R_e is the equilibrium internuclear distance in the state $v=0$, $J=0$. In order for (4) to converge, the coefficients $q^{(0)}$, $q^{(1)}$, $q^{(2)}$, must all be of the same order of magnitude. Expressed in terms of measured quantities, these coefficients have the form

$$q^{(0)}=\bar{q}-\tfrac{1}{2}q^{(v)}, \quad q^{(1)}=q^{(J)}(\omega_e/2B_e)^2,$$
$$q^{(2)}=q^{(v)}(\omega_e/2B_e)-\tfrac{3}{2}q^{(1)}(1+\alpha_e\omega_e/6B_e^2), \quad (5)$$

where B_e, ω_e, α_e are the usual molecular constants[7] in units of cm^{-1}. To show that the assumption that $|q^{(0)}|\sim|q^{(1)}|\sim|q^{(2)}|$ for the molecules investigated in this paper and in I is valid, these coefficients have been computed and are presented in Table II. α_e, however, is known only for TlCl. For all the other molecules given in Table II, α_e has been estimated from the Morse potential. For this reason the values of $q^{(2)}$ are much less precise than are those of $q^{(0)}$ or $q^{(1)}$.

Hughes and Grabner[8] have obtained the value of eqQ for Rb^{87} in $Rb^{87}F$ for molecules in the zeroth vibrational state and in the first two rotational states. Since the variation of eqQ with rotational state is small, a comparison of $e\bar{q}Q$ obtained for Rb^{87} in $Rb^{87}F$ in this experiment with the value obtained by Hughes and Grabner is valid. The value of $e\bar{q}Q=33.96\pm 0.02$ Mc in this experiment agrees well with the value of $eqQ=34.00\pm 0.06$ Mc obtained by Hughes and Grabner.

We are indebted to Professor I. I. Rabi for suggesting this problem and for his guidance throughout the course of the experiment. Professor T. Y. Wu was of great help during the early stages of the experiment. We wish to thank Professor P. Kusch and the members of the molecular beams laboratory for many helpful discussions.

[7] G. Herzberg, *Spectra of Diatomic Molecules* (D. Van Nostrand Company, Inc., New York, 1950), second edition.

Total Cross Sections of 60-Mev Mesons in Hydrogen and Deuterium*

P. J. Isaacs, A. M. Sachs, and J. Steinberger
Columbia University, New York, New York

(Received November 16, 1951)

The total cross sections of positive and negative mesons of average energy 58 Mev have been measured in hydrogen and deuterium. The results are

$\sigma(\pi^+ + p) = 27.8 \pm 2.5$ mb
$\sigma(\pi^- + p) = 17.6 \pm 2.2$ mb
$\sigma(\pi^+ + d) = 38.3 \pm 3.1$ mb
$\sigma(\pi^- + d) = 32.8 \pm 3.1$ mb.

The deuteron cross sections are related to the elementary scattering amplitudes in the impulse approximation, and the observed interference is compared to that predicted in weak coupling meson theory.

TOTAL interaction cross sections of π^- and π^+ mesons with average energy of 58 Mev in hydrogen and deuterium have been measured, using the scintillation counter arrangement and analysis of the beams described in a previous report on total cross sections of 85-Mev π^- mesons.[1] In the present experiment, the final 4½-inch diameter counter was placed 5½ inches behind the center of the absorber, so that "total cross section" applies to all interactions except those in which a meson is scattered into a forward angle of less than 22 degrees.

The hydrogen cross sections were found from CH_2-C subtractions, and the results were combined with those of D_2O-H_2O subtractions to yield the deuterium cross sections. The mesons enter the hydrogenous materials with an energy of 72 Mev, and leave with an energy of 40 Mev. The carbon and polyethylene absorbers contain the same weight of carbon. A strong energy dependence found experimentally for the total cross section of π^- mesons in carbon[2] leads to a substantial correction in the results of the CH_2-C subtraction.[3] The results, corrected also for a measured 6 percent μ-meson beam component which is assumed noninteracting, are as follows:

$\sigma(\pi^+ + p)$	$\sigma(\pi^+ + d)$
27.8 ± 2.5 mb	38.3 ± 3.1 mb
$\sigma(\pi^- + p)$	$\sigma(\pi^- + d)$
17.6 ± 2.2 mb	32.8 ± 3.1 mb.

The errors combine statistical standard deviation and an estimated 20 percent maximum error in the energy dependence correction. The cross section for positive pions in hydrogen is greater than that for negative pions, outside of possible experimental error. This is perhaps surprising, since the charge exchange scattering is possible only for negative pions. It is not in conflict, however, with a possible charge symmetry: $\pi^+ + p \leftrightarrow \pi^- + n$, etc. In fact, the deuterium cross sections for positive and negative mesons are approximately equal within experimental error, and we therefore assume charge symmetry.

The following reactions may contribute appreciably to the deuterium cross section: 1. Scattering $\pi^+ + d \rightarrow n + p + \pi^+$ (inelastic), $\pi^+ + d \rightarrow d + \pi^+$ (elastic). 2. Charge exchange $\pi^+ + d \rightarrow \pi^0 + p + p$. 3. Radiative absorption $\pi^+ + d \rightarrow \gamma + p + p$. 4. Absorption $\pi^+ + d \rightarrow p + p$.

The last reaction has been measured independently,[4] and has a total cross section of 7 ± 1 mb for mesons of this energy. The first three reactions therefore contribute $36 - 7 = 29 \pm 3$ mb. These reactions occur also with single nucleons, and except for interference effects, we would have

$$\sigma_d - \sigma_d^{\text{absorption}} = \sigma_p + \sigma_n = 45 \pm 3.5 \text{ mb}.$$

There exists therefore an interference in the deuteron of 16 ± 5 mb, or 35 percent of the combined cross section of neutron and proton.

The analysis of this interference is possible from a phenomenological point of view, if it is assumed that the interaction amplitudes of the neutron and proton are linearly superposable and that the several possible interactions do not interfere with each other. The last assumption is probably justifiable, provided the cross sections in question are small compared to the deuteron, and this is actually the case. The problem is similar to that of photomeson production in deuterium. This has been treated by Chew and Lewis,[5] and we follow their

* Research supported by joint program of the ONR and AEC.

[1] Chedester, Isaacs, Sachs, and Steinberger, Phys. Rev. **82**, 958 (1951).

[2] The total π^- cross section in carbon (not including elastic scattering into smaller angles than 50°) is 314 ± 10 mb at 85 Mev, 237 ± 10 mb at 60 Mev, and 195 ± 10 mb at 40 Mev. The energy variation has also been measured in the geometry of the subtraction experiments for π^- mesons. The π^+ variation is assumed to be the same for the purpose of the corrections.

[3] This correction must also be applied to the previously reported result at 85 Mev (see reference 1). This raises the cross section of π^- mesons on hydrogen from 13 mb to approximately 21 mb. This value is somewhat in doubt because the variation of the carbon cross section has not been mesured as well in this energy region.

[4] Durbin, Loar, and Steinberger, Phys. Rev. **84**, 581 (1951).

[5] G. Chew and H. W. Lewis, Phys. Rev. **84**, 779 (1951). The method has also been applied to the meson scattering in deuterium by Fernbach, Green, and Watson, University of California Radiation Laboratory Report No. 1443 and to charge exchange scattering by B. Segall, Phys. Rev. **83**, 1247 (1951).

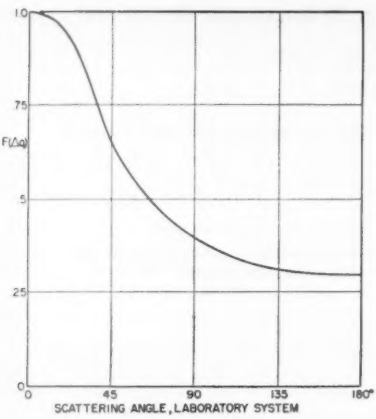

FIG. 1. The form factor $F(\Delta q)$.

treatment entirely, stating only the result and referring to their article for the justification of the method.

We write the elementary interactions of the positive pion and nucleon

$$I_s = s^p + \mathbf{S}^p\cdot\boldsymbol{\sigma}^p + s^n + \mathbf{S}^n\cdot\boldsymbol{\sigma}^n \text{ (scattering)},$$
$$I_c = c^n + \mathbf{C}^n\cdot\boldsymbol{\sigma}^n \text{ (charge exchange scattering)},$$
$$I_r = r^n + \mathbf{R}^n\cdot\boldsymbol{\sigma}^n \text{ (radiative absorption)},$$

where $\boldsymbol{\sigma}^n$ and $\boldsymbol{\sigma}^p$ are the Pauli spin operators for neutron and proton, $\mathbf{S}$, $\mathbf{C}$, $\mathbf{R}$ are the spin interaction amplitudes, and s, c, r are the spin independent amplitudes. s, c, r, $\mathbf{S}$, $\mathbf{C}$, and $\mathbf{R}$ are functions of meson energy and reaction product angle. They are normalized so that the free nucleon cross sections are simply

$$d\sigma^p/d\omega = |s^p|^2 + |\mathbf{S}^p|^2, \quad d\sigma_s^n/d\omega = |s^n|^2 + |\mathbf{S}^n|^2,$$
$$d\sigma_c^n/d\omega = |c^n|^2 + |\mathbf{C}^n|^2, \quad d\sigma_r^n/d\omega = |r^n|^2 + |\mathbf{R}^n|^2.$$

If, in the scattering on deuterium, we are not interested in the state of the final nucleon system, then it is valid[5] to apply a closure approximation in summing over the final nucleon states. Neglecting the deuteron D states, the result is

$$d\sigma_s^d/d\omega = d\sigma_s^p/d\omega + d\sigma_s^n/d\omega + 2F(\Delta q)[\mathrm{Re}(s^{p*}s^n) + \tfrac{1}{3}\,\mathrm{Re}(\mathbf{S}^{p*}\cdot\mathbf{S}^n)], \quad (1)$$

$$d\sigma_c^d/d\omega = d\sigma_c^n/d\omega - F(\Delta q)[\,|c^n|^2 + \tfrac{1}{3}|\mathbf{C}^n|^2], \quad (2)$$

$$d\sigma_r^d/d\omega = d\sigma_r^n/d\omega - F(\Delta q)[\,|r^n|^2 + \tfrac{1}{3}|\mathbf{R}^n|^2], \quad (3)$$

where

$$F(\Delta q) = \int \mu_d^2(r) e^{i\Delta\mathbf{q}\cdot\mathbf{r}} d\mathbf{r},$$

Δq = |momentum of incoming pion—momentum of outgoing pion or γ-ray|,

μ_d = deuteron wave function (in the calculations we use $\mu_d(r) \propto (e^{-\alpha r} - e^{-\beta r})$, $\alpha = (ME_b/\hbar)^{\frac{1}{2}}$, $\beta = 7\alpha$),

E_b = deuteron binding energy.

$F(\Delta q)$ is the form factor which measures the interference of the nucleons, either because of the Pauli principle (reactions 2 and 3), or because the scattering takes place on two centers (reaction 1). $F(\Delta q)$ has been evaluated as a function of the angle of the outgoing meson (Fig. 1). For reaction 3 the angular dependence of $F(\Delta q)$ is slightly different, but, as will be seen, this reaction contributes very little.

Because the angular dependence of the interference terms is not known, the angular integration can only be carried out approximately. We note, however, that

$$(1/4\pi)\int F(\Delta q)\, d\omega = 0.46;$$

$$(3/4\pi)\int F(\Delta q)\cos^2\theta\, d\omega = 0.51;$$

$$(3/8\pi)\int F(\Delta q)\sin^2\theta\, d\omega = 0.44.$$

No great error is introduced if these angular distributions are replaced by their average. We therefore write tentatively

$$\sigma^d = \sigma^p + \sigma^n + \sigma(\text{absorption}) + 0.46\times 4\pi[2\,\mathrm{Re}(s^{p*}s^n) + \tfrac{2}{3}\,\mathrm{Re}(\mathbf{S}^{p*}\cdot\mathbf{S}^n) - \overline{|c^n|^2} - \tfrac{1}{3}\overline{|\mathbf{C}^n|^2} - \overline{|r^n|^2} - \tfrac{1}{3}\overline{|\mathbf{R}^n|^2}].$$

The only interference terms for which independent evidence exists are r and R. In this case the inverse reaction has been measured[6] and gives the total cross section by detailed balance, as well as evidence that $r^n \ll |R^n|$. We therefore set

$$4\pi\overline{|\mathbf{R}^n|^2} = \sigma_r^n = 0.8\pm 0.2 \text{ mb}.$$

Then

$$4\pi\times 0.46[2\,\mathrm{Re}(\overline{s^{p*}s^n}) + \tfrac{2}{3}\,\mathrm{Re}(\overline{\mathbf{S}^{p*}\cdot\mathbf{S}^n}) - \overline{|c^n|^2} - \tfrac{1}{3}\overline{|\mathbf{C}^n|^2}] = -16\pm 5 \text{ mb}.$$

The charge exchange term contributes always destructively to the interference, from between 15 to 45 percent of the elementary charge exchange cross section σ^c, depending only on the relative importance of the spin

[6] J. Steinberger and A. S. Bishop, Phys. Rev. (to be published).

dependent and independent terms.[7] The scattering terms may be either destructive or constructive. We point out only that in the pseudoscalar perturbation theory with pseudoscalar coupling,

$$4\pi \operatorname{Re}(s^{p*}s^{n}) = \sigma^{p} = \sigma_{s}^{n}; \quad \operatorname{Re}(\mathbf{S}^{p*}\cdot\mathbf{S}^{n}) = 0.$$

The interference is expected to be strongly constructive, in disagreement with the experimental result. The pseudovector coupling results, neglecting nuclear recoil, are

$$4\pi \operatorname{Re}(s^{p*}s^{n}) = -\sigma^{n}\cos^{2}\theta = -\sigma^{n}\cos^{2}\theta,$$

$$4\pi \operatorname{Re}(\mathbf{S}^{p}\cdot\mathbf{S}^{n}) = \sigma^{p}\sin^{2}\theta = \sigma^{n}\sin^{2}\theta,$$

$$2\int d\omega F(\Delta q)[\operatorname{Re}(s^{p*}s^{n}) + \tfrac{1}{3}\operatorname{Re}(\mathbf{S}^{n*}\cdot\mathbf{S}^{n})] = -0.1\sigma^{p} = -0.1\sigma^{n} \approx -2.5 \text{ mb}.$$

The net interference is destructive, but smaller than the experimentally observed interference.

[7] The charge exchange cross section is necessarily less than the cross section of π^- on p; the interference due to the charge exchange reaction is therefore at most 8 mb, and this only if all scattering of negative pions or protons were charge exchange.

PHYSICAL REVIEW VOLUME 85, NUMBER 5 MARCH 1, 1952

The Beta-Spectrum of RaD

G. M. Insch, J. G. Balfour, and S. C. Curran
Department of Natural Philosophy, University of Glasgow, Glasgow, Scotland
(Received October 15, 1951)

The electronic radiations from a very thin source of RaD are analyzed by means of a proportional counter, operating as a 2π spectrometer. The β-rays of the continuum which coincide with the photoelectrons of highest energy form the tail on the pulse distribution which is analyzed to isolate the β-particles and to compare their spectrum with Fermi theory. The disintegration energy is found to be 64.5 ± 2.5 kev and the limiting energy of the β-rays $=18\pm2.5$ kev. The form of the spectrum agrees with the theoretical shape for an allowed transition and $E_0=18$ kev. The presence of a complex system of soft photoelectron peaks, probably emitted mostly in cascade, is deduced from the remarkable shape of the pulse spectrum at low energies (5 to 25 kev).

INTRODUCTION

THE unsatisfactory situation existing as late as 1949 in our understanding of the decay of RaD has been well summarized by Feather.[1] Isolation of the continuous β-spectrum had not been achieved and the rather large number of low intensity γ-rays detected (energies 7.3, 16.1, 23.2, 31.3, 37, 42.6, 46.7 kev) did not readily suggest a unique system of levels. Feather, however, points out two significant groupings of quantum energies. Very recent work by Cranberg,[2] Frilley *et al.*,[3] and Butt and Brodie[4] has extended knowledge of the decay, but they have not been concerned with the main objective of the present work, which was the examination of the β-spectrum. Most observers[5,6] agree that the β-rays are very soft, but even the limiting energy has not been well defined, estimates ranging from ~15 to ~40 kev.

The proportional tube spectrometer is clearly suited to the study of the soft radiations of RaD and has been employed in examining the L x-rays and soft γ-rays.[7] Early work on the particles proved somewhat difficult, mainly on account of difficulties in preparing gaseous or solid sources effectively free of RaE and RaF, both of which contributed very large disturbing pulses. More recently, however, relatively clean sources (~97 percent) have been separated following the method used by Cranberg[2] and this has greatly assisted in the successful application of the instrument. It has been found possible, by direct examination of the particles emitted from a thin source (~20 μg of chloride) mounted on thin foils (Nylon ~50 μg/cm^2 and aluminium ~1.6 mg/cm^2), to separate the β-rays from the relatively very intense and complex system of photoelectron lines of low energy. The separation was sufficiently good to permit comparison of the shape of the spectrum with Fermi theory. The tube with source at an aperture in the cathode constitutes a spectrometer of 2π acceptance angle.

APPARATUS

The proportional counter, 1.4 inches in diameter and 8 inches in fully operating length[8] was enclosed in a cylindrical vessel C, Fig. 1, into which the thin source could be slipped. The vessel was filled to a pressure of one atmosphere and the mixture (ethylene+16 cm of argon) was such that the efficiency of the L x-rays of RaE from the source was <5 percent. The spectrometer was thus rendered responsive chiefly to photoelectrons and β-rays, but it was, of course, sensitive to the very soft M x-radiations. It integrated the ionizing events

[1] N. Feather, Nucleonics **5**, 28 (1949).
[2] L. Cranberg, Phys. Rev. **77**, 155 (1950).
[3] M. Frilley *et al.*, Compt. rend. **232**, 50 and 157 (1951).
[4] D. K. Butt and W. D. Brodie, Proc. Phys. Soc. (London) **A64**, 791 (1951).
[5] H. O. W. Richardson and A. Leigh Smith, Proc. Roy. Soc. (London) **A160**, 454 (1937).
[6] *Nuclear Data*, National Bureau of Standards Circular 499.
[7] Curran, Angus, and Cockroft, Phil. Mag. **40**, 36 (1949).
[8] A. L. Cockroft and S. C. Curran, Rev. Sci. Instr. **22**, 37 (1951).

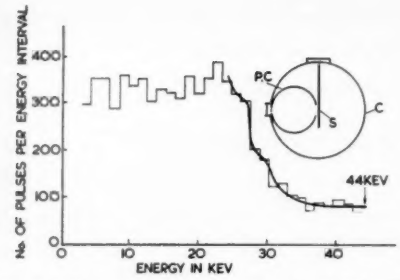

FIG. 1. Pulse spectrum shape between ~4 and 40 kev using source of counting rate 2.5×10^5 c/min mounted on aluminum, 1.6 mg/cm². The counter is shown in the inset. The source S is at an aperture in the proportional tube spectrometer $P.C.$

which occurred within ~10 μsec of each other. The counting rate was usually between 2×10^4 and 3×10^4 c/min. Calibration was achieved with fluorescence x-rays of Cu $K\alpha$ of energy 8.04 kev, the amplifier gain being increased by a factor of 4. The output pulses from the amplifier were analyzed by means of the cathode-ray tube and moving film technique.

RESULTS

The total range of the pulse spectrum was covered in two overlapping parts, from ~4 to 40 kev, Fig. 1, and from 33 to beyond 80 kev. This region is shown separately in Fig. 2, and the final end point occurs at 62±2.5 kev. This value was verified by critical examination of the spectrum shape between 50 and 70 kev with improved statistical data.

The shape of the distribution is very remarkable, but it has been confirmed in several different experimental arrangements of counter and source. The nearly flat plateau between 4 and 26 kev shows definitely significant peaks around 10 and 23 kev. Independent work in this department, using scintillation spectrometers, confirms these results and suggests that the form of the curve arises from the emission of homogeneous photoelectrons of various energies, produced by internal conversion of soft γ-rays in the L and M shells of RaE, which are frequently emitted in cascade so that the pulse spectrum is produced mainly by different combinations of β-rays and photoelectrons. The presence of the associated β-rays is largely responsible for the nearly complete failure to resolve the many groups. We do not propose to discuss further this part of the curve.

Beyond the main plateau two plateaus of shorter length are clearly observed. These terminate at energies of nearly 30 kev and about 44 kev and are ascribed to the presence of the two well-established lines in the photoelectric spectrum (L and M shell conversion of the hardest γ-ray, energy 46.7 kev). The energies are close to the expected values if some allowance is made for energy loss of the photoelectrons in the source and the possibility of simultaneous detection of M x-radiations in the case of the second. The smooth drop of the curve above each plateau suggests the presence of β-particles of the continuum since these can be detected simultaneously if the life of the excitation level at 46.7 kev does not exceed 10 μsec. Four combinations of β-particle and photoelectron e^- are possible: (a) β and e^- backward, neither detected; (b) β forward into counter, e^- back, β alone detected; (c) e^- forward, β back, e^- alone detected; (d) β and e^- forward, both detected as a single ionizing event.

Case (b) gives rise to β-rays which are merged in the general distribution at low energies. Case (c) gives a tendency to peak at about 30 and 44 kev, while (d) is chiefly responsible for tails at energies above the peaks. We expect, therefore, that close examination of the shape of the curve from around 44 kev to 62 kev will give a clear picture of the β-spectrum associated with

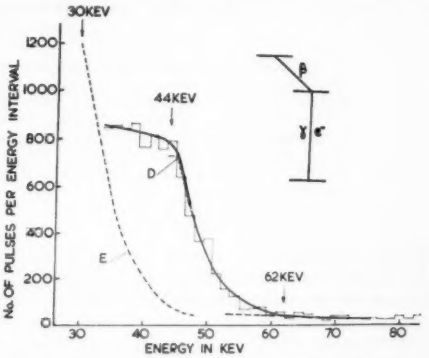

FIG. 2. Curve D shows modification of end of spectrum obtained by using curve E which represents the combination of photoelectrons, ~30 kev in energy, with β-rays.

the level at 46.7 kev. This part of the curve must necessarily represent the β-distribution closely.

ANALYSIS OF THE β-SPECTRUM

A theoretical Fermi distribution $F(Z=83$, allowed) for an energy limit E_0 of 18 kev was evaluated. This value of E_0 followed from the facts that the over-all end-point of Fig. 2 occurs at 62 kev and the photoelectron peak due to M-shell conversion at 44 kev. The curves of Fig. 3 indicate the method of using F. Thus curve P, centered at 44 kev, and representing the form that a homogeneous group of electrons of this energy would take as experimentally analyzed by the tube (based on observations with γ-rays of energy 46.7 kev) was constructed so that the areas under P and F (not shown) were equal. Using P and F (and weighting properly in accordance with their shapes), curve A was drawn to represent the distribution observed by recording simultaneously any one electron of group P

and any β-particle of group F. Now in the spectrometer, P and A, which enclose the same areas, correspond to cases (c) and (d) above. They combine to produce the pulse distribution S of Fig. 3, which is then the derived curve which can be used for comparison with the results shown in Fig. 2 to check the extent of the agreement of our results with Fermi theory.

In Fig. 2, therefore, a curve D (dashed line) is drawn coinciding exactly with the observed distribution from 62 to (62–14), i.e., 48 kev, and below this energy differing from the experimental curve by an amount corresponding to the tail of the curve increased in the ratio $\frac{3}{2}$ (the heights of the 30- and 44-kev plateaus are as $\frac{3}{2}$).

The final test of agreement between theory and experiment is obtained by checking how well the modified experimental curve D above 44 kev fits the corresponding part of the derived curve S. The comparison

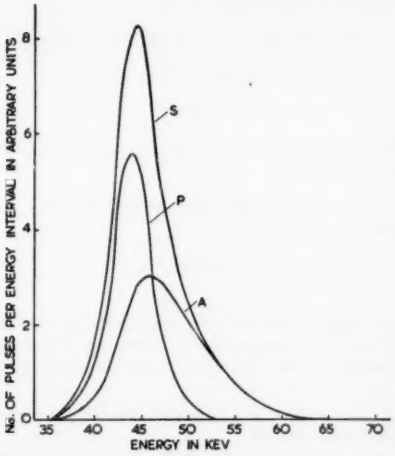

FIG. 3. Illustration of the method of deriving the curve S from curves P and A. Curve P represents photoelectrons alone, curve A photoelectrons+β-rays, and S the composite curve.

is shown in Fig. 4 and the close fitting of the two curves is very satisfactory. The agreement appears to confirm that the region of the observed spectrum above 44 kev corresponds to the combination of β-rays of limiting energy 18 kev with photoelectrons. It is somewhat unfortunate that the photopeak is not really accurately defined (sometimes the x-rays are associated) as this would give additional accuracy to E_0, but the limiting energy would appear to be stated within fairly conservative limits by:

$$E_0 = 18 \pm 2.5 \text{ kev}.$$

CONCLUSIONS

It appears that the disintegration energy of RaD is 64.5±2.5 kev and that the main mode of decay consists of the emission of β-rays of limiting energy $E_0 = 18$ kev

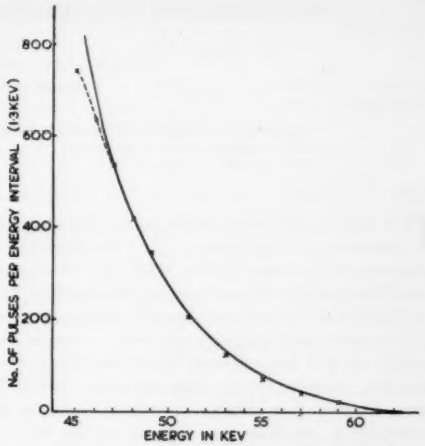

FIG. 4. Comparison of the derived curve S with the experimental results. The experimental points are shown by crosses.

leaving the RaE nucleus excited to 46.7 kev. This value of E_0 gives $\log ft = 5.5$, which definitely classifies the transition as allowed unfavored[9] rather than first forbidden which follows from previous data[10] on E_0.

Although direct de-excitation to the ground state occurs, by internal conversion in the L and M shells, frequently cascade processes of internal conversion take place. The lack of resolution of the corresponding peaks in the lower energy part of the pulse spectrum, Fig. 1, arises partly from the complexity of these photoelectron radiations, and the presence of Auger electrons, but mainly it is due to the accompanying β-rays which smooth out the distribution. It is difficult to make an accurate assessment of the probability of direct de-excitation because of this smoothing. The average energy of the observed pulses is 18 kev, but this figure is defined almost entirely by the photoelectrons and not by the β-rays.

Beta-transitions to levels of RaE other than that at 46.7 kev, if not entirely negligible, would appear to be of rather low intensity, and this is particularly true of the ground to ground transitions of energy 64.5 kev in view of the success of our analysis which assumes its absence.

Finally, it is noteworthy that β-emission of such low energy in a heavy nucleus should apparently correspond rather closely with Fermi theory and gratifying to find that the rather radical modifications of the process which have been suggested[11,12] do not seem to have any justification in fact, at least in this particular case.

[9] E. Feenberg and G. Trigg, Revs. Modern Phys. **22**, 399 (1950).
[10] A. M. Feingold, Revs. Modern Phys. **23**, 10 (1951).
[11] Frilley, Surugue, and San-Tsiang, J. phys. et radium **7**, 350 (1946).
[12] D. Ivanenko and V. Lebedev, J. Exp. Theor. Phys. U.S.S.R. **20**, 91 (1950).

The Spontaneous Magnetization of a Two-Dimensional Ising Model

C. N. YANG
Institute for Advanced Study, Princeton, New Jersey
(Received September 18, 1951)

The spontaneous magnetization of a two-dimensional Ising model is calculated exactly. The result also gives the long-range order in the lattice.

IT is the purpose of the present paper to calculate the spontaneous magnetization (i.e., the intensity of magnetization at zero external field) of a two-dimensional Ising model of a ferromagnet. Van der Waerden[1] and Ashkin and Lamb[2] had obtained a series expansion of the spontaneous magnetization that converges very rapidly at low temperatures. Near the critical temperature, however, their series expansion cannot be used. We shall here obtain a closed expression for the spontaneous magnetization by the matrix method which was introduced into the problem of the statistics of a two-dimensional Ising model by Montroll[3] and Kramers and Wannier.[4] Onsager gave in 1944 a complete solution[5] of the matrix problem. His method was subsequently greatly simplified by Kaufman,[6] and the result has been used to calculate the short-range order in the crystal lattice.[7]

The Onsager-Kaufman solution of the matrix problem will be used in the present paper to calculate the spontaneous magnetization. In Sec. I we define the specific magnetization I and express it as an off diagonal element in the matrix problem. By introducing an artificial limiting process its calculation is reduced to an eigenvalue problem in Sec. II. This is solved in the next three sections and the final result given in Sec. VI. The relation between I and the usual long-range order is discussed in Sec. I.

It will be seen that the final expression for the spontaneous magnetization is surprisingly simple, although the intermediate steps are very complicated. Attempts to find a simpler way to arrive at the same result have, however, failed.

I. SPONTANEOUS MAGNETIZATION

Using Kaufman's notation[6] we have for the two-dimensional square lattice the following expression for the partition function:

$$Z=(2\sinh 2H)^{n/2}\,\mathrm{trace}(\mathbf{V}_2\mathbf{V}_1)^m, \tag{1}$$

where

$$\mathbf{V}_1=\exp\{H^*\sum_1^n \mathbf{C}_r\}, \tag{2}$$

and

$$\mathbf{V}_2=\exp\{H\sum_1^n \mathbf{s}_r\mathbf{s}_{r+1}\}. \tag{3}$$

H^* and H are given by

$$e^{-2H}=\tanh H^*=\exp[-(1/kT)\{V_{\uparrow\downarrow}-V_{\uparrow\uparrow}\}]. \tag{4}$$

The following abbreviation will be useful:

$$x=e^{-2H}. \tag{5}$$

If a weak magnetic field is introduced the partition function becomes

$$Z_{\mathfrak{H}}=(2\sinh 2H)^{n/2}\,\mathrm{trace}(\mathbf{V}_3\mathbf{V}_2\mathbf{V}_1)^m, \tag{6}$$

where

$$\mathbf{V}_3=\exp\{\mathfrak{H}\sum_1^n \mathbf{s}_r\}. \tag{7}$$

For a large crystal only the eigenvector of $\mathbf{V}=\mathbf{V}_3\mathbf{V}_2\mathbf{V}_1$ with the largest eigenvalue is important. We shall be interested in the limiting form of this eigenvector as $\mathfrak{H}\to 0$.

It has been shown by Onsager[5] that below the critical temperature, i.e., for

$$x<\sqrt{2}-1,$$

the largest eigenvalue of $\mathbf{V}_2\mathbf{V}_1$ is doubly degenerate. This is evidently also true of the symmetrized matrix $\mathbf{V}_1^{\frac{1}{2}}\mathbf{V}_2\mathbf{V}_1^{\frac{1}{2}}$. Let ψ_+ and ψ_- be the even and odd eigenvectors corresponding to the largest eigenvalue λ.

$$\mathbf{V}_1^{\frac{1}{2}}\mathbf{V}_2\mathbf{V}_1^{\frac{1}{2}}\psi_+=\lambda\psi_+, \quad \mathbf{V}_1^{\frac{1}{2}}\mathbf{V}_2\mathbf{V}_1^{\frac{1}{2}}\psi_-=\lambda\psi_-. \tag{8}$$

The even eigenvector remains unchanged when the spins of all atoms are reversed while the odd eigenvector changes sign. Introducing the operator

$$\mathbf{U}=\mathbf{C}_1\mathbf{C}_2\cdots\mathbf{C}_n,$$

that reverses the spins of all atoms we have

$$\mathbf{U}\psi_+=\psi_+, \quad \mathbf{U}\psi_-=-\psi_-. \tag{9}$$

With the introduction of the magnetic field $\mathfrak{H}$ the degeneracy is removed. Since we are only interested in the limit as $\mathfrak{H}\to 0$, we may perform a perturbation cal-

[1] B. L. van der Waerden, Z. Physik **118**, 473 (1941).
[2] J. Ashkin and W. E. Lamb, Jr., Phys. Rev. **64**, 159 (1943).
[3] E. Montroll, J. Chem. Phys. **9**, 706 (1941).
[4] H. A. Kramers and G. H. Wanner, Phys. Rev. **60**, 252, 263 (1941).
[5] L. Onsager, Phys. Rev. **65**, 117 (1944).
[6] B. Kaufman, Phys. Rev. **76**, 1232 (1949).
[7] B. Kaufman and L. Onsager, Phys. Rev. **76**, 1244 (1949).

culation and consider the largest eigenvalue of

$$\mathbf{V}_1^{\frac{1}{2}}\mathbf{V}\mathbf{V}_1^{-\frac{1}{2}}=\mathbf{V}_1^{\frac{1}{2}}\mathbf{V}_3\mathbf{V}_2\mathbf{V}_1^{\frac{1}{2}}$$
$$=\mathbf{V}_1^{\frac{1}{2}}\mathbf{V}_2\mathbf{V}_1^{\frac{1}{2}}+3\mathcal{C}\mathbf{V}_1^{\frac{1}{2}}(\sum_1^n \mathbf{s}_r)\mathbf{V}_2\mathbf{V}_1^{\frac{1}{2}}. \quad (10)$$

The last term is a matrix that anticommutes with $\mathbf{U}$. It has, therefore, no diagonal matrix element with respect to either ψ_+ or ψ_-. It is, besides, a real symmetrical matrix. Ordinary perturbation theory shows immediately that the eigenvector of (10) with the largest eigenvalue approaches, as $3\mathcal{C}\to 0$

$$\psi_{\max}=(1/\sqrt{2})(\psi_+ +\psi_-), \quad (11)$$

if the phases of ψ_+ and ψ_- are so chosen that they are real and that[8]

$$\psi_+'\mathbf{V}_1^{\frac{1}{2}}(\sum_1^n \mathbf{s}_r)\mathbf{V}_2\mathbf{V}_1^{\frac{1}{2}}\psi_-\geqq 0. \quad (12)$$

The average magnetization per atom is, from the general definition of the matrix method,

$$I=\frac{1}{mn}\frac{m\,\mathrm{trace}(\mathbf{V}_3\mathbf{V}_2\mathbf{V}_1)^m\sum_1^n \mathbf{s}_r}{\mathrm{trace}(\mathbf{V}_3\mathbf{V}_2\mathbf{V}_1)^m}$$
$$=\frac{1}{n}\frac{\mathrm{trace}(\mathbf{V}_1^{\frac{1}{2}}\mathbf{V}_3\mathbf{V}_2\mathbf{V}_1^{\frac{1}{2}})^m(\mathbf{V}_1^{\frac{1}{2}}\sum_1^n \mathbf{s}_r\mathbf{V}_1^{-\frac{1}{2}})}{\mathrm{trace}(\mathbf{V}_1^{\frac{1}{2}}\mathbf{V}_3\mathbf{V}_2\mathbf{V}_1^{\frac{1}{2}})^m}$$
$$=\frac{1}{n}\psi_{\max}'\mathbf{V}_1^{\frac{1}{2}}(\sum_1^n \mathbf{s}_r)\mathbf{V}_1^{-\frac{1}{2}}\psi_{\max}.$$

As $3\mathcal{C}\to 0$ this becomes by (11)

$$I=\frac{1}{2n}(\psi_+'+\psi_-')\mathbf{V}_1^{\frac{1}{2}}(\sum_1^n \mathbf{s}_r)\mathbf{V}_1^{-\frac{1}{2}}(\psi_+ +\psi_-).$$

But $\mathbf{V}_1^{\frac{1}{2}}(\sum \mathbf{s}_r)\mathbf{V}_1^{-\frac{1}{2}}$ anticommutes with $\mathbf{U}$, and therefore has no diagonal matrix element with respect to either ψ_+ or ψ_-. Besides, by the use of (8), one shows easily that

$$\psi_-'\mathbf{V}_1^{\frac{1}{2}}(\sum_1^n \mathbf{s}_r)\mathbf{V}_1^{-\frac{1}{2}}\psi_+=\frac{1}{\lambda}\psi_-'\mathbf{V}_1^{\frac{1}{2}}(\sum_1^n \mathbf{s}_r)\mathbf{V}_2\mathbf{V}_1^{\frac{1}{2}}\psi_+,$$
$$\psi_+'\mathbf{V}_1^{\frac{1}{2}}(\sum_1^n \mathbf{s}_r)\mathbf{V}_1^{-\frac{1}{2}}\psi_-=\frac{1}{\lambda}\psi_+'\mathbf{V}_1^{\frac{1}{2}}(\sum_1^n \mathbf{s}_r)\mathbf{V}_2\mathbf{V}_1^{\frac{1}{2}}\psi_-, \quad (13)$$

which are obviously equal. Hence at zero magnetic field the spontaneous magnetization is

$$I=\frac{1}{n}\psi_-'\mathbf{V}_1^{\frac{1}{2}}(\sum_1^n \mathbf{s}_r)\mathbf{V}_1^{-\frac{1}{2}}\psi_+, \quad (14)$$

which is always positive by (13) and (12).

[8] We use the notation $A'=A$ transposed.

Intuitively one would infer that the summation $\sum \mathbf{s}_r$ in (14) can be replaced by $n\mathbf{s}_1$ so that

$$I=\psi_-'\mathbf{V}_1^{\frac{1}{2}}\mathbf{s}_1\mathbf{V}_1^{-\frac{1}{2}}\psi_+. \quad (15)$$

This can also be shown in detail by introducing the orthogonal operator $\mathbf{L}$ that is equivalent to the cyclic permutation of the n spins:

$$\mathbf{L}\sigma_i\mathbf{L}^{-1}=\sigma_{i+1}, \quad \mathbf{L}\sigma_n\mathbf{L}^{-1}=\sigma_1.$$

Evidently $\mathbf{L}$ commutes with $\mathbf{V}_1$, $\mathbf{V}_2$, and $\mathbf{U}$. Therefore $\mathbf{L}\psi_+$ is also an even eigenvector of $\mathbf{V}_2\mathbf{V}_1$ with eigenvalue λ. Hence

$$\mathbf{L}\psi_+=a\psi_+.$$

$\mathbf{L}$ and ψ_+ are real. Therefore a is real. Since further $\mathbf{L}^n=1$, we have $a=1$, and

$$\mathbf{L}\psi_+=\psi_+. \quad (16)$$

Similarly

$$\mathbf{L}\psi_-=\psi_-.$$

Now

$$\mathbf{s}_r=\mathbf{L}^{(r-1)}\mathbf{s}_1\mathbf{L}^{-(r-1)}.$$

Substituting this into (14) and using (16) we obtain (15).

The spontaneous magnetization I per atom is exactly the usual long-range order parameter s which may be defined as the average of the absolute value of the total spin of the lattice divided by the number of atoms. That I is equal to s is easily seen from the fact that the introduction of a vanishingly weak positive magnetic field merely cuts out all states of the lattice for which the total spin is negative.

One may ask, as Zernike[9] did, what is the average value of the total spin of the lattice if it is known that at a given lattice point the spin is $+1$. We can show that the answer is NI^2 in the following way: The total spin is either $+NI$ or $-NI$. If a given lattice point has a spin $+1$, it assumes the former value more frequently than the latter in the ratio of $\frac{1}{2}(1+I):\frac{1}{2}(1-I)$. Hence the average total spin is

$$NI(1+I)/2-NI(1-I)/2=NI^2.$$

The long-distance order can also be investigated as the limit of the short-distance order which has been studied by Kaufman and Onsager. Onsager[10] has done this and obtained the correlation of the spins of two atoms in one row at an infinite distance from each other. It can be shown that the long-distance order can be obtained from this, and the result agrees with the findings of this paper.

II. REDUCTION TO EIGENVALUE PROBLEM

A.

To calculate the spontaneous magnetization as given by (15) we notice that it is the off-diagonal ele-

[9] F. Zernike, Physica **7**, 565 (1938).

[10] L. Onsager, unpublished; see also Nuovo cimento **6**, Suppl. p. 261 (1949). The author wishes to thank Bruria Kaufman for showing him her notes on Onsager's work.

ment of the matrix $\mathbf{V}_1^{\frac{1}{2}}\mathbf{s}_1\mathbf{V}_1^{-\frac{1}{2}}$ between the vectors ψ_+ and ψ_-. Onsager and Kaufman[7] have shown how to calculate diagonal elements by reducing the $2^n\times 2^n$ matrix problem to one of $2n\times 2n$. Their method, however, does not apply to off-diagonal elements. To resolve this difficulty we shall in the present section introduce an artificial limiting process and reduce the problem to an eigenvalue problem of an $n\times n$ matrix.

From Kaufman's[6] Eq. (60) we have, except for a multiplicative phase factor:

$$\psi_- = \mathbf{S}^{-1}(\mathbf{T}_-)\tau, \tag{17}$$

where

$$\tau = \mathbf{g}\begin{pmatrix}1\\0\\0\\:\\0\end{pmatrix} = 2^{-n/2}\begin{pmatrix}1\\1\\:\\1\end{pmatrix}. \tag{18}$$

Similarly

$$\psi_+ = \mathbf{S}^{-1}(\mathbf{T}_+)\tau.$$

Now since $\mathbf{T}_-$ is real it follows that $\mathbf{S}(\mathbf{T}_-)$ is unitary. Hence taking the complex conjugate transposed of Eq. (17) we obtain

$$\psi_-{}' = \tau'\mathbf{S}(\mathbf{T}_-).$$

The reality condition of ψ_- has been used. Eq. (15) therefore assumes the form

$$I = \tau'\mathbf{S}(\mathbf{T}_-)\mathbf{V}_1^{\frac{1}{2}}\mathbf{s}_1\mathbf{V}_1^{-\frac{1}{2}}\mathbf{S}^{-1}(\mathbf{T}_+)\tau. \tag{19}$$

As we have just mentioned, if the expression were of the form

$$\tau'\mathbf{S}(\mathbf{T}_-)\cdots\mathbf{S}^{-1}(\mathbf{T}_-)\tau,$$

it would have been easy to reduce because $\mathbf{S}(\mathbf{T}_-)\cdots\times\mathbf{S}^{-1}(\mathbf{T}_-)$ induces a rotation in the $2n$ dimensional space formed by the Γ's.[11] We could, however, in the present case still utilize this reduction by first writing

$$I = \mathrm{trace}\mathbf{V}_1^{\frac{1}{2}}\mathbf{s}_1\mathbf{V}_1^{-\frac{1}{2}}\mathbf{S}^{-1}(\mathbf{T}_+)\tau\tau'\mathbf{S}(\mathbf{T}_-). \tag{20}$$

Now

$$\tau\tau' = (1/2^n)(\mathbf{1}+\mathbf{C}_1)(\mathbf{1}+\mathbf{C}_2)\cdots(\mathbf{1}+\mathbf{C}_n), \tag{21}$$

does not induce a rotation. But we notice that

$$\mathbf{1}+\mathbf{C}_1 = \lim_{a\to i\infty}(\cos a)^{-1}(\cos a - i\mathbf{C}_1\sin a) = \lim_{a\to i\infty}(\cos a)^{-1}\exp(-ia\mathbf{C}_1), \tag{22}$$

and $\exp(-ia\mathbf{C}_1)$ does induce a rotation. Write

$$\mathbf{M} = \begin{pmatrix}\cos 2a & \sin 2a & & & 0\\ -\sin 2a & \cos 2a & & & \\ & & \cos 2a & \sin 2a & \\ & & -\sin 2a & \cos 2a & \\ 0 & & & & \ddots\end{pmatrix} \tag{23}$$

so that

$$\exp(-ia\sum_1^n \mathbf{C}_r)\mathbf{\Gamma}_\alpha\exp(ia\sum_1^n \mathbf{C}_r) = \sum_\beta M_{\beta\alpha}\mathbf{\Gamma}_\beta. \tag{24}$$

[11] The $\mathbf{\Gamma}$'s are defined in Kaufman's paper (see reference 6). There is a mistake of sign in her Eq. (11) which should read $\mathbf{\Gamma}_{2r} = -\mathbf{C}\times\mathbf{C}\times\cdots\times i\mathbf{s}\mathbf{C}\times\mathbf{1}\times\mathbf{1}\times\cdots = \mathbf{Q}_r$.

We have from (21) and (22)

$$\tau\tau' = \lim_{a\to i\infty}(2\cos a)^{-n}\exp(-ia\sum_1^n \mathbf{C}_r) = \lim_{a\to i\infty}(2\cos a)^{-n}\mathbf{S}(\mathbf{M}).$$

Substitution back into (20) gives

$$I = \lim_{a\to i\infty}(2\cos a)^{-n}\,\mathrm{trace}\mathbf{V}_1^{\frac{1}{2}}\mathbf{s}_1\mathbf{V}_1^{-\frac{1}{2}}\mathbf{S}(\mathbf{T}_+^{-1}\mathbf{M}\mathbf{T}_-). \tag{25}$$

B.

This can easily be calculated if we know the eigenvalues and eigenvectors of the $2n$-dimensional rotation $\mathbf{T}_+^{-1}\mathbf{M}\mathbf{T}_-$. The rotations $\mathbf{T}_+$ and $\mathbf{M}$ have determinants equal to 1 while $\mathbf{T}_-$ has a determinant equal to -1. Thus $\mathbf{T}_+^{-1}\mathbf{M}\mathbf{T}_-$ is an improper rotation and must have eigenvalues $1,\ -1,\ e^{\pm i\theta_2},\ e^{\pm i\theta_3},\ \cdots e^{\pm i\theta_n}$. Let ζ be an orthogonal matrix that transforms $\mathbf{T}_+^{-1}\mathbf{M}\mathbf{T}_-$ into the canonical form

$$\zeta\mathbf{T}_+^{-1}\mathbf{M}\mathbf{T}_-\zeta^{-1} = \begin{pmatrix}1 & & & & & 0\\ & -1 & & & & \\ & & \cos\theta_2 & \sin\theta_2 & & \\ & & -\sin\theta_2 & \cos\theta_2 & & \\ & & & & \cos\theta_3 & \sin\theta_3 \\ & & & & -\sin\theta_3 & \cos\theta_3 \\ 0 & & & & & \ddots\end{pmatrix} = \mathbf{W}. \tag{26}$$

$\mathbf{W}$ is evidently orthogonal. We shall compute, first, instead of (25), the more general expression

$$\mathrm{trace}\mathbf{\Gamma}_j\mathbf{S}(\mathbf{T}_+^{-1}\mathbf{M}\mathbf{T}_-), \tag{27}$$

where $\mathbf{\Gamma}_j$ is as defined in Kaufman's paper.[11] By (26)

$$\mathrm{trace}\mathbf{\Gamma}_j\mathbf{S}(\mathbf{T}_+^{-1}\mathbf{M}\mathbf{T}_-) = \mathrm{trace}\mathbf{\Gamma}_j\mathbf{S}(\zeta^{-1})\mathbf{S}(\mathbf{W})\mathbf{S}(\zeta) = \mathrm{trace}\mathbf{S}(\zeta)\mathbf{\Gamma}_j\mathbf{S}(\zeta^{-1})\mathbf{S}(\mathbf{W}). \tag{28}$$

Now

$$\mathbf{S}(\zeta)\mathbf{\Gamma}_j\mathbf{S}(\zeta^{-1}) = \sum \zeta_{\alpha j}\mathbf{\Gamma}_\alpha,$$

where $\zeta_{\alpha j}$ are the matrix elements of ζ. Moreover, the explicit form of $\mathbf{S}(\mathbf{W})$ is known:

$$\mathbf{S}(\mathbf{W}) = i\mathbf{P}_1(\mathbf{P}_2\mathbf{Q}_2)(\mathbf{P}_3\mathbf{Q}_3)\cdots(\mathbf{P}_n\mathbf{Q}_n)\exp(\tfrac{1}{2}\sum_2^n \theta_\beta\mathbf{P}_\beta\mathbf{Q}_\beta).$$

(28) therefore reduces to

$$\begin{aligned}&\mathrm{trace}\mathbf{\Gamma}_j\mathbf{S}(\mathbf{T}_+^{-1}\mathbf{M}\mathbf{T}_-)\\ &= i\,\mathrm{trace}(\textstyle\sum \zeta_{\alpha j}\mathbf{\Gamma}_\alpha)\mathbf{P}_1(\prod_2^n \mathbf{P}_\alpha\mathbf{Q}_\alpha)\exp(\tfrac{1}{2}\textstyle\sum\theta_\beta\mathbf{P}_\beta\mathbf{Q}_\beta)\\ &= i\zeta_{1j}\,\mathrm{trace}\prod_2^n \mathbf{P}_\alpha\mathbf{Q}_\alpha\exp(\tfrac{1}{2}\theta_\alpha\mathbf{P}_\alpha\mathbf{Q}_\alpha)\\ &= i(-1)^{n-1}2^n\zeta_{1j}\prod_2^n\sin(\theta_\alpha/2).\end{aligned} \tag{29}$$

Returning to (25) we notice that

$$\mathbf{V}_1^{\frac{1}{2}}\mathbf{s}_1\mathbf{V}_1^{-\frac{1}{2}} = \mathbf{P}_1\cosh H^* - i\mathbf{Q}_1\sinh H^*. \tag{30}$$

(25), (29), and (30) give

$$I=(\prod_{2}^{n}\lambda_a)i(\xi_{11}\cosh H^*-i\xi_{12}\sinh H^*), \tag{31}$$

where

$$\lambda_a=\operatorname*{Lim}_{a\to i\infty}(-\cos a)^{-1}\sin(\theta_a/2), \tag{32}$$

and

$$\xi_{\alpha\beta}=\operatorname*{Lim}_{a\to i\infty}(\cos a)^{-1}\zeta_{\alpha\beta}. \tag{33}$$

C.

In this subsection we shall derive a formula for λ_a as the eigenvalue of an $n\times n$ matrix.

The matrices $\mathbf{T}_+$ and $\mathbf{T}_-$ are real, so that we can write

$$\mathbf{T}_+^{-1}\mathbf{M}\mathbf{T}_-=\tfrac{1}{2}\mathbf{G}\exp(-2ia)+\tfrac{1}{2}\mathbf{G}^*\exp(2ia), \tag{34}$$

where * means complex conjugate, and $\mathbf{G}$ is *independent* of a and is given by

$$\mathbf{G}=\mathbf{T}_+^{-1}\begin{pmatrix}1 & i & & & 0\\ -i & 1 & & & \\ & & 1 & i & \\ & & -i & 1 & \\ 0 & & & & \ddots\end{pmatrix}\mathbf{T}_-. \tag{35}$$

Now in Eq. (34) the eigenvalues of the left-hand side are $1, -1, e^{\pm i\theta_2}, e^{\pm i\theta_3}, \cdots e^{\pm i\theta_n}$. As $a\to i\infty$, the second term of the right-hand side becomes negligible, and we see that

$$\operatorname*{Lim}_{a\to i\infty}2e^{2ia}e^{i\theta_\alpha}=l_\alpha,$$

where $l_2, l_3, \cdots l_n$ are the nonvanishing eigenvalues of $\mathbf{G}$. A relation between the l's and the λ's is found by squaring (32):

$$\begin{aligned}\lambda_a^2&=\operatorname*{Lim}_{a\to i\infty}(\cos a)^{-2}\sin^2(\theta_a/2)=\operatorname*{Lim}_{a\to i\infty}4e^{2ia}\sin^2(\theta_a/2)\\ &=-\tfrac{1}{2}l_a.\end{aligned} \tag{36}$$

We therefore want to find the eigenvalues of the $2n\times 2n$ matrix $\mathbf{G}$ defined by (35). Now explicit matrix elements of $\mathbf{T}_+$ and $\mathbf{T}_-$ have been exhibited by Kaufman.[6] Using these matrix elements and rearranging the rows and columns of all $2n\times 2n$ matrices so that the order of the Γ's is changed into $\mathbf{P}_1, \mathbf{P}_2\cdots\mathbf{P}_n, \mathbf{Q}_1, \mathbf{Q}_2\cdots\mathbf{Q}_n$, we arrive at the following expression for $\mathbf{G}$:

$$\mathbf{G}=\begin{pmatrix}\mathbf{D}_+^{-1} & 0\\ 0 & -i\mathbf{D}_+^{-1}\end{pmatrix}\begin{pmatrix}\mathbf{p}_+^{-1} & \\ & \mathbf{p}_+\end{pmatrix}\begin{pmatrix}\mathbf{p}_- & \mathbf{p}_-^{-1}\end{pmatrix}\begin{pmatrix}\mathbf{D}_- & 0\\ 0 & i\mathbf{D}_-\end{pmatrix}, \tag{37}$$

where

$$\mathbf{D}_-=n^{-\frac{1}{2}}\begin{pmatrix}\epsilon^2 & \epsilon^4\cdots\epsilon^{2n}\\ \epsilon^4 & \epsilon^8\cdots\epsilon^{4n}\\ \cdots & \cdots\quad\cdots\\ \cdots & \cdots\quad\cdots\\ \epsilon^{2n} & \epsilon^{4n}\cdots\epsilon^{2nn}\end{pmatrix},\quad \epsilon=\exp(\pi i/n), \tag{38}$$

$$\mathbf{D}_+=\mathbf{D}_-\begin{pmatrix}\epsilon^{-1} & & & 0\\ & \epsilon^{-2} & & \\ & & \ddots & \\ 0 & & & \epsilon^{-n}\end{pmatrix}, \tag{39}$$

$$\mathbf{p}_-=\begin{pmatrix}e^{i\delta_2'/2} & & & 0\\ & e^{i\delta_4'/2} & & \\ & & \ddots & \\ 0 & & & e^{i\delta_{2n}'/2}\end{pmatrix}, \tag{40}$$

and

$$\mathbf{p}_+=\begin{pmatrix}e^{i\delta_1'/2} & & & 0\\ & e^{i\delta_3'/2} & & \\ & & \ddots & \\ 0 & & & e^{i\delta_{2n-1}'/2}\end{pmatrix}. \tag{41}$$

The quantities δ' are defined in Kaufman's paper. Explicit expressions for them will be given later in Eq. (60). The four matrices $\mathbf{D}_-$, $\mathbf{D}_+$, $\mathbf{p}_-$, and $\mathbf{p}_+$ are all unitary. Writing the eigenvector of $\mathbf{G}$ as $\begin{pmatrix}\phi\\ \eta\end{pmatrix}$ and by the use of (37) one obtains the following eigenvalue problem

$$\mathbf{D}_+^{-1}\mathbf{p}_+^{-1}(\mathbf{p}_-\mathbf{D}_-\phi+i\mathbf{p}_-^{-1}\mathbf{D}_-\eta)=l\phi, \tag{42}$$

$$-i\mathbf{D}_+^{-1}\mathbf{p}_+(\mathbf{p}_-\mathbf{D}_-\phi+i\mathbf{p}_-^{-1}\mathbf{D}_-\eta)=l\eta. \tag{43}$$

If $l\neq 0$, this shows that

$$\mathbf{p}_+\mathbf{D}_+\phi=i\mathbf{p}_+^{-1}\mathbf{D}_+\eta.$$

With the aid of this, η could be eliminated and the eigenvalue problem is finally reduced to

$$(\mathbf{D}+\mathbf{p}_-^{-2}\mathbf{D}\mathbf{p}_+^2)\phi_1=l(\mathbf{p}_-^{-1}\mathbf{p}_+)\phi_1, \tag{44}$$

where

$$\phi_1=\mathbf{D}_+\phi,$$

and

$$\mathbf{D}=\mathbf{D}_-\mathbf{D}_+^{-1}. \tag{44a}$$

D.

The calculation of $\xi_{1\beta}$ will be reduced in this subsection to the eigenvector problem of an $n\times n$ matrix.

From the definition of ζ in (26) we see that the column matrix

$$\zeta_1=\begin{pmatrix}\zeta_{11}\\ \zeta_{12}\\ \vdots\end{pmatrix}$$

which is the first column of $\boldsymbol{\zeta}^{-1}$ is an eigenvector of $\mathbf{T}_+^{-1}\mathbf{M}\mathbf{T}_-$ with the eigenvalue $+1$:

$$(\mathbf{T}_+^{-1}\mathbf{M}\mathbf{T}_-)\zeta_1=\zeta_1. \tag{45}$$

It is easily shown that if a column matrix ξ_1 could be found such that

$$\mathbf{G}\xi_1=0, \tag{46a}$$

and

$$\mathbf{G}\xi_1^*=2\xi_1, \tag{46b}$$

then in virtue of (34)

$$\zeta_1=\tfrac{1}{2}(e^{-ia}\xi_1+e^{ia}\xi_1^*) \tag{47}$$

does satisfy (45). It is to be emphasized that the ξ_1

defined by (46) is *independent* of a so that as $a\to i\infty$ (47) shows that ζ_1 becomes proportional to ξ_1, and the first column of the matrix $\|\xi_{\alpha\beta}\|$ is exactly ξ_1.

We now tackle Eqs. (46). Equations (37) and (46a) lead to

$$\begin{pmatrix}\mathbf{p}_-\mathbf{p}_-^{-1}\end{pmatrix}\begin{pmatrix}\mathbf{D}_- & 0\\ 0 & i\mathbf{D}_-\end{pmatrix}\xi_1=0,$$

showing that there exists an $n\times 1$ column matrix y such that

$$\begin{pmatrix}\mathbf{D}_- & 0\\ 0 & i\mathbf{D}_-\end{pmatrix}\xi_1=\begin{pmatrix}\mathbf{p}_-^{-1}\\ -\mathbf{p}_-\end{pmatrix}y, \tag{48}$$

which is both necessary and sufficient for the fulfillment of (46a). Solving (48) for ξ_1 and substituting into (46b) one obtains

$$\mathbf{D}_+^{-1}\mathbf{p}_+^{-1}(\mathbf{p}_-\mathbf{D}_-^2\mathbf{p}_-+\mathbf{p}_-^{-1}\mathbf{D}_-^2\mathbf{p}_-^{-1})y^*=2\mathbf{D}_-^{-1}\mathbf{p}_-^{-1}y, \tag{49}$$

$$-\mathbf{D}_+^{-1}\mathbf{p}_+(\mathbf{p}_-\mathbf{D}_-^2\mathbf{p}_-+\mathbf{p}_-^{-1}\mathbf{D}_-^2\mathbf{p}_-^{-1})y^*=2\mathbf{D}_-^{-1}\mathbf{p}_-y. \tag{50}$$

We shall show that

$$\mathbf{p}_-\mathbf{D}_-^2\mathbf{p}_-=\mathbf{p}_-^{-1}\mathbf{D}_1^2\mathbf{p}_-^{-1}. \tag{51}$$

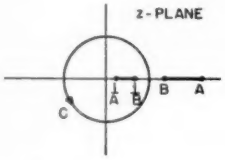

FIG. 1. Cuts in z-plane.

First, from (38)

$$\mathbf{D}_-^2=\begin{pmatrix}0 & 1 & & 0\\ & \ddots & \ddots & \\ & & \ddots & 1\\ 1 & & & \\ 0 & & & 0\end{pmatrix}. \tag{51a}$$

But from Kaufman's definition of δ',

$$\delta_{2r}'=-\delta_{2n-2r}', \tag{52}$$

and

$$\exp(i\delta_{2n}')=-1, \quad T<T_C. \tag{53}$$

Hence by (40) $\mathbf{D}_-^2\mathbf{p}_-^2\mathbf{D}_-^2=\mathbf{p}_-^{-2}$; and using $\mathbf{D}_-^4=1$ one immediately proves (51). (49) and (50) now simplifies to

$$\mathbf{D}\mathbf{p}_+^{-1}\mathbf{p}_-\mathbf{D}_-^2\mathbf{p}_-y^*=\mathbf{p}_-^{-1}y, \tag{54}$$

$$-\mathbf{D}\mathbf{p}_+\mathbf{p}_-\mathbf{D}_-^2\mathbf{p}_-y^*=\mathbf{p}_-y. \tag{55}$$

Elimination of y^* and simplification leads finally to

$$(\mathbf{D}^{-1}+\mathbf{p}_+^{-2}\mathbf{D}^{-1}\mathbf{p}_-^2)(\mathbf{p}_-^{-1}y)=0. \tag{56}$$

Equations (54) and (56) together determine y, which in turn gives ξ_1 through (48).

The normalization of ξ_1 is determined by substitution of (47) into

$$\zeta_1'\zeta_1=1. \tag{57}$$

This results in

$$\xi_1'\xi_1=0, \tag{58}$$

and

$$\xi_1'\xi_1^*=2. \tag{59}$$

(58) is automatically satisfied by virtue of (48), (51), and the fact that $\mathbf{D}_-$ and $\mathbf{p}_-$ are symmetrical matrices.

E.

To summarize the results of this section: The spontaneous magnetization I is given by (31), in which the λ's are related through Eq. (36) to the eigenvalues l of Eq. (44), and in which ξ_{11} and ξ_{12} are the first and the $(n+1)$th element of the column matrix ξ_1 calculated through (48) from the column matrix y which in turn is determined by (54) and (56). ξ_1 is to be normalized according to (59).

III. LIMIT FOR INFINITE CRYSTAL

A.

The procedure just outlined simplifies greatly when we approach the limit of an infinite crystal. To show this let us first introduce the variable

$$z=e^{i\omega} \quad (\omega=r\pi/n, r=1, 2, \cdots n). \tag{59a}$$

The relationship between δ' and ω is given by Kaufman's Eq. (52). In terms of z this can be reduced to

$$e^{2i\delta'}=\frac{\tanh^2H^*(z-\coth H\coth H^*)(z-\tanh H\coth H^*)}{(z-\coth H\tanh H^*)(z-\tanh H\tanh H^*)}. \tag{60}$$

From this we obtain $e^{i\delta'}$ and we shall write it as

$$\Theta(z)=e^{i\delta'}=(1/AB)^{\frac{1}{2}}[(z-A)(z-B)/(z-\mathrm{A}^{-1})(z-\mathrm{B}^{-1})]^{\frac{1}{2}} \tag{61}$$

where

$$A=\coth H\coth H^*=[(1+x)/x(1-x)],$$
$$B=\tanh H\coth H^*=[(1-x)/x(1+x)]. \tag{62}$$

For $T<T_C$, $A>B>1$. $\Theta(z)$ is analytic everywhere except at the points $z=A$, B, $1/A$, or $1/B$ where it has branch points. The square root in (61) is defined to be that branch of the function that takes the value -1 at $z=1$, in accordance with (53). (See Fig. 1.)

Consider Eq. (44). For a very large crystal

$$\mathbf{p}_-=\mathbf{p}_+=\mathbf{p},$$

and we have

$$(\mathbf{D}+\mathbf{p}^{-2}\mathbf{D}\mathbf{p}^2)\phi_1=l\phi_1. \tag{63}$$

By the definition of $\mathbf{D}$, Eq. (44a), the matrix elements of $\mathbf{D}$ are

$$(\mathbf{D})_{rs}=\frac{1}{n}\sum_{t=1}^{n}\epsilon^{2rt}\epsilon^{t}\epsilon^{-2ts}=-\frac{2}{n}\frac{1}{1-\epsilon^{2s-2r-1}}.$$

Hence $\mathbf{D}$ operating on any vector ϕ gives

$$(\mathbf{D}\phi)_r=\sum(\mathbf{D})_{rs}\phi_s=-\frac{2}{n}\sum_{s=1}^{n}\phi_s\left[1-\exp\frac{\pi i}{n}(2s-2r-1)\right]^{-1}$$

$$=-\frac{2}{n}\sum_{s=1}^{n}\frac{\phi_s}{1-z_{2s}/z_{2r}\epsilon}, \tag{64}$$

where z is the variable defined in (59a). For $s=1, 2, \cdots n$ the values assumed by z_{2s} are the n nth roots of unity. As $n\to\infty$ the summation in (64) therefore becomes an integral around the unit circle:

$$(\mathbf{D}\phi)_r=-2\int_C\frac{1}{2\pi i}\frac{dz}{z}\frac{\phi(z)}{1-(z/z_r)}, \tag{65}$$

where

$$z=\exp(2\pi is/n) \quad \text{and} \quad z_r=\exp(2\pi ir/n).$$

The contour C is the unit circle. At the point $z=z_r$ the principle value of the integral is to be taken. This is necessary because of the factor ϵ in the expression (64) which prevents the denominator from assuming the value zero. Alternately, we might make a detour around the point z_r and make up the difference by adding a term to (65):

$$(\mathbf{D}\phi)_t=-\frac{1}{\pi i}\int_{C'}\frac{dz}{z}\frac{\phi(z)}{1-(z/t)}+\phi(t). \tag{66}$$

We have here used the more convenient notation t for z_r. With this definition it is evident that the point t does not have to be on the unit circle. If, however, t is inside the unit circle, it is more convenient to use the following equivalent of (66):

$$(\mathbf{D}\phi)_t=-\frac{1}{\pi i}\int_{C''}\frac{dz}{z}\frac{\phi(z)}{1-(z/t)}-\phi(t), \tag{66a}$$

where C'' is as shown in Fig. 2.

The definitions (66) and (66a) for $\mathbf{D}$ are valid when $\mathbf{D}$ operates on any function $\phi(z)$ that is analytic in a region that contains the circumference of the unit circle in its interior. It is important to notice that this region does not have to be singly connected.

We quote a few interesting properties of the operator $\mathbf{D}$:

$$\begin{aligned}&\mathbf{D}z^m=t^m \quad \text{for } m=\text{integer}\geqq 1,\\ &\mathbf{D}z^m=-t^m \text{ for } m=\text{integer}\leqq 0,\end{aligned} \tag{67}$$

$$\mathbf{D}^2=1. \tag{68}$$

Now return to Eq. (63). Since $\mathbf{p}^2$ is a diagonal matrix with diagonal element $\Theta(z)$ given by (61), it is evident that (63) reduces to

$$2\phi_1(t)-\frac{1}{\pi i}\int_{C'}\frac{dz}{z}\frac{\phi_1(z)}{1-(z/t)}\left(1+\frac{\Theta(z)}{\Theta(t)}\right)=l\phi_1(t). \tag{69}$$

This integral equation will be solved in the next two sections.

B.

There still remains, according to the results of the last section, the problem of solving (54) and (56). By virtue of (68), (56) reduces to the same form as (63) with $l=0$. Thus $p_-^{-1}y$ is proportional to that eigenvector $\phi_1=\Phi$ of (69) belonging to the eigenvalue $l=0$:

$$2\Phi(t)-\frac{1}{\pi i}\int_{C'}\frac{dz}{z}\frac{\Phi(z)}{1-(z/t)}\left(1+\frac{\Theta(z)}{\Theta(t)}\right)=0. \tag{70}$$

For the convenience of normalization we shall write

$$\mathbf{p}_-^{-1}y=n^{-k}\Phi. \tag{71}$$

Then by virtue of (48), Eq. (59) reduces to

$$(1/n)\Phi'\Phi^*=1,$$

or

$$\frac{1}{2\pi i}\int_C|\Phi(z)|^2\frac{dz}{z}=1. \tag{72}$$

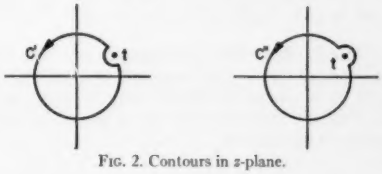

FIG. 2. Contours in z-plane.

The first and $(n+1)$th elements of ξ_1 are, according to (48) and (71):

$$\begin{aligned}\xi_{11}&=-\frac{1}{n}\sum_{s=1}^{n}\epsilon^{-2s}\Phi_s=\frac{1}{2\pi i}\int_C\frac{dz}{z^2}\Phi(z),\\ \xi_{12}&=-\frac{i}{n}\sum_{s=1}^{n}\epsilon^{-2s}\Theta(\epsilon^{2s})\Phi_s=\frac{1}{2\pi}\int_C\frac{dz}{z^2}\Theta(z)\Phi(z).\end{aligned} \tag{73}$$

The question of the fulfillment of Eq. (54), which now reduces to

$$\mathbf{D}\mathbf{D}_-{}^2\Phi^*=\Phi,$$

is best discussed with the aid of the introduction of the function $\Phi^\dagger(z)$ defined by

$$\Phi^\dagger(z)=[\Phi(z^*)]^*. \tag{74}$$

If Φ is analytic in a region containing the circumference of the unit circle in its interior, $\Phi^\dagger$ would be analytic in a similar region. Equation (51a) shows that

$$(\mathbf{D}_-{}^2\Phi^*)_s=[\Phi(z^*)]^*=\Phi^\dagger(z).$$

Thus (54) is fulfilled if

$$\Phi^\dagger(t)-\frac{1}{\pi i}\int_{C'}\frac{dz}{z}\frac{\Phi^\dagger(z)}{1-z/t}=\Phi(t). \tag{75}$$

C.

The integral equation (70) is easily solved by inspection:

$$\Phi(z)=Fz[(A-z)(B-z)]^{-\frac{1}{2}}, \tag{76}$$

where F is a normalization factor. F will turn out to be real, so that according to (74)

$$\Phi^{\dagger}(z)=\Phi(z).$$

It is easy to prove that (75) is satisfied. This completes the verification that (73) does indeed give the correct matrix elements of ξ_1.

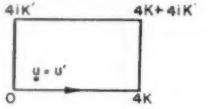

FIG. 3. Contour in u-plane.

To find F we substitute (76) into (72) and obtain

$$\frac{F^2}{2\pi i}\int_C \frac{dz}{[(A-z)(B-z)(Az-1)(Bz-1)]^{\frac{1}{2}}}=1. \tag{76a}$$

In the integrand the sign of the square root is to be so taken that at $z=1$ the integrand is positive. The integral is a complete elliptic integral and can be reduced to the standard form by a projective transformation. The result is

$$F^{-2}=\frac{4}{\pi}\frac{1}{A-B}k_{-1}^{\frac{1}{2}}K(k_{-1}),$$

where

$$k_{-1}=\left[\frac{(A^2-1)^{\frac{1}{2}}-(B^2-1)^{\frac{1}{2}}}{A(B^2-1)^{\frac{1}{2}}+B(A^2-1)^{\frac{1}{2}}}\right]^2, \tag{77}$$

and K is the complete elliptic integral of the first kind.[12] It is convenient to change the modulus and define[13]

$$k=2k_{-1}^{\frac{1}{2}}/(1+k_{-1})=4x^2/(1-x^2)^2=\sinh^{-2}2H. \tag{78}$$

Then

$$F^{-2}=2kK(k)/\pi(A-B). \tag{79}$$

The values of ξ_{11} and ξ_{12} are obtained from (73) and (76):

$$\xi_{11}=F(AB)^{-\frac{1}{2}},\quad \xi_{12}=0.$$

Substitution of these into (31), with the use of (36), leads to

$$I^4=[\prod_2^{\infty}(l_a^2/4)]F^4A^{-2}B^{-2}\cosh^4H^*.$$

We have here taken the fourth power of I to eliminate the undetermined phase factor that was introduced into the expression for I as early as Eq. (17). When the explicit expressions for A, B, F, and H^* are introduced, the expression for I^4 further simplifies to

$$I^4=\left(\prod_2^{\infty}\frac{l_a^2}{4}\right)\frac{\pi^2}{4}\left[\frac{1}{K(k)}\right]^2. \tag{80}$$

IV. ELLIPTIC TRANSFORMATION

It remains to find the eigenvalues l from (69) and substitute into (80). To do this we first introduce an elliptic transformation[12] that was essentially the one used in evaluating the integral in (76a):

$$z=-(\mathrm{cn}u-i[1+k]^{\frac{1}{2}}\,\mathrm{sn}u)(\mathrm{dn}u-i[k+k^2]^{\frac{1}{2}}\,\mathrm{sn}u)/(1+k\,\mathrm{sn}^2u), \tag{81}$$

the modulus k being given by (78).[13] This is the same transformation as was used by Onsager,[6] and Kaufman and Onsager[7] in their calculations. It serves to eliminate the square root in the function Θ:

$$\Theta=e^{iu'}=\mathrm{cn}u+i\,\mathrm{sn}u. \tag{82}$$

It is easy to verify that

$$\frac{1}{z}\frac{dz}{du}=-i\frac{1-k^2}{(1+k)^{\frac{1}{2}}}\frac{1}{\mathrm{dn}u-k^{\frac{1}{2}}\,\mathrm{cn}u}. \tag{83}$$

We shall need the following properties of the transformation (81): (A) z is doubly periodic in u with periods $4K$ and $4iK'$.

(B) z is everywhere analytic, except at $u=iK'/2$, $3iK'/2$ (mod. $4K$, $4iK'$), where $z=\infty$.

(C) In a unit cell in the complex u-plane, to every value of z there correspond exactly two values of u, except for $z=A$, B, $1/B$ or $1/A$ for which there corresponds only one value of u, namely, $u=+iK'$, $2K+iK'$, $2K-iK'$ or $-iK'$ (mod. $4K$, $4iK'$).

(D) If for a value of z there correspond in a unit cell two values of u, then at those two values Θ assume equal values but have different signs. Thus a unit cell of the u plane corresponds to both sheets of the Riemann surface in the z plane of Fig. 1 with respect to the function $\Theta(z)$.

The substitution, suggested by (76), into (69), of

$$\phi_1(z)=z[(z-A)(z-B)]^{\frac{1}{2}}\phi$$

gives, with the use of (81), (82), and (83)

$$2\phi(u')+\int_0^{4K}J(u',u)\phi(u)du=l\phi(u'), \tag{84}$$

where

$$J=\mathbf{I}\,\mathbf{II}\,\mathbf{III}\,\mathbf{IV}; \tag{85}$$

and

$$\mathbf{I}=[1-z(u)/z(u')]^{-1}, \tag{86}$$

$$\mathbf{II}=1+\Theta(z)/\Theta(z')=1+(\mathrm{cn}u+i\,\mathrm{sn}u)/(\mathrm{cn}u'+i\,\mathrm{sn}u'), \tag{87}$$

$$\mathbf{III}=\frac{z(u)}{z(u')}\left[\frac{\{z(u')-A\}\{z(u')-B\}}{\{z(u)-A\}\{z(u)-B\}}\right]^{\frac{1}{2}}, \tag{88}$$

[12] E. T. Whitaker and G. N. Watson, *Modern Analysis* (Cambridge University Press, London, 1927), fourth edition.

[13] The modulus k is the same as that used in references 5 and 7.

and

$$\mathbf{IV}=-\frac{1}{\pi}\frac{1-k^2}{(1+k)^{\frac{1}{2}}\,\mathrm{dn}u-k^{\frac{1}{2}}\,\mathrm{cn}u}.$$

V. SOLUTION OF INTEGRAL EQUATION (84)

We proceed by investigating the analytic behavior of $J(u', u)$ *with respect to the variable* u.

(*A*) **I**, **II**, and **IV** are all doubly periodic with periods $4K$ and $4iK'$. But **III** is doubly periodic with periods $4K$ and $8iK'$. It changes sign at periods $4iK'$:

$$\mathbf{III}(u+4iK)=-\mathbf{III}(u). \tag{89}$$

(*B*) **III** is analytic everywhere except at $z=A$ or $z=B$, i.e., $u=iK'$ or $2K+iK'$ (mod. $4K$, $4iK'$) where **III** has simple poles.

(*C*) **II** is analytic everywhere except at $u=-iK'$ or $2K-iK'$ (mod. $4K$, $4iK'$) where it has simple poles.

(*D*) **IV** is analytic everywhere except at

$$u=\pm iK'/2, \quad \pm 3iK'/2(\text{mod. } 4K, 4iK'),$$

where it has simple poles.

(*E*) **I** is analytic everywhere except at $z(u)=z(u')$. According to the last section in each cell there are, in general, two values of u where this exception occurs. At these two points **I** has simple poles.

However, there is *only one pole* for J in each unit cell ($4K$ by $4iK'$). This is so because of the following considerations:

(*F*) At $u=\pm iK'$, $\pm iK'+2K$ (mod. $4K$, $4iK'$), **IV** has simple zeros.

(*G*) At $u=iK'/2$, $3iK'/2$ (mod. $4K$, $4iK'$), $z(u)=\infty$, so that **I** has simple zeros.

(*H*) At $u=-iK'/2$, $-3iK'/2$ (mod. $4K$, $4iK'$), $z(u)=0$, so that **III** has simple zeros.

(*I*) According to property *D*, Sec. IV, in a unit cell ($4K$ by $4iK'$) at one of the solutions of $z(u)=z(u')$, $\Theta(u)=\Theta(u')$ so that $\mathbf{II}=2$. At the other solution, **II** has a zero.

Thus inside the rectangle in Fig. 3, J has only one pole at $u=u'$ which we assume to be inside of the rectangle. In the neighborhood of this pole $\mathbf{II}=2$, $\mathbf{III}=1$, and $\mathbf{I}-\mathbf{IV}=i\pi^{-1}(u-u')^{-1}$. Hence the residue of J at $u=u'$ is $2i/\pi$.

The solution of (84) is given by

$$\phi=\exp(im\pi u/2K), \quad m=\pm\text{integer}. \tag{90}$$

To show that this is indeed a solution we note that ϕ is periodic with period $4K$. Hence calling

$$g=\int_0^{4K} J(u', u)\phi(u)du,$$

one obtains by performing a contour integration around the rectangle of Fig. 3:

$$2\pi i(2i/\pi)\phi(u')=g[1+\exp(-2m\pi K'/K)]. \tag{91}$$

[The integration along the two vertical sides cancel each other and that along the top reduces to g multiplied by a factor, in virtue of (89).] This gives

$$g=-4\phi(u')/(1+q^{2m}), \tag{92}$$

where

$$q=\exp(-\pi K'/K). \tag{93}$$

(84) is therefore satisfied with

$$l=2-4/(1+q^{2m})=2(q^{2m}-1)/(q^{2m}+1). \tag{94}$$

For $m=0$ this gives, as expected, the solution $l=0$ which was already found by inspection in Sec. IIIC.

Knowing all the nonvanishing eigenvalues we can now calculate

$$\prod_2^\infty \frac{l_a^2}{4}=\prod_{\substack{m=-\infty\\ m\neq 0}}^{\infty}\left(\frac{1-q^{2m}}{1+q^{2m}}\right)^2=\prod_1^\infty\left(\frac{1-q^{2m}}{1+q^{2m}}\right)^4.$$

This infinite product can be[14] expressed in terms of the ϑ functions which are related to K. We get finally

$$\prod_2^\infty \frac{l_a^2}{4}=\frac{4}{\pi^2}[K(k)]^2(1-k^2)^{\frac{1}{2}}=\frac{4}{\pi^2}K^2\frac{1+x^2}{(1-x^2)^2}(1-6x^2+x^4)^{\frac{1}{2}}. \tag{95}$$

VI. FINAL RESULTS

The spontaneous magnetization I is obtained from (95) and (80) as

$$I=\left[\frac{1+x^2}{(1-x^2)^2}(1-6x^2+x^4)^{\frac{1}{2}}\right]^{\frac{1}{4}}. \tag{96}$$

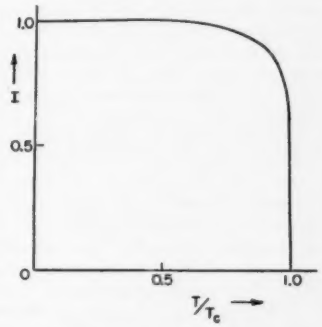

FIG. 4. Spontaneous magnetization.

At low temperatures this gives the same expansion in powers of x as obtained in previous works of Van der Waerden[1] and Ashkin and Lamb:[2]

$$I=1-2x^4-8x^8-34x^{12}-152x^{16}-714x^{20}-\cdots.$$

This series is convergent all the way up to the critical

[14] See reference 11, especially p. 472.

point, where

$$x=x_C=\sqrt{2}-1.$$

Near the critical point, I has a branch point:

$$I\cong[4(\sqrt{2}+2)(x_C-x)]^{1/8}.$$

In Fig. 4, I is plotted against the temperature.

This work was completed in the summer of 1951 while the author was at the University of Illinois. He wishes to take this opportunity to thank the staff of the Department of Physics, University of Illinois for the hospitality extended him during his stay. He also wishes to thank Bruria Kaufman for many stimulating discussions.

PHYSICAL REVIEW VOLUME 85, NUMBER 5 MARCH 1, 1952

High Energy Induced Fluorescence in Organic Liquid Solutions (Energy Transport in Liquids). III*†

MILTON FURST AND HARTMUT KALLMAN
Physics Department, New York University, New York, New York

(Received November 20, 1951)

Experimental results on the fluorescence of a large number of efficient solutions under both gamma-ray and alpha-particle excitation are presented. These results are compared with the theory to be found in Part I, and very good agreement is obtained in almost all cases. The physical efficiencies of some of these solutions under gamma-ray excitation are found to be quite high when compared with an anthracene crystal. The light output for the same amount of absorbed energy is considerably less for alpha-particle excitation than for gamma-rays in all of the solutions. The experimental data are discussed in conjunction with the theoretical considerations, and the physical processes involved in the large fluorescence of the solutions are analyzed.

A. EXPERIMENTAL RESULTS

SOME experimental and theoretical results on the fluorescence of organic liquid solutions using gamma-ray excitation have previously been reported.[1-3] This paper presents results under alpha-particle excitation in addition to further findings with gamma-ray bombardment. The light intensities of all the solutions were measured as a function of the solute concentrations, using mainly a RCA 1P28 photomultiplier with both types of excitation. In most cases, in order to minimize errors, the identical solutions were used for both excitations in comparing their effects. The light emission in the case of gamma-ray excitation is referred to the emission of an anthracene crystal of the same mass and in the same geometrical setting. Such relative fluorescence values at the optimum concentration are described here by the term relative physical efficiencies. These efficiencies differ somewhat from the practical efficiencies published previously,[3] as a consequence of the use of a nonreflecting container in the present measurements to minimize effects caused by different amounts of reflection at the walls of the container because of the spectral differences in the emission of the solutions. The values listed in Table I still depend to some extent on the spectral distribution of the emitted light because of the non-uniform spectral response of the photomultiplier. To determine the importance of such effects, measurements were made using two photomultipliers with different spectral responses (RCA 1P28 and 1P21), after the emission spectra of many of the solutions were determined.[2] A measure of the importance of this spectral effect is given in the last column of Table I, where the ratios of the intensities in the two photomultipliers for the different solutions are presented. The gamma-ray results for all the solutions are referred to the same mass, which means approximately the same amount of absorbed gamma-ray energy since the number of electrons per gram is essentially the same for all these organic solutions (see below).

It is to be noted that some of the light emission efficiencies are quite high; this is particularly the case for *p*-terphenyl which in phenylcyclohexane and xylene has an efficiency about half as great as an anthracene crystal. Since an anthracene crystal converts about 15 percent of the absorbed energy into light (measurements on a naphthalene crystal show about 5 percent conversion and anthracene is better by a factor of about 3),[4] this indicates that with the solutions as much at about 7 percent of the absorbed gamma-energy may be transformed into light. Another feature to be noted is that fairly generally a solute showing a relatively high efficiency in one solvent exhibits a rather high light emission in the other efficient solvents.

For alpha-particles the values are also referred to a standard measurement with an anthracene crystal or a zinc sulfide powder. Here there is the difficulty that the anthracene crystal surface deteriorates rather quickly under the alpha-particle bombardment (a 10-mC

* This work was supported by the Signal Corps Engineering Laboratories, Fort Monmouth, New Jersey.

† This is part of a dissertation (M.F.) in partial fulfillment of the requirements for the PhD degree at New York University.

[1] H. Kallmann and M. Furst, Phys. Rev. **79**, 857 (1950).

[2] H. Kallmann and M. Furst, Phys. Rev. **81**, 853 (1951).

[3] H. Kallmann and M. First, Nucleonics **8**, 32 (1951).

[4] Broser, Kallmann, and Martius, Z. Naturfursch. **4a**, 204 (1949).

TABLE I. Relative physical efficiencies of solutions.

	Xylene	Benzene	Cumene	*p*-Cymene	*p*-Dioxane	Phenetole	Phenyl cyclo-hexane	Phenyl ether	Toluene	Av. ratio 1P21/1P28*
Anthracene	0.060	0.046	0.042	0.039	0.025	0.048	0.059	0.045	0.047	0.98
Anthranilic acid	0.15	0.11	0.10	0.12	0.082	0.13	0.16	0.13	0.13	0.97
Diphenylbutadiene	0.12	0.058	0.078	0.069	0.019	0.067	0.14	0.093	0.081	0.95
Diphenylhexatriene	0.14	0.11	0.090	0.064	0.042	0.12	0.21	0.091	0.13	0.95
Durene	0.048	0.078	...	...	...	...	0.12	0.044	...	0.39
Fluoranthene	0.075	0.070	0.080	0.073	0.057	0.061	0.079	0.078	0.070	0.97
Methyl *p*-aminobenzoate	0.062	0.049	0.039	0.036	0.022	0.051	0.059	0.054	0.051	0.88
Methyl anthranilic acid	0.13	0.085	0.086	0.089	0.097	0.11	0.11	0.10	0.11	0.97
Phenyl α-naphthylamine	0.23	0.20	0.17	0.12	0.091	0.20	0.28	0.24	0.22	0.97
p-Terphenyl	0.48	0.38	0.39	0.34	0.27	0.32	0.48	0.41	0.43	0.92
Carbazole	0.12	...	...	...	...	...	...	...	...	...
Fluorene	0.15	...	...	...	...	...	...	...	...	...
Naphthalene	0.032	0.029	...	...	...	...	...	...	...	...
α-Naphthylamine	0.17	...	...	...	...	...	...	...	...	...
β-Naphthylamine	0.13	...	...	...	...	...	...	...	...	...
Pyrene	0.086	...	...	...	...	...	...	...	...	...
Stilbene	0.038	...	...	...	...	...	...	...	...	...
m-Terphenyl	0.20	...	...	...	...	...	...	...	...	...

* Ratio of anthracene crystal taken as 1.

polonium source was used). The crystal surface had to be renewed (by scraping or dissolving off the top layer) in order to obtain consistent measurements. The arrangement for the alpha-particle solution measurements is shown in Fig. 1; the instrumental portion is the same as for the gamma-ray measurements. A small amount of solution (0.7 cc) in a brass container with a quartz plate window was placed above the photographic shutter. The alpha-particle source was situated above the solution and separated from it by a very thin aluminum foil. This was necessary to avoid the light excited in the air in the vicinity of the alpha-particle source; this light was found to be comparable to the emission from the solution if the air gap was considerable.

Some typical results are reproduced in Figs. 2 to 6, where the indicated points give the experimental values and the drawn lines represent the curves which are calculated to fit the experimental points closely by means of the three parameters occuring in our theory[1,2] (see below). All of the experimental results of light intensity as a function of concentration are presented in summary form in Tables II to X by means of these parameters.‡ From the measured intensities no direct comparison can be made between the relative light efficiencies of gamma-rays and alpha-particles. They represent the readings of the measuring instrument with quite different exciting energies. It is, however, possible to refer these readings to the same amount of absorbed energy by calculation. It is then found that the light efficiencies under alpha-particle excitation are smaller than those under gamma-ray excitation by a factor of about 40 when comparing the maximum light emission from solutions of terphenyl in xylene. From this value all the alpha-particle intensities obtained from the parameters can be referred to the gamma-ray intensities. This value coincides in order of magnitude with the values given by Broser, Kallmann, and Martius[4] for the ratio between the gamma-ray and alpha-particle excitation efficiencies of organic crystals.

The curves and tables show a further difference in the effect of gamma-ray and alpha-particle excitation. All the alpha-particle curves have their maxima shifted to larger concentrations than the gamma-ray maxima. The degree of shift is not the same for all the solutions, but quite definite differences occur with the different solutions. A tentative explanation for such a behavior will be given below.

B. THEORETICAL CONSIDERATIONS

To explain the observed variations light with concentration variations and the large amount of light

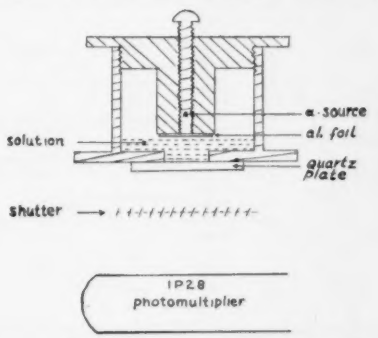

FIG. 1. Arrangement where an alpha-particle source excites a solution which emits light through a quartz window to a photomultiplier.

‡ Note: These values are calculated for concentrations in grams per liter. It would be somewhat more meaningful to use moles per liter. The relative P, Q, and R values would then be somewhat increased for the lighter solute molecules. The P/R values would remain unchanged.

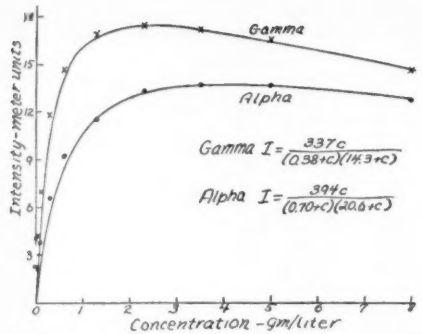

FIG. 2. Variation of emitted light intensity for various concentrations of diphenylbutadiene in benzene showing the experimental points and the agreement of the theory (curve) for both gamma-ray and alpha-particle excitations.

emission under high energy radiation, a theory has been proposed by us[1] which describes the light intensity I for a concentration c, by the equation

$$I=Pc/[(Q+c)(R+c)]. \tag{1}$$

The theory assumes that there is a transfer of energy from the excited solvent molecules to the solute, where this energy is trapped. The probability of this transfer and trapping is measured by αc. The energy transfer is counteracted by a quenching in the solvent molecules, the probability of which per unit time is described by $1/\tau_0$. The constant Q in the above formula is then given by

$$Q=1/(\alpha\tau_0). \tag{2}$$

After the excitation energy has been transferred to the solute and localized there, it is no longer exposed to the internal quenching in the solvent. In the solute the energy may then be subjected to three processes which must be considered: (1) The process of light emission; the probability of this per unit time is $1/\tau_e$. (2) The

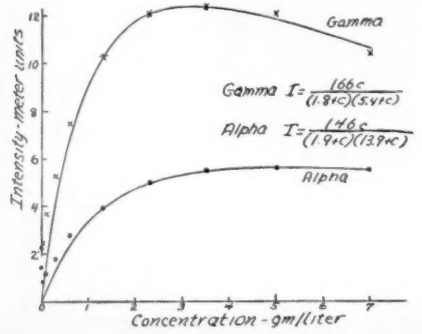

FIG. 3. Same as Fig. 2 except diphenylhexatriene in p-dioxane.

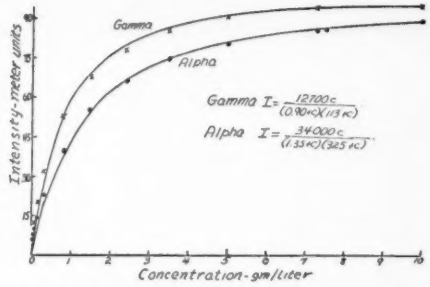

FIG. 4. Same as Fig. 2 except terphenyl in phenetole.

light energy process is counteracted by an internal quenching process in the solute, the probability of which is denoted by $1/\tau_i$. (3) There is also another process which competes with the light emission described in the literature by self-quenching which only occurs at higher concentrations; the probability of this per unit time is described by βc. From these, the parameters P and R are, respectively,

$$P=\eta_e\delta/\beta\tau_e \tag{3}$$

and

$$R=(1/\beta)(1/\tau_i+1/\tau_e), \tag{4}$$

where η_e describes the number of electrons of the solvent excited per unit time which are capable of transferring their energy to the solute, and δ is a constant which transforms the number of emitted quanta into meter units. The result, that mainly solutions made with solvents containing double bonds are the ones which have large fluorescent intensities under high energy radiation, suggests that the energy transfer is connected mainly with the electrons in these double bonds. The maximum intensity emitted by a solution measured in meter units and the maximum concentration in grams per liter can be calculated, respectively, from the values

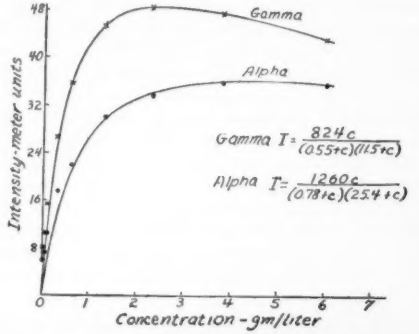

FIG. 5. Same as Fig. 2 except anthranilic acid in phenylcyclohexane.

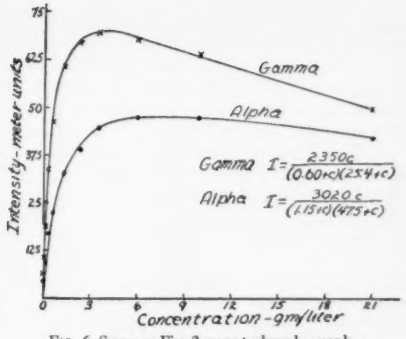

FIG. 6. Same as Fig. 2 except phenyl α-naphthylamine in xylene.

listed in Tables II to X by the formulas

$$I_{max}=P/(Q^{\frac{1}{2}}+R^{\frac{1}{2}})^2 \quad (5)$$

and

$$C_{max}=(QR)^{\frac{1}{2}}. \quad (6)$$

In these meter units, an anthracene crystal of the same mass as the solutions has a reading of 300 for gamma-ray excitation.

The curves of Figs. 2–6 show that on the whole the proposed theory fits the experimental results very well. There are definite systematic variations at low concentrations. These deviations arise from the fact that in our theory it is assumed that the solvent shows no emission, whereas in reality the solvents do fluoresce to an extent comparable with the emission intensities of the efficient solutions at very low concentrations. One might attempt to deduct these solvent emission values

TABLE II. Solution parameters—solvent: benzene.

Gamma-excitation: Solute	P	Q	R	P/R
Anthracene 1[a]	106	0.40	4.6	23
Anthracene 2	87	0.42	3.7	24
Anthranilic acid 1[a]	467	0.45	9.4	50
Anthranilic acid 2	450	0.52	9.5	47
Diphenylbutadiene	337	0.38	14.3	24
Diphenylhexatriene	225	0.55	3.55	63
Durene 1[a]	3000	0.75	133	23
Durene 2	6900	0.85	265	26
Fluoranthene 1[a]	9020	0.45	405	22
Fluoranthene 2	8570	0.42	402	21
Methyl anthranilic acid	1235	0.55	38.4	32
Methyl p-aminobenzoate	63	0.38	2.08	30
Phenyl α-naphthylamine 1[a]	1760	0.44	23.3	76
Phenyl α-naphthylamine 2[b]	1975	0.40	28.9	68
Phenyl α-naphthylamine 3[b]	2950	0.48	40.3	73
p-Terphenyl 1[a]	5610	0.57	41	137
p-Terphenyl 2	7100	0.61	51	139
Alpha-excitation:				
Anthracene 2	257	0.75	19.3	13
Anthranilic acid 2	375	0.75	13.7	27
Diphenylbutadiene	394	0.70	20.6	19
Diphenylhexatriene	141	0.65	5.0	28
Durene 2	19100	1.6	1270	15
Fluoranthene	10800	1.0	730	15
Methyl p-aminolbenzoate	56.7	0.80	3.0	19
Methylanthranilic acid	540	0.90	26.4	20
Phenyl α-napththylamine 2	3480	0.77	91.5	38
Phenyl α-napththylamine 3	3875	0.81	85	45
p-Terphenyl	10250	1.8	80	128

[a] No corresponding alpha-curve.
[b] Especially purified.

TABLE III. Solution parameters—solvent: cumene.

Gamma-excitation: Solute	P	Q	R	P/R
Anthracene 1[a]	109	0.75	4.3	25
Anthracene 2[b]	109	0.70	5.4	20
Anthranilic acid	542	1.1	10.2	53
Diphenylbutadiene	452	1.25	10.7	42
Diphenylhexatriene	173	0.95	2.43	71
Fluoranthene 1[a]	7570	0.85	301	25
Fluoranthene 2[b]	22800	1.55	885	26
Methyl p-aminobenzoate	75	0.80	2.81	27
Methylanthranilic acid	1413	1.05	40.2	35
Phenyl α-naphthylamine 1[a]	1603	1.0	20.7	77
Phenyl α-naphthylamine 2[b]	1550	1.9	21.6	72
Phenyl α-naphthylamine 3[b]	1250	1.3	19.2	65
Terphenyl 1[a]	5700	1.3	34.5	165
Terphenyl 2[b]	4010	1.2	33.1	121
Alpha-excitation:				
Anthracene 2	239	0.7	17.5	14
Anthranilic acid	615	1.5	18.8	33
Diphenylbutadiene	583	1.18	19.7	30
Diphenylhexatriene	127	1.3	2.79	46
Fluoranthene 2	20100	2.7	1245	16
Methyl p-aminobenzoate	159	0.9	7.2	22
Methylanthranilic acid	970	1.2	44.3	22
Phenyl α-naphthylamine 2	2483	1.95	47.7	49
Terphenyl 2	4060	2.4	31.2	130

[a] No corresponding alpha-curve.
[b] Change in solvent properties probably caused by absorption of oxygen.

TABLE IV. Solution parameters—solvent: p-cymene.

Gamma-excitation: Solute	P	Q	R	P/R
Anthracene	118	1.15	4.2	28
Anthranilic acid 1[a]	558	2.7	5.4	104
Anthranilic acid 2[b]	467	3.6	9.3	50
Diphenylbutadiene	496	2.6	10.4	48
Diphenylhexatriene 1[a]	243	1.9	2.12	115
Diphenylhexatriene 2[b]	209	2.5	2.3	75
Fluoranthene 1[a]	7300	0.85	320	23
Fluoranthene 2[b,c]	7950	1.5	308	26
Methyl p-aminobenzoate	88	1.0	3.24	27
Methylanthranilic acid	1380	1.4	35	40
Phenyl α-naphthylamine 1[a]	1068	1.3	17.0	63
Phenyl α-naphthylamine 2[b]	715	3.0	12.4	57
p-Terphenyl 1[a]	5550	1.3	37.5	148
p-Terphenyl 2[b]	3620	2.1	25.0	145
Alpha-excitation:				
Anthracene	123	1.5	6.0	21
Anthranilic acid 2	503	4.0	14.0	36
Diphenylbutadiene	482	2.7	13.3	36
Diphenylhexatriene 2	192	2.5	4.5	43
Fluoranthene 2	12930	2.0	800	16
Methyl p-aminobenzoate	199	0.9	9.4	21
Methylanthranilic acid	1275	1.4	52	24
Phenyl α-naphthylamine 2	1230	2.4	35	35
p-Terphenyl 2	8050	2.65	74	109

[a] No corresponding alpha-curve.
[b] Greater purification.
[c] Change in solvent properties probably caused by oxygen absorption.

TABLE V. Solution parameters—solvent *p*-dioxane.

Gamma-excitation: Solute	*P*	*Q*	*R*	*P/R*
Anthracene 1[a]	91	2.0	6.85	13
Anthracene 2	108	2.0	5.8	19
Anthranilic acid 1[a]	1370	1.8	37	37
Anthranilic acid 2	1565	1.8	47	33
Diphenylbutadiene 1[a]	385	2.5	44	9
Diphenylbutadiene 2	300	2.3	40	8
Diphenylhexatriene 1[a]	158	2.0	6.1	26
Diphenylhexatriene 2	166	1.8	5.4	32
Fluoranthene 1[a]	11080	4.3	704	16
Fluoranthene 2[b]	15900	4.5	800	20
Methyl *p*-aminobenzoate	102	0.8	9.1	11
Methylanthranilic acid	4030	2.45	104	39
Phenyl α-naphthylamine 1[a]	1760	3.8	44.5	40
Phenyl α-naphthylamine 2	1650	4.0	33	50
p-Terphenyl 1[a]	11400	6.0	113	101
p-Terphenyl 2	15700	5.5	132	119
Alpha-excitation:				
Anthracene 2	123	2.1	11.4	11
Anthranilic acid[c]	2150	2.6	118	18
Anthranilic acid 2	2140	2.4	127	17
Diphenylbutadiene 2	268	4.5	38	7
Diphenylhexatriene 2	146	1.9	13.9	10
Fluoranthene 2	19400	7.0	2060	9
Methyl *p*-aminobenzoate	600	0.4	73	8
Methylanthranilic acid	3190	4.5	150	21
Phenyl α-naphthylamine[c]	3800	5.3	159	24
Phenyl α-naphthylamine 2	2980	5.2	125	24
Terphenyl[c]	11950	6.5	222	54
Terphenyl 2	12800	5.8	236	54

[a] No corresponding alpha-curve.
[b] Further purified.
[c] No corresponding gamma-curve.

from the intensities of the solutions; but this cannot be done unambiguously since the emission of the solvent already very likely originates in tiny amounts of fluorescent impurities,[1] and since it was also found that in solutions containing several fluorescent solutes the intensity of one solute may be changed by tiny amounts of the other solutes.[2] There are a small number of rather efficient solutes such as fluorene, pyrene, and

TABLE VI. Solution parameter—solvent: phenetole.

Gamma-excitation: Solute	*P*	*Q*	*R*	*P/R*
Anthracene	129	0.85	4.38	29
Anthranilic acid	563	0.60	9.6	59
Diphenylbutadiene	362	0.45	13	28
Diphenylhexatriene	249	0.65	2.9	86
Fluoranthene	7650	0.48	390	20
Methyl *p*-aminobenzoate	158	0.38	6.8	23
Methylanthranilic acid	732	0.45	16.2	45
Phenyl α-naphthylamine	2320	0.68	28.4	82
p-Terphenyl	12700	0.90	113	112
Alpha-excitation:				
Anthracene	189	0.90	11.4	17
Anthranilic acid	630	0.68	20.0	32
Diphenylhexatriene	197	0.95	4.0	49
Diphenylbutadiene	545	0.60	24	23
Fluoranthene	8780	0.85	795	11
Methyl *p*-aminobenzoate	377	0.38	19.2	20
Methylanthranilic acid	675	0.67	22.7	30
Phenyl α-naphthylamine	2360	0.90	52.8	45
p-Terphenyl	34000	1.35	325	105

TABLE VII. Solution parameters—solvent: phenylcyclohexane.

Gamma-excitation: Solute	*P*	*Q*	*R*	*P/R*
Anthracene	154	0.50	5.13	30
Anthranilic acid 1[a]	627	0.65	8.2	77
Anthranilic acid 2	824	0.55	11.5	72
Anthranilic acid 3	860	0.57	11.9	72
Diphenylbutadiene 1[a]	953	0.38	16.5	58
Diphenylbutadiene 2	632	0.40	11.5	55
Diphenylbutadiene 3	726	0.40	13.2	55
Diphenylhexatriene 1[a]	254	1.0	1.7	150
Diphenylhexatriene 2	428	0.90	2.8	144
Durene 1[a]	6340	1.25	205	31
Durene 2	10430	1.15	250	42
Fluoranthene 1[a]	2580	0.37	104	25
Fluoranthene 2	3700	0.35	140	26
Methyl *p*-aminobenzoate	94	0.42	2.72	35
Methylanthranilic acid	576	0.50	12.5	46
Phenyl α-naphthylamine 1[a]	2100	0.50	22.4	94
Phenyl α-naphthylamine 2[b]	2840	0.55	25.5	111
Phenyl α-naphthalamine 3[b]	3010	0.45	28	107
p-Terphenyl 1[a]	6000	0.53	33	182
p-Terphenyl 2	5300	0.55	29.2	182
Alpha-excitation				
Anthracene	327	0.60	16	20
Anthranilic acid 2	1260	0.77	25.4	50
Anthranilic acid 3	1230	0.80	26.4	47
Diphenylbutadiene 2	455	0.75	9.7	47
Diphenylbutadiene 3	666	0.70	14.2	47
Diphenylhexatriene[c]	243	0.90	3.6	68
Diphenylhexatriene 2	308	0.90	3.85	80
Durene 2	11230	1.3	445	25
Fluoranthene 2	16600	0.50	880	19
Methyl *p*-aminobenzoate	123	0.45	5.3	23
Methylanthranilic acid	1120	0.80	30	37
Phenyl α-naphthylamine 2	3890	1.35	38.4	100
Phenyl α-naphthylamine 3	4200	1.15	40	105
p-Terphenyl 2	15950	1.10	100	160

[a] No corresponding alpha-curve.
[b] Further purified.
[c] No corresponding gamma-curve.

TABLE VIII. Solution parameters—solvent: phenyl ether.

Gamma-excitation: Solute	*P*	*Q*	*R*	*P/R*
Anthracene 1[a]	214	0.55	10.5	20
Anthracene 2	214	0.55	10.5	20
Anthranilic acid[a]	1060	0.60	19.3	55
Diphenylbutadiene	645	0.70	15.8	41
Diphenylhexatriene 1[a]	544	0.90	5.62	97
Diphenylhexatriene 2	409	0.82	4.05	101
Fluoranthene	5550	0.70	206	27
Methyl *p*-aminobenzoate	232	0.48	9.6	24
Methylanthranilic acid	1315	0.60	33.7	39
Phenyl α-naphthylamine 1[a]	2930	0.72	33.4	88
Phenyl α-naphthylamine 2[b]	4100	0.73	44.5	92
p-Terphenyl 1[a]	19800	1.1	142	140
p-Terphenyl 2	21900	1.15	152	144
Alpha-excitation:				
Anthracene 2	458	0.80	21	22
Anthranilic acid[c]	1212	0.80	31	39
Diphenylbutadiene	619	0.75	22.5	28
Diphenylhexatriene 2	347	0.80	5.65	61
Fluoranthene	24200	1.05	1170	21
Methyl *p*-aminobenzoate	477	0.55	23.4	20
Methylanthranilic acid	875	1.25	30	29
Phenyl α-naphthylamine 2	4880	1.3	64	76
p-Terphenyl 2	44850	1.7	340	132

[a] No corresponding alpha-curve.
[b] Further purified.
[c] No corresponding gamma-curve.

m-terphenyl where the agreement between theory and experiment is not so good. In some of these cases, additional purifications have corroborated the idea that at least part of the discrepancy is due to small amounts of impurity which may become quite effective, especially at higher concentrations. For pyrene, however, impurities are not responsible for the deviations, but rather its weak fluorescence which reaches a maximum at such high concentrations (because self-quenching is very weak) that other effects such as the direct excitation of the solute molecules by the incident radiation must be taken into account.

After our theory on solutions was published, a somewhat different theory proposed originally for crystals was applied to some of our results with solutions.[5] It is not felt that this other theory gives any better fit in view of the circumstance that the underlying physical ideas seem to be inapplicable to solutions.

An informative extrapolation can be made from the knowledge of the parameters. Thus the light intensity which a solution would emit if self-quenching would not reduce the light emission at higher concentrations, can be calculated by letting β approach zero. Then the asymptotic intensity that would be reached at infinite concentration is given by

$$I_{\text{ext}}=P/R=\delta\eta_e/[1+(\tau_e/\tau_i)]; \qquad (7)$$

in this expression the value of β no longer appears.

The values of the parameters show that I_{ext} of some of the solutions compared to an anthracene crystal are as high as 0.6 for terphenyl in xylene; $I_{\max}$ in this case was 0.48. For diphenylhexatriene in phenylcyclohexane there is a particularly large increase of I_{ext} over $I_{\max}$ from 0.21 to 0.5. If these extrapolated intensities are calculated for the same number of double bonds per gram of solvent (these may be mostly responsible as remarked above, for the energy transfer and fluorescence) rather than for the same mass, the extrapolated intensities relative to an anthracene crystal are considerably larger for phenylcyclohexane solutions; and for a solution of terphenyl in phenylcyclohexane, in particular, this intensity is greater than that of an anthracene crystal (see also below).

There is another point which requires discussion. From the analysis of the experimental curves, two parameter values are obtained which are identified with Q and R. Since, however, these values occur symmetrically in Eq. (1), there is ambiguity as to which value should be ascribed to R and which to Q. We have always, however, identified the larger of these constants with R for the following reasons. For some solutions the

TABLE IX. Solution parameters—solvent: toluene.

Gamma-excitation: Solute	P	Q	R	P/R
Anthracene	99.5	0.56	3.65	27
Anthranilic acid	655	0.60	11.3	58
Diphenylbutadiene	327	0.47	8.9	37
Diphenylhexatriene	231	0.53	3.0	77
Fluoranthene	5300	0.45	231	23
Methyl *p*-aminobenzoate	77.9	0.40	2.6	30
Methylanthranilic acid	866	1.15	16.0	54
Phenyl α-naphthylamine	1810	0.49	20.9	87
p-Terphenyl 1	5680	0.72	33.3	171
p-Terphenyl 2	6050	0.85	36.0	168
Alpha-excitation:				
Anthracene	183	0.65	11.2	16
Anthranilic acid	842	0.65	32.6	26
Diphenylbutadiene	407	0.60	18.7	22
Diphenylhexatriene	140	0.70	3.9	36
Fluoranthene	6180	1.0	400	15
Methyl *p*-aminobenzoate	95.5	0.55	5.25	18
Methylanthranilic acid	577	1.75	15.5	37
Phenyl α-naphthylamine	2105	0.83	42.2	50
Terphenyl 1	7110	1.30	57	125
Terphenyl 2	7980	1.35	62.7	127

[5] P. D. Johnson and F. E. Williams, Phys. Rev. **81**, 146 (1951).

TABLE X. Solution parameters—solvent: xylene.

Gamma-excitation: Solute	P	Q	R	P/R
Anthracene 1[a]	106	0.55	3.15	34
Anthracene 2	130	0.53	3.7	35
Anthranilic acid 1[a]	646	0.80	8.6	75
Anthranilic acid 2	595	0.75	9.0	66
Carbazole	342	0.55	5.6	61
Diphenylbutadiene 1[a]	630	0.45	14.0	45
Diphenylbutadiene 2	480	0.63	8.4	57
Diphenylhexatriene 1[a]	240	0.80	2.2	109
Diphenylhexatriene 2	218	0.75	2.1	104
Fluoranthene 1[a]	4770	0.35	206	24
Fluoranthene 2	6700	0.40	275	24
Fluorene 1[b]	155	0.80	1.8	86
Fluorene 2[b,c]	577	0.35	8.7	66
Methyl *p*-aminobenzoate	76	0.55	1.64	46
Methylanthranilic acid	972	1.1	16.0	61
α-naphthylamine	567	0.60	6.7	78
β-naphthylamine	1048	0.36	21.5	49
Phenyl α-naphthylamine 1[a]	1780	0.75	18.2	98
Phenyl α-naphthylamine 2[c]	2350	0.60	25.4	93
Pyrene[b]	105200	2.6	3850	27
Stilbene	838	0.38	63	13
p-Terphenyl 1[a]	7900	0.58	44.8	176
p-Terphenyl 2[a]	7870	0.60	43.3	182
p-Terphenyl 3	8050	0.55	45.5	177
Alpha-excitation:				
Anthracene[d]	123	0.65	7.6	16
Anthracene 2	134	0.70	6.2	22
Anthranilic acid 2	685	0.70	21.7	32
Carbazole	1840	0.55	77	24
Diphenylbutadiene	600	0.70	16	38
Diphenylhexatriene[d]	148	0.90	3.6	41
Diphenylhexatriene 2	191	0.95	4.0	48
Fluoranthene 2	18100	0.80	1130	16
Fluorene 1[b]	197	1.0	3.6	55
Fluorene 2[b]	6900	0.60	17.1	40
Methyl *p*-aminobenzoate	98.5	0.75	3.4	29
Methylanthranilic acid	3020	1.05	115	29
α-naphthylamine	770	0.70	19.5	39
β-naphthylamine	2470	0.48	85	29
Phenyl α-naphthylamine[d]	1885	1.3	31.5	60
Phenyl α-naphthylamine 2	3020	1.15	47.5	64
Pyrene[b]	159500	6.0	8000	20
Stilbene	5290	0.53	570	9
Terphenyl 3	9550	1.2	70.5	135

[a] No corresponding alpha-curve.
[b] Poor over-all fit.
[c] Further purified.
[d] No corresponding gamma-curve.

constant thus identified as R is found to be very large; nevertheless, the value P/R lies in the normal range of intensities. If, however, the identification were interchanged, the extrapolated intensities for vanishing self-quenching would be far too large and would in some cases give an energy larger than the energy absorbed. Therefore in a considerable number of cases our identification is certainly without ambiguity. Since now the values identified as Q (these are always the smaller ones) group around a certain value with relatively small variation when different solutes are put into the same solvent and Q is associated mainly with the solvent; it is felt that our identification is the correct one in all cases.

The values obtained for the parameters give some information about the magnitudes of the physical quantities occurring in the theory. Consider P/R which according to (7) depends only on the number of excited solvent electrons or perhaps mainly on those associated with the double bonds, and the ratio of τ_i/τ_e. If now the P/R ratios for a given solvent using different solutes are compared, the relative values of τ_i/τ_e for the different solutes may be obtained. And if the assumption that the number of effective excited electrons either is constant for a given mass or is proportional to the number of double bonds in that mass is valid, information may be gained about the dependence on the solvent of τ_i/τ_e by comparing the P/R values of a given solute in different solvents. The values for Q give the ratio between the internal quenching in the solvent and the probability of energy transfer (trapping) per unit concentration. For a given solvent they are surprisingly constant for different solutes, which indicates that the mechanism of energy transfer is essentially similar for all the solutes. For durene, which has a fair fluorescence within the solvents benzene and phenylcyclohexane but only a poor fluorescence with the other solvents, the explanation is certainly associated with the emission spectrum of this substance which extends relatively far into the ultraviolet. On the other hand, the values of Q looked upon as a function of the solvent show considerably more variation. Thus values of Q for cumene, p-cymene, and especially for dioxane are considerably greater with all solutes than they are for the other solvents listed in the tables. In some cases the Q values for a solute in p-dioxane are as much as 10 times larger than for an example in benzene. This indicates that the internal quenching $(1/\tau_q)$ of this solvent is larger than for any of the others.

The P and R values are quite erratic and change considerably for the same solute in different solvents, sometimes by a factor of 5. If P and R are considered as a function of the solute, however, the variations are very much larger (in some cases they vary by a factor of 500). This indicates that these parameters are chiefly a property of the solute which is, however, to some extent influenced by the solvent. These strong changes from solute to solute are due mainly to variations in the self-quenching coefficient β; without a detailed theory of self-quenching, however, no conclusions can be made about these variations. According to Eq. (3) P depends upon η_e, β, and τ_e. Now η_e does not change very much, as can be seen from the P/R values; τ_e can be evaluated theoretically[6] and certainly does not change so drastically as P. Thus the large variation in P must be attributed to variations in β.

There is another source of information on the magnitudes of τ_e and τ_i. This is the measurement of the decay time τ of the light flashes which is given for dilute solutions and organic crystals by

$$1/\tau=(1/\tau_i)+(1/\tau_e). \tag{8}$$

These lifetimes τ have been measured to be of the order of 3 to 5×10^{-9} sec for the solutions; for crystals the lifetimes are mostly considerably longer.[7,8] If now the lifetime and the relative light emission [proportional to $1/(1+\tau_e/\tau_i)$] are known the time constants τ_i and τ_e can be individually evaluated. In an anthracene crystal, the absolute efficiency of converting the absorbed gamma-ray energy into light is so high that the internal quenching must be small, which means that τ_i may be assumed to be probably larger than or about the same as τ_e. For the best solutes it may then be assumed that τ_i is also about the same as τ_e since their efficiencies in certain solutions are close to that of anthracene. The measurements of τ for crystals then indicate that in the crystal both τ_i and τ_e are greater than for solutions, since $1/\tau$ is smaller and essentially determined in such a case by $1/\tau_e$. For τ_i such an increase in crystals seems reasonable because the smaller interaction between neighboring molecules will most likely have the effect of decreasing the internal quenching. The fact that τ_e is larger in a crystal than for the relatively isolated solute molecules in a dilute solution shows that this emission time is prolonged in crystals, probably because of interference of the excited wave functions. Another suggestion that τ_e may be larger for crystals is obtained from considering the fluorescent emission of a naphthalene crystal excited by gamma-rays. Its efficiency is about $\frac{1}{3}$ that of anthracene, but the decay time is 3 times as long. This means that the observed τ is given practically by τ_i and is of the order of 6×10^{-8} sec[8] and that τ_e as calculated from the smaller efficiency is of the order of 1×10^{-7} sec; whereas for the best solution (terphenyl in phenylcyclohexane) τ_e is of the order of 5×10^{-9} sec. This may indicate that perhaps in perfect crystals τ_e would tend to still higher values and only the distortions in the lattice produce these smaller lifetimes of 1×10^{-7} sec in naphthalene and 2×10^{-8} sec in anthracene.

[6] R. S. Mulliken, J. Chem. Phys. **7**, 14, 121 (1939).
[7] G. B. Collins, Phys. Rev. **74**, 1543 (1948); C. G. Kelley and M. Goodrich, Phys. Rev. **77**, 138 (1950); R. F. Post and N. S. Shiren, Phys. Rev. **78**, 80 (1950).
[8] See Annual Report (May 1951) of U. S. Signal Corps, Contract No. DA 36-039 sc-35; these measurements were made by L. Bittman.

TABLE XI. (P/R) values for same mass/or same number of double bonds per gram.[a]

Gamma-excitation:	Benzene	Cumene	Cymene	Dioxane	Phenetole	Phenyl cyclohexane	Phenyl ether	Toluene	Xylene
Anthracene	24	20	28	19	29	30	20	27	35
	24	31	48	—	45	62	22	32	48
Anthranilic acid	47	53	50	33	59	72	55	58	66
	47	82	86	—	92	148	60	68	90
Diphenylbutadiene	24	42	48	8	28	58	41	37	57
	24	65	83	—	44	119	45	44	78
Diphenylhexatriene	63	71	75	31	86	153	101	77	104
	63	109	129	—	135	310	110	91	142
Durene	26	...	...	...	...	42	...	...	...
	26					86			
Fluoranthene	21	26	26	20	20	26	27	23	24
	21	40	45	—	31	53	30	27	33
Methyl *p*-aminobenzoate	30	27	27	11	23	35	24	54	46
	30	42	47	—	36	72	26	64	63
Methylanthranilic acid	32	35	40	39	45	46	39	30	61
	32	54	69	—	70	94	43	35	83
Phenyl α-naphthylamine	73	77	57	50	82	111	92	87	93
	73	119	98	—	128	228	101	103	127
p-Terphenyl	139	121	145	119	112	182	144	171	177
	139	187	250	—	175	374	157	202	241
Alpha-excitation:									
Anthracene	13	14	21	11	17	20	22	16	22
	13	22	36	—	27	41	24	19	30
Anthranilic acid	27	33	36	17	32	50	39	26	32
	27	51	62	—	50	103	43	31	44
Diphenylbutadiene	19	30	36	7	23	47	28	22	38
	19	46	62	—	36	97	31	26	52
Diphenylhexatriene	28	46	43	10	49	80	61	36	48
	28	71	74	—	77	164	67	42	65
Durene	15	...	...	...	...	25	...	...	...
	15					51			
Fluoranthene	15	16	16	9	11	19	21	15	16
	15	25	28	—	17	39	23	18	22
Methyl *p*-aminobenzoate	19	22	21	8	20	37	29	18	29
	19	34	36	—	31	76	32	21	40
Methylanthranilic acid	20	22	24	21	30	23	20	37	29
	20	34	41	—	47	47	22	44	40
Phenyl α-naphthylamine	45	49	35	24	45	100	76	50	64
	45	76	60	—	70	206	83	59	87
p-Terphenyl	128	130	109	54	105	160	132	125	135
	128	200	188	—	164	330	144	147	184

[a] Relative to the number of double bonds per gram of anthracene.

Considering now the solutions, the lifetimes in these are mostly given by τ_i if the solution is not of the highest efficiency. (Though in the case of p-terphenyl solutions the measured τ may be practically given by τ_e.) It would be interesting if such an effect of decreasing lifetimes in the less efficient solutions could be observed. The lifetime of emission can be roughly calculated from theory or obtained from the absorption coefficients of these solute molecules in different solvents. The absorption coefficients increase in some instances nearly linearly with the number of double bonds,[9] and thus the lifetime τ_e decreases with the increasing number of double bonds.

If the P/R values are now considered more fully (Table XI), some further information about τ_e/τ_i may be obtained. Thus for different solutes in a given solvent, a strong variation is found which indicates that τ_e/τ_i, which is essentially the internal quenching, is smallest for terphenyl, phenyl α-naphthylamine, and diphenylhexatriene; but for anthracene solutions it is relatively large, although in the anthracene crystal, τ_e/τ_i must be small as is shown by the large light emission. If, instead, the P/R values for the same solute but varying solvents are considered, it is found that in some cases they are quite similar; however, in others there are noticeable differences in this ratio. Thus, for instance, the P/R values of terphenyl in different solvents for gamma-ray excitation are rather constant, whereas those for diphenylhexatriene are not. If the ratios for terphenyl and diphenylhexatriene are formed, it is found that in benzene it is 2.2, in phenylcyclohexane it is 1.2, in phenyl ether it is 1.4, in xylene 1.7, and in p-dioxane 3.8. This shows clearly that the internal quenching depends to some extent on the solvent. It may be emphasized that in this respect p-dioxane always behaved somewhat erratically, as can be seen for instance by comparing the values for diphenylbutadiene in benzene, dioxane, and phenylcyclohexane. A better insight into this situation could be obtained from the comparison of the P/R values for one solute in different solvents, but here the method of determining the variation of η_e from solvent to solvent is uncertain. The upper figures in Table XI are calculated by assuming that these numbers of excited electrons available for energy transfer are proportional to the mass of the solvent being excited. For the lower figures it is assumed that η_e is proportional to the number of double bonds per gram of solvent. This latter assumption was suggested by the observation that mostly dilute solutions with solvents containing double bonds exhibit large fluorescence under gamma excitation. There are solvents like hexane and paraffin oil with no double bonds which show some energy transfer, though very much smaller than the efficient solvents. The only exception found is p-dioxane, which is a rather efficient solvent though it contains no double bonds; it does, however, contain a ring structure.

[9] Hausser, Kuhn, and Seitz, Z. physik. Chem. **B29**, 397 (1935).

On the assumption that double bonds are mostly responsible for the fluorescence, the values of Table XI show that τ_e/τ_i changes by a factor of 5 between different solvents. From a theoretical point of view one would assume that this change comes about by a change of τ_i and not τ_e. One could try to go still further and assume that the light emission of the most efficient solution, namely, p-terphenyl in phenylcyclohexane, is practically unquenched. In such a case τ_e would be identical with the τ measured from the decay of light flashes to be 4×10^{-9} sec. Once τ_e is determined, τ_i can be calculated for other substances from the P/R values in the table by assuming that η_e is proportional to either the mass or the double bonds and evaluating the relative values of τ_e for the other substances from known absorption coefficients. Such a method of treatment could most easily be accomplished if P/R values in chemically similar molecules are considered; as for example, in the series of diphenylpolyenes consisting of stilbene, diphenylbutadiene, diphenylhexatriene, and diphenyloctatetraene. In this series τ_e decreases with increasing number of double bonds fairly linearly,[9] and the P/R values and thus τ_i/τ_e increase with the number of double bonds in the line up to three; then τ_i/τ_e begins to decrease (diphenyloctatetraene is worse than diphenylhexatriene). It is therefore concluded that for larger numbers of double bonds the internal quenching is increased. A similar conclusion can be made by considering the series benzene, naphthalene, anthracene, and napthacene; and the series benzene, diphenyl, terphenyl, and quaterphenyl. Again, in these series the τ_e decreases with the number of double bonds, but the P/R values increase up to three rings and then decreases. (The measurements show that for quaterphenyl and naphthacene I_{max} are definitely smaller than for terphenyl and anthracene, respectively, though the actual P/R values have not been calculated.) This is only a tentative preliminary approach to unveil the underlying processes, and it is to be noted that for crystals such a relationship does not hold, since, for example, solid stilbene is considerably better for high energy fluorescence than diphenylhexatriene.

These conclusions with respect to internal quenching could be checked by optical measurements if the absolute quantum efficiency of these solute materials when optically excited were determined. Up to now there is only a small amount known in this field.[10] Some of our measurements on absorption inside of the solution further support the above conclusions. For instance, small amounts of anthracene are found to absorb the p-terphenyl radiation and then quench it; this occurs because the internal quenching of anthracene in xylene is much higher than that of p-terphenyl. Diphenylhexatriene, which also absorbs the terphenyl radiation, however, quenches the radiation energy from the terphenyl molecules only slightly, especially in phenyl-

[10] P. Pringsheim, *Fluorescence and Phosphorescence* (Interscience Publishers, Inc., New York, 1949).

cyclohexane, in agreement with the results that the P/R values of diphenylhexatriene in phenylcyclohexane are close to those of terphenyl. If the above mentioned optical experiments could be performed, they would provide another method of determining τ_i/τ_e, and then it would be possible to determine the relative η_e values from our P/R values.

If the relative physical efficiencies (essentially maximum intensities) are looked at, the influence of Q is also present [see Eq. (5)]. However, the variations of these values stem in many instances mostly from changes in P/R. For example, the difference between the efficiencies of diphenylhexatriene in benzene and xylene come mainly from the smaller internal quenching of this substance in xylene. There is another outstanding effect which may be noted: it is the fluorescent behavior of *p*-, *m*-, and *o*-terphenyl solutions. Of these *p*-terphenyl is the most efficient, *m*-terphenyl has a relative physical efficiency compared to *p*-terphenyl of about 40 percent and *p*-terphenyl has practically zero efficiency. These differences are most probably due to an increase of internal quenching from *p* to *m* to *o*, since all three molecules have essentially the same absorption coefficient and thus the same τ_e, and the self-quenching is less in *m* and probably *o*-terphenyl. It may be that this change in internal quenching is correlated with the change in angular orientation of the benzene rings; in *p*-terphenyl the rings lie in a straight line in one plane while in *m*- and *o*- there is a successive increase in angle with this line and the rings are not situated in the same plane.

If analogous considerations are made for the P, Q, and R parameters with alpha-particle excitation, many similarities (though some differences) are found in the relative behavior of the different solutions. Thus, for instance, if the P/R values for a certain solution are arbitrarily set equal for alpha-particle and gamma-ray excitation, all the others essentially coincide; whereas the Q and R values are both increased in almost all cases, the R values showing greater relative increases in most instances. Some deviations from this latter rule appear to be the result of detrimental changes in solvent properties produced by chemical reaction of the solvents with the air.

The most notable feature of the alpha-particle experiments is, however, the lower efficiency of the conversion of the absorbed energy into light emission by a factor of certainly more than 10. The explanation for this smaller efficiency is believed to lie in the much higher density of excitation with the alpha-particles. Inside the channel where an alpha-particle excites the solvent, the density of excited solvent molecules is so high (of the order of 10^{20} molecules/cm^3) that there exists a high probability that one excited molecule "collides" with another excited molecule before the energy transfer (described above) or light emission has occurred. If one assumes that each such collision leads to a quenching of excitation energy, then the strong decrease in the alpha-particle excited efficiency compared to that of gamma-rays can be understood, not only for the solutions but also for organic crystals where a similar decrease in alpha-particle efficiency is found. In the crystals the interaction between two excited molecules may come about by means of a migration of the excitation energy through the crystal; in the solutions, in addition to such a migration of excitation energy, the motion of the excited molecules may be important. See also reference 1. The question now arises as to the reason why this large quenching does not show up so strongly in the Q values because of changes in the $1/\tau_e$ values. The answer lies in the fact that the strong quenching coefficient produced by the high excitation density of a single alpha-particle is a function of time, and thus quenching decreases progressively with the decrease of the density of the excited molecules. After most of the excited molecules have decayed, the quenching coefficient becomes quite normal and only comparatively slightly increased compared to gammas.

The fact that the R values are also increased can perhaps be explained as follows: The R values give the ratio between the internal quenching and light emission probabilities, and the self-quenching coefficient. Since the τ_i/τ_e values are not changed very much, as can be concluded from the small change in the relative P/R values for α-particles as compared to gamma-rays, this change in R must be due to variations in self-quenching. Here the same considerations of the increased density of excitation may help in the understanding. The density of excitation, even after most of the excitation has decayed, is still high enough inside the channel of excitation has decayed, is still high enough inside the channel of excitation so that many of the solute molecules are excited. Thus the number of unexcited solute molecules which are responsible for the self-quenching is decreased, and this shows up as an increase in R.

Interactions of High Energy Nucleons with Nuclei.* Part I

G. BERNARDINI, E. T. BOOTH, AND S. J. LINDENBAUM†
Columbia University, New York, New York
(Received October 23, 1951)

Goldberger attempted to explain the interaction of high energy nucleons (~90 Mev) with heavy nuclei on the basis of a nucleonic cascade in a nucleon Fermi gas. The experimental test of this model was indecisive. In order to check the model at the higher energies available at the Nevis cyclotron, the interactions of 300–400 Mev protons and neutrons with the G-5 emulsion nuclei were analyzed. The experimental results are given and general evidence for the nucleonic cascade mechanism is presented.

I. INTRODUCTION

THE ideas set forth by Serber[1] concerning the inelastic interaction of a high energy nucleon with a heavy nucleus were extended by Goldberger[2] and developed into a detailed model for the behavior of a nucleon inside nuclear matter. The heavy nucleus was represented by a zero temperature Fermi gas of nucleons in a potential well of depth equal to the maximum Fermi energy plus the average nucleon binding energy. The incoming high energy nucleon was considered to be well localized (since its wavelength is much less than nuclear diameter) and to interact with the nucleon gas by a series of single nucleon-nucleon scatterings. The free nucleon-nucleon scattering cross sections were employed but were appropriately reduced by the Pauli exclusion principle, which excludes scatterings into momentum states within the filled Fermi sphere. The struck nucleons interacted similarly and in this way an internal nucleonic cascade was generated which proceeded until either the moving nucleons reached the edge of the nucleus and escaped or fell below the nuclear barrier (including Coulomb) and were thermally captured. Finally, there were some immediately ejected fast nucleons and a thermally excited nucleus which subsequently evaporated in a manner described by the Weisskopf[3] thermodynamical theory.

To treat complex cascades of this type and retain all the natural statistical fluctuations, Goldberger employed the Monte Carlo method. The evaluations were performed for the interaction of 90-Mev neutrons with a Pb nucleus. An experimental check of Goldberger's evaluation by Hadley and York[4] was interpreted to be at best only in partial qualitative agreement. The discrepancies may have been caused by the failure of the model at these low energies for which pick-up effects, multiple nucleon interactions, and refraction effects could be important. However, the assumed p-p and n-n cross sections which were later shown to be erroneous and some approximations in the calculations are also at least partly responsible. The broadness of the neutron beam energy spectrum and the difficulties in comparing in detail the calculations and the experiment could also be partly responsible for the differences.

The Fermi gas nuclear model has had a fair degree of success in explaining nuclear shell structure, and has also been successful in explaining nuclear transparency via the concept of a mean free path in nuclear matter.[5]

The Goldberger model is essentially based on extension of these concepts. Therefore, in spite of its apparent failure, or perhaps it is better to say indecisive test at 90 Mev, it was felt that it is worthwhile to check the model at the higher energies of 300–400 Mev protons and neutrons available at the Nevis cyclotron.

The model would be expected to be intrinsically better at these energies since the free nucleon scattering cross sections become much less than the nucleon cross section, even without the action of the Pauli exclusion principle, and also edge refraction effects, etc., become much less important.

Also, with a bombarding energy in the region of 300–400 Mev it is still possible to neglect meson production,[6] but at the same time one would expect rather large internal nucleonic cascades which provide a more definitive check of the basic features of the model.

The recent determinations of n-p and p-p scattering cross sections up to energies of about 300–350 Mev make a new set of Goldberger type of evaluations possible.

Since the calculations yield the detailed information about the properties of the nucleons emanating from the individual nuclear events, a most sensitive comparison of the theory and experiment can be made when the individual nuclear events are studied experimentally, and their fluctuations as well as the over-all mean distributions are compared to the theory, This is possible with the electron sensitive emulsions. since all charged particles emanating from the individual nuclear events are visible.

* This project was jointly supported by the ONR and AEC.
† Now at the Brookhaven National Laboratory, Upton, New York.
[1] R. Serber, Phys. Rev. **72**, 1114 (1947).
[2] M. L. Goldberger, Phys. Rev. **74**, 1269 (1948).
[3] V. Weisskopf, Phys. Rev. **52**, 295 (1937).
[4] J. Hadley and H. York, Phys. Rev. **80**, 345 (1950).
[5] Fernbach, Serber, and Taylor, Phys. Rev. **75**, 1352 (1949).
[6] An experimental estimate of meson production cross sections by the 385-Mev Nevis proton beam has been made by Block, Havens, and Passman [Phys. Rev. **83**, 167 (1951)]. These results indicate that less than 2–3 percent of the 350–400 Mev proton-induced nuclear interactions should be affected by meson production.

There is the disadvantage of a mixture of heavy (Ag-Br) and light (gelatin) nuclei. However, this has not proven too serious since it has been calculated (and checked experimentally) that at least 80 percent of the inelastic nuclear events occur in Ag-Br nuclei of average mass number ~ 100. There are other ways of separating the gelatin effects which will be discussed later.

II. PROTON-INDUCED NUCLEAR INTERACTIONS

A. Experimental Procedure

Four-hundred-micron Ilford G5 plates (3 inches by 1 inch) were exposed to the proton beam of the Nevis cyclotron. The exposures were made inside the vacuum chamber with the emulsion surface parallel to but $1\frac{1}{4}$ inches below the median plane. The plates were positioned such that the 3-inch dimension was bisected by the $n=0.2$ point, and with only the arc filament operating, the R.F. was switched on for a 5-sec period.

The plates were developed using the amidol, two-temperature method.[7] The development was uniform and a minimum ionization grain density of 33 grains per 100 microns was observed. The halves of the plates inside the $n=0.2$ point were covered by a more or less uniform flux of $2-4\times10^5$ fast proton tracks per cm^2 with an average length in the emulsion of about 5 mm. These tracks were almost parallel to the beam direction with an angular distribution of half-width equal to one degree.

Since the grain density of 400-Mev protons changes very slowly with energy, it was not practicable to determine the energy spectrum of the protons by grain counting. However, a check of the mean energy by grain density measurements gave the expected value of 1.5 minimum corresponding to 400 Mev.

A finer method of obtaining the energy spectrum was developed using cyclotron beam orbit theory. A statistical corelation between the angular distribution of the proton tracks in the plates and the maximum energy spread in the beam was developed. An evaluation based on this fixed the energy spectrum between the limits of 350–400 Mev. Actually, it may well be narrower than this, since part of the angular spread in the plate is because of Coulomb scattering in the plate, and this was not corrected.

Another approach to justify this estimate was an analysis of how the beam is lost as a function of radial and vertical oscillations introduced by the multiple traversals in our target geometry. The results of this calculation supported the previous estimate of a proton beam spectrum between 350–400 Mev. An independent analysis of multiple traversal phenomena was performed by Knox[8] and was checked experimentally at Berkeley by a different method. The results obtained were in agreement with the above conclusions.

[7] Dilworth, Occhialini, and Vermaesen, Bulletin du Centre de Physique Nucleare, Bruxelles **13a**, part I (1950).
[8] W. Knox, Phys. Rev. **81**, 693 (1951).

B. Terminology

To observe all inelastic nuclear interactions and to determine the corresponding mean free path in emulsion, proton tracks were individually followed. Only those regions of tracks at least 50 microns from either surface were used. In 1820 cm of proton track 34 inelastic events were observed. All observable nuclear events were recorded and classified phenomenologically in the following categories:

Star Production

The sudden ending of the incoming proton at a point from which either 2 or more tracks of any given grain density emerge, or only one track of grain density >3 times minimum emerges was defined as star production. Twenty-nine cases of star production were observed. The star tracks, to adhere to the usual notation, were classified into three groups.

(1) Gray—denotes prongs of grain density less than three times minimum.

(2) Sparse black—denotes prongs of grain density between about three and six times minimum.

(3) Black—denotes prongs of grain density greater that about six times minimum. In order to exclude recoil nuclei only those black prongs of range greater than 10 microns were recorded.

These grain density ranges correspond, respectively, to proton energies greater than 100 Mev, between 100 Mev and 30 Mev, and less than 30 Mev.

Scatterings

A scattering was defined as a sudden change of direction of the incoming proton with the scattered proton remaining as a gray prong (grain density <3 times minimum). Seven scatterings by a polar angle of less than 10° with no apparent change in grain density were observed. These are attributable to elastic shadow and Coulomb scatterings. Three scatterings greater than 10° were observed and these are probably attributable to inelastic nuclear interactions, since the cutoff of the elastic shadow scattering for the emulsion elements has been calculated to be about 10°. The cross section for Coulomb scatterings greater than 10° is negligible compared to the geometric.

Stops

Sudden disappearance of a proton in a region of the emulsion of full sensitivity was defined as a stop. Two cases were observed and both had a characteristic blob which is probably a nuclear recoil.

The above results are summarized in Table I.

C. Mean Free Path for Inelastic Nuclear Interactions

The experimental measurement error in proton track length is estimated to be of the order of 1 percent.

TABLE I. Distribution of events found scanning along proton tracks.

Event	Scattering $>10^\circ$	Stops in flight	Stars[a] 0	1	2	3	4	5	6	7	Prongs
Number	3	2	1	8	5	4	5	4	0	2	

[a] Stars are classified according to the number of non-gray prongs, i.e., number of black plus sparse black prongs.

The mean free path for all inelastic nuclear interactions is

$$\lambda_{in}=1820/34=54\pm9 \text{ cm}.$$

This result clearly indicates the phenomenon of nuclear transparency for 350–400 Mev protons, since the mean free path for G5 emulsion corresponding to a geometrical nuclear cross section is 25 cm. In the case of neutrons the phenomenon has been clearly established by Cook *et al.*[9] for 90-Mev neutrons and later by Fox *et al.*[10] and DeJuren[11] for 270-Mev neutrons.

To obtain large enough statistics for the distribution of the events by scanning along individual proton tracks would have been prohibitive from the point of view of time, and so a standard scanning "per area" with high resolution oil objective was employed. This scanning also gave us a check of the cross section based on better statistics. It was found by cross-checking two observers that all stars of at least one or more non-gray prongs would be reliably and consistently found in the normal scanning method. Therefore, a determination of the cross section for one or more non-gray prong stars was made using the method of track length sampling in conjunction with the normal scanning.

Based on 404 stars, a mean free path of $\lambda_{star}=56\pm9$ cm was found, where the errors include the statistical one (±3) and the experimental one (±6). In order to obtain the mean free path for all inelastic nuclear interactions, corrections must be made in some way for the events missed in the normal scanning. It was observed that the experimental numbers of 1, 2, and 3 prong stars (of the 404) are about the same. It therefore seems reasonable to assume the same frequency for the events missed (which correspond to the zero prong stars).[12] This leads to a multiplying factor of 0.81 ± 0.06 which is consistent with the data of Table I, showing that 28 of the 34 inelastic events listed are of the type which would be seen in normal scanning. Using this factor one finds as the mean free path for all inelastic nuclear interactions $\lambda=45\pm9$ cm. This agrees with the value found by scanning along individual tracks. The corresponding cross section is $\sigma=(0.56\pm0.11)\sigma_{geom}$.

Inelastic cross section measurements[9,10] with high energy neutrons have shown that the total inelastic cross section for light and heavy nuclei can be approximately computed[5] by considering the nucleus as a Fermi gas of noninteracting nucleons and attributing to it an absorption coefficient based upon the density of nucleons and the experimental scattering cross sections, which are appropriately reduced to satisfy the Pauli exclusion principle.

A calculation of this type for the interaction of 350–400 Mev protons with emulsion was performed by extrapolating experimentally measured cross sections to 350–400 Mev. The calculated inelastic cross section for emulsion is $\sigma_{in}\approx0.6\sigma_{geom}$.[13] This agrees very well with the measured value.

Using the results of this calculation, the ratio of the total inelastic cross section of the Ag-Br to that of the gelatin in the emulsion is 4:1. Therefore, it is to be expected that about 80 percent of the stars are Ag-Br events.

D. Proton Star Characteristics and Distribution Curves

Only those stars which clearly exhibited an incoming proton of the proper grain density and directed in the well-collimated region of $\pm2^\circ$ from the beam direction

TABLE II. Proton star characteristics.

A. Mean prong numbers

Type of prong	Black	Gray	Sparse black
Mean prong number	3.1 ± 0.15 correcting for zero prong stars: 2.5 ± 0.2	0.42 ± 0.04	0.35 ± 0.04

B. Gray prong distribution.

Number of gray prongs	0	1	2	3	4
Percentage of events	$(57\pm4)\%$	$(40\pm4)\%$	$(2.5\pm1)\%$	0	0

C. Fast (sparse black or gray) prong distribution.

Number of fast prongs	0	1	2	3	4
Percentage of events	$(35\pm3)\%$	$(54\pm4)\%$	$(9\pm2)\%$	$(1.7\pm0.7)\%$	0

[9] Cook, McMillan, Peterson, and Sewell, Phys. Rev. **75**, 7 (1949).

[10] Fox, Leith, Wouters, and MacKenzie, Phys. Rev. **80**, 23 (1950).

[11] J. DeJuren, Phys. Rev. **80**, 27 (1950).

[12] The term, "zero prong star" would refer to what was previously defined as a stop or a scattering and also to stars consisting of two or more gray prongs only.

[13] This result is not very sensitive to the extrapolation for the following reasons. The p-p cross section is known and does not change from 120 Mev to 340 Mev [Chamberlain, Segrè, and Weigand, Phys. Rev. **81**, 661 (1950)], and therefore should very probably be the same at 400 Mev. The n-p cross section is known from 40 to 270 Mev [Hadley, Kelly, Leith, Segrè, Weigand, and York, Phys. Rev. **75**, 351 (1950); Kelly, Leith, Segrè, and Weigand, Phys. Rev. **79**, 96 (1950)], and is continuously decreasing with energy somewhat more slowly than a $1/E$ law. Provided that it does not change its behavior too drastically in the region of 270–400 Mev, the calculated result will be close to the measured one, because the nuclear transparency is a slowly varying function of cross section in this region.

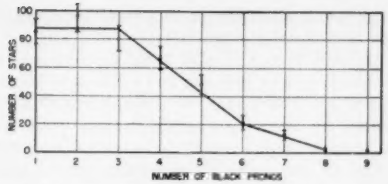

FIG. 1. Black prong distribution curve based on 412 stars induced in G-5 emulsion by 350–400 Mev protons.

were considered. The identification of different types of prongs was made visually after the training of the observers. A systematic check of the gray-sparse black border by grain counting showed that the distinction was included in the range 80–120 Mev.[14] The sparse black to black border was checked by using the range-grain density relations found for prongs ending in the emulsion and π-μ decays. The maximum variation in the black to sparse black classification was from 25–35 Mev. The lower end of this range was always identifiable as black and the upper end as sparse black.

Hereafter for simplicity the border divisions will be considered to be at 30 Mev and 100 Mev. Gray or sparse black prongs will be called "fast prongs."

In Fig. 1 the proton star distribution curve is given as a function of the number of black prongs only. It is based on 412 stars.

Figure 2 presents the percentages of stars in each star size group (determined by the number of black prongs) which exhibit outgoing fast prongs. The solid curve represents stars with at least one outgoing gray prong. The dotted curve represents stars with at least one outgoing gray or sparse black prong. Table II presents characteristic data.

These distribution curves and data can be considered as primarily representative of the processes occurring in Ag-Br nuclei. As previously calculated, the percentage of events occurring in gelatin is at most 20 percent. An experimental determination of the ratio of the gelatin events to Ag-Br events for 300-Mev neutrons incident upon G5 emulsion has been performed by Blau,[15] employing stratified emulsions. The result was that only 17 ± 3 percent of the visible stars induced in the emulsion occur in gelatin. The gelatin star distribution curve was found to be predominantly confined to the small stars (<5 black prongs). Only about 5 percent of the large stars (5 or more black prongs) were found to be attributable to gelatin events. Hence, the large stars are almost exclusively Ag-Br events.

A similar result might reasonably be expected for proton-induced stars. This will become evident when neutron and proton stars are compared later and are shown to be equivalent.

The effective cutoff of the black prong distribution curve is at about 8 black prongs. Assume that this represents the complete transfer of 400 Mev to an Ag-Br nucleus and that the relationship is linear. Then an approximate estimate of the average energy transferred to the nucleus per black prong is 50 Mev. This is not to be construed as pure thermal energy transfer, but merely as an energy dissipation in low energy nucleons or groups of nucleons.

The cutoff of stars with a *gray* prong at 6 prongs also supports this view, since a 6-prong star would represent 300-Mev energy transfer, which would leave 100 Mev, or just about enough energy for a border gray prong. The decrease of the percentage of gray prongs (Fig. 2) with increasing star size is probably a result of the decrease of the energy available for a gray prong with increasing star size.

Similar considerations can be made by also treating the sparse black prongs as fast knock-on protons,[16] i.e., the dashed curve of Fig. 2.

The difference between the dashed and solid curves in Fig. 2 represents the percentage of stars with sparse black prongs only. The ratio of the percentage of stars with sparse black prongs only to the percentage of stars with a gray prong can be seen from Fig. 2 to increase from ~0.2 to ~3 from the 1 to 7 prong stars. This also clearly indicates the increasing dissipation of available energy into black prongs with increasing star size and in particular the more or less complete dissipation of the available energy in the large stars. This implies the generation of a nucleonic cascade in a heavy nucleus, since it is to be expected that the light nuclei could split before the dissipation of so much energy.

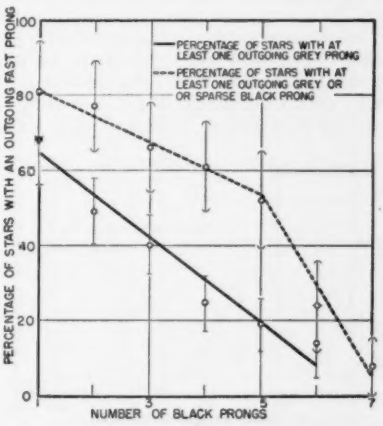
PERCENTAGE OF STARS WITH AT LEAST ONE OUTGOING GREY PRONG
PERCENTAGE OF STARS WITH AT LEAST ONE OUTGOING GREY OR OR SPARSE BLACK PRONG
PERCENTAGE OF STARS WITH AN OUTGOING FAST PRONG
NUMBER OF BLACK PRONGS

FIG. 2. Percentage of stars with outgoing fast prongs as a function of the number of black prongs, based on 412 stars induced in G-5 emulsion by 350–400 Mev protons.

[14] The tracks were followed completely. In the doubtful cases the grains were counted.

[15] M. Blau (private communication). We are very much indebted to Dr. Blau for this information.

[16] This will be justified by angular distribution measurements.

TABLE III. Energy of gray proton prongs from proton-induced stars.

Energy in Mev	100–200	200–300	300–400
Number of gray prongs	15	7	4

The clear inference of all these considerations is that in practically all of the stars with less than 7 or 8 black prongs one or more fast nucleons carry away the energy not transferred to the slow nucleons.

The energies of 26 outgoing gray prongs long enough to count at least 500 grains were determined. The results, grouped in 100-Mev intervals, are given in Table III.

A rough estimate of the total energy in the outgoing visible prongs is thus possible. The average disappearance of energy amounted to about one-half the initial energy or about 200 Mev. This means that on the average about half the energy is carried away by neutrons, even in the stars with outgoing gray prongs.

E. Angular Distribution of Proton Star Prongs

The angular distribution of gray, sparse black, and black prongs was determined in terms of the angle between the beam direction and the prong projection upon a plane parallel to the beam direction. The angular distributions of gray (solid curve) and sparse black (dashed curve) prongs are given in Fig. 3. The black prong angular distribution for all stars and large stars only is given in Fig. 4.

The evaporation prongs are expected to be isotropic and even for excitation energies of 400 Mev to be predominantly confined to the 0–30-Mev energy region.[17] The gray prongs are very sharply projected in the forward direction and are clearly directly ejected knock-ons. The sparse black prongs are less sharply projected, but they also seem to be almost exclusively directly ejected knock-ons. The higher energy gray prongs are more sharply collimated than the lower energy sparse black prongs, in a manner suggestive of a few nucleon-nucleon scatterings.

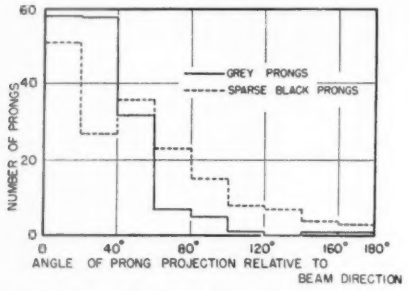

FIG. 3. Angular distribution of gray and sparse black prongs from stars induced by 350–400 Mev proton.

[17] K. J. LeCouteur, Proc. Phys. Soc. (London) **A63**, 259 (1950).

The black prongs (Fig. 4) could be considered as a superposition of an isotropic and a forwardly projected distribution. The maximum isotropic contribution is obtained by assuming that the average value in the backward 60° region is entirely because of an isotropic component, and extending this value over all angular intervals. In this way one finds that at the most, 60 percent of the black prongs of all stars (curve *I*) are isotropic.

The evaporation prongs must be isotropically emitted in the center-of-mass system of the thermally evaporating nucleus. If all the momentum of the incoming proton is transferred to the Ag-Br nuclei, the velocity of the nucleus c.m. system would still be small (~5 percent) compared to the velocities corresponding to the characteristic energy (~10 Mev) of the evaporation prongs. However, when we consider that most of the momentum of the incoming proton is carried off by the forwardly collimated directly ejected prongs, the evaporation prongs from Ag-Br nuclei are expected to be isotropically emitted, also in the laboratory system.

Since at most 60 percent of the black prongs of all stars are isotropic, at least 40 percent have an origin other than that of the evaporation products of Ag-Br nuclei.

It has been previously concluded that the stars with 5 or more black prongs should be almost exclusively Ag-Br events. Curve II of Fig. 4 represents the angular distribution of black prongs based on stars with 5 or more black prongs. The maximum isotropic distribution is again found to be about 60 percent. Curve III is based on stars of six or more black prongs in order to assure even further that the light element stars are excluded. Although in this case the statistics are poorer, one still finds the value of 60 percent as the maximum isotropic contribution. Therefore it is clear that at least 40 percent of the black prongs of large Ag-Br stars have a knock-on origin. For the smaller stars, considering the percentage of prongs caused by the light elements, at least 25 percent[18] of the black prongs from Ag-Br stars are knock-ons.

III. NEUTRON-INDUCED NUCLEAR INTERACTIONS

A. Exposure

In order to study the high energy proton interactions in more detail it would be desirable to be able to

[18] It was previously shown that at most 20 percent of the stars are due to gelatin nuclei. Because the mean prong number of gelatin stars is about 3 (see reference 15) (probably because of their expected preference for dissociation into α-particles), no more than 20 percent of the black prongs observed in the emulsion stars originate in light nuclei. Therefore even the extreme assumption that all of these light nuclei black prongs are forwardly projected could only account for half of the observed forwardly projected black prongs. Hence, one concludes that at least 20 percent of the black prongs are knock-ons from Ag-Br nuclei. Since at most 60 percent of the black prongs could be due to

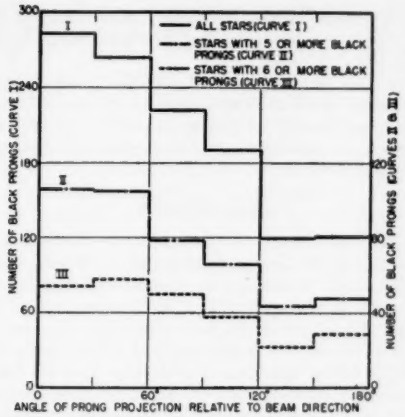
ALL STARS(CURVE I)
STARS WITH 5 OR MORE BLACK PRONGS (CURVE II)
STARS WITH 6 OR MORE BLACK PRONGS (CURVE III)
NUMBER OF BLACK PRONGS (CURVE I)
NUMBER OF BLACK PRONGS (CURVES II & III)
ANGLE OF PRONG PROJECTION RELATIVE TO BEAM DIRECTION

FIG. 4. Angular distribution of black prongs of stars induced by 350–400 Mev protons.

measure directly the characteristics of the emitted neutrons as well as those of the protons. This is obviously impossible with the photographic technique. However, there is a sort of mirror image symmetry predicted by the Goldberger model for the interactions of high energy protons and neutrons of similar energy with the emulsion. This is caused by the fact that there are approximately equal numbers of neutrons and protons (at most 5 neutrons to 4 protons) and it is generally assumed that $\sigma_{n-n} \approx \sigma_{p-p}$.[19] Hence it would be expected that the protons directly ejected as a result of neutron bombardment should be equivalent in all respects to the neutrons directly ejected under proton bombardment. And conversely, the protons directly ejected from proton-induced stars should be equivalent to the neutrons directly ejected in neutron-induced stars. Thus the results of the two experiments should be complimentary to each other in a very useful way.

In order to compare the properties of neutron-induced stars with the proton stars, 400 micron G5 plates were exposed to the Nevis high energy neutron beam. The neutron beam was sharply collimated to select only those neutrons directly ejected in the forward direction from a beryllium target bombarded by the proton beam at the maximum energy orbit, which corresponds to a proton energy of 385 Mev.

The energy spectrum of the neutrons was determined from CH_2 proton recoils with triple coincidence proportional counter telescopes by Goodell.[20]

evaporation of Ag-Br nuclei, it follows that at least 25 percent of the black prongs originating in Ag-Br have a knock-on origin.

[19] This assumption is essentially that of the charge independence of nuclear forces. Its approximate validity can be deduced from the neutron cross-section measurements described in footnotes 9–11.

[20] W. Goodell, Nevis Cyclotron Laboratory, quarterly report, June 15, 1951. The spectrum has a definite peak at about 300 Mev and the average energy is also ~300 Mev.

B. Neutron Star Characteristics

The plates were processed in the same way as the proton plates. The terminology used for the grouping of the proton star prongs will also be used for the neutron star data. In order to avoid confusion with Coulomb scatterings, only those two-prong stars which exhibited a difference in prong grain density were recorded. All three-prong or larger stars were clearly neutron-induced events and were recorded. There is the possibility of the inclusion of background stars induced by cosmic rays. The background because of cosmic-ray stars was estimated to be at most 2 percent of the observed stars, and was neglected.

In Fig. 5 the neutron star, black prong distribution is compared to the proton star distribution curve. The proton curve was normalized to correspond to the same total number of three or more black prong stars. The proton curve is shifted toward higher prong numbers. This is most likely a result of the fact that the average neutron energy (300 Mev) is less than the average proton energy (375 Mev). The magnitude of the shift, about 1–2 prongs, corresponds, as was previously discussed, to about 50–100 Mev. This is in agreement with the difference in the average proton and neutron energies.

In order to compare the numbers and distribution of stars with an outgoing fast (sparse black or gray) prong, the events not recorded in the neutron stars were deleted from the proton star data. Thus all proton stars with either one prong only or with only two black prongs were not considered for the comparison.[21] The remaining events which were observed in both cases are compared in Fig. 6. The proton curve is normalized to

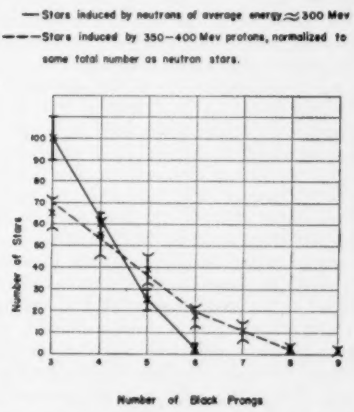
—Stars induced by neutrons of average energy ≈ 300 Mev
– – –Stars induced by 350–400 Mev protons, normalized to some total number as neutron stars.
Number of Stars
Number of Black Prongs

FIG. 5. Comparison of neutron and proton star black prong distributions.

[21] It has to be noted that they represent only about 10 percent of all proton stars.

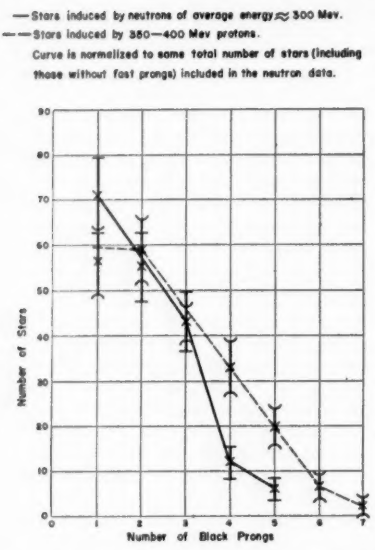
—Stars induced by neutrons of average energy≈ 300 Mev.
——Stars induced by 350—400 Mev protons.
Curve is normalized to some total number of stars (including those without fast prongs) included in the neutron data.
Number of Stars
Number of Black Prongs

FIG. 6. Comparison of distribution of neutron and proton stars with a fast prong.

correspond to the same number of stars as the neutron curve. The proton curve is again shifted toward higher prong numbers by 1–2 prongs.

Table IV compares characteristic data for proton and neutron stars. The mean numbers of black prongs are the same within statistical limits. Also, the mean numbers of fast (>30 Mev) protons agree within statistics. However, in the case of the neutron stars there are somewhat more sparse black than gray prongs, while the reverse is true for the protons. This could be attributed to the sensitivity of the number of gray (>100 Mev) prongs to the differences in bombarding energy and to the charge of the incoming nucleon.

A comparison of the distribution of events with fast prongs for the proton and neutron stars is made iy Table V. Within statistical limits there are practically no differences in the two distributions. The angular distributions of gray, sparse black, and black prongs from neutron and proton-induced stars are compared in Fig. 7(a), (b), and (c). The proton curves were normalized to the same area as that of the neutron curve. The frequency of occurrence of each type of prong for neutron and proton-induced events is given in Table IV. Here again the two distributions are about the same. The energy balance for the neutron events also indicated that about one-half the incoming energy was carried away by neutrons. This result is again similar to the proton star case. Hence we must finally conclude that except for the differences found in the star distribution curves which are attributable to the lower neutron energy, the many characteristics of the two types of interactions that have been examined are essentially the same.

In view of the previously discussed mirror image symmetry of the two experiments we can conclude that the characteristics of the neutrons emitted in both experiments are identical to those determined for the visible protons.

IV. DISCUSSION

The best evidence for the internal nucleonic cascade mechanism will be presented in Part II of this report, where it will be shown that the model calculations are in quantitative agreement with the experimental results. A brief account of these calculations has already been published.[22] However, many of the remarks previously made in various parts of the text provide a direct experimental basis for the interpretation of the so-called stars as mainly the result of an internal nucleonic cascade. It would be difficult to find a simpler explanation of the following facts:

(a) The correlation of the angular distribution of gray (>100 Mev), sparse black (30–100 Mev) and black[23] (<30 Mev) prongs with their respective energy ranges seems to be characteristic of the results of a few single nucleon-nucleon scatterings.

(b) The abundance of black knock-on prongs (at least 25–40 percent) implies a much longer mean free path in nuclear matter for these low energy nucleons than that corresponding to free scattering cross sections, and hence indicates the action of the Pauli exclusion principle which lengthens the mean free path of these low energy nucleons. The large percentage of these low energy knock-ons demonstrates that the usual interpretation of black prongs as mostly a result of the evaporation process is probably wrong.

(c) The steady transfer of energy from the fast nucleons to the black nucleons as star size increases and in particular the almost complete degradation of the energy into black prongs in the largest stars also indicates that the broadness of the distribution curves is determined by cascade fluctuations rather than by

TABLE IV. Comparison of neutron and proton star mean prong numbers.

Type of prong	Black	Sparse black	Gray	Fast (gray and sparse black)
Mean prong No. for proton stars	3.2±0.2	0.39±0.04	0.46±0.04	0.85±0.07
Mean prong No. for neutron stars	2.9±0.2	0.41±0.04	0.33±0.05	0.74±0.07

[22] Bernardini, Booth, and Lindenbaum, Phys. Rev. **83**, 669 (1951).

[23] Only the probable knock-on component is considered.

the fluctuations in the emission of visible prongs in an evaporation process.

(d) The agreement between the observed nuclear transparency for 350–400-Mev protons with the model prediction implies that at least for the first collision the calculated mean free path is correct.

(e) The similarity found for the fast directly-ejected prongs in the neutron and proton-induced interactions, and the implied similarity of the properties of directly ejected neutrons and protons in both types of events is understandable in the case of a cascade of single nucleon-nucleon collisions. The n-p cross section has been experimentally observed to be symmetrical around 90° in the center-of-mass system, and it is assumed that $\sigma_{n-n} \approx \sigma_{p-p}$. Furthermore, there are approximately equal numbers of neutrons and protons in the emulsion nuclei. Hence it is obvious from these symmetry conditions that the cascades of nucleons induced by protons and neutrons of equal energy would be identical in all respects provided that the ejected neutrons and protons are considered as nucleons only, without any distinction between the two. However, in the present experiments only the protons were detected and so in general one would expect an asymmetry between the protons ejected under proton and neutron bombardment. This asymmetry depends inversely upon both the ratio $\sigma_{n-p}/\sigma_{p-p}$ and the number of collision stages the cascade has gone through inside the nucleus. Using the experimentally determined cross sections it has been estimated that an average of 2–3 collision stages per event would reduce the asymmetry enough to explain the observed similarity of the neutron and proton interactions. This is about what one gets from the model calculations (to be given in Part II).

It has been tacitly assumed throughout the foregoing discussions that the sparse black and gray prongs are predominantly protons. The direct ejection of groups of nucleons such as deuterons and tritons has been recently extensively studied. The theory of these phenomena, or so-called pick-up processes, has been investigated in detail by Chew and Goldberger[24] and Heidmann.[25] A simple description of the theory can be given in the following terms: When a fast nucleon traverses the nucleus, it has a certain probability of passing close enough to a group of nucleons of proper space and momentum characteristics to form a stable aggregate such as a deuteron, triton, or alpha-particle. Then there is a corresponding probability for the aggregate to reach the edge of the nucleus undisturbed and escape. For 400-Mev protons this effect is calculated to be negligible.[25] However, the development of nucleonic cascades inside the target nuclei leads to secondary

TABLE V. Frequencies of stars *versus* number of their fast prongs.

Number of fast protons	Percentage of stars induced: By neutrons	By protons
0	30±4%	29±3%
1	63±5%	60±4%
2	7±2%	9±2%
3	0%	2±1%

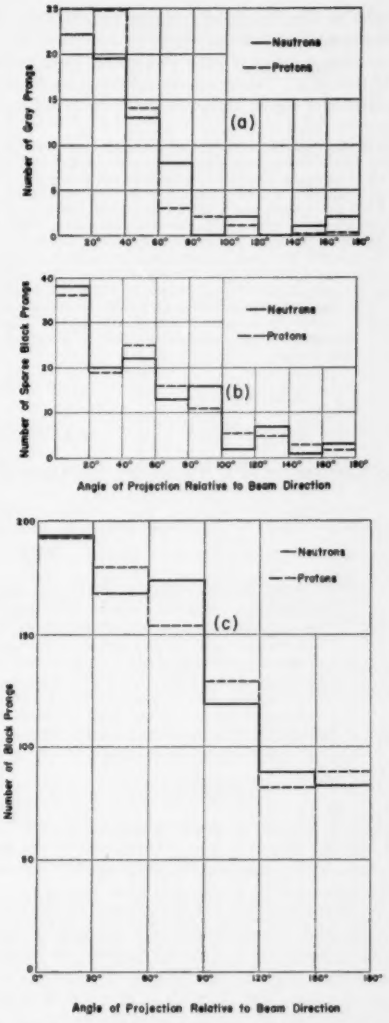

FIG. 7. (a) Comparison of neutron and proton gray prong angular distributions; (b) comparison of neutron and proton sparse black prong angular distributions; (c) comparison of neutron and proton black prong angular distributions.

[24] G. Chew and M. Goldberger, Phys. Rev. **77**, 470 (1950).
[25] J. Heidmann, Phys. Rev. **80**, 171 (1950).

nucleons in the low energy region (~100 Mev) for which these effects are not negligible.

The mean number of gray plus sparse black prongs is 0.77 (Table II). Taking into account relative numbers of gelatin and Ag-Br stars, we can roughly estimate[26] that at the most 6–8 percent of the gray or sparse black prongs could be pick-up deuterons and 1 percent could be pick-up tritons. These effects are small and do not affect any of the general conclusions reached treating all gray and sparse black prongs as protons.

[26] J. Hadley and H. York (see reference 4) have investigated deuterons and tritons ejected from carbon, copper, and lead nuclei by 90-Mev neutrons. The ratios of deuteron production cross sections to total inelastic cross sections were found to be 0.12 for carbon, 0.067 for copper, and 0.042 for lead. The cross section for tritons was found to be one-tenth that for deuterons and effectively zero for heavier particles. The assumption that these ratios are the same for the 400-Mev case is a reasonable upper limit. Therefore, one would expect that the mean number of pick-up deuterons and tritons per gelatin stars (using carbon value) would be at the most 0.12 and 0.01, respectively. In Ag-Br we would expect something intermediate between copper and lead or approximately 0.05 and 0.005 as the mean number of deuterons and tritons, respectively.

ACKNOWLEDGMENTS

The authors wish to thank Dr. Marietta Blau for several interesting discussions. We also thank Miss Elizabeth Wimmer for her invaluable assistance and cooperation in the photographic plate analysis. Mrs. Josephine Bielk generously aided and advised the authors on plate processing techniques. We also wish to thank the engineering staff of the Nevis Cyclotron Laboratories, in particular Mr. Julius Spiro and Mr. George Rosenbaum, for their help.

PHYSICAL REVIEW VOLUME 85, NUMBER 5 MARCH 1, 1952

The Formation of a Boundary between Normal-Conducting and Superconducting Metal*†

M. P. GARFUNKEL‡ AND B. SERIN
Physics Department, Rutgers University, New Brunswick, New Jersey

(Received November 6, 1951)

An experiment is described in which a superconducting sample is arranged so that part of it is in the normal state and part of it is superconducting. The boundary surface is thus a single, large area rather than the complicated boundaries that exist between normal and superconducting regions when a sample is in the intermediate state. We find that there is a large difference between the magnetic field at which the superconducting-normal state transition occurs and the magnetic field at which the normal-state-superconducting transition occurs. These results are in agreement with the thermodynamic theory of the phase transition. The thermodynamic theory, coupled with an assumption about the nature of the surface energy between superconducting and normal metal is used to show how the hysteresis determines the ratio of this surface energy to a characteristic dimension of the superconductor. A measure of this ratio is given in the temperature region between 3.37°K and 3.68°K for superconducting tin.

I. INTRODUCTION

BELOW the critical temperature, the normal state can be restored in a superconductor by the application of a sufficiently large magnetic field.[1] The nature of the transition to the normal state depends on the details of the geometry of the sample relative to the magnetic field. For the special case of a large diameter, infinite cylinder in a uniform, longitudinal magnetic field, the transition occurs abruptly at a definite value of the magnetic field. This value of the field is called the critical field H_c and for a given metal depends only on the temperature. (At the critical temperature T_c, the critical field H_c is zero.) For other geometries, such as an ellipsoid, or a cylinder in a transverse field, the conditions are somewhat different. The magnetic field is distorted around the edges of the superconductor and thus has greater values at some points on the surface than at others. The complications which arise when the sample does not have a zero demagnetization require the introduction of a new state—the intermediate state.[2] The intermediate state is not a pure state, but is a complicated structure of superconducting and normal domains.[3–5] The domains were observed by Meshkovsky and Shalnikov[5] to have diameters of about 0.1 cm.

Since all experiments to determine the critical field are carried out on finite cylinders, which have nonzero demagnetization, the transition from the superconducting to the normal state in a longitudinal field for such cylinders occurs with the formation of an intermediate state, usually at the ends of the cylinder. Since the intermediate state consists of small domains of superconducting and normal regions, the transition

* This work has been supported by the joint program of the ONR and AEC, the Rutgers University Research Council, and by the Radio Corporation of America.

† Based on the Ph.D. thesis submitted by M. P. Garfunkel to the Graduate Faculty of Rutgers University.

‡ Now at Westinghouse Research Laboratories, East Pittsburgh, Pennsylvania.

[1] H. Kammerlingh Onnes, Leiden Comm. **122b** (1911); Leiden Comm. **124c** (1911); Leiden Comm. Suppl. **35** (1913).

[2] C. J. Gorter and H. Casimir, Physica **1**, 305 (1934).

[3] L. Landau, Nature **141**, 688 (1938).

[4] A. Shalnikov, J. Phys. U.S.S.R. **9**, 202 (1945).

[5] A. Meshkovsky and A. Shalnikov, J. Phys. U.S.S.R. **11**, 1 (1947).

can take place by the growth of the final phase from an already established nucleus of that phase, and the corresponding displacement of a superconducting-normal boundary. Thus, the transition of a finite cylinder in a longitudinal magnetic field does not take place abruptly over the complete cylinder but grows from an established nucleus of the final phase.

The experiments of deHaas, Voogd, and Jonker,[6] Misener,[7] and more recently Desirant and Shoenberg[8] show that the creation of the intermediate state in a long cylinder in a transverse magnetic field requires more energy than is expected from the simple thermodynamic argument. It is assumed that the additional energy is required to create the surfaces between the normal and superconducting phases. Landau[3,9] has shown that the existence of the domain structure of the intermediate state depends on the surface energy between the normal and the superconducting phases. Andrew[10] has analyzed the transition of a long cylindrical conductor in a transverse field and explained the results of Desirant and Shoenberg,[8] who observed that the transition from the superconducting state to the intermediate state occurs at a slightly higher external magnetic field than is required to create the critical field at the surface of the cylinder. The aforenamed authors also observed a hysteresis in the transition; that is the field at which the transition from the superconducting state to the intermediate state takes place is greater than the field at which the reverse transition takes place.

In view of the complicated structure of the intermediate state, it is of interest to investigate the normal-superconducting transition with the creation of a single surface between the normal and superconducting metal, and with the growth of the final phase taking place without the benfit of a small domain of that phase to act as a nucleus. The experiment to be described has accomplished this by the application of a small, constant magnetic field h over a small central section of a long cylindrical sample, while the sample as a whole has been carried through the transition from the superconducting to the normal state by the application of an additional uniform longitudinal magnetic field H over the whole sample.

Neglecting the surface energy between phases, one would expect that when the sum of the two fields, H and h, reaches the critical field the central section would make a transition from the superconducting state to the normal state while the remainder of the sample would remain superconducting until the field H reached the critical value H_c, at which point the whole sample would pass into the normal state. On decreasing H, the transitions would be expected to occur at the same field values.[11]

The experiment to be described consisted of an investigation of the superconducting-normal transition in both increasing and decreasing magnetic field H, with several different values of the field h, and at several different temperatures as shown in Table I.

TABLE I. Hysteresis in transition field.

Temperature[a] (°K)	H_0 (oersteds)	h (oersteds)	V_s/V	Sample coil nos.[b]	Δh (oersteds)
3.681	6.9	2.77	0.25	2 and 3	1.3
3.681	6.9	2.77	0.25	2 and 3	0.9
3.681	6.9	5.54	0.25	2 and 3	0.6
3.679	7.5	2.16	0.125	3	1.3
3.679	7.5	2.70	0.25	2 and 3	1.2
3.675	7.9	1.35	0.125	2	1.2
3.675	8.0	1.35	0.125	1	1.2
3.675	8.0	1.35	0.125	3	1.2
3.675	8.1	1.35	0.125	4	1.3
3.675	8.2	2.70	0.125	1	1.9
3.659	10.5	1.62	0.25	2 and 3	1.5
3.659	10.1	2.70	0.25	1 and 2	1.8
3.649	12.0	2.70	0.125	2	2.4
3.649	12.0	2.70	0.125	3	2.4
3.647	12.0	5.40	0.125	2	1.8
3.647	11.9	5.54	0.25	2 and 3	1.6
3.608	14.6	2.77	0.25	2 and 3	1.2
3.608	16.4	2.77	0.25	2 and 3	1.0
3.608	16.6	2.82	0.625	1, 2, 3, 4, 5	1.0
3.605	18.0	5.54	0.25	2 and 3	1.6
3.566	23.8	5.54	0.25	2 and 3	1.7
3.541	27.5	2.07	0.25	2 and 3	1.8
3.541	27.5	8.31	0.25	2 and 3	1.3
3.372	51.3	2.77	0.25	2 and 3	1.9
3.372	51.3	13.75	0.25	2 and 3	1.2
3.372	51.3	27.7	0.25	2 and 3	1.3
3.372	51.3	27.7	0.25	2 and 3	1.5

[a] Temperatures were obtained from helium vapor pressure-temperature scale published by Royal Society Mond Laboratory, Cambridge, June, 1949, and are described by H. van Dijk and D. Shoenberg, Nature **164**, 151 (1949).
[b] The column labeled Sample coil nos. indicates which sections of the sample coils carried the current, and thus which section of the sample was in the field h.

II. EXPERIMENTAL DETAILS

(a) *Samples.*—The samples were prepared from Johnson-Matthey spectroscopically pure tin (99.998 percent Sn). They were cast in glass capillaries of diameter 0.15 cm and were 8.0 cm long. After the samples were grown into single crystals, five coils (each having a 1.0 cm length) were wound over the central five centimeters of each sample. These coils were used to supply the field h. They will be referred to as the sample coils.

(b) *Measurements.*—The transitions were observed by changes in the average susceptibility of the sample, which was deduced from measurements of the magnetic moment of the sample in a longitudinal field. The magnetic moment was measured by determining the change

[6] deHaas, Voogd, and Jonker, Physica **1**, 281 (1934).
[7] A. D. Misener, Proc. Roy. Soc. (London) **A166**, 43 (1938).
[8] M. Desirant and D. Shoenberg, Proc. Roy. Soc. (London) **A194**, 63 (1948).
[9] L. Landau, J. Phys. U.S.S.R. **7**, 99 (1943).
[10] E. R. Andrew, Proc. Roy. Soc. (London) **A194**, 98 (1948).
[11] In this case, since we are neglecting surface energy, there would be no Meissner effect, as is pointed out by F. London, *Superfluids* (John Wiley and Sons, Inc., New York, 1950), Vol. I, Sec. 21.

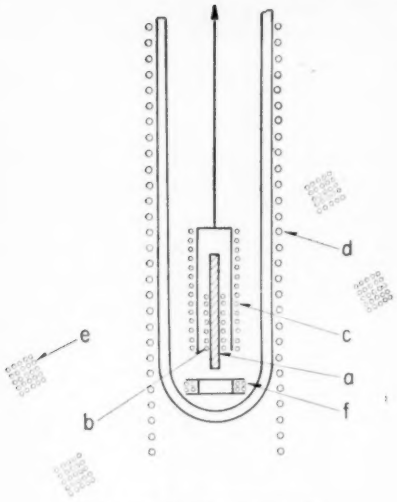

FIG. 1. Experimental arrangement.

in flux through a pick-up coil, as the pick-up coil was moved from a position enclosing the sample to a position not enclosing the sample.[12] The change in flux was measured with a ballistic galvanometer.

The general arrangement is shown in Fig. 1. A sample *a* was mounted inside a helium Dewar with the sample coils *b*. The pick-up coil *c* was arranged so that it could slide over the sample. Around the helium Dewar was a long solenoid *d* to supply the field H. Surrounding the whole apparatus was a large pair of Helmholtz coils *e* which was used to cancel the earth's magnetic field over the region of the sample. A heater *f* was placed in the bottom of the helium Dewar insuring thermal equilibrium throughout the liquid helium bath.

The data were taken by determining the magnetic moment of the sample at constant temperature (as given in Table I), and at various values of the magnetic field H. Care was taken to determine any hysteresis by changing the field H in one direction only. This was done at several values of the temperature, and for several values of the field h, applied over different central sections of the sample from 1 to 5 cm in length. The temperature was maintained constant by monitoring the vapor pressure over the helium bath, to within 0.2 mm of Hg. The pressure was measured with a mercury manometer.

III. EXPERIMENTAL RESULTS

The data observed in the manner described in Sec. II are shown plotted in Figs. 2 and 3. All the curves have sample-susceptibility as ordinate and the magnetic field H as abscissa. From these figures, with the exception of 3(*b*) and 3(*c*), it is clear that the sample is not always in the same state at a given value of the field H, but that it can exist in two different states, corresponding to greatly different susceptibilities, over a large range of values of the field H.

Figure 2(*a*) shows the transition for the field h equal to zero and is the usual type of transition curve in a longitudinal magnetic field. The transition is very sharp, going from the superconducting state to the normal state in about 0.2 oersted. There is no hysteresis in this transition, the points for decreasing field following the curve for increasing field.§ The critical field, H_0, as can be seen from this figure, is 11.8 oersteds.

Figure 2(*b*) is plotted from data taken at the same temperature but with the sample field h equal to 5.40 oersteds, over a one centimeter length of the sample. It is to be noted that between 6.6 oersteds and 9.0 oersteds the whole sample remains superconducting, in increasing field, even though the field on a one centimeter section exceeds the critical field at that temperature by as much as 2.4 oersteds. At 9.0 oersteds a transition is made to a mixed state, where the section inside the sample coil goes into the normal state and the remainder of the sample stays superconducting. Since the coil producing the field h covers about 25 percent of the part of the sample covered by the pick-up coil, we note that the susceptibility value of about 0.75 $(-1/4\pi)$ corresponds to the value expected for the mixed state. As the field H approaches the critical field the susceptibility increases to zero corresponding to the whole sample being in the normal state. On decreasing the field H, the transition to the mixed state occurs when H equals the critical field just as in the increasing field case. The transition from the mixed state to the superconducting state, however, does not occur until the field on the section in the sample coil drops to the critical field, corresponding to $H=H_0-h$.

Figures 2(*c*) and 2(*d*) show the same form as 2(*b*), but in the cases represented, the field h is 2.70 oersteds causing the transitions to the mixed state to occur at higher values of the field H, but at the same values of the total field on the section in the sample coil. The data plotted in Figs. 2(*c*) and 2(*d*) were taken on different sections of the sample, to check on the possibility of the effect being caused by a characteristic of a particular section. No effect was found. Other sections of the sample were also used with the same negative result.

Figure 3(*a*) is a curve plotted with data obtained with the field h over a 2.0 centimeter length of the sample. It is to be noted that the mixed state has a susceptibility corresponding to a normal region of twice the size of the mixed state shown in Figs. 2(*b*), 2(*c*), and 2(*d*) with

[12] The essential features of this method are described by D. Shoenberg, Proc. Roy. Soc. (London) **A175**, 49 (1940).

§ *Note added in proof.*—Mr. W. H. Wright has recently conducted experiments using the same sample. He has found that if the magnetic field is brought to several times the critical value and allowed to remain there for a sufficient time, the subsequent decreasing field magnetization curve shows supercooling. This is in agreement with the thermodynamic arguments.

the 1.0 centimeter coil, in agreement with our model of the mixed state. The other characteristics of the curve are the same as those in Figs. 2(*b*), 2(*c*), and 2(*d*) except that the temperature is slightly lower, and thus the critical field slightly greater.

The data shown in the curves of Figs. 3(*b*) and 3(*c*) were obtained under somewhat different conditions. The full 5.0 centimeter length of the sample solenoid was used and the field h was in the opposite direction to the field H. This arrangement is equivalent to having the sample coils on the ends of the sample. Thus, for these two cases the normal region could grow out from the ends where there was an intermediate state, and therefore, a nucleus of the normal state at fields well below the critical field. The transitions in Figs. 3(*b*) and 3(*c*) from the superconducting state to the mixed state occur just at the point where the field on the end sections reaches the critical field in both increasing and decreasing field h, thus differing markedly from the results obtained with the sample coil at the center. Although there is no hysteresis in the value of the field H at which the transitions occur, there is a large hysteresis in the value of the susceptibility for increasing and decreasing field. In the case of decreasing field, when the transition from the normal state to the mixed state occurs, there must be formed in some region of the sample an intermediate state, thereby giving the observed smaller value of the susceptibility in decreasing field than in increasing field. This intermediate state region remains even after the section on the ends goes into the superconducting state. Data were not taken for lower field values to determine where the intermediate state disappeared and whether it disappeared discontinuously. At very small values of the field, however, the sample was completely superconducting and no frozen-in magnetic moment was observed.

Figure 3(*d*) shows part of a curve plotted from data taken when the sample was mechanically shocked at each value of the field H. The jarring made no essential difference in the characteristics of the curves.

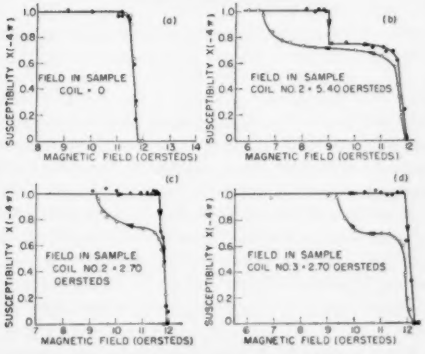

FIG. 2. Experimental curves of susceptibility *versus* magnetic field H.

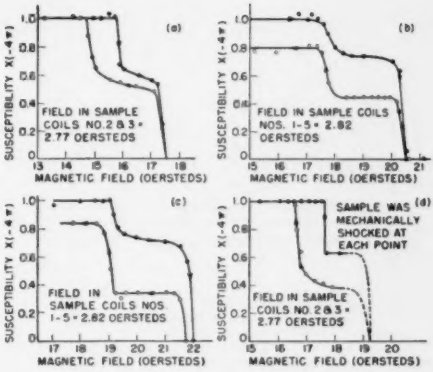
(a)
FIELD IN SAMPLE COILS NO.2 & 3 = 2.77 OERSTEDS
(b)
FIELD IN SAMPLE COILS NOS. 1-5 = 2.82 OERSTEDS
(c)
FIELD IN SAMPLE COILS NOS. 1-5 = 2.82 OERSTEDS
(d)
SAMPLE WAS MECHANICALLY SHOCKED AT EACH POINT
FIELD IN SAMPLE COILS NO. 2 & 3 = 2.77 OERSTEDS
SUSCEPTIBILITY X(-4π)
MAGNETIC FIELD (OERSTEDS)

FIG. 3. Experimental curves of susceptibility *versus* magnetic field H.

We call the difference in the values of the field H, at which the superconducting-mixed-state transition occurs in increasing and decreasing magnetic field, the width of the hysteresis Δh. Table I shows the values of Δh obtained under various experimental conditions. We note that Δh is essentially constant and is apparently independent of the temperature, the dimensions of the sample coil, and the value of the field h. There may be a small change in Δh with temperature, but the scatter in the values is so large that any small changes are not detectable. It should be noted that in all of the figures, except Figs. 3(*b*) and 3(*c*), the transition from the superconducting state to the mixed state in increasing field H is discontinuous; while the transition in the opposite direction, while sharp, is not discontinuous.

IV. DISCUSSION

A. Thermodynamic Theory of the Superconducting-Normal State Transition

We shall follow the thermodynamic theory of the superconducting-normal state transition developed by Gorter and Casimir.[2] The most stable phase of any system at constant temperature and magnetic field,[13] is that phase which has the minimum value of the Gibbs free energy. London[11] gives for the Gibbs free energy per unit volume of the normal phase g_n and the superconducting phase g_s of an infinite cylinder of large radius in a longitudinal field H,

$$8\pi g_s = 0, \quad 8\pi g_n = H_c^2 - H^2. \tag{1}$$

We omit the same term in each expression which depends on temperature only. These latter terms are not sig-

[13] The thermodynamic variables considered here are magnetic field, temperature, and magnetization per unit volume.

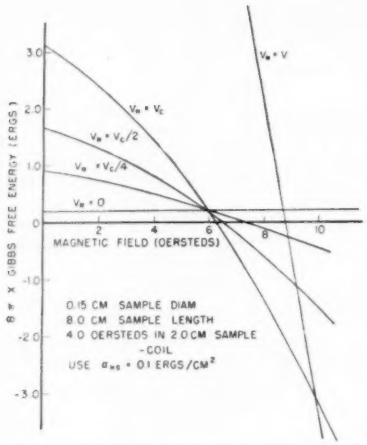

FIG. 4. Gibbs free energy of the mixed state *versus* magnetic field for various volumes in the normal state.

nificant because we are interested only in differences between g_n and g_s. H_c is the critical field at any given temperature, and H is the applied field.

We apply these equations to the case of interest and consider a finite cylinder of volume V and surface S in a uniform longitudinal field H with an additional uniform field h on a central section having a volume V_c and a surface S_c. We obtain for the total Gibbs free energies

$$8\pi G_s = 8\pi\alpha_s S,$$
$$8\pi G_n = [H_c^2-(H+h)^2]V_c+(H_c^2-H^2)(V-V_c)+8\pi\alpha_n S,$$

where α_s and α_n are the surface energy densities at a superconducting-insulator boundary and a normal conductor-insulator boundary, respectively. We must now consider a third possible phase—the mixed phase. This phase is not to be confused with the intermediate state which is sometimes called the mixture state, but rather refers to that configuration where the volume V_s is normal, and the remainder of the cylinder is superconducting. The Gibbs free energy for this mixed phase is given by

$$8\pi G_m = [H_c^2-(H+h)^2]V_c+8\pi\alpha_n S_c + 8\pi\alpha_s(S-S_c)+8\pi\alpha_{ns}A_{ns},$$

where α_{ns} is the surface energy density on a superconducting-normal surface, and A_{ns} is the total area between normal and superconducting material.

It is convenient to select the zero of Gibbs free energy as the free energy of the superconducting phase. This is done by subtracting $\alpha_s S$ from each of the three free energies. The expressions become

$$8\pi G_s = 0,$$
$$8\pi G_n = [H_c^2-(H+h)^2]V_c + (H_c^2-H^2)(V-V_c)-8\pi(\alpha_s-\alpha_n)S,$$
$$8\pi G_m = [H_c^2-(H+h)^2]V_c+8\pi\alpha_{ns}A_{ns}-8\pi(\alpha_s-\alpha_n)S_c.$$

If H_0 is the value of H at which the transition from superconducting to normal phase occurs for $h=0$, then

$$H_0^2 V = H_c^2 V - 8\pi(\alpha_s-\alpha_n)S,$$
$$H_0^2 V_c = H_c^2 V_c - 8\pi(\alpha_s-\alpha_n)S_c,$$

where we assume that the area of the ends of the sample are small compared to the total area.

Thus, we have

$$8\pi G_s = 0,$$
$$8\pi G_n = [H_0^2-(H+h)^2]V_c+(H_0^2-H^2)(V-V_c), \quad (2)$$
$$8\pi G_m = [H_0^2-(H+h)^2]V_c+8\pi\alpha_{ns}A_{ns}.$$

The most stable phase at any value of the magnetic field can now be determined by observing which of Eqs. (2) has the smallest value. Clearly any other mixed phase that can be formulated will have a larger free energy, at any value of the magnetic field H, than at least one of the three phases assumed.

The theory outlined above is the usual thermodynamic theory. We see that this theory predicts that the superconducting-mixed-state transition will occur at a value of the field H slightly greater than H_0-h, and that the transition will occur at the same value of the field H in both increasing and decreasing magnetic field. The experimental results given in Sec. III are in contradiction to these conclusions.

B. Mechanism of the Superconducting-Normal-State Transition

The experimental results force us to appreciate that it is not sufficient to know only the most stable phase at any given magnetic field. It is also necessary to consider the mechanism by which a transition is made from one phase to a second phase. We can expect the transition to occur only if the system can go from one phase to the other phase without increasing its free energy anywhere on the path.

If we consider the transition that takes place in going from the superconducting phase to the mixed phase, we see that this must occur by the growth of a small normal region out to the volume V_c. Thus we must consider the Gibbs free energy everywhere along this path.

For a volume V_n in the normal state, we see from the third of Eqs. (2) that the free energy of the mixed

state G_m is given by

$$8\pi G_m=\begin{cases}[H_0^2-(H+h)^2]V_n+8\pi\alpha_{ns}A_{ns}, & V_n\lesssim V_c\\ [H_0^2-(H+h)^2]V_c+(H_0^2-H^2)(V_n-V_c) & \\ \qquad +8\pi\alpha_{ns}A_{ns}, & V_n\gtrsim V_c.\end{cases} \quad (3)$$

As long as the normal volume extends over a region of the sample that is long compared to the diameter of the sample, the area A_{ns} remains constant. However, when V_n gets very small the shape of the normal region will take a shape which will reduce the surface energy to as small a value as possible while still keeping the energy stored in the magnetic field small. This shape will be assumed to be approximately a hemisphere with a flat surface on the surface of the cylinder.

Figure 4 is a plot of the Gibbs free energy as a function of the magnetic field H, for various values of the normal volume V_n. For simplicity, A_{ns} is taken as constant and equal to the area of a sphere with the same diameter as the sample. The surface energy density used is the value 0.1 erg per square centimeter as determined by the thin measurements of Pontius.[14] This value is not reliable for this purpose, but it serves to illustrate the argument. The curves show that even above that field at which G_m is less than G_s for $V_n=V_s$ there are curves of $G_m>G_s$ for smaller values of V_n. Thus, the path that must be taken in going from the superconducting state to the mixed state requires an increase in the free energy.

The argument aforementioned is somewhat oversimplified. We have considered that the surface energy appears on a mathematical surface. This is not actually the case, as can be realized from the consideration of the usual penetration depth, which indicates a transition region between normal and superconducting regions. If we now ascribe a characteristic length R_0 to this transition region, then for all regions V_n having a radius smaller than R_0, the "surface" energy is distributed over the whole volume of the region and is no longer to be considered a surface energy but must be considered a volume energy.

We can now rewrite the first of Eqs. (3) for regions V_n small compared to R_0^3. The shape of the regions is assumed to be hemispherical. We have

$$8\pi G_m=[H_0^2-(H+h)^2]V_n+24\pi V_n\alpha_{ns}/R_0, \qquad V_n<R_0^3. \quad (4)$$

Figure 5 is a plot of the free energy *versus* the volume in the normal state, using Eqs. (3) for large V_n and Eq. (4) for small V_n. The shape of the boundary is taken to be constant for large V_n, changing to a hemisphere when the volume V_n becomes the order of magnitude of the cube of the radius of the sample.

C. Analysis of Experimental Results

We now discuss our experimental observations in terms of the theory preceding.

[14] Pontius, Phil. Mag. **24**, 787 (1937).

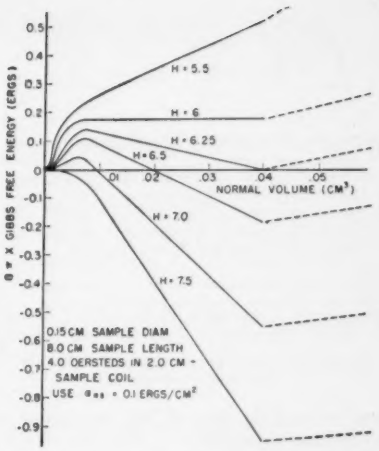

FIG. 5. Gibbs free energy of the mixed state *versus* volume in the normal state for various values of the magnetic field.

The transition from the superconducting state to the mixed state cannot occur when the mixed state has the same free energy as the superconducting state if there is a surface energy, since the path from the superconducting state to the mixed state requires an increase in the free energy. The transition cannot occur until the field H is so large that the free energy decreases everywhere along the path. Thus, the observed hysteresis is expected. This value of field, H_1, can be found by setting $dG_m/dV_n=0$ at $V_n=0$. This yields $(H_1+h)^2-H_0^2=24\pi\alpha_{ns}/R_0$, or, since $H_1+h=H_0+\Delta h$,

$$2H_0(\Delta h)+(\Delta h)^2=24\pi\alpha_{ns}/R_0.$$

In the approximation $\Delta h\ll H_0$,

$$H_0(\Delta h)=12\pi\alpha_{ns}/R_0. \quad (5)$$

The values of H_0 and H_1 can be found accurately experimentally since H_0 is the transition field when h is equal to zero [Fig. 2(*a*)], and H_1 is the field at which the transition from the superconducting to the mixed state takes place. The former is quite sharp, occurring in a region of less than 0.2 oersted, and the latter is discontinuous. However, the spread in the values from experiment to experiment indicates that there are other factors which may critically effect Δh. The most important factor may be the magnitude of the transverse component of field in the region of the sample. This is determined by the percentage cancellation of the earths field and by the alignment of sample in the field H. These two factors may easily have given a variation of from 0.1 to 0.2 oersted in the transverse component of field from one experiment to the next. In addition small temperature drifts between the time H_0 was

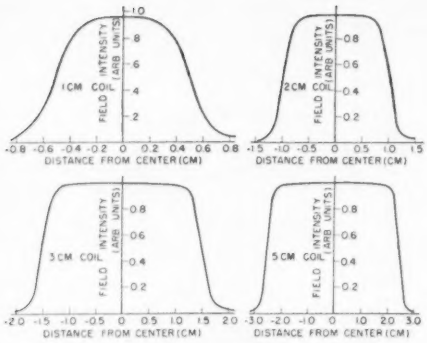

FIG. 6. Field intensity as a function of distance from the center of the sample coil.

determined and the time H_1 was determined would cause the observed scatter.

From Fig. 5 we see the reason for the fact that the transition from the superconducting state ot the mixed state is discontinuous. Consider the transition occuring for H equal to 7.5 oersteds. At this value of field the free energy of the mixed state is considerably smaller than the free energy of the superconducting state, and the slope of the free energy *versus* normal volume curve is very steep as soon as V_n is slightly greater than zero. We therefore expect a discontinuous transition from the superconducting state to the mixed state, since as soon as a small volume becomes normal the transition proceeds rapidly, decreasing free energy all along the path. If we now consider the transition from the mixed state to the superconducting state in decreasing field H, we see that the transition cannot occur when the free energy of the two states are equal since the path requires an increase in the free energy. In this case, the transition cannot occur until the field $H=H_2$ is so small that the free energy decreases everywhere on the path or for $dG_m/dV_n=0$, for $V_n=V_c$. This yields

$$H_2+h=H_0, \tag{6}$$

since for large V_n, A_{ns} is a constant. We have always observed the reverse transition to occur at precisely this field value.

The reason that the transition is not discontinuous in this last case is not apparent from this analysis. We note, however, that we have been assuming that the field h is constant over the region V_c. This is not quite correct as may be seen from Fig. 6, in which appear the magnetic field distributions for various sample-coil lengths. The field h has a maximum value at the center and decreases very slowly until it reaches the width of the sample coil, at which point there is a sharp decrease in field. The small nonuniformity over the center section slightly modifies the family of curves plotted in Fig. 5, causing the straight portion of each of them to become concave upwards. As a result, the relative minima which occur in Fig. 5 at V_n equal to V_c do not occur at exactly that value, but move to smaller values of V_n as the field H is decreased. In the neighborhood of $H=H_2$ the relative minimum moves rapidly to smaller values of V_n until the minimum disappears completely at $H=H_2$. This discussion does not appreciably affect the transition in increasing field since the free energy curve is very steep at the field H_1.

Equation (5), taken with the result that Δh is essentially constant over the range of temperatures considered, indicates that α_{ns}/R_0 varies approximately as H_0, or approximately as the critical field. At $H_0=30$ oersteds, $\alpha_{ns}/R_0\sim 1$ erg/cm^3. If we now relate the dimension R_0 to the region of long-range order suggested by Pippard[15,16] and Bardeen,[17] we find that $\alpha_{ns}\sim 10^{-4}$ ergs/cm^2 at $H_0=30$ gauss and for $R_0\sim 10^{-4}$ cm. And if R_0 is assumed to remain approximately constant, then the surface energy varies approximately as the critical field.

In conclusion, we review some implications of this experiment. There seems to be ambiguity in the usual definition of the critical field. This experiment gives reason to believe that in the ideal case of an infinite cylinder, there will be two different transitions, one in increasing field and one in decreasing field, neither occuring at the value of field where the two phases are in equilibrium. This ambiguity can readily be removed by the usual expedient of using long but finite cylinders. In addition the experiment implies that there is a maximum amount of supercooling or superheating that can be attained in a superconductor and that this can be determined from the ratio α_{ns}/R_0. We might expect that the velocity at which superconductivity (or normal conductivity) is propagated from the point of nucleation is related to the gradient of the Gibbs function, and thus to the degree of supercooling (or superheating), as has been shown by Faber.[18]

We are very grateful to Dr. C. A. Reynolds and Dr. P. R. Weiss for many valuable discussions during the course of this experiment. We also acknowledge the assistance of Mr. J. Teza, Mr. L. B. Nesbitt, and Mr. R. Campbell for their helpful advice regarding the construction of the apparatus; and finally we thank Mr. W. H. Wright, Mr. J. Gittleman, and Mr. C. Lohman for their help in the conduction of the experiments.

[15] A. B. Pippard, Proc. Roy. Soc. (London) **A203**, 210 (1950).
[16] A. B. Pippard, Proc. Cambridge Phil. Soc. **47**, 617 (1951).
[17] J. Bardeen, Phys. Rev. **81**, 1070 (1951).
[18] T. E. Faber, Nature **164**, 277 (1949).

Electromagnetic Properties of Spin-One Particles

DANIEL LEENOV
Department of Physics, University of Chicago, Chicago, Illinois
(Received November 13, 1951)

In this paper an analysis of the electromagnetic properties of a charged particle with spin 1 is made from two standpoints. Part I contains a phenomenological treatment, in which the methods of field theory are used to investigate scattering processes involving a particle with spin 1 and magnetic moment $1-\gamma$ magnetons, where γ is arbitrary. A calculation of the scattering cross section for unpolarized particles is obtained, differing from the result of Laporte (see reference 4) through the presence of the terms containing γ. Using this formula for the cross section, it is shown that studies of the multiple scattering of high energy particles of this type will give a small but perhaps measurable indication of their spin and magnetic moment. Also, this theory shows that low energy vector particles are not significantly depolarized when passing through matter, considering only electromagnetic effects.

The μ-pair theory has been used by Wentzel (see reference 7) as a description of the π-meson in order to predict certain of its properties. In Part II this theory has been generalized to the case of a vector particle made up of a spinor pair, and descriptions are given of the computation of the magnetic dipole moment and the electric quadrupole moment, as well as the cross sections for scattering and for dissociation because of interaction with a Coulomb field, here including the case of a pseudoscalar π-meson. These results, it must be noted, cannot be considered quantitative, owing to the cut-off method used; however, they may give useful qualitative information.

I. PHENOMENOLOGICAL THEORY

WHEN investigating interactions of a spin 1 particle with the electromagnetic field, using the methods of field theory, one usually starts with the following expression for the Lagrangian density[1,2]

$$L=-\tfrac{1}{2}\sum_{\mu\nu}(\partial_\mu^*\psi_\nu^*-\partial_\nu^*\psi_\mu^*)(\partial_\mu\psi_\nu-\partial_\nu\psi_\mu) -m^2\sum_\nu\psi_\nu^*\psi_\nu,$$

where

$$\partial_\nu\equiv\partial/\partial x_\nu-ie\phi_\nu;\quad \partial_\nu^*\equiv\partial/\partial x_\nu+ie\phi_\nu. \tag{1.1}$$

Here ϕ_ν represents a given Maxwell field. The magnetic moment computed from this Lagrangian would be one magneton. In order to investigate the properties of a spin 1 particle with arbitrary magnetic moment, one adds an additional term, namely[3]

$$\tfrac{1}{2}\gamma ieF_{\mu\nu}(\psi_\mu^*\psi_\nu-\psi_\nu^*\psi_\mu)$$

where

$$F_{\mu\nu}=\partial\phi_\nu/\partial x_\mu-\partial\phi_\mu/\partial x_\nu, \tag{1.2}$$

which corresponds to a particle having a magnetic moment of $1-\gamma$ magnetons. Using standard methods,[1] one may obtain the Hamiltonian density, which contains, in addition to the zero-order terms present when there is no electromagnetic field, terms of first order in the vector potential. In the case which is of interest here, namely in the presence of a static electric potential ϕ_0, the interaction part of the Hamiltonian density is given by

$$ie\phi_0(\pi_i^*\psi_i^*-\pi_i\psi_i)+ie\gamma F_{4\mu}(\psi_4\psi_\mu^*-\psi_4^*\psi_\mu). \tag{1.3}$$

This may be converted into the momentum space representation by expanding the space functions Ψ, Π and ϕ_0 into Fourier series as follows,

$$\Psi=V^{-\frac{1}{2}}\textstyle\sum_{\mathbf{k}}\mathbf{q}_{\mathbf{k}}e^{i\mathbf{k}\cdot\mathbf{x}};\quad \Pi=V^{-\frac{1}{2}}\sum_{\mathbf{k}}\mathbf{p}_{\mathbf{k}}e^{-i\mathbf{k}\cdot\mathbf{x}};\quad \phi_0=\textstyle\sum_{\mathbf{k}}A_{\mathbf{k}}{}^0e^{i\mathbf{k}\cdot\mathbf{x}} \tag{1.4}$$

where V is the periodicity volume over which these expansions are carried out. Integration over coordinate space gives for the interaction part of the Hamiltonian the following,

$$H'=ie\textstyle\sum_{\mathbf{k}}\sum_{\mathbf{k}'}A_{\mathbf{k}'-\mathbf{k}}{}^0[\mathbf{p}_{\mathbf{k}}^*\cdot\mathbf{q}_{\mathbf{k}'}^*-\mathbf{p}_{\mathbf{k}'}\cdot\mathbf{q}_{\mathbf{k}} -\gamma m^{-2}(\mathbf{k}'-\mathbf{k})\cdot(\mathbf{k}\cdot\mathbf{p}_{\mathbf{k}}^*\mathbf{q}_{\mathbf{k}'}^*+\mathbf{k}'\cdot\mathbf{p}_{\mathbf{k}'}\mathbf{q}_{\mathbf{k}})]. \tag{1.5}$$

The longitudinal and transverse components of $\mathbf{q}_{\mathbf{k}}$, $\mathbf{p}_{\mathbf{k}}$, $\mathbf{q}_{\mathbf{k}}^*$, and $\mathbf{p}_{\mathbf{k}}^*$ are now to be expressed in terms of the corresponding absorption and emission operators $a_{\mathbf{k}}^{(l)}$, $a_{\mathbf{k}}^{(l)*}$, $a_{\mathbf{k}}^{(r)}$, $a_{\mathbf{k}}^{(r)*}$ where (l) refers to longitudinal, and (r) to transverse components. The details may be found in references.[1] In terms of these operators, H' takes the form,

$$H'=e\sum_{\mathbf{k},\mathbf{k}'}\sum_{r,r'}A_{\mathbf{k}'-\mathbf{k}}{}^0[\mathbf{e}_{\mathbf{k}}{}^r\cdot\mathbf{e}_{\mathbf{k}'}{}^{r'}\zeta_{\mathbf{k},\mathbf{k}'}{}^{r,r'}a_{\mathbf{k}'}{}^{r'*}a_{\mathbf{k}}{}^r +(\gamma/2m^2)(\mathbf{k}'-\mathbf{k})\cdot(-\mathbf{k}\cdot\mathbf{e}_{\mathbf{k}}{}^r a_{\mathbf{k}}{}^r\mathbf{e}_{\mathbf{k}'}{}^{r'}a_{\mathbf{k}'}{}^{r'*} +\mathbf{k}'\cdot\mathbf{e}_{\mathbf{k}'}{}^{r'}a_{\mathbf{k}'}{}^{r'*}\mathbf{e}_{\mathbf{k}}{}^r a_{\mathbf{k}}{}^r)];\quad r,r'=1,2,3. \tag{1.6}$$

Here

$$\zeta^{r,r}=\zeta^{2,3}=\zeta^{3,2}=1;$$

$$\zeta^{1,2}=\zeta^{2,1}=\zeta^{1,3}=\zeta^{3,1}=[(k^4/4\omega^2m^2)+1]^{\frac{1}{2}}\quad\text{for}\quad|\mathbf{k}'|=|\mathbf{k}|,$$

where

$$\omega=(k^2+m^2)^{\frac{1}{2}}.$$

This expression may be used to compute matrix elements for transitions between any two states of polarization of the particle when it is scattered by the electric field given by ϕ_0. From the matrix element the cross section for the given scattering process is obtained in the first Born approximation. It is of interest, in particular, to obtain the cross section for Coulomb

[1] G. Wentzel, *Quantum Theory of Fields* (Interscience Publishers, Inc., New York, 1949), Chapter III.
[2] The system of units to be used throughout is that in which $\hbar=c=1$.
[3] H. C. Corben and J. Schwinger, Phys. Rev. **58**, 953 (1940).

scattering of unpolarized particles, in which case $|H'|^2$ is averaged over initial states and summed over final states. The desired expression is

$$|H'|^2=\tfrac{1}{2}\sum_{r,r'}|H'(a_{\mathbf{k}'r'},a_{\mathbf{k}r})|^2.$$

For this purpose it is convenient to choose the basis vector $\mathbf{e}_2$ to be in the plane of scattering, and $\mathbf{e}_3$ perpendicular to this plane. Let θ be the scattering angle, given by

$$\cos\theta=\mathbf{k}'\cdot\mathbf{k}/k^2.$$

One then obtains for the cross section, per unit solid angle,

$$\sigma_{sc}=\left[1+\frac{k^4}{6\omega^2m^2}\sin^2\theta+\frac{2}{3}\gamma\frac{k^2}{m^2}\right]\left\{\left(1+\frac{k^4}{4\omega^2m^2}\right)^{\frac{1}{2}}\frac{m}{\omega}-\sin^2\theta-\cos\theta(1-\cos\theta)\right\}+\gamma^2\frac{k^4}{3m^4}\left\{(1-\cos\theta)^2+\frac{m^2}{2\omega^2}\sin^2\theta\right\}\left[\frac{Z^2e^4}{4k^2v^2}\frac{1}{\sin^4\frac{1}{2}\theta}.\quad(1.7)\right.$$

This expression differs from the result previously obtained,[4] owing to the presence of terms containing γ. It is seen that all terms inside the square brackets, other than the first, contain functions of θ; it would be of interest to see if these terms, and in particular those containing γ, produce an effect which might be detected by some experiment, such as the observation of multiple scattering. It would then be possible to test the validity of (1.7), as well as obtain an indication of the spin and magnetic moment of the particle.

Since the angular dependent terms of (1.7) all contain powers of the quantity k/m as factors, it is to be expected that the effect of these terms will be most pronounced at high energies. Writing (1.7) in the limiting case of relativistic energies, one obtains

$$\sigma_{sc}\cong\frac{Z^2e^4}{4k^2v^2}\frac{1}{\sin^4\frac{1}{2}\theta}\left[1+\frac{k^2}{6m^2}\sin^2\theta+\frac{1}{3}\gamma\frac{k^2}{m^2}(1-\cos\theta)^2+\frac{\gamma^2}{3}\left\{\frac{k^4}{m^4}(1-\cos\theta)^2+\frac{k^2}{2m^2}\sin^2\theta\right\}\right].\quad k/m\gg1.\quad(1.8)$$

The magnitude of multiple scattering will be determined by the quantity $\int\sin^2\theta\sigma_{sc}d\Omega$, where σ_{sc} is given by (1.8). However, the evaluation of this integral is subject to the following considerations. Owing to the screening effect of the electrons in the atoms of the scattering material, σ_{sc} does not increase indefinitely as θ approaches zero; rather, it approaches a finite value; this effect may be taken into account by changing the lower limit of the integration over θ from zero to a minimum angle θ_0 given $\theta_0=1/kr_a$, where r_a is an average atomic radius. Similarly, owing to the finite extension of the nucleus, there is a maximum scattering angle θ_1 given by $\theta_1=1/kr_n$, where r_n is the nuclear radius. Using these as the limits of the integration over scattering angles, one finds

$$\int\theta^2\sigma_{sc}(\theta)d\Omega\cong8\pi(1-v^2)\left(\frac{Ze^2}{mv^2}\right)^2\left[\log\frac{\theta_1}{\theta_0}+\frac{k^2}{12m^2}\theta_1^2+\frac{\gamma^2}{3}\left(\frac{k^4}{16m^4}\theta_1^4+\frac{k^2}{4m^2}\theta_1^2\right)\right].\quad(1.9)$$

This may be compared with the corresponding expression for spin 0 particles,

$$\int\theta^2\sigma_{sc}(\theta)d\Omega=8\pi(1-v^2)(Ze^2/mv^2)^2\log(\theta_1/\theta_0).\quad(1.9')$$

The ratio of (1.9) to (1.9′), upon inserting numerical values (taking $r_a=2.1\times10^{-9}$ cm, $r_n=4.8\times10^{-13}$ cm for oxygen as a particular case), becomes, for $m\cong300$ electron masses

$$1+5\times10^{-4}(1+\gamma^2).\quad(1.10)$$

Unless $\gamma^2\gg1$, this ratio is very close to unity. Nevertheless, the small terms in (1.10) may have some relevance for accurate mass determinations based on multiple scattering measurements.

Another question of interest is the depolarization of low energy (nonrelativistic) vector particles traveling through matter. Such a result is useful in the case that the state of polarization of the particle is to be determined, and it must travel through a certain amount of matter before the polarization is measured. Then the extent of depolarization is one of the factors limiting the feasibility or accuracy of this measurement.

For this calculation, reference is made to Eq. (1.6). First, it should be noted that for $k\gtrsim m$, the depolarization is strong because certain of the ζ's, such as $\zeta^{1,2}$, $\zeta^{1,3}$ then become proportional to k/m, roughly. The following discussion, however, will be confined to low energies, and in the calculations only terms up to the order $(k/m)^2$ will be retained. Then $\zeta^{r,r'}$ may be set equal to one for all indices r and r', and one may conveniently introduce in (6) the vectors,

$$\mathbf{a}_{\mathbf{k}}\cong\sum_r\mathbf{e}_{\mathbf{k}}{}^r a_{\mathbf{k}}{}^r.\quad(1.11)$$

In terms of these, (1.6) becomes

$$H'=c\sum_{\mathbf{k},\mathbf{k}'}A_{\mathbf{k}'-\mathbf{k}}{}^0[\mathbf{a}_{\mathbf{k}'}{}^*\cdot\mathbf{a}_{\mathbf{k}}+(\gamma/2m^2)(\mathbf{k}'-\mathbf{k})\cdot(-\mathbf{k}\cdot\mathbf{a}_{\mathbf{k}}\mathbf{a}_{\mathbf{k}'}{}^*+\mathbf{k}'\cdot\mathbf{a}_{\mathbf{k}'}{}^*\mathbf{a}_{\mathbf{k}})].\quad(1.12)$$

Consider now a scattering process involving a change in polarization. Let the initial polarization vector be $\mathbf{n}$, and the final one be $\mathbf{n}'$, with $|\mathbf{n}|=|\mathbf{n}'|=1$. Then calculating the matrix element for a scattering process $\mathbf{k},\mathbf{n}\rightarrow\mathbf{k}',\mathbf{n}'$ amounts to rewriting H' in Eq. (12) with $\mathbf{a}_{\mathbf{k}}$, $\mathbf{a}_{\mathbf{k}'}{}^*$ replaced by $\mathbf{n}$, $\mathbf{n}'$ respectively; that is,

$$\langle\mathbf{k}',\mathbf{n}'|H'|\mathbf{k},\mathbf{n}\rangle=n_i'f_{ij}n_j$$

[4] O. Laparte, Phys. Rev. **54**, 905 (1938).

where

$$f_{ij}=eA_{\mathbf{k}'-\mathbf{k}}{}^{0}(\delta_{ij}+\epsilon_{ij}) \tag{1.13}$$

and

$$\epsilon_{ij}=(\gamma/2m^2)[-(k_i'-k_i)k_j+k_i'(k_j'-k_j)].$$

The magnitude of the depolarization angle resulting from a scattering process will be defined by

$$\sin\delta=\frac{\text{amplitude of scattered wave with } \mathbf{n}' \text{ perpendicular to } \mathbf{n}}{\text{total amplitude of scattered wave}}$$

or, more specifically,

$$\sin\delta=|\mathbf{n}\times(\boldsymbol{\epsilon}\cdot\mathbf{n})|/|(\boldsymbol{\delta}+\boldsymbol{\epsilon})\cdot\mathbf{n}|$$

$$\delta^2\cong\sin^2\delta\cong|\mathbf{n}\times(\boldsymbol{\epsilon}\cdot\mathbf{n})|^2=|\boldsymbol{\epsilon}\cdot\mathbf{n}|^2-(\mathbf{n}\cdot\boldsymbol{\epsilon}\cdot\mathbf{n})^2,$$

assuming that $\boldsymbol{\epsilon}$ is small, and remembering that $\mathbf{n}$ is a vector of unit length. Splitting the tensor ϵ_{ij} into its symmetric and skew-symmetric parts $(\epsilon_{ij}\pm\epsilon_{ji})/2$, one readily sees that the symmetric part is proportional to $|\mathbf{k}'-\mathbf{k}|^2$, or to $\sin^2\theta$, and it may be neglected because of the prevalence of small angle scattering in the Coulomb case. Then,

$$\delta^2\cong\tfrac{1}{4}|\textstyle\sum_j(\epsilon_{ij}-\epsilon_{ji})n_j|^2,$$

or in the average over all initial polarizations $\mathbf{n}$:

$$\langle\delta^2\rangle_{\mathbf{n}}=(1/12)\textstyle\sum_{ij}(\epsilon_{ij}-\epsilon_{ji})^2=\frac{1}{6}\gamma^2v^4\theta^2, \tag{1.14}$$

where $\mathbf{v}=\mathbf{k}/m$ is the velocity of the scattered particle.

According to this theory, then, $\langle\delta^2\rangle_{\mathbf{n}}$ is proportional to γ^2. On the other hand, one may calculate the same quantity classically for a particle with a magnetic moment of $1-\gamma$ magnetons, using the following procedure. Letting $\mathbf{a}$ be the classical polarization vector, where $|\mathbf{a}|=1$, one has[5]

$$\partial\mathbf{a}/\partial t=-(e/2m)(1-\gamma)\mathbf{H}\times\mathbf{a}$$

where

$$\mathbf{H}=-\mathbf{v}\times\mathbf{E}.$$

The traversal of the atomic field results in a change of $\mathbf{a}$ by

$$|\boldsymbol{\delta}|=\left|\int(\partial\mathbf{a}/\partial t)dt\right|$$

$$=(e/2m)|1-\gamma|\left|\int(\mathbf{v}\times\mathbf{E})\times\mathbf{a}dt\right|. \tag{1.15}$$

Integration over the entire Keplerian orbit, taking $\mathbf{v}\times\mathbf{E}$ to be in the z direction, gives

$$|\boldsymbol{\delta}|=|1-\gamma|v^2[\tan\tfrac{1}{2}\theta-\tfrac{1}{2}(\pi-\theta)\tan^2\tfrac{1}{2}\theta](a_x^2+a_y^2)^{\frac{1}{2}}, \tag{1.16}$$

and for small scattering angles θ

$$\langle\delta^2{}_{\text{class}}\rangle_{\mathbf{n}}\cong\langle(a_x^2+a_y^2)\rangle_{\mathbf{n}}(1-\gamma)^2v^4\theta^2/4$$

$$=\tfrac{1}{8}(1-\gamma)^2v^4\theta^2, \tag{1.17}$$

which is similar to (1.14), except that γ^2 is here replaced by $(1-\gamma)^2$. No explanation can be offered for this difference, except that agreement between the results of quantum-mechanical and of classical calculations may not always be expected to occur.

To give an indication of the rate of depolarization, the quantity $\iint\langle\delta^2\rangle_{\mathbf{n}}\sigma_{sc}d\Omega$ is computed, using

$$\sigma_{sc}=\tfrac{1}{4}(Ze^2/mv^2)^2(\sin^2\tfrac{1}{2}\theta+\alpha^2)^{-2}, \tag{1.18}$$

where α accounts for the screening by electrons [see Eq. (1.9)], and it is given by $\alpha\cong1/2kr_a$. One finds

$$\iint\langle\delta^2\rangle_{\mathbf{n}}\sigma_{sc}d\Omega\cong(4\pi/3)\gamma^2(Ze^2/m)^2[\log(1/\alpha)-1] \tag{1.19}$$

for $\alpha\ll1$. This result includes the effects of elastic scattering by the nucleus and the atomic electrons. Additional contributions to the depolarization may come from inelastic collisions with the electrons; these may occur in two ways, by interaction of the particle's magnetic moment with the electronic charge, and with the intrinsic magnetic moments of the electrons. These effects have been computed and combined with (1.19). Subsequently an estimate of the total depolarization is given in terms of the rate of change of $\Delta^2\equiv\sum\langle\delta^2\rangle_{\mathbf{n}}$ per unit distance traveled. Since the dependence of this quantity on velocity is logarithmic only, the value $v=1/10$ has been used. The result is

$$d(\Delta^2)/ds=\tfrac{2}{3}\pi.N\gamma^2(e^2/m)^2(17Z^2+11Z) \tag{1.20}$$

where $N=$ number of atoms/cm^3. The term proportional to Z represents, of course, the contribution of the inelastic collisions.

Equation (1.20) is valid only for nonrelativistic velocities, the region in which the approximations discussed above may be used.

II. PAIR THEORY

A. General Discussion

The pair theory of the π-meson has been introduced in order to simplify the status of elementary particles, by assuming the pion to be a compound particle composed of two μ-mesons.[6,7] In the case of a charged pion, the pair is taken to be a charged muon combined with a neutral anti-muon, the muons being treated as Dirac particles. The binding energy of the pair is taken to result from the virtual process which yields a nucleon pair, the latter consisting of a proton and an anti-neutron in case of a positive pion. An analogous process results in a binding energy between neutron and proton, namely, the exchange of a virtual muon pair between the two nucleons.

Leaving the specific identity of the particles open, one may choose for the interaction between the pairs of

[5] G. Wentzel, Phys. Rev. **75**, 1810 (1949).

[6] This theory is to be contrasted with that of Fermi and Yang, in which the π-meson is assumed to be made up of a nucleon pair. E. Fermi and C. N. Yang, Phys. Rev. **76**, 1739 (1949).

[7] G. Wentzel, Phys. Rev. **79**, 710 (1950).

spin ½ particles any one of the usual five interaction types used in beta-decay theory, yielding a particle with either spin 0 or spin 1, depending on the coupling type.

The advantages of a pair theory lie in the possibility thus afforded to predict certain specific properties of a Bose particle. In this paper the following are computed: the magnitudes of the magnetic dipole and electric quadrupole moments in the case of vector particles; the spatial charge distribution and the cross sections for scattering and for dissociation for a pion, using pseudoscalar coupling.

A disadvantage of the theory lies in the fact that its results are essentially qualitative, owing to the lack of an invariant method of applying a cutoff to the momentum space integrals which appear. In actual practice the calculations are carried out in the center-of-mass system, and the integrals are cut off at some value of the magnitude of the momentum. In spite of this disadvantage, it appears that the pair theory can give useful orders of magnitude for certain processes, which in some cases may be capable of comparison with experiment. An example is the dissociation of a pion into a muon pair by an atomic collision.

A brief discussion of the theory as applied to the pion will now be given. The four particles, proton, neutron, positive muon, and neutral muon or nuon, are assumed to be coupled by the interaction Hamiltonian

$$(2\pi)^3\sum_\alpha \eta \int d^3x(N^*A_\alpha P)(\mu^*A_\alpha\nu)+\text{comp. conj.}, \quad (2.1)$$

where η is a coupling constant, the symbols N, P, μ, and ν stand for the spinor field operators of the corresponding particles, and A is one of the five Dirac operators. The momentum space cutoffs mentioned above will be introduced in the form of the functions $g(p)$ and $G(P)$, which will be defined by

$$g(p)=\exp(-\alpha^2p^2/4); \quad G(P)=\exp(-A^2P^2/4) \quad (2.2)$$

where

$$\int g^4(p)d^3p=(4\pi/3)k^3; \quad \int G^4(P)d^3P=(4\pi/3)k^3.$$

It is found that these cutoffs should be assigned roughly the values k = mesonic mass and K = nucleon mass. The use of this nonrelativistic cut-off method leads to the requirement that calculations should be done in the rest frame of the center of mass of the pion.

Now the matrix element (1) becomes after integration

$$\eta\delta(\mathbf{P}_0-\mathbf{P}+\mathbf{p}-\mathbf{p}_0)G(P_0)G(P)g(p)g(p_0) \times\sum_\alpha\langle\mathbf{P}_0\Lambda_0|A_\alpha|\mathbf{P}\Lambda\rangle\langle\mathbf{p}\lambda|A_\alpha|\mathbf{p}_0\lambda_0\rangle \quad (2.3)$$

where $|\mathbf{P}\Lambda\rangle$, $\langle\mathbf{P}_0\Lambda_0|$, $|\mathbf{p}\lambda\rangle$, $\langle\mathbf{p}_0\lambda_0|$ represent the momentum and spin states of the proton, neutron, muon, and nuon, respectively. It should be noted that $\mathbf{P}_0$ and $\mathbf{p}_0$ represent the momenta of the vacant states of the neutral particles; hence, the particle momenta are $-\mathbf{P}_0$ and $-\mathbf{p}_0$.

For the purpose of describing a pion at rest, the Schroedinger function Ψ may be considered as a superposition of state functions, each corresponding to a given set of values for the momenta and the spins of the particles making up the pair. The function Ψ is then a sum containing each such state function multiplied by its probability amplitude. In this discussion these probability amplitudes will be represented by $f(\mathbf{p}\lambda\lambda_0)$ for the presence of a pair consisting of a muon with momentum $\mathbf{p}$ and spin λ and of an anti-nuon with momentum $-\mathbf{p}$ and spin λ_0; similarly, $F(\mathbf{P}\lambda\lambda_0)$ is for the presence of a proton and anti-neutron pair with the indicated momenta and spins.

The desired properties of the π-meson of this theory may be calculated once the amplitudes f and F have been determined. This is accomplished by solving a pair of coupled integral equations which these amplitudes satisfy, namely

$$\begin{aligned}0=&[-\epsilon+(m^2+p^2)^{\frac{1}{2}}+(m_0^2+p^2)^{\frac{1}{2}}]f(\mathbf{p}\lambda\lambda_0)\\&+\eta g^2(p)\sum_\alpha\langle\mathbf{p}\lambda|A_\alpha|\mathbf{p}\lambda_0\rangle\int d^3PG^2(P)\\&\times\sum_{\Lambda\Lambda_0}\langle\mathbf{P}\Lambda_0|A_\alpha|\mathbf{P}\Lambda\rangle F(\mathbf{P}\Lambda\Lambda_0);\\0=&[-\epsilon+(M^2+P^2)^{\frac{1}{2}}+(M_0^2+P^2)^{\frac{1}{2}}]F(\mathbf{P}\Lambda\Lambda_0)\\&+\eta G^2(P)\sum_\alpha\langle\mathbf{P}\Lambda|A_\alpha|\mathbf{P}\Lambda_0\rangle\int d^3pg^2(p)\\&\times\sum_{\lambda\lambda_0}\langle\mathbf{p}\lambda_0|A_\alpha|\mathbf{p}\lambda\rangle f(\mathbf{p}\lambda\lambda_0).\end{aligned} \quad (2.4)$$

These equations are approximate in the sense that they do not include virtual states in which more than one meson and/or nucleon pair are present. However, since this treatment will be approximate in any case, these additional states will not be considered.

From these equations the following solutions are obtained for a bound state. (For simplicity the masses of the two nucleons are taken equal to M, and those of the two muons equal to m.)

$$\begin{aligned}f(\mathbf{p}\lambda\lambda_0)&=[g^2(p)/(2e_p-\epsilon)]\textstyle\sum_\alpha\langle\mathbf{p}\lambda|A_\alpha|\mathbf{p}\lambda_0\rangle u_\alpha,\\F(\mathbf{P}\Lambda\Lambda_0)&=[G^2(P)/(2E_P-\epsilon)]\textstyle\sum_\alpha\langle\mathbf{P}\Lambda|A_\alpha|\mathbf{P}\Lambda_0\rangle U_\alpha,\end{aligned} \quad (2.5)$$

where $e_p=(p^2+m^2)^{\frac{1}{2}}$, $E_P=(P^2+M^2)^{\frac{1}{2}}$, and ϵ is the binding energy of the pion. Inserting these solutions into Eqs. (2.4), one finds the conditions

$$u_\alpha+\eta\textstyle\sum_\beta C_{\alpha\beta}U_\beta=0, \quad U_\alpha+\eta\sum_\beta c_{\alpha\beta}u_\beta=0 \quad (2.6)$$

where

$$c_{\alpha\beta}=\int\frac{d^3pg^4(p)}{2e_p-\epsilon}\sum_{\lambda\lambda_0}\langle\mathbf{p}\lambda_0|\bar{A}_\alpha|\mathbf{p}\lambda\rangle\langle\mathbf{p}\lambda|A_\beta|\mathbf{p}\lambda_0\rangle$$
$$C_{\alpha\beta}=\int\frac{d^3PG^4(P)}{2E_p-\epsilon}\sum_{\Lambda\Lambda_0}\langle\mathbf{P}\Lambda_0|\bar{A}_\alpha|\mathbf{P}\Lambda\rangle\langle\mathbf{P}\Lambda|A_\beta|\mathbf{P}\Lambda_0\rangle. \quad (2.7)$$

From the foregoing relations, together with the normalization condition,

$$\int d^3p\sum_{\lambda\lambda_0}|f(\mathbf{p}\lambda\lambda_0)|^2+\int d^3P\sum_{\Lambda\Lambda_0}|F(\mathbf{P}\Lambda\Lambda_0)|^2=1, \quad (2.8)$$

it is possible to calculate the magnitudes of the amplitudes $\mathbf{u}$ and $\mathbf{U}$ in (2.5) in terms of the cut-off values k and K.

B. Magnetic Dipole Moment

Consider a vector particle in a weak, constant magnetic field $\mathbf{H}$. The change in energy of the particle, which is $-\boldsymbol{\mu}\cdot\mathbf{H}$, may be calculated by a first-order perturbation treatment, from which the value of the magnetic moment is then obtained. Expressing the field in terms of a vector potential $\mathbf{A}$, the perturbation term is

$$-\mathbf{H}\cdot\boldsymbol{\mu}=-e\int\int\psi^*\mathbf{A}(\mathbf{r}_+)\cdot\boldsymbol{\alpha}_+\psi d^3r_+d^3r_0$$
$$=\tfrac{1}{2}e\int\int\psi^*\mathbf{H}\cdot\boldsymbol{\alpha}_+\times\mathbf{r}_+\psi d^3r_+d^3r_0$$

or

$$\boldsymbol{\mu}=-\tfrac{1}{2}e\int\int\psi^*\boldsymbol{\alpha}_+\times\mathbf{r}_+\psi d^3r_+d^3r_0. \quad (2.9)$$

Here ψ may be expressed in terms of the momentum amplitudes as

$$\psi=\frac{1}{(2\pi)^3}\int d^3Pa(\mathbf{P})e^{\frac{1}{2}i\mathbf{P}\cdot(\mathbf{r}_++\mathbf{r}_0)}$$
$$\times\sum_{\lambda\lambda_0}\int d^3p\chi_{\mathbf{p}\lambda}f(\mathbf{p}\lambda\lambda_0)\chi_{\mathbf{p}\lambda_0}{}^*\cdot e^{i\mathbf{p}\cdot(\mathbf{r}_+-\mathbf{r}_0)}, \quad (2.10)$$

where $\mathbf{P}$ represents the momentum of the combined particle and $a(\mathbf{P})$ represents the corresponding probability amplitude, while $\mathbf{p}$ and $-\mathbf{p}$ are, respectively, the momenta of the charged and neutral spin $\frac{1}{2}$ particles, referred to the center of mass. Writing

$$d^3r_+d^3r_0\rightarrow d^3[\tfrac{1}{2}(\mathbf{r}_++\mathbf{r}_0)]d^3(\mathbf{r}_+-\mathbf{r}_0)$$
and
$$\boldsymbol{\alpha}\times\mathbf{r}_+=\tfrac{1}{2}[\boldsymbol{\alpha}_+\times(\mathbf{r}_+-\mathbf{r}_0)+\boldsymbol{\alpha}_+\times(\mathbf{r}_++\mathbf{r}_0)], \quad (2.11)$$

it is clear that the second term, referring to the center-of-mass motion, cannot contribute to $\boldsymbol{\mu}$ in the case of a stationary particle ($a(\mathbf{P})$ spherically symmetric). In the remaining part, all factors in $\boldsymbol{\mu}$ pertaining to the center-of-mass motion reduce to $\int d^3P|a(P)|^2=1$;

TABLE I. Numerical values of the coefficients in Eq. (2.14).

Coupling type, A	Type of particle	a	b
Vector	Vector	1	$-\frac{1}{3}$
Tensor	Vector	1	$-\frac{2}{3}$
	Axial vector	0	
Pseudovector	Axial vector	0	

therefore, with $\mathbf{r}_+-\mathbf{r}_0\equiv\mathbf{r}$, and making the substitution $\mathbf{r}\rightarrow i(\partial/\partial\mathbf{p})$,

$$\boldsymbol{\mu}=-\frac{ie}{4}\int d^3r\int d^3p'\int d^3p$$
$$\times\sum_{\lambda\lambda_0}\sum_{\lambda'\lambda_0'}\left\{f^*(\mathbf{p}\lambda\lambda_0)\left(\mathbf{p}\lambda\left|\boldsymbol{\alpha}\times\frac{\partial}{\partial\mathbf{p}'}\right|\mathbf{p}'\lambda'\right)\right.$$
$$\left.\times f(p'\lambda'\lambda_0')\langle\mathbf{p}'\lambda_0'|1|\mathbf{p}\lambda_0\rangle\right\}e^{i(\mathbf{p}-\mathbf{p}')\cdot\mathbf{r}}$$
$$=\frac{ie}{4}\int d^3p\lim_{\mathbf{p}'\rightarrow\mathbf{p}}\left\{\frac{\partial}{\partial\mathbf{p}'}\times\left[\sum_{\lambda\lambda_0}\sum_{\lambda'\lambda_0'}f^*(\mathbf{p}\lambda\lambda_0)\right.\right.$$
$$\left.\left.\times\langle\mathbf{p}\lambda|\boldsymbol{\alpha}|\mathbf{p}'\lambda'\rangle f(\mathbf{p}'\lambda'\lambda_0')\langle\mathbf{p}'\lambda_0'|1|\mathbf{p}\lambda_0\rangle\right]\right\}. \quad (2.12)$$

On substituting the values of $f(\mathbf{p}\lambda\lambda_0)$ and of $f^*(\mathbf{p}\lambda\lambda_0)$ given in (2.5), one obtains

$$\boldsymbol{\mu}=\frac{ie}{4}\int d^3p\lim_{\mathbf{p}'\rightarrow\mathbf{p}}\left\{\frac{\partial}{\partial\mathbf{p}'}\times\left[\sum_{\lambda\lambda_0}\sum_{\lambda'\lambda_0'}\sum_{\alpha\beta}\frac{g^2(p)g^2(p')u_\alpha{}^*u_\beta}{(2e_p-\epsilon)(2e_{p'}-\epsilon)}\right.\right.$$
$$\times\langle\mathbf{p}\lambda_0|\bar{A}_\alpha|\mathbf{p}\lambda\rangle\langle\mathbf{p}\lambda|\boldsymbol{\alpha}|\mathbf{p}'\lambda'\rangle$$
$$\left.\left.\times\langle\mathbf{p}'\lambda'|A_\beta|\mathbf{p}'\lambda_0'\rangle\langle\mathbf{p}'\lambda_0'|1|\mathbf{p}\lambda_0\rangle\right]\right\} \quad (2.13)$$

where $\bar{A}$ is the conjugate transpose of A. The summation over spins is accomplished in the usual fashion, remembering that λ is to be summed only over positive energies and λ_0 only over negative energies. In all coupling cases which lead to bosons of spin 1, one finds the general result,

$$\boldsymbol{\mu}=-\frac{ie}{2}\mathbf{u}^*\times\mathbf{u}\int\frac{d^3pg^4(p)}{(2e_p-\epsilon)^2}\frac{1}{e_p}\left(a+b\frac{p^2}{e_p{}^2}\right). \quad (2.14)$$

The values of a and b are given in Table I. They are the same as those obtained when carrying out the normalization,[2] using Eq. (2.8), which involves the expression,

$$\mathbf{u}^*\cdot\mathbf{u}\sum_{\lambda\lambda_0}\sum_\alpha\langle\mathbf{p}\lambda_0|\bar{A}_\alpha|\mathbf{p}\lambda\rangle\langle\mathbf{p}\lambda|A_\alpha|\mathbf{p}\lambda_0\rangle$$
$$=2(a+bp^2/e_p{}^2)\mathbf{u}^*\cdot\mathbf{u}.$$

In addition to the above contribution to the magnetic moment by the pair of light particles, one should, for completeness, consider the contribution of the virtual nucleon pair. The latter will include a term similar to

TABLE II. Numerical values of the quantities related to spatial extension.

Coupling type, A	Type of boson	$\langle r^2\rangle_M$	$\alpha\|u\|^2$	$\beta\|u\|^2$
Vector	Vector	$1.6\epsilon^{-2}$	$0.6\epsilon^{-2}$	$0.05\epsilon^{-2}$
Tensor	Vector	$1.4\epsilon^{-2}$	$0.5\epsilon^{-2}$	$-0.04\epsilon^{-2}$
	Axial vector	$2.8\epsilon^{-2}$	$0.9\epsilon^{-2}$	$0.4\epsilon^{-2}$
Pseudovector	Axial vector	$2.7\epsilon^{-2}$	$0.9\epsilon^{-2}$	$-0.2\epsilon^{-2}$
Pseudoscalar	Pseudoscalar	$1.6\epsilon^{-2}$	—	—

(2.12), with $f(\mathbf{p}\lambda\lambda_0)$ replaced by $F(\mathbf{P}\Lambda\Lambda_0)$, and will also contain contributions from the anomalous magnetic moments of the neutron and the proton. However, the contributions from this admixture are small, relatively, for, because of the high energy associated with such a state, it "exists for a much smaller fraction of the time."

The magnitude of the magnetic moment is obtained from (2.14) by choosing circular polarization (e.g., $u_1=0$, $u_2=iu_3\neq 0$), in which case

$$|\mathbf{u}^*\times\mathbf{u}|=\mathbf{u}^*\cdot\mathbf{u}.$$

A numerical calculation was carried out for the various types of coupling which yield a vector particle, using, for the cutoff, parameters defined in Eq. (2), $k=m$ and $K=M$. In all cases, the magnetic moment was found to be approximately one-half the normal moment, $e/2\epsilon$, corresponding to $\gamma\cong\frac{1}{2}$ [see Eq. (1.2)].

C. Electric Charge Distribution

In the center-of-mass system of the pair-formed boson, the electric charge density is given by $e\psi^*\psi$, where ψ is given by (2.10) again neglecting the contribution from the nucleon pair, which will be small, and confined to a smaller region. Rather than obtain an expression for $\psi^*\psi$ in a closed form, the nature of the charge distribution will be illustrated by calculations of the mean-square-radius and of the quadrupole moment for various types of coupling. This amounts to computing the components of the tensor $\langle r_{+i}r_{+j}\rangle_M$, where $\mathbf{r}_+=\frac{1}{2}(\mathbf{r}_+-\mathbf{r}_0)$ is the vector distance of a charge element from the center of mass. Using the momentum amplitudes $f(\mathbf{p}\lambda\lambda_0)$, introduced above, and making the operator substitutions $r_{+i}\rightarrow\frac{1}{2}i\partial/\partial p_i$, leads to the following

$$\langle r_{+i}r_{+j}\rangle_M=-\tfrac{1}{4}\sum_{\lambda\lambda_0}\sum_{\lambda'\lambda_0'}\sum_{\rho\sigma}\int d^3p\Big[f^*(\mathbf{p}\lambda\lambda_0)\chi_{\mathbf{p}\lambda,\rho}{}^*\times\frac{\partial^2}{\partial p_i\partial p_j}\{\chi_{\mathbf{p}\lambda',\rho}f(p\lambda'\lambda_0')\chi_{\mathbf{p}\lambda_0',\sigma}{}^*\}\chi_{\mathbf{p}\lambda_0,\sigma}\Big]. \quad (2.15)$$

From this one may calculate either

$$\langle r_+{}^2\rangle_M=\sum_i\langle r_{+i}{}^2\rangle_M$$

or

$$Q_{ij}=\langle r_{+i}r_{+j}\rangle_M-\tfrac{1}{3}\delta_{ij}\langle r_+{}^2\rangle_M.$$

It will be of interest to give first a discussion of the nature of the integrands obtained for the two different cases $i=j$ and $i\neq j$. In general the integrand in (2.15), after averaging over the directions of $\mathbf{p}$, has the form

$$A(p)\delta_{ij}\textstyle\sum_k u_k{}^*u_k+B(p)(u_i{}^*u_j+u_j{}^*u_i-\frac{2}{3}\delta_{ij}\sum_k u_k{}^*u_k), \quad (2.16)$$

where $A(p)$ and $B(p)$ are functions of the magnitude of $\mathbf{p}$ only. It is seen from this that the nondiagonal components of the quadrupole moment tensor Q will vanish in the following two cases:

$$\begin{aligned}&(1)\ u_1\neq 0,\quad u_2=u_3=0\quad\text{(linear polarization)}\\&(2)\ u_1=0,\quad u_2=iu_3\neq 0\quad\text{(circular polarization).}\end{aligned} \quad (2.17)$$

The first corresponds to having the axis of symmetry in the direction of the polarization vector $\mathbf{u}$, the second to having the axis of symmetry along the direction of the spin vector $i\mathbf{u}^*\times\mathbf{u}$.

The values of $A(p)$ and $B(p)$ were computed for the four spin 1 particles which can be obtained from vector, tensor, and pseudovector coupling; they were then integrated over momentum, using for the cut-off parameter the value $k=m$. Let α and β represent, respectively, these integrated values; then setting $\sum_k u_k{}^*u_k=|u|^2$,

$$\begin{aligned}\langle r_{+i}r_{+j}\rangle_M&=\alpha|u|^2\delta_{ij}+\beta(u_i{}^*u_j+u_j{}^*u_i-\tfrac{2}{3}|u|^2\delta_{ij})\\&=\alpha|u|^2\delta_{ij}+\beta|u|^2(a_i{}^*a_j+a_j{}^*a_i-\tfrac{2}{3}\delta_{ij}),\end{aligned} \quad (2.18)$$

where a_i is a new polarization vector such that $\sum_i|a_i|^2=1$. In particular

$$\langle r_+{}^2\rangle_M=\textstyle\sum_i\langle r_{+i}{}^2\rangle_M=3\alpha|u|^2.$$

In the special cases (2.17), we have, for $a_1=1$, $a_2=a_3=0$:

$$\begin{aligned}\langle r_1{}^2\rangle_M&=[\alpha+(4/3)\beta]|u|^2\\\langle r_2{}^2\rangle_M&=\langle r_3{}^2\rangle_M=(\alpha-\tfrac{2}{3}\beta)|u|^2\\Q&\equiv\langle r_1{}^2\rangle_M-\tfrac{1}{2}(\langle r_2{}^2\rangle_M+\langle r_3{}^2\rangle_M)=2\beta|u|^2\\\langle r_1{}^2\rangle_M/\langle r_2{}^2\rangle_M&=1+2\beta/(\alpha-\tfrac{2}{3}\beta)\end{aligned}$$

and for $a_1=0$, $a_2=ia_3=1/\sqrt{2}$:

$$\begin{aligned}\langle r_1{}^2\rangle_M&=(\alpha-\tfrac{2}{3}\beta)|u|^2\\\langle r_2{}^2\rangle_M&=\langle r_3{}^2\rangle_M=(\alpha+\tfrac{1}{3}\beta)|u|^2\\Q&=-\beta|u|^2\\\langle r_1{}^2\rangle_M/\langle r_2{}^2\rangle_M&=1-\beta/(\alpha+\tfrac{1}{3}\beta).\end{aligned}$$

In Table II are tabulated the quantities of interest for the four types of spin 1 particles, as well as the value of $\langle r^2\rangle_M$ for the case of pseudoscalar coupling. It should, of course, be noted that the spatial extension of the boson, as computed above, results directly from the cut-off procedure, which eliminates indefinitely large magnitudes of the momentum, and the numerical values given depend on the choice $k=m$.

D. Elastic Coulomb Scattering at Low Velocities

The extension in space of the π-meson, as predicted by the pair theory, suggests an investigation of the

Coulomb scattering of the particle to seek any effects resulting from this property. Strictly speaking, however, it is not correct to treat the scattering of a pion by means of Eqs. (2.5) to (2.8), since this representation is only valid for the center-of-mass frame, and in a scattering process, the velocity of this frame undergoes a change. Because of the non-invariant character of the cut-off method, it is reasonable to assume that correction terms of the order $(v/c)^2$ ($\mathbf{v}$ = pion velocity) may not be uniquely determined, and the terms we are looking for are all of this type. Nevertheless, a qualitative estimate may be attempted.

In computing the matrix element for a scattering process, the wave function for the pion moving initially with a small velocity $\mathbf{v}$ with respect to the scattering center is obtained by a Lorentz transformation of the wave function referred to the rest frame of the pion. In the latter form it may be written

$$\psi=(2\pi)^{-3}\int d^3p\,\chi_{\mathbf{p},\lambda}f(\mathbf{p}\lambda\lambda_0)\chi_{\mathbf{p},\lambda_0}{}^*e^{i\mathbf{p}\cdot(\mathbf{r}_+-\mathbf{r}_0)-i\epsilon t}. \quad (2.19)$$

Taking $\mathbf{v}$ to be in the z direction, one has

$$\begin{aligned} z_+&=(\bar z_+-v\bar t)/(1-v^2)^{\frac12},\\ z_0&=(\bar z_0-v\bar t)/(1-v^2)^{\frac12},\\ t&=[\bar t-\tfrac12 v(\bar z_++\bar z_0)]/(1-v^2)^{\frac12}\\ x_+&=x_0=\bar x,\quad y_+=y_0=\bar y. \end{aligned} \quad (2.20)$$

Here $\bar x$, $\bar t$, etc., are referred to the rest frame of the Coulomb field.

The transformations of the amplitudes $\chi_{\mathbf{p},\lambda}$, $\chi_{\mathbf{p},\lambda_0}{}^*$ are made in the following way.

$$\chi_{\mathbf{p},\lambda}\rightarrow T_{\mathbf{p}}{}^+(\mathbf{v})\chi_{\mathbf{p},\lambda};\quad \chi_{\mathbf{p},\lambda_0}{}^*\rightarrow\chi_{\mathbf{p},\lambda_0}{}^*T_{\mathbf{p}}{}^-(\mathbf{v}), \quad (2.20')$$

where

$$\begin{aligned} &T_{\mathbf{p}}(\mathbf{v})=S(\mathbf{v})/N_{\mathbf{p}}{}^{\pm}(\mathbf{v});\\ &S(\mathbf{v})=S^*(\mathbf{v})=\cosh\tfrac12\xi-\tfrac12\boldsymbol{\alpha}\cdot\mathbf{v}\sinh\tfrac12\xi;\\ &\sinh\xi=v/(1-v^2)^{\frac12}\\ &[N_{\mathbf{p}}{}^+(\mathbf{v})]^2=\langle\mathbf{p}\lambda|S^*S|\mathbf{p}\lambda\rangle;\\ &[N_{\mathbf{p}}{}^-(\mathbf{v})]^2=\langle\mathbf{p}\lambda_0|S^*S|\mathbf{p}\lambda_0\rangle. \end{aligned}$$

The wave functions for the initial and final states (with corresponding velocities $\mathbf{v}$ and $\mathbf{v}'$), as referred to the rest frame of the Coulomb field, now may be written

$$\begin{aligned} \bar\psi&=(2\pi)^{-3}e^{\frac{i}{\hbar}\mathbf{P}\cdot(\bar{\mathbf{r}}_++\bar{\mathbf{r}}_0)-i\epsilon_P\bar t}\int d^3pT_{\mathbf{p}}{}^+(\mathbf{v})\\ &\quad\times\chi_{\mathbf{p},\lambda}f(\mathbf{p}\lambda\lambda_0)\chi_{\mathbf{p},\lambda_0}{}^*T_{\mathbf{p}}{}^-(\mathbf{v})e^{\frac{i}{\hbar}\mathbf{p}\cdot(\bar{\mathbf{r}}_+-\bar{\mathbf{r}}_0)}\\ \bar\psi'^*&=(2\pi)^{-3}e^{-\frac{i}{\hbar}\mathbf{P}'\cdot(\bar{\mathbf{r}}_++\bar{\mathbf{r}}_0)+i\epsilon_{P'}\bar t}\\ &\quad\times\int d^3p'T_{\mathbf{p}'}{}^-(\mathbf{v}')\chi_{\mathbf{p}',\lambda_0'}f^*(\mathbf{p}'\lambda'\lambda_0')\\ &\quad\times\chi_{\mathbf{p}',\lambda'}{}^*T_{\mathbf{p}'}{}^+(\mathbf{v}')e^{-\frac{i}{\hbar}\mathbf{p}'\cdot(\bar{\mathbf{r}}_+-\bar{\mathbf{r}}_0)} \end{aligned} \quad (2.21)$$

where $\mathbf{P}=\epsilon\mathbf{v}/(1-v^2)^{\frac12}$, $\epsilon_P=\epsilon/(1-v^2)^{\frac12}$, $\bar p_{1\mathbf{v}}=p_{1\mathbf{l}}/(1-v^2)^{\frac12}$, $\bar p_{\lambda\mathbf{v}}=p_{\lambda\mathbf{l}}$, and similarly for the final state.

The matrix element for an elastic collision,

$$H_{\mathbf{P}'-\mathbf{P}'}=\int\bar\psi_{\mathbf{P}'}{}^*V(\bar{\mathbf{r}})\bar\psi_{\mathbf{P}}d^3\bar rd^3\bar r_0 \quad (2.22)$$

may now be computed; this has been done for the case of pseudoscalar coupling (pseudoscalar pion). After carrying out the necessary summations over spin states, the expression (2.22) may be reduced to the following form, retaining only terms up to the second power of the velocities,

$$\begin{aligned} H_{\mathbf{P}'-\mathbf{P}'}=V_{\mathbf{P}'-\mathbf{P}}(1-v^2)^{\frac12}\Big[1-\tfrac12|\mathbf{v}'-\mathbf{v}|^2\\ \times\int d^3q\Big\{\varphi^2(q)\Big(1+\frac{\epsilon^2}{4e_q{}^2}\Big)\Big(1-\frac{q^2}{3e_q{}^2}\Big)\\ +\frac{\epsilon^2}{6}\varphi'^2(q)\Big\}\Big] \end{aligned} \quad (2.23)$$

where

$$\varphi(q)\equiv|u|\,g^2(q)/(2e_q-\epsilon),\quad \varphi'=d\varphi/dq,$$

and

$$V_{\mathbf{P}'-\mathbf{P}}=\langle\mathbf{P}'|V(\bar{\mathbf{r}})|\mathbf{P}\rangle.$$

Using for the cut-off parameter defined in (2.2) the value $k=m$, one obtains the numerical result,

$$H_{\mathbf{P}'-\mathbf{P}'}=V_{\mathbf{P}'-\mathbf{P}}(1-v^2)^{\frac12}[1-0.53|\mathbf{v}'-\mathbf{v}|^2]. \quad (2.24)$$

The quadratic term in $\mathbf{v}'-\mathbf{v}$ may be interpreted tentatively as the effect of the spatial extension of charge of the pion.

As a means of comparison, the matrix element for scattering may be computed by the use of a phenomenological theory. Consider a particle with spatial extension, whose Schroedinger wave function is given by

$$\Psi_{\mathbf{p}}=f(\mathbf{r})e^{i\mathbf{p}\cdot\mathbf{r}_c}$$

where $\mathbf{r}_c$ gives the position of the center of mass of the particle, and $\mathbf{r}$ gives the position relative to the center of mass. The matrix element,

$$H_{\mathbf{p}'-\mathbf{p}'}=\int\psi_{\mathbf{p}'}{}^*V(\mathbf{r})\psi_{\mathbf{p}}d^3\mathbf{r}_cd^3\mathbf{r},$$

is evaluated by expanding $V(\mathbf{r})$ into powers of $\mathbf{r}$, and, assuming $\bar{\mathbf{r}}=0$, the matrix element reduces to

$$H_{\mathbf{p}'-\mathbf{p}}=V_{\mathbf{p}'-\mathbf{p}}[1-\tfrac12\textstyle\sum_{ij}\langle r_ir_j\rangle_{\mathrm{Av}}(p_i'-p_i)(p_j'-p_j)+\cdots].$$

In the case of spherical symmetry, one has

$$H_{\mathbf{p}'-\mathbf{p}'}=V_{\mathbf{p}'-\mathbf{p}}[1-\tfrac16\langle r^2\rangle_{\mathrm{Av}}|\mathbf{p}'-\mathbf{p}|^2+\cdots]. \quad (2.25)$$

Equation (2.25) should represent the case of a pseudoscalar particle. Comparing with (2.24), one sees that there is qualitative, but not quantitative agreement. Indeed, the factor 0.53 is somewhat larger than

$\langle r^2\rangle_{Av}\epsilon^2/6=0.26$ (see Table II). From the calculation it appears that this is because the elastic scattering requires some readjustment of the internal structure (spins) of the pion which is as effective in reducing the cross section as is the extension in space.

E. Dissociation of a Pi-Meson

The Coulomb scattering of a pion moving with a sufficiently high velocity may lead to dissociation into two muons, according to the pair theory. This problem is conveniently treated by considering the pion at rest, acted on by a moving Coulomb field. For this purpose the potential may be expressed in terms of its Fourier components as follows,

$$V(\mathbf{r},t)=\frac{Ze}{2\pi^2}(1+\boldsymbol{\alpha}\cdot\mathbf{v})\int d^3q\frac{e^{i\mathbf{q}\cdot(\mathbf{r}+\mathbf{v}t)}}{q^2-(\mathbf{v}\cdot\mathbf{q})^2}. \quad (2.26)$$

Again neglecting the presence of a nucleon pair, the matrix element for dissociation of the pion into a muon with momentum $\mathbf{p}$ and spin λ, and an anti-nuon with momentum $-\mathbf{p}$ and spin λ_0 is given by

$$H'=\frac{Ze^2}{2\pi^2}\sum_{\lambda'}\frac{\langle\mathbf{p}\lambda|1+\boldsymbol{\alpha}\cdot\mathbf{v}|\mathbf{p}_0\lambda'\rangle f(\mathbf{p}_0\lambda'\lambda_0)}{|\mathbf{p}-\mathbf{p}_0|^2-[\mathbf{v}\cdot(\mathbf{p}-\mathbf{p}_0)]^2}e^{i\omega t} \quad (2.27)$$

where

$$\omega=e_p+\mathbf{v}\cdot\mathbf{p}+e_{p0}-\mathbf{v}\cdot\mathbf{p}_0-\epsilon$$

and $\omega=0$ corresponds to energy conservation in the rest frame of the Coulomb center. To obtain the total cross section for the dissociation process, $|H'|^2$ must be summed over the final spins and momenta of the two outgoing particles. For the sum over spins the expression for $f(\mathbf{p}\lambda\lambda_0)$ is introduced and the summations over positive energy states of the muon and negative energy states of the anti-nuon are carried out in the usual way. The result of summing over spins is

$$|H'|^2=g^4(p_0)\frac{Z^2e^4}{4\pi^4}\frac{u_\alpha^*u_\beta}{(2e_{p0}-\epsilon)^2}\times\frac{\mathrm{Sp}\{\bar{A}_\alpha(e_{p0}+H_{p0})A_\beta(e_{p0}+H_{p0})\}}{8e_{p0}{}^3e_p}\times\frac{2(e_p+\mathbf{p}\cdot\mathbf{v})(e_{p0}+\mathbf{p}_0\cdot\mathbf{v})+(1-v^2)(\mathbf{p}\cdot\mathbf{p}_0+m^2-e_pe_{p0})}{\{|\mathbf{p}-\mathbf{p}_0|^2-[\mathbf{v}\cdot(\mathbf{p}-\mathbf{p}_0]^2\}^2}. \quad (2.28)$$

In terms of $|H'|^2$ the dissociation cross section is then given by the usual expression,

$$\sigma_{\mathrm{diss}}=(2\pi)^4v^{-1}\int d^3p\int d^3p_0|H'|^2\delta(\omega).$$

The integrations over the momenta have not been carried out exactly. Instead, the cross section has been estimated in the region of high energies of the pion in order to determine its dependence on energy in this region. The first step was to carry out exact integrations over the directions of $\mathbf{p}_0$. Then the integration over the magnitude of $\mathbf{p}_0$ was approximated by the use of the average values

$$\bar{p}_0\cong m,\quad \bar{e}_{p0}\cong\sqrt{2}m\cong\epsilon,$$

as well as of the normalization condition (2.8) in the form

$$|u|^2\int\sum_\alpha\frac{\mathrm{Sp}\{\bar{A}_\alpha(e_{p0}+H_{p0})A_\alpha(e_{p0}-H_{p0})\}}{4e_{p0}{}^2(2e_{p0}-\epsilon)^2}=1,$$

neglecting the term with $F(\mathbf{P}\Lambda\Lambda_0)$. The remaining integral over $\mathbf{p}$ space was approximated by making the following assumptions: (1) terms containing $1-v^2$ as a factor can in some cases be neglected (already at the threshold $1-v^2=0.42$); (2) since the integrand has a fairly strong maximum value for directions of $\mathbf{p}$ corresponding to a certain angle θ with the direction of $\mathbf{v}$, the integrand may be treated as a delta-function with respect to the variable θ. The expression for σ_{diss} then reduces to merely

$$\frac{2\pi m^2Z^2e^4}{(1-v^2)v^2\epsilon}\int_m^\infty\frac{de_p}{e_p{}^4}\left(\frac{m}{e_p}+\frac{\epsilon}{m}\right) \quad (2.29)$$

where m is the muon mass and ϵ is the pion mass. Equation (2.29) holds for all coupling types A. Performing this integration, one obtains as an order of magnitude for high energies ($v\cong1$)

$$\sigma_{\mathrm{diss}}\cong5.5(Ze^2/\epsilon)^2(E_\pi/\epsilon)^2=5.8\times10^{-30}Z^2(E_\pi/\epsilon)^2\ \mathrm{cm}^2. \quad (2.30)$$

As a particular example, consider pions with a kinetic energy of 250 Mev; one then finds for the total cross section

$$\sigma_{\mathrm{diss}}\cong5\times10^{-29}Z^2\ \mathrm{cm}^2.$$

A consideration of the relation between the angle of emission, and the energy of the emitted muons may give an indication of the experimental conditions under which the disintegration process might be investigated. In obtaining (2.29), it was found that there is a rough correlation between the direction and the energy of the muon as observed in the rest frame of the pion, namely $\cos\theta\cong-p/e_pv$. (Actually, this correlation is not strong except for $(1-v^2)^{\frac{1}{2}}\ll1$.) Expressed in terms of θ', the angle of emission as observed in the laboratory (Coulomb center) frame, this relation becomes $\sin\theta'\cong(p/mv)(1-v^2)^{\frac{1}{2}}$ in terms of the muon momentum measured in the rest frame of the pion, or $\cos\theta'\cong p'/e_{p'}v$ in terms of the momentum measured in the laboratory frame. The latter of these two expressions gives a rough connection between the energy and the angle of emission of the muon. The former, together with (2.29), may be

used to compute the cross section for a disintegration process leading to emission of a muon having θ' within any particular angular range.

A numerical example will now be given. The cross section for obtaining muons with angles $\theta' \geq 30°$ is found to be

$$\sigma_{\text{diss}}(\theta' \geq 30°) \cong 2.0 \times 10^{-30} Z^2 \text{ cm}^2,$$

assuming that one starts with 250-Mev pions. The kinetic energy of these muons will be $\lesssim$150 Mev. On the other hand one may compare this with the cross section for scattering of the pions into an angle $\theta' \geq 30°$, which is found to be

$$\sigma_{\text{scat}}(\theta' \geq 30°) = 7.7 \times 10^{-30} Z^2 \text{ cm}^2.$$

These scattered pions would have an energy of 250 Mev, of course, and since the two cross sections are at least of the same order of magnitude, it should not be difficult to detect the muons, if they are actually emitted. Unfortunately, however, the cross section in both cases is quite small.

I wish to express my sincere gratitude to Professor G. Wentzel, both for suggesting these problems and for many helpful discussions during the course of the work.

PHYSICAL REVIEW VOLUME 85, NUMBER 5 MARCH 1, 1952

The Yield of Gamma-Rays and Neutrons from the Proton Bombardment of Fluorine*

H. B. Willard, J. K. Bair, J. D. Kington, T. M. Hahn,† C. W. Snyder, and F. P. Green
Oak Ridge National Laboratory, Oak Ridge, Tennessee

(Received November 21, 1951)

The excitation function of gamma-rays produced by the proton bombardment of fluorine has been extended from 2.1 to 5.4 Mev with a resolution of 0.1 percent. 17 new resonances were observed with maxima at 2.32, 2.51, 2.63, 2.80, 3.02, 3.19, 3.49, 3.92, 4.00, 4.29, 4.49, 4.57, 4.71, 4.78, 4.99, 5.07, and 5.20 Mev. The $F^{19}(p,n)Ne^{19}$ threshold was determined to be 4.253±0.005 Mev, and the neutron yield in the forward direction was extended to 5.3 Mev. Maxima occur at 4.29, 4.46, 4.49, 4.57, 4.62, 4.71, 4.78, 4.99, 5.07, and 5.20 Mev. The $Ne^{19}-F^{19}$ mass difference was calculated from the threshold measurement to be 0.00349$_9$ amu.

I. INTRODUCTION

THE excitation function of gamma-rays produced by the proton bombardment of fluorine has been previously measured with good resolution in the region from 0 to 1.5 Mev.[1,2] The 15 resonances observed have natural widths which vary from less than 1.2 to 37 kev. Three additional resonances have been reported between 1.5 and 2.1 Mev.[3] It has been shown[4] that these gamma-rays arise from the following reaction:

$$\begin{aligned} &F^{19}+H^1 \rightarrow (Ne^{20})^* \rightarrow {}^*O^{16}+He^4+Q_1, \\ &{}^*O^{16} \rightarrow O^{16}+h\nu+Q_2. \end{aligned} \tag{1}$$

An analysis of the energy spectra of these gamma-rays[5] resolves them into two lines at 6.1 and 7.0 Mev. No lines between 8 and 18 Mev exist having an intensity of greater than one percent of the 6.1-Mev line. The resonances in this reaction are of sufficient sharpness and intensity to serve as useful calibration points on an absolute voltage scale.[2,6,7]

The $F^{19}(p,n)Ne^{19}$ reaction is endothermic with a measured threshold of 4.18±0.25 Mev.[8] The excitation function has not been reported previously with good resolution.

The new Van de Graaff accelerator at Oak Ridge[9] is capable of producing magnetically analyzed protons up to 5.5 Mev. In order to determine the energy resolution and calibrate the absolute voltage scale of this machine, the known gamma-ray resonances in fluorine were measured. The excitation function was then extended to 5.4 Mev. The $F^{19}(p,n)Ne^{19}$ threshold was determined and the excitation function was measured up to 5.3 Mev.

II. EXPERIMENTAL PROCEDURE

Ordinary 15-mil tantalum sheet was found to have a very thin surface layer of TaF_5 (the average stopping power was about 100 ev for 1-Mev protons), and was used for targets in the calibration experiments. For measurements above 2 Mev, thin layers of CaF_2 were evaporated on 15-mil tantalum (the stopping power was 5 kev for 2-Mev protons). The gamma-ray and neutron backgrounds were determined from an evapo-

* We are indebted to the United States Air Force for the financing of the 5.5-Mev Van de Graaff used in this research.

† Summer research participant on leave from the University of Kentucky.

[1] T. W. Bonner and J. E. Evans, Phys. Rev. **73**, 666 (1948).

[2] Chao, Tollestrup, Fowler, and Lauritsen, Phys. Rev. **79**, 108 (1950).

[3] Hornyak, Lauritsen, Morrison, and Fowler, Revs. Modern Phys. **22**, 356 (1950).

[4] McLean, Becker, Fowler, and Lauritsen, Phys. Rev. **55**, 796 (1939).

[5] R. L. Walker and B. D. McDaniel, Phys. Rev. **74**, 315 (1948).

[6] A. H. Morrish, Phys. Rev. **76**, 1651 (1949).

[7] Herb, Snowdon, and Sala, Phys. Rev. **75**, 246 (1949).

[8] Creutz, White, Delsasso, and Fox, Phys. Rev. **56**, 207 (1939).

[9] Robinson, McIntosh, and Nygard, Phys. Rev. **83**, 233 (1951).

rated calcium metal target of proper thickness. The evaporations were carried out by Dr. H. E. Banta of the High Voltage Group.

The gamma-rays were detected with a single crystal NaI scintillation counter biased to count only gamma-rays above approximately 3 Mev. The crystal was positioned one cm from the target along the beam axis. The neutron yield, in the forward direction, was obtained with a long counter[10] spaced 50 cm from the target. For the determination of the $F^{19}(p,n)Ne^{19}$ threshold a counter sensitive to low energy neutrons (about 10 kev for this particular reaction) similar to that described by Bonner and Butler[11] was employed. Electronic circuits were conventional. The yield was monitored by a beam current integrator of the Watt type.[12]

Protons accelerated by the 5.5-Mev electrostatic generator at Oak Ridge enter the analyzing magnet through two adjustable pairs of perpendicular entrance slits, are bent through 105° (in the vertical plane) with a radius of 37.7 cm, and leave through two similar pairs of exit slits. The entrance slits for the present work were set 4 mm apart, while the exit slits were limited to 1.5 mm, thus permitting a resolution of better than 0.2 percent. The beam voltage is stabilized by corona current using an error signal taken at the mass-one exit slits. This maintains the focused beam sufficiently well-centered to permit the somewhat better resolution of 0.1 percent as determined experimentally from the known gamma-ray resonances in fluorine. These were observed with their natural widths as reported elsewhere.[3] By making use of the monatomic, diatomic, and triatomic hydrogen beams (ranging from 1 to 3μa) the proton energy may be varied continuously from 0.15 to 5.5 Mev.

The absolute proton energy scale was determined by calibrating the current supplied to the magnet with known resonances in fluorine. The three hydrogen beams available give 31 calibration points ranging from 0.3404 Mev (mass-one) to 5.524 Mev (the 1.381-Mev resonance on mass-two). The magnet was carefully recycled between runs. The 0.222-Mev resonance was too weak to be observed with the present beam intensities at low voltages. The TaF_5 target was found, by comparison of its yield with the somewhat thicker CaF_2 targets, to have a thickness much less than the natural width of any of these resonances. Deposits of carbon were noted after many hours of operation, but were not thick enough to shift the resonances by more than 0.05 percent. The 31 points are fitted with an accuracy of 0.1 percent by an equation of the form

$$E_p = aI^2 - bI^3 \qquad (2)$$

where E_p is the proton energy in Mev and I is the magnet current in amperes. However, shifts in the magnet current amounting to 0.2 percent have occurred over a three-month interval, and all energies except the

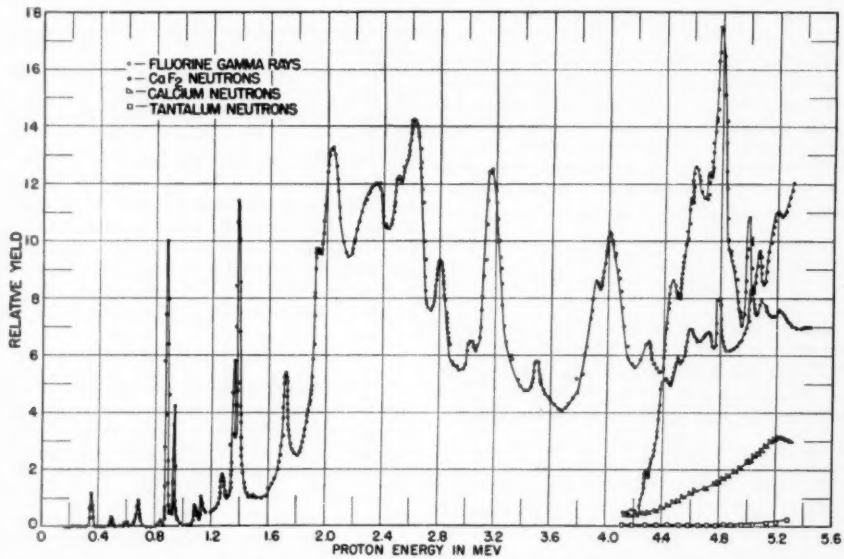

FIG. 1. Resonances in the yield of gamma-rays and neutrons (in the forward direction) from the proton bombardment of fluorine. The relative neutron background yields of calcium and tantalum are included.

[10] A. O. Hanson and J. L. McKibben, Phys. Rev. **72**, 673 (1947).
[11] T. W. Bonner and J. W. Butler, Phys. Rev. **83**, 1091 (1951).
[12] B. E. Watt, Rev. Sci. Instr. **17**, 334 (1946).

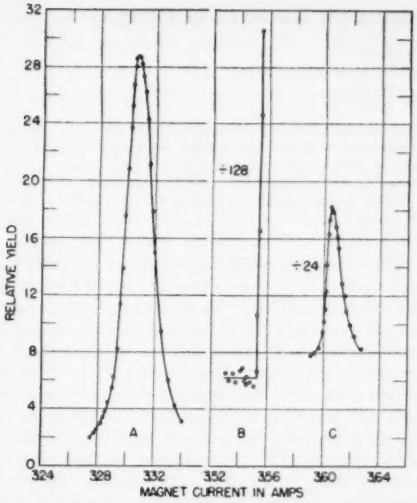

FIG. 2. Typical run for the $F^{19}(p,n)Ne^{19}$ threshold determination. *A* is the 0.9353-Mev fluorine gamma-ray resonance observed with the mass-two beam at the mass-one equivalent magnet current setting of 3.741 Mev. *B* is the mass-one beam neutron threshold. *C* is the 0.486-Mev fluorine gamma-ray resonance observed with the mass-three beam at the mass-one equivalent magnet setting of 4.374 Mev.

(p,n) threshold are reported with this accuracy relative to the resonance energies of the fluorine gamma-ray calibration points. The $F^{19}(p,n)Ne^{19}$ threshold was obtained with 0.1 percent accuracy by measurement of the 0.9353-Mev gamma-ray resonance on mass-two just below, and the 0.486-Mev resonance on mass-three just above threshold in a single magnet cycling (repeated numerous times).

III. RESULTS

Figure 1 shows the yield of gamma-rays produced by the proton bombardment of fluorine from 0.15 to 5.4 Mev, the yield of neutrons, in the forward direction, from threshold to 5.3 Mev, and the neutron backgrounds from calcium and tantalum (thick target yield). The gamma-ray background from these elements was negligible.

The gamma-ray yield below 2.1 Mev contains the known resonances with the exception of the one at 0.222 Mev which was not observed because of insufficient intensity. Above 2.1 Mev, 17 new maxima are observed at 2.32, 2.51, 2.63, 2.80, 3.02, 3.19, 3.49, 3.92, 4.00, 4.29, 4.49, 4.57, 4.71, 4.78, 4.99, 5.07, and 5.20 Mev. The experimental resolution is 0.1 percent, but the levels are so closely spaced that the resonances are not isolated, and hence an accurate assignment of their energy cannot be made. A rough analysis with a scintillation spectrometer indicates that up to 5.3 Mev most of the gamma-rays arise from reaction (1).

The neutron yield exhibits the same maxima above threshold at 4.29, 4.49, 4.57, 4.71, 4.78, 4.99, 5.07, and 5.20 Mev, and two additional ones at 4.46 and 4.62 Mev. To check that the neutron and gamma-ray maxima coincided, the yields were re-run simultaneously with the long counter at 0° and the scintillation counter at 90° with respect to the proton beam. The (p,n) threshold was determined, with an accuracy of 0.1 percent relative to the 0.9353-Mev mass-two and 0.486-Mev mass-three gamma-ray resonances, to be 4.253 Mev. A typical run is shown in Fig. 2. The $Ne^{19}-F^{19}$ mass difference obtained from this threshold is 0.00349_9 amu, taking the mass difference $(n-H^1)$ from Li, Whaling, Fowler, and Lauritsen.[13] The positron from Ne^{19} has been observed to have an end point of 2.20 Mev.[14] The maximum energy for this disintegration is calculated from the present threshold to be 2.24 Mev.

TABLE I. Resonances in the gamma-ray and neutron yields from the proton bombardment of fluorine. $E_{m\gamma}$ is the measured maximum in the gamma-ray yield. E_{mn} is the measured maximum in the neutron yield (at 0°). Γ_A and Γ_B are rough estimates of the full level widths at half-maximum in gamma-ray and neutron yields, respectively. $E_{exc}(Ne^{20})$ is the calculated excitation energy for the level in the compound nucleus (Ne^{20}).

Number	$E_{m\gamma}$ (Mev)	E_{mn} (Mev)	Γ_A (kev)	Γ_B (kev)	E_{exc} (Mev)
1	1.69	···	30	···	14.26
2	1.94	···	15	···	14.49
3	2.03	···	60	···	14.58
4	2.32	···	85	···	14.85
5	2.51	···	30	···	15.04
6	2.63	···	90	···	15.15
7	2.80	···	60	···	15.31
8	3.02	···	30	···	15.53
9	3.19	···	80	···	15.68
10	3.49	···	40	···	15.97
11	3.92	···	30	···	16.38
12	4.00	···	110	···	16.45
13	4.29	4.29	50	45	16.73
14	···	4.46	···	80	16.89
15	4.49	4.49	30	20	16.92
16	4.57	4.57	30	20	16.99
17	···	4.62	···	60	17.04
18	4.71	4.71	30	25	17.13
19	4.78	4.78	35	45	17.19
20	4.99	4.99	20	20	17.39
21	5.07	5.07	35	30	17.47
22	5.20	5.20	70	70	17.59

Table I summarizes the resonances observed in the gamma-ray and neutron yields, their estimated level widths, and the excitation energies in the compound nucleus Ne^{20}, calculated from

$$E_{exc}=[12.646+(19.0044/20.0126)E_m]\text{ Mev}. \quad (3)$$

The proton binding energy 12.646 Mev was obtained from the mass values of Mattauch and Flammersfeld.[15]

It is a pleasure to acknowledge the efforts of the staff of the High Voltage Engineering Corporation who constructed the very fine accelerator used in these experiments. Thanks are also due to W. T. Newton, W. W. Werner, and A. J. Hamilton for their assistance in maintaining and operating the machine and allied experimental equipment.

[13] Li, Whaling, Fowler, and Lauritsen, Phys. Rev. **83**, 512 (1951).
[14] White, Delsasso, Fox, and Creutz, Phys. Rev. **56**, 512 (1939).
[15] J. Mattauch and A. Flammersfeld, Z. Naturforsch. (special edition) 1949.

The Hypothesis of Charge Independence for Nuclear Phenomena

KENNETH M. WATSON
Physics Department, Indiana University, Bloomington, Indiana
(Received November 29, 1951)

The hypothesis of charge independence for nuclear phenomena is a symmetry condition which leads to nontrivial relationships to be satisfied by an extensive class of meson-nucleon interactions. Application of the principle to meson production by nucleon collisions and by photons and to meson scattering leads to a number of sensitive tests of the hypothesis. No contradictions are found from the present rather limited experimental data. Extension of the principle to heavy unstable particles (such as V-particles) is discussed.

I. INTRODUCTION

THE equivalence of the nuclear forces between two protons, two neutrons or a proton and neutron as suggested by low energy scattering experiments and the binding energies of light nuclei raises the question whether this may reflect some general symmetry principle in nature.[1] Such a principle should presumably be extended to include not only the phenomena involving just nucleons, but also to those involving other particles whose existence is related to nuclear forces (supposedly π-mesons, for instance). This hypothetical symmetry principle has been called the hypothesis of charge independence.

As is well known, the formal expression for the charge independence of nuclear forces is that the interaction energy V[2] between any two nucleons be a function of $\boldsymbol{\tau}^{(a)}\cdot\boldsymbol{\tau}^{(b)}$, where the $\boldsymbol{\tau}$'s are the isotopic spin operators of the respective nucleons "a" and "b". That is,

$$V=f(\boldsymbol{\tau}^{(a)}\cdot\boldsymbol{\tau}^{(b)}). \tag{1}$$

Equation (1) is equivalent to invariance with respect to rotations in the space of the τ-operators. The rotations through an infinitesimal angle ϵ in this space are effected by the operator

$$R_a=1+\tfrac{1}{2}i\epsilon\sum_{n=1}^{N}\hat{a}\cdot\boldsymbol{\tau}, \tag{2}$$

where $\hat{a}$ is the axis of the rotation and the summation is carried over interacting nucleons.

The physical content of this hypothesis is that neutrons and protons represent different states of the same particle and have identical properties (obvious limitations to this will be discussed below). Indeed, any unitary transformation which introduces a linear combination of these states will also represent a state with identical properties.

It seems highly probable that π-mesons contribute to the nuclear forces, so it is quite natural to attempt to extend this hypothesis to phenomena involving π-mesons. The physical content here is that the three charge states of π-mesons, i.e., positive, negative, and neutral, have identical physical properties (again there are, of course, some obvious limitations).

When we consider such processes as the production and absorption of mesons by nucleons, it is clear that the result of applying the transformation (2) to the nucleon variables must induce a unitary transformation on the meson field variables if the physical properties are to be unchanged. That is, a particle which is a proton after the transformation was a mixture of neutron and proton states before the transformation, and the mesons which it can emit will be a linear combination of the mesons which were emitted by the proton and neutron states before the transformation. This transformation is a three-dimensional representation of the three-dimensional rotation group, since there are three types of mesons. It is further irreducible: it cannot consist of three one-dimensional representations, since the mixing of states actually does occur; it cannot consist of a two-dimensional and a one-dimensional representation, since then it would not be possible to describe the emission of a meson by a single nucleon in an invariant manner. Therefore, the representation is irreducible.

Because of this, we can choose a representation such that the meson wave functions ω_i (corresponding to a meson of type "i" with $i=1, 2, 3$) transform as the components of a vector. We can relate the indices "i" to those for positive, negative, and neutral mesons by considering such elementary processes as the emission of a meson by a single nucleon. Consider

$$(i,\rho|M|\sigma),$$

the matrix element for the emission of a meson of type "i" by a nucleon which makes a transition from an isotopic spin state σ to a state ρ. Since "i" is taken to be a vector index, we can write M as the vector $\mathbf{M}$. Then, as argued above, if the transformation (2) is to induce a vector transformation on $\mathbf{M}$, we must have

$$R_a\mathbf{M}R_a^{-1}=\mathbf{M}+\tfrac{1}{2}i\epsilon[\hat{a}\cdot\boldsymbol{\tau},\mathbf{M}]=\mathbf{M}+\epsilon\hat{a}\times\mathbf{M}, \tag{3}$$

or

$$\hat{a}\times\mathbf{M}=\tfrac{1}{2}i[\hat{a}\cdot\boldsymbol{\tau},\mathbf{M}]. \tag{4}$$

This is the commutation rule for $\boldsymbol{\tau}$ itself, so $\mathbf{M}$ is proportional to $\boldsymbol{\tau}$. Choosing τ_3 diagonal with eigenvalue plus one when operating on a neutron state, it follows that the created meson for the transition from a proton to a neutron state will have the wave function

$$\omega(1^+)=(1/\sqrt{2})(\omega_1-i\omega_2). \tag{5}$$

[1] G. Breit and E. Feenberg, Phys. Rev. **50**, 850 (1936).
[2] More generally, this condition should be imposed on the phase shifts of the partial waves involved in the scattering.

This is to be interpreted as a positive meson and relates its state to the vector representation ω_i $(i=1, 2, 3)$. Similarly,

$$\omega(1^-)=-(1/\sqrt{2})(\omega_1+i\omega_2), \quad \text{and} \quad \omega(1^0)=\omega_3 \qquad (6)$$

represent the states of negative and neutral mesons, respectively.[3]

This completes the formal development of the symmetry hypothesis as applied to π-mesons. However, to obtain a convenient mechanism for constructing the rotation operators, we introduce meson creation and absorption operators U_i^+, U_j $(i, j=1, 2, 3)$ which satisfy the commutation rules

$$[U_i, U_j^+]=\delta_{ij}, \qquad (7)$$

(other combinations commuting) and which transform like vectors in charge space.

We next define the quantity

$$\mathbf{l}=i\mathbf{U}\times\mathbf{U}^+ \qquad (8)$$

(using vector notation) in terms of which we can express the rotation operator for the ω_i's (or the U_i's) as

$$R_\alpha=1+i\epsilon\hat{\alpha}\cdot\mathbf{l}. \qquad (2')$$

If we are interested in a system with several nucleons and several mesons (in different quantum states), we assign to the kth nucleon the variables $\boldsymbol{\tau}^{(k)}$ and to the nth meson the variables $\mathbf{U}^{(n)}$, $\mathbf{U}^{+(n)}$. Thus

$$\mathbf{T}=\tfrac{1}{2}\sum_k \boldsymbol{\tau}^{(k)}, \quad \mathbf{L}=\sum_n i\mathbf{U}^{(n)}\times\mathbf{U}^{+(n)} \qquad (9)$$

play roles analogous to spin and orbital angular momentum operators, respectively (they of course satisfy the corresponding commutation rules).

Furthermore,

$$\mathbf{J}=\mathbf{T}+\mathbf{L} \qquad (10)$$

has the properties of a total angular momentum. We can therefore speak of the isotopic spin, the isotopic angular momentum, and the total isotopic angular momentum of a system. The total charge of the system containing N nucleons is given in units of the charge on a proton by the eigenvalue of

$$Q=\tfrac{1}{2}N-J_3. \qquad (11)$$

The charge independence hypothesis implies the invariance of physical quantities with respect to the rotation $R_\alpha=1+i\epsilon\hat{\alpha}\cdot\mathbf{J}$, or the conservation of total isotopic angular momentum. These properties are, of course, familiar from Kemmer's charge symmetric meson theory;[4] however, the symmetry principle has here been developed in a general way independent of specific meson theories.

As was stated above, the charge independence hypothesis is obviously not satisfied exactly in nature. If it were, there would be no electromagnetic interactions, for instance, and thus no means of determining the charge of a particle. The validity of the hypothesis can be only approximate, therefore, and it can be applied only to phenomena in which electromagnetic effects are small—or else occur in a simple manner.

For instance, if the matrix element of some operator M (not primarily of an electromagnetic nature) can be expanded in powers of the electronic charge, e, we would have

$$M=M_0+(e^2/\hbar c)M_1+(e^2/\hbar c)^2M_2+\cdots. \qquad (12)$$

In this case we might reasonably expect to apply the charge-independence condition to M_0, i.e.,

$$[\mathbf{J}, M_0]=0. \qquad (13)$$

For a large class of nuclear phenomena this should be a satisfactory approximation to $[\mathbf{J}, M]=0$.

Again, even for some processes which do directly involve electromagnetic interactions, the symmetry restrictions may be useful. Consider

$$M'=[e/(\hbar c)^{\frac{1}{2}}][M_1'+(e^2/\hbar c)M_2'+\cdots]. \qquad (14)$$

If it happens that M_1' is the matrix element of an electromagnetic interaction whose rotation properties in charge space are known, then the quantity $[\mathbf{J}, M_1']$ will be known and can be used to establish certain restrictions on M_1'.

There may be further limitations on the validity of the charge independence hypothesis. To illustrate such a possible limitation, let us suppose that nuclear forces are due to π- and τ-mesons and further that the π-meson field, but not the τ-meson field, satisfies the charge independence hypothesis. It might then be not unreasonable to think that low energy nuclear events would be due mostly to the π-meson field and would consequently exhibit charge independence, while higher energy events would depend upon both types of fields and would no longer show this symmetry property.

It must, indeed, be admitted that there is no very convincing evidence in favor of charge independence—but there is also no convincing evidence that it does not have an approximate validity. Because of its intuitive appeal and because of the importance of recognizing general symmetry properties of nature, it seems worthwhile to investigate in detail some of the consequences of this hypothesis in an attempt to find what range of validity that it may have.

The implications drawn from high energy nucleon-nucleon scattering[5] have been extensively discussed in the literature.[6] The results seem inconclusive at present and will not be pursued here.

As recently discussed,[7] the charge independence hypothesis places stringent restrictions on the differ-

[3] The phase of $\omega(1^-)$ is chosen in accordance with the customary notation for the spherical harmonics. The results (5) and (6) would have been obtained directly from an equation of the type (3) if we had chosen a spherical harmonic (rather than a vector) representation for M.

[4] N. Kemmer, Proc. Cambridge Phil. Soc. **34**, 354 (1938).

[5] See, for instance, Chamberlain, Segrè, and Wiegand, Phys. Rev. **81**, 284 (1951); and **83**, 923 (1951) for further references.

[6] R. Jastrow, Phys. Rev. **81**, 165 (1951). K. M. Case and A. Pais, Phys. Rev. **80**, 203 (1950).

[7] K. M. Watson and K. A. Brueckner, Phys. Rev. **83**, 1 (1951).

ential cross sections for meson production in nucleon-nucleon collisions. No disagreement with experiment was found, but the experimental data are too limited at present to impose a severe test of the theory.

In what follows, we shall consider further consequences of the hypothesis. The condition of invariance is conservation of the "isotopic angular momentum" **J**, except for processes of the form (14) where special considerations are involved.

II. MULTIPLE MESON PRODUCTION

Fermi[8] has proposed a theory of multiple meson production by very high energy nucleon collisions in which it is supposed that the produced mesons reach thermal equilibrium within a certain volume of space during the collision process. One of the conclusions reached was that there should be approximately equal numbers of positive, negative, and neutral mesons produced.

This result is in agreement with observations by Carlson, Hooper, and King[9] of high energy nuclear events in photographic plates. Denoting the average number of positive, negative, and neutral mesons by $\bar{N}^+$, $\bar{N}^-$, and $\bar{N}^0$, respectively, these observers found

$$\bar{N}^0/(\bar{N}^+ + \bar{N}^-) = 0.45 \pm 0.10. \tag{15}$$

Since the charge independence hypothesis imposes a constraint on the manner in which mesons may be produced, it is of interest to see if this will modify Fermi's conclusions. That such will not happen follows from Fermi's arguments with respect to conservation of ordinary angular momentum. There only the Z-component of angular momentum entered into the theory, due to the vanishing of the average values of the other components. For the isotopic angular momentum, only the "3" component enters—or charge conservation—so nothing new is obtained by imposing charge independence.

However, it is of some interest that the result (15) can be understood on the basis of charge independence alone.[10] For the production of N mesons in the collision of two nucleons the isotopic angular momentum eigenvalue, j, must be either zero or one, corresponding to whether the nucleons were initially in a singlet or triplet isotopic spin state. From Eqs. (5) and (6) we see that each meson carries an isotopic angular momentum of unity; i.e., the meson wave functions transform as the spherical harmonics of order one:

$$\omega(1^-) \rightarrow Y_1^{+1}, \quad \omega(1^0) \rightarrow Y_1^0, \quad \omega(1^+) \rightarrow Y_1^{-1}. \tag{16}$$

Charge independence then implies that the resultant j value for the final two nucleons and the N mesons be zero or one, depending on the initial state. This restriction does not seem extremely severe due to the large number of $j=0$ and 1 representations possible when N is large. (For six mesons, for instance, there are 34 representations with $L=1$.) We shall therefore seek properties which are independent of the representation.

For the ith meson we introduce the operators (Eq. (8))

$$\begin{aligned} n_i^+ &= \tfrac{1}{2}[-l_3^{(i)} + (l_3^{(i)})^2], \\ n_i^0 &= \tfrac{1}{2}\mathbf{l}^{(i)} \cdot \mathbf{l}^{(i)} - (l_3^{(i)})^2, \\ n_i^- &= \tfrac{1}{2}[l_3^{(i)} + (l_3^{(i)})^2]. \end{aligned} \tag{17}$$

n_i^+ operating on the wave function of the ith meson has the eigenvalue unity if the meson is positive, but otherwise the eigenvalue zero. n_i^0 and n_i^- have similar properties with respect to neutral and negative mesons.

We now consider states for which N mesons have been produced, Ψ_j^m, having total isotopic angular momentum j and eigenvalue m for J_3. We shall not for the moment impose the condition that $j=0$, 1.

The following theorem will prove useful.[11] Let $T_{j'}^{\sigma}$ be an operator transforming according to an irreducible representation of dimension $(2j'+1)$ of the three-dimensional rotation group. Then

$$\sum_{m=-j}^{+j} (\Psi_j^m, T_{j'}^{\sigma} \Psi_j^m) = 0 \tag{18}$$

unless $j'=0$ and thus $T_{j'}^{\sigma}$ is a scalar. Now l_3 does not contain a scalar and l_3^2 contains the scalar $\frac{1}{3}I^2$. I^2 operating on Ψ_j^m has the eigenvalue 2, so we have

$$\bar{n}_i^+ \equiv \frac{1}{2j+1} \sum_{m=-j}^{+j} (\Psi_j^m, n_i^+ \Psi_j^m) = \tfrac{1}{3} = \bar{n}_i^0 = \bar{n}_i^-. \tag{19}$$

Defining

$$N^+ = \sum_{i=1}^{N} n_i^+,$$

etc., we then obtain

$$\bar{N}^+ = \sum_{i=1}^{N} \bar{n}_i^+ = \frac{N}{3} = \bar{N}^- = \bar{N}^0 \tag{20}$$

for the respective average number of positive, negative, and neutral mesons present, when the average is carried over m.

Letting $N(\pm) \equiv N^+ + N^-$, and applying Eq. (18), we obtain, for $j=1$,

$$\sum_{m=-1}^{+1} (\Psi_1^m, N(\pm) J_3 \Psi_1^m) = \bar{N}(\pm)_{m=+1} - \bar{N}(\pm)_{m=-1} = 0, \tag{21}$$

where $\bar{N}(\pm)_{m=+1}$ is the expectation value of $N(\pm)$ for $m=+1$, etc. Similarly, we have

$$\bar{N}_{m=+1}{}^0 = \bar{N}_{m=-1}{}^0. \tag{22}$$

[8] E. Fermi, Prog. Theor. Phys. **5**, 570 (1950); and Phys. Rev. **81**, 683 (1951).

[9] Carlson, Hooper, and King, Phil. Mag. **41**, 701 (1950).

[10] The author is indebted to Dr. A. Pais for the original suggestion that charge independence might lead to a restriction on the relative numbers of charged and neutral mesons created in multiple production events.

[11] See, for example, E. Wigner, *Gruppentheorie* (Edwards Brother, Inc., Ann Arbor, 1944), p. 263, from which the theorem can be immediately deduced.

If $j=0$, then Eq. (20) states that the collision will lead on the average to equal numbers of positive, negative, and neutral mesons.

For $j=1$, we argue as follows: Let us suppose the incident particle to be a proton (the argument is unchanged if it is a neutron) impinging on a nucleus, and make the simplifying assumption that the nucleus contains equal numbers of protons and neutrons. Then a proton-proton collision ($j=1$) will be twice as probable as an isotopic triplet proton-neutron collision since by the charge independence hypothesis the cross sections are equal, but the latter involves just one-half the incoming neutron-proton states. For the sum $N(\pm)=N^+ + N^-$ and for N^0 we can treat one-half the proton-proton collisions as if they had been neutron-neutron collisions, however, by Eqs. (21) and (22). This is equivalent to an average over azimuthal states m as was done in Eq. (19).

Then for either a $j=0$ or 1 state, we have*

$$\bar{N}^0/(\bar{N}^+ + \bar{N}^-) = \tfrac{1}{2}.$$

III. MESON SCATTERING

The consequences of the charge independence hypothesis for meson scattering have been developed by Heitler.[12] We shall quote them, however, since meson scattering has recently become feasible experimentally.

We follow Heitler's notation and designate the matrix element for the process $n+\pi^+ \rightarrow p+\pi^0$ (n means a neutron; p, a proton) by (n_+p_0), etc. Then Heitler obtained the following relations

$$\begin{aligned} &(n_+p_0)=(p_0n_+)=(p_-n_0)=(n_0p_-),\\ &(p_+p_+)=(n_-n_-),\\ &(n_+n_+)=(p_-p_-),\\ &(n_0n_0)=(p_0p_0). \end{aligned} \tag{23}$$

These are fairly obvious. Heitler's further relations are less so:

$$\begin{aligned} (p_0p_0)&=\tfrac{1}{2}[(p_+p_+)+(p_-p_-)],\\ (1/\sqrt{2})(p_-n_0)&=\tfrac{1}{2}[(p_+p_+)-(p_-p_-)]. \end{aligned} \tag{24}$$

From Eqs. (24) Heitler obtained a relation between the cross sections:

$$\tfrac{1}{2}d\sigma(p_-n_0)+d\sigma(p_0p_0)=\tfrac{1}{2}[d\sigma(p_+p_+)+d\sigma(p_-p_-)]. \tag{25}$$

This expression is not very useful because of the experimental difficulties involved in the measurement of $d\sigma(p_0p_0)$. However, the second of Eqs. (24) may lead to a test of the hypothesis if at certain energies and angles it turns out that the charge exchange scattering cross section is much less than that for the simple scattering. Then $(p_-n_0)\simeq 0$, and it follows that at these angles and energies

$$d\sigma(p_+p_+)\simeq d\sigma(p_-p_-). \tag{26}$$

A further test of the hypothesis should be obtained from the scattering of π^+ and π^- mesons by deuterons. Here the cross sections for π^+ and π^- mesons, except for Coulomb effects, should be equal. The scattering by deuterons should also lead to a knowledge of the relative phases of the matrix elements (p_+p_+) and (n_+n_+)[13]—and consequently (p_-p_-) by Eqs. (23). By the use of the second of Eqs. (24), the exchange scattering cross section can then be predicted. Furthermore, the relative magnitudes of the absorption cross sections for positive and negative mesons on protons and deuterons are also restricted by the charge independence principle.[14]

IV. PHOTOMESON PRODUCTION

For photomeson production the transition matrix element is of the type (14). This is not of the form of an invariant with respect to rotations in charge space, so our conclusions will be somewhat more dependent upon the model assumed. Because of the smallness of the electronic charge, we may keep only the first term in Eq. (14). It seems highly reasonable to expect this to be of the form

$$M'=(\Psi_{j'}{}^{m'}, H'\Psi_j{}^m), \tag{27}$$

where (by our hypothesis) the Ψ's are eigenstates of a charge invariant nucleonic-mesonic system and

$$H'=-\int \mathbf{j}\cdot\mathbf{A}d^3x. \tag{28}$$

Here $\mathbf{j}$ is the current density of the charged particles present (real or virtual) and $\mathbf{A}$ is the vector potential of the electromagnetic field.

In meson theories the meson current density vector, $\mathbf{j}_\mu$, arises in connection with the concept of invariance with respect to gauge transformations (i.e., rotations about the "3" axis in charge space). In the Kemmer[4] charge symmetric theory, invariance with respect to rotations about the "1" and "2" axes also leads to two additional current vectors, each satisfying the usual conservation law. These three current vectors transform among themselves as the components of a vector in charge space. In particular, the physically significant current occurring in Eq. (28) is the "3" component of this vector. For example, in pseudoscalar meson theory with pseudovector coupling, one has

$$\mathbf{j}_\mu/e=(\varphi_2\nabla\varphi_1-\varphi_1\nabla\varphi_2)+(f/\kappa)(\varphi_2\tau_1-\varphi_1\tau_2)\boldsymbol{\sigma} \tag{29}$$

where $\boldsymbol{\sigma}$ is the nucleon spin, f the coupling constant, κ^{-1} the meson Compton wavelength, and φ_1, φ_2 the charged meson field variables in a Kemmer[4] repre-

* The generality of the above arguments should be noted. The number of mesons produced in a single collision was not specified to be large or small. π-mesons need not be the only particles produced in the collision; that is, the wave function $\psi_j{}^m$ can also contain other particles carrying an arbitrary isotopic spin (such as K-mesons), if the production of these other particles is consistent with charge independence. Finally, the π's need not have been produced directly in the collision, but can be the decay products of intermediate particles (again as long as these do not violate charge independence).

[12] W. Heitler, Proc. Roy. Irish Acad. **51**, 33 (1946).

[13] Fernbach, Green, and Watson, Phys. Rev. **84**, 1084 (1951).

[14] K. A. Brueckner has made an extensive analysis of these relationships for the various meson scattering cross sections (to be published).

sentation. The nucleonic current density is

$$\mathbf{j}_N/e=\tfrac{1}{2}(1-\tau_3)\boldsymbol{\alpha} \tag{30}$$

where $\boldsymbol{\alpha}$ is the Dirac matrix. In theories for which the nucleon is treated relativistically the transformation properties in charge space of Eqs. (29) and (30) are unchanged.

We shall investigate the consequences for Eq. (27) of current vectors having the transformation properties of Eqs. (29) and (30). It may be that the rotation properties of these operators are more general than the specific types of theories which have been so far developed.

If it be thought that the anomalous nucleon magnetic moments do not arise entirely from the π-meson field, one might add to H' in Eq. (27) the expression

$$H''=-\boldsymbol{\mu}\cdot\mathbf{H} \tag{31}$$

where $\mathbf{H}$ is the magnetic field and $\boldsymbol{\mu}$ is

$$\boldsymbol{\mu}_p(1-\tau_3)/2+\boldsymbol{\mu}_n(1+\tau_3)/2. \tag{32}$$

$\boldsymbol{\mu}_p$ and $\boldsymbol{\mu}_n$ are anomalous magnetic moments for the proton and neutron, respectively.

In any case, we see that H', or $H'+H''$, can be decomposed into the sum of two terms, V_3 and S, which rotate in charge space respectively as the "3" component of a vector and as a scalar: i.e., we have

$$V_3+S \tag{33}$$

for the form of the interaction.

It is interesting that if we were to consider only the mesonic current, $\mathbf{j}_\mu$, as contributing appreciably to photomeson production, then the interaction would be of the simple type

$$V_3. \tag{33'}$$

For photomeson production, the initial nucleon state (i.e., nucleon plus meson field in an eigenstate) will be $j=\frac{1}{2}$, $m=\pm\frac{1}{2}$. The final state will consist of a meson and a nucleon plus mesonic self-field and can be a $j'=\frac{3}{2}$, or $\frac{1}{2}$ state, with the appropriate m' values [see Eq. (27)]. We thus have[15]

$$(\tfrac{1}{2}, m'\,|\,V_3\,|\,\tfrac{1}{2}, m)=\delta_{mm'}T_1m \tag{34}$$

and

$$(\tfrac{3}{2}, m'\,|\,V_3\,|\,\tfrac{1}{2}, m)=\delta_{mm'}T_2[(\tfrac{3}{2})^2-m^2]^{\frac{1}{2}}, \tag{35}$$

where T_1 and T_2 depend upon other variables. For S, in Eq. (33), we have

$$(j', m'\,|\,S\,|\,j, m)=\delta_{jj'}\delta_{mm'}S_0, \tag{36}$$

where S_0 depends upon other variables.

We relate eigenstates of charge for the individual particles to the j, m representation by the usual vector addition formulas, such as

$$(n, 1^0)=(1/\sqrt{3})[\sqrt{2}\Psi_{\frac{3}{2}}{}^1-\Psi_{\frac{1}{2}}{}^1],$$

where $(n, 1^0)$ means a state containing a neutron and a neutral meson, etc.

If we make the assumption (33') that only the meson current contributes to meson production, we obtain the rather obvious relations between the differential cross sections,

$$\begin{aligned} d\sigma[n\to p+\pi^-]&=d\sigma[p\to n+\pi^+],\\ d\sigma[n\to n+\pi^0]&=d\sigma[p\to p+\pi^0]. \end{aligned} \tag{37}$$

This is not satisfied by experimental cross sections[16] so we conclude that we must also include nucleon current interactions—a result which is not surprising.

Including nucleon current interactions, and introducing the abbreviations,

$$A\equiv(1/\sqrt{3})(2T_2-\tfrac{1}{2}T_1),\quad B\equiv(1/\sqrt{3})[\sqrt{2}T_2+(1/\sqrt{2})T_1],$$
$$S_0'\equiv(1/\sqrt{3})S_0,$$

we obtain the following relations between the matrix elements for photomeson production:

$$\begin{aligned} M'(n\to n+\pi^0)&=A-S_0',\\ M'(p\to p+\pi^0)&=A+S_0',\\ M'(n\to p+\pi^-)&=B+\sqrt{2}S_0',\\ M'(p\to n+\pi^+)&=B-\sqrt{2}S_0'. \end{aligned} \tag{38}$$

The four matrix elements are expressed in terms of three parameters so are not independent. The relations between the cross sections are considerably more complicated, however, since the quantities A, B, and S_0' are in general complex.

There are several possible ways to obtain information which may enable one to test the relations (38). One might measure the photoproduction cross sections in deuterium in order to obtain information on the relative phases of A and S_0'.

Again, it is known that the cross section $d\sigma[p\to p+\pi^0]$ is much smaller than the charged meson cross sections near threshold.[17] If it should also turn out that

$$d\sigma[n\to n+\pi^0]$$

is similarly small near threshold, one could conclude that at such energies $A\simeq S_0'\simeq 0$. This would imply that the π^-/π^+ ratio,

$$|B+\sqrt{2}S_0'|^2/|B-\sqrt{2}S_0'|^2, \tag{39}$$

is nearly unity at these energies.

If a certain set of energies and angles of emission are known to correspond to a π^-/π^+ ratio of unity, then either S_0' is zero or there is no interference in the cross section between S_0' and B. In the former case, we would have $d\sigma[n\to n+\pi^0]=d\sigma[p\to p+\pi^0]$. Conversely, the equality of the latter cross section at certain energies and angles plus knowledge of the phases of A and S_0' from the photoproduction in deuterium should enable one to predict those values of energy and angle for which the π^-/π^+ ratio is unity.

V. NUCLEON MAGNETIC MOMENTS

If π-mesons are assumed responsible for the anomalous magnetic moments of nucleons, the question arises as to whether the charge independence condition gives any restrictions on these. The magnetic moment

[15] E. U. Condon and G. H. Shortley, *Theory of Atomic Spectra* (Macmillan Company, New York, 1935), p. 63.

[16] McMillan, Peterson, and White, Science **110**, 579 (1949).

[17] J. S. Steller and W. K. H. Panofsky, Phys. Rev. **81**, 649 (1951).

operator is

$$\mathbf{M}=\tfrac{1}{2}e\int \mathbf{x}\times\mathbf{j}d^3x \tag{40}$$

where $\mathbf{j}$ is the current operator considered in the previous section. We see that in charge space $\mathbf{M}$ is of the form (33), i.e.,

$$V_3+S. \tag{33''}$$

The expectation value of M_Z gives the proton and neutron magnetic moments:

$$M(\text{proton})=\tfrac{1}{2}T_1+S_0,\quad M(\text{neutron})=-\tfrac{1}{2}T_1+S_0, \tag{41}$$

where T_1 and S_0 are given essentially by Eqs. (34) and (36). (They, are not, of course, the same as the T_1 and S_0 of Sec. IV.)

This does not therefore impose any restriction on the magnetic moments. If, on the other hand, we had assumed that only the meson current, $\mathbf{j}_\mu$, were responsible for the anomalous moments, we would have found that the anomalous magnetic moments of the neutron and proton were equal in magnitude and opposite in sign—a conclusion analogous to that of Eq. (37).

VI. UNSTABLE HEAVY PARTICLES

Although the decay schemes for V-particles and τ- and κ-mesons are far from unambiguously known, it is of interest to see what restrictions charge independence would place on these particles according to some of the hypothetical decay schemes.

It is to be noted that the charge independence of the other processes considered in this paper does not necessarily imply such a restriction for these new particles, for there may be different mechanisms involved than just π-meson—nucleon interactions. However, if some of these particles decay only into π-mesons, or into π-mesons and nucleons, it is not unreasonable to investigate here also the consequences of the charge independence hypothesis. This would seem to be especially pertinent if the V-particle is considered to be an excited state of the π-meson field about a nucleon.

Let us suppose that the V^0 particle decays into a proton and a π^- meson. Then we might have charge states corresponding to $j=\frac{1}{2}$ or $\frac{3}{2}$. In the former case there would be V^0 and V^+ particles, but no V^- particles. In the latter case, there would be particles with charges $(-|e|, 0, +|e|, +2|e|)$. If the decay is into two π-mesons and a nucleon, then we might expect $j=\frac{1}{2}, \frac{3}{2}$, or $5/2$ with a corresponding number of charge states. Conservation of j implies that particles in the $j=5/2$ state could not be produced singly in a nucleon-nucleon collision. We note that it is not possible to obtain just a single V-particle (for instance, with neutral charge). There must be an even number of such particles. (The asymmetry in charge would be removed, if it be supposed that there are negative protons, however.)

If the τ-meson decays into three π-mesons, we can have $j=3$, 2, 1, or 0. There will always be an odd number of such particles, symmetric in positive and negative charges, and always including a neutral particle.

Knowledge of the decay schemes and the assumption of a value of j for these particles should also enable one to make predictions concerning their relative abundances and the relative rates of competing decay mechanisms.

VII. THE LESS RESTRICTIVE CHARGE SYMMETRY CONDITION

Invariance with respect to rotations about the "3" axis in charge space implies just charge conservation and is consequently expected to be a characteristic of any theory. However, the meson theories which have been used possess another symmetry condition—i.e., invariance with respect to an interchange in the definition of neutron and proton states when a corresponding interchange is made with respect to positive and negative mesons. This is a weaker condition than is that given by charge independence and has been called charge symmetry. Integration of the differential rotation (2) shows that the charge symmetry condition corresponds to invariance with respect to a rotation of 180° about either the "1" or "2" axis in charge space (except for phase factors) and consequently does not impose new conditions on the charge independence principle.

The consequences of the charge symmetry principle are fairly obvious. It implies the equality of the neutron-neutron force and the proton-proton force (but not of these to the neutron-proton force) and the relations (23), for instance.

VIII. CONCLUSIONS

The physical basis of the charge independence hypothesis is seen to rest essentially on the assumption that neutrons and protons have very similar properties. From this it extends itself to particles interacting with nucleons, to particles interacting with these additional particles, and so on, until it is finally violated (witness the electromagnetic interactions). It is not quite satisfying to find so far-reaching a symmetry principle with only an approximate validity, which leads one to expect possibly that the present analysis is only an approximate formulation of a more comprehensive and rigorous set of symmetry operations involving quite general classifications of elementary particles and their interactions.

In this connection it would seem that one must refrain from trying to draw very stringent restrictions on natural phenomena (such as rigorous selection rules for the decay of particles, etc.) from charge independence as now formulated. For instance, the mass of the neutral π-meson is about 3 percent less than that of the charged π-mesons.

The author is indebted to Professor K. A. Brueckner for several very stimulating discussions concerning this paper.

Decay of Te^{125m} *

J. C. Bowe† and P. Axel
Department of Physics, University of Illinois, Urbana, Illinois

(Received November 12, 1951)

The two-step isomeric transition in Te^{125m} has been studied with proportional counters in coincidence, a NaI crystal scintillation spectrometer and a thin lens beta-ray spectrometer. The following branching fractions were determined: 110-kev transition: K conversion $=0.54\pm0.01$, other conversion $=0.46$, unconverted gamma-ray $=0.0034\pm0.0005$; 35.5-kev transition: K conversion $=0.80\pm0.05$, L conversion $=0.11\pm0.02$, M conversion $=0.02\pm0.004$, unconverted gamma-ray $=0.07\pm0.02$.

These data are shown to confirm completely the level assignments in Te^{125} as $s_{1/2}$, $d_{3/2}$, and $h_{11/2}$. In addition, comparison with theoretical conversion coefficients show an agreement between experiment and extrapolated theoretical values. The second transition (35.5 kev) is almost entirely magnetic dipole; an upper limit of about 1 percent can be placed on the electric quadrupole admixture.

INTRODUCTION

THE 58-day isomer,[1] Te^{125m}, decays by two successive transitions. The first radiation emitted is a highly converted 109.7-kev gamma-ray.[2] The second transition has an energy of 35.5 kev[3] and follows the 110-kev transition with a delay of less than 4×10^{-9} sec.[4]

This paper reports the relative amounts of conversion electrons and unconverted gamma-rays for each of these transitions. The quantitative results are included in the decay scheme shown in Fig. 1. The different experimental techniques which were used to determine the branching ratios, are summarized in the following two paragraphs.

Two measurements were made to study the 110-kev gamma-rays: (1) A NaI crystal scintillation spectrometer was used to find the ratio of the number of unconverted 110-kev gamma-rays to the total number of K x-rays. (2) The fraction of 110-kev transitions which emits K conversion electrons was found by observing the electron spectrum both in a proportional counter and in a thin lens beta-ray spectrometer.

Three measurements were used to establish the branching of the 35.5-kev transition: (1) The fraction of these transitions that are K converted was determined from x-x and x-35.5-kev gamma-coincidence data. The coincidences were measured by using two proportional counters as detectors. (2) The numbers of L and M conversion electrons were found from the electron spectrum taken with the lens spectrometer. (3) The number of unconverted 35.5-kev gamma-rays was derived from the photon spectrum taken with a proportional counter.

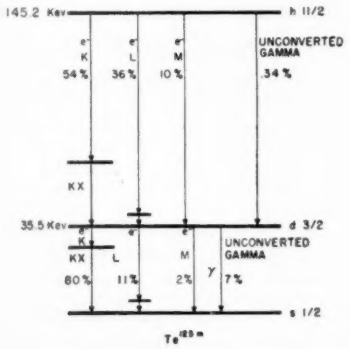

FIG. 1. Decay scheme of Te^{125m}.

SOURCE AND EQUIPMENT

The Te^{125m} was provided by the Isotopes Division of the Atomic Energy Commission at Oak Ridge. The Te had been chemically separated from Sb^{125} and was shipped in solution. Despite this, it was not possible to obtain very thin sources since there was a considerable amount of inactive material present when the solution was evaporated.

The scintillation spectrometer consisted of a 16-mm thick NaI crystal and an RCA 5819 phototube. The pulses from the phototube were amplified linearly and then analyzed with a single channel, pulse-height selector. This selector used two vacuum diodes as discriminators and a 6AS6 for an anticoincidence tube. The noise from both the phototube and the amplifier was negligible above 6 kev.

The double thin lens beta-ray spectrometer had a resolution of about 2.2 percent and a transmission of about 1 percent. A Geiger-counter detector was used with amyl acetate vapor filling; Nylon windows of 50 and 150 mg/cm² were used.

Two identical proportional counters were made from 6-inch diameter brass tubing. A 175 mg/cm² circular beryllium window 1 inch in diameter permitted photons

* Assisted by the joint program of the ONR and AEC.

† Now at Argonne National Laboratory, Chicago, Illinois. The material contained in this paper was submitted in partial fulfillment of the requirements for the degree of Doctor of Philosophy.

[1] Friedlander, Goldhaber, and Scharff-Goldhaber, Phys. Rev. **74**, 981 (1948).

[2] Hill, Scharff-Goldhaber, and Friedlander, Phys. Rev. **75**, 324 (1949).

[3] R. D. Hill, Phys. Rev. **76**, 333 (1949).

[4] F. K. McGowan, Oak Ridge National Laboratory Report 952, unpublished.

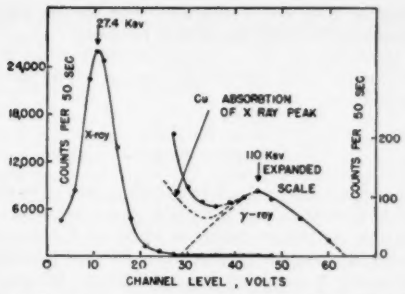

FIG. 2. Photon spectrum, NaI crystal detector. Expanded scale on right applies to gamma-ray. Partial absorption of x-ray by Cu shown by dashed curve. *Note added in proof.*—The expanded scale on the right of Fig. 2 is in error; the number of counts should be one-half of the values listed. This error was pointed out by Dr. A. W. Sunyar.

to enter with a minimum of attenuation. Each counter was 20 inches long and contained 9.2 liters of a mixture of 90 percent argon and 10 percent methane at atmospheric pressure. The counters were operated with a battery voltage of 2500 v on the 4-mil central wire, corresponding to a gas multiplication of about 1000.

The counter voltage pulses were amplified by a factor of 7000 by means of a non-overloading linear amplifier with a rise time of 0.8 μsec and a clipping time of 4 μsec. The amplified pulses were sorted by single channel pulse-height selectors; the output of each selector was a blocking oscillator pulse which activated the coincidence circuit. The coincidence circuit had four independent channels each of which had a different adjustable delay and an adjustable resolving time.[5] The multichannel delay feature constantly showed that the resolving time was sufficiently large to detect all true coincidences. With a resolving time of 1.85 μsec, the first three channels (0, 0.25, and 0.60 μsec delays) always counted the same number of coincidence pulses; the fourth channel was delayed by 1.70 μsec and it recorded fewer coincidence events.

CONVERSION OF 110-KEV GAMMA-RAY

The photon distribution observed with a NaI scintillation spectrometer is shown in Fig. 2. The expanded intensity scale on the right is necessary to show the weak unconverted 110-kev gamma-ray. The detection of this unconverted gamma-ray had not been reported by earlier investigators. Copper absorption curves were taken to ascertain the contribution to the gamma-ray peak made by pulses from the high energy tail of the x-ray distribution. The effect of a thin copper absorber is shown by the dashed curve on the expanded scale. The absorption measurements showed that the x-ray contribution to the upper half of the gamma-ray peak was negligible. Therefore, the relative intensity was determined by comparing the areas of only the upper half of each peak. It was assumed that all of the impinging gamma-rays contribute to the photoelectric peak. Although 9 percent of the gamma-rays undergo a primary Compton process, it is reasonable to expect the crystal to detect almost all of the secondary gamma-rays.

The ratio of the counts due to x-rays to those due to gamma-rays was found to be 320±20. From experiments described below it was found that the fraction of 110-kev and 35.5-kev transitions which decay by K conversion are 0.54 and 0.80, respectively. Using these figures and an x-ray fluorescent yield of 0.82,[6] the K conversion coefficient of the 110-kev transition is 160±20.

110 KEV K TO $(L+M)$ RATIO

The ratio of the K to $(L+M)$ conversion was determined from electron-spectra taken both in a proportional counter and in the lens spectrometer. The proportional counter data, which was taken with a thin internal source, gave a ratio of 1.15±0.08. The lens spectrometer data shown in Fig. 3 gave a K to $(L+M)$ ratio of 1.15±0.05. These results are in excellent agreement with those of previous investigators: 1.17,[3] 1.2[7] and 1.10.[8] This K to $(L+M)$ ratio of 1.15 and the very low intensity of the unconverted gamma-ray indicate that 54 percent of the 110-kev transitions are K converted.

The separation of the L and M conversion electrons has been reported only by Hill *et al.*;[2] they give the L to M ratio as 3.5.

K CONVERSION OF THE 35.5-KEV GAMMA-RAY

The most direct determination of the fraction of 35.5-kev transitions which were K converted involved an

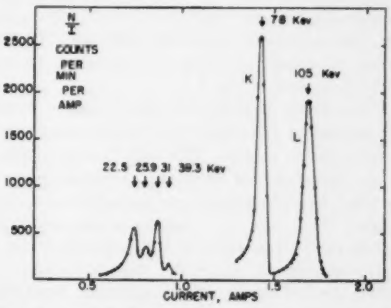

FIG. 3. Electron spectrum taken with lens spectrometer. The 78- and 105-kev lines are due to K and $(L+M)$ conversion electrons from the 110-kev gamma-ray.

[5] We wish to thank Dr. Sherman Frankel of the University of Pennsylvania, who designed and tested the pulse-height selector and the multichannel coincidence circuit.

[6] H. Tellez-Plasencia, J. phys. et radium **10**, 14 (1949); Steffen, Huber, and Humbel, Helv. Phys. Acta **22**, 167 (1949).
[7] Kern, Mitchell, and Zaffarano, Phys. Rev. **76**, 94 (1949).
[8] Siegbahn and Forsling, Ark. Fys. Bd. 1 **No. 24**, 505 (1949).

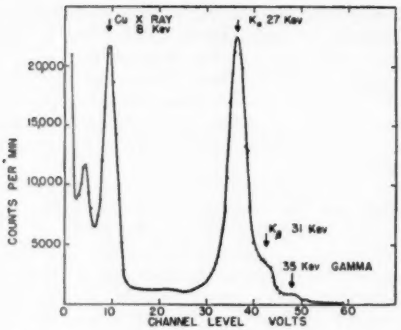

FIG. 4. Photon spectrum, proportional counter detector. The Cu x-ray originates in the counter wall.

analysis of the photon-photon coincidences. The K conversion electrons had too low an energy to be detected conveniently.

Each of the proportional counters was placed with its Be window facing the source. The geometry and detection efficiency of each counter were such that about 1.5 percent of the emitted Te K-x-rays gave pulses in the x-ray peak of the spectrum. Figure 4 shows a typical spectrum obtained with a proportional counter and its pulse-height selector. In addition to the Te K x-rays and the 35.5-kev gamma-ray, the spectrum shows the Te L x-ray and the fluorescent Cu x-ray originating in the counter wall.

During the coincidence measurements, one of the pulse-height selectors was constantly sensitive only to pulses contributing to the lower half of the Te K x-ray peak. The other selector accepted pulses in a three volt channel which had an adjustable level. As this channel level was varied over the x-ray peak x-x coincidences were recorded; when the variable channel level was increased it became sensitive to the 35.5-kev gamma-ray, and x-γ coincidences were detected. The experimental data from a typical coincidence run are shown in the lower half of Fig. 5.

The analysis of these coincidence data is based on the number of coincidences per single count recorded in the variable channel. This ratio is a direct measure of the probability of detecting a coincident event in the fixed channel for each event recorded in the variable channel. Thus, the x-γ coincidence rate per 35.5-kev gamma-ray is a measure of the probability that a K x-ray was emitted during the 110-kev transition preceding the low energy gamma-emission. Similarly the x-x coincidence rate per x-ray is a measure of the probability that a K x-ray was emitted in coincidence with the K x-ray detected in the variable channel level. The number of coincidences per single is plotted in the upper portion of Fig. 5. Since the x-x coincidences per x-ray exceed the x-γ coincidences per gamma-ray, there must be more x-rays associated with the low energy transition than with the 110-kev transition.

Quantitatively, if a_1 and a_2 are the fractions of K conversions in the first (110 kev) and second transitions, respectively,

$$\frac{N_{xx}/N_x}{N_{x\gamma}/N_\gamma}=\frac{2}{1+a_1/a_2}.$$

The experimental value for this fraction was determined as 1.16 ± 0.06. Using the value given above for the fraction of 110-kev transitions which are K converted, $a_1=0.54$; therefore, the fraction of 35.5 kev transitions which are K converted is $a_2=0.75\pm0.09$. This experimental result is a quantitative extension of the earlier qualitative coincidence experiments of Bowe and Goldhaber.[9]

BRANCHING OF 35.5-KEV TRANSITION

A more precise value of the K conversion coefficient can be derived from this preliminary value together with measurements of the other modes of decay. The $L+M$ conversion can be deduced from the ratio of $L+M$ electrons to the Auger electrons. A typical set of lens spectrometer data on these low energy electrons is shown in Fig. 6. After these data are corrected for source and window absorption the ratio is found to be 0.52 ± 0.08. The assigned error includes allowance for uncertainty in the correction factors. From the K conversion results described above and the known fluorescent yield the number of Auger electrons per disintegration is established as 0.23 ± 0.02. These results combine to show that $L+M$ conversion occurs in 13 ± 2 percent of the 35.5-kev transitions.

The number of unconverted gamma-rays was determined from the proportional counter photon spectrum shown in Fig. 7. The ratio of pulses in the $K\alpha$ x-ray

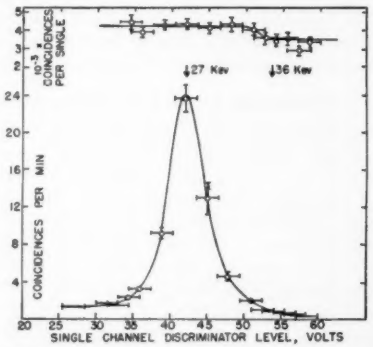

FIG. 5. Photon-photon coincidences. The channel level of one proportional counter is the abscissa. The selector of the other proportional counter detected one-half of the x-ray pulses.

[9] J. C. Bowe and G. Scharff-Goldhaber, Phys. Rev. **76**, 437 (1949).

peak to those in the gamma-ray peak was measured as 29; the $K\beta$ x-ray to 35.5-kev ratio was 3. When these values are corrected for relative efficiencies in argon and for the fluorescent yield, the ratio of all K conversion to the number of 35.5-kev gamma-rays is 20 ± 4. The large uncertainty in this value is mainly because of the uncertainty of the shapes of the individual overlapping peaks. This value is consistent with the value of 17 determined by Friedlander *et al.*[10] The K conversion data indicate that the fraction of the K x-rays originating from the 35.5-kev transition is 0.58 ± 0.03. The 35.5-kev K conversion coefficient is therefore 58 percent of 20 or 11.6 ± 2.5. This in turn implies a 7 ± 2 percent branch of unconverted gamma-ray.

A combination of all of these results gives a more precise value for the K branch; the final branching values are: K conversion $=0.80\pm0.05$; L conversion $=0.11\pm0.02$; M conversion $=0.02\pm0.004$ and unconverted gamma $=0.07\pm0.02$. The indicated accuracy includes a liberal estimate of possible systematic errors.

COMPARISON OF RESULTS WITH THEORY

The spin of the ground state of Te^{125} is known to be $\frac{1}{2}$.[11] The assignments of the spins and parities to the other levels of Te^{125} had been suggested by earlier investigators.[3,9] These assignments were given almost irrefutable support by the classification of nuclear isomers made by Goldhaber and Sunyar.[12] Their classification emphasizes the agreement between shell structure, empirical K/L ratios and the theory of transition rates, particularly for magnetic 2^4 pole ($M4$) radiation.

The data which were determined in this experiment do more than simply add proof to this well-established aspect of isomer classification. These data give information both about internal conversion coefficients where the theory has been previously unchecked and about the $M1$ character of the radiation between the $d_{\frac{3}{2}}$ and the $s_{\frac{1}{2}}$ levels.

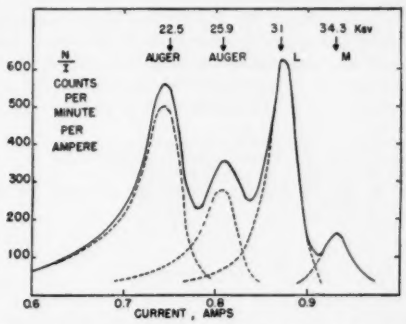

FIG. 6. Low energy electron spectrum taken with lens spectrometer. Dashed curves show the contributions of the four electron groups.

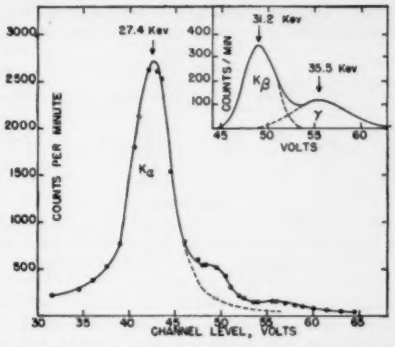

FIG. 7. Analysis of proportional counter photon spectrum.

In order to compare experimental conversion coefficients with theory, it is necessary to use five different sources of theoretical calculations. Each of these sources has limitations. (1) Rose *et al.*[13] have calculated K conversion coefficients relativistically for all multipolarities but only for energies above 150 kev. In order to apply these to the energies in Te^{125} a logarithmic extrapolation was made to energies below this value. (2) Hebb and Nelson[14] have made nonrelativistic calculations of K and L conversion coefficients but only for electric type transitions. They used the formula derived by Dancoff and Morrison[15] for K conversion and derived an analogous formula for L conversion. These calculations do not appear to be very inaccurate for low energies.[16] (3) Axel and Goodrich[16] extrapolated the results of Rose *et al.*, to very low energies for magnetic radiation by using the approximate calculations of Drell.[17] The extrapolation procedure is quite questionable. (4) Reitz[18] has calculated $E1$, $E2$ and $M1$ conversion coefficients for $Z=49$ (as well as $Z=84$ and $Z=92$) for low energies. These calculations are very accurate (about 1 percent) and include both relativistic and screening effects. However, the Z dependence might require of the order of a 30 percent increase in Reitz's $Z=49$ value to make it applicable to Te ($Z=52$). In the results quoted below, no attempt is made to correct for this unknown Z dependence. (5) Gellman, Griffith, and Stanley[19] have made accurate relativistic

[10] Friedlander, Perlman, and Scharff-Goldhaber, Phys. Rev. **80**, 1103 (1950).
[11] G. R. Fowles, Phys. Rev. **78**, 744 (1950).
[12] M. Goldhaber and A. W. Sunyar, Phys. Rev. **83**, 906 (1951).
[13] Rose, Goertzel, Harr, Spinrad, and Strong, Phys. Rev. **83**, 79 (1951).
[14] M. H. Hebb and E. Nelson, Phys. Rev. **58**, 486 (1940).
[15] S. M. Dancoff and P. Morrison, Phys. Rev. **55**, 122 (1939).
[16] P. Axel and R. F. Goodrich, Technical Report on Internal Conversion, University of Illinois, unpublished.
[17] S. D. Drell, Phys. Rev. **75**, 132 (1949).
[18] J. R. Reitz, Phys. Rev. **77**, 10 (1950).
[19] Gellman, Griffith, and Stanley, Phys. Rev. **80**, 866 (1950).

TABLE I. Conversion coefficients for 110-kev gamma-ray.

Radiation type	Theoretical *K* shell: Hebb and Nelson[a]	Theoretical *K* shell: Rose[b] *et al.* (extrapolated)	*K*/*L* ratio Hebb and Nelson[a]
*E*4	24.7	27	0.49
*E*5	134	140	0.20
*M*3		26	
*M*4		190	
*M*5		1100	
	Experimental		
	160±20		1.15±0.08

[a] See reference 14. [b] See reference 13.

TABLE II. Conversion coefficients for 35.5-kev gamma-ray.

Radiation type	Theoretical *K* shell: Hebb and Nelson	Theoretical *K* shell: Reitz (for $Z=49$)	Theoretical *K* shell: Axel and Goodrich	Theoretical *L* shell: Hebb and Nelson	Theoretical *L* shell: Gellman *et al.* (L_I subshell only)
*E*1	2.8	3.1		0.4	0.4
*E*2	17	21		35	2.0
*E*3	38			2900	
*M*1		10	8		1.45
*M*2			190		
	Experimental				
	11.7±2.5			$1.6^{+1.2}_{-0.7}$	

calculations for *E*1, *E*2, and *M*1 conversion coefficients for $Z=49$ and only for the L_I subshell. These calculations did not take screening into account but this neglect probably tends to compensate for the unknown Z dependence.

The comparison of the experimental conversion coefficient with theory for the 110-kev gamma-ray is shown in Table I. The conversion coefficient restricts the possible multipolarities to *E*5 and *M*4. However, the lifetime energy relationship and the K to L ratio both eliminate the *E*5 possibility.[12] (The empirical lifetime energy relationship of Goldhaber and Sunyar is strongly supported by the transition rate formulas published by Moszkowski[20] and by Weisskopf.[21])

The conversion coefficient of 160 is the highest to have been reported experimentally. Since the theoretical *M*4 value is an extrapolation, the slight discrepancy between experiment and theory is negligible. It is, in fact, gratifying to find the degree of agreement that does exist and it can be concluded that extrapolations into this energy range introduce only slight errors.

The theoretical values of the conversion of the 35.5-kev gamma-ray are shown in Table II. The K conversion coefficient indicates a preference for *M*1 radiation. Reitz's theoretical values require some upward correction due to the Z dependence. From the experimental results it can be concluded that this correction is less than 50 percent and, therefore, in the expected range.

The L conversion coefficients are more sensitive to electric quadrupole (*E*2) admixture. From the L_I subshell results alone it seems that *M*1 and *E*2 transitions have comparable conversion. However, the *E*2 result of Hebb and Nelson should be accurate. In addition, when the Hebb and Nelson result is separated into subshells,[22] the L_I value is quite close to the value given by Gellman *et al.* It is thus reasonable to conclude that the L_I shell contributes only of the order of 6 percent to the *E*2 conversion. On the other hand, the L_I subshell might well contribute the major share to *M*1 conversion. This is supported by the agreement in the *E*1 transitions and by an analogous case[23] in Sn^{119} where only L_I conversion has been observed by Hill.[24] This is further supported by Mihelich and Church[25] who also find that *M*1 conversion is predominantly due to L_I subshell while *E*2 conversion comes mainly from the L_{II} and L_{III} subshells.

The value of the experimental L conversion coefficient indicates that the L_I contribution is predominant in this case (unless the theory contains gross errors). In addition, if the listed, theoretical values are accepted, the greatest amount of allowable *E*2 admixture would be less than one percent.

We wish to thank Mr. Robert Baer for his assistance in taking and analyzing some of the experimental data. We are also indebted to Dr. Sherman Frankel of the University of Pennsylvania for discussions and aid pertaining particularly to electronic problems.

[20] S. A. Moszkowski, Phys. Rev. **83**, 1071 (1951).
[21] V. F. Weisskopf, Phys. Rev. **83**, 1073 (1951).
[22] R. F. Goodrich (private communication).
[23] J. C. Bowe and P. Axel, Phys. Rev. **84**, 939 (1951).
[24] R. D. Hill, Phys. Rev. **83**, 865 (1951).
[25] J. W. Mihelich and E. L. Church, Bull. Am. Phys. Soc. **26**, No. 6, 37 (1951).

Mean Free Path of Neutral Penetrating Shower-Producing Radiation*

H. W. BOEHMER†
Department of Physics, University of Colorado, Boulder, Colorado

AND

H. S. BRIDGE
Department of Physics and Laboratory for Nuclear Science and Engineering, Massachusetts Institute of Technology, Cambridge, Massachusetts

(Received November 2, 1951)

The collision mean free path has been measured in carbon and in lead for neutral particles capable of producing penetrating showers.

Several types of events are selected with different multiplicities of particles in the penetrating shower. For the events with highest multiplicity the mean free path is 85 ± 12 g cm^{-2} in carbon, and 143 ± 30 g cm^{-2} in lead.

INTRODUCTION

THE measurements reported here are a continuation of experiments on the production of charged secondaries by neutral particles in the cosmic radiation. This work was initiated by Rossi and Regener[1] and extended by Janossy and Rochester.[2] In principle, the method allows a determination of the collision mean free path for penetrating shower production by the neutral radiation. The present experiment was undertaken to improve the statistical accuracy of the previous results and to remove some of the uncertainties resulting from various sources of background. An experiment similar to this has been performed recently by Walker, Walker, and Greisen.[3] Our results agree closely with theirs, but since the experimental conditions and methods of analysis are rather different, it seems worthwhile to describe the present experiment in some detail.

EXPERIMENTAL METHOD

A schematic diagram of the apparatus is given in Fig. 1. The Geiger-Müller counters were of the metal type filled with an alcohol-argon self-quenching mixture. The effective area of each of the A tray counters was 1 in.$\times$20 in. while that of the counters in the B, C, D, E, and F trays was 1 in.$\times$10 in. Trays B, C, D, and E make up the penetrating shower detector. The counters in trays B and E were connected to addition circuits that made it possible to record coincidences of the type B_mCDE_n, wherein m or more counters were discharged in the B tray, one or more counters in the C and D trays, and n or more counters in the D tray. Normally the penetrating charged particles were required to

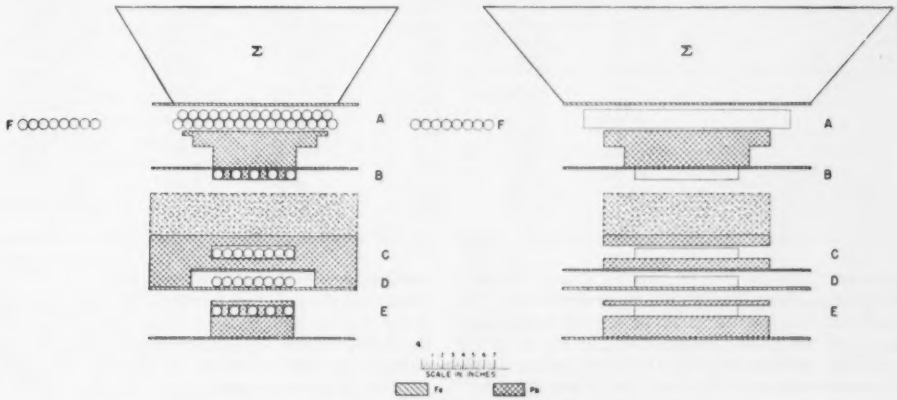

FIG. 1. Experimental arrangement of counters and absorbers.

* This work was supported in part by the joint program of the ONR and AEC.
† Now on leave at Massachusetts Institute of Technology, Cambridge, Massachusetts.
[1] B. Rossi and V. H. Regener, Phys. Rev. **58**, 837 (1940).
[2] L. Janossy and G. D. Rochester, Proc. Roy. Soc. (London) **A182**, 180 (1943).
[3] Walker, Walker, and Greisen, Phys. Rev. **80**, 546 (1950).

TABLE I. Penetrating shower rates for event P_{21}.

Absorber Σ g/cm²	Detector penetration	$P_{21}-A$ counts/hr	$P_{21}F-A$ counts/hr	$P_{21}-A-F$ counts/hr	Barom. corr. factor	$P_{21}-A-F$(corr) counts/hr
Zero	I	8.67	0.23	8.44±0.27	0.982	8.29±0.27
Zero	II	4.83	0.17	4.67±0.13	0.973	4.54±0.13
36 g/cm² C	I	5.60	0.22	5.38±0.23	1.003	5.40±0.23
36 g/cm² C	II	3.11	0.11	3.00±0.15	0.968	2.90±0.15
72 g/cm² C	I	4.34	0.25	4.08±0.16	1.030	4.20±0.16
72 g/cm² C	II	2.50	0.11	2.39±0.11	0.985	2.35±0.11
108 g/cm² C	I	3.09	0.25	2.84±0.14	1.080	3.07±0.14
108 g/cm² C	II	1.82	0.12	1.70±0.10	0.979	1.66±0.10
5 g/cm² Fe	I	8.05	0.60	7.45±0.61	1.041	7.76±0.61
28.5 g/cm² Pb+5 g/cm² Fe	I	6.92	0.52	6.40±0.50	1.018	6.52±0.50
57 g/cm² Pb+5 g/cm² Fe	I	5.74	0.39	5.35±0.42	1.009	5.40±0.42
171 g/cm² Pb+5 g/cm² Fe	I	3.92	0.15	3.77±0.31	1.062	4.00±0.31
285 g/cm² Pb+5 g/cm² Fe	I	2.99	0.17	2.82±0.23	1.041	2.94±0.23

TABLE II. Penetrating shower rates for event P_{22}.

Absorber Σ g/cm²	Detector penetration	$P_{22}-A$ counts/hr	$P_{22}F-A$ counts/hr	$P_{22}-A-F$ counts/hr	Barom. corr. factor	$P_{22}-A-F$(corr) counts/hr
Zero	I	2.42	0.11	2.31±0.14	0.982	2.27±0.14
Zero	II	1.11	0.07	1.04±0.06	0.973	1.01±0.06
36 g/cm² C	I	1.44	0.11	1.33±0.12	1.003	1.33±0.12
36 g/cm² C	II	0.66	0.02	0.64±0.07	0.968	0.62±0.07
72 g/cm² C	I	1.10	0.09	1.01±0.08	1.030	1.04±0.08
108 g/cm² C	I	0.92	0.10	0.82±0.08	1.080	0.89±0.08
108 g/cm² C	II	0.32	0.04	0.28±0.04	0.979	0.27±0.04
5 g/cm² Fe	I	2.50	0.45	2.05±0.32	1.041	2.13±0.32
28.5 g/cm² Pb+5 g/cm² Fe	I	1.96	0.20	1.76±0.27	1.018	1.79±0.27
57 g/cm² Pb+5 g/cm² Fe	I	1.77	0.19	1.58±0.23	1.009	1.59±0.23
171 g/cm² Pb+5 g/cm² Fe	I	1.04	0.08	0.96±0.16	1.062	1.02±0.16
285 g/cm² Pb+5 g/cm² Fe	I	0.63	0.10	0.53±0.10	1.041	0.55±0.10

TABLE III. Penetrating shower rates for event P_{32}.

Absorber Σ g/cm²	Detector penetration	$P_{32}-A$ counts/hr	$P_{32}F-A$ counts/hr	$P_{32}-A-F$ counts/hr	Barom. corr. factor	$P_{32}-A-F$(corr) counts/hr
Zero	I	0.92	0.04	0.88±0.09	0.982	0.86±0.09
Zero	II	0.43	0.01	0.42±0.04	0.973	0.41±0.04
36 g/cm² C	I	0.48	0.01	0.47±0.07	1.003	0.47±0.07
36 g/cm² C	II	0.23	0.00	0.23±0.04	0.968	0.22±0.04
72 g/cm² C	I	0.30	0.01	0.29±0.04	1.030	0.30±0.04
72 g/cm² C	II	0.21	0.01	0.20±0.03	0.985	0.20±0.03
108 g/cm² C	I	0.28	0.03	0.25±0.04	1.080	0.27±0.04
108 g/cm² C	II	0.11	0.01	0.10±0.02	0.979	0.10±0.02
5 g/cm² Fe	I	0.75	0.00	0.75±0.20	1.041	0.78±0.20
28.5 g/cm² Pb+5 g/cm² Fe	I	0.88	0.04	0.84±0.20	1.018	0.86±0.20
57 g/cm² Pb+5 g/cm² Fe	I	0.52	0.03	0.49±0.13	1.009	0.49±0.13
171 g/cm² Pb+5 g/cm² Fe	I	0.28	0.00	0.28±0.08	1.062	0.30±0.08
285 g/cm² Pb+5 g/cm² Fe	I	0.10	0.00	0.10±0.05	1.041	0.10±0.05

penetrate 71 g cm^{-2} of Pb plus 8.7 g cm^{-2} of Fe, a detector penetration which will be referred to as I. An additional lead absorber could be inserted in the region shown by the broken cross-hatching in Fig. 1. In this condition, referred to as II, the total absorber in the detector consisted of 185 g cm^{-2} of Pb plus 8.7 g cm^{-2} of Fe. Range-energy curves indicate that a proton and π-meson must have kinetic energies in excess of about 255 Mev and 135 Mev, respectively, in order to penetrate detector I. In the case of detector II the proton and π-meson energies must exceed 440 Mev and 265 Mev, respectively. Heavy shielding was used wherever possible to protect the trays from side showers. The $\frac{3}{4}$-inch lead spacers which separated the counters in the B and E trays, and the layer of lead immediately over the E tray reduced the background that resulted from multiple electronic secondaries of μ-mesons. The equipment was operated in a trailer, at an altitude of 10,600 ft above sea level.

The events of interest in the measurements reported here were B_mCDE_n coincidences that were unaccompanied by the discharge of tray A. Such events (B_mCDE_n-A), hereafter designated by $P_{mn}-A$, are presumably a result of high energy neutral particles

which traverse the absorber Σ and tray A undetected and produce nuclear interactions in the 100 g cm^{-2} lead layer located between tray A and tray B. The experimental method employed is similar to that of other investigators and consists in measuring the rate of occurrence of the above events as a function of the variable absorber thickness Σ. It is presumed that a high energy neutral particle, which undergoes a nuclear collision in the absorber, either disappears or if it survives the encounter produces secondary charged particles capable of discharging tray A. In both cases the incident particle can no longer give rise to a $P_{mn}-A$ event. On the other hand, a neutral particle that does not have a collision in the absorber is just as likely to produce a $P_{mn}-A$ event as if the absorber were not there. Thus from the rate of decrease of the counting rate with increasing absorber thickness, one can determine the collision mean free path of the high energy neutral particles in the material of the absorber.

In order to discriminate against spurious events caused by air showers, two extension trays, F, were placed at the sides of the penetrating shower detector (see Fig. 1) and coincidences, $P_{mn}F-A$, between the anticoincidences, $P_{mn}-A$, and the discharges of the F trays were recorded. The corresponding counting rate was then subtracted from the counting rate of the $P_{mn}-A$ events to obtain the corrected counting rate, $P_{mn}-A-F$. Admittedly this method of discrimination is open to criticism, since it may rule out events that should be accepted. For example, a neutron may produce in the lead below tray A a nuclear interaction in which a secondary charged particle is projected sideways through one of the F trays. The procedure used is justifiable only because the correction is small. In fact the most important purpose achieved by the use of the extension trays was to prove that air showers do not have a significant effect upon the present experiment.

It is apparent that inefficiency in the anticoincidence tray A would give rise to a troublesome constant background in the recorded anticoincidence rate. For this reason the counters in this tray were stacked in a double layer and divided into four groups with each group feeding its associated fast amplifier and output circuits. The pulses from the four groups were then mixed to form the total A tray output. In this manner serious inefficiency caused by the dead time of the amplifiers and output circuits was reduced to a minimum. Frequent measurements showed that the A tray had an efficiency of about 99.5 percent.

RESULTS

Tables I through IV present a summary of the data for the different events aforementioned. A barometric correction factor was used to normalize the data to the average barometric pressure during the experiment. This correction factor was based on an absorption thickness of the N-component in air equal to 120 g cm^{-2}. The corrected data are plotted in Figs. 2 and 3. One sees that the absorption curves are exponential within the experimental errors. The solid lines represent data taken with detector penetration I while the dashed lines are the curves for the measurements with detector penetration II.

A complete summary of the results based on the assumption of exponential absorption and obtained by least square analysis is given in Table V. From this table one notices that the apparent mean free path decreases as the multiplicity in the penetrating shower increases. It is evident that higher multiplicity of the particles in the detected event corresponds, on the average, to a higher energy of the incident particle responsible for the event. Thus the results, if taken at face value, would indicate that the mean free path decreases as the energy of the particle producing the nuclear interaction increases. It is important to notice, however, that this effect may be of an instrumental character. For example, a high energy neutron on traversing the absorber Σ may undergo a nuclear interaction in which it loses only a small amount of energy and produces a few low energy charged particles. The charged particles may be stopped by ionization loss before they reach the anticoincidence tray A, while the neutron may go on to produce another nuclear interaction in the material below A. The occurrence of events such as the one described above would make the observed mean free path longer than the actual mean free path. It is reasonable to assume that this source of error is more effective at low neutron energies than at high neutron energies because, as the energy of the neutron increases, the penetration of the secondary charged particles produced in its nuclear interactions also increases. Thus the effect described may possibly explain the energy dependence of the observed mean free paths.

TABLE IV. Penetrating shower rates for event P_{31}.

Absorber Σ g/cm^2	Detector penetration	$P_{31}-A$ counts/hr	Barom. corr. factor	$P_{31}-A$ (corr.) counts/hr
Zero	I	2.29±0.14	0.982	2.25±0.14
Zero	II	1.35±0.06	0.973	1.31±0.06
36 g/cm^2 C	I	1.28±0.12	1.003	1.28±0.12
36 g/cm^2 C	II	0.88±0.08	0.968	0.85±0.08
72 g/cm^2 C	I	1.04±0.08	1.030	1.07±0.08
72 g/cm^2 C	II	0.62±0.06	0.985	0.61±0.06
108 g/cm^2 C	I	0.74±0.07	1.080	0.80±0.07
108 g/cm^2 C	II	0.46±0.05	0.979	0.45±0.05
5 g/cm^2 Fe	I	2.05±0.32	1.041	2.13±0.32
28.5 g/cm^2 Pb +5 g/cm^2 Fe	I	2.20±0.30	1.018	2.24±0.30
57 g/cm^2 Pb +5 g/cm^2 Fe	I	1.40±0.20	1.009	1.41±0.20
171 g/cm^2 Pb +5 g/cm^2 Fe	I	0.86±0.15	1.062	0.91±0.15
285 g/cm^2 Pb +5 g/cm^2 Fe	I	0.61±0.11	1.041	0.64±0.11

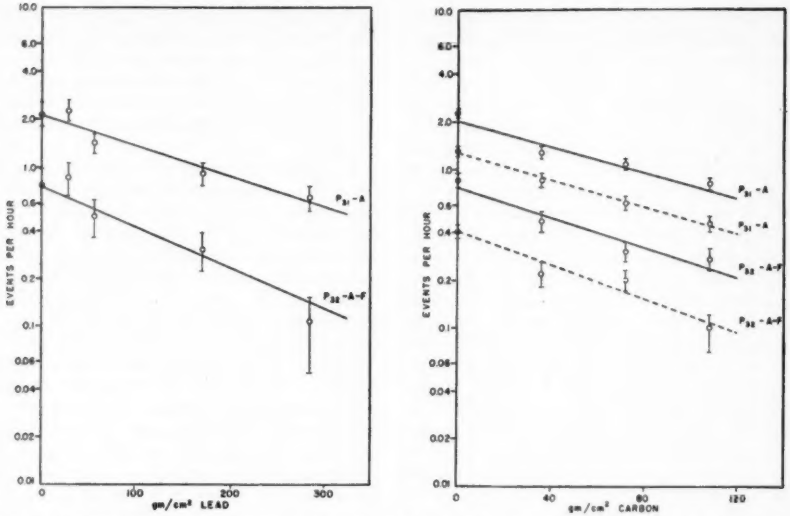

FIG. 2. The rate of occurrence of events $P_{21}-A-F$ and $P_{22}-A-F$ as a function of the thickness Σ of lead and carbon absorbers. The solid and dashed curves represents data with detector penetrations I and II, respectively.

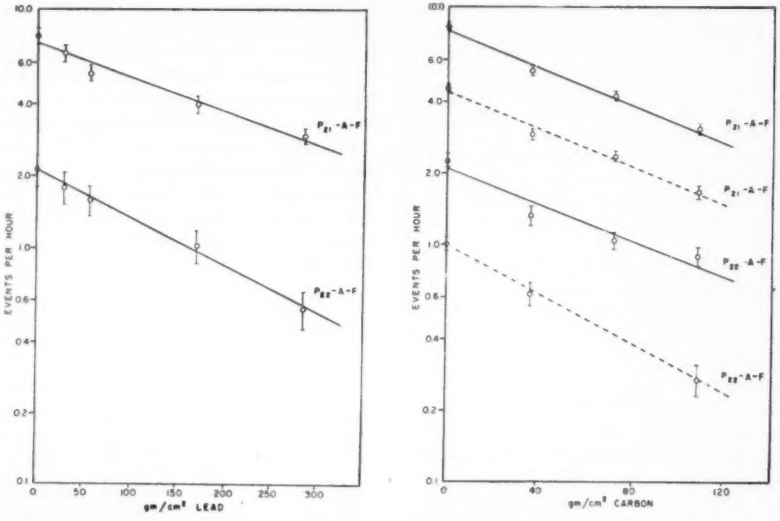

FIG. 3. The rate of occurrence of events $P_{21}-A$ and $P_{22}-A-F$ as a function of the thickness Σ of lead and carbon absorbers. The solid and dashed curves represent data with detector penetrations I and II, respectively.

The aforementioned arguments suggest that the most reliable determinations of the collision mean free path are those corresponding to events of highest multiplicity. Our experimental values for these mean free paths (see Table V) agree well with those obtained by other authors (Walker, Walker, and Greisen).[3] They are also consistent with the present views on the dimensions and structure of nuclei. In fact, if one assumes a nuclear radius $r_n=r_0A^{\frac{1}{3}}$ (with $r_0=1.38\times10^{-13}$ cm and A equal to the atomic number), one finds that the geometrical

mean free path (i.e., the mean free path computed for completely opaque nuclei) is 165 g cm^{-2} in lead and 65 g cm^{-2} in carbon. One sees that the observed mean free path in lead comes close to the geometrical mean free path whereas the observed mean free path in carbon is somewhat longer than the geometrical mean free path. The obvious and reasonable conclusion is that the heavy lead nucleus is completely opaque to high energy neutrons whereas the light carbon nucleus is slightly transparent.

It may be noted that, if one considers instead the events of low multiplicity, the values of the observed mean free paths in lead and carbon are not consistent with the model of partially transparent nuclei. For example, the mean free paths corresponding to $P_{21}-A-F$ events is 108±6 g cm^{-2} in carbon and 311±34 g cm^{-2} in lead. According to the theory of Fernbach, Serber, and Taylor,[4] 311 g cm^{-2} in lead corresponds to 245 g cm^{-2} in carbon. The disagreement confirms our previous assumption that, in the case of low multiplicity events, the mean free path measurements are falsified by the occurrence in the absorber of nuclear interactions in which the neutron survives and no ionizing particles are produced capable of discharging the anticoincidence tray A. For a given energy of the primary neutron, these events probably occur more frequently in lead than in carbon, because the secondary particles from a nuclear interaction in lead are presumably more numerous and less energetic than those arising from a similar interaction in carbon and have thus a greater probability of being reabsorbed before reaching tray A. If the above analysis is correct, one concludes that the difference between the observed and the actual mean free path is greater in lead than in carbon. This conclusion, qualitatively at least, explains the disagreement noted before.

A possible source of error is the production of penetrating showers by particles coming in at large angles from the vertical and thus reaching the lead below tray A without traversing the absorber Σ. Such particles could be either neutral or charged since a charged particle might conceivably strike the producing layer without passing through the anticoincidence tray A. This effect would contribute a background rate independent of the absorber thickness Σ and the observed absorption curves would be of the form $N(x)=N_b+N_0e^{-x/L}$, where $N(x)$ is the counting rate at the absorber thickness, x, L is the mean free path, and N_b and N_0 are constants. In the present experiment such a source of error did not appear to be serious since the counting rates exhibited a simple exponential variation within the limits of statistical accuracy (except perhaps for some of the carbon curves taken with detector penetration I).

[4] Fernbach, Serber, and Taylor, Phys. Rev. **75**, 1352 (1949).

TABLE V. Mean free paths.

Event	Absorber	Detector penetration	Mean free path (g cm^{-2})
$P_{21}-A-F$	C	I	108±6
$P_{21}-A-F$	C	II	108±6
$P_{22}-A-F$	C	I	109±11
$P_{22}-A-F$	C	II	81±9
$P_{21}-A$	C	I	103±10
$P_{21}-A$	C	II	98±9
$P_{22}-A-F$	C	I	85±12
$P_{22}-A-F$	C	II	85±13
$P_{21}-A-F$	Pb	I	311±34
$P_{22}-A-F$	Pb	I	220±35
$P_{21}-A$	Pb	I	218±34
$P_{22}-A-F$	Pb	I	143±30

The possibility of charge exchange represents another possible source of error. For instance, a proton in traversing the absorber may change into a neutron without giving rise to secondary particles of sufficient penetration to discharge the anticoincidence tray. In order to measure this effect an additional tray of counters was placed above the absorber Σ. For absorber thicknesses of approximately half a mean free path of carbon or lead it was found that less than 5 percent of the $P_{\text{mult}}-A$ events could be attributed to protons which undergo charge exchange in the absorber.

This experiment was performed at the Inter-University High Altitude Laboratory at Echo Lake, Colorado. The original instrumentation of the experiment was carried out by Dr. John Tinlot and Dr. Bernard Gregory. We are indebted to them for their initial experimental work to determine the feasibility of the method. It is a pleasure to acknowledge the support and encouragement given to us by Professor Bruno Rossi. We wish to thank both Professor Rossi and Professor R. W. Williams for helpful discussions concerning the results.

The Relativistic Dynamics of a System of Particles Interacting at a Distance

L. H. THOMAS
Watson Scientific Computing Laboratory, Columbia University, New York, New York
(Received November 1, 1951)

The dynamics of a system of particles acting on one another at a distance can be relativistically invariant if the assumption of invariant world-lines is given up. This is shown by constructing a particular dynamics in which invariance over the homogeneous Lorentz group is trivial, but space as well as time displacement requires the solution of equations of motion or of a Schroedinger equation. This particular dynamics reduces in the nonrelativistic limit to the most general dynamics of a system of interacting particles admitting the Newtonian group.

I. INTRODUCTION: DIFFICULTIES WITH WORLD LINES

THE Newtonian equations of motion of two interacting particles are, in one dimension of space,

$$m_1\ddot{x}_1=-\partial V/\partial x_1, \quad m_2\ddot{x}_2=-\partial V/\partial x_2,$$

where

$$V=V(x_2-x_1). \tag{1.1}$$

These keep the same form if we change to a frame of reference in uniform relative motion by the equation

$$x'=x-ut, \tag{1.2}$$

and in such an inertial frame of reference the accelerations of the particles depend only on their relative position. This assumes a common time t, but does not identify points of space at one time with points of space at any other time (see Fig. 1).

In relativity theory we replace $x'=x-ut$ by

$$\begin{aligned} x'&=(x-ut)/\sqrt{(1-u^2/c^2)},\\ t'&=(t-ux/c^2)/\sqrt{(1-u^2/c^2)}, \end{aligned} \tag{1.3}$$

c being the speed of light. A relation between x and t, transformed from frame to frame by these formulas, specifies a world-line for the motion of a particle (see Fig. 2), but when we try to generalize the equations of motion we immediately run into difficulty. In (1.1), $\ddot{x}_1(t)$ and $\ddot{x}_2(t)$ depend on $x_2(t)-x_1(t)$, and this is invariant for the transformation (1.2); but with (1.3), $t_2=t_1$ does not lead to $t_2'=t_1'$ unless $x_2=x_1$. There is, indeed, no reason why any property of the motion of particle 1 at a definite location on its world-line should depend on any one location of the second particle rather than on any other which can be made simultaneous with the location of the first particle by the transformation (1.3).

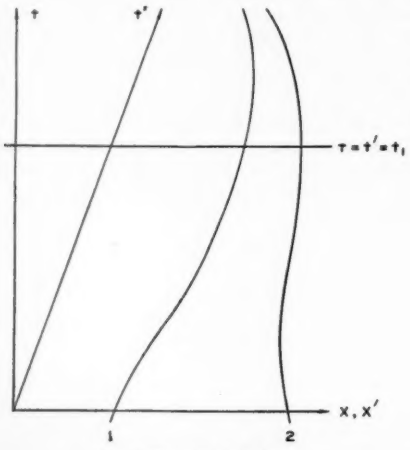

FIG. 1. Nonrelativistic theory.

The current methods of avoiding this difficulty are to deal only with collisions, or with the interactions between particles and fields, for which we can take $x_2=x_1$; or to use retarded interactions, $x_1-x_2=c(t_1-t_2)$ leading to $x_1'-x_2'=c(t_1'-t_2')$. When these methods are applied in detail, consistent finite results are not obtained, and one seems to be led to noncausal theories, or to discontinuous space and time.[1]

There is, however, in the above discussion an assumption that does not seem to be logically necessary, the assumption of invariant world lines. We may quite logically give up this assumption and suppose that the state of the system is specified relative to any observer in terms of canonically conjugate dynamical variables, q_1 and p_1 for the first particle, q_2 and p_2 for the second particle, and that these variables transform to the corresponding variables relative to any other observer, displaced in time, position, and velocity, by the transformations of a group given in canonical form. (See Fig. 3.) While $q_1(t)$ may be regarded as giving a world line for the first particle relative to a series of observers displaced only in time, there is no reason why this should be exactly the same line as that given by $q_1'(t')$ for a relatively moving series of observers.

This paper will be devoted to developing a relativistic theory of particles interacting at a distance by giving up the assumption of invariant world lines.

II. KINEMATICS AND DYNAMICS

We shall adopt the general point of view of quantum mechanics, and a notation briefly symmarized as follows.

[1] P. G. Bergmann, *An Introduction to the Theory of Relativity* (Prentice-Hall, Inc., New York, 1942), p. 85.

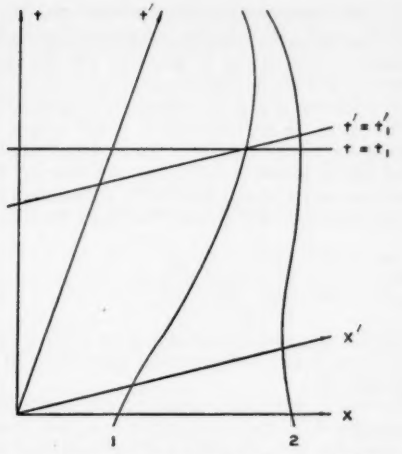

FIG. 2. Relativistic theory with invariant world lines.

Relative to any one observer the world is described in terms of basic dynamical variables a, b, $\cdots$, that can be represented by Hermitian matrices, various representations being obtained from one another by unitary transformations. A real function of the basic variables is in general a Hermitian matrix depending on the matrices representing the dynamical variables in a manner covariant over the unitary transformations. In particular $\lambda a+\mu b$ where λ and μ are numbers, and $\frac{1}{2}(ab+ba)$, are functions of a and b in this sense, and so is their Poisson bracket

$$(a, b)=(ab-ba)/\imath\hbar, \tag{2.1}$$

while the trace $\langle f\rangle$ of any matrix f is invariant. Any property of the system may be described by such a function of the basic variables. A statistical state of the system is also described by a function $P(a, b, \cdots)$ of the dynamical variables, of unit trace, but it must be analyzable into a sum with positive coefficients over pure states, or a limit of such a sum, the statistical matrix describing a pure state being the open product of a column φ and the complex conjugate row φ^*

$$A=\varphi\varphi^*. \tag{2.2}$$

The kinematics of the system is given by one set of representations of the basic variables, or by relations between them sufficient to determine their representations up to a unitary transformation. Expected values of properties for a state of the system are given by the trace of the product of the matrices describing the property and the state.

A continuous series of observers, referred to by the parameters s, describe the world in terms of basic dynamical variables $a(s)$, $b(s)$, $\cdots$, defined by each observer relative to himself, for example, in the non-relativistic case, Cartesian coordinates, momenta, and spins, of the various particles in that observer's frame of reference. We shall suppose that for all the observers the system has the same kinematics. The representations used by the observers can be chosen so that to the same statistical state they give the same matrix. For such a Heisenberg set of representations the matrices representing the dynamical variables, $a(s)$, will in general be different for each observer, and the change from one observer to a neighboring observer of any function of the basic variables not explicitly depending on the observer can be put in canonical form

$$df/ds=(f, S), \tag{2.3}$$

where S is also a matrix function. These equations go over to the classical equations of motion by replacing the quantum Poisson bracket by a classical Poisson bracket. Again the representations can be chosen so that the basic variables are given by the same matrices whatever the observer. For such a Schrödinger set of representations, the matrices $P(s)$ representing a statistical state must in general be different, and the change from one observer to a neighboring observer can be put in the form

$$\partial P(s)/\partial s=(S, P), \tag{2.4}$$

where S must be the previous matrix of (2.3) transformed to the new set of representations. For a column describing a pure state we have, perhaps after adjusting the phases of the representations,

$$\partial\varphi/\partial s=S\varphi/\imath\hbar, \tag{2.5}$$

the Schrödinger equation.

The above point of view is familiar enough if our observers' descriptions are the usual descriptions in non-relativistic theory at different times, s being the time

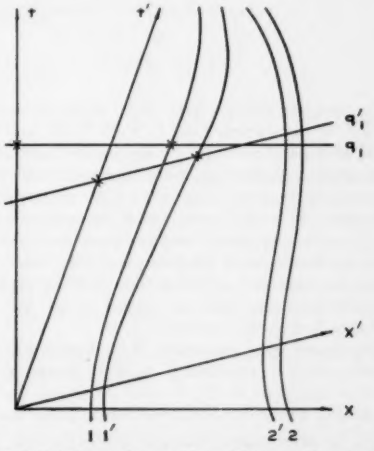

FIG. 3. Relativistic theory with world lines not invariant.

variable t, and S the Hamiltonian function H.[2] We shall extend this point of view to relativity theory by treating in this displacements of the observer in position, orientation, and velocity, as well as in time. Thus position in space and time, as well as orientation and velocity, will be regarded as properties of observers, who form a ten-parameter family, with the structure of the inhomogeneous Lorentz group. The dynamical variables are not regarded as directly related to space position, and there is no need to introduce many times.

III. THE INHOMOGENEOUS LORENTZ GROUP

We may define the rate of displacement along a series of observers with change of parameter s by the component rates of displacement in position, $\partial x/\partial s$, $\partial y/\partial s$, $\partial z/\partial s$ along the x, y, and z directions, in orientation, $\partial l/\partial s$, $\partial m/\partial s$, $\partial n/\partial s$, about the x, y, and z axes, in velocity $\partial u/\partial s$, $\partial v/\partial s$, $\partial w/\partial s$, in the x, y, and z directions, and in time $\partial t/\partial s$, relative to each observer. We then have rates of change like (2.3) in a Heisenberg set of representations or (2.4) in a Schrödinger set, with

$$S=H\frac{\partial t}{\partial s}+U\frac{\partial u}{\partial s}+V\frac{\partial v}{\partial s}+W\frac{\partial w}{\partial s}-L\frac{\partial l}{\partial s}-M\frac{\partial m}{\partial s}-N\frac{\partial n}{\partial s}-X\frac{\partial x}{\partial s}-Y\frac{\partial y}{\partial s}-Z\frac{\partial z}{\partial s}, \tag{3.1}$$

where the signs have been taken so that H can be identified with the energy, X, Y, and Z, with the components of linear momentum, and L, M, and N, with the components of angular momentum of the whole system.

Here the ten matrices, H, U, V, W, L, M, N, X, Y, and Z, will be functions of the basic dynamical variables and in general of the observer, but if the system is a complete isolated system, satisfying the same physical laws for each observer, they should be explicitly independent of the observer and should be given by the same matrices for all observers in a Schrödinger set of representations.

Further, in order that we should return to the same description of the system on completing a closed circuit of observers, it is necessary and sufficient that the Poisson brackets of these matrices may take the forms, corresponding to the structure of the inhomogeneous Lorentz group,

$$\begin{array}{llll}(L,M)=N & (L,M)=-M & (L,U)=0 & (L,V)=W \\ & (M,N)=L & (M,U)=-W & (M,V)=0 \\ & & (N,U)=V & (N,V)=-U \\ & & & (U,V)=-N/c^2\end{array}\qquad\begin{array}{l}(L,W)=-V \\ (M,W)=U \\ (N,W)=0 \\ (U,W)=M/c^2 \\ (V,W)=-L/c^2,\end{array} \tag{3.2}$$

$$\begin{array}{llll}(L,X)=0 & (L,Y)=Z & (L,Z)=-Y & (L,H)=0 \\ (M,X)=-Z & (M,Y)=0 & (M,Z)=X & (M,H)=0 \\ (N,X)=Y & (N,Y)=-X & (N,Z)=0 & (N,H)=0 \\ (U,X)=H/c^2 & (U,Y)=0 & (U,Z)=0 & (U,H)=X \\ (V,X)=0 & (V,Y)=H/c^2 & (V,Z)=0 & (V,H)=Y \\ (W,X)=0 & (W,Y)=0 & (W,Z)=H/c^2 & (W,H)=Z,\end{array} \tag{3.3}$$

$$\begin{array}{llll}(X,Y)=0 & (X,Z)=0 & (X,H)=0 \\ & (Y,Z)=0 & (Y,H)=0 \\ & & (Z,H)=0.\end{array} \tag{3.4}$$

The first set of equations, (3.2), gives the Poisson brackets of the six functions, U, V, W, L, M, and N, in terms of themselves only, giving the structure of the homogeneous Lorentz group for changes of orientation and velocity between observers at the same point of space-time. U, V, W, L, M, and N themselves form a six-vector for this group, and the conditions that any other six functions of the basic variables form a six-vector are equations obtained from (3.2) by replacing the right-hand side and one variable on the left-hand side of each with the new set.

The second set of equations, (3.3), gives the Poisson brackets of the six functions U, V, W, L, M, and N, with the four functions H, X, Y, and Z; shows that the latter form a four-vector for the homogeneous Lorentz group; and gives the changes in the former in space-time displacements of the observer. Any other set of four functions of the basic variables form a four-vector if they satisfy similar equations.

Lastly, Eqs. (3.4), stating that H, X, Y, and Z commute with each other, complete the conditions that the functions H, U, V, W, L, M, N, X, Y, and Z of the basic variables give a dynamical theory admitting the inhomogeneous Lorentz group.[3]

IV. THE DYNAMICAL EQUATIONS

In choosing basic dynamical variables and kinematical relations between them to represent a single

[2] P. A. M. Dirac, *Quantum Mechanics* (Oxford University Press, London, 1930), Chap. VI.

[3] Similar theory dealing with a single particle or a system not necessarily composed of particles is to be found in E. Wigner, *Annals of Mathematics* **40**, 145 (1939); C. Møller, Communications Dublin Institute for Advanced Studies 3 (1949), and M. H. L. Pryce, Proc. Roy. Soc. (London) **A195**, 621 (1948).

particle, we may be guided by the consideration that for a single particle by itself we should be able to construct matrices satisfying the relations (3.2), (3.3), and (3.4). This can be done giving them in terms of more special variables, of variables equivalent to this set, or of more general variables. We shall adopt the second possibility and simply take a particle to be described by basic dynamical variables satisfying the relations (3.2), (3.3), and (3.4).

For n particles, then, we take n sets of variables,

$$\mathrm{H}_r, \mathrm{U}_r, \mathrm{V}_r, \mathrm{W}_r, \mathrm{L}_r, \mathrm{M}_r, \mathrm{N}_r, \mathrm{X}_r, \mathrm{Y}_r, \mathrm{Z}_r, \quad r=1, \cdots, n, \tag{4.1}$$

each set satisfying the conditions (3.2), (3.3), and (3.4), and with zero Poisson brackets for variables from different particles.

In general, a relativistic theory could be given by any ten functions L, M, N, U, V, W, X, Y, Z, and H of the basic variables, satisfying (3.2), (3.3), and (3.4), but this would be far too general for our purpose.

If we examine customary constructions, we see that they usually introduce invariance over space displacements and rotations implicitly, the construction making this trivial; the effect of time displacement is the main one to be described, by a Hamiltonian or otherwise, and invariance for velocity displacement requires proof. Thus we may take

$$\begin{aligned} &\mathrm{X}=\Sigma\mathrm{X}_r, \quad \mathrm{Y}=\Sigma\mathrm{Y}_r, \quad \mathrm{Z}=\Sigma\mathrm{Z}_r, \\ &\mathrm{L}=\Sigma\mathrm{L}_r, \quad \mathrm{M}=\Sigma\mathrm{M}_r, \quad \mathrm{N}=\Sigma\mathrm{N}_r, \end{aligned} \tag{4.2}$$

so that invariance over space displacements and rotations is trivial, choose a Hamiltonian function H which commutes with X, Y, Z, L, M, and N, and prove relativistic invariance, which is equivalent to constructing functions U, V, and W to give infinitesimal velocity displacements, such that the whole set X, Y, Z, L, M, N, H, U, V, and W satisfy (3.2), (3.3), and (3.4).

We shall depart from this scheme and instead make trivial the homogeneous Lorentz transformations, space rotations, and changes of velocity for a fixed space-time position. This seems to be more elegant mathematically and to lead to simpler results, and has the further advantage that it will extend directly to the usual form of the general theory of relativity, where just the homogeneous Lorentz group of transformations at each space-time position is taken trivial.[4]

Thus we assume to start with

$$\begin{aligned} &\mathrm{L}=\Sigma\mathrm{L}_r, \quad \mathrm{M}=\Sigma\mathrm{M}_r, \quad \mathrm{N}=\Sigma\mathrm{N}_r, \\ &\mathrm{U}=\Sigma\mathrm{U}_r, \quad \mathrm{V}=\Sigma\mathrm{V}_r, \quad \mathrm{W}=\Sigma\mathrm{W}_r, \end{aligned} \tag{4.3}$$

which, it is trivial, satisfy (3.2). We need in addition functions H, X, Y, and Z, satisfying (3.3) and (3.4). The conditions (3.4) require that they shall mutually commute. The conditions (3.3) require that they are four functions of the basic variables L_r, M_r, N_r, U_r, V_r, W_r, H_r, X_r, Y_r, and Z_r, $r=1, \cdots, n$, forming a four-vector for the transformations of the homogeneous Lorentz group. Any four-vector function of the basic variables with mutually commuting components will give us a relativistically invariant dynamics.

[4] L. H. Thomas, Revs. Modern Phys. **17**, 182 (1945); P. M. Dirac, Revs. Modern Phys. **21**, 392 (1949).

V. CONSTRUCTION OF A SPECIAL DYNAMICS

Assume

$$\begin{aligned} \mathrm{X}&=\tfrac{1}{2}(\mu\Sigma\mathrm{X}_r+\Sigma\mathrm{X}_r\mu), \\ \mathrm{Y}&=\tfrac{1}{2}(\mu\Sigma\mathrm{Y}_r+\Sigma\mathrm{Y}_r\mu), \\ \mathrm{Z}&=\tfrac{1}{2}(\mu\Sigma\mathrm{Z}_r+\Sigma\mathrm{Z}_r\mu), \\ \mathrm{H}&=\tfrac{1}{2}(\mu\Sigma\mathrm{H}_r+\Sigma\mathrm{H}_r\mu), \end{aligned} \tag{5.1}$$

where μ is a single function of the basic variables, a scalar for the homogeneous Lorentz group; then X, Y, Z, and H will be Hermitian and will form a four-vector satisfying Eqs. (3.3). In order that the expressions (5.1) should commute, it is sufficient that μ should commute with the ratios of $\Sigma\mathrm{X}_r$, $\Sigma\mathrm{Y}_r$, $\Sigma\mathrm{Z}_r$, and $\Sigma\mathrm{H}_r$.

$$\Sigma\mathrm{X}_r\mu\Sigma\mathrm{Y}_r=\Sigma\mathrm{Y}_r\mu\Sigma\mathrm{X}_r, \quad \text{etc.} \tag{5.2}$$

Thus μ may be any scalar function of expressions that have this property, in particular of X_r, Y_r, Z_r, and H_r, $r=1, \cdots, n$, and of expressions constructed by the following method. Take any determinant D with five rows and columns, with rows chosen out of the $6n+1$ rows

$$\begin{matrix} \Sigma\mathrm{X}_r, & \Sigma\mathrm{Y}_r, & \Sigma\mathrm{Z}_r, & \Sigma\mathrm{H}_r, & 0, \\ (\Sigma\mathrm{X}_r, \mathrm{Q}), & (\Sigma\mathrm{Y}_r, \mathrm{Q}) & (\Sigma\mathrm{Z}_r, \mathrm{Q}), & (\Sigma\mathrm{H}_r, \mathrm{Q}), & \mathrm{Q}, \end{matrix} \tag{5.3}$$

where Q is one of L_r, M_r, N_r, U_r, V_r, or W_r, $r=1, \cdots, n$. For all these Poisson brackets when evaluated contain only X_r, Y_r, Z_r, and H_r, $r=1, \cdots, n$, which commute with each other. Thus, for example,

$$(\Sigma\mathrm{X}_r, \mathrm{D})\Sigma\mathrm{Y}_r-(\Sigma\mathrm{Y}_r, \mathrm{D})\Sigma\mathrm{X}_r,$$

where D is one of these determinants, is a determinant with corresponding rows and columns from

$$\begin{matrix} \Sigma X_r, & \Sigma\mathrm{Y}_r, & \Sigma\mathrm{Z}_r, & \Sigma\mathrm{H}_r, & \\ (\Sigma\mathrm{X}_r, \mathrm{Q}), & (\Sigma\mathrm{Y}_r, \mathrm{Q}), & (\Sigma\mathrm{Z}_r, \mathrm{Q}), & (\Sigma\mathrm{H}_r, \mathrm{Q}), & \\ & & & 0, & \\ & & & (\Sigma\mathrm{X}_r, \mathrm{Q})\Sigma\mathrm{Y}_r-(\Sigma\mathrm{Y}_r, \mathrm{Q})\Sigma\mathrm{X}_r, & \end{matrix}$$

and, since all these terms commute, is seen by combining the columns to vanish, and this is just the condition required. In this way we obtain, in all, $10n-4$ allowed combinations of the original $10n$ variables, which is as many as we should expect.

We may arrange these more symmetrically as the components of four-vectors.

(a) X_r, Y_r, Z_r, and H_r, $r=1, \cdots, n$. (5.4)

The length of this four-vector may be regarded as the rest-mass of the particle.

(b) $\mathrm{L}_r\mathrm{H}_r/c^2+W_r\mathrm{Y}_r-\mathrm{Y}_r\mathrm{Z}_r$, $\mathrm{M}_r\mathrm{H}_r/c^2+\mathrm{U}_r\mathrm{Z}_r-\mathrm{W}_r\mathrm{X}_r$, $\mathrm{N}_r\mathrm{H}_r/c^2+\mathrm{V}_r\mathrm{X}_r-\mathrm{U}_r\mathrm{Y}_r$, and $\mathrm{L}_r\mathrm{X}_r+\mathrm{M}_r\mathrm{Y}_r+\mathrm{N}_r\mathrm{Z}_r$, $r=1, \cdots, n$. (5.5)

The factors of the terms of the four-vector (b) commute. The components of the four-vector (b) commute with X_r, Y_r, Z_r, and H_r. The four-vector (b) has zero scalar product with the four-vector (a), and it may be regarded as the product of the rest-mass of the particle and its spin angular momentum.

(c) Differences for different values of r of the ratios of

$$U_r\Sigma H_s+M_r\Sigma Z_s-N_r\Sigma Y_s,\quad V_r\Sigma H_s+N_r\Sigma X_s-L_r\Sigma Z_s,$$
$$W_r\Sigma H_s+L_r\Sigma Y_s-M_r\Sigma Z_s,$$

and

$$U_r\Sigma X_s+V_r\Sigma Y_s+W_r\Sigma Z_s,$$
$$\text{to } H_r\Sigma H_s/c^2-X_r\Sigma X_s-Y_r\Sigma Y_s-Z_r\Sigma Z_s. \quad (5.6)$$

The factors of terms of these four-vectors do not commute, but the changes made in them by taking the factors in the opposite order are proportional to X_r, Y_r, Z_r, and H_r. The four-vectors have zero scalar product with ΣX_s, ΣY_s, ΣZ_s, and ΣH_s.

Thus to give our dynamics we take for μ any scalar function of the four-vectors (5.4), (5.5), and (5.6), which means any function of their lengths and scalar products, and the expressions (5.1) will commute so that (3.2), (3.3), and (3.4) will all be satisfied.

VI. THE NONRELATIVISTIC APPROXIMATION[5]

If
$$m_r^2c^4=H_r^2-c^2(X_r^2+Y_r^2+Z_r^2), \quad (6.1)$$

m_r is a scalar and commutes with all the other variables. The nonrelativistic limit for the basic variables is obtained by keeping all except H_r, $r=1, \cdots, n$, finite as c tends to infinity, but putting

$$H_r-m_rc^2\rightarrow\frac{1}{2m_r}(X_r^2+Y_r^2+Z_r^2), \quad (6.2)$$

following (6.1).

In the limit, U_r, V_r, and W_r commute, and $(U_r, X_r)=(V_r, Y_r)=(W_r, Z_r)=m_r$, so we can write

$$U_r=m_rx_r,\quad V_r=m_ry_r,\quad W_r=m_rz_r, \quad (6.3)$$

where x_r, y_r, and z_r are canonically conjugate to X_r, Y_r, and Z_r.

$$(x_r, X_r)=1,\quad (y_r, Y_r)=1,\quad (z_r, Z_r)=1. \quad (6.4)$$

We then find that if we write

$$\begin{aligned}L_r&=\lambda_r+m_r(y_rZ_r-z_rY_r),\\ M_r&=\mu_r+m_r(z_rX_r-x_rZ_r),\\ N_r&=\nu_r+m_r(x_rY_r-y_rX_r),\end{aligned} \quad (6.5)$$

λ_r, μ_r, and ν_r have Poisson brackets as for components of angular momentum,

$$(\lambda_r, \mu_r)=\nu_r,\quad (\mu_r, \nu_r)=\lambda_r,\quad (\nu_r, \lambda_r)=\mu_r. \quad (6.6)$$

[5] The equations given by C. G. Darwin, Phil. Mag. **39**, 537 (1920), and G. Breit, Phys. Rev. **34**, 553 (1929); **51**, 248 (1937); **53**, 153 (1938), may be regarded as approximations to order v^3/c^3.

The remaining Poisson brackets of x_r, y_r, z_r, X_r, Y_r, Z_r, λ_r, μ_r, ν_r, and m_r vanish.

Thus x_r, y_r, z_r, X_r, Y_r, Z_r, λ_r, μ_r, ν_r, and m_r have just the right Poisson brackets to be interpreted as the Cartesian coordinates, components of linear momentum, spin angular momentum, and mass of a nonrelativistic particle, with kinetic energy $H_r-m_rc^2$, and angular momentum components L_r, M_r, and N_r, while Eqs. (2.4) and (3.1) will give its displacement as an isolated particle in space, time, orientation, or velocity, correctly.

If we further write

$$\mu=1+V/\Sigma m_rc^2, \quad (6.7)$$

we find in the nonrelativistic limit,

$$\begin{aligned}L&=\Sigma L_r=\Sigma\{m_r(y_rZ_r-z_rY_r)+\lambda_r\},\\ M&=\Sigma M_r=\Sigma\{m_r(z_rX_r-x_rZ_r)+\mu_r\},\\ N&=\Sigma N_r=\Sigma\{m_r(x_rY_r-y_rX_r)+\nu_r\},\end{aligned} \quad (6.8)$$

$$\begin{aligned}U&=\Sigma U_r=\Sigma m_rx_r,\\ V&=\Sigma V_r=\Sigma m_ry_r,\\ W&=\Sigma W_r=\Sigma m_rz_r,\end{aligned} \quad (6.9)$$

and

$$X=\Sigma X_r,\quad Y=\Sigma Y_r,\quad Z=\Sigma Z_r, \quad (6.10)$$

with finally

$$H-\Sigma m_rc^2=\Sigma\frac{1}{2m_r}(X_r^2+Y_r^2+Z_r^2)+V, \quad (6.11)$$

where V has to be constructed out of the limiting principal parts of scalar products of the four-vectors (5.4), (5.5), and (5.6).

These four-vectors take the forms

(a) $X_r,\ Y_r,\ Z_r,\ m_rc^2+(X_r^2+Y_r^2+Z_r^2)/2m_r,$

(b) $\lambda_r,\ \mu_r,\ \nu_r,\ X_r\lambda_r+Y_r\mu_r+Z_r\nu_r,$

and (c) differences for two different values of r of

$$x_r,\ y_r,\ z_r,\ x_r(\Sigma X_s/\Sigma m_s)+y_r(\Sigma Y_s/\Sigma m_s)+z_r(\Sigma Z_s/\Sigma m_s).$$

The limiting principal parts reduce to scalar products of (a) differences for different values of r of the three-vectors

$$X_r/m_r,\ Y_r/m_r,\ Z_r/m_r, \quad (6.12)$$

(b) the three-vectors

$$\lambda_r,\ \mu_r,\ \nu_r, \quad (6.13)$$

and (c) differences of the three-vectors

$$x_r,\ y_r,\ z_r. \quad (6.14)$$

Thus in nonrelativistic limit we have the usual theory with a potential energy any scalar function of the relative positions, relative velocities, spin angular momenta, and masses of the particles.

The Reaction $Cl^{37}(p,n)A^{37}$; Excited States in A^{38}*

W. A. SCHOENFELD,† R. W. DUBORG,† W. M. PRESTON, AND C. GOODMAN
Laboratory for Nuclear Science and Engineering, Massachusetts Institute of Technology, Cambridge, Massachusetts
(Received November 12, 1951)

The relative neutron yield of the reaction $Cl^{37}(p,n)A^{37}$ has been observed from the threshold, at 1641±2 kev, up to a proton energy of 2510 kev. Over 100 resonances are found; these correspond to excited states in the compound nucleus A^{38}, with an average separation of about 5 kev.

A. INTRODUCTION

THIS is the third in a series of papers on the p,n reaction on light-intermediate weight elements. By observing resonances in the neutron yield, with the best resolution which seemed practical, we have attempted to estimate level widths and level densities in several compound nuclei in the range of excitation somewhat above the neutron binding energy. In our previous work, with targets of Mn^{55},[1] and of Cr^{53} and Cr^{54},[2] the observed average level spacing was only two to three times the experimental resolution width, and it is probable that a substantial number of levels were unresolved. For the present work we have chosen Cl^{37}, which is the lightest stable isotope, above O^{18}, with a p,n reaction threshold known to be below 3.5 Mev. It was hoped that the level spacing would be substantially greater than with Mn and Cr and hence the degree of resolution more complete.

The reaction $Cl^{37}(p,n)A^{37}$ has been studied by Richards, Smith, and Browne,[3] who found the threshold to be at 1640±4 kev. They report that many resonances were found at higher energies, without giving further details. Since the completion of our work Brostrom, Madsen, and Madsen[4] have reported an investigation of the p,n, the p,γ, and the p,α reactions on Cl^{37}. Our p,n results are in good general agreement, but we find many more resonances as a result of the higher resolution which we have employed.

B. EXPERIMENTAL METHODS

The experimental conditions and procedures were similar to those described in reference 2; protons were accelerated by the Rockefeller electrostatic generator and neutrons detected by a paraffin-surrounded, BF_3 proportional counter.

Targets were prepared by evaporating NaCl onto 10-mil tantalum disks‡ which fit on our rotating target. The p,n thresholds of Cl^{35} and Na^{22} are estimated from disintegration data to lie well above 4 Mev. The highest energy covered in this work was 2.5 Mev, which is also below the p,n thresholds of the common target contaminants carbon, nitrogen, and oxygen. We therefore believe that all resonances observed should be attributed to $Cl^{37}(p,n)$.

A number of different targets were used. At first we had difficulty from gradual evaporation of the thin NaCl. By restricting proton currents to 3 μa and by cooling the back side of the target with a fine water spray we were able to operate for many hours with little deterioration of the target.

C. EXPERIMENTAL RESULTS

The neutron yield spectrum was studied over the proton energy range from 1640 (threshold) to 2510 kev, using several targets ranging from about 1.4- to 4.0-kev stopping power. Two sections of this range were examined carefully with a single thin target; the results are shown in Figs. 1 and 2. Experimental points were taken between 0.7 and 0.8 kev apart, and the entrance and exit slit widths of the 38-cm radius magnetic analyzer were set at 0.5 mm, giving an effective energy spread of the incident proton beam of about 0.8 kev.

Figure 3 shows a resonance near 1813 kev, used as a control. The solid dots and the crosses represent readings taken before and after the data reproduced in Fig. 1: the triangles were taken after the run of Fig. 2. Target deterioration and energy-scale shift due to build-up of contamination during the two runs were negligible,§ so that the data should all be consistent.

Table I lists the observed peaks. The column headed "E_r" gives the resonance energies in kilovolts, corrected for target thickness and relativistic change of mass. No particular care was taken in calibrating the energy scale of the generator for this work, so the energies may be consistently in error by as much as 0.1 percent relative to the $Li^7(p,n)$ threshold standard, which is taken to be 1882.2 kev. The absolute error of the standard itself has been estimated as 0.1 percent.[5]

Those resonances covered in Fig. 1 or Fig. 2, and a

* This work was supported by the Bureau of Ships and the ONR.

† Lt. Commanders, U.S.N. This work was submitted in partial fulfillment of the requirements for the degree of Master of Science in Physics, at MIT by these authors.

[1] J. J. G. McCue and W. M. Preston, Phys. Rev. **84**, 1150 (1951).
[2] Lovington, McCue, and Preston, Phys. Rev. **85**, 585 (1952).
[3] Richards, Smith, and Browne, Phys. Rev. **80**, 524 (1950).
[4] Brostrom, Madsen, and Madsen, Phys. Rev. **83**, 1265 (1951).

‡ The NaCl, prepared by Johnson, Matthey, and Company, Ltd. of London and obtained through the Jarrell Ash Company of Boston, was extremely pure and certified "spectrographically standardized." The evaporation was performed by Baird Associates, Cambridge, Massachusetts.

§ It must be remarked that this degree of reproducibility is not typical; it is the most fortunate of our experience.

[5] Herb, Snowdon, and Sala, Phys. Rev. **75**, 246 (1949).

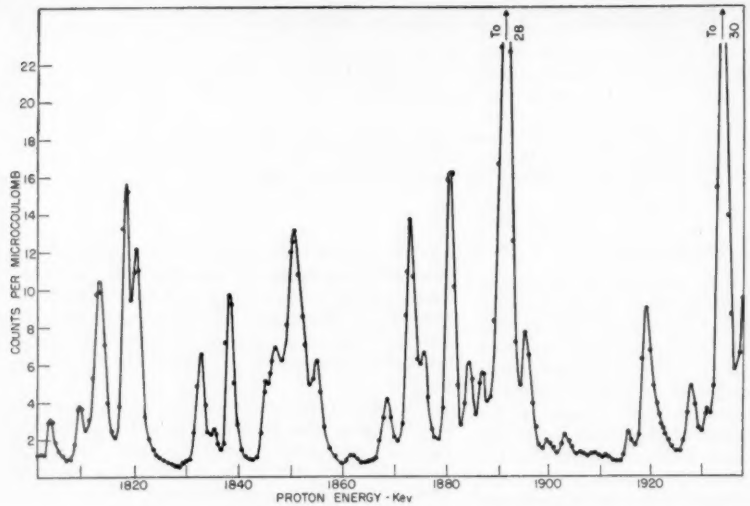

FIG. 1. Relative neutron yield from the reaction $Cl^{37}(p,n)A^{37}$ in the range of proton energy from 1803 to 1940 kev, effective resolution 1.4 kev.

few others measured with the same target, are designated by the letter "A" in column 2 of Table I. All data for these resonances are more reliable than for the others. In column 3 the letters G (good), M (medium), and P (poor) indicate the degree of resolution of each peak from its neighbors. Column 4 gives the relative observed maximum yield Y_m at the peak of each resonance, without correction for imperfect resolution. The measured yields of resonances covered only with targets other than A have been adjusted to roughly the same scale as A in order to be comparable.

The average observed width Γ_0 of the four narrowest resonances in Fig. 1 is 1.4 kev. We have set the resolution width $\Delta = 1.4$ kev at this energy. (If the natural width Γ is not negligible for these resonances, Δ may actually be somewhat less.) From the calculated energy spread in the proton beam and the variation with proton energy of energy loss in the target, Δ can be estimated for other energies. For the other targets, which were all thicker than A, the target thickness could be set equal to Γ_0 of any narrow resonance, with little error. Values of Δ are listed in column 5 of Table I.

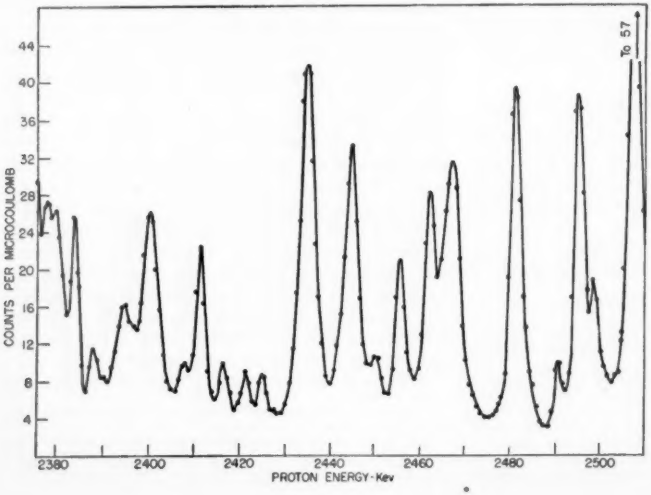

FIG. 2. Relative neutron yield from the reaction $Cl^{37}(p,n)A^{37}$ in the range from 2370 to 2510 kev, estimated effective resolution 1.6 kev.

TABLE I. Proton energies at resonance, E_r; relative maximum yields, Y_m; and estimated natural half-widths, Γ, of resonances in A^{38} from the reaction $Cl^{37}(p,n)A^{37}$. The data for resonances marked "*A*" in column 2 are more reliable than for others. In column 3 the letters *G*, *M*, and *P* designate, respectively, good, medium, or poor resolution of a particular resonance from its neighbors. Column 5 gives the estimated experimental resolution, usually set by the finite target thickness.

(1) E_r(kev)	(2)	(3)	(4) Y_m	(5) Δ	(6) Γ	(1) E_r(kev)	(2)	(3)	(4) Y_m	(5) Δ	(6) Γ
1643.0		*G*	0.8	3.7		2063.0		*G*	17	3.0	
1654.6		*G*	0.8	3.7		2075.4		*P*	4	3.0	
1664.3		*P*	0.2	3.7		2080.3		*P*	3	3.0	
1667.7		*P*	0.2	3.7		2083.7		*P*	5	3.0	
1685.0		*M*	3.2	3.7		2088.7		*P*	25	3.0	
1690.8	*A*	*G*	7.3	1.4	1.5	2094.0		*P*	32	3.0	
1702.7		*G*	3.1	3.7		2097.8		*P*	···	3.0	
1721.5		*M*	2.1	3.7		2104.1		*P*	3	3.0	
1727.7		*M*	4.0	3.7		2112.0		*G*	25	3.0	
1733.2		*M*	5	3.7		2123.5		*P*	34	3.0	
1739.8		*P*	0.6	3.7		2128.9		*P*	34	3.0	
1745.3		*M*	12	3.7		2135.0		*P*	7	3.0	
1750.1		*P*	3	3.7		2145.7		*P*	2	3.0	
1754.5		*M*	11	3.7		2148.7		*M*	5	3.0	
1763.0		*M*	7	3.7		2158.8		*M*	7	3.0	
1772.4	*A*	*G*	10	1.4	1.6	2165.7		*M*	10	3.0	
1777.6		*M*	2.4	3.8		2172.7		*M*	9	3.0	
1783.8		*P*	0.6	3.8		2179.6		*M*	6	3.0	
1788.0		*M*	3.6	3.8		2184.6		*M*	3.4	3.0	
1794.7		*M*	3.6	3.8		2189.2	*A*	*G*	30	1.5	2.7
1803.7	*A*	*M*	3.4	1.4	<1.0	2208.6		*G*	13	3.0	
1809.3	*A*	*M*	3.4	1.4	<1.0	2214.1		*P*	3	3.0	
1812.9	*A*	*G*	10	1.4	1.6	2221.5		*M*	19	3.0	
1817.8	*A*	*M*	16	1.4	<1.0	2226.1		*M*	20	3.0	
1819.9	*A*	*M*	11	1.4	1.6	2237.1		*G*	20	3.0	
1831.8	*A*	*M*	6.5	1.4	1.3	2248.8		*P*	2	3.0	
1834.9	*A*	*P*	1.5	1.4		2255.6	*A*	*P*	···	1.6	
1837.7	*A*	*G*	9.5	1.4	<1	2259.6	*A*	*G*	70	1.6	3.5
1844.8	*A*	*P*	1.0	1.4		2265.4	*A*	*P*	5	1.6	
1846.4	*A*	*P*	5	1.4	2.2	2277.9		*M*	20	2.0	
1850.0	*A*	*M*	12	1.4	2.5	2286.6		*G*	36	2.0	
1854.2	*A*	*P*	5	1.4	2.2	2302.8		*M*	14	2.0	
1863.0	*A*	*P*	0.5	1.4		2308.0		*M*	20	2.0	
1868.0	*A*	*M*	3.5	1.4	1.6	2314.0		*M*	18	2.0	
1872.3	*A*	*M*	13	1.4	<1	2323.1	*A*	*M*	34	1.6	
1875.0	*A*	*P*	6	1.4	<1	2328.6		*M*	18	2.0	
1880.0	*A*	*G*	16	1.4	<1	2348.6		*M*	10	2.0	
1883.9	*A*	*M*	5	1.4		2355.9		*P*	6	2.0	
1885.9	*A*	*M*	4	1.4		2360.3		*M*	8	2.0	
1890.9	*A*	*G*	28	1.4	2.3	2365.2		*M*	10	2.0	
1894.7	*A*	*M*	6	1.4		2370.8		*P*	12	2.0	
1899.2	*A*	*P*	1	1.4		2374.0		*M*	24	2.0	
1902.5	*A*	*M*	1.5	1.4		2376.5	*A*	*P*	15	1.6	
1914.9	*A*	*M*	2	1.4		2378.5	*A*	*P*	15	1.6	
1918.3	*A*	*M*	8	1.4		2382.5	*A*	*M*	22	1.6	
1920.3	*A*	*P*	···	1.4		2386.5	*A*	*M*	7	1.6	
1927.3	*A*	*M*	4	1.4		2393.4	*A*	*M*	10	1.6	3.3
1933.1	*A*	*G*	30	1.4	1.5	2399.1	*A*	*M*	25	1.6	4.1
1941.0	*A*	*G*	40	1.4	2.3	2406.3	*A*	*P*	6	1.6	2.5
1946.1		*M*	13	1.1		2410.0	*A*	*M*	21	1.6	1.8
1953.3		*P*	···	1.1		2414.8	*A*	*M*	8	1.6	1.8
1955.8		*M*	6	1.1		2419.9	*A*	*M*	8	1.6	
1959.4		*M*	9	1.1		2423.4	*A*	*M*	7	1.6	
1964.2		*M*	23	1.1		2433.6	*A*	*G*	42	1.6	3.1
1979.3		*P*	19	1.1		2443.2	*A*	*G*	32	1.6	3.3
1986.1	*A*	*M*	63	1.5	3.8	2448.7	*A*	*P*	6	1.6	1.8
1990.2		*P*	12	1.1		2454.0	*A*	*M*	20	1.6	2.4
1995.9		*M*	4	1.1		2460.8	*A*	*M*	22	1.6	2.1
1999.6		*M*	12	3.0		2465.4	*A*	*M*	31	1.6	4.3
2010.1		*M*	10	3.0		2479.7	*A*	*G*	40	1.6	2.4
2017.6		*G*	22	3.0		2489.0	*A*	*M*	8	1.6	
2026.5	*A*	*G*	47	1.5	4.4	2493.5	*A*	*M*	36	1.6	2.5
2042.0	*A*	*P*	10	1.5		2496.8	*A*	*M*	10	1.6	
2045.2	*A*	*M*	30	1.5		2505.9	*A*	*G*	56	1.6	2.6
2051.6		*M*	17	3.0							

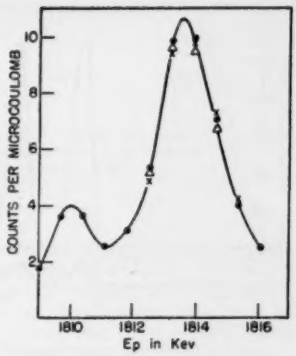

FIG. 3. A resonance near 1813 kev, used to check target deterioration and energy calibration shift. The solid dots and crosses were taken before and after the run shown in Fig. 1, the triangles after the run of Fig. 2.

Column 6 gives the natural width Γ computed from $\Gamma=(\Gamma_0^2-\Delta^2)^{\frac{1}{2}}$. In view of the approximations involved, values of Γ are not considered significant unless $\Gamma_0 \geqslant \sqrt{2}\Delta$.

Figure 4 shows the neutron yield near the p,n reaction threshold, taken with a target about 4 kev thick. An upper limit for the threshold is $E_T=1641\pm2$ kev, which agrees well with the value of 1640 ± 4 kev given by Richards *et al.*[3] Below $16\frac{1}{2}$1 kev, the scatter in the background counting rate is within the statistical error. Clearly, the true threshold (energetically speaking) may be somewhat lower if by chance there is no intervening resonance level for the emission of neutrons with low angular momentum. This illustrates the point that reaction yield thresholds do not necessarily yield accurate *Q*-values; it is necessary, in addition, to measure the energy of the emitted particles. It is likewise clear from Fig. 5 that there is often no advantage in using thick targets for precise threshold determinations. The large variations in the size and separation of resonances would make it impossible in the present case to extrapolate a thick target yield-curve to zero yield.

TABLE II. Observed average level spacing, D, in A^{38}. ΔE is the energy interval in kev, N the observed number of levels, and $D=(37/38)\times(\Delta E/N)$.

Interval	ΔE	N	D(kev)	
1643–1733	90	9	9.7	
1733–1795	62	10	6.0	
1795–1846	51	10	5.0	Region of Fig. 1 (good resolution)
1846–1891	45	10	4.4	average $D=4.9$
1891–1946	55	10	5.4	
1946–2010	64	10	6.2	
2010–2089	79	10	7.7	
2089–2159	70	10	6.8	Poorer resolution
2159–2237	78	10	7.6	average $D=7.1$
2237–2323	86	10	8.4	
2323–2383	60	10	5.8	
2383–2443	60	10	5.8	Region of Fig. 2 (good resolution)
2443–2506	63	9	6.8	average $D=6.3$
1643–2506	863	128	6.5	

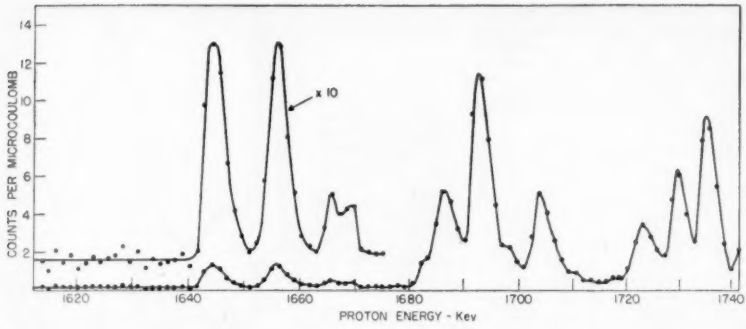

FIG. 4. Neutron yield from $Cl^{37}(p,n)A^{37}$ near the reaction threshold. The threshold is at 1641 ±2 kev, relative to the $Li(p,n)$ threshold taken as 1882 kev.

D. DISCUSSION

Table II gives the average observed level spacing, D, for successive groups of 10 levels each. The fluctuations are probably partly statistical and partly experimental. In general, two adjacent resonances will be counted as one unless their separation is equal to or greater than the observed width Γ_0 of the narrower resonance. The fraction of the total number missed will be some function of Γ_0/D. The average observed value of D is 4.9 kev for 30 levels in Fig. 1 (mean proton energy 1870 kev) and 6.3 kev for 19 levels in Fig. 2 (mean proton energy 2440 kev); both these regions were covered carefully and with approximately equal resolution, but the average value of Γ_0 of peaks in the higher energy region is greater. The average D for 60 levels in between is 7.1 kev, in a region covered with poorer resolution. It seems likely, therefore, that a value $D\sim 5$ kev is closer to the true average for the whole region covered than the observed value of 6.5 kev.

In the region 2370–2510 kev, of Fig. 2, the natural widths of the broadest resonances are significantly greater than the experimental resolution, and run from 3 to 4 kev. The partial width for emission of a particle a with angular momentum l may be expressed as $\Gamma_a{}^l = T_a{}^l(D_J/2\pi)$, where $T_a{}^l$ is the centrifugal and Coulomb barrier penetration factor and D_J is a nuclear factor related to the average spacing between levels in the compound nucleus of spin J and the same parity. The widest levels observed will involve neutron emission with $l=0$; for these levels, the total half-width $\Gamma \approx \Gamma_n{}^0$, since the penetration factor for $l=0$ neutrons is considerably larger than for $l=0$ protons or α-particles, and Γ_γ is negligible. At $E_p=2440$, neutrons emitted to the ground state of A^{37} have an energy $E_n=780$ kev, and $T_n{}^0=0.55$.[6] If we set $\Gamma_n=3.5$ kev, the experimental value,

$$D_J \approx (2\pi\Gamma_n/T_n{}^0) = 40 \text{ kev}.$$

The number of states which may be formed by protons of $l=0$, 1, or 2 with the Cl^{37} nucleus ($I=\frac{3}{2}$), and differing in J and parity, is 9. If there is any significance in so literal an interpretation of the quantities D, our result that $D_J/D\approx 8$ indicates that the observable resonances from which D has been computed include those formed by protons up to $l=2$. This is reasonable on the basis of calculated values for the barrier penetration factors, which indicate that transitions from states formed by $l=3$ protons should be unobservably weak under our experimental conditions.

The result that the average level spacing in A^{38} is about 5 kev may be compared with data for Mn^{54}, Mn^{55}, and Fe^{56}, shown in Fig. 6 of reference 2. The binding energy of a proton in A^{38} is 10.14 Mev.[7] Our value of $D=5$ kev is averaged over a small region 1.80 Mev above the proton binding energy. The excitation energy in A^{38} is therefore 11.94 Mev above the ground state, or 9.75 Mev above the reference level "R" from which the excitation energy should more properly be measured, according to Hurwitz and Bethe.[8] If we measure excitation energy from "R," the regions investigated in A^{38} and in Mn^{55} and Fe^{56} are rather closely comparable. The observed level spacing is about the same, whereas one would expect the two heavier nuclei to have a much smaller level spacing. It is possible that Mn^{55} and Fe^{56}, since they have only two more neutrons than the closed shell of 28, have smaller level densities than might otherwise be expected. Alternatively, our estimates of D for the heavier nuclei may have been considerably too large because of the less favorable ratio of resolution width to natural width.

We wish to express our appreciation to Mr. Donald Thompson and to Mr. I. E. Slawson for their invaluable aid with the Rockefeller generator.

[6] From curves in *Report of the Fast Neutron Data Project*, Nuclear Development Associates, by B. T. Feld *et al.*, January 31, 1951. We assume a nuclear radius $R=1.54^{\frac{1}{3}}\times 10^{-13}$ cm.

[7] Calculated from $Cl^{37}+n\rightarrow Cl^{38}+6.11$ Mev [Kinsey, Bartholomew, and Walker, Phys. Rev. **78**, 481 (1950)] and $Cl^{38}\rightarrow A^{38}+4.81$ Mev [L. M. Langer, Phys. Rev. **77**, 50 (1950)].

[8] H. Hurwitz and H. A. Bethe, Phys. Rev. **81**, 898 (1951).

Angular Momentum in Nonlocal Field Theory*

D. R. YENNIE†‡
Columbia University, New York, New York
(Received October 1, 1951)

The decomposition of arbitrary nonlocal fields into irreducible parts is discussed. It is shown that the spin of a nonlocal particle is made up of two parts arising, respectively, from the transformation properties and from the nonlocal nature of the field; the two parts combine vectorially to give the total spin.

IN field theory, the concept of an elementary particle is intimately associated with the notion of irreducible types of fields. In this paper we shall be concerned primarily with the decomposition of arbitrary nonlocal fields into irreducible parts and the association of these irreducible parts with particles of a given mass and spin. The decomposition of scalar and spinor nonlocal fields has already been discussed by Yukawa.[1] He found that the scalar nonlocal field could be decomposed into irreducible parts characterized by four invariant quantities which could be interpreted as the mass, spin, internal radius, and the time component of the internal extension of a resting particle. Yennie[2] derived the invariant internal angular momentum operator δ for scalar nonlocal fields; δ has the property that an irreducible part of the scalar nonlocal field is an eigenfunction of δ with eigenvalue $\hbar^2 l(l+1)$, where l is the integral spin of the particle. The present paper will present such an operator for more general types of nonlocal fields.

Fierz[3] has pointed out the essential equivalence of the different irreducible parts of the scalar nonlocal field with irreducible local tensor fields. This equivalence is based, of course, purely on the transformation properties of the fields concerned. This idea can be extended further; namely, if we decompose an arbitrary nonlocal field (e.g., a nonlocal spinor or tensor field) into its irreducible parts, each of these irreducible parts will be found to transform after one of the irreducible unitary representations of the inhomogeneous Lorentz group,[4] and to have a definite spin (integral or half-integral). Thus, as Fierz asserts, for free fields the variable r is nothing more than a spin variable; however, it is still conceivable that interactions between fields could be introduced in such a way that the variable r would really represent an internal extension of the particle.

In decomposing the internal structure of the particle into irreducible parts, it is important to note that we must consider the transformation properties of the field with respect to the inhomogeneous Lorentz group, rather than just the homogeneous Lorentz group. Physically, this means that the mass motion of the particle defines a preferred reference frame, the rest frame, which may be used in the description of the internal structure of the particle. Use of the irreducible representations of the homogeneous Lorentz group to describe the internal structure would correspond to dealing with a particle whose four-momentum is identically zero. In this paper we shall restrict ourselves to particles of nonvanishing mass so that a rest frame will always exist.

We shall now turn to a general discussion of the decomposition of nonlocal fields into irreducible parts. This discussion will be based largely on the results of a paper by Bargmann and Wigner.[5] For convenience, we give here some of the results of that paper which are important for the present applications. Briefly, their method of approach is as follows: If we have the wave functions for a free particle satisfying a relativistic wave equation, there is a correspondence between the wave functions describing the same state in different Lorentz frames. Denoting two Lorentz frames by l and l', the wave functions in the two frames are connected by

$$\psi_{l'} = U(L)\psi_l, \tag{1}$$

where $U(L)$ is a linear unitary operator which depends on the Lorentz transformation leading from l to l' (L includes inhomogeneous Lorentz transformations). The operators U form a single- or double-valued representation of the inhomogeneous Lorentz group. Bargmann and Wigner work in the Heisenberg representation, but the time development of the wave function in the Schrödinger representation may be obtained with the aid of (1) by letting L be an inhomogeneous transformation in which the time changes. The problem is to

* Publication assisted by the Ernest Kempton Adams Fund for Physical Research of Columbia University.
† AEC Predoctoral Fellow in the Physical Sciences.
‡ Now at the Institute for Advanced Study, Princeton, New Jersey.
[1] H. Yukawa, Phys. Rev. **80**, 1047 (1950).
[2] D. R. Yennie, Phys. Rev. **80**, 1053 (1950).
[3] M. Fierz, Phys. Rev. **78**, 184 (1950); Helv. Phys. Acta **23**, 412 (1950).
[4] The homogeneous Lorentz group consists of Lorentz transformations of the form

$$x' = \Lambda x \text{ (or } x_\mu' = \Lambda_\mu^\nu x_\nu),$$

while the inhomogeneous Lorentz group consists of Lorentz transformations with a change of origin

$$x' = \Lambda x + a \text{ (or } x_\mu' = \Lambda_\mu^\nu x_\nu + a_\mu).$$

We shall restrict ourselves to transformations which may be generated by infinitesimal transformations starting with the identity; i.e., we exclude time reversals and space reflections. The notation employed in this paper will be the same as in references 1 and 2.
[5] V. Bargmann and E. P. Wigner, Proc. Natl. Acad. Sci. **34**, 211 (1948).

discover and classify all of the irreducible (single- or double-valued) representations of the inhomogeneous Lorentz group; this then gives a classification of all possible relativistic wave equations.

The states of a given irreducible representation are specified by a momentum vector k_μ and a spin variable ξ, which in our case is discrete. Bargmann and Wigner require that k_μ be not identically zero, thus ruling out the representations of the homogeneous Lorentz group as being not physically significant for this application. For a given irreducible representation, all of the states satisfy $k_\mu k^\mu + \kappa^2 = 0$, with κ independent of the state (we shall assume in this discussion that $\kappa \neq 0$, although Bargmann and Wigner also consider the case in which the mass vanishes). For every Lorentz transformation

$$x' = \Lambda x + a \quad (x_\mu' = \Lambda_\mu^{\ \nu} x_\nu + a_\mu) \tag{2}$$

there is a unitary operator defined by

$$U(L)\psi(k, \xi) = \exp(-ia_\mu k^\mu) Q(k, \Lambda)\psi(\Lambda^{-1}k, \xi), \tag{3}$$

where $Q(k, \Lambda)$ is a unitary operator which may depend on k but acts only on ξ.[6] The subgroup of Lorentz transformations obtained by keeping some momentum vector k_0 invariant is called a "little group." Little groups defined by different arbitrary vectors k_0 are isomorphic to each other and to the three-dimensional rotation group. The $Q(k_0, \xi)$ form an irreducible representation of the little groups. The irreducible representations of the inhomogeneous Lorentz group are completely characterized by the value of κ, the sign of k^4, and by the irreducible representations of the three-dimensional rotation group. The momentum p_μ and the angular momentum $M_{\mu\nu}$ are introduced as the infinitesimal generators of translations and rotations, respectively.

Let us now apply these results to nonlocal field theory. Consider a very general type of nonlocal field:

$$U_i(X, \mathbf{r}).$$

The subscript i denotes that this is the ith component of some tensor or spinor quantity having a transformation equation of the type:

$$Z_i' = \sum_j B_{ij}(\Lambda) Z_j. \tag{4}$$

The transformation equation for the nonlocal field under the Lorentz transformation (2) is:

$$U_i'(X', \mathbf{r}') = \sum_j B_{ij} U_j(X, \mathbf{r}). \tag{5}$$

In the momentum representation this is

$$u_i'(k, \mathbf{r}') = \sum_j B_{ij}(\Lambda) u_j(\Lambda^{-1}k, \Lambda^{-1}\mathbf{r}') \exp(-ik_\mu a^\mu). \tag{6}$$

For an irreducible representation this should reduce to the form (3); a reducible representation should reduce to a direct sum of representations of the form (3).

To carry out the reductions we turn to the identification of the infinitesimal operators in configuration space. The momentum is the generator of the infinitesimal translation

$$x_\mu' = x_\mu + \epsilon_\mu. \tag{7}$$

The defining equation for the momentum operator is:

$$\begin{aligned} -(i/\hbar)\epsilon_\mu P^\mu U_i(X, \mathbf{r}) &= U_i'(X, \mathbf{r}) - U_i(X, \mathbf{r}) \\ &= U_i(X - \epsilon, \mathbf{r}) - U_i(X, \mathbf{r}), \end{aligned}$$

yielding

$$P_\mu = (\hbar/i)(\partial/\partial X^\mu). \tag{8}$$

For the angular momentum, we consider the infinitesimal homogeneous transformation

$$x_\mu' = x_\mu + \epsilon_{\mu\nu} x^\nu, \quad \epsilon_{\mu\nu} = -\epsilon_{\nu\mu}. \tag{9}$$

The angular momentum operator is defined by:

$$\begin{aligned} \tfrac{1}{2}(i/\hbar)\epsilon_{\mu\nu} M^{\mu\nu} U_i(X, \mathbf{r}) &= U_i'(X, \mathbf{r}) - U_i(X, \mathbf{r}) \\ &= \{\textstyle\sum_j B_{ij} U_j(\Lambda^{-1}X, \Lambda^{-1}\mathbf{r})\} - U_i(X, \mathbf{r}). \end{aligned}$$

For an infinitesimal transformation, B_{ij} takes the form

$$B_{ij} = \delta_{ij} + \tfrac{1}{2}\epsilon_{\mu\nu}\{\beta_{ij}{}^{\mu\nu} - \beta_{ij}{}^{\nu\mu}\}.$$

The total angular momentum may be expressed as the sum of an orbital part and a spin part:

$$(M^{\mu\nu})_{ij} = (M_0{}^{\mu\nu})_{ij} + (S^{\mu\nu})_{ij}, \tag{10}$$

where

$$M_0{}^{\mu\nu} = (h/i)(X^\mu \partial/\partial X_\nu - X^\nu \partial/\partial X_\mu) \tag{11}$$

is the orbital part, and

$$\begin{aligned} (S^{\mu\nu})_{ij} &= (S_r{}^{\mu\nu})_{ij} + (S_{\mathbf{r}}{}^{\mu\nu})_{ij} \\ &= (h/i)(r_\mu \partial/\partial r_\nu - r^\nu \partial/\partial r_\mu)\delta_{ij} + (h/i)(\beta_{ij}{}^{\mu\nu} - \beta_{ij}{}^{\nu\mu}) \end{aligned} \tag{12}$$

is the spin part.

In order to carry out the reduction of a nonlocal field into irreducible parts, we next consider the little group obtained by holding a momentum vector k_0 fixed. We choose

$$(k_0)_1 = (k_0)_2 = (k_0)_3 = 0, \quad (k_0)^4 = \kappa. \tag{13}$$

The little group then reduces to the group of rotations in ordinary three-dimensional space. In this Lorentz system, we now look at the particular field component which represents a particle at rest, namely:

$$u_i(k_0, \mathbf{r}).$$

These quantities form a basis for a (reducible) representation of the rotation group. To carry out the reduction of this representation, we use the spin operators (12). The infinitesimal generators of the little group are now related to a three-dimensional angular momentum vector by

$$\{S_x, S_y, S_z\} \equiv \{S^{23}, S^{31}, S^{12}\}. \tag{14}$$

These operators satisfy the usual angular momentum

[6] Q is a matrix operator:
$$Q\psi(k, \xi) = \Sigma_\eta Q(k, \Lambda)_{\xi\eta}\psi(k, \eta).$$
E. P. Wigner, Ann. Math. **40**, 149 (1939) gives a derivation of (3).

commutation rules:

$$[S_x, S_y]=ihS_z, \text{ etc.} \tag{15}$$

The eigenfunctions and eigenvalues of these operators satisfy:

$$\begin{aligned} S_z\chi(s,m)&=\hbar m\chi(s,m),\\ [(S_x)^2+(S_y)^2+(S_z)^2]\chi(s,m)&=\hbar^2 s(s+1)\chi(s,m),\end{aligned} \tag{16}$$

also

$$(S_x\pm iS_y)\chi(s,m)=\hbar[(s\mp m)(s\pm m+1)]^{\frac{1}{2}}\chi(s,m\pm 1). \tag{17}$$

The set of functions with fixed s and $-s\leqslant m\leqslant s$ form the basis for an irreducible representation of the rotation group; s may have the values 0, $\frac{1}{2}$, 1, $\frac{3}{2}$, 2, $\cdots$. This decomposition may be applied to the r and β parts of the spin separately, and the results combined according to the rules for addition of angular momenta.

The simplest case is the scalar nonlocal field. In that case i takes on only one value, which may be omitted; the β part of the spin is zero. Introducing spherical coordinates

$$\begin{aligned} r_1&=a\sin\theta\cos\varphi, \quad r_2=a\sin\theta\sin\varphi,\\ r_3&=a\cos\theta, \quad r^4=r^4,\end{aligned} \tag{18}$$

the field component may be expanded in spherical harmonics

$$u(k_0,r)=\sum_{l,\,m,\,\alpha} u_{l,m,\alpha}(k_0)f_{l,\alpha}(r^4,a)Y_{l,m}(\theta,\varphi). \tag{19}$$

Each value of l yields a different irreducible representation and a spin l. Using the scalar nonlocal field, it is possible to obtain only integral values for the spin; half-integral spins, represented by double-valued functions, may be ruled out by arguments given by Pauli.[7] In a quantized field theory, the $u_{l,m,\alpha}(k_0)$ would become creation and destruction operators.

There is no criterion available by which the functional form of $f_{l,\alpha}(r^4,a)$ may be determined. It is possible that for each value of l there are several functions $f_{l,\alpha}$ (possibly some sort of a complete set); i.e., the representation corresponding to spin l may be contained several times in a nonlocal scalar field. The different $f_{l,\alpha}$, would then presumably correspond to different values of some intrinsic physical property of the particle such as charge or mass, designated in the sum by α. One possible way of defining $f_{l,\alpha}$ has been given by Yukawa:[1]

$$f_{l,\lambda,M}=\delta(r_\mu r^\mu-\lambda^2)\delta(r_\mu k^\mu-M) \tag{20}$$

where λ is the radius of the particle and (M/κ) is the time component of the internal extension of the resting particle. As far as transformation properties are concerned, (20) is quite arbitrary, and we shall leave the form of $f_{l,\alpha}$ unspecified in the remainder of this discussion.

The next case yielding integral spin is the vector nonlocal field. With respect to β the vector field may be split into two irreducible parts whose bases are[8]

$$\{u_1, u_2, u_3\}, \tag{21a}$$

$$\{u^4\}. \tag{21b}$$

Under the little group, (21b) transforms as a scalar and contributes zero to the spin; it may be handled in the same manner as the scalar field. Under a rotation, (21a) transforms as an ordinary three-vector and gives a contribution of one to the β-part of the spin. As in the case of the scalar field, the r part of the spin is l, a nonnegative integer. For a given l, the total intrinsic spin may have three values

$$s=l+1,\ l,\ l-1 \quad (s\not<0).$$

Also, a given $s(\neq 0)$ may be obtained in three different ways using

$$l=s-1,\ s,\ s+1.$$

In order to specify the representation completely, we must therefore give the value of l as well as s. The different states (with a given l and s) are specified by m_s, the projection of s on the z axis. The expansion of (21a) into irreducible parts accordingly takes the form:

$$u_i(k_0,r)=\sum_{s,\,m_s,\,l,\,m_l,\,\alpha} u_{s,\,m_s,\,l,\,\alpha}(k_0)f_{s,\,l,\,\alpha}(r^4,a) \times c_{i,\,s,\,m_s,\,l,\,m_l}Y_{l,\,m_l}(\theta,\varphi). \tag{22}$$

The c's are not arbitrary, but must be properly chosen to give the desired representation. The expansion coefficient is $u_{s,\,m_s,\,l,\,\alpha}$, which becomes a creation or destruction operator when the field is quantized.

In order to obtain half odd integral spins, we must take u_i to be a spinor quantity. For example, a four-component spinor satisfying the Dirac equation represents a particle of spin one-half (for $k^4>0$ only two of the components are independent as far as transformation properties are concerned, provided reflections of coordinates are not included in the group of transformations). If l is the r part of the spin, the total spin will be $l+\frac{1}{2}$, or $l-\frac{1}{2}$. Each total spin can be formed in two ways.

The preceding process can evidently be carried through for an arbitrary nonlocal field. We therefore assume that we know the irreducible parts of the quantities $u_i(k_0, r)$ in the system specified by (13). Let us consider a particular representation with total spin s, and r-spin l; then the known representation has components of the form $u_{i,\alpha}{}^{(0)}(k_0, m_s, r)$, where m_s takes on

[7] W. Pauli, Helv. Phys. Acta **39**, 147 (1939).

[8] The separation (21) applies only in the rest system. In an arbitrary Lorentz frame, (21) becomes:

$$v_\mu=u_\mu-(1/\mathrm{K}^2)(\partial^2 u_\nu/\partial X_\nu\partial X^\mu), \tag{21'a}$$

$$B=(i/\mathrm{K})\partial u_\mu/\partial X_\mu. \tag{21'b}$$

(21'a) satisfies:

$$\partial v_\mu/\partial X_\mu=0.$$

If u_μ were a local field, B would transform as a scalar field and v_μ as an irreducible vector field. Thus (21') gives a decomposition of $u_\mu(X, r)$ into irreducible parts with respect to the β-part of the transformation.

$2s+1$ discrete values; s, $s-1$, $\cdots$, $-s$. These components are expressible in the form

$$u_{i,\alpha}{}^{(0)}(k_0, m_s, r) = u_{s, m_s, l, \alpha}(k_0) f_{s, l, \alpha}(r^4, a) \times \sum_{m_l} c_{i, s, m_s, l, m_l} Y_{l, m_l}(\theta, \varphi) \quad (23)$$

$$= u_{s, m_s, l, \alpha}(k_0) \chi_{i,\alpha}{}^{(0)}(k_0, m_s, r).$$

The c's are not arbitrary constants, but must be specially chosen so that $u_{i,\alpha}{}^{(0)}(k_0, m_s, r)$ will have the desired properties. The $u_{s, m_s, l, \alpha}$ are the expansion coefficients which become creation and destruction operators in quantized field theory. (23) holds in the special Lorentz frame (13). In an arbitrary Lorentz frame we define:

$$\chi_{i,\alpha}{}'(k, m_s, r) = \sum_j B_{ij}(\Lambda) \chi_{j,\alpha}{}^{(0)}(\Lambda^{-1}k, m_s, \Lambda^{-1}r) \quad (24)$$

where Λ is a Lorentz transformation such that $\Lambda^{-1}k = k'$, with the space parts of k' equal to zero. There is a certain arbitrariness in this definition since $R\Lambda^{-1}k = k'$ also (where R is a rotation of three-space) and $\chi_{j,\alpha}{}^{(0)}(k', m_s, \Lambda^{-1}r) \neq \chi_{j,\alpha}{}^{(0)}(k', m_s, R\Lambda^{-1}r)$; generally, however, we would have an expression of the form:

$$\chi_{i',\alpha}{}'(k, m_s{}', r) = \sum_{j, m_s} \alpha_{m_s' m_s}(\Lambda) B_{i'j}(\Lambda) \times \chi_{j,\alpha}{}^{(0)}(\Lambda^{-1}k, m_s, \Lambda^{-1}r) \quad (24')$$

where $\det(\alpha_{m_s' m_s}) \neq 0$. Equation (24′) differs from (24) only by a similarity transformation. Similarly, for a different momentum $\bar{k}$:

$$\chi_{i'',\alpha}{}''(k, m_s{}'', r) = \sum_{j, m_s} \alpha_{m_s'' m_s}(\bar{\Lambda}) B_{i''j}(\bar{\Lambda}) \times \chi_{j,\alpha}{}^{(0)}(\bar{\Lambda}^{-1}\bar{k}, m_s, \bar{\Lambda}^{-1}r).$$

The $\chi^{(0)}$'s may now be eliminated, leaving

$$\chi_{i'',\alpha}{}''(\bar{k}, m_s{}'', r) = \sum_{i', m_s'} A_{m_s'' m_s'}(\bar{\Lambda}\Lambda^{-1}) \times B_{i''i'}(\bar{\Lambda}\Lambda^{-1}) \chi_{i',\alpha}{}'(\Lambda\bar{\Lambda}^{-1}k, m_s', \Lambda\bar{\Lambda}^{-1}r) \quad (25)$$

where the A's arise as a result of the elimination of the $\chi^{(0)}$'s. The over-all transformation is now:

$$\bar{k} = (\bar{\Lambda}\Lambda^{-1})k = \Lambda' k.$$

This removes the restriction of a special Lorentz frame specified by k_0. It should be pointed out that when k and m_s are given, the r dependence and the β dependence of $\chi_{i,\alpha}(k, m_s, r)$ are determined. We may accordingly write (25) (somewhat symbolically) in the form

$$\chi_\alpha{}''(k, m_s{}'') = \sum_{m_s} A_{m_s'' m_s'}(\Lambda') \chi_\alpha{}'([\Lambda']^{-1}k, m_s') \quad (26)$$

in agreement with (3).

So far the infinitesimal operators of the little group have been defined only in the rest system. These operators may be considered to be the components of a tensor operator $J_{\mu\nu}$, which has the following special form in the rest system:

$$\{J_{23}, J_{31}, J_{12}\} \equiv \{S_{23}, S_{31}, S_{12}\}, \quad \{J_{14}, J_{24}, J_{34}\} \equiv \{0, 0, 0\}. \quad (27)$$

This may be expressed in the covariant form:

$$J_{\mu\nu} = S_{\mu\nu} + (1/(P_\sigma P^\sigma))(S_{\nu\lambda}P_\mu - S_{\mu\lambda}P_\nu)P^\lambda. \quad (28)$$

In the rest system, the square of the spin is given by:

$$S^2 = (S_x)^2 + (S_y)^2 + (S_z)^2.$$

From (27) and (28), this may be expressed as an invariant operator:

$$S^2 = \tfrac{1}{2}J_{\mu\nu}J^{\mu\nu} = \tfrac{1}{2}S_{\mu\nu}S^{\mu\nu} - S_{\mu\nu}S^{\lambda\nu}P_\lambda P^\mu (P_\sigma P^\sigma)^{-1}. \quad (29)$$

We may form an S^2 operator for the r and β parts of the spin separately, and for the total spin. The irreducible part of the field is then characterized by three numbers l, t, and s, which have the following significance:

$S_r{}^2$ has eigenvalues $\hbar^2 l(l+1)(l = 0, 1, 2, \cdots)$,

$S_\beta{}^2$ has eigenvalues $\hbar^2 t(t+1)(t = 0, \tfrac{1}{2}, 1, \tfrac{3}{2}, \cdots)$,

S^2 has eigenvalues $\hbar^2 s(s+1) \times (s = |l+t|, |l+t-1|, \cdots |l-t|)$.

S^2 is the generalization of δ which was mentioned in the introductory paragraph.

In conclusion, it should be emphasized again that the preceding considerations apply only to free fields. It has been shown that an arbitrary nonlocal field can be decomposed into irreducible parts whose transformation properties are determined by the irreducible representations of the inhomogeneous Lorentz group. As far as transformation properties are concerned, an irreducible part of a nonlocal field is therefore equivalent to some type of local field, as asserted by Fierz.[3] This equivalence can be removed only by introducing an interaction between fields in a way which depends on the nonlocal character of the fields involved. Although it is unsatisfactory in certain respects, such an interaction scheme has been introduced by Yukawa;[1] in his formalism, the nonlocal character of the field is manifested in the occurence of convergence factors,[2] demonstrating that r is more than a spin variable. However, we must admit that it may not be possible to find a completely satisfactory interaction scheme which will have physical consequences depending on the internal structure. In that case, nonlocal field theory would give only a new method of introducing particles of different spins, and it might not be possible to distinguish the two types of spin individually.

The author is deeply indebted to Professor H. Yukawa for encouragement and guidance in this work, and to Professors N. Kroll and G. Yevick for criticisms of the manuscript.

Multiple Compton Scattering of Low Energy Gamma-Radiation

R. C. O'ROURKE
Electricity Division, Naval Research Laboratory, Washington, D. C.

(Received November 14, 1951)

This paper contains solutions to several problems of multiple Compton scattering of low energy gamma-radiation ($E \ll 1$ Mev). The results have been obtained by an approximate method proposed by Chandrasekhar. The solutions indicate an appreciable broadening of a primary monochromatic spectral distribution after it has passed through relatively small distances in the scattering medium.

The results for the forward scattering spectral distributions exhibit small shifts to the violet because of an approximation employed (*viz.*, a Taylor series development). Chandrasekhar proposed that the area of this violet shift be used as a criterion of error. If this is accepted, then the error is less than 15 percent at a distance of $x=1$ and decreases rapidly with increasing x. The corresponding results for the backscattering spectral distributions exhibit negative intensities near the source, i.e., for small x. Again the area of this negative portion of the spectral distribution curves becomes negligible as x increases. It requires a great deal of graphical integration to plot the results for the backscattering in the plane parallel media over the required range of wavelength shifts which is some 20–30 Compton units. One can exhibit the negative intensities, however, by plotting the results over a range of zero to about 5 Compton units. In the case of a point source in an infinite spherical medium the backscattering spectral distribution was obtained in closed form and Fig. 5 shows the results for two values of x. One can see from Fig. 5 that the area of negative intensity becomes negligible as x increases.

The method of Chandrasekhar seems to yield qualitatively correct results if one uses only distances x which are greater than about $x=2$. One cannot check the results, however, since one cannot carry out the higher approximations in any practical manner. In brief, if one tries to include either the higher derivatives in the Taylor series or to go to the higher approximations of the Gauss and Radau methods, or both, one is lead to a system of partial differential equations of high order which cannot be solved by any practical method.

SECTION 1. THE TRANSPORT EQUATION

THE following well-known transport equation governs the multiple scattering of gamma-radiation for energies below those critical energies above which secondary Compton electrons and pairs can produce additional gammas by bremmstrahlung.[1]

Plane Parallel Media

$$\mu\frac{\partial}{\partial z}I(z,\mu,\sigma)+N\pi r_0^2\phi_T(\sigma)I(z,\mu,\sigma)=N\int_{-1}^{+1}\int_0^{2\pi}\frac{r_0^2}{2}\left(\frac{\sigma'}{\sigma}\right)^2\left\{\frac{\sigma'}{\sigma}+\frac{\sigma}{\sigma'}-\sin^2\Theta\right\}\times I(z,\mu',\sigma')d\mu'd\varphi', \quad (1.01)$$

where

$$E=\epsilon mc^2;\quad \sigma=\frac{1}{\epsilon}=\frac{mc}{k}\equiv\frac{1}{\lambda}$$

$$\sigma'=\sigma-1+\cos\Theta;\quad \mu=\cos\vartheta$$

$$\cos\Theta=\mu\mu'+(1-\mu^2)^{\frac{1}{2}}(1-\mu'^2)\cos\varphi'.$$

$\pi r_0^2\phi_T(\sigma)$ = total cross section (photoelectric+Compton+pair production) per electron

N = number of electrons per cm^3

r_0 = electron radius.

Axial symmetry has been assumed so that $\varphi=0$ is allowed; but, of course, $\varphi'=0$. The corresponding transport equation for spherical symmetry is

$$\mu\frac{\partial}{\partial r}I(r,\mu,\sigma)+\frac{1-\mu^2}{r}\frac{\partial}{\partial\mu}I(r,\mu,\sigma)+N\pi r_0^2\phi_T(\sigma)I(r,\mu,\sigma)=N\int_{-1}^{+1}\int_0^{2\pi}\frac{r_0^2}{2}\left(\frac{\sigma'}{\sigma}\right)^2\left\{\frac{\sigma'}{\sigma'}+\frac{\sigma}{\sigma'}-\sin^2\Theta\right\}\times I(r,\mu',\sigma')d\mu'd\varphi', \quad (1.02)$$

where the notation is the same as above.

[1] L. Foldy, Phys. Rev. **81**, 395 (1951).

It is rather too ambitious at the present time to attempt to find explicit solutions of these integro-differential equations. Instead only the corresponding transport equations for multiple Compton scattering of low energy gammas will be considered in this article. The Klein-Nishina differential cross section can be replaced by that of Thompson. Equations (1.01) and (1.02) reduce to

$$\mu\frac{\partial}{\partial z}I(z,\mu,\sigma)+\frac{8}{3}N\pi r_0^2I(z,\mu,\sigma)=N\int_{-1}^{+1}\int_0^{2\pi}\frac{r_0^2}{2}(1+\cos^2\Theta)I(z,\mu',\sigma')d\mu'd\varphi' \quad (1.03)$$

and

$$\mu\frac{\partial}{\partial r}I(r,\mu,\sigma)+\frac{1-\mu^2}{r}\frac{\partial}{\partial\mu}I(r,\mu,\sigma)+\frac{8}{3}N\pi r_0^2I(r,\mu,\sigma)=N\int_{-1}^{+1}\int_0^{2\pi}\frac{r_0^2}{2}\{1+\cos^2\Theta\}I(r,\mu',\sigma')d\mu'd\varphi', \quad (1.04)$$

respectively.[2] In this first paper, the method of Chandrasekhar will be employed; he replaces the normalized differential cross section by unity; that is,

$$\tfrac{3}{4}(1+\cos^2\Theta)=1. \quad (1.05)$$

A second paper based on the spherical harmonic method of Marshak is being prepared in which one does not have to make this approximation. The question is whether it is fair to ignore the partial polarization of the multiply scattered gammas and keep the differential cross section.[2] For the present then, the following variables are to be used:

$$\tau=(8/3)N\pi r_0^2\cdot z;\quad \rho=(8/3)N\pi r_0^2\cdot r. \quad (1.06)$$

[2] S. Chandrasekhar, *Radiative Transfer* (Oxford University Press, London, 1950), p. 329.

Equations (1.03) and (1.04) become

$$\mu\frac{\partial}{\partial\tau}I(\tau,\mu,\sigma)+I(\tau,\mu,\sigma)=\frac{1}{4\pi}\int_{-1}^{+1}\int_{0}^{2\pi}I(\tau,\mu',\sigma')d\mu'd\varphi' \quad (1.07)$$

and

$$\mu\frac{\partial}{\partial\rho}I(\rho,\mu,\sigma)+\frac{1-\mu^2}{\rho}\frac{\partial}{\partial\mu}I(\rho,\mu,\sigma)+I(\rho,\mu,\sigma)=\frac{1}{4\pi}\int_{-1}^{+1}\int_{0}^{2\pi}I(\rho,\mu',\sigma')d\mu'd\varphi', \quad (1.08)$$

respectively.

SECTION 2. THE METHOD OF CHANDRASEKHAR

The method of Chandrasekhar[3] will be employed to solve Eqs. (1.07) and (1.08). He has published the solution of Eq. (1.07) for a plane parallel finite medium with a source on one side $\tau=0$, say, which radiates uniformly over all angles. This section will present the solutions to the semi-infinite parallel medium obtained by two different methods, namely, the methods of Gauss and Radau for numerical quadratures. Also Chandrasekhar's problem of a finite medium will be obtained by the usual method of separation of variables, thus avoiding the use of Green's functions. Chandrasekhar's method of approach is as follows: One first develops $I(\tau,\mu',\sigma')$ in a Taylor series

$$I(\tau,\mu',\sigma')=I(\tau,\mu',\sigma)-(1-\cos\Theta)(\partial/\partial\sigma)I(\tau,\mu',\sigma)+\cdots; \quad (2.01)$$

then the transport equation becomes

$$\mu\frac{\partial}{\partial\tau}I(\tau,\mu,\sigma)+I(\tau,\mu,\sigma)=\frac{1}{2}\int_{-1}^{+1}d\mu'\left\{I(\tau,\mu',\sigma)-(1-\mu\mu')\frac{\partial}{\partial\sigma}I(\tau,\mu',\sigma)\right\}. \quad (2.02)$$

One then applies either of two well-known formulas for numerical quadratures which allows one to replace Eq. (2.02) by a system of partial differential equations of first order. The first of these methods is a result of Gauss.

The Method of Gauss

$$\int_{-1}^{+1}f(\mu)d\mu\cong\sum_{i=1}^{m}a_jf(\mu_j), \quad (2.03)$$

where $f(\mu)$ need not be a polynomial [the relation (2.03) would then be exact if polynomial has degree $\leq 2m-1$]. The Christoffel numbers a_j are given by

$$a_j=\frac{1}{P_m'(\mu_j)}\int_{-1}^{+1}\frac{P_m(\mu)}{\mu-\mu_j}d\mu; \quad '\equiv\frac{d}{d\mu} \quad (2.04)$$

and μ_j are roots of

$$P_{2n}(\mu)=0, \quad n=1,2,\cdots. \quad (2.05)$$

One has the following first approximation values which are to be used below:

$$\mu_{\pm1}=\pm(1/\sqrt{3}); \quad a_{\pm1}=1. \quad (2.06)$$

A second method is due to Radau.

The Method of Radau

$$\int_{-1}^{+1}f(\mu)d\mu\cong\frac{2}{m(m+1)}\sum_{i=1}^{m+1}\frac{f(\mu_j)}{[P_m(\mu_j)]^2}, \quad (2.07)$$

where

$$a_j=[2/m(m+1)][P_m(\mu_j)]^{-2} \quad (2.08)$$

and μ_j are roots of $(1-\mu^2)P_m'(\mu)=0$. Radau's method has the great advantage that in all orders of approximation $\mu_{\pm1}=\pm1$ are roots. This means that one can in principle study the convergence of the higher approximations to the exact value of $I(\tau,\mu=\pm1,\sigma)$. In Gauss' method the μ_j all change and one never finds the solution for the same $I(\tau,\mu_j,\sigma)$ in all orders of approximation. Finally, since only the first approximation to the present problem can be readily carried out, it is advantageous to use both the method of Gauss and Radau. This will indicate the angular dependence of the multiply scattered radiation to some extent. The first values of μ_j, a_j in the method of Radau are

$$\mu_{\pm1}=1; \quad a_{\pm1}=1. \quad (2.09)$$

Proceeding then, first with the method of Gauss, Eq. (2.02) becomes

$$\mu_i\frac{\partial}{\partial\tau}I_i(\tau,\sigma)+I_i(\tau,\sigma)=\frac{1}{2}\sum_{j=1}^{m}a_j\left\{I_j(\tau,\sigma)-(1-\mu_i\mu_j)\frac{\partial}{\partial\sigma}I_j(\tau,\sigma)\right\}, \quad (2.10)$$

where

$$I_i(\tau,\sigma)=I(\tau,\mu_i,\sigma); \quad m=2; \quad \mu_{\pm1}=\pm1/\sqrt{3}; \quad a_{\pm1}=1$$

one finds the following system of equations,

$$\begin{aligned}(\sqrt{3}/2)(\partial/\partial x)(I_{+1}-I_{-1})&=-\tfrac{3}{2}(\partial/\partial y)(I_{+1}+I_{-1})\\(\sqrt{3}/2)(\partial/\partial x)(I_{+1}+I_{-1})&=\tfrac{1}{2}(\partial/\partial y)(I_{+1}-I_{-1})\\&\quad-(I_{+1}-I_{-1}),\end{aligned} \quad (2.11)$$

where

$$x=\tfrac{3}{2}\tau; \quad y=\tfrac{3}{2}(\sigma-\sigma_0)$$

and $\sigma_0=\gamma^{-1}\lambda_0$, where λ_0 is the primary wavelength of the source. From the first of Eqs. (2.11), one can

[3] See reference 2, Chapter II.

introduce

$$I_{+1}-I_{-1}=\sqrt{3}\partial S(x,y)/\partial y$$
$$I_{+1}+I_{-1}=-\partial S(x,y)/\partial x. \tag{2.12}$$

The second Eq. (2.11) then yields

$$\partial^2 S/\partial x^2+\partial^2 S/\partial y^2=2\partial S/\partial y \tag{2.13}$$

which reduces to

$$\partial^2 f/\partial x^2+\partial^2 f/\partial y^2-f=0, \tag{2.14}$$

where

$$f(x,y)=e^{-y}S(x,y).$$

Expressing $I_{\pm 1}(x,y)$ in terms of $f(x,y)$ one has

$$I_{+1}(x,y)=\tfrac{1}{2}e^{y}\{-\partial f/\partial x\pm\sqrt{3}(f+\partial f/\partial y)\}. \tag{2.15}$$

For the semi-infinite problem, the method of separation of variables gives

$$f(x,y)=\int_{-\infty}^{\infty}A(\alpha)\exp[-(1+\alpha^2)^{\frac{1}{2}}x+i\alpha y]d\alpha, \tag{2.16}$$

which has been chosen so that the solutions will behave properly at infinity. The boundary condition which determines $A(\alpha)$ is

$$I_{+1}(0,y)=1\cdot\delta(\sigma-\sigma_0)=\tfrac{2}{3}\delta(y). \tag{2.17}$$

One then has the following equality

$$\int_{-\infty}^{\infty}A(\alpha)\{(1+\alpha^2)^{\frac{1}{2}}+\sqrt{3}(1+i\alpha)\}e^{i\alpha y}d\alpha = \frac{3}{2\pi}\int_{-\infty}^{\infty}e^{i\alpha y}d\alpha \tag{2.18}$$

or

$$A(\alpha)=\frac{3}{2\pi}\frac{1}{(1+\alpha^2)^{\frac{1}{2}}+\sqrt{3}(1+i\alpha)}. \tag{2.19}$$

Substituting (2.19) into (2.15), (2.16) one obtains the following results:

$$I_{+1}(x,y)=\frac{3}{4\pi}e^{y}\int_{-\infty}^{\infty}\exp[-(1+\alpha^2)^{\frac{1}{2}}x+i\alpha y]d\alpha$$
$$I_{-1}(x,y)=\frac{3}{4\pi}e^{y}\int_{-\infty}^{\infty}\frac{(1+\alpha^2)^{\frac{1}{2}}-\sqrt{3}(1+i\alpha)}{(1+\alpha^2)^{\frac{1}{2}}+\sqrt{3}(1+i\alpha)} \times\exp[-(1+\alpha^2)^{\frac{1}{2}}x+i\alpha y]d\alpha. \tag{2.20}$$

The first of these integrals can be performed explicitly; the result is

$$I_{+1}(x,y)=-\tfrac{3}{4}e^{y}x(x^2+y^2)^{-\frac{1}{2}}H_1^{(1)}[i(x^2+y^2)^{\frac{1}{2}}]. \tag{2.21}$$

The other integral can be evaluated by graphical methods. In real form it reads

$$I_{-1}(x,y) = I_{+1}(x,y)-\frac{3\sqrt{3}}{2\pi}e^{y}\int^{\infty}\left\{\frac{1+\sqrt{3}(1+\alpha^2)^{\frac{1}{2}}}{\sqrt{3}+2(1+\alpha^2)^{\frac{1}{2}}}\cos\alpha y - \frac{\alpha\sin\alpha y}{\sqrt{3}+2(1+\alpha^2)^{\frac{1}{2}}}\right\}\exp[-(1+\alpha^2)^{\frac{1}{2}}x]d\alpha. \tag{2.22}$$

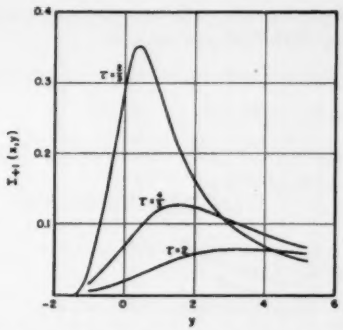

FIG. 1. Spectral distribution of forward scattered radiation in a semi-infinite medium for $\mu=+1/\sqrt{3}$ in terms of a unit intensity at $x=0$. The abscissa $y=\frac{3}{4}(\sigma-\sigma_0)$. Curves are labeled by $\tau=\frac{3}{4}x$, where $x=1$, 2, and 3 and $\tau=(8/3)(N\pi r_0^2 z)$.

The results for $I_{+1}(x,y)$ are shown in Fig. 1 for $x=1$, 2, 3; the curves for $I_{+1}(x,y)$ indicate an appreciable broadening of the primary monochromatic radiation even for $x=1$. There is a "violet shift" which is physically unsatisfactory. If one uses the area of the spectral distribution curve to the left of $y=0$ (i.e., violet shift) as a criterion of error, then this error is always less than about 15 percent for $x>1$. The curves for $I_{-1}(x,y)$ for x small cannot be obtained in any practical manner by graphical integration because of the large values of y which become important. If one does not have a monochromatic source, but a continuous distribution $\psi(\sigma)$ or $\psi(y)$, one can write for the general solution

$$I_{\pm 1}(x,y;\psi(y))=\int_{-\infty}^{\infty}I_{\pm 1}(x,y-\eta;\delta(y))\psi(\eta)d\eta, \tag{2.23}$$

where $I_{\pm 1}(x,y;\delta(y))$ is the result given above.

The problem of a finite medium[4] of thickness x_1, can easily be solved by taking

$$f(x,y)=\int_{-\infty}^{\infty}\{A(\alpha)\exp[-(1+\alpha^2)^{\frac{1}{2}}x] + B(\alpha)\exp[+(1+\alpha^2)^{\frac{1}{2}}x]\}e^{i\alpha y}d\alpha \tag{2.24}$$

and the boundary conditions

$$I_{+1}(0,y)=\tfrac{2}{3}\delta(y),\quad I_{-1}(x_1,y)\equiv 0 \tag{2.25}$$

[4] S. Chandrasekhar, Proc. Roy. Soc. (London) **A192**, 508 (1948).

i.e., vacuum for $x>x_1$. The boundary conditions just determine $A(\alpha)$, $B(\alpha)$; one has again

$$I_{\pm1}(x, y)=\tfrac{1}{2}e^{y}\{-\partial f/\partial x\pm\sqrt{3}(f+\partial f/\partial y)\}. \quad (2.26)$$

Applying Eq. (2.25) leads to

$$\begin{aligned}&\{\beta+\sqrt{3}(1+i\alpha)\}A(\alpha)-\{\beta-\sqrt{3}(1+i\alpha)\}B(\alpha)=3/2\pi\\&\{\beta-\sqrt{3}(1+i\alpha)\}e^{-\beta x_1}A(\alpha)\\&\qquad-\{\beta+\sqrt{3}(1+i\alpha)\}e^{\beta x_1}B(\alpha)=0,\end{aligned} \quad (2.27)$$

where

$$\beta=(1+\alpha^2)^{\frac{1}{2}}$$

whose solutions are

$$\begin{aligned}A(\alpha)&=(3/2\pi)\xi e^{\beta x_1}/(\xi^2e^{\beta x_1}-\eta^2e^{-\beta x_1})\\B(\alpha)&=(3/2\pi)\eta e^{-\beta x_1}/(\xi^2e^{\beta x_1}-\eta^2e^{-\beta x_1}),\end{aligned} \quad (2.28)$$

where

$$\xi=\beta+\sqrt{3}(1+i\alpha), \quad \eta=\beta-\sqrt{3}(1+i\alpha).$$

After some rather tedious algebra one finds,

$$\begin{aligned}A(\alpha)=\frac{3}{8\pi}\frac{e^{\beta x_1}}{\beta(p^2+\alpha^2q^2)}&\{[(1+\sqrt{3}\beta)p-\alpha^2q]\\&-i[\alpha(p+q)+\sqrt{3}\alpha\beta q]\}\end{aligned} \quad (2.29)$$

$$\begin{aligned}B(\alpha)=\frac{3}{8\pi}\frac{e^{-\beta x_1}}{\beta(p^2+\alpha^2q^2)}&\{[(1-\sqrt{3}\beta)p-\alpha^2q]\\&-i[\alpha(p+q)-\sqrt{3}\alpha\beta q]\},\end{aligned}$$

where

$$p=\sqrt{3}\beta\cosh\beta x_1+2\sinh\beta x_1; \quad q=\sinh\beta x_1$$

and

$$\begin{aligned}&A(\alpha)e^{-\beta x_1}+B(\alpha)e^{\beta x_1}\\&\quad=(3/4\pi)[(p-\alpha^2q)-i\alpha(p+q)]/\beta(p^2+\alpha^2q^2).\end{aligned}$$

The values of $A(\alpha)$, $B(\alpha)$ in (2.29) allow one to calculate $I_{\pm1}(x, y)$ for all points in the medium by using (2.25),

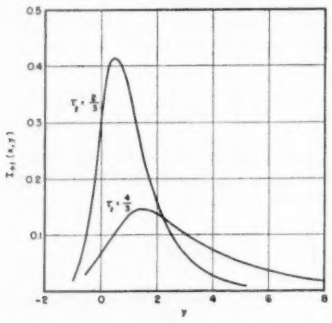

FIG. 2. Spectral distribution for finite medium and $\mu=1/\sqrt{3}$. These are Chandrasekhar's curves except for a factor $\frac{3}{4}$ in the ordinate. The ordinates are in terms of unit intensity at $x=0$. Abscissas are given by $y=\frac{3}{2}(\sigma-\sigma_0)$. Curves are labeled for two thicknesses $x_1=1$, $x_1=2$, where $x_1=\frac{3}{4}\tau_1=\frac{3}{4}(8/3)(N\pi r_0^2 z)$.

(2.26). One has for $I_{+1}(x_1, y)$ the result

$$I_{+1}(x_1, y)=\frac{3}{2}\frac{\sqrt{3}}{2\pi}e^{y}\int_0^\infty d\alpha\frac{\beta(p\cos\alpha y+\alpha q\sin\alpha y)}{p^2+\alpha^2q^2}. \quad (2.30)$$

Chandrasekhar's result does not have the factor $\frac{3}{4}$ since he apparently uses $\delta(y)$ for his boundary condition instead of the physical $\delta(\sigma-\sigma_0)=\frac{3}{2}\delta(y)$ because $y=\frac{3}{2}(\sigma-\sigma_0)$. His results must be multiplied by $\frac{3}{4}$. Two particular curves are shown in Fig. 2, for $x_1=1$, 2. One sees that the results do not differ appreciably from those for a semi-infinite medium shown in Fig. 1.

This section will be concluded with the corresponding results which can be derived from Radau's method. Only the semi-infinite medium will be discussed, although the finite can be carried out just as above. One begins with Eqs. (2.10) and to first approximation

$$a_{\pm1}=1; \quad \mu_{\pm1}=\pm1, \quad (2.31)$$

which leads to

$$\begin{aligned}(\partial/\partial\tau)(I_{+1}-I_{-1})&=-(\partial/\partial\sigma)(I_{+1}+I_{-1})\\(\partial/\partial\tau)(I_{+1}+I_{-1})&=(\partial/\partial\sigma)(I_{+1}-I_{-1})\\&\quad-(I_{+1}-I_{-1}).\end{aligned} \quad (2.32)$$

Introducing the new variables, $x=\tau$, $y=\sigma-\sigma_0$

$$\begin{aligned}I_{+1}+I_{-1}&=-(\partial/\partial x)\Lambda(x, y)\\I_{+1}-I_{-1}&=(\partial/\partial y)\Lambda(x, y)\end{aligned} \quad (2.33)$$

and

$$f(x, y)=e^{-y/2}\Lambda(x, y),$$

one arrives at the following partial differential equation

$$\partial^2f/\partial x^2+\partial^2f/\partial y^2-\tfrac{1}{4}f=0. \quad (2.34)$$

Separation of variables leads to the solution

$$f(x, y)=\int_{-\infty}^{\infty}A(\alpha)\exp[-(\tfrac{1}{4}+\alpha^2)^{\frac{1}{2}}x+i\alpha y]d\alpha. \quad (2.35)$$

Carrying out the calculation of $A(\alpha)$ in the same way as before, one obtains

$$\begin{aligned}I_{+1}(x, y)&=\frac{e^{y/2}}{2\pi}\int_{-\infty}^{\infty}\exp[-(\tfrac{1}{4}+\alpha^2)^{\frac{1}{2}}x+i\alpha y]d\alpha\\I_{-1}(x, y)&=\frac{e^{y/2}}{2\pi}\int_{-\infty}^{\infty}\frac{(\frac{1}{4}+\alpha^2)^{\frac{1}{2}}-(\frac{1}{2}+i\alpha)}{(\frac{1}{4}+\alpha^2)^{\frac{1}{2}}+(\frac{1}{2}+i\alpha)}\\&\qquad\times\exp[-(\tfrac{1}{4}+\alpha^2)^{\frac{1}{2}}x+i\alpha y]d\alpha.\end{aligned} \quad (2.36)$$

The first integral is known, so

$$I_{+1}(x, y)=-\tfrac{1}{4}x(x^2+y^2)^{-\frac{1}{2}}e^{y/2}H_1^{(1)}[(i/2)(x^2+y^2)^{\frac{1}{2}}]. \quad (2.37)$$

This result is shown in Fig. 3 for $x=2/3$, $4/3$, 2 since x is different here than in Gauss' solution above.

SECTION 3. POINT SOURCE IN AN INFINITE SPERICAL MEDIUM

The solution for a monochromatic point isotropic (in angle) source in an infinite medium will now be

solved by the method of Chandrasekhar. First, again, Gauss' formula for numerical quadratures will be employed. If the source is not monochromatic, one can solve the problem by superposition as in Eq. (2.23). Using Eqs. (1.08) and (2.01) one has

$$\mu\frac{\partial}{\partial\rho}I+\frac{1-\mu^2}{\rho}\frac{\partial}{\partial\mu}I+I=\frac{1}{2}\int_{-1}^{+1}\left\{I(\rho,\mu',\sigma)-(1-\mu\mu')\frac{\partial}{\partial\sigma}I(\rho,\mu',\sigma)\right\}d\mu'. \quad (3.01)$$

In the nth approximation (Gauss), one has

$$\mu_i\frac{\partial}{\partial\rho}I_i+\frac{1-\mu_i^2}{\rho}\left(\frac{\partial I}{\partial\mu}\right)_{\mu=\mu_i}+I_i=\tfrac{1}{2}\sum_j a_j\left\{I_j-(1-\mu_i\mu_j)\frac{\partial}{\partial\sigma}I_j\right\}$$
$$i,j=\pm1,\cdots,\pm n. \quad (3.02)$$

One needs an expression for $(\partial I/\partial\mu)_{\mu=\mu_i}$. Chandrasekhar has obtained this desired relation for another purpose. One considers[5]

$$Q_l(\mu)\equiv\frac{1-\mu^2}{l(l+1)}P_l'(\mu)=\frac{1}{2l+1}\left[P_{l-1}(\mu)-P_{l+1}(\mu)\right] \quad (3.03)$$
$$Q_l'(\mu)=-P_l(\mu);\quad Q_l(\pm1)=0;\quad '\equiv\frac{d}{d\mu}.$$

Then one has

$$\int_{-1}^{+1}\frac{(1-\mu^2)P_l'(\mu)}{l(l+1)}\frac{\partial}{\partial\mu}I\,d\mu=\int_{-1}^{+1}P_l(\mu)I\,d\mu \quad (3.04)$$

by one partial integration, or one can apply Gauss' method and write

$$\sum_j a_j(1-\mu_j^2)P_l'(\mu_j)(\partial I/\partial\mu)_{\mu=\mu_j}=l(l+1)\sum_j a_jP_l(\mu_j)I_j. \quad (3.05)$$

Therefore one multiplies (3.02) by

$$\sum_i a_iP_l'(\mu_i)$$

and obtains

$$\frac{\partial}{\partial\rho}\sum_i a_i\mu_iP_l'(\mu_i)I_i+\frac{l(l+1)}{\rho}\sum_i a_iP_l(\mu_i)I_i+\sum_i a_iP_l'(\mu_i)I_i=\tfrac{1}{2}\sum_i a_iP_l'(\mu_i)\sum_j a_j\left\{I_j-(1-\mu_i\mu_j)\frac{\partial}{\partial\sigma}I_j\right\}. \quad (3.06)$$

[5] See reference 2, p. 365.

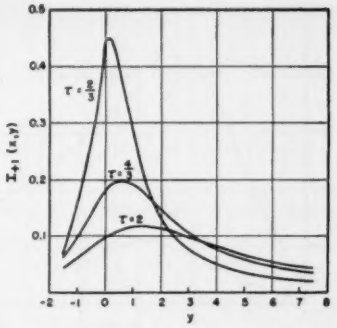

FIG. 3. Spectral distribution for forward scattered radiation $\mu=1$ in a semi-infinite medium. Ordinates are in terms of unit intensity at $x=0$. Abscissas are given by $y=(\sigma-\sigma_0)$. Curves labeled by $x=\tau=2/3, 4/3, 2$.

The first approximation consists in letting $l=1$, 2. This leads to

$$l=1:\ \frac{\partial}{\partial\rho}\sum_i a_i\mu_iI_i+\frac{2}{\rho}\sum_i a_i\mu_iI_i+\sum_i a_iI_i=\tfrac{1}{2}\sum_i a_i\sum_j a_j\left\{I_j-(1-\mu_i\mu_j)\frac{\partial}{\partial\sigma}I_j\right\}$$
$$l=2:\ \frac{\partial}{\partial\rho}\sum_i a_i\mu_i^2I_i+\frac{1}{\rho}\sum_i a_i(3\mu_i^2-1)I_i+\sum_i a_i\mu_iI_i=\tfrac{1}{2}\sum_i a_i\mu_i\sum_j a_j\left\{I_j-(1-\mu_i\mu_j)\frac{\partial}{\partial\sigma}I_j\right\}, \quad (3.07)$$

or, putting

$$a_{\pm1}=1;\quad \mu_{\pm1}=\pm1/\sqrt{3}$$
$$\frac{1}{\sqrt{3}}\frac{\partial}{\partial\rho}(I_{+1}-I_{-1})+\frac{2}{\sqrt{3}}\frac{1}{\rho}(I_{+1}-I_{-1})=-\frac{\partial}{\partial\sigma}(I_{+1}+I_{-1}) \quad (3.08)$$
$$\frac{1}{\sqrt{3}}\frac{\partial}{\partial\rho}(I_{+1}+I_{-1})+(I_{+1}-I_{-1})=\frac{1}{3}\frac{\partial}{\partial\sigma}(I_{+1}-I_{-1}).$$

One can introduce a function $S(\rho,\sigma)$ such that

$$\rho^2(I_{+1}-I_{-1})=-\sqrt{3}\partial S(\rho,\sigma)/\partial\sigma$$
$$\rho^2(I_{+1}+I_{-1})=\partial S(\rho,\sigma)/\partial\rho, \quad (3.09)$$

which gives

$$\partial^2S/\partial\rho^2-(2/\rho)\partial S/\partial\rho=-\partial^2S/\partial\sigma^2+3\partial S/\partial\sigma. \quad (3.10)$$

Introducing new variables

$$x=\tfrac{3}{4}\rho,\quad y=\tfrac{3}{2}(\sigma-\sigma_0) \quad (3.11)$$

and applying the usual separation of variables, one is

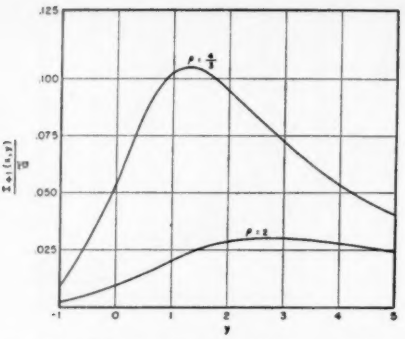

FIG. 4. Spectral distribution for $\mu=1/\sqrt{3}$ from a point isotropic source in an infinite spherical medium. Ordinates are in terms of a primary source strength $\mathcal{Q}=Q/4\pi(\frac{3}{2})^3(8/3)(N\pi r_0^2)^2$. Abscissas are in terms of $y=\frac{3}{2}(\sigma-\sigma_0)$. Curves are labeled by $\rho=\frac{3}{2}x=4/3$, 2 (i.e., $x=2$, 3) where $\rho=(8/3)(N\pi r_0^2 r)$.

lead to the following solution:

$$S(x, y)=\int_{-\infty}^{\infty} A(\alpha)x^{\frac{1}{2}}Z_{\frac{1}{2}}[i(1+\alpha^2)^{\frac{1}{2}}x]e^{y+i\alpha y}d\alpha \quad (3.12)$$

and

$$I_{\pm 1}(x, y)=(\tfrac{3}{2})^3(1/2x^2)\{\partial S/\partial x\mp\sqrt{3}\partial S/\partial y\}. \quad (3.13)$$

The boundary conditions for the determination of $A(\alpha)$ and the cylinder function are assumed, for the present, to be given by the following:

$$I_{+1}(0, y)=(Q/4\pi r^2)\delta(\sigma-\sigma_0)=(\mathcal{Q}/x^2)\delta(y)$$

$$\mathcal{Q}=\frac{Q}{4\pi}\left(\frac{3}{2}\right)^3\left(\frac{8}{3}N\pi r_0^2\right)^2 \quad (3.14)$$

and

$$\lim_{x\to\infty} I_{\pm 1}(x, y)=0.$$

There is a difficulty in defining $I(r, \mu=1/\sqrt{3}, \sigma)$ near $r=0$ since only $I(r, \mu=1, \sigma)$ exists at that point. This will be discussed more fully in the following. This fixes the cylinder function as a spherical Hankel function of first kind; *viz.*,

$$Z_{\frac{1}{2}}[i(1+\alpha^2)^{\frac{1}{2}}x]=H_1^{(1)}[i(1+\alpha^2)^{\frac{1}{2}}x]$$
$$=[(2/\pi)i(1+\alpha^2)^{\frac{1}{2}}x]^{\frac{1}{2}}h_1^{(1)}[i(1+\alpha^2)^{\frac{1}{2}}x]. \quad (3.15)$$

One then has

$$S(x, y)=\int_{-\infty}^{\infty}\mathfrak{A}(\alpha)x^2h_1^{(1)}[i(1+\alpha^2)^{\frac{1}{2}}x]e^{y+i\alpha y}d\alpha. \quad (3.16)$$

An examination of $I_{+1}(0, y)$ leads one to the following result:

$$\mathfrak{A}(\alpha)=\frac{i}{\sqrt{3}\pi}\mathcal{Q}(\tfrac{3}{2})^3(1-i\alpha) \quad (3.17)$$

so that the final answer is

$$I_{\pm 1}(x, y)=\frac{i\mathcal{Q}}{\sqrt{3}}\frac{1}{2\pi x^2}\left(\frac{\partial}{\partial x}\mp\sqrt{3}\frac{\partial}{\partial y}\right)\int_{-\infty}^{\infty}(1-i\alpha)x^2h_1^{(1)}$$
$$\times[i(1+\alpha^2)^{\frac{1}{2}}x]e^{y+i\alpha y}d\alpha. \quad (3.18)$$

This integral can be evaluated explicitly by simple manipulations on the known results (2.21); one finds

$$I_{\pm 1}(x, y)=\frac{\mathcal{Q}}{2\sqrt{3}}\frac{e^y}{(x^2+y^2)}\left\{(y\pm\sqrt{3}x)iH_0^{(1)}[i(x^2+y^2)^{\frac{1}{2}}]\right.$$
$$\left.-\left[\frac{x^2+y^2+2y\pm 2\sqrt{3}x}{(x^2+y^2)^{\frac{1}{2}}}\right]H_1^{(1)}[i(x^2+y^2)^{\frac{1}{2}}]\right\}. \quad (3.19)$$

These results are shown in Figs. 4 and 5 for $x=2$, 3. The curves are very poor for $x=1$. For $x>2$, $I_{+1}(x, y)$ seems to be qualitatively correct if one invokes the "violet shift" as a criterion of error. The negative intensities which occur in $I_{-1}(x, y)$ are completely negligible if their area is used as a criterion of error at least for large enough values of x. It is easily seen that the trouble for small x lies in the concept of an isotropic in angle point source. Since the above solutions (3.19) are for $\mu=\pm 1/\sqrt{3}$, one cannot really establish a boundary condition for $I_{+1}(x, y)$ as $x\to 0$ since in the immediate vicinity of the singularity the radiation is characterized by $\mu=1$. Somewhere near the source there is a peculiar discontinuity in the angular distribution of the radiation. This can be avoided usually by subtracting off the unscattered and first scattered components of the multiply scattered radiation which are always singular. The radiation scattered more than once is then described by a continuous function.[6]

One can, however, solve this spherical problem with Radau's method which gives a result identical to the above plane case except for an inverse square term, and the boundary conditions are correct, for large enough x,

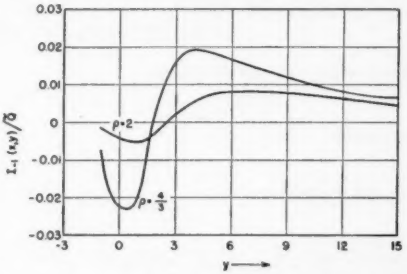

FIG. 5. Spectral distribution for $\mu=-1/\sqrt{3}$ from a point isotropic source in an infinite spherical medium. Notation same as Fig. 4.

[6] Cave, Corner, and Liston, Proc. Roy. Soc. (London) **A204**, 223 (1950).

say $x>2$. Also the $I_{-1}(x, y)$ for $\mu=-1$ doesn't exhibit large negative intensities. This will now be carried out.

Setting $a_{+1}=a_{-1}=1$ and $\mu_{+1}=-\mu_{-1}=1$ in Eqs. (3.07), one has

$$\begin{aligned}\partial/\partial\rho(I_{+1}-I_{-1})+2/\rho(I_{+1}-I_{-1})&\\ =-\partial/\partial\sigma(I_{+1}+I_{-1})&\\ \partial/\partial\rho(I_{+1}+I_{-1})+2/\rho(I_{+1}+I_{-1})&\\ =\partial/\partial\sigma(I_{+1}-I_{-1})-(I_{+1}-I_{-1}).&\end{aligned}\tag{3.20}$$

Introducing the new variables

$$x=\rho;\quad y=\sigma-\sigma_0;\quad S_{\pm}=I_{+1}\pm I_{-1}\tag{3.21}$$

one has

$$\begin{aligned}S_{+}(x, y)&=-x^{-2}\partial\Lambda(x, y)/\partial x\\ S_{-}(x, y)&=x^{-2}\partial\Lambda(x, y)/\partial y\end{aligned}\tag{3.22}$$

and letting

$$\begin{aligned}\Lambda(x, y)&=e^{y/2}f(x, y)\\ \partial^2 f/\partial x^2+\partial^2 f/\partial y^2-\tfrac{1}{4}f&=0.\end{aligned}\tag{3.23}$$

This is the same as the plane parallel problem solved by Radau's method in Sec. I. The result is

$$\begin{aligned}f(x, y)&=\int_{-\infty}^{\infty}A(\alpha)\exp[-(\tfrac{1}{4}+\alpha^2)^{\frac{1}{2}}x+i\alpha y]d\alpha\\ I_{\pm1}(x, y)&=(1/2x^2)e^{y/2}(-\partial f/\partial x\pm(\tfrac{1}{2}f+\partial f/\partial y)).\end{aligned}\tag{3.24}$$

Again, the boundary conditions are proper behavior at infinity and

$$I_{+1}(0, y)=(\mathcal{Q}/x^2)\delta(y);\quad \mathcal{Q}=(Q/4\pi)(8N\pi r_0^2/3)^2,\tag{3.25}$$

which gives

$$A(\alpha)=\frac{\mathcal{Q}}{\pi}\frac{1}{(\frac{1}{4}+\alpha^2)^{\frac{1}{2}}+(\frac{1}{2}+i\alpha)}\tag{3.26}$$

and

$$\begin{aligned}I_{+1}(x, y)&=-\frac{1}{4}\frac{\mathcal{Q}}{x(x^2+y^2)^{\frac{1}{4}}}e^{y/2}H_1^{(1)}\left[\frac{i}{2}(x^2+y^2)^{\frac{1}{2}}\right]\\ I_{-1}(x, y)&=\frac{\mathcal{Q}}{x^2}e^{y/2}\frac{1}{2\pi}\int_{-\infty}^{\infty}\frac{(\frac{1}{4}+\alpha^2)^{\frac{1}{2}}-(\frac{1}{2}+i\alpha)}{(\frac{1}{4}+\alpha^2)^{\frac{1}{2}}+(\frac{1}{2}+i\alpha)}\\ &\quad\times\exp[-(\tfrac{1}{4}+\alpha^2)^{\frac{1}{2}}x+i\alpha y]d\alpha.\end{aligned}\tag{3.27}$$

These results are the same as the above Radau solution for the plane case except for the factor $\mathcal{Q}/x^2$.

This section will be closed with an interesting example in which the above problem of a plane parallel semi-infinite medium will be solved without the Taylor series assumption. The result will be paradoxical in the sense that it is physically correct but yields a spectral distribution which is discrete. This implies that the Taylor series approximation smears this physically correct discrete spectrum into a qualitatively correct continuous distribution. One begins with

$$\begin{aligned}&\mu\frac{\partial}{\partial\tau}I(\tau, \mu, \sigma)+I(\tau, \mu, \sigma)\\ &\quad=\frac{1}{4\pi}\int_{1}^{+1}\int_{0}^{2\pi}I(\tau, \mu', \sigma-1+\cos\Theta)d\mu' d\varphi'.\end{aligned}\tag{3.28}$$

First, $I(\tau, \mu, \sigma)$ is expressed as a Fourier integral

$$I(\tau, \mu, \sigma)=\int_{-\infty}^{\infty}M(\tau, \mu, \alpha)e^{i\alpha(\sigma-\sigma_0)}d\alpha.\tag{3.29}$$

Then Eq. (3.28) becomes

$$\begin{aligned}&\mu\frac{\partial}{\partial\tau}M+M\\ &\quad=\frac{1}{4\pi}\int_{-1}^{+1}\int_{0}^{2\pi}e^{-i\alpha(1-\cos\Theta)}M(\tau, \mu', \alpha)d\mu' d\varphi'.\end{aligned}\tag{3.30}$$

The φ'-integration is the integral representative of $J_0[(1-\mu^2)^{\frac{1}{2}}(1-\mu'^2)^{\frac{1}{2}}\alpha]$ so that

$$\begin{aligned}\mu\frac{\partial}{\partial\tau}M+M&=\frac{1}{2}\int_{-1}^{+1}e^{-i\alpha(1-\mu\mu')}J_0[(1-\mu^2)^{\frac{1}{2}}(1-\mu'^2)^{\frac{1}{2}}\alpha]\\ &\quad\times M(\tau, \mu', \alpha)d\mu'.\end{aligned}\tag{3.31}$$

Applying Radau's method and the fact that $J_0(0)=1$, one obtains in first approximation

$$\begin{aligned}dM_{+1}/d\tau+M_{+1}&=\tfrac{1}{2}\{M_{+1}+e^{-2i\alpha}M_{-1}\}\\ -dM_{-1}/d\tau+M_{-1}&=\tfrac{1}{2}\{M_{-1}+e^{-2i\alpha}M_{+1}\}.\end{aligned}\tag{3.32}$$

The solution for $I_{+1}(\tau, \sigma)$ can be written then in the form

$$I_{+1}(\tau, \sigma)=\int_{-\infty}^{\infty}A(\alpha)e^{i\alpha(\sigma-\sigma_0)-s(\alpha)\tau}d\alpha,\tag{3.33}$$

where

$$s(\alpha)=\tfrac{1}{2}(1-e^{-4i\alpha})^{\frac{1}{2}}.$$

The boundary condition is the usual

$$I_{+1}(0, \sigma)=\delta(\sigma-\sigma_0);\quad A(\alpha)=1/2\pi,\tag{3.34}$$

so that

$$I_{+1}(\tau, \sigma)=\frac{1}{2\pi}\int_{-\infty}^{\infty}e^{i\alpha(\sigma-\sigma_0)-s(\alpha)\tau}d\alpha.\tag{3.35}$$

Expanding the exponential $e^{-s(\alpha)\tau}$ and the resulting factor $(1-e^{-4i\alpha})^{n/2}$ one has

$$e^{-s(\alpha)\tau}=\sum_{n=0}^{\infty}\frac{(-)^n\tau^n}{2^n n!}\sum_{\kappa=0}^{\infty}(-)^{\kappa}\binom{n/2}{\kappa}e^{-4i\kappa\alpha}.$$

One finds the interesting result

$$I_{+1}(\tau, \sigma) = \sum_{n=0}^{\infty} \frac{(-)^n \tau^n}{2^n n!} \sum_{\kappa=0}^{\infty} (-)^\kappa \binom{n/2}{\kappa} \delta(\sigma - \sigma_0 - 4\kappa). \quad (3.36)$$

This solution, which should be more exact than those obtained with the Taylor series assumption, gives a discrete spectrum in contrast to the solutions presented in previous sections of this paper.

One interprets this result as follows. The method of Radau replaced an integral over μ' by two terms only; *viz.*, $\mu' = \pm 1$, i.e., $\vartheta' = 0, \pi$. The above solution is for $\mu = 1$ so the result should contain only those contributions of gammas which are unscattered, twice scattered through π, four times scattered through π, etc. Since each scattering through π involves a wavelength increase of two Compton units, the spectral distribution should contain the following wavelengths only (along the direction $\mu = 1$), $\lambda = \lambda_0$, $\lambda = \lambda_0 + 4\gamma$, $\lambda = \lambda_0 + 8\gamma$, etc. where $\gamma = h/mc$.

The author would like to thank Mr. J. H. Hancock, Mr. C. F. Ravilious, and the Computation Group at the Naval Research Laboratory for carrying out the numerical work.

PHYSICAL REVIEW VOLUME 85, NUMBER 5 MARCH 1, 1952

Angular Correlation of Electrons in Double Beta-Decay*

H. PRIMAKOFF
Washington University, St. Louis, Missouri

(Received October 1, 1951)

Angular correlation functions for the emitted electrons with corresponding electron energy spectra are obtained, assuming the Majorana theory of the neutrino, for allowed and first-forbidden nuclear double beta-transitions. The associated decay mean lives are estimated $\approx 10^{12}$ yr, and $\approx 10^{16}$ yr, respectively, for $Z \approx 50$, and an atomic mass difference ≈ 1.5 Mev. A brief discussion is given of the reported experimental observations of double beta-decay in the light of the deduced angular correlation functions, electron energy spectra, decay mean lives, and selection rules; the improbability of actual occurrence of the allowed 10^{12}-yr transitions is pointed out.

INTRODUCTION

THE phenomenon of nuclear double beta-decay has been investigated theoretically by Goeppert-Mayer[1] on the basis of the original Fermi description, i.e., with Dirac neutrinos and antineutrinos, while Furry[2] has studied the problem on the assumption of Majorana neutrinos. The Furry treatment, which entails the simultaneous emission of two electrons without any accompanying neutrinos, predicts half-lives 10^9–10^{11} times shorter (for comparable degree of forbiddenness and energy release) than that of Goeppert-Mayer, which necessitates the simultaneous emission of two electrons and two neutrinos. Experimental observations of nuclear double beta-decay have been reported by Fireman[3] and Inghram and Reynolds;[4] these yield half-lives $\approx 10^{16}$ yr and $\approx 10^{21}$ yr for the double beta-process in ${}_{50}Sn^{124}$ and in ${}_{52}Te^{130}$, respectively. It is, however, not yet known whether the sum of the energies of the different pairs of electrons, emitted by the different decaying nuclei of a double beta-active substance, is or is not the same in all individual decays; experimental decision between these two possibilities would at once indicate either the Majorana or the Dirac theory.

In the present note we have calculated, assuming the Majorana theory,[5] the transition probabilities—selection rules, mean lives, electron energy spectra, and angular correlation functions—for allowed and for first-forbidden double beta-transitions. The selection rules, mean lives, and electron energy spectra for the allowed and for some of the first-forbidden transitions have previously been obtained by Furry.[2] Our expressions differ from his in yielding more explicit formulas for the various transition nuclear matrix elements as a

* Assisted by the joint program of the ONR and AEC.

[1] M. Goeppert-Mayer, Phys. Rev. **48**, 512 (1935).

[2] W. H. Furry, Phys. Rev. **56**, 1184 (1939); see also, B. Touschek, Z. Physik **125**, 108 (1948–1949).

[3] E. L. Fireman, Phys. Rev. **75**, 323 (1949).

[4] M. G. Inghram and J. H. Reynolds, Phys. Rev. **76**, 1265 (1949); **78**, 822 (1950); M. G. Inghram, Chicago Conference, September, 1951.

[5] The quantized amplitude of the Dirac neutrino-antineutrino field ψ (which together with the quantized amplitude of the Dirac electron-positron field enters the β-decay nucleon-lepton interaction Hamiltonian, $\mathcal{H}_{\text{inter}}$) involves both destruction operators for positive energy neutrinos and creation operators for positive energy antineutrinos of various spin orientations and linear momenta; each of these destruction, creation operators is multiplied by the corresponding positive energy, spin orientation, linear momentum eigenspinor ϕ, and $(C\phi)^*$, respectively (C=charge conjugation operator). For the purposes of a theory of β-decay, the quantized amplitude of the Majorana neutrino field can then be obtained from ψ merely by replacing the various creation operators for the positive energy antineutrinos by the corresponding creation operators for positive energy neutrinos. Such a formulation enables the usual techniques employed in calculations with Dirac particles, e.g., the projection operator procedure for summing over the two possible spin orientations associated with a given linear momentum, to be immediately used with Majorana neutrinos as well.

consequence of the use of closure in the sum over the intermediate (virtual) nuclear states; this results in several cases in an assignment of a degree of forbiddenness one unit larger than Furry's. We have, in addition, also obtained the double beta angular correlation function of the two emitted electrons; this quantity may conceivably become susceptible to experimental observation. Comparison of any such experiments with the various forms for the double beta angular correlation function would then serve as a test of the assumptions regarding (1) the fundamental coupling between nucleons and leptons and (2) the nuclear spin and parity change in the double beta-transitions. Studies of this type in double beta-decay would obviously supplement analogous theoretical[6] and experimental[7] investigations into electron-neutrino angular correlation in single beta-decay.

RESULTS

As regards our quantitative results, they may be summarized as follows: Let $P(E, E', \theta)dEdE'2\pi \sin\theta d\theta$ represent the double beta-decay transition probability per unit time for emission of the two electrons with momenta making an angle one with the other between θ and $\theta+d\theta$, and with energies between mc^2E and $mc^2(E+dE)$, and between mc^2E' and $mc^2(E'+dE')$, respectively; also let $F(\theta)\cdot\frac{1}{2}\sin\theta d\theta$, $S(E)dE$, and τ, denote the angular correlation function, the electron energy spectrum, and the decay mean life. We then find as a result of a second-order perturbation calculation with $\mathfrak{IC}_{\text{inter}}$,[5] performed in accordance with the general scheme of Furry:[2] initial nucleus→intermediate (virtual) nucleus+(virtual) neutrino+electron→final nucleus+two electrons,[8]

$$P(E, E', \theta)dEdE'2\pi\sin\theta d\theta$$
$$=2^{-6}\pi^{-5}G^4(mc^2/\hbar)\left|\int\Psi_{\text{fin}}{}^*\sum_{k,j}(Q_kQ_j/x_{kj}{}^3)A_{kj}\Psi_{\text{ini}}\right|^2$$
$$\times\left(\frac{2\pi Z}{137}\frac{E}{p}\right)\left(\frac{2\pi Z}{137}\frac{E'}{p'}\right)$$
$$\times pEp'E'f_1(E, E')\delta(E_0-E-E')$$
$$\times\{1+[f_2(E, E')/f_1(E, E')]\cos\theta\}dEdE'\tfrac{1}{2}\sin\theta d\theta \quad (1)$$

$$F(\theta)=1+\{f_2(E, E')/f_1(E, E')\}\cos\theta$$
$$S(E)dE=dE\int\int P(E, E', \theta)dE'2\pi\sin\theta d\theta$$
$$=\text{const}E^2(E_0-E)^2f_1(E, E_0-E)dE$$
$$\tau^{-1}=\int_1^{E_0-1}S(E)dE,$$

with

$$A_{kj}=(\boldsymbol{\sigma}_k\times\boldsymbol{\sigma}_j)\cdot\mathbf{x}_{kj}/x_{kj};\quad f_1(E, E')=(1+1/EE');$$
$$f_2(E, E')=(p/E)(p'/E');$$
$$\textit{allowed};\ \Delta J=0,\ \text{"yes"};\ T, A. \quad (2)$$

$$A_{kj}=\tfrac{1}{2}(\boldsymbol{\sigma}_k\cdot\boldsymbol{\sigma}_j)^nx_{kj};\quad f_1(E, E')=(E-E')^2(1-1/EE')$$
$$+(2/n')(E-E')(p^2/E-p'^2/E')+(1/n')^2$$
$$\times([p^2+p'^2](1+1/EE')-2(p^2/E)(p'^2/E));$$
$$f_2(E, E')=(1+2/n')(E-E')^2(p/E)(p'/E')$$
$$+(1/n')^2\{[p^2+p'^2](p/E)(p'/E')$$
$$-2pp'(1+1/EE')\};$$
$$\textit{first-forbidden};\ \Delta J=0,\ \text{"no"};$$
$$T(n=1, n'=9),\ A(n=1, n'=-9),$$
$$V(n=0, n'=3),\ S(n=0, n'=-3) \quad (3)$$

$$[\mathbf{A}_{kj}]_T=-(\boldsymbol{\sigma}_k\times\boldsymbol{\sigma}_j)B_{kj}+(\boldsymbol{\sigma}_k\times\boldsymbol{\sigma}_j)\cdot(\mathbf{x}_{kj}/x_{kj})$$
$$\times\{(\mathbf{x}_k+\mathbf{x}_j)/|\mathbf{x}_k+\mathbf{x}_j|\}\left(\frac{1}{2}\frac{Z}{137}\right)$$
$$-\tfrac{1}{3}(\boldsymbol{\alpha}_k\cdot\boldsymbol{\sigma}_j-\boldsymbol{\alpha}_j\cdot\boldsymbol{\sigma}_k)(\mathbf{x}_{kj}/x_{kj}),$$
$$[\mathbf{A}_{kj}]_A=(\boldsymbol{\sigma}_k\times\boldsymbol{\sigma}_j)B_{kj}+(\boldsymbol{\sigma}_k\times\boldsymbol{\sigma}_j)\cdot(\mathbf{x}_{kj}/x_{kj})$$
$$\times\{(\mathbf{x}_k+\mathbf{x}_j)/|\mathbf{x}_k+\mathbf{x}_j|\}\left(\frac{1}{2}\frac{Z}{137}\right)$$
$$+(1/3i)(\boldsymbol{\alpha}_k\cdot\boldsymbol{\sigma}_k\boldsymbol{\sigma}_j-\boldsymbol{\alpha}_j\cdot\boldsymbol{\sigma}_j\boldsymbol{\sigma}_k)\times(\mathbf{x}_{kj}/x_{kj}),$$
$$[\mathbf{A}_{kj}]_V=(\boldsymbol{\alpha}_k-\boldsymbol{\alpha}_j)\times(\mathbf{x}_{kj}/x_{kj});$$
$$f_1(E, E')=(1-1/EE');$$
$$f_2(E, E')=-\tfrac{1}{3}(p/E)(p'/E');$$
$$\textit{first-forbidden};\ \Delta J=0,\pm1,$$
$$\text{but not } 0\to0,\ \text{"no"};\ T, A, V. \quad (4)$$

In Eqs. (1)–(4), S, T, V, A denote scalar, vector, tensor, and axial vector couplings, respectively; $p=(E^2-1)^{\frac{1}{2}}$, $p'=[(E')^2-1]^{\frac{1}{2}}$; $mc^2(E_0-2)$ is the energy equivalent of the atomic mass difference available for the transition; G is the dimensionless nucleon-lepton coupling constant; we take $G=4\times10^{-12}$ on the basis of the theory of single beta-decay and the observed 12.8-min neutron half-life.[9] Within the square of the nuclear matrix element,[10] Ψ_{ini} and Ψ_{fin} are the wave functions

[6] E. Grueling and M. L. Meeks, Phys. Rev. **82**, 531 (1951); M. E. Rose, Phys. Rev. **75**, 1444 (1949); D. R. Hamilton **71**, 456 (1947).

[7] C. S. Sherwin, Phys. Rev. **82**, 52 (1951); Allen, Paneth, and Morrish, Phys. Rev. **75**, 570 (1949).

[8] Our double beta-decay transition probability amplitude, P.A., calculated in accordance with the above scheme, involves a sum over all linear momenta and spin orientations of the (virtual) neutrino and over all intermediate (virtual) nuclear states, n; the latter sum is performed by closure, after the energy eigenvalues of the various states n in the energy denominators of the second-order perturbation expression for the P.A. are replaced by an average effective energy (see reference 12). As a consequence, the operator connecting Ψ_{ini} and Ψ_{fin} in the ultimate formula for the P.A. involves a product of two sums in the individual nucleon position, spin, and charge operators, i.e., involves, as is seen in Eqs. (1)–(4), a sum of terms each of which refers to a pair of nucleons.

[9] J. M. Robson, Phys. Rev. **83**, 349 (1951). In our numerical estimate of G, the dominant nucleon-lepton interaction has been taken as tensor (or axial vector), see reference 14.

[10] Summed over all final nuclear spin orientation substates and averaged over all such initial substates.

of the initial and final nuclear states involved in the decay; Q_k, Q_j; σ_k, σ_j; α_k, α_j; $(\hbar/mc)x_{kj}=(\hbar/mc)|\mathbf{x}_k-\mathbf{x}_j|$ are the neutron-to-proton transformation operators, the Pauli spin operators, the Dirac velocity operators and the distance vectors, for the kth and jth nucleons;[11] $\langle B_{kj}\rangle_{Av}=-\langle B_{jk}\rangle_{Av}\approx[(m/2M)\langle x_{kj}\rangle_{Av}]$.[12] The effect of the nuclear Coulomb field on the spinor wave functions of the emitted electrons, and so on the energy spectrum and the angular correlation function, has been considered and is approximately described (for $Z/137\approx\frac{1}{4}-\frac{1}{3}$, and $E_0\approx 3-6$) by the Z-containing terms in Eqs. (1)–(4); in particular in Eq. (4) we take:

sum of last two terms of $\langle[A_{kj}]_T\rangle_{Av}$ or of $\langle[A_{kj}]_A\rangle_{Av}$

$$\gg\langle(\boldsymbol{\sigma}_k\times\boldsymbol{\sigma}_j)\cdot(\mathbf{x}_{kj}/x_{kj})(\mathbf{x}_k+\mathbf{x}_j)\cdot(\mathbf{p}+\mathbf{p}')\rangle_{Av},$$

which results in an $F(\theta)$ independent of Z.

In the case more or less relevant to the experiments: $Z\approx 50$, and $mc^2(E_0-2)\approx 1.5$ Mev, the Eqs. (1)–(4) yield $\tau\approx 10^{12}$ yr and $\tau\approx 10^{16}$ yr, for the allowed and first-forbidden transitions, respectively.[13] These values of τ are some hundred times shorter than those given by Furry,[2] in all cases where the corresponding matrix elements are similarly estimated; the discrepancy is largely due to his use of the too small value of G which was then current.

DISCUSSION

Recent work in single beta-decay indicates that the dominant nucleon-lepton coupling type is either axial vector or tensor, and in fact, more probably the latter.[14] Moreover, it is expected from considerations of nuclear stability that both the parent and the daughter nuclei in all double beta-processes are of the even-even type, and indeed, the two examples reported thus far conform to this rule. Now the ground states of all even-even nuclei have $J=0$ and, quite probably, even parity; the ground state→ground state double beta-transition is then not allowed but rather first forbidden, with $F(\theta)$ and $S(E)$ given by Eqs. (1), (3)—i.e., in rough approximation, $F(\theta)\approx 1+\cos\theta$. The reported 10^{16}-yr ${}_{50}\mathrm{Sn}^{124}\rightarrow{}_{52}\mathrm{Te}^{124}$ transition[3] may well be either of this first-forbidden type or of the first-forbidden type of Eq. (4); in the latter case the transition goes to an excited state of the daughter nucleus and has $F(\theta)=1-\frac{1}{3}(p/E)(p'/E')(1-1/EE')^{-1}\cos\theta\approx 1-\frac{1}{3}\cos\theta$; $S(E)=\mathrm{const}E^2(E_0-E)^2[1-1/E(E_0-E)]$. The reported 10^{21}-yr ${}_{52}\mathrm{Te}^{130}\rightarrow{}_{54}\mathrm{Xe}^{130}$ transition[4] can be understood as a first-forbidden double beta-process with Majorana neutrinos, if we make the admittedly improbable assumption that the available energy is much less than 1.5 Mev; e.g., this transition may be of the ground state→ground state type with $mc^2(E_0-2)\approx 150$ kev [Eqs. (1), (3)]. In addition, we may remark that it is unlikely that it will be possible to observe the 10^{12}-yr allowed transition of Eq. (2) since low-lying states in even-even nuclei with $J=0$ and odd parity, in particular first-excited states of this kind, seem to be very rare.[15]

One further comment should be made. The 10^{21} yr-${}_{52}\mathrm{Te}^{130}\rightarrow{}_{54}\mathrm{Xe}^{130}$ decay fits the half-life expected from the Dirac neutrino theory[1] if $G=4\times 10^{-12}$ is used, if $mc^2(E_0-2)\approx 2$ Mev, and if a ground state→ground state transition (which is allowed on the Dirac theory) is assumed. Allowed double beta-decay half-lives$\approx 10^{21}$-yr would, of course, make double beta-angular correlation experiments quite impracticable for a long time to come, so that a decision on the feasibility of such experiments seems to rest on any future laboratory confirmation or refutation of Fireman's 10^{16}-yr result.†

[11] Strictly speaking, one should write $\beta_k\boldsymbol{\alpha}_k$, $\beta_j\boldsymbol{\alpha}_j$ instead of $\boldsymbol{\alpha}_k$, $\boldsymbol{\alpha}_j$ in the last term of $[\mathbf{A}_{kj}]_T$ since the nonrelativistic form of the former is different from that of the latter.

[12] The quantity $\langle B_{kj}\rangle_{Av}$ is, in order of magnitude, essentially the average effective energy of the intermediate (virtual) nuclear states, divided by $mc^2\epsilon_{Av}$, the average effective energy of the (virtually) emitted and reabsorbed neutrino associated with the neutron to proton transformation of the kth and jth nucleons. As is most easily seen from the uncertainty principle, one has $\epsilon_{Av}\approx\{\langle x_{kj}\rangle_{Av}\}^{-1}$. As indicated in footnote 8, B_{kj} enters into Eqs. (1), (4) as a result of our use of closure in the sum over the intermediate (virtual) nuclear states. To obtain a numerical estimate, we have: $\langle B_{kj}\rangle_{Av}\approx(mc\epsilon_{Av})^2/2Mmc^2\epsilon_{Av}\approx m/2M\langle x_{kj}\rangle_{Av}\approx 1/75$, with M the nucleon mass, and $\langle x_{kj}\rangle_{Av}$ taken $\approx\{$nuclear radius for $Z=50\}+(\hbar/mc)\approx 1/50$. Thus all of the individual terms in $\langle[A_{kj}]_T\rangle_{Av}$, $\langle[A_{kj}]_A\rangle_{Av}$, $\langle[A_{kj}]_V\rangle_{Av}$, of Eq. (4) are, to within a factor of perhaps 10, of the same order of magnitude, which, moreover, is about that of $\langle A_{kj}\rangle_{Av}$ in Eq. (3). In Furry's estimates (see reference 2), however, the quantity analogous to $\langle B_{kj}\rangle_{Av}$ is, in effect, taken ≈ 1; as a result the tensor or axial vector transition in Eq. (4) is classified by him as allowed rather than first forbidden.

[13] We are not writing out here our calculated $P(E,E',\theta)$ for first-forbidden transitions with $\Delta J=2$, 3, 4, "no." These also have $\tau\approx 10^{16}$ yr. We have not considered nucleon-lepton pseudoscalar coupling since its need for the interpretation of single beta-decay is as yet unsettled (see however, A. G. Petschek and R. E. Marshak, Phys. Rev. **85**, 698 (1952)). On the other hand, a dominant pseudoscalar coupling is completely ruled out since it would give a free neutron decay spectrum quite different in shape from the Fermi allowed, in contradiction to the experiment of reference 9. In the interest of simplicity, we have not considered various possible linear combinations of the couplings.

[14] L. M. Langer and R. J. D. Moffat, Phys. Rev. **82**, 635 (1951); H. W. Fulbright and J. C. D. Milton, Phys. Rev. **82**, 635 (1951). However, E. Feenberg and G. Trigg have stressed that the interpretation of the comparative half-lives in the single beta-decay allowed-favored transitions demands an appreciable admixture of vector and/or scalar coupling. Direct experimental evidence for such an admixture has recently been adduced by R. Sherr's discovery of single beta-transitions in C^{10} and O^{14}, most reasonably interpreted as $0\rightarrow 0$.

[15] This is indicated, at least for first-excited states, in M. Goldhaber and A. W. Sunyar, Phys. Rev. **83**, 906 (1951), Sec. V and Fig. 17.

† *Note added in proof.*—Very recent mass spectroscopic determinations of the mass of ${}_{52}\mathrm{Te}^{130}$ [Duckworth, Kegley, Olson, and Stanford, Phys. Rev. **83**, 1114 (1951)] and of the mass of ${}_{54}\mathrm{Xe}^{130}$ [Halsted, Bull. Am. Phys. Soc. **26**, No. 6 (1951), paper L13; Hays, Richards, and Goudsmit, Phys. Rev. **84**, 824 (1951)] yield $mc^2(E_0-2)=1.8$ Mev, thus providing evidence in favor of the Dirac theory. Further possible evidence in favor of the Dirac theory is provided by the work of W. Libby (reported by Inghram, reference 4) and by that of J. S. Lawson, Jr. [Phys. Rev. **81**, 299 (A)(1951)] who have obtained negative results in a study of the double beta-decay of ${}_{50}\mathrm{Sn}^{124}$, with corresponding estimated lower limits on its half-life of 10^{17}-yr and 10^{18}-yr, respectively.

The Emission of Slow Positive and Negative Mesons from Nuclear Disruptions Produced by Cosmic Radiation*

HERMAN YAGODA
Experimental Biology and Medicine Institute of the National Institutes of Health, Public Health Service, Bethesda, Maryland
(Received October 31, 1951)

Microscopic examination of 76 cc of thick (300 to 1800 microns) nuclear emulsion exposed in the stratosphere has revealed 168 events in which slow mesons are created and terminate their range in the recording medium. Basing the identification of sign on either π-μ decay or σ-star formation at the range terminus, 26 of the ejected particles were π^+ mesons and 145 π^-. The small value of the π^+/π^- ratio is attributed chiefly to the production of the ejected mesons by neutral radiation. The observational frequency of the ejected π^- mesons increases rapidly with star size and is approximately proportional to the square of the excitation energy of the parent star. In two events initiated by charged primaries several slow negative mesons were ejected as the wide angle members of large showers of particles. In general, the energy of the slow mesons is between 0.3 and 40 Mev. Corrected for escape from the emulsion the average frequency of the π^- meson production is proportional to $E^{0.6}$ for $E \leq 8$ Mev and to $E^{2.4}$ for energies between 8 and 40 Mev. Comparison of the data on ejected mesons with that available on cyclotron mesons indicates close similarity in the form of the secondary star spectra, the π^+/π^- ratio and the energy distribution of slow π^- mesons.

I. INTRODUCTION

SINCE the first description by Lattes, Occhialini, and Powell[1] of a double star in which the members are connected by the characteristic track of a slow negatively meson coming to rest in the emulsion, several similar events have been reported by other investigators[2–6] employing nuclear emulsions in the study of cosmic radiation. In particular, a group of 31 of these rare events has been discussed by Powell[7] in all of which the ejected meson is negatively charged. Failure to observe the emission of a slow positive meson from a star produced in thin emulsions has been attributed by the Bristol investigators to the added kinetic energy imparted to the particle by Coulomb repulsion. This increases the range and thus tends to diminish the probability of the positive meson coming to rest in the emulsion with opportunity for observation of the π-μ decay process.

The availability of thick plates and of cylindrical emulsion castings[8] of about 2-mm thickness affords better opportunity for the detection of ejected slow mesons. A systematic survey of these preparations, exposed in a series of stratosphere balloon flights, has resulted in the observation of 168 events exhibiting the ejection and termination of positive and negative mesons in the recording medium. The number of the latter is adequate for the evaluation of the frequency of slow π^- meson production, and the ranges of the particles, corrected for escape, provide several points on the energy distribution curve. While the statistics on the positive particles are still inadequate for a similar analysis, their number permits an approximate evaluation of the star-ejected π^+/π^- ratio and a comparison with the charge ratio of the cosmic-ray mesons incident from the atmosphere and the charge ratio of mesons produced by cyclotron bombardment.

II. EXPERIMENTAL

Ilford G5 plates coated 300 and 600 microns thick and emulsion castings prepared from gel of the same composition were flown in a series of stratosphere balloon flights at Minnesota ($\lambda = 55°$N) described in Table I. The thick preparations were developed uniformly by means of low temperature imbibition of a bufferred amidol solution, followed by a warm stage in an aqueous medium termed an "ionic environment" which is devoid of developer but contains salts for maintaining a fixed pH and compounds to inhibit swelling of the gelatin. Details of this method, employed successfully in the uniform development of 2 mm thick castings, will be described elsewhere. All emulsions scanned recorded the tracks of fast singly charged particles at or close to the minimum of ionization.

The plates were examined with a 6.4 mm achromatic objective and 10× wide field oculars. In order to secure sufficient clarity near the bottom layers of the thick castings it was necessary to resort to oil immersion

TABLE I. Stratosphere balloon flight characteristics.

Flight	Maximum altitude, ft	Av. altitude above 60,000 ft	Time above 60,000 ft
76S	93,000	85,500	6.8 hr
83	95,000	91,700	6.9
110	106,000	98,500	7.3
97	99,000	90,500	6.8
108	90,000	85,200	6.7

* A preliminary report of this work was presented at the American Physical Society Meeting in New York, January, 1951 [H. Yagoda, Phys. Rev. **82**, 336 (1951)].

[1] Lattes, Occhialini, and Powell, Nature **160**, 453, 486 (1947).
[2] G. P. S. Occhialini and C. F. Powell, Nature **162**, 168 (1948).
[3] L. Leprince-Ringuet, Revs. Modern Phys. **21**, 42 (1949).
[4] Cosyns, Dilworth, Occhialini, and Schönberg, Nature **164**, 129 (1949).
[5] E. Pickup and A. Morrison, Phys. Rev. **75**, 686 (1949).
[6] I. Barbour, Phys. Rev. **78**, 522 (1950).
[7] C. F. Powell, *Cosmic Radiation-Colston Papers* (Interscience Publishers, Inc., New York, 1949), p. 91.
[8] H. Yagoda, Phys. Rev. **79**, 207 (1950); **80**, 753 (1950).

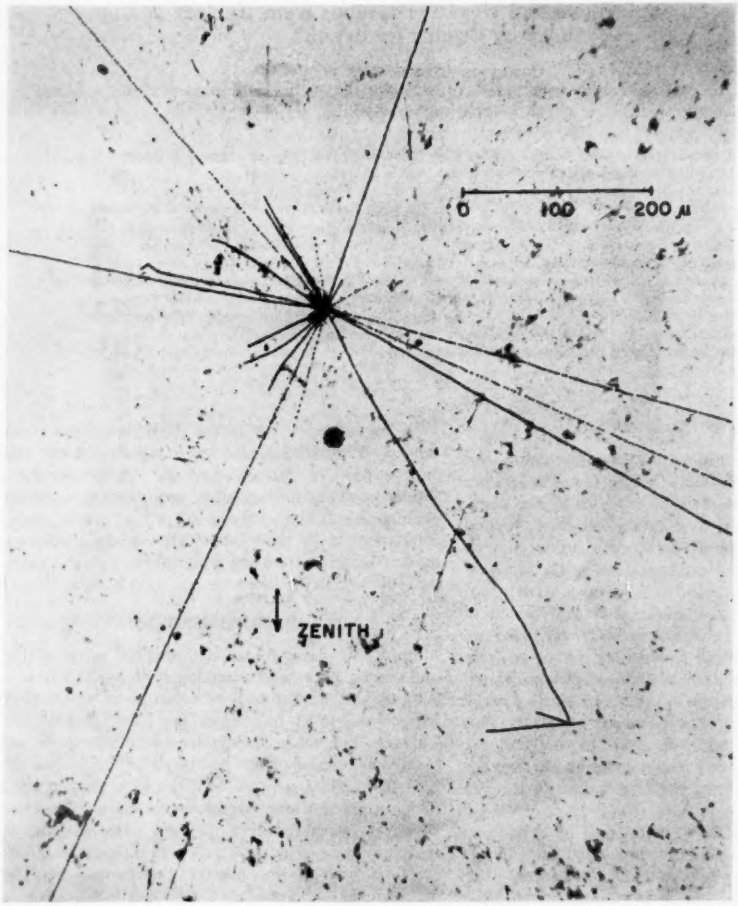

FIG. 1. Disruption of a heavy emulsion nucleus accompanied by the ejection of a 4.2-Mev π^- meson which is captured at the end of its range with the formation of a 3-prong star.

All the star illustrations are photodrawings prepared by inking pertinent detail on an enlargement print from a low power photomicrograph. The grain densities of the tracks are not perfect facsimiles of the original developed structures.

objectives. The castings were scanned with a 26× immersion objective (N.A. 0.5, W.D. 2 mm) and details of individual events were studied with a 45× immersion objective (N.A. 0.85, W.D. 1.5 mm). In all instances the entire volume of the recording medium was examined by successive linear traversals with overlapping fields.

All stars encountered in the field of view were examined for the presence of slow meson tracks (range 6 to 300 microns) basing the identification on scatter and σ-star formation at the rest point of π^- particles, and of the characteristic π-μ decay for those of positive charge. Particles ejected with ranges exceeding 300 microns were usually located at points remote from the parent star by tracing back all meson tracks observed to be near the end of their range to their points of origin. The detection efficiency of the mesons ejected from stars was therefore dependent chiefly on the ability to discern σ-stars and π-μ events. This feedback scanning mechanism is advantageous in that it avoids the tracing of all star tracks, and tends to equalize the detection probability of long-ranged mesons ejected from both small and large stars. A duplicate scanning of a 600 micron plate showed that the detection efficiency was about 80 percent under the particular conditions of microscopy. The visibility of tracks located near the bottom of very thick gelatin layers is poor owing to the scattering of the light by the silver structures in the upper layers and hence the detection efficiency is probably lower in the 1200 and 1800 micron emulsion castings.

Studies by Adelman and Jones[9] of the tracks of negative mesons produced by the Berkeley cyclotron show that 26.8 percent of the particles produce a heavy blob of several grains at the track terminus and the remaining mesons created small stars of one to five prongs. In our observations a small number of ejected mesons were also observed to terminate in a grain cluster. However, it was decided to exclude this category from the statistics, as it is not always possible to identify a meson by inspection of its scatter, and the number of random small grain clusters in the field were too numerous for use of the blob at the rest point as an auxiliary aid in the identification.

It is also difficult to detect negative mesons when the capture of the particle results in the emission of only a single track. To avoid possible confusion with protons undergoing a large angle scatter near the end of their range, the event was not accepted unless the multiple small-angle scatter was very pronounced and the emitted prong had a range exceeding 25 microns. Also, when the range of the ejected meson was less than 300 microns, short straight tracks at the apparent rest point of the particle were interpreted as an emitted prong only when of very heavy grain density accompanied by a detectable thin-down. When the track of the 1-prong star failed to terminate the identity of the meson was determined from considerations of the grain density and small angle scatter along the recorded portion. Mesons which produce stars of more than one prong can be identified readily when the range of the ejected particle exceeds about 50 microns and the star prongs have a recorded range of at least 5 microns. A typical example of this unambiguous category is illustrated in Fig. 1. When ejected at small angles with the emulsion plane, mesons with a range of only 5 microns can be detected when their capture results in a secondary star with more than 1-prong.

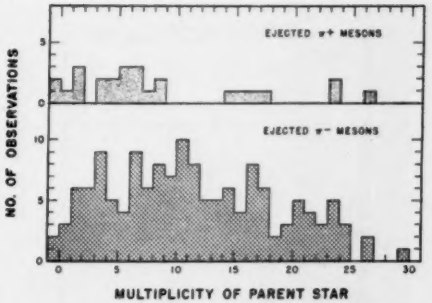

FIG. 3. Histogram of the number of events with ejected mesons as a function of the multiplicity (sum of black and gray tracks) of the parent star.

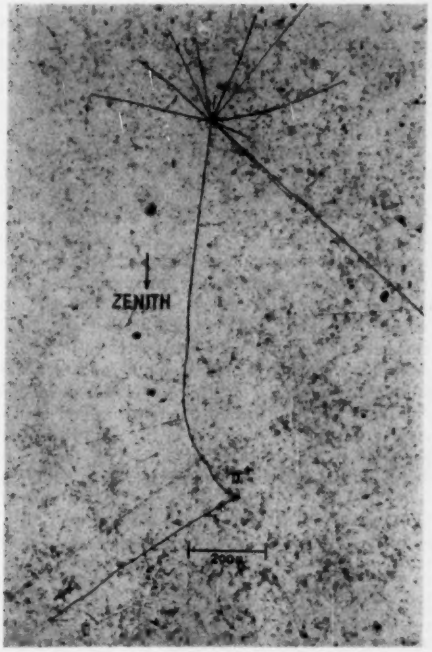

FIG. 2. Star showing the ejection of a 6.3-Mev π^+ meson which comes to rest in the emulsion and undergoes π-μ decay. The electron track from the decay of the μ^+ particle is recorded at a steep angle and appears of high grain density in the horizontal projection.

[9] F. L. Adelman and S. B. Jones, Phys. Rev. **75**, 1468 (1949).

The mesons of positive charge were identified by the characteristic π-μ decay process. In many instances, as shown in Fig. 2, the track of a minimum ionization electron could also be discerned at the rest point of the μ^+ meson. In a few events the μ^+ meson track escaped from the recording medium. These were tallied only when the variation of grain density and scatter over the recorded length permitted a differentiation from the tracks of fast protons or deuterons which occasionally are produced by the capture of a slow negative meson.

The data secured by these criteria is summarized in Fig. 3 in which the number of events showing the emission of mesons of opposite charge are arranged in the order of the parent star size. In assigning a multiplicity to the parent star only black and gray tracks were counted. The multiplicity does not include the track of the ejected meson, the tracks of minimum ionization shower particles, or the track of the incident particle when its trajectory was unambiguous. The star size may thus be employed as an approximate index for differentiating between heavy (Ag, Br, I) and light (H, C, O, N) groups of nuclei by assuming that all stars of multiplicity >6 originate from the heavy nuclei.

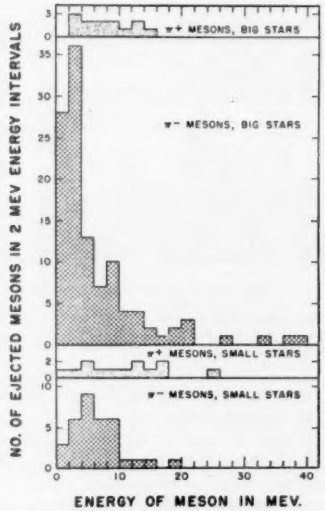
π+ MESONS, BIG STARS
π⁻ MESONS, BIG STARS
π+ MESONS, SMALL STARS
π⁻ MESONS, SMALL STARS
NO. OF EJECTED MESONS IN 2 MEV ENERGY INTERVALS
ENERGY OF MESON IN MEV.

FIG. 4. Classification of mesons emitted from nuclear disruptions as a function of the ejection energy of the particles.

This subdivision of the data into small and large stars is exhibited in Fig. 4 as a function of the kinetic energy of the ejected mesons. The energies were computed from the measured range in the emulsion basis a mass of $276m_e$ for pions employing the relationship $E_\pi = 0.250(m_\pi/m_p)^{0.419}R^{0.581}$ derived by the Berkeley group.[10]

III. THE RATIO OF POSITIVE AND NEGATIVE MESONS EJECTED FROM STARS

The observations indicate that in the low energy region under consideration (<40 Mev) the ratio of π^+/π^- ejection from all the emulsion nuclei is 0.18. On the basis of origin from large and small stars the observational charge ratio is estimated at 0.15 for heavy target nuclei and 0.37 for the light nuclei of the gelatin component. It is to be noted that ejected negative mesons terminating without visible star formation are not included in the statistics, and if it be assumed that these constitute 26.8 percent of the negative mesons, as indicated by the observations of Adelman and Jones,[9] the π^+/π^- ratios would be reduced correspondingly by a factor of 0.79.

The charge ratio of the ejected mesons is strikingly small when compared with available data on the corresponding ratio of mesons incident on plates exposed to cosmic radiation in the stratosphere. For the latter Barbour[6] observed values ranging between 1.8 and 1.4 in a series of flights with the plates exposed between the poles of a 65-lb magnet. In our flights No. 108 and 110 (Table I) a total of 520 π-μ events and 542 σ-mesons were observed to enter and terminate in the emulsions, suggesting that in essentially unscreened plates the π^+/π^- incident ratio is close to unity. In a flight at 60,000 ft elevation Fry[11] observed a π^+/π^- ratio for externally created mesons of 0.35.

The discrepancy between the ejected and the incident meson charge ratios may originate from the following factors:

(1) Geometric limitations: A study of the 26 events exhibiting the ejection of a positive meson shows that in 24 instances the μ^+ decay particle also terminated and that in the remaining two events the recorded range (about 400 microns) was adequate for the identification. The large fraction of completely terminating π-μ events suggests that the observations were limited chiefly to those events in which the decay particle was recorded at small angles with the emulsion plane. This is further indicated by the analysis in Table II which shows that the observational ratio of π^+/π^- mesons ejected from stars increases progressively with the thickness of the recording medium. Application of escape corrections to the μ^+ particle indicates that the 26 events noted microscopically probably correspond to 47 occurrences of an ejected positive meson, and that the ratio thus corrected is increased to 0.32 when all nuclei in the emulsion are considered.

(2) Ejection energies: In leaving the nucleus positive mesons will acquire an additional energy by Coulomb repulsion $E_c = Z_1Z_2e^2/d$. This evaluates to 9.8 and 8.1 Mev for silver and bromine nuclei, and 2.6 to 3.2 Mev for nuclei of charge 6 to 8 if it be assumed that d is of the order of the nuclear radius $1.45\times10^{-13}A^{\frac{1}{3}}$ cm. Thus, if mesons of both charges were initially created with the same energy distributions the positive particles ejected from heavy nuclei would have their ranges extended by an amount corresponding to about 9 Mev, and hence a smaller number would terminate in the emulsion. Examination of Fig. 4 shows that this factor is not evident in our present observations, and that in contrast, a large fraction 9/13 of the positive mesons ejected from heavy nuclei appear in the laboratory system with kinetic energies well below the minimum

TABLE II. Observational intensities of ejected mesons.

Flight	Emulsion thickness microns	Volume scanned cc	No. of events with ejected mesons π^+	π^-	π^+/π^-	Intensity[a] cc per day	Total star intensity >2 prongs
76S	300	20.2	none	15	0.13	2.62	2460
83	300	15.8	3	9		2.65	2270
110	600	25.4	9	65	0.14	9.58	2680
97	1200	3.8	4	14	0.29	16.7	2540
108	1800	11.2	10	42	0.24	16.6	1910

[a] Sum of π^+ and π^- ejected mesons.

[10] H. Bradner, University of California Radiation Laboratory Report 486 (October 19, 1949), p. 60.

[11] W. F. Fry, Phys. Rev. **82**, 749 (1951).

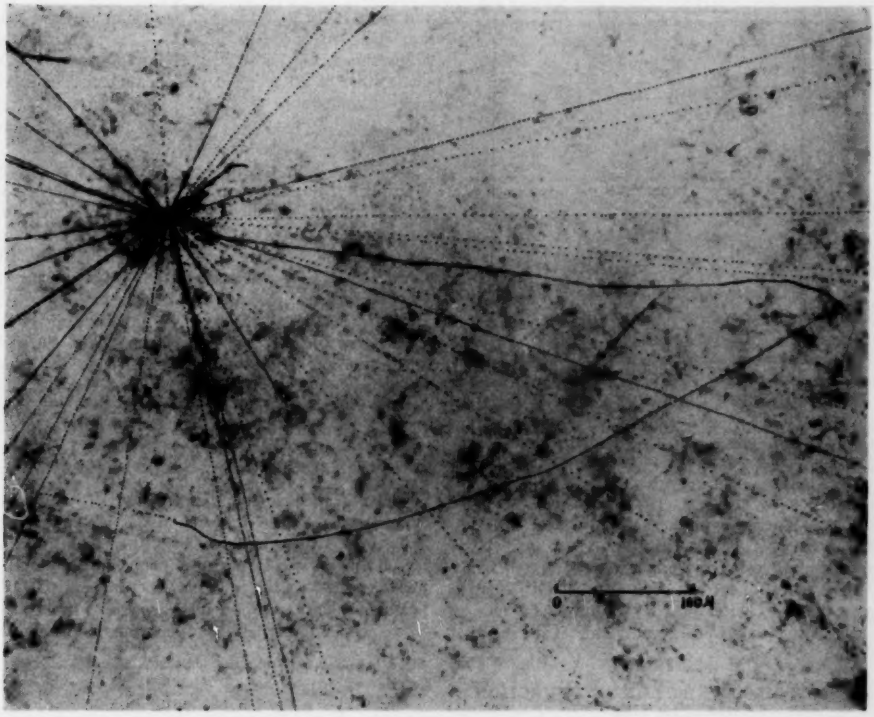

FIG. 5. Emission of a slow π^+ particle in the disruption of a heavy nucleus. The ejected meson has a kinetic energy of 4 Mev, a value markedly smaller than that imposed by the Coulomb barrier of silver or bromine nuclei. While apparently emerging in the same direction as the fast shower particles, it is probably a member of an independent group of slow mesons.

energy imposed by the Coulomb barrier.[12] Figures 2 and 5 are examples of positive meson ejection from heavy nuclei with energies less than E_c, the latter example is particularly striking in that the meson appears to emerge within the angular cone of the fast shower particles (see Sec. VI).

A low yield of positive mesons is to be anticipated if the parent stars are produced chiefly by neutrons. Thus, Bradner, O'Connel, and Rankin[12] observed a π^+/π^- ratio of 0.11 for the mesons produced by the bombardment of a carbon target with 270-Mev neutrons. The observational π^+/π^- ratio of 0.18 (or 0.32 when corrected for μ^+ escape) for mesons ejected from all the emulsion nuclei is explicable if it is assumed that most of the disruptions were initiated by non-ionizing radiation. Examination of the parent stars shows that only 13 percent of the events were initiated by a charged particle.

The charge ratio of slow mesons produced by the bombardment of targets of different nuclear charge by 390-Mev alpha-particles has been measured by Barkas.[10,14] His observations on relative meson yields, over an energy interval of 2 to 5 Mev, summarized in Fig. 6, indicates that the charge ratio falls rapidly with increasing nuclear charge and that no positive mesons were observed from indium or lead targets. Restricting our observations on mesons ejected from cosmic ray stars to an energy less than 6 Mev, yields π^+/π^- ratios of 4/18 and 5/77 for the light and heavy nuclear components of the emulsion. As seen in Fig. 6, these

[12] In a discussion with Dr. M. M. Shapiro he has suggested that lowering of the Gamow barrier for the escape of a π^+ meson might occur: (1) in a violent, more or less head-on collision of an incident particle with the target nucleus (a) if disintegration precedes the escape of the slow meson, or (b) through an increase in nuclear diameter resulting from the high excitation: (2) in a collision which imparts a high angular momentum to the target nucleus. Penetration by leaking through the Gamow barrier, which is more probable for a pion than for a heavier particle with the same energy, may account for a small proportion of the observations. Finally, the detector geometry contributes in an essential way: once a low energy meson does emerge, its chance of stopping in the emulsion is much greater than that of longer-range mesons.

[12] Bradner, O'Connel, and Rankin, Phys. Rev. **79**, 720 (1950).

[14] W. H. Barkas, Phys. Rev. **75**, 1467(A) 1949.

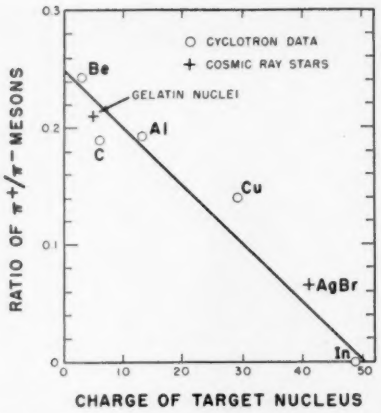

FIG. 6. Comparison of the observational π^+/π^- ratio for slow mesons produced by the cyclotron and ejected from cosmic-ray stars as a function of the nuclear charge of the target atoms.

charge ratios are in good agreement with the yield of positive and negative mesons produced by 390-Mev alpha-particles. This is rather unexpected, in that the slow mesons of cosmic-ray origin were produced chiefly by high energy neutrons and this would seem to suggest that the charge ratio of very low energy mesons is not sensitive to the energy or charge of the incident radiation.

IV. SLOW MESON EJECTION AS A FUNCTION OF STAR SIZE

Examination of Fig. 3 shows that slow mesons are ejected from stars of 2 to 18 prongs with about equal frequency. As is well known from numerous investigations of star size distribution in emulsions exposed to cosmic radiation, small stars predominate and, in general, the relative frequency diminishes exponentially with increasing star multiplicity. Our observations therefore indicate that the probability of slow meson ejection increases very rapidly with the complexity of the parent star. In order to evaluate the form of this ejection probability function an estimate was made of the total number of stars in each multiplicity class S_n (black and gray prongs) recorded in the volume of emulsion scanned for ejected mesons. On the basis of the star intensities recorded in Table II and the duration of the respective stratosphere flights it is estimated that 53,800 stars with 3 or more prongs were recorded in the volume scanned. S_n was estimated with the aid of the star spectrum based on 15,300 events analyzed in plates flown at 68,000 ft by the Bristol group,[15] and the probability $P_n=(S_\pi/S)_n$ was computed for each star class. As shown in Fig. 7, P_n is approximately proportional to the square of the multiplicity. For giant stars of 20 or more prongs there is about a 2 percent probability of a slow negative meson ($E<40$ Mev) being ejected and terminating in thick emulsions. The available data on ejected positive mesons is indicative of a similar trend in the variation of P_n with multiplicity, but the form of the function must await more abundant statistics. On the basis of ejection from large and small stars the relative observational frequency for negative mesons is 3.15 ± 0.6. Within the limitations of the present statistics slow positive mesons are observed with about equal frequency from both large and small stars. In so far as the multiplicity is a measure of the star excitation energy, and since the star excitation energy has been shown[15] to be a linear function $E_n=155n-100$, it follows that the probability of slow meson ejection is approximately proportional to the square of the excitation energy.

V. MESONS FROM STARS OF <3 PRONGS

The observations summarized in Fig. 3 show that slow mesons are also produced in simple nuclear interactions constituted of only 1 or 2 prongs, and that the meson track may begin at a point in the emulsion unassociated with the tracks of other ionizing particles, i.e., multiplicity zero. In all 4 events of multiplicity zero the points of meson origin were well embedded

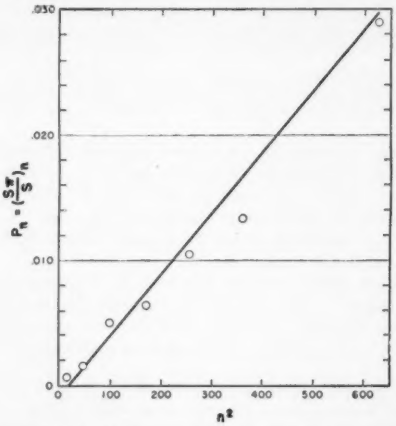

FIG. 7. Relationship between the probability of slow π^- meson ejection from a star with n-prongs and the square of the multiplicity, n^2. Because of the small number of events in individual multiplicity groups, the data has been grouped into units of three successive multiplicities. The average statistical uncertainty for the plotted points is ±25 percent on the basis of the numbers of ejected mesons in each category.

[15] Preliminary manuscript by Camerini, Davies, Fowler, Franzinetti, Lock, Perkins, and Yekutieli to be published in Phil. Mag. The star spectrum based on black and gray tracks does not vary significantly with altitude between 68,000 and 100,000 ft, as indicated by a comparison of the star size distribution of 500 stars recorded in our high altitude plates with the more statistically significant work of the Bristol group at the lower altitude.

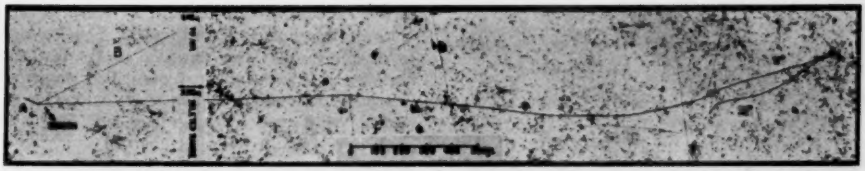

FIG. 8. Interaction exhibiting the emission of an 18.5-Mev π^+ meson, associated with a black track A and a gray track B. The latter leaves the emulsion after traversing 1300 microns without an appreciable change in grain density (less than 4× minimum); its specific ionization is indicative of either a 47-Mev pion, or a 300-Mev proton. The short black track also leaves the emulsion at a steep angle and its charge is not determinant.

within the emulsion layer and the initial grain densities of the trajectories were considerably above the lower recording limit for singly charged particles. The two positively charged mesons originating from stars of zero multiplicity are readily explicable on the basis of the interaction of neutrons or gamma-rays with hydrogen nuclei, $n+\mathrm{H}\rightarrow 2n+\pi^+$ or $h\nu+\mathrm{H}\rightarrow n+\pi^+$. The negatively charged particles, however, are not readily reconcilable with known mechanisms of meson production. The possibility must be considered that minimum ionization particles may have been associated with the π^- meson tracks, but that owing to localized fluctuations in sensitivity or unfavorable angles of incidence the tracks could not be discerned microscopically. The interpretation of these negative meson tracks must await the accumulation of more abundant statistics.

The several events constituting multiplicity groups 1 and 2 can be classified according to the charge of the ejected meson and the grain density of the associated tracks as shown in Table III. Most of these events can be interpreted in terms of meson production by nucleon-nucleon interaction processes. In several instances, however, where a black track is associated at the origin of the meson particle it must be postulated that the energy of the incident nucleon was only slightly above the threshold value for meson production and that the black prong represents the emergence of a slow proton. A typical example of the parent star class in which a black and a gray prong is associated with the meson track is illustrated in Fig. 8.

VI. MULTIPLE SLOW MESON EJECTION

The present observations also include two stars exhibiting the emission and termination of more than one slow meson. The first event of this character, described in detail in an earlier publication,[16] was initiated by a relativistic proton, and the two negative mesons of 3.3 and 18.4 Mev appeared as wide angle members of a collimated shower of 8 fast singly charged particles. In the second example of multiple slow meson creation, reproduced as a projection drawing in Fig. 9, three slow negative mesons were ejected from a giant star initiated by a heavy primary whose charge is estimated at 11 ± 1 by delta-ray counts. The slow mesons emerge along an independent shower axis at an average angle of 90° to the main collimated shower of about 30 relativistic particles. One of the slow mesons σ_1 appears in the horizontal projection of the event as part of the fast group, but it is directed upward at a steep angle with the principal shower axis.

It is noteworthy that in both instances of multiple slow meson ejection the nuclear disruption shows a collimated shower of fast singly charged particles and that the slow mesons are emitted at large angles with the fast shower axis. In general, showers of fast particles (4 or more minimum ionization tracks recorded over an angular spread of $<60°$), are evident only in about 20 percent of the stars which exhibit the track of a single slow meson, and this particle is invariably the wide angle member. This orientation of the slow mesons with respect to the fast shower axis, taken in conjunction with the two instances of multiple slow meson ejection which have been observed, suggests that in stars with a fast collimated shower more than one slow meson may be produced in a fair proportion of the events, but that owing to the limited thickness of the recording medium the termination of more than one is observed very infrequently. The two occurrences suggest a lower observational limit for this process of the order of 0.09 per cc per day of exposure in the stratosphere.

The emission of a slow positive meson as a member of a group of slow mesons has not been directly ob-

TABLE III. Classification of the simple meson production processes.

Star multiplicity	Ejected meson charge	Associated tracks	Possible origin	Number of occurrences
0	+	none	$h\nu+p\rightarrow\pi^++n$ $n+p\rightarrow\pi^++n$	2
0	−	none		2
1	+	1 gray	$p+n\rightarrow n+n+\pi^+$	1
1	−	1 gray	$n+n\rightarrow n+p+\pi^-$	1
1	−	1 black		2
2	+	2 gray	$p+p\rightarrow n+p+\pi^+$	1[a]
2	+	1 black+1 gray		2
2	−	1 black+1 gray	$n+p\rightarrow p+p+\pi^-$	4
2	−	2 black		2

[a] An event similar to this, but in which the ejected meson is of negative charge, has recently been described by S. J. Goldsack and N. Page, Phil. Mag. 42, 570 (1951). They attribute the meson production to a $n+p\rightarrow p+p+\pi^-$ reaction.

[16] M. M. Shapiro and H. Yagoda, Phys. Rev. 80, 283 (1950).

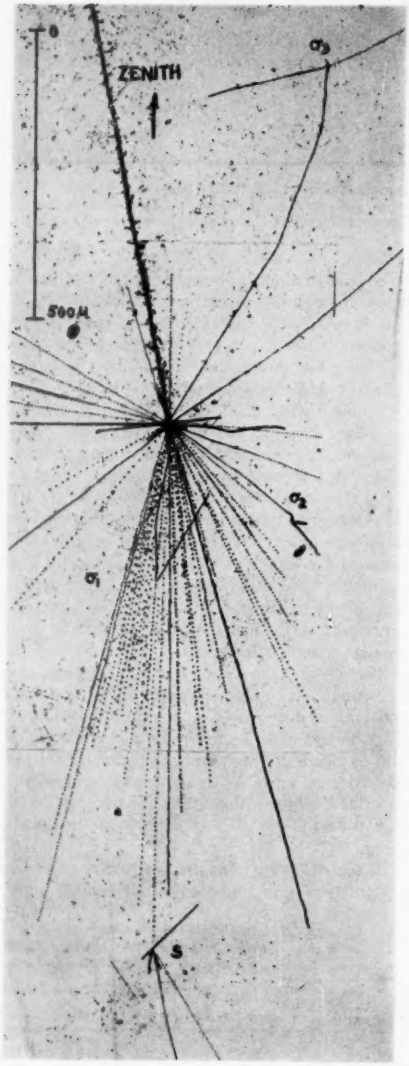

FIG. 9. Giant star initiated by a heavy primary of estimated charge 11±1, constituted of 31 black and gray tracks and about 30 relativistic particles, the latter collimated in a broom of 52° angular spread. One of the fast shower particles is captured in flight and produces a 7-prong star S. In this interaction of the incident particle with a heavy nucleus, possibly silver, three slow mesons are also ejected with energies of $\sigma_1=3$ Mev, $\sigma_2=4.9$ Mev, and $\sigma_3=8.2$ Mev. The slow mesons emerge over an angular spread of 155° and their axis is at an angle of 90° with that of the fast shower.

A number of tracks, directed at large angles with the emulsion plane, have been omitted from the horizontal projection of the event.

served. The orientation of the π^+ track in Fig. 5, however, is indicative of this process. This track seems to emerge in the same direction as the fast shower particles. It is reasonable to assume that this direction is coincidental, and that like track σ_1 of Fig. 8, the ejected positive meson belongs to an independent group of slow mesons the other members of which failed to terminate.

VII. ENERGY DISTRIBUTION OF THE EJECTED π^- MESONS

The data on slow meson ejection accumulated from observations in recording media of different thickness exposed on independent flights. Only in the exposures of flights 110 and 108 were a sufficient number of events observed to permit a rough estimate of the production rate by correcting the data for those meson tracks which originated in stars but failed to terminate in the sensitive layer. In applying geometric escape corrections it has been assumed that the probability of a meson track originating in an emulsion of thickness t and producing a σ-star or a μ^+ decay particle at the end of its range R is:

$$P_1=[1-(R+k)/2t], \quad \text{when} \quad (R+k)<t \qquad (1)$$

and

$$P_2=t/[2(R+k)], \quad \text{when} \quad (R+k)>t. \qquad (2)$$

A length k must be added to the range in order to establish the production of a secondary event at the meson track terminus. This correction is only appreciable for positive mesons where a length k of about 400 microns must be recorded to identify the secondary track as that of a μ^+ particle. For mesons of negative charge, k resides between 5 and 25 microns depending on the secondary star size and is in general negligible for most all values of R in the thick emulsions under consideration.

Equations (1) and (2) assume that R is small compared to the linear dimensions of the recording medium, and hence are not applicable to the data of flight No. 108. In the region of 10 to 40 Mev the long ranges of the mesons necessitate an additional correction owing to the limited size of the castings (diameter 5 cm). For cylindrical disks of diameter D and thickness t the probability of a particle of range $R>t$ terminating is as a first approximation:

$$P_3=(t/2R)[(D-R)/D]^1. \qquad (3)$$

Application of these corrections to the data observed in the 600 micron plates and the 1800 micron thick castings shows (Fig. 10) that within the limitations of the available statistics the yield of negative mesons increases progressively with their ejection energy. The close agreement between points from the two flights indicates that the meson ejection phenomenon is of a reproducible character, and that the form of the spectrum is independent of altitude between 90,000 and

106,000 ft. Points *A*, *B*, and *C* on Fig. 10 are from the energy spectrum of π^- mesons produced by 390-Mev alpha-particles on a carbon target measured by Jones and White and described in the Bradner Report,[10] normalized to the stratosphere data. This comparison indicates a close similarity in the form of the negative meson spectra over the region of 3.8 to 12.5 Mev suggesting that the distribution is not sensitive to the charge of the target and projectile nuclei.

A detailed analysis of the present data is not warranted owing to the limited statistics. It appears, however, that even in the region below 40 Mev, the spectrum cannot be fitted by a single power law. The negative meson production frequency in the region between 8 to 40 Mev is significantly greater than for the 1 to 8 Mev region. The points below 8 Mev are based on good statistics, the geometric escape corrections are small and hence the relationship $I_\pi \propto E^{0.6}$ is dependable for the production intensity of negative mesons ejected with energies ≤ 8 Mev. For energies >9 Mev the intensity appears to be proportional to $E^{2.3}$, but the statistical uncertainty is large and the significance of the rapid increase in intensity must await more abundant observations.[17] The intensities of meson production in the stratosphere shown in Fig. 10 have not been corrected for those particles which stop in the emulsion without visible star formation, or for the over-all factors which govern the detection efficiency as discussed in Sec. II.

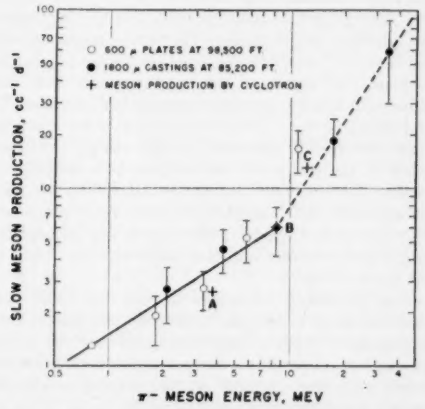

FIG. 10. Slow π^- meson production intensity, corrected for escape, as a function of meson ejection energy. Points *A*, *B*, and *C* from the energy distribution of cyclotron mesons (intensity in arbitrary units) have been normalized to the stratosphere cosmic-ray data at point *B*.

[17] Disks of emulsion 2.5 mm thick and 90 mm in diameter have been cast and processed successfully. One of these has been recovered after a level flight at 95,000 ft. Measurements on this preparation should improve the statistics in the region of 8 to 40 Mev and provide some additional points on the range distribution of ejected mesons with energies up to about 80 Mev.

TABLE IV. Star size distributions produced by ejected and cyclotron mesons.

Exposure No. of events	Stratosphere 148	Cyclotron 3366
	percentage of stars	
1-prong	32.4 ±4.7	32.4±1.0
2-	26.3 ±4.2	32.7±1.0
3-	27.0 ±4.3	22.3±0.8
4-	12.2 ±2.9	10.5±0.6
5-	1.35±1.0	2.0±0.2
6-	0.68[a]	0.1±0.1

[a] Based on only a single observation. Combining the data on 5- and 6-prong stars indicates a frequency of 2.0 and 2.1 percent for σ-stars produced by cosmic-ray and cyclotron mesons, respectively.

VIII. SECONDARY STARS PRODUCED BY THE CAPTURE OF EJECTED MESONS

The distribution of secondary stars produced at the range terminus of the 148 negative mesons ejected from cosmic-ray disruptions is compared with the prong size distribution obtained with π^- cyclotron mesons in Table IV. The latter data is taken from a compilation by Adelman[18] based on a total of 3366 σ-stars recorded in plates exposed to the negative mesons produced by the Berkeley cyclotron. Within the limitations of the comparatively scant cosmic-ray statistics the two groups of observations appear to be comparable. This can be interpreted that most all of the mesons ejected from cosmic ray disruptions are identical in mass with the π^- mesons produced by the cyclotron, as a large admixture of heavy mesons ($\sim 1000 m_e$) might favor the production of the more complex σ-stars constituted of 4 to 6 prongs.

In the course of these observations more than 2000 meson tracks were followed back to their points of origin. No examples of the decay of a heavy τ-meson into 3 light mesons were detected by this scanning mechanism.[19] In descriptions of τ-meson occurrences[20,21] the plates were exposed at mountain altitudes surrounded by large thicknesses of lead or ice. It thus appears that the production of τ-mesons is favored by

[18] F. L. Adelman, University of California Radiation Laboratory Report 1005 (1951).

[19] The decay of a $1000 m_e$ particle at rest into three π-mesons releases 86 Mev available as kinetic energy. If shared equally, the decay particles will have ranges of about 10 mm and a termination probability of only 0.072 per track in the 1800 micron castings. When the energy is shared unequally the probability of detecting the slower decay particles is considerably improved ($P=0.3$ to 1 for energies of 12 to 1 Mev). If the three respective ranges are considered equally probable, the average detection probability per event is estimated at about 0.5. Since no instance of ternary τ-meson decay was noted the upper limit for the process is of the order of 1 per 500 π-μ decays.

[20] Brown, Camerini, Fowler, Muirhead, Powell, and Ritson, Nature **163**, 82 (1949).

[21] J. B. Harding, Phil. Mag. **41**, 405 (1950).

a preponderance of secondary radiation, and that very few interactions at stratosphere elevations result in the formation of π-mesons.

ACKNOWLEDGMENTS

Opportunity is taken to thank the ONR and the aeronautical staff of General Mills for the exposure and recovery of the several emulsion preparations. The casting of emulsion disks of adequate sensitivity was greatly facilitated by Dr. C. Waller of Ilford Limited through provision of a supply of G5 gel. Appreciation is expressed to Dr. M. M. Shapiro for many helpful discussions of meson production mechanisms, and for providing space in the gondola on several balloon flights.

PHYSICAL REVIEW VOLUME 85, NUMBER 5 MARCH 1, 1952

Emulsion Cloud-Chamber Study of a High Energy Interaction in the Cosmic Radiation*

M. KAPLON, B. PETERS,† AND D. M. RITSON
University of Rochester, Rochester, New York
(Received November 16, 1951)

A new technique is described for studying high energy interactions utilizing photographic emulsions as detectors. A detailed study has been made with this technique of one very high energy mixed shower. Evidence is obtained for the multicore structure of the soft component at depths of several radiation lengths in this mixed shower, along with the existence of a finite lifetime for the decay of the neutral π-meson into two photons of the order of 1×10^{-14} sec.

HIGH energy nuclear interactions lead to the production of mixed showers of mesons, nucleons, and electronic components. Such interactions with energies above 10^{12} ev have been previously studied both by observing the resultant electronic and nucleonic cascades in Auger showers and by directly observing the primary interactions in the photographic emulsions. Observations on Auger showers are necessarily indirect. While on the other hand the photographic plate allows a detailed study of the primary interaction to be made as to distribution and multiplicity, the energies of the products cannot be determined, and the primary energy can only be approximately estimated from kinematic considerations. Hitherto, such events have very rarely been found and only in the course of random surveys.

We have made observations with a technique which allows a much more detailed study to be made of the interactions, and at the same time permits the events to be found with relative ease. The events are observed in a so-called emulsion cloud chamber consisting of alternate layers of photographic emulsions and absorber. An interaction in the stack starts a mixed shower. The plates near the interaction show just the charged mesons and nucleons formed in the primary interaction. Later in the stack the electronic component begins to multiply and form well-marked electronic cores. From these cores and their degree of multiplication can be determined the numbers, and energies of the neutral mesons resulting from the initial interaction. It is further possible to measure the lifetime of the neutral mesons from the finite path lengths they transverse at high energies. To find such an event, one of the emulsions in the emulsion cloud chamber is scanned for high energy electronic cores. If the plates are well aligned it is possible to predict the position of a core in succeeding and preceding plates and thus trace the event back to the first plate in which it appears; this plate is usually near the origin of the shower and the tracks reproject back to the point of origin.

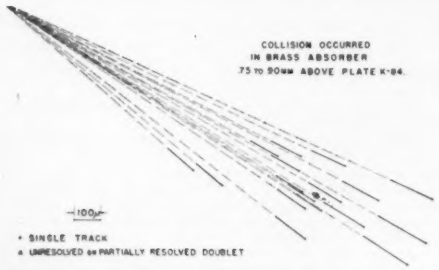

FIG. 1. Target diagram of hard shower in first plate (plate 8) showing reprojection of tracks to a common origin.

One important advantage of this technique over cloud-chamber techniques is the high resolution of the photographic plate in which tracks are resolved within $\frac{1}{2}\mu$ and cores of electronic showers can be resolved which would completely "swamp" a cloud chamber and permit no detailed structure to be discernible.

The energy range for which the technique is applicable depends on the material of which the stack is constructed. The core of an electronic shower does not show above the background of random tracks in the experiment described below unless its energy is in excess of 10^{11} ev. If we had used a stack exclusively of photographic plates, this limit would have been about 5×10^{12} ev; with high Z materials the limit would have been as low as 10^{10} ev.

* This work was supported by the AEC.
† Now at Tata Institute, Bombay, India.

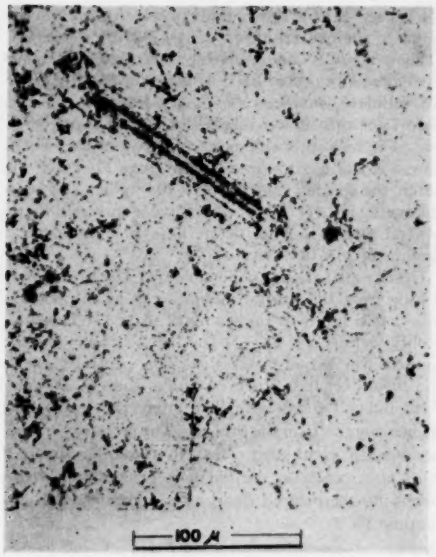

FIG. 2. Microphotograph of main target area in plate 15, 2.7 radiation lengths from origin of shower. The two resolved electronic cores AA' are believed to originate from the decay of a neutral meson into two photons. The photograph is a single shot in one focal plane taken with a ×20 objective.

We describe in the following section the application of this technique to measurements of a high energy interaction, the so-called T-star.

EXPERIMENTAL

The apparatus used has been described previously.[1] It consisted of a stack of twenty 6 in.×4 in. 100-μ Ilford G5 emulsions each separated by a 3-mm brass plate. The effective radiation length from emulsion to emulsion in this stack calculated for the mixture of materials used was 2.4 cm. The T-star started in the brass plate above plate 8 and was inclined at such an angle that it traversed 0.94 cm or 0.39 radiation lengths, from one plate to the next. The cores can be followed through to plate 20, thus covering a total of 4.7 radiation lengths in the stack.

Figure 1 shows the target diagram of the first plate on which the event is found. The coordinates of the entrance and exit points of the tracks into the emulsion were found from the stage motions of the microscope, and are plotted on the diagram. Figure 1 thus shows the projections of the tracks in the emulsion on the plane of the glass. It will be noted that there are 36 minimum ionization tracks about half of which are in a wide core, and half in a narrow core, and that the tracks clearly project back to a single origin. The origin lies about 0.1 cm back in the brass or 0.06 of a radiation unit. Further down in the stack rapid cascade multiplication occurs and various cores become visible. Later these cores begin to "wash" one into the other, and resolution between the cores is lost.

Plate 7 was scanned for the primary which caused the interaction. One track of minimum ionization with the right length, direction, and position was found, but no tracks of greater ionization were found. With the background of random minimum tracks, we are not certain that the interaction was caused by a charged primary, but we can be sure that the charge of the primary was less than two.

Figure 2 is a microphotograph of part of the target area of plate 15, 2.7 cascade units from the origin of the shower; the most striking feature is the two very close electronic cores marked A and A'. These cores which under higher magnification consist of bundles of minimum ionization tracks can first be seen resolved on plate 14 and can be traced through to plate 18. On plates 19 and 20 the cores are no longer resolved. Figure 3 shows a microphotograph of plate 20. The region of high density marked AA' corresponds to the double cored structure on plate 15, now no longer resolved. In addition a new barely resolved double-cored structure

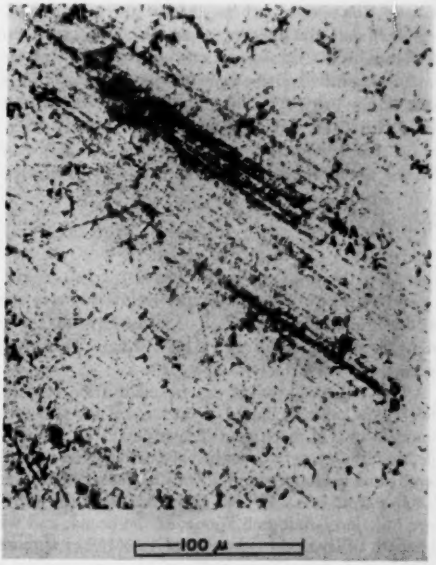

FIG. 3. Microphotograph of main target area in plate 20, 4.7 radiation lengths from origin of shower. The region AA' represents the now unresolved cores AA' of plate 15 and the barely resolved cores BB' represent the soft showers from the decay of a more energetic neutral meson. The photograph is a single shot in one focal plane taken with a ×20 objective.

[1] M. F. Kaplon *et al.*, Phys. Rev. **85**, 295 (1952).

can be seen to the left of the main core. This second double core BB' is first visible on plate 17 and is unresolved on plates 17, 18, and 19.

In addition to these well-marked cores we can distinguish eight other cores of smaller density which are resolved on three or more plates. In order to make energy estimates, we made counts of the numbers of tracks within 25μ and 50μ of the shower axis on each core.

Most of the cores are not resolved from the over-all background. After plate 15, AA' and BB' are resolved from other cores down to plate 20 and another core is resolved until plate 17. The cores only resolved to plate 15 contained about ten tracks in a twenty-five micron radius on plate 15. The core resolved down to plate 17 contained twenty-six tracks. AA' contained forty tracks on plate 20, and BB' contained thirty-four tracks on plate 20 within a twenty-five micron radius.

INTERPRETATION

a. Lifetime of the Neutral Meson

In the previous section two double-scored showers, AA' and BB', were described. These showers are of higher energy and appear to start later in the stack than the other γ-rays that materialize. We interpret these showers as a result of neutral mesons that have decayed after a finite path length each into two photons.

Shower AA' first appears on plate 12, and is resolved on plates 14–18. The separations on the various plates can be measured and the cores reprojected back to the point of the origin. The origin appears to be between plates 10 and 11, about 2.5 cm from the primary interaction. The energy of the shower can be estimated in two ways. The angle between the two photons emitted by a neutral π-meson of mass μc^2 and energy $\mu c^2\gamma_0$ is given by

$$\sin\tfrac{1}{2}\theta=(1/2\gamma_0)(r^{\frac{1}{2}}+r^{-\frac{1}{2}}),$$

where r is the ratio of the energies of the two γ-rays. θ can be directly measured and r estimated from the ratio of the numbers of electrons in the two cores: r is from 2:1 to 5:1 and $\theta=2.1\times10^{-4}$ radian. This gives an energy for AA' of $1.4-1.8\times10^{12}$ ev.

A less reliable estimate can be made from cascade theory. We have calculated on the basis of the structure function of Fernbach and Eyges[2] and the electron spectra,[3] the expected number of particles for various depths and primary energies. On this basis, the shower has an energy of 4×10^{12} ev. The behavior of the structure function is not well known at the origin, and we therefore believe that the value of 1.5×10^{12} ev is more reliable and that the cascade calculations should be changed by a factor of the order of two to give agreement with experiment. The path length of 2.5 cm and the energy of 1.6×10^{12} ev leads to a lifetime in the rest frame of the neutral meson of $\tau_0=7\times10^{-15}$ sec.

Shower BB' is only resolved on one plate and cannot therefore be projected back. It is first seen on plate 17. An estimate from cascade theory leads to a higher energy for this shower relative to AA' of the order of two. The most probable point of decay of the neutral meson is half a cascade unit from plate 17. Using this value, the opening angle is 1.35×10^{-4} radian and hence the energy is 2.4×10^{12} ev. The distance traversed by the neutral meson is 7 cm before decaying, leading to a lifetime of 13×10^{-15} sec.

Other explanations are possible: (1) The two photons arising from the neutral meson decay at the point of interaction failed to convert until plate 17. The probability for this is $1:10^3$. (2) The BB' neutral meson was formed in a second interaction. This neutral meson is the highest energy observed in the shower. It would seem difficult for a secondary interaction to produce higher energies than the primary. The primary produces besides AA', eight other cores. No cores other than BB' start after plate 17. We therefore believe that we are observing the delayed decay of a neutral meson with lifetime 1×10^{-14} sec.[4,5]

b. The Energy Balance and Spectrum of Neutron Mesons in the Core

In Sec. a, we have given energies for showers AA' of 1.6×10^{12} ev and BB' of 2.4×10^{12} ev. Using the cascade theory modified by the factor of two (see preceding section) a shower core of 5×10^{11} ev can be recognized and about seven cores with energies of the order of 10^{11} ev-3×10^{11} ev. The neutral meson spectrum is thus consistent with one neutral meson of 2.4×10^{12} ev, one of 1.6×10^{12} ev, one of 6–8×10^{11} ev, and about four of energies 2–4×10^{11} ev. An examination of isolated pairs outside the core within an opening angle of 0.03 radian on plate 9 (average separations 5μ) leads to an average energy of 2.5×10^{10} ev for the photons[6] and thus an average energy of 5×10^{10} ev for the neutral mesons outside the core. Adding this contribution for ten neutral mesons outside the core to the previous energies in the core we find the total energy in the soft component is thus 6×10^{12} ev. Using a 2:1 partition between the charged and neutral meson component (see Sec. c) the total energy is 1.8×10^{13} ev.[7]

[2] S. Fernbach, Phys. Rev. **82**, 288 (1951).
[3] L. Janossy and H. Messel, Proc. Roy. Irish Acad. **54**, 31 (1951).

[4] H. L. Bradt *et al.*, Helv. Phys. Acta **23**, 24 (1950); A. G. Carlson *et al.*, Phil. Mag. **41**, 701 (1940); and J. J. Lord *et al.*, Phys. Rev. **80**, 970 (1950). Bradt gives $\tau_0\leq3\times10^{-13}$; Carlson gives $\tau_0\leq5\times10^{-14}$ and Lord gives $\tau_0\leq2\times10^{-13}$.
[5] This is to be contrasted with the theoretical prediction for the *PS-PV* theory which gives $\tau_0=0.3\times10^{-17}/(g^2/\hbar c)\cdot(g^2/\hbar c\sim\frac{1}{4})$. J. Schwinger, Phys. Rev. **82**, 664 (1951).
[6] H. L. Bradt *et al.*, Helv. Phys. Acta **23**, 24 (1950). See definitions and formula 2a.
[7] If nucleons and antinucleons are also produced in the interaction, this energy estimate could be raised as a result of the presence of non-ionizing nucleonic component.

The energy of the star can also be estimated from kinematic considerations. If the mesons and nucleons are formed in a single collision symmetric about the 90° line in the c.m. system, we have the following relation between the laboratory angles θ_f containing a fraction f of the particles, θ_{1-f} containing a fraction $1-f$ and $\bar{\gamma}$ the energy in units of the rest mass of a nucleon in the c.m. system.[6]

$$\bar{\gamma}^2 = 1/\theta_f \theta_{1-f}.$$

The approximation is made that the particles in the c.m. system have moderate velocities. Figure 4 shows θ_f plotted against f. The curve appears symmetric about $f=0.5$. Taking the value corresponding to $\theta_{0.5}$, which has the highest statistical weight, gives $\bar{\gamma}=50$ or an energy of 6.5×10^{12} ev. The accuracy of such a determination depends on two assumptions, the validity of assuming a single nucleon-nucleon collision, and the statistical accuracy inherent in determining $\theta_{0.5}$ with thirty-six tracks. By assuming a Poissonian fluctuation. the experimental value of $\theta_{0.5}$ can correspond to theoretical values of $\theta_{0.5\pm0.08}$, thus giving an error in the energy determination of a factor of 4. The opening angle is thus consistent with energies from $1.6\times10^{12}-2.6\times10^{12}$ ev.

We assume that the estimate from the energy balance 1.8×10^{13} ev is correct. If the angular distribution was the result of plural processes, and energetic neutral mesons had escaped detection by decaying outside the stack the energy might be higher.

c. Charged Particles to Neutral Meson Rate

In plate 8, any γ-rays formed directly in the primary interaction[8] and from the decay photons from slow neutral mesons have not as yet materialized, the shower starting 0.06 radiation units back. A count on this plate gives a total number of thirty-six charged particles. We considered an area enclosing the primary core containing twenty-five tracks in plate 8 and scanned the corresponding area on plate 9 for minimum ionization tracks satisfying our length and angle criteria. The number of tracks found was forty-five, an increase of twenty tracks in 0.39 cascade unit. An estimate taking into account cascade multiplication gave a total of twenty-four γ-rays at the start of the shower corresponding to twelve neutral mesons. Allowing for the finite lifetime of the neutral meson, we have to add four neutral mesons decaying further down in the stack. Thus we obtain a neutral to charged ratio of 0.6 ± 0.2.[9]

[8] R. E. Marshak, Phys. Rev. **74**, 1736 (1949). Marshak shows that the contribution of directly produced γ-rays should be negligible in such an event.

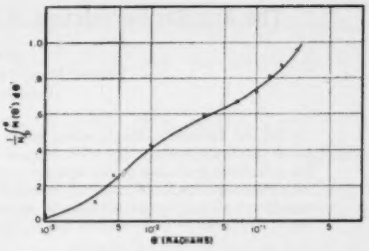

FIG. 4. Integral angular distribution in the laboratory system of the hard shower in the first plate.

DISCUSSION

The total multiplicity of thirty-six charged particles plus approximately eighteen neutral mesons giving a total of fifty-four particles cannot be interpreted in terms of pure plural processes, even though the collision occurs in brass. An estimate based on a simple three generation model indicates multiplicities of at least four if the mesons are assumed to be interacting, and of seven if the mesons are assumed to be noninteracting.

We intend, in a later publication, to give a fuller account of our results and to compare them in detail with other experimental results available and with theoretical predictions.

We wish to thank Dr. H. L. Reynolds for his assistance in the early stages of this work and Professor R. E. Marshak for many valuable discussions.

[9] The ratio of 0.6 ± 0.2 strictly speaking, is the ratio of neutral mesons to total number of charged particles. As the charged particle beam must contain some nucleons (and possibly antinucleons), the ratio

$$\rho = N(\pi^0)/[N(\pi^+)+N(\pi^-)] > 0.6\pm0.2.$$

The Angular Correlation of Two Successive Nuclear Radiations*

STUART P. LLOYD
Institute for Advanced Study, Princeton, New Jersey
(Received Novermber 12, 1951)

A general formula is derived, using group-theoretic methods, which gives the correlation as series in Jacobi polynomials whose argument depends on the angle between the radiations. The coefficients factor into quantities depending on the separate nuclear transitions, and the factors are worked out explicitly for the directional correlation cases where one of the interfering radiation angular momenta is the lowest or next-lowest allowed by conservation of angular momentum. Correction factors are given for converting lowest multipole $\gamma-\gamma$ correlations into an extensive class of directional correlations.

1. INTRODUCTION

THE theoretical aspects of the problem of the angular correlation of successive nuclear radiations have been treated by many authors, several of whom have presented results in numerically tractable form.[1–4] The problem is now well known, and we refer the reader to (FU) for a detailed general examination of the theory, as well as references to earlier work. Briefly, the problem is the following. A nucleus in an excited level E_1 decays to excited level E by emitting radiation R_1. The intermediate nucleus in E then decays to level E_2 by emitting radiation R_2, and one wants to find the relative angular distribution of R_2 with respect to R_1 in terms of the total angular momenta J_1, J, and J_2 (and perhaps other nuclear properties) of the successive levels E_1, E, and E_2, respectively. This relative angular distribution is called the angular correlation of R_1 and R_2.[5]

In the initial form for the angular correlation function, the form given by quantum-mechanical perturbation theory, the nuclear matrix elements appearing are those for emission of the radiations into plane wave states, but for computational purposes these matrix elements must be expanded in terms of those for emission into angular momentum eigenstates. The resulting expression for the angular correlation function contains summations involving many magnetic quantum numbers of various nuclear and radiation states; several of these summations are not trivial. In this paper we show that most of these summations can be eliminated by use of the formulas of Racah[6] for certain sums of products of vector-addition coefficients, so that the angular correlation function can be simplified to the point where the main considerations in its evaluation in a given case are physical in character, e.g., the dependence of a correlation on β-ray energy or on the relative amplitudes of simultaneously emitted γ-ray multipoles, etc. Put another way, the complicated sums over magnetic quantum numbers are geometrical entities, having to do with the properties of the three-dimensional rotation group,[7] and the geometrical problem of obtaining a closed form for these sums has already been solved by Racah in connection with the theory of complex spectra. Numerically tractable results obtained previously without the use of Racah's formulas have been in general limited to those cases where the angular momenta of the radiations do not exceed two units or where the initial or final nuclear spin is zero.

A general correlation formula is derived in Sec. 3, together with the directional correlation formula resulting from it. The directional correlation is set up to make use of existing $\gamma-\gamma$ numerical tables[8] as far as possible; formulas for coefficients not to be found in reference 8 are given in Secs. 4 and 5. The explicit formulas are limited to those cases where, in each transition, one of the interfering particle multipole orders is the lowest or next lowest allowed by conservation of angular momentum. The final directional correlation formula is Eq. (31), Sec. 6, where a summary of results is given for the benefit of those readers who are mainly interested in the application of the formula to practical problems.

2. PRELIMINARIES

We give here a general proof for the multipole expansion of nuclear matrix elements assumed in (FU).

* This paper is an exposition of results described in: S. P. Lloyd, Phys. Rev. **80**, 118 (1950) and Phys. Rev. **81**, 307 (1951). The preliminary stages of the work were performed while the author held an AEC Predoctoral Fellowship. Much of the present material is part of: S. P. Lloyd, thesis submitted in partial fulfillment of the requirements for the degree of Doctor of Philosophy in Physics in the Graduate College of the University of Illinois, 1951.

[1] D. R. Hamilton, Phys. Rev. **58**, 122 (1940).

[2] D. S. Ling, Jr., and D. L. Falkoff, Phys. Rev. **76**, 1639 (1949), to be referred to as (LF).

[3] D. L. Falkoff and G. E. Uhlenbeck, Phys. Rev. **79**, 323 (1950), referred to hereafter as (FU).

[4] J. W. Gardner, Proc. Roy. Soc. (London) **A62**, 763 (1949). Our list is not complete.

[5] It is assumed that: (a) the initial nucleus is randomly oriented, (b) the intermediate nucleus is not disturbed by extranuclear fields before it emits R_2, and (c) effects caused by nuclear recoil are neglected.

[6] G. Racah, Phys. Rev. **62**, 439 (1942), referred to hereafter as (R).

[7] Or more precisely, with the properties of the group {P} of unitary unimodular two-dimensional matrices, the group of the Pauli electron. The group theory used in our derivations can be found in: E. Wigner, *Gruppentheorie usw* (Vieweg, Braunschwieg, 1931), referred to hereafter as (W), or in: C. Eckart, Revs. Modern Phys. **2**, 305 (1930).

[8] S. P. Lloyd, Phys. Rev. **83**, 716 (1951).

The matrix element for the emission of radiation R into a state specified by a set of quantum numbers A in the nuclear transition $J_i m_i \rightarrow J_f m_f$ will be denoted by $(J_f m_f | A | J_i m_i)$. A set A includes the direction Ω of the detected particle of R, and in the conversion electron case, for example, it includes the quantum numbers of the hole left by the ejected electron. We omit all nuclear quantum numbers except the total angular momentum quantum number J and its magnetic quantum number (z-projection) m.

Under the operations of $\{P\}$ these matrix elements transform according to

$$(J_f m_f | A | J_i m_i) = \Sigma_{m_i' m_f'} (m_f | P^{-1} | m_f')^{J_f} \times (J_f m_f' | PA | J_i m_i') (m_i' | P | m_i)^{J_i}, \quad (1)$$

where the $(m|P|m')^J$ are the usual $(2J+1)$-dimensional unitary irreducible representations of $\{P\}$.[9] Equation (1) is obtained simply by evaluating the matrix element in a rotated coordinate system and using the scalar property of the perturbation Hamiltonian describing the emission of R. The product of matrix elements $(\ |\ |\ )^J$ of $\{P\}$ in Eq. (1) can be reduced (Clebsch-Gordan series[10]):

$$\begin{aligned}
&(m_f | P^{-1} | m_f')^{J_f} (m_i' | P | m_i)^{J_i} \\
&= (-1)^{m_f - m_f'} (-m_f' | P | -m_f)^{J_f} (m_i' | P | m_i)^{J_i} \\
&= (-1)^{m_f - m_f'} \Sigma_{LM'} (J_f J_i - m_f' m_i' | J_f J_i L - M') \\
&\quad \times (J_f J_i - m_f m_i | J_f J_i L - M) (-M' | P | -M)^L \\
&= \Sigma_{LM'} [(2L+1)/(2J_f+1)] (J_i L m_i' M' | J_i L J_f m_f') \\
&\quad \times (J_i L m_i M | J_i L J_f m_f) (M' | P | M)^{L*} \quad (2)
\end{aligned}$$

to give

$$\begin{aligned}
&(J_f m_f | A | J_i m_i) \\
&= \Sigma_{LM} (2J_f+1)^{-1} (J_i L m_i M | J_i L J_f m_f) G_L^M(A)^*, \quad (3)
\end{aligned}$$

where

$$\begin{aligned}
G_L^M(A)^* &\equiv \Sigma_{m_i' m_f' M'} (2J_f+1)^{-1} (2L+1) \\
&\quad \times (J_i L m_i' M' | J_i L J_f m_f') (M' | P | M)^{L*} \\
&\quad \times (J_f m_f' | PA | J_i m_i') \\
&= \Sigma_{m_i m_f} (2J_f+1)^{-1} (2L+1) \\
&\quad \times (J_i L m_i M | J_i L J_f m_f) (J_f m_f | A | J_i m_i). \quad (4)
\end{aligned}$$

Various symmetry properties given in (W) for $(\ |\ |\ )^J$ and in (R) for vector-addition coefficients have been used in Eqs. (2)–(4). It is easy to verify from their definition, Eq. (4), that the $G_L^M(A)$ belong to $(\ |\ |\ )^L$ as indicated by the indices, i.e.:

$$G_L^M(A) = \Sigma_{M'} G_L^{M'}(PA) (M' | P | M)^L. \quad (5)$$

Hence, if $\mathfrak{S}$ denotes the $(\{P\}$-invariant) summation over the angular variables in set A, the $G_L^M(A)$ are unitary-orthogonal under $\mathfrak{S}$, and one can write

$$\mathfrak{S} G_L^M(A)^* G_{L'}^{M'}(A) = \delta_{LL'} \delta_{MM'} |(J_f \| L \| J_i)|^2, \quad (6)$$

where

$$\begin{aligned}
|(J_f \| L \| J_i)|^2 &\equiv (2L+1)^{-1} \Sigma_M \mathfrak{S} |G_L^M(A)|^2 \\
&= \mathfrak{S} |G_L^M(A)|^2, \quad \text{(all } M\text{)}. \quad (7)
\end{aligned}$$

Numbers $(J_f \| L \| J_i)$, independent of angles, are determined by Eq. (7) to within a phase factor, so that if one puts

$$G_L^M(A) = (J_f \| L \| J_i)^* \mathcal{Y}_L^M(A), \quad (8)$$

the $\mathcal{Y}_L^M(A)$ belong to $(\ |\ |\ )^L$ and are unitary orthonormal under $\mathfrak{S}$. Usually the $\mathcal{Y}_L^M(A)$ will be those whose phases are fixed by convention or convenience, e.g., the (CS) spherical harmonics, so that Eq. (8) is to be thought of as determining the phases of the $(J_f \| L \| J_i)$.

The rate of emission of R in the transition $J_i \rightarrow J_f$ will be proportional to

$$\begin{aligned}
I &= (2J_i+1)^{-1} \Sigma_{m_i m_f} \mathfrak{S} |(J_f m_f | A | J_i m_i)|^2 \\
&= (2J_i+1)^{-1} \Sigma_{LM} (2L+1)^{-1} \mathfrak{S} |G_L^M(A)|^2 \\
&= (2J_i+1)^{-1} \Sigma_L |(J_f \| L \| J_i)|^2, \quad (9)
\end{aligned}$$

so that $|(J_f \| L \| J_i)|^2$ is simply the relative probability that R is emitted with angular momentum L. It will be convenient in the following to use a different normalization for these scalar amplitudes. Put

$$(J_f :: L :: J_i) = (J_f \| L \| J_i) / (\Sigma_L |(J_f \| L \| J_i)|^2)^{\frac{1}{2}}.$$

Then $\Sigma_L |(J_f :: L :: J_i)|^2 = 1$, and the $|(J_f :: L :: J_i)|^2$ are actual probabilities.

3. A GENERAL TWO-STEP CORRELATION FORMULA

We start with the usual expression

$$\begin{aligned}
W(A_1; A_2) &= a \Sigma_{m_1 m_2} |\Sigma_m (J_2 m_2 | A_2 | Jm) (Jm | A_1 | J_1 m_1)|^2 \\
&= a \Sigma_{m_1 m_2 mm'} (J_2 m_2 | A_2 | Jm) (Jm | A_1 | J_1 m_1) \\
&\quad \times (J_2 m_2 | A_2 | Jm')^* (Jm' | A_1 | J_1 m_1)^* \quad (10)
\end{aligned}$$

for the angular correlation function $W(A_1; A_2)$.[11] The normalization constant a will be chosen later. Multipole expansion of the nuclear matrix elements after Eq. (3) gives:

$$W(A_1; A_2) = a \Sigma_{(LM)} \mathfrak{S} \Sigma_{m_1 m_2 mm'} \mathfrak{U}, \quad (11a)$$

where we abbreviate

$$\begin{aligned}
&(LM) = L_1, M_1, L_1', M_1', L_2, M_2, L_2', M_2' \\
&\mathfrak{S} = G_{L_1}^{M_1}(A_1)^* G_{L_1'}^{M_1'}(A_1) \\
&\quad \times G_{L_2}^{M_2}(A_2)^* G_{L_1'}^{M_2'}(A_2), \\
&\mathfrak{U} = [(2J_2+1)(2J+1)]^{-1} (J_1 L_1 m_1 M_1 | J_1 L_1 J m) \\
&\quad \times (J_1 L_1' m_1 M_1' | J_1 L_1' J m') \\
&\quad \times (J L_2 m M_2 | J L_2 J_2 m_2) \\
&\quad \times (J L_2' m' M_2' | J L_2' J_2 m_2). \quad (11b)
\end{aligned}$$

[9] The $(m|P|m')^J$ are the $D^{(J)}(P)_{mm'}$ of (W).

[10] We use the vector-addition coefficients of (W), but in the Condon and Shortley notation. See E. U. Condon and G. H. Shortley, *The Theory of Atomic Spectra* (Cambridge University Press, Cambridge, 1935), Chapter III. This work will be referred to as (CS).

[11] G. Goertzel, Phys. Rev. **70**, 897 (1946), treats the $\gamma-\gamma$ case and his results are easily generalized.

We have used the fact that the vector-addition coefficients are real. It is known that Eq. (11) can be considerably simplified by assuming that one of the particles is emitted along the z axis-of-quantization;[11] a further reduction is possible when the correlation is expressed in terms of the matrix elements for emission of both particles along the z axis, as follows.

The angular correlation is a scalar function of the whole set A_1 plus A_2, so that without loss of generality one can assume that the $(+z)$ axis lies along the direction Ω_1 of the detected particle in the first transition and that the z-$(+x)$ half-plane contains Ω_2 of the second-transition particle. Let P_{21} be the rotation by angle θ, $0 \leq \theta \leq \pi$, around the $(-y)$ axis which rotates Ω_2 (in these axes) into the z axis, so that θ is the angle between Ω_1 and Ω_2. Denote by $A_1{}^z$ the values of the A_1 in these axes and by $A_2{}^z$ the values of the A_2 after P_{21} has been performed on them: $A_2{}^z = P_{21}A_2$. The $G_{L_2}{}^{M_2}(A_2)$ belong to $(\ |\ |\ )^{L_2}$, so that[12]

$$\begin{aligned}
\mathfrak{G} &= G_{L_1}{}^{M_1}(A_1{}^z)^* G_{L_1'}{}^{M_1'}(A_1{}^z) G_{L_2}{}^{M_2}(A_2)^* G_{L_2'}{}^{M_2'}(A_2) \\
&= \Sigma_{N_2 N_2'} G_{L_1}{}^{M_1}(A_1{}^z)^* G_{L_1'}{}^{M_1'}(A_1{}^z) G_{L_2}{}^{N_2}(A_2{}^z)^* \\
&\quad \times G_{L_2'}{}^{N_2'}(A_2{}^z)(N_2|\,P_{21}\,|M_2)^{L_2*}(N_2'|\,P_{21}\,|M_2')^{L_2'} \\
&= \Sigma_{N_2 N_2'}(-1)^{N_2 - M_2} G_{L_1}{}^{M_1}(A_1{}^z)^* G_{L_1'}{}^{M_1'}(A_1{}^z) \\
&\quad \times G_{L_2}{}^{N_2}(A_2{}^z)^* G_{L'}{}^{N_2'}(A_2{}^z) \Sigma_{\lambda\mu_1\mu_2}(L_2 L_2' \\
&\quad - N_2 N_2'|\,L_2 L_2' \lambda\mu_2)(L_2 L_2' - M_2 M_2'|\,L_2 L_2' \lambda - \mu_1) \\
&\quad \times (\mu_2|\,P_{21}\,|-\mu_1)^{\lambda}. \qquad (12)
\end{aligned}$$

Two more vector-addition coefficients have been introduced into the formula for $W(A_1; A_2)$, but they are the ones that make Racah's formulas applicable. The sums over (M_2, M_2', m_2) and (m_1, m, m') can be eliminated, in that order, using Eq. (R41) and others, to give:

$$\begin{aligned}
W(A_1; A_2) &= a \Sigma_{(L)} (-1)^{L_2' - L_2} (-1)^{J_1 - L_1 - J_2 + L_2} \\
&\quad \times \Sigma_{\lambda\mu_1\mu_2} (-1)^{\lambda + \mu_2} d^{(\lambda)}(\theta)_{\mu_2, -\mu_1} \cdot \{W(L_1 J L_1' J; J_1 \lambda) \\
&\quad \times \Sigma_{M_1} (-1)^{L_1 + M_1} (L_1 L_1' - M_1 M_1'|\,L_1 L_1' \lambda \mu_1) \\
&\quad \times G_{L_1}{}^{M_1}(A_1{}^z)^* G_{L_1'}{}^{M_1'}(A_1{}^z)\} \cdot \{W(L_2 J L_2' J; J_2 \lambda) \\
&\quad \times \Sigma_{M_2} (-1)^{L_2 + M_2} (L_2 L_2' - M_2 M_2'|\,L_2 L_2' \lambda \mu_2) \\
&\quad \times G_{L_2}{}^{M_2}(A_2{}^z)^* G_{L_2'}{}^{M_2'}(A_2{}^z)\}, \qquad (13)
\end{aligned}$$

where $(L) = (L_1, L_1', L_2, L_2')$, with the sum unrestricted, and $W(abcd; ef)$ is defined in Eqs. (R36).[13]

The $d^{(\lambda)}(\theta)_{\mu_2, -\mu_1}$ are the Jacobi polynomials given in (W):

$$\begin{aligned}
&d^{(\lambda)}(\theta)_{\mu_2, -\mu_1} \\
&= \sum_{\kappa} \frac{(-1)^{\kappa} [(\lambda+\mu_1)!(\lambda-\mu_1)!(\lambda+\mu_2)!(\lambda-\mu_2)!]^{\frac{1}{2}}}{(\lambda-\mu_2-\kappa)!(\lambda-\mu_1-\kappa)!\kappa!(\kappa+\mu_1+\mu_2)!} \\
&\quad \times (\cos\tfrac{1}{2}\theta)^{2\lambda - \mu_1 - \mu_2 - 2\kappa} (\sin\tfrac{1}{2}\theta)^{2\kappa + \mu_1 + \mu_2};
\end{aligned}$$

the sum on κ is over all integral values for which the arguments of the factorials are not negative.

Let us consider the $(2\lambda+1)$quantities

$$\begin{aligned}
U_{\lambda}{}^{\mu}(A) &= \Sigma_M (-1)^{L+M} (LL' - MM'|\,LL' \lambda\mu) \\
&\quad \times G_L{}^M(A)^* G_{L'}{}^{M'}(A), \qquad (14)
\end{aligned}$$

$\mu = -\lambda, -\lambda+1, \cdots, \lambda$. From their definition and the transformation properties of the $G_L{}^M(A)$, it can be shown easily that the $U_{\lambda}{}^{\mu}(A)$ belong to $(\ |\ |\ )^{\lambda}$, as indicated by the notation. Let S denote the ($\{P\}$-invariant) summation over all angular variables in set A except for the direction Ω of the detected particle. Since S is invariant, the quantities $SU_{\lambda}{}^{\mu}(A)$ belong to $(\ |\ |\ )^{\lambda}$ or vanish identically. Their angular dependence is on Ω only, and from parity considerations they are even functions of Ω. Also, since $L+L'$ will always be an integer, λ is an integer. These conditions fix the $SU_{\lambda}{}^{\mu}(A)$ rather thoroughly, and one must have[14]

$$\begin{aligned}
SU_{\lambda}{}^{\mu}(A) &= u_{\lambda} Y_{\lambda}{}^{\mu}(\Omega), \quad \lambda \text{ even}, \\
&= 0, \qquad\qquad \lambda \text{ odd}; \\
SU_0{}^0(A) &= (2L+1)^{\frac{1}{2}} |\,(J_f \| L \| J_i)\,|^2 \delta_{LL'}/(4\pi),
\end{aligned}$$

where $Y_{\lambda}{}^{\mu}(\Omega)$ are the (CS) spherical harmonics and u_{λ} is a constant independent of μ. When Ω is along the z axis the spherical harmonics $Y_{\lambda}{}^{\mu}(\Omega)$ vanish unless $\mu = 0$. The terms $\mu_1 \neq 0$ or $\mu_2 \neq 0$ in Eq. (13) thus describe only the dependence of the correlation on the polarization of the first or second radiation, respectively, since these terms drop out when the correlation is summed over the corresponding polarization.

For directional correlations [the function $W(\theta) = S_1 S_2 W(A_1; A_2)$] with which the following will be mainly concerned, one needs only then that $d^{(\lambda)}(\theta)_{0,0} = P_{\lambda}(\cos\theta)$, so that the directional correlation has been obtained as a series of even Legendre polynomials. One sees from Eq. (13) that the coefficients of $P_{\lambda}(\cos\theta)$ factor into quantities depending on each transition separately. It is convenient to put

$$\begin{aligned}
a_{\lambda}(LL'; JJ')_M &= a_{\lambda}(L'L; JJ')_M \\
&= (-1)^{L'-L} a_{\lambda}(LL'; JJ')_{-M} \\
&= (2 - \delta_{LL'})(-1)^{J'-J+M+\frac{1}{2}} [(2L+1)(2L'+1)(2J+1)/ \\
&\quad (2\lambda+1)]^{\frac{1}{2}} W(LJL'J; J'\lambda)(LL' - MM|\,LL'\lambda 0) \qquad (15)
\end{aligned}$$

[11] J. A. Spiers, Phys. Rev. **80**, 491 (1950), gives an equivalent form which differs considerably in appearance from Eqs. (11)–(12), but which can also be used to obtain Eq. (13), following. The essential point is the reduction of the outer product of $(\ |\ |\ )^J$ which appear. This is a generalization of the method used by Gardner to obtain nonrelativistic conversion electron (spinless particle) correlations, reference 4.

[12] The derivation to this point is similar to one shown to the author by Professor Racah (private communication). The summations were performed in a different order in Lloyd's thesis (see footnote to title). [*Note added in proof.*—See G. Racah, Phys. Rev. **84**, 910 (1951), where a semiclassical interpretetion of the various quantities appearing in Eq. (13) (Eq. (8) of Racah's paper) is given.]

[14] Suppose $f_{\lambda}{}^{\mu}(\Omega)$ belong to $(\ |\ |\ )^{\lambda}$. By considering rotations around the z axis, $f_{\lambda}{}^{\mu}(\Omega^z) = \delta_{\mu 0} f_{\lambda}{}^0(\Omega^z)$. Also, $f_{\lambda}{}^{\mu}(\Omega) = \Sigma_{\mu'} f_{\lambda}{}^{\mu'}(\mathrm{P}\Omega)(\mu'|\,\mathrm{P}\,|\mu)^{\lambda} = f_{\lambda}{}^0(\Omega^z)(0|\,\mathrm{P}\,|\mu)^{\lambda}$, where P is any rotation of Ω which brings it to the z axis. From the known form of the $(\ |\ |\ )^{\lambda}$, $f_{\lambda}{}^{\mu}(\Omega) = [4\pi/(2\lambda+1)]^{\frac{1}{2}} f_{\lambda}{}^0(\Omega^z) Y_{\lambda}{}^{\mu}(\Omega)$.

and also, after (LF),

$$S\,\mathcal{Y}_L{}^M(\mathrm{A})^*\,\mathcal{Y}_{L'}{}^M(A) = [(2L+1)(2L'+1)]^{\frac{1}{2}}(4\pi)^{-1}F_{LL'}{}^M(\beta), \quad (16)$$
$$F_{LL'}{}^M = F_{LL'}{}^M(\beta=0) = F_{L'L}{}^{M*},$$

where β is the angle the detected particle makes with the z axis. This notation is intended to be that of (FU), except that the specific normalization

$$\Sigma_M F_{LL'}{}^M(\beta) = \delta_{LL'},$$
$$\int F_{LL'}{}^M(\beta)\,d(\cos\beta) = (L+\tfrac{1}{2})^{-1}\delta_{LL'}, \quad (\text{all } M) \quad (17)$$

is required.[15] In terms of these the directional correlation takes the form[16]

$$W(\theta) = 1 + \sum_{L_1\le L_1'}\sum_{L_2\le L_2'}(-1)^{L_2'-L_2}\sum_{\lambda}(2\lambda+1) \times P_\lambda(\cos\theta)\cdot\Sigma_{M_1}a_\lambda(L_1L_1';JJ)_{M_1} \times \mathrm{R.P.}[(J_1{:}L_1{:}J)(J_1{:}L_1'{:}J)^*F_{L_1L_1'}{}^{M_1}] \cdot\Sigma_{M_2}a_\lambda(L_2L_2';JJ)_{M_2} \times \mathrm{R.P.}[(J_2{:}L_2{:}J)(J_2{:}L_2'{:}J)^*F_{L_2L_2'}{}^{M_2}]. \quad (18)$$

The normalization constant has been given the value $a=(4\pi)^2((2J_1+1)I_1I_2)^{-1}$ to normalize $W(\theta)$ to unit average. The angular correlation selection rules appear as properties of Racah's coefficient $W(abcd;ef)$; the sum on λ in Eq. (18) is over the even integers satisfying simultaneously: $L_1'-L_1\le\lambda\le L_1+L_1'$; $L_2'-L_2\le\lambda\le L_2+L_2'$; $2\le\lambda\le 2J$. There is no correlation if $J=0$ or $J=\frac{1}{2}$. (These are the multipole mixture modifications of Yang's rules.[17])

For spinless particles the $\mathcal{Y}_L{}^M(A)$ can be only the spherical harmonics $Y_L{}^M(\Omega)$, so that $F_{LL}{}^M=\delta_{M0}$. For γ-rays, from (LF) $F_{LL}{}^M=\frac{1}{2}\delta_{|M|1}$; also, $(LL-11\,|\,LL\lambda0)=(LL1-1\,|\,LL\lambda0)$, λ even. In most cases of physical interest the L's will be integers, i.e., spinless particle, β-ray, γ-ray, conversion electron (exception: single nucleons), so that in Eq. (18), considering only the pure multipole terms, the quantities in square brackets are the fractions of the radiations that behave as 2^L-pole: spinless particles ($M=0$), γ-rays ($|M|=1$), massless quanta of spin-two ($|M|=2$), etc.—at any rate for directional correlation purposes. The quantities in square brackets are the physics of the problem and involve through the $F_{LL'}{}^M$, the type of radiation, and through the $(J_f{:}L{:}J_i)$, the particular nucleus emitting it. The quantities $a_\lambda(LL';JJ')_M$ are simply numerical coefficients and can be obtained from formulas in (R). The calculations for $a_\lambda(LL';JJ')_M$ are rather simple if one of the radiation angular momenta L, L' is the lowest ($L=|J-J'|$) or next lowest ($L=|J-J'|+1$) allowed by conservation of angular momentum, provided also that $|M|$ is not too large. The coefficients for these cases are given explicitly in the next section. The quantities in square brackets in Eq. (18) are discussed in Sec. 5.

4. THE GEOMETRICAL COEFFICIENTS

(a) Dependence on M

We observe first that the $a_\lambda(LL';JJ')_M$ as defined in Eq. (15) depend on M through the vector-addition coefficient only. Since the $\gamma-\gamma$ correlation coefficients ($|M_1|=|M_2|=1$) are already tabulated as functions of nuclear angular momentum,[8] it is convenient to introduce, for integral L and L', the ratios

$$\xi_\lambda(LL')_M = (-1)^{L'-L}\xi_\lambda(LL')_{-M} = a_\lambda(LL';JJ')_M/a_\lambda(LL';JJ')_1 = (-1)^{M-1}(LL'-MM\,|\,LL'\lambda0)/(LL'-11\,|\,LL'\lambda0). \quad (19)$$

From Eqs. (R3) and (R5),

$$\xi_\lambda(LL')_0 = \frac{2[L(L+1)L'(L'+1)]^{\frac{1}{2}}}{L(L+1)+L'(L'+1)-\lambda(\lambda+1)}, \quad L+L'=\text{even}$$
$$\xi_\lambda(LL')_0 = 0, \quad L+L'=\text{odd}$$
$$\xi_\lambda(LL')_2 = -\frac{(L-1)L(L+1)(L+2)+(L'-1)L'(L'+1)(L'+2) -\lambda(\lambda+1)[2(L-1)(L+2)+2(L'-1)(L'+2)-(\lambda-2)(\lambda+3)]}{((L-1)(L+2)(L'-1)(L'+2))^{\frac{1}{2}}[L(L+1)+L'(L'+1)-\lambda(\lambda+1)]}, \quad L+L'=\text{even}, \quad (20)$$
$$\xi_\lambda(LL')_2 = \frac{(\lambda-1)(\lambda+2)-(L-1)(L+2)-(L'-1)(L'+2)}{((L-1)(L+2)(L'-1)(L'+2))^{\frac{1}{2}}}, \quad L+L'=\text{odd},$$

[15] The summation in Eq. (17) is $-\min(L,L')\le M\le\min(L,L')$.

[16] The pure multipole terms in Eq. (18) have been given by K. Alder, Phys. Rev. **83**, 1266 (1951), and, for a special case, by Biedenharn, Arfken, and Rose, Phys. Rev. **83**, 586 (1951), who also consider triple cascade correlations.

[17] C. N. Yang, Phys. Rev. **74**, 764 (1948).

and in particular, for the pure multipole terms $L'=L$:

$$\xi_\lambda(LL)_0=\left[1-\frac{\lambda(\lambda+1)}{2L(L+1)}\right]^{-1},$$

$$\xi_\lambda(LL)_2=\left[1-\frac{2\lambda(\lambda+1)}{L(L+1)}+\frac{(\lambda-2)\lambda(\lambda+1)(\lambda+3)}{2(L-1)L(L+1)(L+2)}\right]\xi_\lambda(LL)_0, \tag{21}$$

$$\xi_\lambda(LL)_3=\left[1-\frac{9\lambda(\lambda+1)}{2L(L+1)}+\frac{3(\lambda-2)\lambda(\lambda+1)(\lambda+3)}{(L-1)L(L+1)(L+2)}-\frac{(\lambda-4)(\lambda-2)\lambda(\lambda+1)(\lambda+3)(\lambda+5)}{2(L-2)(L-1)L(L+1)(L+2)(L+3)}\right]\cdot\xi_\lambda(LL)_0.$$

The $\xi_\lambda(LL')_0$, $\xi_\lambda(LL')_2$, $\cdots$ are the factors which convert the L,L' terms in a γ-ray correlation into the corresponding terms in spinless particle, spin-two quantum, . . . correlations, and, as it turns out, the ones given in Eqs. (20)–(21) cover the spinless particle, β-ray to second-forbidden, and K and L conversion electron cases.

(b) The γ-Ray Coefficients

The lowest and next lowest γ-ray coefficients are, from Eq. (R36) and others, with $L\leq L'$ and $L=\pm(J-J')$ or $L=\pm(J-J')+1$:

$L+L'=$even:

$$a_\lambda(LL';JJ')_1=(2-\delta_{LL'})(-1)^{\frac{1}{2}(L'-L)}a_\lambda(LL')u(LL';JJ')v_\lambda(LL';JJ')[w_\lambda(J)]^{\pm\frac{1}{2}} \tag{22}$$

with

$$a_\lambda(LL')=\frac{\left(\frac{\lambda+L+L'}{2}\right)!(\lambda+L'-L)!\left(\frac{(2L'+1)(L+L')(L'-L+1)(L+L')!(2L+1)!}{(2L)(L'-L)!}\right)^{\frac{1}{2}}}{\left(\frac{\lambda+L+L'}{2}\right)!\left(\frac{\lambda+L'-L}{2}\right)!\left(\frac{L+L'-\lambda}{2}\right)!(\lambda+L+L'+1)!\xi_\lambda(LL')_0},$$

$$u(LL';JJ')=\left[\frac{(J+J'-L)!(J+J'+L+1)!}{(J+J'-L')!(J+J'+L'+1)!}\right]^{\pm\frac{1}{2}}, \tag{23}$$

$$w_\lambda(J)=\frac{(2J-\lambda)!(2J+\lambda+1)!}{(2J)!(2J+1)!},$$

$$v_\lambda(LL';JJ')=1 \text{ for } L=\pm(J-J'),$$

$$v_\lambda(LL';JJ')=1-\frac{(J'+\frac{1}{2}\mp\frac{1}{2})\lambda(\lambda+1)}{(J+\frac{1}{2}\pm\frac{1}{2})(L+L')(L'-L+1)} \text{ for } L=\pm(J-J')+1;$$

in particular, the pure multipole coefficients are

$$a_\lambda(LL;JJ')_1=a_\lambda(LL)v_\lambda(LL;JJ')[w_\lambda(J)]^{\pm\frac{1}{2}},$$

$$a_\lambda(LL)=\left[1-\frac{\lambda(\lambda+1)}{2L(L+1)}\right]\frac{(2L+1)!\lambda![L+(\lambda/2)]!}{(2L+\lambda+1)![(\lambda/2)!]^2[L-(\lambda/2)]!}, \tag{24}$$

$$v_\lambda(LL;JJ')=1 \text{ for } L=\pm(J-J'),$$

$$v_\lambda(LL;JJ')=1-\frac{(J'+\frac{1}{2}\mp\frac{1}{2})\lambda(\lambda+1)}{2L(J+\frac{1}{2}\pm\frac{1}{2})} \text{ for } L=\pm(J-J')+1.$$

$L+L'=$odd:

$$a_\lambda(LL';JJ')_1=\zeta_\lambda(LL';JJ')a_\lambda(LL'';JJ')_1$$

where $L''=L'-1$ (and $L\leq L''$), and

$$\zeta_\lambda(LL';JJ')=\frac{1}{(2-\delta_{LL''})}x(LL';JJ')y_\lambda(LL')z_\lambda(LL';JJ'), \tag{25}$$

with

$$x(LL';JJ')=\pm\left[\frac{J+J'-L'+1}{J+J'+L'+1}\right]^{\pm\frac{1}{2}} \text{ for } L=\pm(J-J') \text{ or } =\pm(J-J')+1,$$

$$y_\lambda(LL')=(\lambda+L-L'')(\lambda+1+L''-L)\left[\frac{(L+L''+1)(2L''+3)}{L(L+1)(L''+1)(L''+2)(2L''+1)(L''+1-L)}\right]^{\frac{1}{2}}\xi_\lambda(LL'')_0,$$

$$z_\lambda(LL';JJ')=1 \text{ for } L=\pm(J-J'),$$

$$z_\lambda(LL';JJ')=\left[\frac{(L+L')(L'-L+1)}{(L+L'')(L''-L+1)}\right]^{\frac{1}{2}}\frac{v_\lambda(LL';JJ')}{v_\lambda(LL'';JJ')}, \text{ for } L=\pm(J-J')+1.$$

In particular, if $L'=L+1$

$$y_\lambda(LL+1)=\frac{\lambda(\lambda+1)}{(L+1)}\left[\frac{(2L+3)}{L(L+2)}\right]^{\frac{1}{2}}\left[1-\frac{\lambda(\lambda+1)}{2L(L+1)}\right]^{-1},$$

$$x(LL+1;JJ')=\mp\left[\frac{J'+\frac{1}{2}\mp\frac{1}{2}}{J+\frac{1}{2}\pm\frac{1}{2}}\right], \tag{26}$$

$$x(12;JJ)z_2(12;JJ)=[(2J-1)(2J+3)/3]^{-\frac{1}{2}},$$

this last giving the dipole-quadrupole interference in $J'=J\to J$. Thus the $L+L'=$ odd type interference terms are given in terms of the lower $L+L'-1=L+L''=$ even type terms.

Note that the factor $v_\lambda(LL';JJ')$ is all that is needed to obtain pure next lowest multipole terms from a complete tabulation of pure lowest multipole terms. For example, if $L_1=\pm(J-J_1)+1$, the $J_1(L_1)J(X)J_2$ correlation, with $X=$ any radiation, is

$$W(\theta)=1+\Sigma_\lambda v_\lambda(L_1L_1;JJ_1)C_\lambda P_\lambda(\cos\theta)$$

if the coefficients of the $J_1\mp1(L_1)J(X)J_2$ correlation are C_λ. Similarly, the coefficients C_λ' of the X-(2^{L_2}-pole) correlation for $J_1\to J\to J_2\mp1$ yield the $J_1(X)J(L_2)J_2$ correlation

$$W(\theta)=1+\Sigma_\lambda v_\lambda(L_2L_2;JJ_2)C_\lambda' P_\lambda(\cos\theta)$$

when $L_2=\pm(J-J_2)+1$.

Equations (19)–(26) will give most of the correlations of physical interest in the γ-ray, β-ray, and conversion electron cases. In the α-particle case the $(J_f\,?\,L\,?\,J_i)$ are not always sharply decreasing with increasing L;[18] and comparison with experiment might require the use of several of the higher terms in: $|J_i-J_f|\leq L, L'\leq J_i+J_f$.

5. THE PHYSICAL PARAMETERS

The analysis in Sec. 3 shows that the natural parameters for $F_{LL'}{}^M(\beta)$ are simply $F_{LL'}{}^M=F_{LL'}{}^M(\beta=0)$. Different parameterizations have been used elsewhere, however, so we collect here various properties of the $F_{LL'}{}^M(\beta)$ which will prove useful in obtaining, for example, β-ray correlations from the work of Fuchs[19] or Falkoff and Uhlenbeck.[20]

In the first place, the $F_{LL'}{}^M$ always occur in the combination $\Sigma_M(-1)^M(LL'-MM\,|\,LL'\lambda 0)F_{LL'}{}^M$, and it is convenient to introduce a special notation for it. Put, for integral L and L',

$$B_\lambda(LL')=\sum_{-\nu}^{\nu}\xi_\lambda(LL')_M F_{LL'}{}^M,\ \nu=\min(L,L'). \tag{27}$$

Particular cases are

$$B_2(11)=(4\lambda)/(3+\lambda)=(-2B)/(3A+B) \tag{28a}$$

if $F_{11}{}^0(\beta)\sim A+B\cos^2\beta$ and λ is the $L=1$ parameter of (FU).

$$\begin{aligned}B_2(22)&=(14+12\mu_2)/\nu_1=(2-42k_2)/\nu_2\\&=(14B+12C)/\nu_3,\\B_4(22)&=(-2\mu_2)/\nu_1=2/\nu_2=(-2C)/\nu_3,\\\nu_1&=5+15\mu_1+3\mu_2,\quad \nu_2=2-15k_1-30k_2,\\\nu_3&=15A+5B+3C,\end{aligned} \tag{28b}$$

if $F_{22}{}^0(\beta)\sim A+B\cos^2\beta+C\cos^4\beta$ and (μ_1,μ_2) or (k_1,k_2) are the $L=2$ parameters of (FU). [Equation (FU20) should read

$$F_2{}^{\pm2}(\vartheta)=\mu_1+\tfrac{1}{2}\mu_2+\tfrac{2}{3}-(\mu_2+1)\cos^2\vartheta+\tfrac{1}{6}\mu_2\cos^4\vartheta.]^{21}$$

For $L=L'=3$, if

$$\begin{aligned}F_{33}{}^0(\beta)&=A+B\cos^2\beta+C\cos^4\beta+D\cos^6\beta,\\B_2(33)&=10(7B+6C+5D)/\nu,\\B_4(33)&=8(11C+15D)/\nu,\\B_6(33)&=-16D/(5\nu),\\\nu&=105A+35B+21C+15D.\end{aligned} \tag{28c}$$

For γ-rays, the polarized spherical harmonics of Eq. (8) are, with the direction $\mathbf{\Omega}^z$ of the quantum along

[18] See H. A. Bethe, Revs. Modern Phys. **9**, 69 (1937), Secs. 66-73; in particular, Table XXXIII, p. 172 and Table XXXIV, p. 179.

[19] M. Fuchs, thesis, University of Michigan, 1951.

[20] D. L. Falkoff and G. E. Uhlenbeck, Phys. Rev. **79**, 334 (1950).

[21] As a result of this misprint the results involving the (μ_1,μ_2) parameters given in Lloyd's thesis (see footnote to title) are incorrect.

the z axis,

$$\mathcal{Y}_L^{\pm 1}(\mathbf{\Omega}^r, \boldsymbol{\varepsilon}) = \mp\tfrac{1}{2}[(2L+1)/(4\pi)]^{\frac{1}{2}} i^L e^{\pm i\varphi}, \text{ (el)}$$
$$\mathcal{Y}_L^{\pm 1}(\mathbf{\Omega}^r, \boldsymbol{\varepsilon}) = \tfrac{1}{2}[(2L+1)/(4\pi)]^{\frac{1}{2}} i^{L-1} e^{\pm i\varphi}, \text{ (mag)} \quad (29)$$
$$\mathcal{Y}_L^{\pm 1}(\mathbf{\Omega}^r, \boldsymbol{\varepsilon}) = 0, \quad |M| \neq 1, \text{ (el or mag)},$$

where φ is the angle the linear polarization vector $\boldsymbol{\varepsilon}$ of the quantum makes with the x axis; in Eq. (13), φ is the angle that $\boldsymbol{\varepsilon}$ (in either transition) makes with the plane containing the directions of both particles. The S process is simply:

$$Sf(\mathbf{\Omega}^r, \varphi) = f(\mathbf{\Omega}^r, \varphi) + f(\mathbf{\Omega}^r, \varphi + \tfrac{1}{2}\pi).$$

One finds that

$$F_{LL'}{}^{\pm 1} = \tfrac{1}{2}(-1)^{\frac{1}{2}(L'-L)}, \quad L+L' = \text{even } (e-e \text{ or } m-m)$$
$$F_{LL'}{}^{\pm 1} = \pm\tfrac{1}{2}(-1)^{\frac{1}{2}(L_e-L_m-1)},$$
$$L+L' = \text{odd } (e-m \text{ or } m-e),$$

so that, for γ-rays,

$$B_\lambda(LL') = (-1)^{\frac{1}{2}(L'-L)}, \qquad L+L' = \text{even},$$
$$B_\lambda(LL') = (-1)^{\frac{1}{2}(L_e-L_m-1)}, \quad L+L' = \text{odd}. \quad (30)$$

The $(J_f \mathbf{:} L \mathbf{:} J_i)$ in the γ-ray case are real,[22] and theoretical and experimental evidence indicates that all except the one for smallest L are small or negligible.[23]

[22] The phases and normalization used in S. P. Lloyd, Phys. Rev. **81**, 161 (1951) have been changed to conform more closely with those of (FU), but the proof and results remain essentially unchanged. The $(J_f \| L \| J_i)$ for γ-rays in the present article are $(-1)^{\frac{1}{2}J_f - L}(2L+1)^{-\frac{1}{2}}$ times those of Phys. Rev. **81**, 161 (1951). This leads to a change in sign of the interference terms, Eqs. (25)–(26) above, compared to those of reference 7, so that the phases are now the same as those of (LF), i.e., $(J_f \| L-1 \| J_i) = \alpha$, $(J_f \| L \| J_i) = \beta$. A point overlooked by Ling and Falkoff is that the matrix $\alpha\beta^*$ is antiHermitian, so that the interference terms for the first and second transitions must have opposite signs, whatever the choice of phase. The signs in the (LF) tables are those which hold when the first γ-ray is mixed, the second pure, although they claim the converse.

[23] M. Goldhaber and A. W. Sunyar, Phys. Rev. **83**, 906 (1951).

The dipole-quadrupole mixture case may be an exception, and we conclude by remarking that (X)-(mixed dipole-quadrupole γ-ray) correlations can be obtained from the (LF) quadrupole-(dipole-quadrupole) tables as follows. (1) For $J-\Delta j \to J \to J+\Delta J$, express $W(\theta) \doteq Q + R\cos^2\theta + S\cos^4\theta$ as a Legendre series: $W(\theta) = 1 + A_2 P_2(\cos\theta) + A_4 P_4(\cos\theta)$, where

$$A_2 = [\tfrac{2}{3}R + (4S/7)][Q + \tfrac{1}{3}R + (S/5)]^{-1},$$
$$A_4 = (8S/35)(Q + \tfrac{1}{3}R + \tfrac{1}{5}S)^{-1}.$$

(2) Multiply these A_λ by

$$B_\lambda(L_1L_1')\, a_\lambda(L_1L_1'; JJ_1)_1 / a_\lambda(22; JJ-\Delta j)_1.$$

One then has the $(X - 2^{L_1} - 2^{L_1'}\text{-pole})$-(dipole-quadrupole γ-ray) coefficient of $P_\lambda(\cos\theta)$ for $J_1 \to J \to J+\Delta J$. This is independent of the value of Δj chosen, of course, and the calculations will be easiest for $\Delta j = \pm 2$. (3) Multiply by the appropriate scalar matrix elements (taking the real part of the product if necessary), and sum over L_1 and L_1'. (4) Change the sign of the $\alpha\beta^*$ term for the second γ-ray. (See reference 22.) If the (dipole-quadrupole)-γ-ray is first, the procedure is essentially the same, except that the signs in the (LF) tables are applicable as they stand; one obtains $J+\Delta J \to J \to J-\Delta j$, with ΔJ mixed, as $J-\Delta j \to J \to J+\Delta J$ from (LF), keeping the sign, and then performs steps (2) and (3), preceding, but not (4).

6. SUMMARY

It has been shown that the angular correlation function can be expanded naturally as a series in the matrix elements $(\ |\ |\ )^\lambda$ of the Pauli spin group (Jacobi polynomials of $\sin^2\frac{1}{2}\theta$) naturally in the sense that the coefficients are factored into quantities which depend on the first and second transitions in $J_1 \to J \to J_2$ separately. This feature makes it easy to modify, e.g., $\gamma-\gamma$ directional correlations to get other correlations of physical interest.[24] The general formula is Eq. (13), Sec. 3.

The directional correlation is obtained as a series of even Legendre polynomials, the formula intended for numerical use being:

$$W(\theta) = 1 + \sum_{L_1 \le L_1'} \sum_{L_2 \le L_2'} \sum_\lambda \{(-1)^{L_2'-L_2}(2\lambda+1)$$
$$\times a_\lambda(L_1L_1'; JJ_1)_1 a_\lambda(L_2L_2'; JJ_2)_1\} P_\lambda(\cos\theta)$$
$$\cdot \text{R.P.}[(J \mathbf{:} L_1 \mathbf{:} J_1)(J \mathbf{:} L_1' \mathbf{:} J_1)^* B_\lambda(L_1L_1')]$$
$$\cdot \text{R.P.}[(J_2 \mathbf{:} L_2 \mathbf{:} J)(J_2 \mathbf{:} L_2' \mathbf{:} J)^* B_\lambda(L_2L_2')]. \quad (31)$$

The coefficients in curly brackets are the coefficients for $\gamma-\gamma$ correlations, given in Sec. 4, and tabulated for pure lowest multipoles in Lloyd's thesis (see footnote to title). The quantities $(J_f \mathbf{:} L \mathbf{:} J_i)$, introduced in Sec. 3, are relative scalar amplitudes for emission of the radiation in $J_i \to J_f$ with angular momentum L, normalized to $\Sigma_L |(J_f \mathbf{:} L \mathbf{:} J_i)|^2 = 1$. They appear as unknown nuclear parameters in the correlation unless the corresponding radiation is emitted as a pure multipole. The coefficients $B_\lambda(LL')$ are the physical parameters of the emitted radiation. In the γ-ray case they are (± 1), after Eq. (30). In the scalar particle case they have the value $\xi_\lambda(LL')_0$, Eqs. (27) and (20), and again are simply numerical coefficients. The $B_\lambda(LL')$ for conversion electrons are functions of nuclear charge and electron energy, different for each atomic shell; the pure multipole $B_\lambda(LL)$ up to $L=5$ obtained by using Dirac wave functions for the atomic electrons have been given by Rose, Biedenharn, and Arfken for the K shell for certain values of the energy and z.[25] The angular distributions $F_{LL}{}^0(\beta)$ of (FU) have been given by Fuchs[19] for β-decay up to second forbidden; the $B_\lambda(LL)$ are then to be had from Eqs. (28). They are, again, functions of particle energy and nuclear charge.

7. ACKNOWLEDGMENTS

I wish to express my reverence for deeply cherished memories of association with the late Sidney M.

[24] Polarization-polarization $\gamma-\gamma$ correlations, including interference terms, can be obtained from the preceding as soon as one knows $(LL'11\,|\,LL'\lambda 2)/(LL'-11\,|\,LL'\lambda 0)$.

[25] Rose, Biedenharn, and Arfken, to be published. [*Added in proof.*—See Phys. Rev. **85**, 5 (1952). The $b_\nu(Z, k, \pi, L)$ of (RBA) are the $B_\nu(LL)$ of the present article.]

Dancoff, Professor of Physics at the University of Illinois, who stood as constant and friendly guide throughout my graduate studies, as well as in the preparation of my thesis. He was, in every sense, a good and inspiring man.

The many discussions with and the advice of Professor J. M. Blatt of the University of Illinois have been of great benefit. Thanks are also due A. Pais and R. Jost of the Institute for Advanced Study for criticism of the manuscript.

PHYSICAL REVIEW VOLUME 85, NUMBER 5 MARCH 1, 1952

On the Quantum Theory for a Finite-Sized Electron. I

GEORGE J. YEVICK
Stevens Institute of Technology, Hoboken, New Jersey
(Received June 7, 1951)

Section I discusses briefly different types of models for a finite-sized electron from the classical point of view with each model being characterized by a particular type of charge-current distribution. Each of these models can be quantized by the Feynman Lagrangian procedure and the new problems encountered are analyzed in Sec. II. These problems are illustrated in Sec. III which goes into the detailed calculations for the first-order perturbation calculation of a finite-sized electron interacting with an external field.

INTRODUCTION

OUR point of view has been to place emphasis not so much on the elegance of the physical model but rather on the exposing and the understanding of some of the problems of the new quantum-mechanical framework developed by Feynman. We should like to stress the fact that this framework is the most ideally suited at the present time to handle, in a relativistically covariant manner, the Lorentz type of finite-sized electron.

We can consider a finite-sized electron as a worthy subject for investigation for several physical reasons. In reality the electron may not be a point singularity but actually extends over a region in space-time. Or, it may be that the notions which we have concerning space and time, in particular their continuity properties actually are incorrect in the very small but because there is no suitable theory that one can use, the finite-sized electron may, for the time being, introduce the necessary fuzziness. Finally there is the physical possibility that the electron is a complex structure in the extremely small regions of space surrounding its center. This structure may be connected with meson particles concerning whose nature we know nothing at present. The finite-sized electron can serve us then as a useful mechanism for calculating physical processes by lumping our ignorance into a suitable structure function with the hope that an explicit evaluation of the structure function by experiment will give rise to new clues for a deeper insight into the electron.

The present theory of quantum electrodynamics still is in a basically unsatisfactory state because of the existence of well-known legitimate problems which the theory is inherently incapable of solving. These problems perhaps can be separated into two categories which may have little to do with each other. The first category contains the infinities of mass and charge and it is the thesis of this work that a finite-sized electron will solve these problems. The second category pertains to the deeper problems of the fine structure constant, the relationship of the electron to the mesons, and the reason for the great stability of the electron. There has been no indication so far as we know from experiment or theory up to the present time as to how to proceed with the second category of problems and we have not attempted to consider these problems in our analysis.

With regard to the first kind of problems, i.e., the mass and charge infinities, the following point ought not to be ignored. The existence of these infinities is in itself unsatisfactory. But techniques for calculating a physical process involving electrons and photons by subtracting out the infinities have now been developed. Nevertheless, the crucial question still remains open whether this calculated value will agree with experiment at extremely high energies. For example, in the scattering of a moving electron against an electron at rest, we have in mind energies of several billion electron volts, for it is only at such high energies that the classical radius of the electron comes into play.

Now undoubtedly the reason for the infinities in the present theory is that the electron is treated as a point singularity. Our assumption is that if one does not have a point but an extended electron we would not have such infinities. By an extended or finite-sized electron we mean that the electron charge-current density is no longer a point singularity but has some sort of smeared-out distribution. This smeared-out distribution is not rigidly fixed with respect to the center of the electron as the electron moves along its world line, but will change its shape as the motion of the electron changes because of the fundamental requirement of conservation of charge-current density.

The difficulty which one immediately encounters is how to treat quantum mechanically such an extended

electron. The solution to this problem alone is of significance because it furnishes another "tool of analysis" in the study of elementary particles. The reason for this is the following: specifying the position of electrons and field values on a space-like surface and having a Schrödinger differential equation or Tomonaga-Schwinger differential equation to describe the behavior of the system we believe is completely out of the picture here. In the language of Dirac, one is confronted with a "non-developable" system which demands really a new set of analytical tools. All physical systems up to now have been "developable." Yukawa recently has encountered the same far-reaching need for a new set of analytical tools in his work on nonlocal fields.

We believe that one of the outstanding qualities of the lagrangian framework of Feynman wherein processes are considered from an over-all space-time point of view is that it is in principle capable of handling non-developable systems. This point has been emphasized by Feynman and actually furnishes the motivating basis for our present work.

This particular paper is primarily concerned with two things. First an attempt is presented at showing different models of finite-sized electrons along with the general idea of how one can create an entire class of such models. Secondly, what is of more importance, the mathematical tools for treating quantum mechanically non-developable systems are presented. Although only the simplest model of an extended electron is handled for the sake of convenience, the same procedures are applicable to the entire class of models which are possible according to the first part of the paper.

In a second paper we aim to show clearly how the non-developability brings in new features by presenting second-order calculations, in particular the processes which would normally yield the mass and charge infinities. These calculations at the present stage of development are very lengthy and therefore quite unsatisfactory.

Finally, a few words concerning our basic assumptions. We assume first that a free electron propagates from one point in space-time to another by means of the Dirac's Green function. Likewise a photon propagates from one point in space-time to another by means of the Maxwell's Green function. It is only at the vertices of the Feynman diagrams that decisive changes are sought.

I. CLASSICAL CONSIDERATIONS[1]

For all the models of the electron considered here, we have the following form of the action which comprises the basis of the theory:

$$S_p+S_{\text{int}}+S_{\text{ext}}=\sum_i m_i\int\frac{dx_\mu(\tau_i)}{d\tau_i}\frac{dx_\mu(\tau_i)}{d\tau_i}d\tau_i$$
$$+\sum_{i,j}\int\int j_\mu^{(i)}(\boldsymbol{x})\delta_+[(\boldsymbol{x}-\boldsymbol{x}')^2]j_\mu^{(j)}(\boldsymbol{x}')dx^4dx'^4$$
$$+\sum_i\int j_\mu^{(i)}(\boldsymbol{x})A_\mu^{\text{ext}}(\boldsymbol{x})dx^4, \quad (1.1)$$

where $x_\mu(\tau_i)$ is the world line of the ith electron; τ_i is the proper time of the ith electron; $j_\mu^{(i)}(\boldsymbol{x})$ is the charge current density of the ith electron at the space-time point $\boldsymbol{x}$. The conservation of charge current density requires that

$$\partial j_\mu^{(i)}(\boldsymbol{x})/\partial x_\mu=0. \quad (1.2)$$

One can define

$$A_\mu^{(i)}(\boldsymbol{x})=\int\delta_+[(\boldsymbol{x}-\boldsymbol{x}')^2]j_\mu^{(i)}(\boldsymbol{x}')dx'^4. \quad (1.3)$$

Therefore

$$S_{\text{int}}=\sum_{i,j}\int j_\mu^{(i)}(\boldsymbol{x})A_\mu^{(j)}(\boldsymbol{x})dx^4.$$

Different theories of the electron are characterized by different $j_\mu(\boldsymbol{x})$. Thus for a point electron

$$j_\mu^{(i)}(\boldsymbol{x}')=\int d\tau_i\delta(\boldsymbol{x}'-\boldsymbol{x}(\tau_i))dx_\mu(\tau_i)/d\tau_i. \quad (1.4)$$

If one calculates the self-energy of a point electron, one will obtain infinity for an answer. Feynman[2] and Peierls and McManus[3] sought a finite self-energy by altering the $\delta_+[(\boldsymbol{x}-\boldsymbol{x}')^2]$ function into a suitable structure function $f[(\boldsymbol{x}-\boldsymbol{x}')^2]$ which possesses a large value for $(\boldsymbol{x}-\boldsymbol{x}')^2<a_0^2$ where a_0 is the classical radius of the electron and presumably is related to the "fundamental length." There are two equivalent ways of looking at this alteration:

(a) One still has a point electron, but the wave equation for the electromagnetic field has been altered, i.e.,

$$g[\Box^2]A_\mu^{(i)}(\boldsymbol{x}')=\int d\tau_i\delta(\boldsymbol{x}'-\boldsymbol{x}(\tau_i))dx_\mu/d\tau_i; \quad (1.5)$$

(b) Or one does not have a point electron, but a "rigid"[4] extended charge-current distribution with the wave equation for $A_\mu^{(i)}$ being

$$\Box^2A_\mu^{(i)}(\boldsymbol{x}')=j_\mu^{(i)}(\boldsymbol{x}')$$
$$=\int d\tau_i h[(\boldsymbol{x}'-\boldsymbol{x}(\tau_i))^2]dx_\mu/d\tau_i. \quad (1.6)$$

[1] Note on notation: symbols in light-faced German type, e.g., $\mathfrak{k}$, represent $\Sigma\gamma_\mu k_\mu$, where the γ_μ are the same Dirac matrices as employed in Feynman's papers. ∇ represents $\gamma_\mu\partial/\partial x_\mu$, whereas $\nabla\cdot\boldsymbol{k}=k_\mu\partial/\partial x_\mu$. Symbols in boldface italic, e.g., $\boldsymbol{k}$, represent four-vectors.

[2] R. P. Feynman, Phys. Rev. **74**, 939 (1948).

[3] H. McManus, Proc. Roy. Soc. (London) **A195**, 323 (1948).

[4] By "rigid," we mean that regardless of the motion of the particle, the shape of the charge current distribution will not depend upon it.

The relation between g and h is obtained as follows: Let

$$A_\mu(\boldsymbol{x})=\int a_\mu(\boldsymbol{k})\exp(i\boldsymbol{k}\cdot\boldsymbol{x})d\boldsymbol{k}^4$$

$$\delta(\boldsymbol{x}'-\boldsymbol{x}(\tau_i))=\int\exp[i\boldsymbol{k}\cdot(\boldsymbol{x}'-\boldsymbol{x}(\tau_i))]d\boldsymbol{k}^4$$

$$h[(\boldsymbol{x}'-\boldsymbol{x})^2]=\int H(\boldsymbol{k}^2)\exp[i\boldsymbol{k}\cdot(\boldsymbol{x}'-\boldsymbol{x})]d\boldsymbol{k}^4.$$

Dropping the i, Eqs. (1.5) and (1.6) become

$$\int a_\mu(\boldsymbol{k})g(-\boldsymbol{k}^2)\exp(i\boldsymbol{k}\cdot\boldsymbol{x}')d\boldsymbol{k}^4$$

$$=\int d\tau\int\exp[i\boldsymbol{k}\cdot(\boldsymbol{x}'-\boldsymbol{x}(\tau))](dx_\mu/d\tau)d\boldsymbol{k}^4 \quad (1.5^1)$$

$$\int a_\mu(\boldsymbol{k})(-\boldsymbol{k}^2)\exp(i\boldsymbol{k}\cdot\boldsymbol{x}')d\boldsymbol{k}^4$$

$$=\int d\tau\int H(\boldsymbol{k}^2)\exp[i\boldsymbol{k}\cdot(\boldsymbol{x}'-\boldsymbol{x}(\tau))](dx_\mu/d\tau)d\boldsymbol{k}^4. \quad (1.6^1)$$

Solving, we obtain

$$g(-\boldsymbol{k}^2)=-\boldsymbol{k}^2/H(\boldsymbol{k}^2). \quad (1.7)$$

Feynman[5] has quantized this model (the quantization essentially amounting to the alteration of the Green's function for the propagation of a photon from one point in space-time to another as can be seen from Eq. (1.5)), but he has encountered a serious difficulty in that conservation of energy does not exist. Moreover, although the self-energy is finite, the polarization of the vacuum diverges, and one must somewhat artificially resort to altering the Dirac Green's function in order to obtain a finite result for the polarization of the vacuum.

The general ideas guiding us in seeking a modification of the point electron have been the following. We seek a theory wherein the free or virtual electron propagates from one point in space-time to another by means of the Dirac Green's function. Likewise the Maxwell wave equation Green's function governs the propagation of the photon. However we seek a genuine modification of the charge-current density which will give us finite effects.

As an example of a modification in this direction, we should like to exhibit first the model proposed by Bohm, Weinstein, and Kouts.[6]

$$j_\mu(\boldsymbol{x}')=\int d\tau f[(\boldsymbol{x}'-\boldsymbol{x}(\tau))^2]g\left[(\boldsymbol{x}'-\boldsymbol{x}(\tau))\cdot\frac{d\boldsymbol{x}}{d\tau}\right]$$
$$\cdot\left[\frac{dx_\mu}{d\tau}-(x_\lambda'-x_\lambda(\tau))\left(\frac{dx_\mu}{d\tau}\frac{d^2x_\lambda}{d\tau^2}-\frac{dx_\lambda}{d\tau}\frac{d^2x_\mu}{d\tau^2}\right)\right], \quad (1.8)$$

where f and g are arbitrary structure functions and where we have ignored for the sake of simplicity the use of "shape variables." If, e.g.,

$$g[(\boldsymbol{x}'-\boldsymbol{x}(\tau))\cdot d\boldsymbol{x}/d\tau]=\delta[(\boldsymbol{x}-\boldsymbol{x}(\tau))\cdot d\boldsymbol{x}/d\tau]$$

we have what appears to be the most natural covariant extension of the Lorentz electron. It is important to note that S_p in Eq. (1.1) must be altered to include the rotational action of the charge distribution. Bohm[7] has pointed out that in going over to a quantum-mechanical theory, this will alter decisively the Dirac Green's function.

As an example which possesses great heuristic value because it is the simplest type of finite-sized "non-rigid" charge-current distribution that we can envisage, we have

$$j_\mu(\boldsymbol{x}')=\int d\tau\int d\lambda f(\lambda)\delta(\boldsymbol{x}'-\boldsymbol{x}(\tau)-\lambda d\boldsymbol{x}/d\tau)$$
$$\cdot(dx_\mu/d\tau+\lambda d^2x_\mu/d\tau^2), \quad (1.9)$$

where λ is a parameter measuring the distance from the center of the electron. One can picture this crudely as a line charge-current stretched along the four-velocity. This type of charge-current density does not possess a rotational action for S_p and therefore does not alter the Dirac Green's function. The four-acceleration term is necessary in order to guarantee conservation of charge-current density, Eq. (1.2).

One of the obvious failures of model (1.9) from the classical point of view is that the self-energy for an electron at rest diverges in the same manner as a point electron, i.e., $1/r$. Nevertheless it is highly heuristic to analyze such a model quantum mechanically to ascertain what new features will arise. There is no way to tell the quantum-mechanical behavior of a theory from the classical results.

Another model of the electron which quantum mechanically reveals new features is the following:

$$j_\mu(\boldsymbol{x}')=\int d\lambda\int d\tau f(\lambda)\delta(\boldsymbol{x}'-\boldsymbol{x}(\tau)-\lambda d^2\boldsymbol{x}/d\tau^2)$$
$$\cdot(dx_\mu/d\tau+\lambda d^3x_\mu/d\tau^3). \quad (1.10)$$

This model is space-like, whereas model (1.9) is time-like. The reason for this is that $(dx_\mu/d\tau)(d^2x_\mu/d\tau^2)=0$, i.e., the four-acceleration is perpendicular to the four-velocity and therefore always space-like. For both models (1.9) and (1.10), $f(\lambda)=\delta(\lambda)$, we have the point electron again. Moreover if the electron is at rest $d^2x_\mu/d\tau^2=0$ and we have the point electron again with its accompanying self-energy divergence.

From examples (1.6), (1.8), (1.9), and (1.10) it is plain that there are many possible models for the electron. All of these can in principle be treated quantum mechanically by the methods discussed below. However because of the requirement (1.2), the models

[5] R. P. Feynman, Phys. Rev. **76**, 749, 769 (1949).
[6] Bohm, Weinstein, and Kouts, Phys. Rev. **76**, 867 (1949).
[7] Private communication.

rapidly become complicated. For example, we find it no longer easy to determine b_μ in the following model

$$j_\mu(x')=\int d\tau f[(x'-x(\tau))^2]g[(x'-x(\tau))\cdot d^2x/d\tau^2]b_\mu.$$

II. QUANTUM-MECHANICAL CONSIDERATIONS

The starting point of the Feynman formalism is the following:

The amplitude of transition, say, of electron from an initial state of the system $\psi(x_1, \tau_1)$ to a final state of the system $\chi(x_2, \tau_2)$ is given by[8]

$$\int\cdots\int \chi(x_2, \tau_2)\exp[i(S_p+S_{\text{int}})]\psi(x_1, \tau_1)d \text{ paths}, \quad (2.1)$$

where $\hbar=c=1$ and where $\int\cdots\int(\ )\cdot d$ paths represents a special type of integral operation defined, discussed, and illustrated by Feynman.[9] The τ is the proper time and serves primarily as an ordering parameter. We regard τ as playing no essential role for it will disappear from the final results.

Moreover Feynman has shown that if one sums all the possible paths for a free electron properly weighted by $\exp(iS_p)$ from point x_1, τ_1 to point x_2, τ_2 the resultant is simply the Green's function $G(x_2, \tau_2; x_1, \tau_1)$ obtained by standard procedures. For our purposes it suffices to make the assumption that S_p is such that the Green's function for S_p is the Dirac Green's function, i.e.,

$$\gamma_\mu\frac{\partial G}{\partial x_{\mu 2}}(x_2, \tau_2; x_1, \tau_1)-\frac{\partial G}{\partial \tau_2}(x_2, \tau_2; x_1, \tau_1) = -i\delta(x_2-x_1)\delta(\tau_2-\tau_1) \quad (2.2)$$

solving (2.2) we get

$$G(x_2, \tau_2; x_1, \tau_1) = \int\frac{\exp[-i(p\cdot(x_2-x_1)+\pi(\tau_2-\tau_1)]}{p-\pi}dp^4d\pi. \quad (2.3)$$

The Dirac wave equation according to Feynman is

$$\nabla\psi=\partial\psi/\partial\tau \quad (2.4)$$

where Feynman assumes for $\psi(x, \tau)$ a proper time dependence of the form

$$\psi(x, \tau)=\psi(x)e^{-im\tau}. \quad (2.5)$$

Substituting (2.5) into (2.4) yields

$$(i\nabla-m)\psi(x)=0, \quad (2.6)$$

which is the usual expression.

As we have mentioned previously, if one has a finite-sized electron capable of rotation, as e.g., in the Bohm model (1.8), S_p will be quite different.

The only procedure known at the present time for analyzing (2.1) is by means of the perturbation technique developed by Feynman.[9] This procedure consists in expanding $\exp(iS_{\text{int}})$ into a power series and properly performing the required operations. For the case of the point electron (1.4) this has been done by Feynman. Now our first problem is to analyze the first-order perturbation calculation, using the simplest possible model (1.9) with the electron in an external potential. We then have the following

$$i\int\cdots\int e^{iS_p}\int dx'^4\int d\tau\int d\lambda f(\lambda)\delta(x'-x(\tau)-\lambda dx/d\tau) \cdot\left(\frac{dx_\mu}{d\tau}+\lambda\frac{d^2x_\mu}{d\tau^2}\right)A_\mu^{\text{ext}}(x')d \text{ paths}. \quad (2.7)$$

In order to understand (2.7) several new problems must be solved. For heuristic purposes, let us consider a simple fictitious example for S_{int}.

$$S_{\text{int}}=\int B_\mu(x(\tau))[d^3x_\mu(\tau)/d\tau^3]d\tau. \quad (2.8)$$

Where $B_\mu(x(\tau))$ is an arbitrary vector-field. Then the first-order perturbation is

$$i\int\cdots\int e^{iS_p}\int B_\mu(x(\tau))[d^3x_\mu(\tau)/d\tau^3]d\tau d \text{ paths}. \quad (2.9)$$

Using Feynman's methods[10] throughout, let us subdivide τ into intervals of length ϵ. For the derivative of the four-acceleration, we get

$$d^3x_\mu(\tau)/d\tau^3\rightarrow[x_\mu(\tau_i+2\epsilon)-3x_\mu(\tau_i+\epsilon) +3x_\mu(\tau_i)-x_\mu(\tau_i-\epsilon)]/\epsilon^3. \quad (2.10)$$

We obtain for (2.9)

$$\sum_i\epsilon(-1)^i\int\cdots\int e^{iS_p}\epsilon^{-3}\{[x_\mu(\tau_i+2\epsilon) -3x_\mu(\tau_i+\epsilon)+3x_\mu(\tau_i)]B_\mu(x(\tau_i)) -B_\mu(x(\tau_i))x_\mu(\tau_i-\epsilon)\}d \text{ paths}. \quad (2.11)$$

Performing the Feynman integral d paths operation and expressing everything in detail, we get

$$\sum_i\epsilon(-1)^i\int G(x_f, \tau_f; x_i, \tau_i)\epsilon^{-3} \times\{[\exp(2\epsilon\mathbf{H})x_\mu(\tau_i)\exp(-2\epsilon\mathbf{H}) -3\exp(\epsilon\mathbf{H})x_\mu(\tau_i)\exp(-\epsilon\mathbf{H})+3x_\mu(\tau_i)]B_\mu(x(\tau_i)) -B_\mu(x(\tau_i))\exp(\epsilon\mathbf{H})x_\mu(\tau_i)\exp(\epsilon\mathbf{H})\} \times G(x_i, \tau_i; x_0, \tau_0)dx_i^4 \quad (2.12)$$

[8] R. P. Feynman, Revs. Modern Phys. **20**, 367 (1948).
[9] R. P. Feynman, Phys. Rev. **80**, 440 (1950).
[10] We are greatly indebted to Professor Feynman for explaining to us how one obtains higher derivatives by means of slices. See also R. P. Feynman, Revs. Modern Phys. **20**, 367 (1948).

where $\mathbf{H}$ is the operator

$$\mathbf{H}\equiv\gamma_\mu\partial/\partial x_\mu\equiv\nabla. \tag{2.13}$$

Since $\nabla\psi=\partial\psi/\partial\tau$ and the Green's function $G(\boldsymbol{x}_i, \tau_i; \boldsymbol{x}_0, \tau_0)$ obeys the Dirac inhomogeneous wave equation.

Let us consider

$$\exp(2\epsilon\mathbf{H})x_\mu(\tau_i)\exp(-2\epsilon\mathbf{H})=x_\mu(\tau_i)+2\epsilon[\mathbf{H}, x_\mu(\tau_i)]+\frac{(2\epsilon)^2}{2!}[\mathbf{H}, [\mathbf{H}, x_\mu(\tau_i)]]+\cdots. \tag{2.14}$$

Substituting expressions such as (2.14) into (2.13) we get

$$\sum_i\epsilon(-1)^i\int G(\boldsymbol{x}_f, \tau_f; \boldsymbol{x}_i, \tau_i)\epsilon^{-3}\Big\{\tfrac{1}{2}\epsilon^3[\nabla, \gamma_\mu]B_\mu(\boldsymbol{x})-\tfrac{1}{2}\epsilon^2B_\mu(\boldsymbol{x}(\tau_i))\cdot[\nabla, \gamma_\mu]-\frac{5\epsilon^3}{3!}[\nabla, [\nabla, \gamma_\mu]]B_\mu+\frac{\epsilon^3}{3!}B_\mu[\nabla, [\nabla, \gamma_\mu]]+0(\epsilon^4)\Big\}\cdot G(\boldsymbol{x}_i, \tau_i; \boldsymbol{x}_0, \tau_0)d\boldsymbol{x}_i^4. \tag{2.15}$$

Because B_μ does not commute with ∇, we observe that the term zero order in ϵ is not zero. Let us try to eliminate this difficulty by symmetrizing out the zero-order term by taking

$$d^3x_\mu/d\tau^3\rightarrow[x_\mu(\tau_i+\epsilon)-3x_\mu(\tau_i)+3x_\mu(\tau_i-\epsilon)-x_\mu(\tau_i-2\epsilon)]/\epsilon^3. \tag{2.16}$$

This yields

$$\sum_i\epsilon(-1)^i\int d\boldsymbol{x}_i^4G(\boldsymbol{x}_f, \tau_f; \boldsymbol{x}_i, \tau_i)\epsilon^{-3}\Big\{\tfrac{1}{2}\epsilon^3[\nabla, \gamma_\mu]B_\mu(\boldsymbol{x}_i)-\frac{\epsilon^3}{2}B_\mu[\nabla, \gamma_\mu]+\frac{\epsilon^3}{3!}[\nabla, [\nabla, \gamma_\mu]]B_\mu-\frac{5}{3!}\epsilon^3B_\mu[\nabla, [\nabla, \gamma_\mu]]\Big\}G(\boldsymbol{x}_i, \tau_i; \boldsymbol{x}_0, \tau_0). \tag{2.17}$$

Again the term zero order in ϵ is nonvanishing. Moreover adding (2.15) and (2.16) does not produce a cancellation. From this we are forced to conclude that the "mixing" of B_μ into $d^3x_\mu/d\tau^3$ is incorrect. Suppose we take $B_\mu(\boldsymbol{x}(\tau_i))$ and

$$d^3x_\mu(\tau_i)/d\tau^3\rightarrow[x_\mu(\tau_i)-3x_\mu(\tau_i-\epsilon)+3x_\mu(\tau_i-2\epsilon)-x_\mu(\tau_i-3\epsilon)]/\epsilon^3. \tag{2.18}$$

There are now no zero order in ϵ terms; we obtain

$$\sum_i\epsilon(-1)^i\int G(\boldsymbol{x}_f, \tau_f; \boldsymbol{x}_i, \tau_i)B_\mu(\boldsymbol{x}(\tau_i))[\nabla_i, [\nabla_i, \gamma_\mu]]\cdot G(\boldsymbol{x}_i, \tau_i; \boldsymbol{x}_0, \tau_0)d\boldsymbol{x}_i^4. \tag{2.19}$$

However, this is unsymmetrical for *a priori* there is no reason to assume that (2.18) is the only choice; we can also have $B_\mu(\boldsymbol{x}(\tau_i))$ and

$$d^3x_\mu(\tau_i)/d\tau^3\rightarrow[x_\mu(\tau_i+3\epsilon)-3x_\mu(\tau_i+2\epsilon)+3x_\mu(\tau_i+\epsilon)-x_\mu(\tau_i)]/\epsilon^3. \tag{2.20}$$

Averaging (2.19) and (2.20) we finally arrive at what we consider the correct quantum-mechanical expression

$$\tfrac{1}{2}i\int d\tau\int d\boldsymbol{x}^4G(\boldsymbol{x}_f, \tau_f; \boldsymbol{x}, \tau)\{B_\mu(\boldsymbol{x})[\nabla_x, [\nabla_x, \gamma_\mu]]+[\nabla_x, [\nabla_x, \gamma_\mu]]B_\mu(\boldsymbol{x})\}G(\boldsymbol{x}, \tau; \boldsymbol{x}_0, \tau_0). \tag{2.21}$$

We can obtain an insight into this in the following way. For the Dirac electron

$$\begin{aligned} dx_\mu/d\tau&\rightarrow[\nabla, x_\mu]=\gamma_\mu\\ d^3x_\mu/d\tau^3&\rightarrow[\nabla, [\nabla, x_\mu]]=[\nabla, \gamma_\mu]\end{aligned} \tag{2.22}$$

etc., therefore,

$$\exp(\epsilon\mathbf{H})x_\mu(\tau)\exp(-\epsilon\mathbf{H})=x_\mu(\tau+\epsilon)=\sum_{n=0}^{\infty}\frac{\epsilon^n}{n!}\frac{d^nx_\mu(\tau)}{d\tau^n}. \tag{2.23}$$

As a check which can be verified by explicit calculation, consider classically $\dot{x}_\mu(\tau)\dot{x}_\mu(\tau)=1$. By differentiating with respect to proper time, we obtain the well-known relations:

$$\dot{x}_\mu\ddot{x}_\mu=0, \quad \dot{x}_\mu\dddot{x}_\mu+\ddot{x}_\mu\ddot{x}_\mu=0. \tag{2.24}$$

etc.

These have the corresponding quantum-mechanical analogs

$$\begin{aligned}&\gamma_\mu[\nabla, \gamma_\mu]+[\nabla, \gamma_\mu]\gamma_\mu=0\\ &\gamma_\mu[\nabla, [\nabla, \gamma_\mu]]+2[\nabla, \gamma_\mu][\nabla, \gamma_\mu]+[\nabla, [\nabla, \gamma_\mu]]\gamma_\mu=0\end{aligned} \tag{2.25}$$

etc.

One can check (2.25) by explicit calculation. These simple considerations are significant because they determine the ordering of physical quantities. In general for any operator 0, its proper time derivative is given by

$$d0/d\tau\rightarrow[\nabla, 0]. \tag{2.26}$$

In summarizing the above, we now know that "mixing" is not allowed, and moreover the ordering of the physical quantities must be determined by a procedure similar to that which produced (2.25). We shall illustrate these two points in detail by considering the first-order perturbation calculation for the simplest model of the electron (1.9).

III. FIRST BORN APPROXIMATION

For the first-order perturbation theory we obtain Eq. (2.7). Let us consider but one Fourier component of $A_\mu^{ext}(\boldsymbol{x}')$

$$A_\mu^{ext}(\boldsymbol{x}')=a_\mu(\boldsymbol{q})\exp(-i\boldsymbol{q}\cdot\boldsymbol{x}'). \tag{3.1}$$

Now classically

$$\frac{\partial j_\mu(x')}{\partial x_\mu'}=0=\int d\tau\int d\lambda\int dk^4 f(\lambda)\times\exp\left[ik\cdot\left(x'-x(\tau)-\lambda\frac{dx}{d\tau}\right)\right]\cdot ik_\mu\left(\frac{dx_\mu}{d\tau}+\lambda\frac{d^2x_\mu}{d\tau^2}\right)$$

$$=-\int d\tau\int d\lambda\int dk^4 f(\lambda)\exp(ik\cdot x')\times\frac{d}{d\tau}\exp\left[-ik\cdot\left(x(\tau)+\lambda\frac{dx}{d\tau}\right)\right]. \quad (3.2)$$

According to (2.26) this corresponds quantum mechanically to

$$-\int d\tau\int d\lambda\int dk^4 f(\lambda)\exp(ik\cdot x')\times[\nabla,\exp(-ik\cdot x-i\lambda\mathfrak{k})]. \quad (3.3)$$

We can rewrite (3.3) in the following way, remembering that $d/d\tau$ is an operator.

$$\partial j_\mu(x')/\partial x_\mu'\rightarrow-\int dk^4\int d\lambda\int d\tau f(\lambda)\exp(ik\cdot x')\cdot\left(\sum_{n=0}^{\infty}\frac{(-i)^n}{n!}\frac{d}{d\tau}\left\{k\cdot x+\lambda\frac{dx}{d\tau}\right\}^n\right). \quad (3.4)$$

Comparing this with the current density which we rewrite again

$$j_\mu(x')=\int dk^4\int d\lambda\int d\tau f(\lambda)\exp(ik\cdot x')\times\exp[-ik\cdot x(\tau)-i\lambda k\cdot(dx/d\tau)]\cdot\left(\frac{dx_\mu}{d\tau}+\lambda\frac{d^2x_\mu}{d\tau^2}\right). \quad (3.5)$$

We obtain quantum mechanically the following significant expression for the charge current density

$$j_\mu(x')\rightarrow\int dk^4\int d\lambda\int d\tau f(\lambda)\exp(ik\cdot x')\cdot\left(\sum_P\sum_{n=1}^{\infty}\frac{(-i)^{n-1}}{n!}P(\gamma_\mu+\lambda[\nabla,\gamma_\mu])\times(k\cdot x+\lambda\mathfrak{k})^{n-1}\right). \quad (3.6)$$

Where P denotes the operation of inserting the $(\gamma_\mu+\lambda[\nabla,\gamma_\mu])$ factor into the n possible places of the $(k\cdot x+\lambda\mathfrak{k})^{n-1}$ factor. For example for $n=3$ the term in the sum becomes

$$\frac{(-i)^2}{3!}[(\gamma_\mu+\lambda[\nabla,\gamma_\mu])(k\cdot x+\lambda\mathfrak{k})^2+(k\cdot x+\lambda\mathfrak{k})(\gamma_\mu+\lambda[\nabla,\gamma_\mu])\cdot(k\cdot x+\lambda\mathfrak{k})+(k\cdot x+\lambda\mathfrak{k})^2(\gamma_\mu+\lambda[\nabla,\gamma_\mu])].$$

The quantum-mechanical expression (3.6) is of no use as it stands. One must put it into closed form. This can be done for example by moving the $[\nabla,\gamma_\mu]$ and γ_μ operators all the way over to the right. After rather lengthy but straightforward manipulation, we obtain for $j_\mu(x')$

$$j_\mu(x')\rightarrow\int dk^4\int d\lambda\int d\tau f(\lambda)\exp[ik\cdot(x'-x(\tau))]\cdot\left\{\exp(-i\lambda\mathfrak{k})(\gamma_\mu+\lambda[\nabla,\gamma_\mu]\right.$$
$$-2\left(\frac{\sin\lambda\mathfrak{k}}{k^2}-\frac{\lambda\mathfrak{k}}{k^2}\exp(-i\lambda\mathfrak{k})\right)\cdot(\nabla k_\mu-\nabla\cdot k\gamma_\mu)$$
$$\left.+2\left(\frac{\cos\lambda\mathfrak{k}}{k^2}-\frac{\mathfrak{k}\sin\lambda\mathfrak{k}}{\lambda k^4}(\mathfrak{k}k_\mu-k^2\gamma_\mu)\right)\right\}. \quad (3.7)$$

One can check (3.7) for consistency in two ways. (These checks do not determine uniqueness, however.) If $f(\lambda)=\delta(\lambda)$ we should get the quantum-mechanical expression for a point electron, i.e.,

$$\int dk^4\int d\tau\exp[ik\cdot(x'-x(\tau))]\gamma_\mu$$

which we do. In addition, we can take the divergence of (3.7) and it should be equal to (3.3). One finds that this is so. There is a significant observation to be made about (3.7). Every term has a factor of the form $\exp(\pm i\lambda\mathfrak{k})$. This is so because the classical model has $\exp(i\lambda k\cdot dx/d\tau)$. However if we do the same calculation for the acceleration model Eq. (1.10), then instead of the factor $\exp(i\lambda k\cdot dx/d\tau)$ we now have $\exp(i\lambda k\cdot d^2x/d\tau^2)$ and instead of $\exp(\pm i\lambda\mathfrak{k})$ we have $\exp(\pm i\lambda[\nabla,\mathfrak{k}])$. This is an important difference, for the ∇ "couples" into the Dirac Green's function, a fact which is highly desirable in bringing about convergence for the polarization of the vacuum. Unfortunately, the expression for $j_\mu(x')$ for model (1.10) is so lengthy at the present stage of development that it is unwieldy. It is likely that (3.7) can also be put into a simpler, more compact form.

Equation (2.7) which is the first Born approximation

now becomes

$$\int d\lambda \int d\tau \int dx^4 f(\lambda) G(\boldsymbol{x}_f, \tau_f; \boldsymbol{x}, \tau) \exp(-i\boldsymbol{q}\cdot\boldsymbol{x})$$
$$\cdot\Big\{\exp(-i\lambda q)(a+\lambda[\nabla, a])$$
$$\times 2\left(\frac{\sin\lambda q}{q^2}-\frac{\lambda q}{q^2}\exp(-i\lambda q)\right)\cdot(\nabla \boldsymbol{q}\cdot\boldsymbol{a}-\nabla\cdot\boldsymbol{q}a)$$
$$+2\left(\frac{\cos\lambda q}{q^2}-\frac{q\sin\lambda q}{\lambda q^4}\right)(\boldsymbol{q}\cdot\boldsymbol{a}-q^2 a)\Big\}$$
$$\cdot G(\boldsymbol{x}, \tau; \boldsymbol{x}_0, \tau_0). \quad (3.8)$$

For a point electron, $f(\lambda)=\delta(\lambda)$, this reduces to the well-known result.

The above development is justified essentially by arguments of plausibility. Now, then, how does one obtain (3.8) by means of Feynman's "slices" in space-time, i.e., how does one obtain (3.8) in the manner that we obtained (2.21)? The answer to this question is necessary in order to handle the second-order perturbation theory correctly, because in second-order calculations one must explicitly calculate the "overlapping" of slices, a phenomenon which is of great importance in any finite-sized electron theory, but which, as Feynman has shown, does not manifest itself for the point electron theory. The contributions of the overlapping slices are called contact terms and our aim is to present the calculations of such terms in a second paper.

In order to express (3.6) in terms of Feynman's slices, let us write (3.6) explicitly in terms of proper time derivatives which do not in general commute with each other.

$$j_\mu(\boldsymbol{x}')\rightarrow\int dk^4\int d\lambda\int d\tau\exp(i\boldsymbol{k}\cdot\boldsymbol{x}')\Big[\left(\frac{dx_\mu}{d\tau}+\lambda\frac{d^2x_\mu}{d\tau^2}\right)$$
$$+\frac{(-i)}{2!}\left\{\left(\frac{dx_\mu}{d\tau}+\lambda\frac{d^2x_\mu}{d\tau^2}\right)\left(\boldsymbol{k}\cdot\boldsymbol{x}+\lambda\boldsymbol{k}\cdot\frac{d\boldsymbol{x}}{d\tau}\right)\right.$$
$$\left.+\left(\boldsymbol{k}\cdot\boldsymbol{x}+\lambda\boldsymbol{k}\cdot\frac{d\boldsymbol{x}}{d\tau}\right)\left(\frac{dx_\mu}{d\tau}+\lambda\frac{d^2x_\mu}{d\tau^2}\right)\right\}$$
$$+\frac{(-i)^2}{3!}\{\cdots\}+\cdots\Big]. \quad (3.9)$$

The following ordering of slices will certainly give (3.6) but we are not certain whether the contact terms in second Born approximation are uniquely determined or not, namely [omitting the Green's functions to the left and right of (3.10)].

$$j_\mu(\boldsymbol{x}')\rightarrow\int dk^4\int d\lambda f(\lambda)\exp(i\boldsymbol{k}\cdot\boldsymbol{x}')\Big[\left(\frac{x_\mu(\tau_i+\epsilon)-x_\mu(\tau_i)}{\epsilon}\right)$$
$$+\lambda\left(\frac{x_\mu(\tau_i+2\epsilon)-2x_\mu(\tau_i+\epsilon)+x_\mu(\tau_i)}{\epsilon^2}\right)$$
$$+\frac{(-i)}{2!}\left\{\left[\frac{(x_\mu(\tau_i+2\epsilon)-x_\mu(\tau_i+\epsilon))}{\epsilon}\right.\right.$$
$$\left.+\lambda\frac{(x_\mu(\tau_i+3\epsilon)-2x_\mu(\tau_i+2\epsilon)+x_\mu(\tau_i+\epsilon))}{\epsilon^2}\right]$$
$$\cdot\left[\boldsymbol{k}\cdot\boldsymbol{x}(\tau_i)+\lambda\boldsymbol{k}\cdot\frac{(\boldsymbol{x}(\tau_i+\epsilon)-\boldsymbol{x}(\tau_i))}{\epsilon}\right]+\left[\boldsymbol{k}\cdot\boldsymbol{x}(\tau_i+2\epsilon)\right.$$
$$\left.+\lambda\boldsymbol{k}\cdot\frac{(\boldsymbol{x}(\tau_i+3\epsilon)-\boldsymbol{x}(\tau_i+2\epsilon))}{\epsilon}\right]\cdot\left[\frac{x_\mu(\tau_i+\epsilon)-x_\mu(\tau_i)}{\epsilon}\right.$$
$$\left.\left.+\lambda\left(\frac{x_\mu(\tau_i+2\epsilon)-2x_\mu(\tau_i+\epsilon)+x_\mu(\tau_i)}{\epsilon^2}\right)\right]\right.$$
$$\left.+\frac{(-i)^2}{3!}\{\cdots\}+\cdots\right]. \quad (3.10)$$

There are other ways of ordering the operators which give Eq. (3.7). These will be discussed in Part II.

ACKNOWLEDGMENTS

We should like to express our great debt of gratitude to Professor Feynman for explaining and discussing his theories to us. We also would like to thank Dr. Bohm for the talks concerning his model. Finally we appreciate very much the many discussions of the present theory with Dr. Donald Yennie.

Letters to the Editor

PUBLICATION of brief reports of important discoveries in physics may be secured by addressing them to this department. The closing date for this department is five weeks prior to the date of issue. No proof will be sent to the authors. The Board of Editors does not hold itself responsible for the opinions expressed by the correspondents. Communications should not exceed 600 words in length, and should be submitted in duplicate.

The Origin of High Permeability in Permalloy

SŌSHIN CHIKAZUMI

Department of Physics and Chemistry, Gakushuin University, Mejiro, Tokyo, Japan

(Received October 8, 1951)

IT is well known that alloys of the composition near Ni_3Fe have unusual magnetic properties sensitive to heat treatment: (a) when cooled rapidly from 600°C, they develop extremely high initial and maximum permeabilities (μ_0 and μ_{max}); (b) when cooled

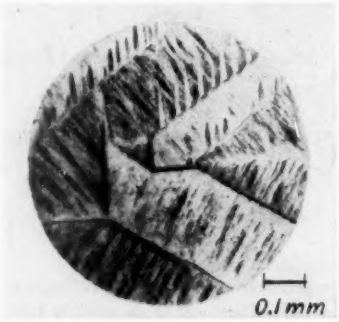

FIG. 1. Domain pattern observed on (110) surface of Ni_3Fe crystal. Nearly perfect order. $K_1 = -28 \times 10^3$ ergs/cc.

slowly or annealed in a magnetic field, they exhibit high μ_{max} only in the direction parallel to the field applied during the heat treatment. The author has investigated these properties in connection with the formation of the superlattice at 490°C, and explained (b) in terms of "directional order."[1]

The principal points are as follows: The fractional contraction $\delta l/l$ observed[1] during the superlattice formation at 490°C was -4.4×10^{-4}. This is considered to correspond to the fractional difference of pair-lengths between like and unlike atom-pairs, because the ordering process means an increase of the unlike atom-pairs. If, therefore, the fractional numbers of unlike atom-pairs, or the degrees of order, are different in different bond directions, the lattice should deform spontaneously to the order of 4.4×10^{-4}. Such an arrangement of atoms, the directional order (d.o.), will be promoted by the ordering process under the influence of the magnetostrictive force, which usually, being counterbalanced by the elastic force, gives rise to but a small amount of strain. As soon as the alloy is cooled and the d.o. frozen, the spontaneous magnetization becomes stable in the same direction as it was during annealing, on account of the interaction between magnetostrictive force and the strain of d.o. The magnitude of strain necessary to explain the observed anisotropy in the case (b) was 1.7×10^{-4}, which is a reasonable value for the strain of d.o.

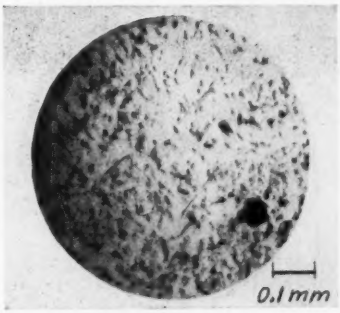

FIG. 2. Domain pattern observed on (110) surface of Ni_3Fe crystal. Partially disordered. $K_1 = -2\times10^3$ ergs/cc.

The origin of the unusually high μ_0 in case (a), however, remains in question. In this respect, the author investigated the variation of domain structure during the disordering process by means of powder pattern technique.[2] A large single crystal (*ca* 2 cc) of the alloy Ni_3Fe[3] was prepared by sudden solidification after supercooling *ca* 100° below the mp to prevent segregation. Two specimens, one for the domain pattern observation and the other for the torquemeter measurement, were cut along a (110) plane. Perfect order was attained by annealing for one week at 490°C and several days below this temperature. The disordering process was carried out by raising the temperature from 490° stepwise to 610°C, the procedure being interrupted several times by quenching for observations. Both specimens were always treated together.

The crystal anisotropy constant K_1 decreased from -29×10^3 ergs/cc to zero during the disordering process, as has been reported by Grabbe.[4] At first the domain patterns showed a structure having 180°, 109°, and 71° boundaries, which was to be expected for a crystal having the easiest magnetization along the ⟨111⟩ direction (Fig. 1). No essential changes were observed until K_1 decreased to -7×10^3, except some slight deformation of linear boundaries which appeared in the later stages. Further disordering baking (at 550°C), however, made the figure rather irregular, in which 180° boundaries were broken and deformed and numerous crooked boundaries appeared (Fig. 2). At this transition K_1 was -2×10^3. When quenched from 610°C, fine crooked and dotted line-like boundaries appeared at a distance of *ca* 0.01 mm (Fig. 3). The irregular movement of these boundaries under

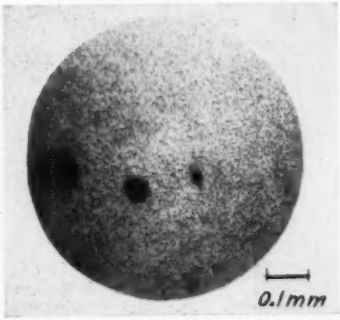

FIG. 3. Domain pattern observed on (110) surface of Ni_3Fe crystal. Nearly perfect disorder. $|K_1| < 0.4\times10^3$ ergs/cc.

the influence of an applied field could be observed only when the size of the colloid particles was adequate.

The fine division of domains thus observed is to be attributed to the random distribution of strains under the condition that $K_1 < (3/2)\lambda E\epsilon$, where λ means the saturation value of magnetostriction, E the Young's modulus and ϵ the strain. There is evidence that the strain is caused by the random generation of d.o. For, if we substitute into the above expression $\lambda = 5\times10^{-6}$, $E = 2\times10^{12}$ dyne/cm^2 and $\epsilon = 1.7\times10^{-4}$, the strain of d.o., we get 2.5×10^5 ergs/cc, which is nearly equal to the actual value of K_1 when the transition of patterns took place.

The fine domain structure described above might, under proper conditions, give rise to high μ, as will be discussed along the following lines: (1) The crooked boundaries in this structure might continuously decrease their area in the process of magnetization, and the resulting decrease of exchange energy could play a role in promoting the magnetization. The exchange energy stored in the demagnetized state was estimated at *ca* 10^5 ergs/cc if we assume a distribution of spin-direction with a period of 0.01 mm. If, therefore, the d.o. were destroyed so much by further disordering that $\lambda E\epsilon$ decreases to 10^5 ergs/cc, magnetization would take place without any external work. This means a high mobility of the boundaries. (2) The influence of inclusions or lattice defects would be nothing but a local one in this structure, without any essential effect on the magnetization as a whole. (3) The contribution to μ_a will be proportional to the total area of the boundaries, which seems to be very large in this structure as compared to usual domain structure.

Too severe disordering will destroy the fine domain structure so as to decrease the exchange energy, again decreasing μ_a. It is experimentally known that the maximum μ_a is attained by a proper rate of quenching for permalloy[5] and by proper prolonged annealing for Mo-permalloy.[6] These treatments are interpreted as means of attaining proper values of the strain.

[1] S. Chikazumi, J. Phys. Soc. (Japan) **5**, 327 (1950).
[2] Williams, Bozorth, and Shockley, Phys. Rev. **75**, 155 (1949).
[3] 25.2 weight percent Fe, 74.8 percent Ni, 0.02 percent Mn, as the result of chemical analysis.
[4] E. M. Grabbe, Phys. Rev. **57**, 728 (1940).
[5] G. W. Elmen, J. Franklin Inst. **207**, 583 (1929).
[6] R. M. Bozorth, *Ferromagnetism* (D. Van Nostrand Company, Inc., New York, 1951), p. 140, and K. Yasukochi, unpublished.

Activation of LiI Crystal Phosphors*

W. Bernstein and A. W. Schardt
Brookhaven National Laboratory, Upton, New York
(Received January 8, 1952)

LITHIUM iodide crystals have been grown[1,2] with different activators and tested for pulse height and resolution with thermal neutrons from the BNL reactor. A collimated beam $\frac{1}{4}$ in. in diameter was used for exploring different parts of the crystals. A $\frac{3}{4}$ in. diameter uniform beam was available for testing over-all response. The crystals, wet with Nujol, were placed on a 5819 photomultiplier inside a $\frac{1}{32}$ in. thick diffuse reflector made from titanium oxide in lucite. The electronics used were essentially the same as described previously.[3] The pulse height has been measured in terms of the gamma-ray energy necessary to produce a photoelectric line at the same pulse height in a standard[3] NaI(Tl) crystal.

In general, single crystals $\frac{1}{2}$-in. diameter and $2\frac{1}{2}$ in. long were grown; then cleaved into one centimeter thick sections. These pieces were cleaved into small (2 mm) cubes if the pulse-height distribution was very nonuniform. Crystals grown at 4 in. per day with an excess of TlI activator (0.5 percent by weight) were clear and colorless with a thin layer of thallous iodide around the outside of the crystal. Spectroscopic analysis[4] of a typical piece from the tip of the crystal gave 0.008 percent by weight of TlI; at the top 0.013 percent was found. The pulse heights from these pieces were in the ratio of 1:2. Two regions of pulse height were

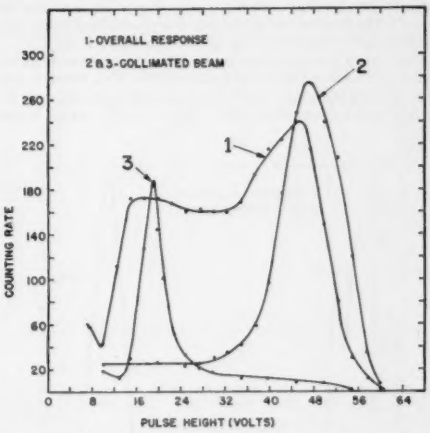

FIG. 1. LiI(Tl) $\frac{1}{2}$ in. $\times\frac{1}{2}$ in. $\times\frac{1}{2}$ in. crystal irradiated with thermal neutrons. (1) Response of whole crystal in uniform beam. (2 and 3) $\frac{1}{4}$ in. beam at characteristic spots in crystal.

favored, 120 to 180 kev, and 300 to 450 kev, NaI(Tl) equivalent. In general pieces of the order of 2 mm^3 gave the resolution found for the equivalent pulse height in NaI. However, larger pieces had either two peaks or a very broad distribution in pulse height (Fig. 1). Exploration with the collimated neutron beam showed that the transition between the two regions occurs within less than $\frac{1}{8}$ inch. Attempts to grow uniformly activated crystals by using growing speeds from 1.7 in. to 7 in. per day were unsuccessful.

From the above it is evident that the pulse height is a function of thallium concentration. Similar variations in thallium concentration were also found by Harshaw[5] in NaI(Tl) crystals (0.1 to 0.5 percent). However, in that case the pulse height was not affected. It seems that the amount of thallium entering the LiI lattice is insufficient for complete activation. A search is being made for other activators which can enter the crystal in sufficient amounts. So far, indium, tin, and silver have been tried. Reagent grade chemicals were used, but small impurities may have an unexpected effect.

LiI(In) behaved very much like LiI(Tl); most of the activator was expelled from the lattice. On neutron irradiation two peaks were found corresponding to 45 and 80 kev. The fluorescence band is a whitish orange and does not match the 5819 spectral response.

A crystal grown with 0.15 percent by weight $SnCl_2 \cdot 2H_2O$ activator was transparent yellow at the tip, becoming more and more opaque yellow toward the top. All but the most opaque part gave a uniform pulse height of 197 kev, and the resolution found with NaI(Tl) for that pulse height (14.5 percent). The decay time is almost the same as that of LiI(Tl). The fluorescence band is in the green.

A crystal grown with 0.3 percent AgI activator was colorless and transparent at the tip, gradually becoming cloudy toward the top. All the activator went into the crystal, since no AgI was found on the surface. The pulse height was the equivalent of 210 kev. Different sections of the crystal showed a pulse-height variation of 20 percent. The fluorescence band is greenish yellow.

The results with the tin activator looked sufficiently promising to grow a larger crystal. A $1\frac{1}{2}$ in. ampule was used and 0.05 percent by weight $SnCl_2 \cdot 2H_2O$ was added. Five parallel crystals starting at the tip grew from this melt. The tip was transparent and slightly yellow; the top was cloudy. Pieces approximately $1\times\frac{3}{4}\times\frac{1}{2}$ inches gave a resolution between 13.7 percent and 16.5 percent, and a pulse height equivalent to 250 kev (Fig. 2). The

pulse height between different pieces varied by less than 10 percent. The proportionality between energy and pulse height was checked within 6 percent by using Cs^{137} gamma-rays (Fig. 2).

From this it is evident that large LiI(Sn) crystals can be grown which give good resolution and pulse height. This makes it possible to build relatively small detectors with high efficiency for thermal and epithermal neutrons. The resolution makes it also

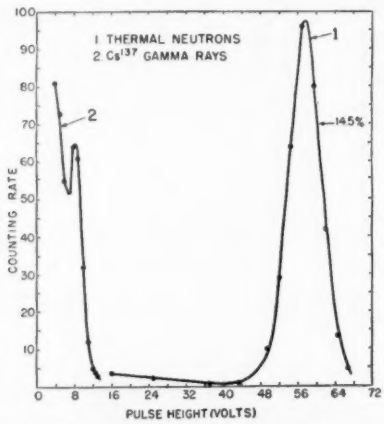

FIG. 2. LiI(Sn) 1 in. × 1 in. × 1 in. crystal response. (1) irradiated with thermal neutrons; (2) Cs^{137} gamma-rays.

possible to use these crystals for rough neutron-energy measurements in the region where the $Li^6(n,\alpha)He^3$ cross section is large enough (~1 barn).

* This work was done under the auspices of the AEC.
[1] Hofstadter, McIntyre, Roderick, and West, Phys. Rev. **82**, 749 (1951).
[2] W. Bernstein and A. W. Schardt, Bull. Am. Phys. Soc. **26**, No. 6, 15 (1951).
[3] A. W. Schardt and W. Bernstein, Rev. Sci. Instr. **22**, 1020 (1951).
[4] We are indebted to Morris Slavin for the spectroscopic analysis.
[5] Harshaw Chemical Company (private communication).

The Graphs for the Kernel of the Bethe-Salpeter Equation

C. A. HURST
Trinity College, University of Cambridge, Cambridge, England
(Received January 9, 1952)

IN view of the recent discussions of Bethe and Salpeter[1] and Low and Gell-mann[2] on the derivation of an integral equation for describing bound states in field theory, it is of interest to see whether this kernel is likely to show any irregular type of convergence. Although it is the intention of these authors to escape some of the limitations of perturbation expansions, particularly when dealing with problems concerning bound states, it has not been found possible to obtain a tractable equation in a closed form, so that the kernel can only be employed in the form of a power series expansion in the coupling constant.

The kernel for the two-particle scattering process is composed of "irreducible" parts. These parts are such that it is not possible, by cutting the two spinor lines carrying the external energy and momentum, to separate the graph into two portions such that each portion has exactly four external spinor lines.

As an indication of the possible convergence of the power series describing the kernel, a lower limit to the number of irreducible graphs is given.

Let $N(n)$ denote the number of graphs of order n, whether reducible or irreducible, and $N_I(n)$ the number of irreducible graphs. Then a difference equation for $N_I(n)$ can be set up, in a manner exactly parallel to the Bethe-Salpeter equation.

$$\frac{N(n)}{n!}=\frac{N_I(n)}{n!}+\frac{N_I(n-2)}{(n-2)!}\frac{N(2)}{2!}+\cdots+\frac{N_I(2)}{2!}\frac{N(n-2)}{(n-2)!}. \quad (1)$$

This equation is obtained by requiring that the last $(n-2r)$ points, as described by the arrows on the spinor lines carrying the external energy and momentum, should form an irreducible graph, while the first $2r$ form a graph which may be reducible.

If

$$\Phi(v)=\sum_{n=0}^{\infty} v^n\frac{N(n)}{n!}, \quad \Psi(v)=\sum_{n=2}^{\infty} v^n\frac{N_I(n)}{n!},$$

Eq. (1), in terms of generating functions, can be written

$$\Phi(v)=1+\Phi(v)\Psi(v), \quad (2)$$

which models the Bethe-Salpeter equation.

Now if "ladder" graphs are considered, for which only virtual boson exchange between the two spinor lines takes place, then we have

$$N(n)/n!=\tfrac{1}{2}(n/2)!,$$

and it is evident that $N(n)\geqslant N_I(n)$.

Also

$$\frac{N_I(n)}{n!}\geqslant\frac{N(n)}{n!}-\sum_{r=1}^{\frac{1}{2}(n-2)}\frac{N(2r)}{2r!}\frac{N(n-2r)}{(n-2r)!}. \quad (3)$$

Then the ratio of succeeding terms in the summation,

$$R_r=\frac{N(2r)N(n-2r)}{N(2r+2)N(n-2r-2)}\frac{(2r+2)(2r+1)}{(n-2r)(n-2r-2)}=\frac{n-2r}{2r+2}>R_{r+1}$$

and $R_1R_2\cdots R_{\frac{1}{2}(n-2)}=1$. Also $R_r=1$ for $(n-2r)/(2r+2)=1$, that is for $r=(n-2)/4$, so that

$$R_r\gtrless 1 \quad \text{for} \quad r\lessgtr(n-2)/4.$$

Then the inequality can be written

$$\frac{N_I(n)}{n!}\geqslant\frac{N(n)}{n!}-\frac{2N(n-2)}{(n-2)!}\frac{N(2)}{2!}-\frac{2N(n-4)}{(n-4)!}\frac{N(4)}{4!}\left(1+\frac{1}{R_4}+\frac{1}{R_4R_6}+\cdots+\frac{1}{R_4\cdots R_{\frac{1}{2}(n-4)}}\right)$$
$$\geqslant\frac{N(n)}{n!}-\frac{2N(n-2)}{(n-2)!}\frac{N(2)}{2!}-nC\frac{N(n-4)}{(n-4)!}\frac{N(4)}{4!},$$

where C is independent of n.

So

$$[N(n)/n!][1-O(1/n)]\leq N_I(n)/n!\leq N(n)/n!.$$

Hence $N_I(n)/n!$ increases as rapidly as $N(n)/n!$, namely $\log[N_I(n)/n!]\sim\frac{1}{2}n\log n+O(n)$. Thus there are, in this sense, as many terms in the kernel of the Bethe-Salpeter equation as in the original perturbation expansion, and so this kernel may very well not form a convergent series in the coupling constant, in the same way as the Born approximation for the S-matrix may not lead to a convergent series.

This result then raises the question of the meaning of the approximate solution of an integral equation, obtained by neglecting further terms in the kernel, when this kernel could not be approximated indefinitely with increasing order. This would be particularly difficult to justify in the case of pseudoscalar meson-nucleon interactions, for which the experimentally determined coupling constant is large.

This result can be modified trivially to fit any of the field theories so far introduced.

[1] H. A. Bethe and E. E. Salpeter, Phys. Rev. **82**, 309 (1951).
[2] M. Gell-mann and F. Low, Phys. Rev. **84**, 350 (1951).

Resistivity of Evaporated Tellurium Films

TAKEMARO SAKURAI AND SEIJI MUNESUE
Research Institute for Scientific Measurements, Tohoku University, Sendai, Japan
(Received December 10, 1951)

A TELLURIUM film was made on a substrate of a silica plate by vacuum evaporation, and its resistivity was measured at various temperatures. The thickness of film was varied from 200 to 5000A. When the substrate was kept at room temperature during evaporation, the film deposited showed high resistivity immediately after the evaporation, but the resistivity decreased with time and reached a finite value. By raising and lowering the temperature, $\log R - 1/T$ curves were obtained, an example of which is shown in Fig. 1. As seen in this figure, the resistivity changed irreversibly when the temperature was raised above that in which the film had ever been placed, but reversibly at the temperature in which the film had been put or lower. It was found that the resistivity R in the reversible region could be expressed by the equation

$$\ln(R-r) = U/2kT + \text{const},$$

by inserting a suitable constant r, where U is the activation energy of a bulk specimen, 0.34 ev. By raising the temperature above that which the film had undergone, the value of r was found to increase and approach a finite value. These facts are indicated in the figure by the decrease of inclination and the increase of curvature in successive reversible courses. The value of r/R was nearly the same for a film with thickness larger than 1000A, but it was less for thinner films. Upon raising the temperature to about 180°C a sudden increase of resistivity set in, and upon lowering the temperature a decrease of r was observed. This feature was conspicuous for thinner films.

When the film was bombarded by electrons of about 10,000 ev after evaporation, the change of resistivity with temperature was entirely reversible, and the constant r showed the value given by the heat treatment. On the other hand, when the tellurium was deposited on a hot substrate about 200°C in temperature, the $\log R - 1/T$ curve of the film was found to be in good accord with that of the bulk specimen, as is shown in Fig. 2. The measured activation energies in the intrinsic and extrinsic ranges were 0.34 and 0.040 ev, respectively.

It seems that the tellurium atoms, deposited on a cold substrate, might wander to make microcrystals but these crystals are buried by amorphous deposit. After evaporation, the crystals grow larger with time and reach an equilibrium at a given temperature. In this case, the resistance of the film is given by the sum of the resistance of microcrystals, the intrinsic semiconductor, and that of the amorphous deposit r which is large in value and has a small temperature coefficient. By heat treatment or electron bombardment, crystals grow larger and amorphous portions diminish; this will result in a decrease of resistance. By the migration of atoms, however, small empty spaces grow in the amorphous portions, which causes the increase of r.

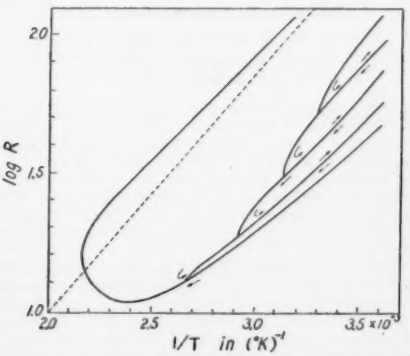

FIG. 1. Resistivity of tellurium film deposited on a cold substrate as a function of temperature. The dashed curve is the result obtained for a bulk specimen.

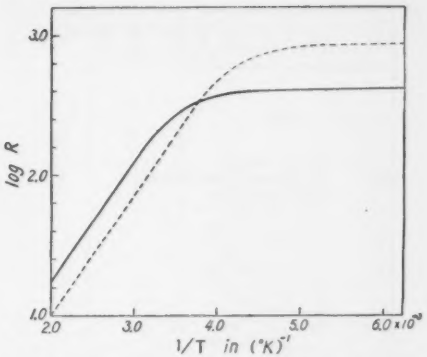

FIG. 2. Resistivity of tellurium film deposited on a hot substrate as a function of temperature. The dashed curve is the result obtained for a bulk specimen.

These phenomena were observed also by means of the electron microscope and electron diffraction. When the substrate is kept at a high temperature, the atoms deposited have sufficient energy to wander and to form crystals during the whole course of evaporation, and hence the largest part of the film is well crystallized. Thus evaporated films prepared by a suitable procedure are quite the same as bulk crystals from the point of view of electrical resistivity; and other experimental data obtained with them, as well as with bulk specimens, seem to be available for theories of semiconductors.

Production Cross Section and Energy Spectrum of the Neutral Mesons in Cosmic Rays*

G. SALVINI AND Y. KIM
Palmer Physical Laboratory, Princeton University, Princeton, New Jersey
(Received January 7, 1952)

WE summarize here our results on the neutral mesons obtained at Echo Lake, Colorado, during the summer of 1951. The nuclear events in which the neutral mesons are created are produced in sodium iodide crystals mounted inside a cloud chamber, and are detected by 1*P*21 photomultipliers (Fig. 1). This method[1] keeps our bias in detection as low as that of the nuclear emulsions, yet gives higher efficiency in detecting the photons into which the π_0 decays.

The distribution of the nuclear events according to the number of the emitted shower particles (ionization $\lesssim$1.5 minimum[2]) is given in Table I, second row. In the third row the number of nuclear events with electromagnetic component is given.

1. *Energy distribution of the neutral mesons.* In most of the cases, the electromagnetic component associated with a nuclear event consisted of two cores diverging from the origin. We regarded the sum of the estimated energies of these two electromagnetic cores as the energy of the π_0 emitted.[3] The main uncertainty in these estimates comes from the fluctuation of the electronic cascade. The results are given in the histogram of Fig. 2.

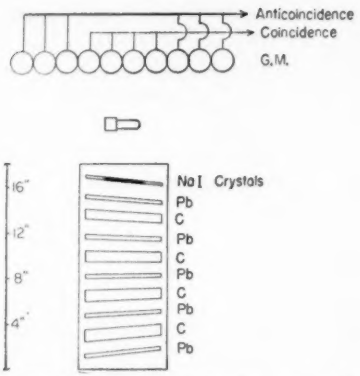

FIG. 1. Experimental disposition; coincidence and anticoincidence Geiger-Mueller counters were used to concentrate on proton-produced events and to cut down air showers.

We have also plotted the points reported by the Bristol Group[4] referring to the charged mesons. The average atomic weight of our crystals almost equals that of the nuclear emulsions. Comparison with the Bristol data[4] on the energy distribution of the π_0 in the air will be discussed in a later paper.

TABLE I. Distribution of nuclear events, N_s, according to the number of shower particles.

No. of shower particles, s:	1	2	3	4	≥ 5
No. of nuclear events, N_s, containing s shower particles:	216	92	45	23	19
No. of nuclear events, N_s, having electromagnetic component:	25	28	29	16	16

2. *Ratio of neutral to charged mesons.* We consider first the events with three or more shower particles. These events show 336 shower particles, and for them we estimate 74 neutral mesons, corresponding to about 22 percent of the shower particles. The shower particles mainly consist of protons and π-mesons, and the π-mesons are about 60 percent of the shower particles.[4]

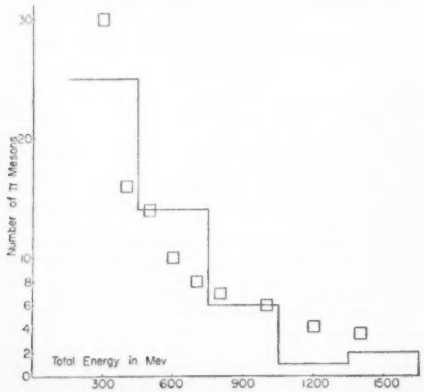

FIG. 2. Differential energy distribution of the π-mesons. Squares: $\pi_+ + \pi_-$; histogram: π_0.

TABLE II. Summary of data on neutral mesons.

Energy of the protons	σ production	Energy distribution	$\pi_0/(\pi_+ + \pi_-)$
0.345 Bev	$\sim 1/200\,\sigma_{\text{geom}}$[7]	...	...
0.8–2 Bev	$0.22 \pm 0.06\,\sigma_{\text{geom}}$	Compare Fig. 2	0.4 ± 0.1
>2 Bev	$0.7 \pm 0.15\,\sigma_{\text{geom}}$		0.37 ± 0.08

This value gives for the ratio of neutral to charged mesons, $R = \pi_0/(\pi_+ + \pi_-) = 0.37 \pm 0.08$, in agreement with the previous observations by Tinlot and Gregory[2] and the earlier results of the Bristol Group.[5]

On the other hand, if we make the corresponding estimate for the events with 1, 2, 3, or 4 shower particles, we find again a similar value, $R = 0.4 \pm 0.1$. This is not in agreement with the recent Bristol value[6] $R = 1 \pm 0.3$ for these events.

3. *Production cross section of the π_0.* We divide the events of Table I into two groups: (a) those with one or two shower particles, or with at least one neutral meson, and (b) those with three or more shower particles.

If we assume that the proton nucleus total cross section for one "nucleus" of sodium iodide is geometrical, σ_{geom}, then we can estimate the cross section $\sigma_{\pi 0}$ for π_0 production for events (a) and (b). For events (a) we find a value $\sigma_{\pi 0} = 0.22 \pm 0.06 \sigma_{\text{geom}}$; for events (b) $\sigma_{\pi 0} = 0.7 \pm 0.15 \sigma_{\text{geom}}$. Recent results[6] on the correlation between the primary proton energy and the size of the nuclear events indicate that events (a) are mostly produced by protons of energy $\sim 0.8-2$ Bev; (b) are by protons of energy ≥ 2 Bev.

In Table II, we summarize the pertinent data on the neutral mesons.

* Assisted by the joint program of the ONR and AEC.

[1] G. Salvini, Nuovo cimento **8**, (1951); G. Reynolds and G. Salvini, Phys. Rev. **83**, 198 (1951).
[2] Brown, Camerini, Fowler, Heitler, King, and Powell, Phil. Mag. **40**, 862 (1949).
[3] J. Tinlot and B. Gregory, Phys. Rev. **81**, 667, 675 (1951); Lovati, Mura, Salvini, and Tagliaferri, Nuovo Cimento **7**, 786 (1950).
[4] Camerini, Fowler, Lock, and Muirhead, Phil. Mag. **41**, 413 (1950).
[5] Carlson, Hooper, and King, Phil. Mag. **41**, 701 (1950).
[6] Camerini, Davis, Fowler, Franzinetti, Muirhead, Lock, Perkins, and Yekutieli, Phil. Mag. **42**, 1241 and 1261 (1951).
[7] Burton J. Moyer, private communication.

The Nuclear Gyromagnetic Ratio of V^{50} and Measurements on Rb^{85} and Cl^{35}*

H. E. WALCHLI, W. E. LEVSHON, AND F. M. SCHEITLIN
Stable Isotope Research and Production Division, Oak Ridge National Laboratory, Oak Ridge, Tennessee

(Received January 8, 1952)

THE nuclear gyromagnetic ratio of vanadium 50 has been determined in a nuclear induction apparatus similar to that described by Proctor[1] and previously reported.[2] An electronically regulated electromagnet with a gap of $1\frac{1}{4}$ inches produced a field homogeneous to 0.1 gauss over the sample volume. Frequency measurements were made with a Signal Corps BC-221 frequency meter calibrated with harmonics from an external 100 kc, crystal-controlled oscillator, which in turn was compared with *WWV* at 10 Mc.

The sample consisted of 271 mg of electromagnetically enriched vanadium as $VOCl_3$, of which an estimated 25 mg was vanadium 50. This enriched sample was preptred from V_2O_5 and was sealed in a small spherical glass vial which was placed in a test tube and surrounded by a saturated solution of RbCl containing 15 percent D_2O. No magnetic catalyst was added.

The vanadium 50 resonance was first observed near 6 Mc at a field of 14,250 gauss. Frequency measurements were made at

nominal fields of 14,250, 11,900, and 10,100 gauss. The frequency ratios for V^{50} relative to Cl^{35}, Rb^{85}, and deuterium gave:

$$\nu(V^{50})/\nu(Cl^{35}) = 1.01758 \pm 0.0001,$$
$$\nu(V^{50})/\nu(Rb^{85}) = 1.03262 \pm 0.0001,$$
$$\nu(V^{50})/\nu(D^{2}) = 0.649527 \pm 0.00007.$$

The sign of the moment of V^{50} has been determined to be positive by direct comparison with Rb^{85} and Cl^{35} resonances. The observed line widths at 10,100 gauss were 1.75, 2.1, and 0.92 gauss for V^{50}, Rb^{85}, and D^{2}, respectively. Using a value of 2.79268 ± 0.00006 nm[2] for the proton moment, and Levinthal's[6] value for the deuteron-to-proton frequency ratio, and a spin of 1 for the deuteron, the nuclear gyromagnetic ratio for vanadium 50 becomes $+0.55690 \pm 0.00006$.

Frequency measurements were made at the same nominal fields for Rb^{85}, Cl^{35}, and D^{2}. The ratios measured with deuterium were converted to those relative to the proton by using Levinthal's deuteron-to-proton frequency ratio of 0.1535059. In Table I, our results are compared with other published values.

TABLE I. Comparison of results.

	Frequency ratio		Method	Reference
$\nu(Rb^{85})/\nu(Cl^{35})$	=0.98545	±0.00042	Indirect	Bitter[a]
	0.98592	±0.0008	Indirect	Chambers and Williams[b]
	0.98541	±0.00015	Direct	This report
$\nu(Rb^{85})/\nu(H^{1})$	=0.096574	±0.00004	Indirect	Bitter[a]
	0.09661	±0.00004	Direct	Chambers and Williams[b]
	0.0965521	±0.0000003	Direct	Yasaitas and Smaller[c]
	0.096554	±0.00001	Indirect	This report
$\nu(Cl^{35})/\nu(H^{1})$	=0.097999	±0.00005	Indirect	Bitter[a]
	0.09799	±0.00007	Direct	Chambers and Williams[b]
	0.097978	±0.00009	Direct	Proctor and Yu[d]
	0.097985	±0.00001	Indirect	This report

[a] F. Bitter, Phys. Rev. **75**, 1326 (1949).
[b] W. H. Chambers and D. Williams, Phys. Rev. **76**, 638 (1949).
[c] E. Yasaitas and B. Smaller, Phys. Rev. **82**, 750 (1951).
[d] W. G. Proctor and F. C. Yu, Phys. Rev. **81**, 20 (1951).

The authors wish to express their gratitude to J. R. McNally, Jr., H. W. Morgan, and other associates for interest and encouragement in this work. Appreciation is also expressed to personnel of the Stable Isotope Research and Production Division who were responsible for the enrichment of the vanadium.

* This paper is based on work performed for the AEC by Carbide and Carbon Chemicals Company, a Division of Union Carbide and Carbon Corporation, Oak Ridge, Tennessee.
[1] W. G. Proctor, Phys. Rev. **79**, 35 (1950).
[2] Walchli, Livingston, and Hebert, Phys. Rev. **82**, 97 (1951).
[3] Sommer, Thomas, and Hipple, Phys. Rev. **80**, 487 (1950).
[4] E. C. Levinthal, Phys. Rev. **78**, 204 (1950).

Tin Activation of LiI

JAMES SCHENCK AND R. L. HEATH*
Oak Ridge National Laboratory, Oak Ridge, Tennessee
(Received January 10, 1952)

CRYSTALS of LiI with thallium activation have been shown[1] to respond to thermal neutrons.

In the course of testing the effect of various activators in LiI, it was found that a strong luminescence occurred under ultraviolet excitation when LiI was activated by tin. In order to determine its response to slow neutrons, crystals of this phosphor containing about 0.1 mole-percent of SnI_2 were grown from the melt. One of these crystals was selected which was about $1 \times 0.5 \times 0.5$ cm in size, irregular in shape, transparent, and ranging in color from faint yellow to nearly colorless. The crystal was ground smooth on one side and optically connected to a 5819 photomultiplier through a 1-inch-diameter by 0.5-inch-long Lucite light piper. White Vaseline was used to join the crystal, Lucite, and photomultiplier. An aluminum can covering the crystal and clamped with an "O" ring to the Lucite served as a reflector and as a means of maintaining the crystal in an atmosphere of dry nitrogen.

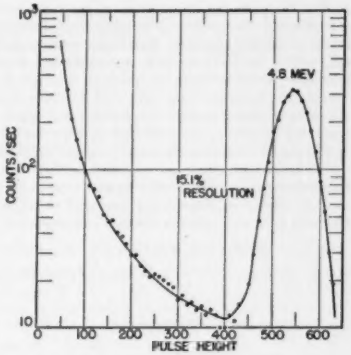

FIG. 1. Slow neutrons on LiI $-SnI_2$.

The crystal was exposed to uncollimated neutrons from an unshielded Po—Be source. A flux of slow neutrons was obtained by placing a block of paraffin behind the source. The measured photomultiplier pulse-height spectrum is shown in Fig. 1. Even in the presence of the γ-rays and fast neutrons emanating from the source, and in spite of the irregularity and nonuniformity of the crystal, the pulse-height spectrum exhibits a resolution of 15.1 percent for the monoenergetic excitation of the phosphor from the reaction of the moderate neutrons with the Li^{6}.

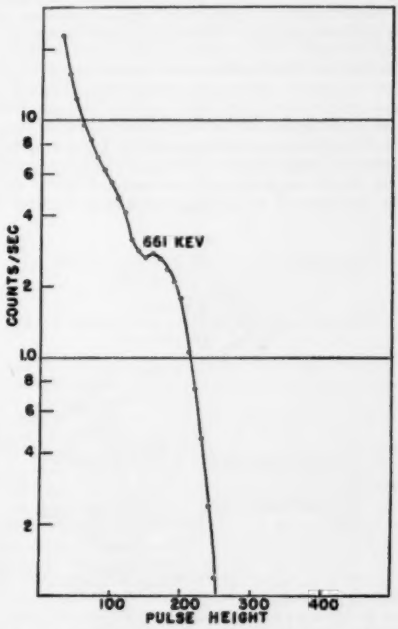

FIG. 2. Cs^{137} γ-rays on LiI $-SnI_2$. The pulse-height scale is twice that of Fig. 1.

Figure 2 is the pulse-height spectrum of the same crystal and mounting showing the peak due to photoelectrons from Cs^{137} γ-radiation. A similar spectrum was taken after replacing the $LiI-SnI_2$ with a $NaI-TlI$ crystal. A comparison of the pulse heights at the photoelectric peaks gives an electron excitation efficiency for $LiI-SnI_2$ relative to $NaI-TlI$ of 1/24.5. A comparison of the pulse heights with $LiI-SnI_2$ for Cs^{137} γ-rays and for neutrons, assuming linearity, gives a Q of 4.5 Mev for the $Li^6(n, \alpha)H^3$ reaction which is 94 percent of the correct value of 4.785 Mev.

The scintillations produced by neutrons on $LiI-SnI_2$ which were detected by the photomultiplier were observed on an oscilloscope, and the decay of fluorescence appeared to be purely exponential with a time constant of about 0.7 microsecond.

* On loan from American Cyanamid Company, Arco Reactor Testing Station.

[1] Hofstadter, McIntyre, Roderick, and West, Phys. Rev. **82**, 749 (1951).

High Energy Photodisintegration of the Deuteron*

T. S. Benedict and W. M. Woodward
Cornell University, Ithaca, New York
(Received January 10, 1952)

THE differential cross section has been measured for protons arising from the photodisintegration of the deuteron at laboratory angles of 60°, 90°, and 120° for γ-ray energies ranging from 80 to 160 Mev. The technique used was essentially that used in a previous experiment[1] on the photodisintegration of He^4. The pressure chamber (Fig. 1) has been modified slightly by introducing an internal collimator and decreasing the solid angles of the counter telescopes. Synchrotron γ-rays of maximum energy 300 Mev were admitted to the chamber and particles were counted which traversed the first crystal and lost at least 20 Mev in the second crystal. The pulses observed in the first crystal are the result of protons arising from photodisintegration and those mesons which produce stars losing more than the required 20 Mev in the second crystal. The two kinds of particles may be separated in the first crystal by a pulse-height analysis. In Fig. 1 the chamber is shown in the position for the 60° and 90° runs. The rear section of the chamber can be reversed to correspond to the 90° and 120° runs. The energy of the protons counted could be varied by inserting various combinations of the movable absorbers mounted in the chamber. The counter telescope was calibrated roughly using a ThC'' source and more exactly by raising the bias on the back crystal until the proton counting rate went to zero. This procedure should give a linear curve for the number of protons vs bias extrapolating to the energy thickness of the crystal.

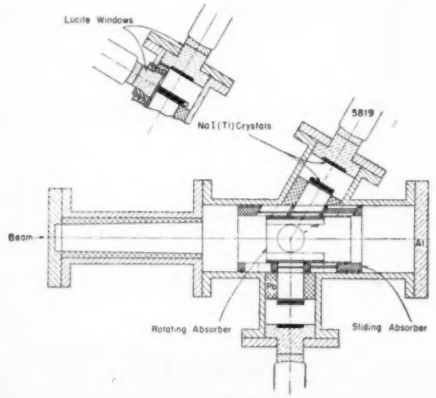

FIG. 1. Schematic diagram of the apparatus.

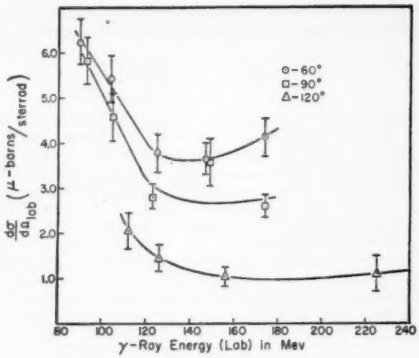

FIG. 2. Differential cross section for photodisintegration of the deuteron vs γ-ray energy at 30°, 60°, and 90° (Lab. system).

With the knowledge of the proton angle and energy one can obtain the energy of the γ-ray causing the photodisintegration. The results obtained are shown in Fig. 2 for laboratory angles of 60°, 90°, and 120°. If one assumes an angular distribution of the form

$$d\sigma/d\Omega=[\sin^2\theta(a+b\cos\theta)+c]/8\pi$$

and converts the results of Fig. 2 into the center-of-mass system, one obtains for the total cross section the values shown in Fig. 3. Along with these is plotted the photoelectric dipole cross section given by Schiff[2] and Marshall and Guth[3] for a Yukawa well of effective range of 1.74×10^{-13} cm with 50 percent exchange force. The errors shown are based on counting statistics alone. The ab-

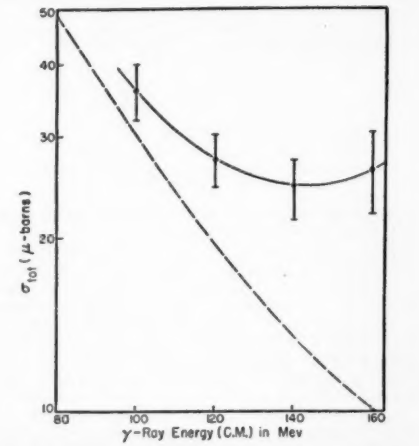

FIG. 3. Total cross section for photodisintegration of the deuteron (cm system). The solid line represents the experimental data. The dashed line is the electric dipole cross section obtained from references 2 and 3.

solute error to be assigned to these points is 30 percent. For the low energy points the measured total cross section is in essential agreement with the calculated cross section; however, in the region of the meson threshold the experimental cross section is higher by a factor of about 2.5. Assuming the angular distributions of references 2 and 3 and that used by Austern[4] in calculations of the isotropic contribution, an estimate can be made of the electric quadrupole cross section which is found to be about 1 percent of the electric dipole cross section in the energy region of this experiment. An estimate of the isotropic contribution is 40 percent of the electric dipole cross section. The errors in these estimates are obviously large, since they are limited by the counting statistics and the fact that observations were made at only three angles.

* Supported by the joint program of the ONR and AEC.
[1] T. S. Benedict and W. M. Woodward, Phys. Rev. **83**, 1269 (1951).
[2] L. I. Schiff, Phys. Rev. **78**, 733 (1950).
[3] J. F. Marshall and E. Guth, Phys. Rev. **78**, 738 (1950).
[4] N. Austern, Phys. Rev. **85**, 283 (1952).

Line Width of Paramagnetic Resonance and Exchange Interaction in Salts Containing Mn^{++} and Fe^{+++}

H. KUMAGAI, K. ÔNO, AND I. HAYASHI
Institute of Science and Technology, University of Tokyo, Tokyo, Japan
(Received December 17, 1951)

IN column 3 of Table I, half-widths $\Delta H_{\frac{1}{2}(\text{obs})}$ of paramagnetic microwave resonance absorption lines, at $\lambda = 3.01$ cm, are shown for nine kinds of polycrystalline salts containing Mn^{++}

TABLE I. Half-widths of paramagnetic microwave resonance absorption lines.

Polycrystals	Crystal symmetry	$\Delta H_{\frac{1}{2}(\text{obs})}$ (oersteds)	$\Delta H_{\frac{1}{2}(\text{calc})}$ (oersteds)	θ (°K)	z(calc)
$FeNH_4(SO_4)_2$	hexa.	580	1680	13[a]	38
$Fe_2(SO_4)_3$	hexa.	180	2300	70[a,b]	33
$MnCl_2$	hexa.	1250	2950	−16[a]	32
$MnCl_2 \cdot 2H_2O$	···	760	···	···	···
$MnCl_2 \cdot 4H_2O$	mono.	1340	1530	$-3(\approx 0)$[c]	···
$MnSO_4$	mono.	655	3400	24[d]	19
$MnSO_4 \cdot H_2O$	mono.	305	2800	···	···
$MnSO_4 \cdot 4H_2O$	mono.	1140	1500	$2(\approx 0)$[c,d]	···
$MnSO_4 \cdot 5H_2O$	tric.	1250	1250	$3(\approx 0)$	···

[a] See reference 3.
[b] See reference 4.
[c] See reference 5.
[d] See reference 6.

and Fe^{+++}. Some of the results have already been reported.[1] When the g value is anisotropic, as in the case of cupric salts, the apparent width for a polycrystalline powder is increased. However, in powders of salts containing Mn^{++} and Fe^{+++}, there is no such effect since these ions are in S states and the g value is almost isotropic.

The theoretical half-width caused by dipolar coupling in a powdered cubic crystal has been calculated by Van Vleck[2] under the assumption that the shape function is Gaussian. The formula thus obtained is

$$\Delta H_{\frac{1}{2}(\text{calc})} \approx 2.35[\langle(\Delta H^2)_{\text{Av}}\rangle]^{\frac{1}{2}} = 2.35 g\beta\{\tfrac{3}{4}S(S+1)\textstyle\sum_{k\neq j} r_{jk}^{-6}\}^{\frac{1}{2}}. \quad (1)$$

As we have little knowledge of the detailed structure of crystals in the table, we have assumed tentatively, as a first approximation, that the arrangement of ions is simple cubic with lattice constant a. Half-widths calculated by this simplification of (1) are given in the fourth column of the table. In cases where the crystal structure is known from x-ray analysis, as for instance $(NH_4)Fe(SO_4)_2$, the calculated width for the simple cubic arrangement of ions is generally narrower than that calculated allowing for the correct arrangement of ions in the crystals. However, the resulting change in the calculated half-width is by a factor ranging from about 1 to 1.4, so the difference in ionic arrangements has no significant influence on our rather qualitative discussion.

In some cases, the observed width is much smaller than the calculated one on account of the effect of exchange coupling. The fifth column shows the observed values[3-6] of θ in the Curie-Weiss formula for the static susceptibility, $\chi_s = c/(T+\theta)$. The departures of θ from zero are caused by the exchange coupling of electrons and the splitting of electronic levels by the crystalline field. The inference is clear that when $\Delta H_{\frac{1}{2}(\text{calc})}/\Delta H_{\frac{1}{2}(\text{obs})}$ is large, θ is large. This circumstance can be explained in order of magnitude in the following way.

According to Van Vleck's considerations,[2] $\Delta\nu_{\frac{1}{2}}$ under exchange coupling is given by $\Delta\nu_{\frac{1}{2}} \approx \tau_c \langle(\Delta\nu^2)_{\text{Av}}\rangle$, where $\tau_c = h/2J$ and J is the exchange integral. We tentatively set

$$\Delta\nu_{\frac{1}{2}} = \tau_c \langle(\Delta\nu^2)_{\text{Av}}\rangle = (h/2J)\langle(\Delta\nu^2)_{\text{Av}}\rangle, \quad (2)$$

in which $\Delta\nu_{\frac{1}{2}}$ is $\Delta H_{\frac{1}{2}(\text{obs})} \cdot g\beta/h$.

In our cases of Mn^{++} and Fe^{+++}, it is probable that the effect of splitting of electronic levels upon θ is negligible and that θ is caused only by exchange coupling.[7] In this case, θ is connected with J by the relation[8]

$$3k\theta = 2Jz S(S+1), \quad (3)$$

where k is the Boltzmann constant, S is the spin quantum number (in our case $S = 5/2$), and z is the number of nearest neighbors in the lattice.

We can try calculating values of z by using the formula

$$z_{(\text{calc})} = \frac{3k\theta(2.35)^2 \Delta H_{\frac{1}{2}(\text{obs})}}{(\Delta H_{\frac{1}{2}(\text{calc})})^2 g\beta S(S+1)},$$

which follows from Eqs. (1), (2), and (3). The resulting values of z are shown in the sixth column of the table. They show no large divergences from each other, but they are all several times larger than the values of z deduced from the crystal structures. Further elaborations of our rather qualitative considerations would be futile.

A more detailed report will appear in *J. Phys. Soc. Japan*. Our thanks are due Professor T. Mutô for his cordial discussions.

[1] Kumagai, Ono, Hayashi, Abe, Shimada, Shôno, and Ibamoto, Phys Rev. **83**, 1077 (1951).
[2] J. H. Van Vleck, Phys. Rev. **74**, 1168 (1948).
[3] T. Ishiwara, Sci. Repts. Tohoku Univ. **3**, 303 (1914).
[4] P. Théodoridès, J. phys. et radium **3**, 1 (1922).
[5] L. C. Jackson, Proc. Roy. Soc. (London) **A140**, 695 (1933).
[6] H. K. Onnes and E. Oosterhuis, Leiden Comm. **12**, 132e (1913).
[7] J. H. Van Vleck and W. G. Penny, Phil. Mag. **17**, 961 (1934).
[8] J. H. Van Vleck, *The Theory of Electric and Magnetic Susceptibilities* (Clarendon Press, Oxford, 1932), p. 332.

Adiabatic Study of the 128°C Transition in Barium Titanate

SHEPARD ROBERTS
General Electric Research Laboratory, Schenectady, New York
(Received January 9, 1952)

THERE has been much discussion about the nature of the so-called Curie point transition in barium titanate. Some writers have classed it as second order,[1] while others have noticed discontinuities typical of a first-order transition.[2,3] A first-order transition would be characterized by a latent heat which in barium titanate has heretofore escaped direct detection. Blattner and Merz[4] observed a specific heat anomaly amounting to 47 cal/mole; however, this was spread over a range of about 15°C and cannot be cited as evidence that the transition is first order. A more convincing argument may be based on the change of temperature which we find takes place when the transition is induced adiabatically by applying an electric field.

For this analysis ceramic disks of barium titanate of the highest obtainable purity were used. These were attached to suitable connecting wires and thermocouple leads and suspended by these wires in a small oven in which air was circulated. Small changes in temperature were detected by a recording galvanometer in the thermocouple potentiometer circuit. The sensitivity of indication

was better than 0.1°C, although the absolute accuracy was not this great since the thermocouple was not individually calibrated.

A step in the heating curve was observed indicating a thermal anomaly between 128.2 and 128.7°C. Essentially the same temperature limits were observed for different heating rates from 0.32°C per min to 2.8°C per min. Upon cooling, the anomaly was observed in a different temperature range, 126.5 to 127.1°C. These anomalies each occur within a much smaller temperature range than that observed by Blattner and Merz, however, they still do not give unequivocal evidence of a latent heat.

Temperature changes could be observed when an electric field was applied. When the temperature reached 130°C, an electric field of 600 v/mm was suddenly impressed. This produced an immediate temperature rise of 0.5°C. When the voltage was turned off, the temperature fell the same amount. This temperature change may be interpreted as that accompanying an adiabatic transition from the cubic to the tetragonal phase.

Upon cooling to 127.7°C the voltage was applied again for one second. This produced an irreversible temperature rise of about 0.5°C, and the usual thermal anomaly between 126.5 and 127.1°C was not observed as cooling continued. These observations indicate that the electric field in this case produced a permanent transition before the material had cooled enough for the transition to take place spontaneously. The temperature change of 0.5°C indicates that the transition has a latent heat. If this figure is multiplied by the average specific heat,[2,4,5] $c_p = 0.13$ cal/g°C and by the molecular weight, a lower limit of 15 cal/mole is obtained for the latent heat of the transition.

[1] V. Ginsburg, J. Phys. U.S.S.R. **10**, 107 (1946); S. Roberts, Phys. Rev. **71**, 890 (1947); H. D. Megaw, Trans. Faraday Soc. **42A**, 224 (1946); P. W. Forsbergh, Jr., Phys. Rev. **76**, 1187 (1949); A. von Hippel, Revs. Modern Phys. **22**, 221 (1950); W. J. Merz, Phys. Rev. **78**, 52 (1950).
[2] M. G. Harwood *et al.*, Nature **160**, 58 (1947).
[3] A. F. Devonshire, Phil. Mag. (7) **40**, 1040 (1949); W. Kaenzig, Phys. Rev. **80**, 94 (1950); C. Kittel, Phys. Rev. **82**, 729 (1951).
[4] H. Blattner and W. Merz, Helv. Phys. Acta **21**, 210 (1948).
[5] S. Sawada and G. Shirane, J. Phys. Soc. Japan **4**, 52 (1949).

Slow Neutron Liquid Scintillation Detector

C. O. Muehlhause and G. E. Thomas
Argonne National Laboratory, Chicago, Illinois
(Received January 18, 1952)

Aside from the possibility of discovering a fluorescent boron compound, the problem of detecting slow neutrons with boron at very high efficiencies (~100 percent) reduces to the problem of discovering a boron compound which may be introduced into a fluorescent medium without quenching the fluorescence. The series of esters: methyl, ethyl, propyl, etc.—borate when added to a standard fluorescent solution of phenylcyclohexane, terphenyl, and diphenylhexatriene—satisfies the above requirement. The only effect on the "alpha" pulse height due to the addition of these borates to the "phenyl" solution is to reduce it in proportion to the dilution of the original fluorescent solution. Even this loss of pulse height may be regained by addition of more terphenyl.

Enriched (B^{10}) methyl borate contains the least number of extraneous atoms and has the highest density of the series. A one-to-one solution by volume of methyl borate-"phenyl" used in conjunction with a 5819 photomultiplier tube has the following properties: (1) "alpha" pulse height of ~30 electrons at the cathode; (2) neutron lifetime in the medium of ~0.4 μsec.

It should be observed that with this short a lifetime, the presence of hydrogen is no obstacle to the use of such a counter for slow neutron time-of-flight velocity selection. In fact, the presence of hydrogen aids in keeping faster neutrons in the detecting medium. To use the counter in a practical way, however, it is desirable to use either liquid air cooling of the photomultiplier tube or to employ coincidences, and to bias out electrons of ~100 kev and higher in energy.

Relative Probabilities of Diverse Photonuclear Reactions from Zn^{64} and Fe^{54}

Ryokichi Sagane*
Institute for Atomic Research and Department of Physics, Iowa State College, Ames, Iowa
(Received January 11, 1952)

By the use of a high energy x-ray beam from the Iowa State College synchrotron with the maximum energy adjustable up to 67 Mev, measurements have been made leading to relative cross sections as a function of quantum energy for (γ, n), (γ, pn), and $(\gamma, 2np)$ reactions[1] on the same parent isotope Zn^{64} or Fe^{54}. The curves obtained are shown in Figs. 1 and 2.

The values for the integrated cross sections are evaluated and listed in Table I. The values for zinc agree well with the values reported by Strauch[2] from transition curves in lead for 330-Mev bremsstrahlung. The relative values for $\sigma_{\gamma,2n}$ and $\sigma_{\gamma,pn}$ also agree well with those given by Ghoshal,[3] who produced the compound nucleus Zn^{64} by Ni+α and Cu+p reactions. In addition, the shapes

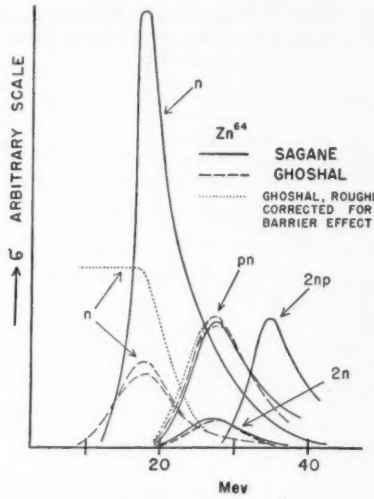

Fig. 1. Relative cross sections *vs* E_{kp} for (γ, n), (γ, pn), $(\gamma, 2n)$, and $(\gamma, 2np)$ reactions on Zn^{64}. Excitation functions for n, pn, and $2n$ emission from the same compound nucleus, Zn^{64*}, as reported by Ghoshal are also given.

of these cross section curves *vs* energy agree with the shapes of Ghoshal's curves. Since he showed that his results are in good accord with the statistical theory of the compound nucleus excited to an energy of the order of 30 Mev, this agreement with the present data shows that competition in the excited nucleus can satisfactorily explain the results for $(\gamma, 2n)$ and (γ, pn) processes. It is also to be noted, however, that the (γ, n) cross section reported here is relatively seven times higher than that obtained by Ghoshal. Since the processes of excitation are different and it is known that the cross section for excitation to 18 Mev by charged particles will be lower than that for excitation to 30 Mev (by a factor of 1.5 to 2, because of the potential barrier which is particularly significant for incoming particles with large l values), this difference in $\sigma_{\gamma,n}/(\sigma_{\gamma,2n}+\sigma_{\gamma,pn})$ must indicate that the cross section for gamma-ray absorption is several times larger at 18 Mev than at 30 Mev. In addition, it is to be noted that, for Zn^{64}, $\sigma_{\gamma,p}$ is probably at least as large as $\sigma_{\gamma,n}$ in the region of 18 Mev.[4] It seems

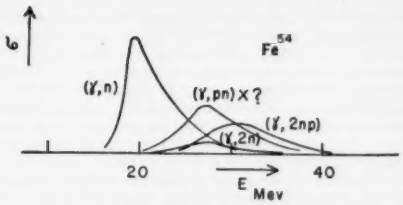

FIG. 2. Relative cross sections *vs* E_{kv} for (γ, n), (γ, pn), $(\gamma, 2n)$, and $(\gamma, 2np)$ reactions on Fe^{54}.

definite, therefore, that the total cross section for gamma-ray absorption by the Zn^{64} nucleus has a peak in the neighborhood of 20 Mev and falls off above this. Such a behavior is suggested by the dipole resonance of Goldhaber and Teller.[5] To state the matter in another way, the results reported here show that the fall-off of the (γ, n) cross section above 20 Mev is caused not only by competition from other reactions, but also by a fall-off in the total cross section for gamma-ray absorption.

TABLE I. Relative integrated cross sections for (γ, n), (γ, pn), $(\gamma, 2n)$, and $(\gamma, 2np)$ reactions on Zn^{64}, Fe^{54}, Ge^{70}, and Ni^{58}, together with the same for $(\gamma, 2p)$ and $(\gamma, 2np)$ for Al^{27}.[a]

Outgoing particle	Product isotope	Half-life	Relative integrated cross sections: Strauch $\sigma_{int.}$	Strauch Rel.	Sagane Measured	Sagane Corrected for $Nh\nu$	Ghoshal
n	Zn^{63}	38 min	0.89	300	500 ± 200	300 ± 150	40
$2n$	Zn^{62}	9.5 hr	0.067	23	23^{+10}_{-5}	23^{+10}_{-5}	24
pn	Cu^{62}	10 min	0.37	125	100	100	100
$2np$[b]	Cu^{61}	3.4 hr	0.17	60	70 ± 20	80 ± 20	
n	Fe^{53}	8.9 min			100	65	
$2n$	Fe^{52}	7.8 hr			14 ± 8	14 ± 8	
pn	Mn^{52}	20 min			8		
		6 day			?	?	
$2np$	Mn^{51}	46 min			20 ± 10	20 ± 10	
$2p$	Na^{25}	60 sec			100		
$2pn$	Na^{24}	14.8 hr			50 ± 25		
n[b]	Ge^{69}	40 hr			100		
$2n$	Ge^{68}	250 day			?		
pn[b]	Ga^{68}	68 min			12		
$2np$	Ga^{67}	78 hr			small		
n[b]	Ni^{57}	36 hr			100		
pn	Co^{56}	80 day			?		
$2np$[b]	Co^{55}	18 hr			2		

[a] Corrections were made for self-absorption, back scattering, and the percentage of K-capture.
[b] Because of the experimental difficulties, the accuracy of these values is poor.

The result of another type of experiment may be of interest. The ratio of production of two isomers, Mo^{91} (70 sec) and Mo^{91} (16 min), by (γ, n) reactions on Mo^{92} was measured over the energy range from 15 Mev to 67 Mev. As shown in Fig. 3, this ratio remains constant for the whole range of measurement, including the region close to 18 Mev where the $Mo^{92}(\gamma, n)$ reaction shows a very sharp resonance.[6] This result may be regarded as an indication that the sharp resonance found in the $Mo^{92}(\gamma, n)$ reaction is not sensitive to the final states.

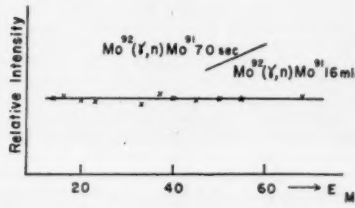

FIG. 3. Relative intensities of the two isomers, Mo^{91} (70 sec) and Mo^{91} (16 min), produced from Mo^{92} by the (γ, n) reaction *vs* the maximum energy of the x-ray beam.

No results similar to those given by Ghoshal are available for Fe^{54} at present. The very high intensity of the (γ, n) reaction, however, appears to indicate a situation similar to that for Zn^{64}.

The author wishes to express his heartiest gratitude to Dr. L. J. Laslett and Dr. D. J. Zaffarano for their continued interest and help given during the course of the experiment. Thanks are also due Dr. A. C. Helmholz and Dr. K. Strauch for detailed information concerning their experimental work.

* On leave from Tokyo University, Tokyo, Japan. Now at the Radiation Laboratory, University of California, Berkeley, California.
[1] R. Sagane, Phys. Rev. **84**, 586 (1951). The $(\gamma, 2np)$ results in the present work are relatively inaccurate.
[2] K. Strauch, Phys. Rev. **81**, 973 (1951).
[3] S. Ghoshal, Phys. Rev. **80**, 939 (1950).
[4] A. K. Mann and J. Halpern, Phys. Rev. **82**, 733 (1951).
[5] M. Goldhaber and E. Teller, Phys. Rev. **74**, 1046 (1948); J. S. Levinger and H. A. Bethe, Phys. Rev. **78**, 115 (1950).
[6] The same measurement has been independently carried out and reported at the Vancouver meeting of the American Physical Society [R. Montalbetti and L. Katz, Phys. Rev. **83**, 892 (1951)].

The Magnetic Moment of Zn^{67}*

S. S. DHARMATTI AND H. E. WEAVER, JR.
Department of Physics, Stanford University, Stanford, California
(Received January 21, 1952)

NUCLEAR induction signals of Zn^{67} with a natural line width at half-maxima of about one gauss were detected in an approximately two molar solution containing the complex ion $Zn(NH_3)_4^{++}$. Signals were also observed in other solutions of Zn salts; e.g., $ZnCl_2$, $ZnSO_4$, and $ZnNO_3$. The resonant frequency was compared to that of N^{14} with the result

$$\nu(Zn^{67})/\nu(N^{14}) = 0.86580 \pm 0.00001. \quad (1)$$

Assuming the spin of Zn^{67} to be 5/2,[1] and with the known value of the magnetic moment of N^{14},[2] the sign and value of the magnetic moment was found to be

$$\mu(Zn^{67}) = +0.87378 \pm 0.00013. \quad (2)$$

No diamagnetic corrections were made in obtaining this value.

The earlier determination of $\mu(Zn^{67}) = +0.9$ by Lyshede and Rasmussen[3] is in agreement with the more precise value of Eq. (2).

The fact that signals of relatively narrow line width were obtained in solutions which did not contain additional paramagnetic ions may be an indication that the necessary relaxation mechanism was provided by the interaction of a relatively weak quadrupole moment of the Zn nucleus with the molecular field gradients.

Careful measurements were made of the signal amplitudes and line widths of Zn^{67} in $ZnSO_4$ and of H^1 in a 0.5-percent solution of D_2O in 8-molar $MnCl_2$. Saturation curves were taken for Zn^{67} in $ZnSO_4$ with the result that the longitudinal and transverse relaxation times were found to have approximately the same value. Applying the phenomenological equation[3] to this case, the spin of Zn^{67} was determined by comparing the obtained signals with those from H^1 and was found to be 2.2 with a standard error of 12 percent. Considering that the nearest other possible spins 3/2 and 7/2 are well outside the experimental value, this result represents a verification of a spin of 5/2[1] for the Zn^{67} nucleus.

The authors wish to express their thanks to Professor F. Bloch for his continued interest in their work.

* Assisted by the joint program of the ONR and AEC.
[1] J. M. Lyshede and E. Rasmussen, Z. Phys. **104**, 375 (1937); O. H. Arroe, Phys. Rev. **74**, 1263 (1948).
[2] W. G. Proctor and F. C. Yu, Phys. Rev. **81**, 20 (1948).
[3] F. Bloch, Phys. Rev. **70**, 460 (1946).

The Reaction $Li^6(t, p)Li^8$

C. D. Moak, W. M. Good, and W. E. Kunz
Oak Ridge National Laboratory, Oak Ridge, Tennessee
(Received January 16, 1952)

THE following reactions have been reported by Pepper, Allen, Almqvist, and Dewan[1] for Li^6 bombarded by tritons:

$$Li^6+H^3\rightarrow Be^{9*}$$

$$Be^{9*}\rightarrow He^4+He^4+n^1+16.03 \text{ Mev} \quad (1)$$

$$Be^{9*}\rightarrow Li^7+H^2+0.98 \text{ Mev} \quad (2)$$

$$Be^{9*}\rightarrow He^5+He^4+15.2 \text{ Mev}. \quad (3)$$

When Li^7 is bombarded by deuterons there is observed not only these same modes of breakup of Be^{9*}, but also the mode

$$Be^{9*}\rightarrow Li^8+H^1+0.80 \text{ Mev} \quad (4)$$

$$\hookrightarrow Be^{9*}+\beta^-+\nu+12.7 \text{ Mev}. \quad (4a)$$

For the sake of completeness it seems worth noting that by bombarding Li^6 with 350-kev tritons, we have confirmed that in this case also the Be^{9*} decays by proton emission to Li^8.

We have experimentally identified the $Li^6(t, p)Li^8$ reaction by observing the β^- rays in (4a) and showing that the half-life matches that of Li^8; in addition, the β^- rays were shown to have an energy end point greater than 10 Mev.

A triton beam of 5μa was accelerated to 350 kev in the Cockroft-Walton accelerator, and after mass analysis, was passed between two electrostatic deflector plates to a thick Li_2SO_4 target mounted on a 5-mil Al window. Directly under the window was a NaI—5819 scintillation-counter used to detect the β-rays. The electrostatic deflector plates were used to sweep the beam away from the vicinity of the target.

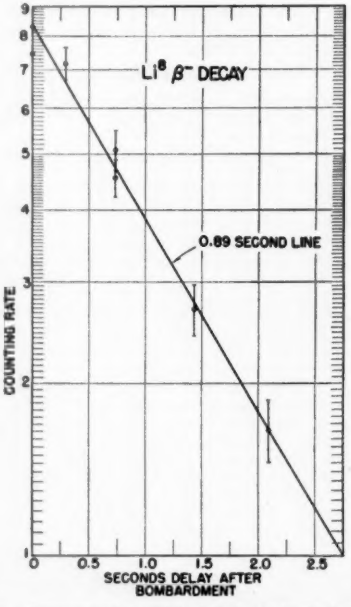

FIG. 1. Decay curve of the activity following the bombardment of Li^6 with tritons.

For the half-life measurement a master timer was used to control the following sequence of events: At $t=-5$ sec the beam was placed on the target; at $t=0$ the beam was swept away by the deflector; at $0\leqslant t\leqslant 3$ sec a scaler was turned on for 0.25 sec, then turned off; at $5=20$ sec the cycle was repeated. A clock was arranged to measure the total on-time of the scaler so that for a given run the same number of cycles was used for each setting of the time-delay after bombardment. A plot of the count rate *versus* the delay after bombardment is shown in Fig. 1.

As a check on the energy of the β-rays the scintillation counting equipment was biased so that pulses corresponding to a β-ray energy of less than 10 Mev were rejected. With this bias setting a β-ray counting rate five times background was still observed. Only three other β-emitters are known with energy end points above 10 Mev. They are:

B^{12}, 0.027 sec; N^{13}, 0.0125 sec; and N^{16}, 7.2 sec.

The accuracy of the half-life determination is sufficient to rule these out as possible contaminations in the experiment.

Identification of the activity is thus accomplished by observing a combination of β-ray energy and half-life found only in Li^8.

[1] Pepper, Allen, Almqvist, and Dewan, Phys. Rev. **81**, 315 (1951).

A Convergent *S*-Matrix Formalism with Correspondence to Ordinary Quantum Mechanics

P. Kristensen* and C. Møller*
Institute for Theoretical Physics, University of Copenhagen, Copenhagen, Denmark
(Received January 14, 1952)

IT has been known for a long time that at least an essential part of the divergences inherent in the usual quantum field theories are due to the use of the point particle picture of the elementary particles. Instead of taking the wave functions of the interacting fields at the same space-time point in the interaction Lagrangian, it has, therefore, repeatedly been proposed to introduce a form factor describing a kind of nonlocalized interaction of the fields.[1] A closer investigation shows, however, that the introduction of a form factor in a relativistically invariant formalism is not possible inside the frame of usual quantum mechanics. A consistent interpretation of a theory of this kind is possible only if one takes an attitude similar to that taken by Heisenberg in his *S*-matrix theory and thus gives up some of the requirements of ordinary quantum mechanics.

In a forthcoming paper[2] in the proceedings of the Danish Academy it is shown that a consistent theory of nucleons in interaction with meson fields can be developed along these lines. The theory allows one to determine the *S*-matrix for such systems and thus to calculate the cross sections for the various elementary processes. Of course the *S*-matrix calculated in this way will depend on the choice of the form factor. The arbitrariness hereby introduced is, however, considerably reduced by the correspondence requirement that the theory must comprise the ordinary quantum-mechanical description in the limit of slowly varying fields. It is shown that the form factor can be chosen in accordance with this requirement in such a way that the self-energies of the elementary particles are finite and small compared with the actual rest energies. Further, the polarization of the vacuum caused by an "external" meson field is investigated and found to be finite.

The correspondence to ordinary quantum mechanics also means that only high energy scattering cross sections are modified by the introduction of the form factor in the theory. In principle a comparison of the results of high energy scattering experiments with the cross sections following from the theory would permit an experimental determination of the form factor.

In the present theory a wider class of transformations—the quasi-canonical transformations—take over the role of the usual canonical transformations which retain their importance only in the limit of slowly varying fields where the conventional theory is valid. Following a proposal by Bloch[3] it is shown that the theory formally can be made gauge invariant in the sense that a gauge transformation is equivalent to a quasi-canonical transformation, which means that a gauge transformation has no effect on the physical predictions derived from the theory.

In the paper quoted above we have considered the consequences of the theory for scattering processes only. In a later paper we shall discuss the properties of composed systems of elementary particles on the basis of this theory. Since the introduction of the form factor effectively means a cutoff, it may be expected that we can avoid the difficulties which in the usual theory of nuclear forces arise from the strong singularities of the potentials.

* Temporarily at Università Degli Studi, Istituto de Fisica "Guglielmo Marconi," Rome, Italy.

[1] W. Pauli, *Handbuch der Physik* (Verlag Julian Springer, Berlin, 1933). Vol. XXIV, p. 271; W. Pauli, *Meson Theory of Nuclear Forces* (Interscience Publishers, Inc., New York, 1946), p. 11; H. McManus, Proc. Roy. Soc. (London) **A195**, 323 (1948); C. Bloch, Prog. Theor. Phys. **5**, 606 (1950). In an unpublished paper C. Bloch has shown that Yukawa's theory of non-local fields with certain restrictions is equivalent to a theory of this kind with a definite form factor. J. Rayski, Proc. Phys. Soc. (London) **A64**, 957 (1951).

[2] P. Kristensen and C. Møller, Kgl. Danske Videnskab. Selskal, Mat.-Fys. Medd. (to be published).

[3] C. Bloch, private communication. (See also a forthcoming paper in Kgl. Danske Videnskab. Selskag, Mat.-Fys. Medd.)

Scattering of 50-Mev Positive Pions by Helium*

A. M. Thorndike, E. C. Fowler, W. B. Fowler, and R. P. Shutt
Brookhaven National Laboratory, Upton, New York
(Received December 28, 1951)

POSITIVE pions of 50-Mev mean energy from the Columbia University Nevis Cyclotron[1] have been observed to undergo nuclear interactions in the gas of a diffusion cloud chamber filled with 15 atmos. of helium and methanol vapor. The procedure was similar to that previously reported.[2] 3400 pictures were taken in which 345 $\pi-\mu$ decays in flight were observed. From this figure the total pion path length is determined to be 935 g/cm² of helium.

A total of 15 interactions were observed, giving an interaction path length of 62 g/cm², or a cross section of 107 millibarns. The geometrical cross section is 150 millibarns. Other investigators have found cross sections approximately equal to geometrical for Li, Be, C, and heavier nuclei.[3-5] Our result is consistent with their work, showing that scattering events are observed reliably in the cloud chamber gas. The smallness of the cross section (3 millibarns) found for 60-Mev negative pions scattered by hydrogen in the diffusion chamber[6] cannot, therefore, be ascribed to a failure to observe the scattering events.

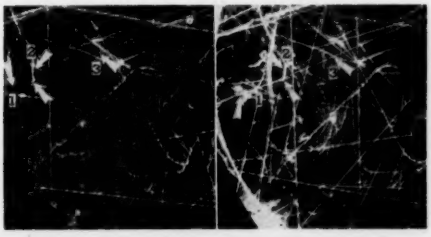

FIG. 1. Interaction of positive pion in helium-filled diffusion cloud chamber. It is probable that three protons and a neutron are emitted, of which protons 1 and 3 are of fairly high energy and in approximately opposite directions. One possible explanation is the absorption of the charge and energy of the pion by a proton-neutron pair. Arrows point to event and individual tracks.

FIG. 2. Interaction of positive pion in helium-filled diffusion cloud chamber, considered to be an elastic scattering. Tracks are coplanar. Angle and range of recoil particle are consistent with those expected for elastic scattering. Arrow points to event.

The interaction of pions with helium may, in principle, take the form of an absorption, elastic scattering, or inelastic scattering with or without charge exchange. Since the cloud chamber employed had no magnetic field, individual events could not always be so classified. Events with three emergent tracks must, however, involve absorption or inelastic scattering. There were 2 such events, one of which is shown in Fig. 1. Events with two emergent tracks may be considered to involve elastic scattering if the angles and lengths of the tracks are consistent with such an assumption. There were 9 such events, of which 5 were quite definitely identified as elastic scatterings. One of these is shown in Fig. 2. The meson scattering angles were 134°, 153°, 151°, 132°, and 125°. The four less definite cases have meson scattering angles of 65°, 15°, 23°, and 19°, being much harder to identify because of the short range of the recoil particle for forward scattering. The rather frequent backward scattering is worth noting; similar observations have been made in nuclear emulsions.[6] The remaining 4 events have two emergent tracks but do not appear to be elastic scatterings, and presumably involve absorption or inelastic scattering. While the number of events observed is small, it appears that elastic scatterings are fairly frequent in He, whereas stars have been observed to be the most common event in carbon.[3]

We are indebted to the Nevis Cyclotron staff for the opportunity to work there and for the generous cooperation of members of the staff and operating crew.

* Work done at Brookhaven National Laboratory under the auspices of the AEC.

‡ Supported jointly by the ONR and AEC.

[3] Shutt, Fowler, Miller, Thorndike, and Fowler, Phys. Rev. **84**, 1247 (1951).

[4] Chedester, Isaacs, Sachs, and Steinberger, Phys. Rev. **82**, 958 (1951).

[5] Camac, Corson, Littauer, Shapiro, Silverman, Wilson, and Woodward, Phys. Rev. **82**, 745 (1951).

[6] Byfield, Kessler, and Lederman, Bull. Am. Phys. Soc. **26**, No. 6, 22 (1951).

[6] Bernardini, Booth, and Lederman, Phys. Rev. **83**, 1277 (1951).

Limits of Isotopic Abundance for Hafnium and Platinum

H. E. Duckworth,* R. F. Woodcock,† G. S. Stanford,‡ A. Coutu, and R. L. Stearns‡
Wesleyan University, Middletown, Connecticut
(Received January 10, 1952)

SOME time ago the Research Corporation made a grant to one of us (H.E.D.) to study the problem of chemical analysis of solids by means of the mass spectrograph. With a portion of this

TABLE I. Limits of isotopic abundance for hafnium and platinum.

Nuclide	Limit of abundance (%)
Hf^{170}, Hf^{171}	0.004
Hf^{173}, Hf^{176}	0.005
Hf^{178}	0.006
Pt^{198}, Pt^{199}	0.002
Pt^{191}	0.004
Pt^{198}	0.009
Pt^{197}	0.010
Pt^{199}	0.008
Pt^{200}	0.007

grant a Dempster-type double-focusing instrument was constructed,[1] but it soon became clear that this apparatus would need to be modified before it would be suitable for use in this work. However, in the process of ascertaining the limitations of the instrument, the two elements hafnium and platinum were examined with a view to setting limits of abundance for certain hypothetical stable isotopes. These limits are listed in Table I.

In this work the abundance of Hf^{174} was assumed[2] to be 0.18 percent and that[3] of Pt^{190}, 0.012 percent. The suggestion to examine hafnium[4] was made to us by M. L. Pool.

The senior author greatly appreciates the generous support of this work by the Research Corporation and regrets that events have so transpired that he has been prevented from continuing the project for which the grant was made.

* Now at McMaster University, Hamilton, Ontario, Canada.
† Now at Brown University, Providence, Rhode Island.
‡ Now at Yale University, New Haven, Connecticut.
§ Now at Case Institute of Technology, Cleveland, Ohio.

[1] R. F. Woodcock, M. A. thesis, Wesleyan University, 1950 (unpublished).
[2] J. Mattauch and H. Ewald, Naturwiss. **31**, 487 (1943).
[3] W. T. Leland, Phys. Rev. **76**, 922 (1949).
[4] We are indebted to Mr. E. B. Meservey for securing the hafnium wire used in these experiments.

Interactions of Remote Impurity Centers in Phosphors

H. W. LEVERENZ AND D. O. NORTH
Radio Corporation of America, RCA Laboratories Division, Princeton, New Jersey
(Received January 14, 1952)

EVIDENCE is presented here which indicates that luminescence centers formed by manganese impurity atoms (ions) in rbhdl.$-Zn_2SiO_4$:Mn interact over several interatomic spacings. The interactions apparently can decrease the thermal activation energy for making nonradiative transitions from the excited state, without greatly affecting the energy difference (spectrum) of radiative transitions.

In the phosphor system symbolized by rbhdl.$-Zn_2SiO_4$:Mn, luminescence centers are produced by Mn activator atoms (ions) which occupy Zn sites substitutionally.[1] Variation of the proportion of manganese atoms N_{Mn} from about 0.001 to 10 percent of the number of Zn sites has a little effect on the spectrum of radiative transitions. This is evidenced by the relative invariance of the emission band peaked near 5250A.[2]

Variation of the Mn content, however, strongly influences the nonradiative transitions. This is indicated in Fig. 1 by concomitant changes in the decay time τ (at 25°C) of the nearly simple exponential decay of emission,[3] and the temperature breakpoint T_B (the operating temperature beyond which luminescence efficiency decreases rapidly).[4] These characteristics are related by

$$\tau=[a+\nu\exp(-\Delta E/kT)]^{-1},$$

where a is the temperature-independent constant for the radiative process, ν is a frequency factor, and ΔE is the thermal activation energy for making nonradiative transitions.[5] When $T=T_B$, the nonradiative Boltzmann term is appreciable relative to a.

As shown in the figure, luminescence efficiency $\mathcal{E}$ (at 25°C) also decreases rapidly beyond $N_{Mn}\approx 1$.[6] (The maximum luminescence output from this system, with intense excitation, occurs for N_{Mn} somewhat greater than 1; i.e., when $\mathcal{E}$, T_B, and τ are all less than their maximum values.) The decline of $\mathcal{E}$ and maxima output can be correlated with the similar variation of τ and T_B by assuming that ΔE decreases with decreasing distance between centers. This behavior is readily described with a conventional energy *vs* configurational-coordinate (x) diagram which shows the localized radiative transition occurring at small values of x and the nonradiative transition occurring at large values of x.[7] The nonradiative transition, then, is more easily affected by a neighboring perturbation, such as another center.

Some insight into the constitutions of the luminescence centers may be obtained from a comparison of the foregoing curves with plots of the probability P of occurrence of isolated pairs of Mn atoms P_2, and isolated single Mn atoms PC_1 (assuming a random distribution of Mn's over Zn sites).[8] As may be seen in the figure, the curves P_2 and PC_1 do not decrease rapidly until $N_{Mn}\simeq 10$; i.e., well above the region where T_B, τ, and $\mathcal{E}$ decrease rapidly. These comparisons indicate that (1) groups of two or more Mn atoms are not important as luminescence centers, in contradiction to

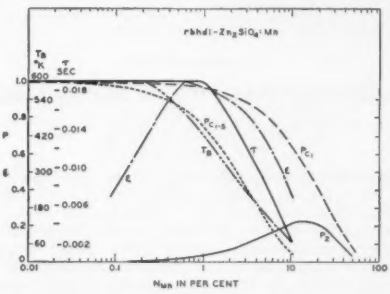

FIG. 1. Temperature breakpoint T_B of photoluminescence, decay time constant τ, and efficiency $\mathcal{E}$ of cathodo-luminescence, and probabilities of occurrence of (1) isolated pairs of Mn atoms P_2, (2) simple isolated Mn atoms PC_1, and (3) isolated Mn atoms without other Mn atoms in the 28 nearest available sites PC_{1-5}, as a function of the proportion of Mn in rbhdl.$-Zn_2SiO_4$:Mn.

hypotheses about clusters of activator atoms,[9] and (2) Mn atoms which have simply no nearest like neighbors (PC_1 at high values of N_{Mn}) may be operative as luminescence centers, but they probably have low values of ΔE which lead to small τ, T_B, and $\mathcal{E}$ as previously outlined.

A rough indication of the minimum remoteness for noninteracting centers was obtained by calculating and plotting the probability of occurrence of Mn atoms having no other Mn atoms anywhere in the five classes of nearest neighbors (C_{1-5}) comprising 28 Zn sites. A plot of this probability

$$PC_{1-5}=(1-0.01N_{Mn})^{28}$$

is shown in the figure. The apparent coincidence of curve PC_{1-5} with curve T_B is probably not of quantitative significance, but the rapid decrease of PC_{1-5} in the same region as T_B and τ suggests that centers of this class represent roughly the degree of isolation required for efficient luminescence.

Such centers, without any other Mn atoms in the nearest 28 available sites, may still be only 12A apart, or less, even when the distance is calculated through intervening atoms. It seems reasonable to expect interaction over such small distances, and it is probable that appreciable interaction occurs over much larger

distances, especially in ZnS-type phosphors where the optimum activator proportion is about 0.01 percent.

[1] Jenkins, McKeag, and Rooksby, Nature **143**, 978 (1939).
[2] H. W. Leverenz and F. Seitz, J. Appl. Phys. **10**, 490 (1939).
[3] J. W. Strange and S. T. Henderson, Proc. Phys. Soc. (London) **58**, Part 4, 378 (1946).
[4] G. R. Fonda and C. Zener, cited by R. P. Johnson, Am. J. Phys. **8**, 150 (1940).
[5] F. A. Kröger *et al.*, Physica **14**, 81, 425 (1948); see reference 6, p. 265.
[6] H. W. Leverenz, *An Introduction to Luminescence of Solids* (John Wiley and Sons, Inc., New York, 1950), Fig. 97, p. 330.
[7] Reference 6, Fig. 16b, p. 132.
[8] By *isolated* it is meant that there are no other Mn atoms in the six nearest Zn sites around a pair of Mn atoms, and none in the four nearest sites around a single Mn atom (see reference 6, Fig. 142, p. 478).
[9] F. A. Kröger and P. Zalm, J. Electrochem. Soc. **98**, 177 (1951); see J. H. Schulman, J. Electrochem. Soc. **98**, 519 (1951).

The Stopping Power of a Metal for Charged Particles

DAVID PINES
Randal Morgan Laboratory of Physics, University of Pennsylvania, Philadelphia, Pennsylvania
(Received January 15, 1952)

THE collective description of electron interactions[1,2] has been applied to the determination of the contribution of the conduction electrons in a metal to its stopping power for a fast nonrelativistic charged particle. This contribution is strongly influenced by the mutual interaction of the conduction electrons. The resulting polarization effect has been treated by Kramers,[3] who used a macroscopic description in which the electrons were treated as a continuum characterized by an effective dielectric constant, and by A. Bohr[4] who gave a microscopic description of certain aspects of the problem. With the aid of the collective description it is possible to obtain a somewhat more accurate expression for the stopping power of the metal, and, in addition, to obtain a more detailed understanding of the physical processes involved.

The conduction electrons are treated as a gas of point electrons embedded in a medium of uniform positive charge, and only the electron-electron interactions are here considered.[5] The interaction between the charged particle and the conduction electrons is analyzed by a classical calculation of the response of the density (or charge) fluctuations of this electron gas to the field of the charged particle. As shown in reference 2, these density fluctuations may be split into two components. One component is associated with organized longitudinal oscillations of the electron gas as a whole, the so-called "plasma" oscillations, which come about as a consequence of the electron-electron interactions. The frequency of these oscillations satisfies the following approximate dispersion relation:

$$\omega^2=\omega_p^2+k^2\langle V^2\rangle_{\text{Av}}, \tag{1}$$

where $\omega_p^2=4\pi ne^2/m$, k is the wave number of the oscillations, and n, m, and $\langle V^2\rangle_{\text{Av}}$ represent respectively the density, mass, and mean square velocity of the conduction electrons. This collective component describes in a natural way the effects of the long range of the electron interactions, and thus the polarization effects in the electron gas. However, due to the random kinetic motion of the individual electrons, the density fluctuations lose their collective behavior above a certain critical wave number k_0. Thus the density fluctuation also possesses an individual particles component, which is associated with the random kinetic motion of the electrons, shows no collective behavior, and may be treated independently of the collective component.

On this picture, the fast charged particle gives up energy to the conduction electrons in two distinct ways. Its long-range Coulomb interaction with the electrons, which may here be described by the collective part of the density fluctuations, results in the excitation of collective oscillations in the form of a wake trailing the particle. This phenomena resembles closely the Čerenkov radiation produced by fast electrons in a dielectric. The energy loss to the collective oscillations is obtained by calculating the reaction of this wake at the position of the particle. By a straightforward extension of the methods developed in reference 2, the energy loss per unit length to the collective oscillations is found to be

$$\left(\frac{dT}{dx}\right)^{(1)}=\frac{\pi nZ^2e^4}{E_0}\ln\left\{\frac{k_0^2[V_F^2-\langle V^2\rangle_{\text{Av}}]}{\omega_p^2}\right\}, \tag{2}$$

where Ze represents the charge of the fast particle, E_0 its energy, and V_0 its speed,[6] which is taken to be $>V_F$, the speed of an electron at the top of the Fermi distribution. The response of the individual particles components of the density fluctuations to the field of the charged particle may be described in terms of short-range collisions between the particle and individual electrons. For the individual particles component represents a collection of individual electrons surrounded by co-moving clouds of charge which screen the electron fields within a distance of $\sim(1/k_0)$.[3] Thus the interaction between the charged particle and the individual electrons may be characterized by a screened Coulomb force of range $1/k_0$. The energy transfer in these short-range collisions may be calculated on the basis of the usual collision theory, and one obtains, for a classical calculation,

$$(dT/dx)^{(2)}=(2\pi nZ^2e^4/E_0)\ln(1.123/k_0b), \tag{3}$$

where b is the minimum impact parameter involved in the collision. (With a suitable choice of b, Eq. (3) also is correct for the appropriate quantum-mechanical calculation.[7])

The total energy loss to the conduction electrons is thus the sum of that expended in the excitation of collective oscillations and that lost in short-range collisions with the individual electrons. We obtain for the total energy loss per unit distance to the conduction electrons,

$$\frac{dT}{dx}=\frac{2\pi nZ^2e^4}{E_0}\ln\left\{\frac{1.123V_0}{\omega_pb}\left[1-\frac{\langle V^2\rangle_{\text{Av}}}{V_0^2}\right]^{\frac{1}{2}}\right\}. \tag{4}$$

Our Eq. (4) differs from the results obtained by Kramers and A. Bohr in the factor $[1-\langle V^2\rangle_{\text{Av}}/V_0^2]^{\frac{1}{2}}$ under the logarithm, which arose from our consideration of the dependence of the dispersion relation, Eq. (1) on the kinetic energy of the conduction electrons. This correction is comparatively small; e.g., for a 1-Mev alpha-particle incident on Be it leads to an increase in the effective average ionization potential of ~5 percent.

It is not expected that a quantum-mechanical description of the density fluctuations will alter the foregoing result appreciably, inasmuch as the dispersion relation is essentially unchanged, and though the cut-off wave number k_0 is somewhat changed from its classical value, this quantity cancels out in our final result.

[1] D. Bohm and D. Pines, Phys. Rev. **82**, 625 (1951).
[2] D. Pines and D. Bohm, Phys. Rev. **85**, 338 (1952).
[3] H. A. Kramers, Physica **13**, 401 (1947).
[4] A. Bohr, Kgl. Danske Videnskab. Selskab, Mat.-fys Medd. **24**, No. 19 (1948).
[5] The corrections due to the bending of the electrons in the lattice and the resistance of the metal are small (~5 percent) for Li and Be, the only metals for which the contribution of the conduction electrons to the stopping power is appreciable. See A. Bohr, reference 4.
[6] In obtaining Eq. (2), we have chosen as the maximum component of the collective oscillation wave vector perpendicular to V_0 a more accurate value than that used in reference 2, *viz.*, $\{k_0^2[1-(\langle V^2\rangle_{\text{Av}}/V_0^2)]-\omega_p/V_0^2\}^{\frac{1}{2}}$.
[7] See N. Bohr, Kgl. Danske Videnskab. Selskab, Mat.-fys. Medd. **18**, No. 8 (1948).

Capture Gamma-Rays from 277-Kev Protons on N^{14}

C. H. JOHNSON, G. P. ROBINSON, AND C. D. MOAK
Oak Ridge National Laboratory, Oak Ridge, Tennessee
(Received January 16, 1952)

THE γ-ray spectrum has been observed for the resonant capture of 277-kev protons by N^{14}. For such protons the only energetically permitted interactions with nitrogen are scattering or capture; thus, an observation of the spectrum yields rather definite information on the compound nucleus O^{15}. In addition a knowledge of the spectrum is useful since nitrogen is often a target contaminant.

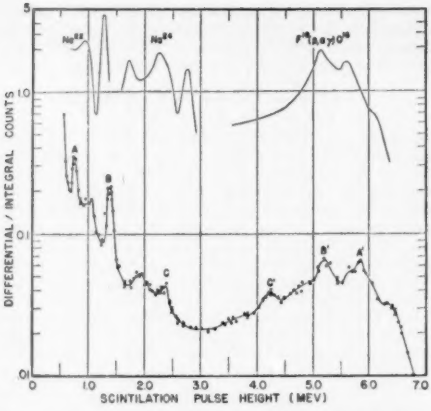

FIG. 1. Scintillation pulse-height spectrum (lower curve) for γ-rays produced by 277-kev protons on N^{14}. The ratio of differential to integral counts is plotted as a function of pulse height in Mev. Standard deviations of all data points are five percent and are indicated for scattering points on the curve. In the upper part of the figure is shown the pulse-height distributions for γ-rays from Na^{22} and Na^{24} and γ-rays from 340-kev protons on F^{19}.

An analyzed proton beam of from 200 to 400 μa from the Cockcroft-Walton generator impinged on a thick TaN target which had been formed by inductively heating a tantalum disk in a nitrogen atmosphere. Gamma-rays were detected by a NaI(Tl) crystal 2 inches long and 1.5 inches in diameter placed at 0° with respect to the proton beam. Scintillations were detected and analyzed by a 5819 photomultiplier, linear amplifier, and a single-channel analyzer.

A thick target yield curve showed a rise near 277 kev in agreement with the $N^{14}(p,\gamma)O^{15}$ resonance observed by Tangen.[1] The proton energy was set about 10 kev above the resonance and the pulse-height distribution in the lower part of Fig. 1 was obtained. Energy calibrations were made using γ-rays from Cs^{137} (0.661 Mev),[2] Na^{22} (1.277 Mev),[3] Na^{24} (2.755 Mev),[4] and the 6.13 Mev[5] γ-ray from 340-kev protons on F^{19}. To aid in the interpretation of the nitrogen spectrum the pulse-height distributions of the various calibration γ-rays is shown in the upper part of Fig. 1. Radiations from Na^{22} and Na^{24} produce photoelectric peaks at the γ-ray energies accompanied by Compton peaks at slightly lower energies. Na^{24} also exhibits a pair group 1.02 Mev below the γ-ray energy. A comparison with the nitroben spectrum indicates that groups B and C of Fig. 1 are photoelectric peaks accompanied in each case by a Compton group of slightly lower energy. Pairs associated with C contribute very little to the peak at B. Peak A is also a photoelectric peak whose Compton group is buried in the background.

In the higher energy region pair production predominates to give a pulse-height distribution which is illustrated by the $F^{19}(p,\alpha\gamma)O^{16}$ spectrum shown in the upper part of Fig. 1. The single γ-ray produces a triple peak by the following process. A part (1.02 Mev) of the γ-ray energy is used for pair production and reappears as annihilation radiation at the end of the positron track. Since the annihilation radiation usually escapes the crystal, the most prominent group of pulses is 1.02 Mev below the γ-ray energy. Occasionally one or both 0.51-Mev annihilation radiations are captured in the crystal so that the observed distribution shows subsidiary peaks 0.51 Mev and 1.02 Mev above the main group.

A comparison of the nitrogen and fluorine distributions indicates that groups A', B', and C' are pair peaks each 1.02 Mev below their γ-ray energies. A subsidiary peak associated with A' is clearly resolved, and there is some indication of subsidiary peaks above B' and C'. Thus the pulse-height distribution of Fig. 1 results from six γ-rays designated as A, B, C, C', B', A', whose energies are 0.75 ± 0.03, 1.39 ± 0.03, 2.38 ± 0.10, 5.29 ± 0.10, 6.21 ± 0.10, and 6.84 ± 0.10 Mev, respectively.

Gamma-rays from protons on nitrogen can arise only from capture followed by positron decay to N^{13}. Positron decay could leave N^{13} with up to 1.68-Mev excitation; however, since the observed positron spectrum is apparently not complex[6] and since no low-lying states are known in N^{13},[7] it is assumed the decay occurs to the ground state and all γ-rays result from direct capture. According to recent mass values,[8] 277-kev protons on N^{14} form O^{15} with 7.60-Mev excitation energy. The six γ-rays contributing to the distribution of Fig. 1 can be attributed to proton capture by nitrogen only if there are three intermediate levels in O^{15} giving rise to three cascade processes of two γ-rays each. These cascade groups are AA', BB', and CC', and their energies add to the total excitation as follows:

$$A+A'=0.75+6.84=7.59\pm0.13 \text{ Mev}$$
$$B+B'=1.39+6.21=7.60\pm0.13 \text{ Mev}$$
$$C+C'=2.38+5.29=7.67\pm0.20 \text{ Mev}.$$

The strongest groups B and B' must certainly be assigned to nitrogen since the integral yield curve shows the 277-kev resonance. The weaker groups (A, A', C, and C') could possibly be attributed to target contaminants; however, the fact that they can be arranged in cascade groups in the above manner is strong evidence that all observed γ-rays come from nitrogen. No direct transition to the ground state was found.

[1] R. Tangen, Kgl. Norske Videnskab. Selskabs. Skr. No. 1 (1946).
[2] L. M. Langer and R. D. Moffat, Phys. Rev. **78**, 74 (1950).
[3] D. E. Alburger, Phys. Rev. **76**, 435 (1949).
[4] J. L. Wolfson, Phys. Rev. **78**, 176 (1950).
[5] R. L. Walker and B. D. McDaniel, Phys. Rev. **74**, 315 (1948).
[6] H. Brown and V. Perez-Mendez, Phys. Rev. **78**, 649 (1950).
[7] Hornyak, Lauritsen, Morrison, and Fowler, Revs. Modern Phys. **22**, 291 (1950).
[8] Li, Whaling, Fowler, and Lauritsen, Phys. Rev. **83**, 512 (1951).

Extremely High Energy Nuclear Interactions*

M. F. KAPLON AND D. M. RITSON
University of Rochester, Rochester, New York
(Received December 26, 1951)

BY utilizing the technique of an "emulsion cloud chamber" to select high energy events[1] we have studied the angular distribution, multiplicity of penetrating particles, and ratio of

TABLE I. Summary of data.

(1) Shower and primary	(2) Number of charged particles (N_{ch})	(3) $\frac{N_{\pi^0}}{N_{ch}}$	(4) $\gamma\times10^{-3}$	(5) X	(6) $\frac{r}{R}$	(7) N_{ch} (Fermi)[b]
$A(\alpha)$	21(84)	0.6 ± 0.2	3	1.17	0.18	15
$178(\alpha)$	23(92)	0.72 ± 0.15	6	2	0.46	14
$R(\alpha)$[a]	14(56)	0.75 ± 0.25	0.48	2.33	0.57	6.6
$77(p)$	24	···	4	1.17	0.18	16.5
$104(p)$	20	0.5 ± 0.3	1.3	1.33	0.23	11.7
$67(p,\pi)$	9	1.2 ± 0.5	4.5	1.33	0.23	16
$60(p,\pi)$	26	···	19.5	1.33	0.23	23
$91(p,\pi)$	16	0.6 ± 0.35	1.3	1.7	0.34	10.8
$17(p)$	24	1.1 ± 0.3	5.1	3.7	0.76	7.9
$59(p)$	24	0.5 ± 0.3	8.9	4	0.78	8.8
$66(p,\pi)$	11	0.75 ± 0.4	0.64	6.67	0.87	2.7
$T(p)$	36	0.6 ± 0.2	19.4	6.67	0.87	6.3
$Z(p,\pi)$	15	0.5 ± 0.25	50	24	~1	≤3.4
$S(p)$[d]	15	···	32	···	~1	≤6
$G-L(p)$[e]	18	···	23	≥9	~1	≤6
		Av. 0.71 ± 0.3				

[a] This ratio is not corrected for secondary nuclear interactions. An approximate estimate for this indicates that the observed ratio can be lowered by as much as 30 percent. The correction will vary for each individual shower.
[b] See reference 4.
[c] Kaplon, Peters, and Bradt, Phys. Rev. **76**, 1735 (1949).
[d] See reference 6.
[e] See reference 7.

neutral mesons to charged particles produced by collisions of cosmic-ray nucleons and α-particles with nuclei of copper. The techniques involved are described in reference 1. The energy per nucleon of the primary causing the event is usually estimated by the kinematical considerations of reference 1. Despite the energy being estimated on the single nucleon-nucleon assumption, in those cases where an accurate check is available by the energy balance method of reference 1, the two methods give agreement within statistical limits.

Table I summarizes the relevant data on the events completely or partially analyzed thus far. Column 1 designates the shower and the incident particle causing the shower (it is not possible in every instance to uniquely determine the primary, but we can be certain that it has either a charge of 0 or 1, or its charge is definitely >1). Column 2 gives the observed charged particle multiplicity per incident nucleon in the initial interaction and column 3 the ratio of neutral π-mesons to charged particles.[2] Column 4 gives the energy per nucleon in the laboratory system (γ) of the primary in units of the nucleon rest mass. Column 5 gives the observed value of the quantity $X=x/x_I$, where $x=\theta_{3/4}/\theta_{1/4}$ is the ratio of the laboratory angles containing a fraction $\frac{3}{4}$ and $\frac{1}{4}$ of the charged particles; x_I is the same ratio for a theoretical multiple process with an isotropic distribution in the center-of-mass system (c.m.) of 2 nucleons. Column 6 gives the impact parameter r/R for the shower corresponding to the Fermi theory,[3] and column 7 gives the charged meson multiplicity as determined from Fermi's theory[4] for a single nucleon-nucleon collision corresponding to an energy of the incident nucleon $E=\gamma mc^2$ and the impact parameter given in column 6.

An examination of column 5 reveals a distribution in values for the quantity X. In a nucleon-nucleon collision isotropic in the c.m. system one should find $X=1$, whereas for nonisotropic distributions in the c.m. system (e.g., such as predicted by the Fermi theory), X should show large deviations from the value 1. As the interactions occur in brass, the showers we observe must in most cases result from successive collisions inside the nuclei.

Such showers resulting from several collisions, each with different impact parameters, would be expected to show on the average similar angular distributions characterized by some average impact parameter. This behavior is not observed for single nucleon produced showers but is observed for α-particle showers, which from their multiplicities appear to involve the interaction of four separate nucleons. The three α-particle showers observed all have similar angular distributions characteristic of some average impact parameter.

We believe this is an indication that at high energies a nucleon-nucleus collision exhibits similar properties to a nucleon-nucleon collision. Multiple production of particles results from the first nucleon-nucleon interaction. These particles than all interact together in any successive collisions inside the nucleus.[5] This is consistent with the Fermi picture and results from the view that at extremely high energies a nucleon interacts in a similar manner whether it is accompanied by a real or virtual group of particles. If this is correct a characteristic impact parameter for a nucleon-nucleus collision is defined by the last target nucleon struck in the nucleus; the multiplicity should be near to that of a pure nucleon-nucleon collision.

On the basis of the foregoing assumptions the observed charged particle multiplicity is compared with that calculated from the Fermi theory (column 7). We note that the agreement is best for low impact parameters but is worse at high impact parameters. It would appear that the idea of impact parameter has meaning in describing the angular distributions in these interactions but that the multiplicity is not a strong function of impact parameter. Independent evidence for the view that a single nucleon-nucleon collision and a nucleon-nucleus collision give the same results at high energy is provided by the similarity of the S-star[6] (which resulted from a nucleon-nucleon collision), the Gerosa and Levi-Setti star[7] (formed in AgBr), and our stars of high impact parameters.[8]

The observed large ratio of neutral π-mesons to charged particles implies within the context of the Fermi theory a relatively small contribution of nucleon-antinucleon pair production as compared to π-meson production in this energy band.

We have also made approximate kinematical estimates of the energy of the showers given by Pickup and Voyvodic[9] (energies of the order of 10^{11} ev) and, by comparing their median energy and multiplicity with that derived from our data, find that the multiplicity of meson production varies as $\gamma^{\frac{1}{4}}$, which is in agreement with the predictions of the Fermi theory.

* This work was supported by the AEC.

[1] Kaplon, Peters, and Ritson, Phys. Rev. **85**, 900 (1952).

[2] We assume that the soft component of mixed showers in its early stages arises exclusively from the 2-photon decay of the neutral π-meson. See R. E. Marshak, Phys. Rev. **74**, 1735 (1949).

[3] E. Fermi, Phys. Rev. **81**, 683 (1951).

[4] The charged particle multiplicity is calculated on the basis of Fermi's theory assuming only π-mesons are produced. If one also allows for the production of nucleon-antinucleon pairs, the calculated charge multiplicity is changed by the same factor (0.985) for each shower independent of the impact parameter.

[5] One can easily show that the c.m. system defined by an assemblage of particles produced by a nucleon of energy $E=\gamma mc^2$ with a nucleon at rest is identical to that formed by the incident nucleon ($E=\gamma mc^2$) and a nucleon at rest.

[6] Lord, Fainberg, and Schein, Phys. Rev. **80**, 970 (1950).

[7] A. Gerosa and P. Levi-Setti, Nuovo cimento **8**, 601 (1951).

[8] A further test of this hypothesis is possible with observations on energetic showers made in a very heavy nucleus such as Pb. Such an experiment is now being planned.

[9] E. Pickup and L. Voyvodic, Phys. Rev. **82**, 265 (1951).

Primary Flux of High Energy Protons and α-Particles*

M. F. Kaplon, D. M. Ritson, and Edythe P. Woodruff
University of Rochester, Rochester, New York
(Received December 26, 1951)

MEASUREMENTS utilizing the emulsion cloud-chamber technique described in the previous letter have been used to obtain flux values in the 10^{12}–10^{13}-ev region.

70 cm^2 of emulsion halfway down in the "cloud chamber" were systematically scanned for all showers crossing the emulsion; a total of fifty-six such showers were found. Many of these showers could only be followed for a short distance and then become too diffuse to follow further. These showers must have come largely from low energy interactions of the order of 10^{11} ev. (Showers with a γ-ray in excess of 3×10^{11} ev can be followed through the entire stack.)

To obtain flux values it was necessary to eliminate those showers which were detected with a low and unknown efficiency. The condition was imposed that all showers must contain at least one secondary electron shower with an energy greater than 3×10^{11} ev. This left a total of fourteen showers. Detailed examination of these events showed that six were γ-ray induced and eight caused by nuclear interactions. The median energy of these eight events estimated from kinematic considerations was 4.5×10^{12} ev. (We can arrive at an independent estimate from our requirement of one secondary electron shower whose energy is in excess of 3×10^{11} ev; we infer from this a median energy of $\sim3\times10^{12}$ ev.) In all these eight cases the primary had a charge $Z\leq1$.

Using an absorption mean free path for nucleons in air of 100 g/cm^2 and a geometric interaction mean free path in the stack, we evaluate the integral primary flux with energy greater than 4.5×10^{12} ev as 0.04 particles per meter^2 per sterad per sec at the top of the atmosphere assuming an isotropic flux. On the assumption of a power law for the integral primary spectrum we find an exponent of 1.45 ± 0.15 using the known values at low energies.[1] The error takes into account the uncertainty of the median energy which we consider to be of the order of 2.

In a less systematic survey of an additional 70 cm^2 we have found two α-particle induced showers with energies per nucleon in the same range as the proton induced showers. It therefore appears

that α-particles constitute about 10 percent of the primary flux and that accordingly the ratio of α-particles to protons remains relatively constant over a large energy range. This seems to be in agreement with results previously reported,[2] which indicate a similar velocity spectrum for all components of the primary beam, and is not in agreement with the predictions of the simple Fermi[3] theory of acceleration of cosmic-ray primaries.

* This research was assisted by the AEC.
[1] Winckler, Stix, Dwight, and Sabin, Phys. Rev. **79**, 656 (1950).
[2] Kaplon, Peters, and Ritson, Phys. Rev. **85**, 900 (1952).
[3] E. Fermi, Phys. Rev. **75**, 1169 (1949). For an integral energy spectrum varying as $N=K/\epsilon^{\gamma}$, where ϵ is the kinetic energy in Bev/nucleon, Fermi gives $\gamma_p/\gamma_\alpha=\lambda_\alpha/\lambda_p$, where λ is the absorption mean free path. As $\lambda_\alpha\approx\frac{1}{4}\lambda_p$, we find $N_p/N_\alpha=(K_p/K_\alpha)\epsilon^{\gamma}$. For the energy region of this experiment one obtains $N_p/N_\alpha\approx 8\times10^2$; $(K_p/K_\alpha\gtrsim 5)$. We believe therefore that our results are significant, notwithstanding the poor statistics.

Neutrons and Gamma-Rays from the Proton Bombardment of Beryllium

T. M. Hahn,* C. W. Snyder, H. B. Willard, J. K. Bair, E. D. Klema, J. D. Kington, and F. P. Green
Oak Ridge National Laboratory, Oak Ridge, Tennessee
(Received December 26, 1951)

THE neutron and gamma-ray yields in the forward direction resulting from the proton bombardment of beryllium have been extended to a maximum proton energy of 5.3 Mev. Voltage calibration of the electrostatic generator has been previously discussed.[1] Targets were thin (approximately 11 kev at threshold) foils obtained through the courtesy of Dr. Hugh Bradner. Neutron yields were measured with a "long" counter placed in the forward direction. Gamma-rays were detected with a large sodium iodide crystal also located along the beam axis. Pulses from the crystal were amplified and fed into two discriminators so that the yields of gamma-rays above approximately 2 and 6 Mev were obtained.

The upper curve of Fig. 1 shows a typical neutron yield. In addition to the geometrical peak and the well-known rise at 2.56 Mev,[2] a third peak is obtained at a proton energy of 4.7 Mev. The existence of a level at high energy had been predicted from work done at the University of Wisconsin.[3] A run, not shown, using a low energy neutron counter similar to that described by Bonner and Butler[4] showed no obvious levels in the residual B^9 nucleus between 2- and 5.3-Mev proton energy.

The middle and lower curves of Fig. 1 show the yield of gamma-rays with energy greater than approximately 6 Mev and 2 Mev, respectively. The level at 2.57-Mev proton energy is observed in both the high and low energy gamma-ray yields. The level at 4.7 Mev does not appear in the low energy yield due to the relatively high intensity of the nonresonant, low energy gammas.

The gamma-ray yield curves are, in this particular case, essentially free of interferences from neutron reactions occurring in the NaI crystal. This is indicated by the considerably narrower resonance in the gamma-ray yield at 2.56 Mev as compared with the corresponding one in the neutron yield. Boron layers placed between the target and the crystal confirmed this hypothesis.

The new level occurs at a proton bombarding energy of 4.72 $\pm$0.01 Mev and has a full width at half-maximum of approximately 0.5 Mev. We find the lower energy level at 2.57$\pm$0.01 Mev. These energies are the averages obtained from several runs.

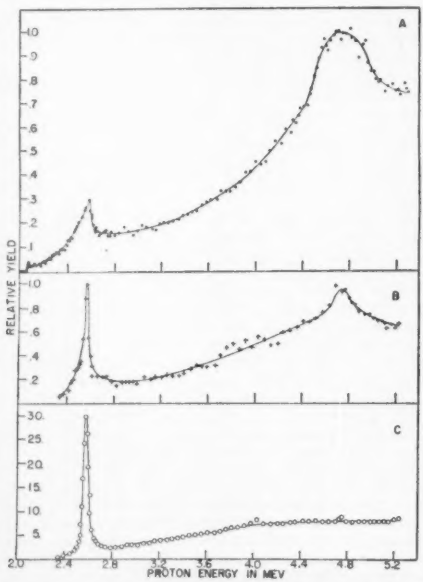

FIG. 1. Yield curves for neutrons and gamma-rays from beryllium bombarded by protons. Top curve, neutron yield; middle curve, gamma-rays of energy greater than approximately 6 Mev; lower curve, gamma-rays of energy greater than approximately 2 Mev. All yields are in arbitrary units.

* Summer research participant on leave from the University of Kentucky.
[1] Willard, Bair, Kington, Hahn, Snyder, and Green, Phys. Rev. **85**, 849 (1952).
[2] W. J. Hushley, Phys. Rev. **67**, 34 (1945); Richards, Smith, and Browne, Phys. Rev. **80**, 524 (1950).
[3] Richards, Laubenstein, Johnson, Ajzenberg, and Browne, Phys. Rev. **81**, 316 (1951).
[4] T. W. Bonner and J. W. Butler, Phys. Rev. **83**, 1091 (1951).

Total Cross Sections of Negative Pions in Hydrogen*

H. L. Anderson, E. Fermi, E. A. Long,†
R. Martin,‡ and D. E. Nagle
Institute for Nuclear Studies, University of Chicago, Chicago, Illinois
(Received January 21, 1952)

THE interaction of negative pions and protons has been investigated by Steinberger and co-workers[1] for pions of 85-Mev energy by transmission measurements and by Shutt and co-workers[2] for pions of 55 Mev by direct observation of pion tracks in a Wilson chamber. Both measurements indicate a surprisingly low value for the cross section in this range of energies. We have undertaken to extend the total cross section measurements to higher energies.

The negative pions are produced in the large Chicago cyclotron by protons of 450 Mev striking a target which in some of the experiments was copper and in others beryllium. The negative pions are bent in the fringing field of the cyclotron and enter channels in a 6-foot steel shield which separates the cyclotron from the experimental room where the measurements are taken. Further monochromatization and purification of the pion beams are carried out by a deflecting magnet located in the experimental room. In this manner one obtains a sharply collimated beam containing pions with energy defined within $\pm$3 percent. In addition to the pions this beam contains some muons and electrons of the same momentum. Their number has been determined from a range curve. The muons amount to between 5 percent and 10 percent. The electrons are present in negligible numbers for beams above 100 Mev. Below this energy the electron contamination increases rapidly. For this reason low energy measurements have been taken by reducing with a beryllium absorber the energy of the 122-Mev beam.

By using various channels we have taken measurements over the energy range from about 80 to 230 Mev.

TABLE I. Total cross sections negative pions on hydrogen.

Energy band Mev	Cross section 10^{-27} cm²
89 ±8	21 ±8
112 ±6	31 ±9
135 ±6	52 ±6
176 ±6	66 ±6
217 ±6	60 ±6

The pion beam is monitored by two scintillation crystals of 1-inch-square cross section separated by a distance of about one meter. The coincidences of these two counters indicate the number of particles entering the equipment. Beyond the second crystal the pions enter the scattering chamber, which is a glass cylinder 3 inches in diameter and 7½ inches long, closed by 0.005-inch copper windows. This chamber can be alternately filled with and emptied of liquid hydrogen. The particles which are not scattered out of the beam are recorded by the coincidences which they give in a pair of liquid scintillation counters, of which one has a 3-inch diameter and the other a 4-inch diameter. The double coincidence rate of the first two scintillators is recorded and at the same time the quadruple coincidence rate of all four scintillators. The attenuation of the beam is obtained from a comparison of the ratio of the quadruple to double coincidence counts with and without the hydrogen and is computed as a cross section.

A number of corrections have been applied to the results on account of the following effects:

(1) Background due to accidentals (usually 1 percent or less).

(2) Angular spread of the beam due to geometry, diffraction scattering, and pi–mu decay. In some experiments the multiple scattering was compensated by means of an equivalent aluminum foil; in others it was computed. This correction is important only at low energies.

(3) Muon and electron component in the original beam. It is assumed that muons and electrons suffer only Coulomb scattering and have no specific nuclear interaction.

(4) Correction for scattered particles recorded by the end counters. This correction was computed on the assumption of isotropic scattering in the center-of-mass system. It amounted to between 4 percent and 2 percent depending on whether the recoil protons are or are not recorded. The correction would be larger if the scattering were predominately forward but smaller if charge exchange scattering were important.[3] The results of the measurement are presented in Table I.

The data show that the cross section rises rather rapidly above 80 Mev until it reaches the "geometrical" value $\pi(\hbar/\mu c)^2$ at 150 Mev, where the cross section seems to level off, or perhaps to go through a maximum, although our measurements do not permit a decision between these two possibilities.

* Research sponsored by the ONR and AEC.
† Institute for the Study of Metals, University of Chicago.
‡ AEC Predoctoral Fellow.
[1] Chedester, Isaacs, Sachs, and Steinberger, Phys. Rev. **82**, 958 (1951).
[2] Shutt, Fowler, Miller, Thorndike, and Fowler, Phys. Rev. **84**, 1247 (1951).
[3] In view of the importance of the charge exchange process reported in the following Letter, it seems likely that the cross sections have been overcorrected by about 2 percent to 3 percent.

Ordinary and Exchange Scattering of Negative Pions by Hydrogen*

E. FERMI, H. L. ANDERSON, A. LUNDBY, D. E. NAGLE, AND G. B. YODH
Institute for Nuclear Studies, University of Chicago, Chicago, Illinois
(Received January 21, 1952)

IN an accompanying letter some experiments on the total cross section of negative pions of various energies in liquid hydrogen have been described. Measurements of total cross sections, of course, do not give any indication as to the actual mechanism of the process. In particular, in the interaction of negative pions in hydrogen the following three processes are considered possible:

$$p+\pi^-\rightarrow p+\pi^- \quad (1)$$

$$p+\pi^-\rightarrow n+\pi^0\rightarrow n+2\gamma \quad (2)$$

$$p+\pi^-\rightarrow n+\gamma. \quad (3)$$

The first two are scattering without or with exchange of charge. The last is the inverse process of the photoproduction of pions by the action of gamma-rays on neutrons. Estimates of the cross section of this last process, based on the principle of detailed balancing, indicate that its cross section must be of the order of magnitude of a few millibarns and is therefore rather small compared to the total cross section, which is of the order of 40 millibarns for pions of 120 Mev.

We have started a series of scattering experiments in order to distinguish between the processes (1) and (2), as well as to give information as to the angular distribution of the scattered particles. We felt that the first results were of sufficient interest to be reported at this time.

The geometry used in this experiment is similar to the one adopted in the study of the total cross sections. The beam of pions enters the experimental space and is deflected by an analyzing magnet. After this, it is recorded by the coincidences of two 1-inch-square crystals and falls on the liquid hydrogen scattering chamber. The scattered products are observed by quadruple coincidences of these two counters with another pair of scintillators located directly under the scattering chamber in a direction at 90° to that of the incident pions. The latter two scintillators had diameters 4 inches and 3 inches and were placed, respectively, 8 inches and 11 inches below the center of the scattering chamber. The 118-Mev beam was chosen because of its high intensity. With 1-inch-square collimating crystals 10 inches apart, the coincidence counting rate was about 150,000 per minute. The count of the scattered particles was instead, of the order of only a few per minute. In order to increase the sensitivity of the scattering detectors to gamma-rays, a lead radiator ½ inch thick was interposed in front of the third counter. A standard measurement involved the observation of the ratio between scattered and incident particles with and without hydrogen in the scattering chamber, and with and without the lead converter of the gamma-radiation. Typical results are given in Table I. The difference with and without liquid hydrogen is due to the scattered particles. With no radiator this difference is $(0.4\pm0.15)\times10^{-4}$; with the radiator it is $(1.02\pm0.11)\times10^{-4}$. The sensitivity of the detector to gamma-rays without lead radiator is small but not negligible, because the radiation goes through the walls of the chamber and part of the third scintillator where it may produce pairs and be recorded. An attempt has been made to separate the number of scattering events recorded due to scattered π^- from those due to gamma-rays. We find the following:

Scattered π^- in the accepted solid angle: $(0.34\pm0.12)\times10^{-4}$.

Photons in the accepted solid angle: $(1.41\pm0.32)\times10^{-4}$.

The conversion of these numbers to a scattering cross section depends on the assumptions made as to the angular distribution. It also depends on the assumption that we have made in this paper that all neutral pions decay immediately into two photons. For example, if we assume that the angular distribution is fairly isotropic in the center-of-mass system and that the gamma-rays are

TABLE I. Scattering of negative pions at 90°.

Liquid hydrogen	½-in. Pb radiator	Ratio quadruple to double coincidence
No	No	$(0.81\pm0.05)\times10^{-4}$
Yes	No	$(1.21\pm0.08)\times10^{-4}$
No	Yes	$(0.71\pm0.06)\times10^{-4}$
Yes	Yes	$(1.73\pm0.09)\times10^{-4}$

produced in pairs by the decay of the neutral pions, the cross sections for the processes (1) and (2) would be $(10\pm4)\times10^{-27}$ and $(20\pm5)\times10^{-27}$ cm². The cross section obtained for the charge exchange process is not very sensitive to the angular distribution adopted. It would be $(29\pm7)\times10^{-27}$ cm² for a $\cos^2\theta$-distribution and $(18\pm4)\times10^{-27}$ cm² for a $\sin^2\theta$-distribution.

* Research sponsored by the ONR and AEC.

Total Cross Sections of Positive Pions in Hydrogen*

H. L. Anderson, E. Fermi, E. A. Long,† and D. E. Nagle
Institute for Nuclear Studies, University of Chicago, Chicago, Illinois
(Received January 21, 1952)

In a previous letter,[1] measurements of the total cross sections of negative pions in hydrogen were reported. In the present letter, we report on similar experiments with positive pions.

The experimental method and the equipment used in this measurement was essentially the same as that used in the case of negative pions. The main difference was in the intensity, which for the positives was much less than for the negatives, the more so the higher the energy. This is due to the fact that the positive pions which escape out of the fringing field of the cyclotron magnet are those which are emitted in the backward direction with respect to the proton beam, whereas the negative pions are those emitted in the forward direction. The difficulty of the low intensity was in part compensated by the fact that the cross section for positive pions turned out to be appreciably larger than for negative pions. The results obtained thus far are summarized in Table I.

In Fig. 1 the total cross sections of positive and negative pions are collected. It is quite apparent that the cross section of the positive particles is much larger than that of the negative particles, at least in the energy range from 80 to 150 Mev.

In this letter and in the two preceding ones,[1,2] the three processes: (1) scattering of positive pions, (2) scattering of negative pions with exchange of charge, and (3) scattering of negative pions without exchange of charge have been investigated. It appears that over a rather wide range of energies, from about 80 to 150 Mev, the cross section for process (1) is the largest, for process (2) is intermediate, and for process (3) is the smallest. Furthermore, the cross sections of both positive and negative pions increase rather rapidly with the energy. Whether the cross sections level off at a high value or go through a maximum, as might be expected if there should be a resonance, is impossible to determine from our present experimental evidence.

Brueckner[3] has recently pointed out that the existence of a broad resonance level with spin 3/2 and isotopic spin 3/2 would give an approximate understanding of the ratios of the cross sections for the three processes (1), (2), and (3). We might point out in this connection that the experimental results obtained to date are also compatible with the more general assumption that in the energy interval in question the dominant interaction responsible for the scattering is through one or more intermediate states of isotopic spin 3/2, regardless of the spin. On this assumption, one finds that the ratio of the cross sections for the three processes should be (9:2:1), a set of values which is compatible with the experimental observations. It is more difficult, at present, to say anything specific as to the nature of the intermediate state or states. If there were one state of spin 3/2, the angular distribution for all three processes should be of the type $1+3\cos^2\theta$. If the dominant effect were due to a state of spin 1/2, the angular distribution should be isotropic. If states of higher spin or a mixture of several states were involved, more complicated angular distributions would be expected. We intend to explore further the angular distribution in an attempt to decide among the various possibilities.

Besides the angular distribution, another important factor is the energy dependence. Here the theoretical expectation is that, if there is only one dominant intermediate state of spin 3/2 and isotopic spin 3/2, the total cross section of negative pions should at all points be less than $(8/3)\pi\lambda^2$. Apparently, the experimental cross section above 150 Mev is larger than this limit, which indicates that other states contribute appreciably at these energies. Naturally, if a single state were dominant, one could expect that the cross sections would go through a maximum at an energy not far from the energy of the state involved. Unfortunately, we have not been able to push our measurements to sufficiently high energies to check on this point.

Also very interesting is the behavior of the cross sections at low energies. Here the energy dependence should be approximately proportional to the 4th power of the velocity if only states of spin 1/2 and 3/2 and even parity are involved and if the pion is pseudoscalar. The experimental observations in this and other laboratories seem to be compatible with this assumption, but the cross section at low energy is so small that a precise measurement becomes difficult.

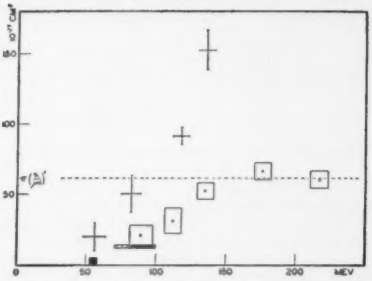

Fig. 1. Total cross sections of negative pions in hydrogen (sides of the rectangle represent the error) and positive pions in hydrogen (arms of the cross represent the error). The cross-hatched rectangle is the Columbia result. The black square is the Brookhaven result and does not include the charge exchange contribution.

Table I. Total cross sections of positive pions in hydrogen.

Energy (Mev)	Cross section (10^{-27} cm²)
56±8	20±10
82±7	50±13
118±6	91± 6
136±6	152±14

* Research sponsored by the ONR and AEC.
† Institute for the Study of Metals, University of Chicago.
[1] Anderson, Fermi, Long, Martin, and Nagle, Phys. Rev., this issue.
[2] Fermi, Anderson, Lundby, Nagle, and Yodh, preceding Letter, this issue, Phys. Rev.
[3] K. A. Brueckner (private communication).

Conductivity of Cold-Worked Metals*

D. L. Dexter
Department of Physics, University of Illinois, Urbana, Illinois
(Received January 17, 1952)

The change in the electrical conductivity of a metal upon cold-working was first calculated by Koehler,[1] on the assumption that the change is primarily due to the dislocations themselves (rather than associated clusters of vacancies, for example). The scattering potential he used was the difference in

the sum of the shielded potentials of the ions, in the strained and unstrained positions, in a lattice containing a pair of edge-type dislocations. Mackenzie and Sondheimer[3] repeated the calculation with the same potential, changing the approximation between the dislocations, and the method of solution of the transport equation. Both K and MS found changes in resistivity of the order of that observed.

In a recent paper with the above title Landauer[3] computed the change in conductivity using as a scattering potential the energy of the bottom of the conduction band, calculated from free-electron theory, in a lattice containing a single edge-type dislocation. His method is somewhat simpler mathematically, avoids convergence difficulties of the type encountered in K and MS (which required the treatment of a positive-negative dislocation pair), and avoids the problem of the discontinuity in the displacement across the plane connecting the pair of parallel dislocation axes.[4] The purposes of this note are to extend and modify the results in L, and to discuss the effect of the singularity in the assumed scattering potential.

Equation (L6) gives the scattering potential (except for an obvious omission of a factor E),

$$V(\mathbf{r})=\frac{aE}{3\pi\epsilon}\left(\frac{1-2\nu}{1-\nu}\right)\frac{\sin\theta}{r}, \tag{1}$$

where the notation is the same as in L. The square of the scattering matrix element between two plane wave states, not explicitly given in L, is here calculated to be

$$|\langle\mathbf{k}'|-eV|\mathbf{k}\rangle|^2=\frac{16}{9}a^2E^2\left(\frac{1-2\nu}{1-\nu}\right)^2\frac{\sin^2(\kappa_x c^2/2)\sin^2\varphi}{\kappa_x^2\kappa_z^2 v^2}, \tag{2}$$

where $\boldsymbol{\kappa}=\mathbf{k}'-\mathbf{k}$, κ_x is the component of $\boldsymbol{\kappa}$ in the xy plane, φ the angle between κ_x and the x axis, and v the volume of the metal.

Now the transport equation[5] can be solved by the method in MS, and the fractional change in resistivity, averaged over direction, is found to be

$$\langle\Delta\rho/\rho\rangle_{\text{Av}}=\frac{1}{27\pi^2}E^2a^2\left(\frac{1-2\nu}{1-\nu}\right)^2\frac{\tau m^*}{\hbar^3}k_0N. \tag{3}$$

This average change in resistivity is equal to that calculated[5a] in L [Eq. (L7)] times $(16\pi^2)^{-1}$. The numerical value for copper becomes

$$\langle\Delta\rho/\rho\rangle_{\text{Av}}=2.23\times10^{-15}N, \tag{4}$$

where we have used the experimental values given in L, and the normal resistivity at 20°C, 1.89×10^{-13} gaussian unit (i.e., 1.69 microhm cm). The reader is referred to K, MS, and L for comparison with experiment. The numerical value of $\langle\Delta\rho/\rho\rangle_{\text{Av}}$ given in Eq. (L9), $2.5\times10^{-15}N$, does not follow either from Eq. (L7) or Eq. (3).

This treatment (as well as those in K and MS) has assumed that the change in density, and hence, the scattering potential, have a singularity on the dislocation axis. It is then of interest to see how much of the scattering is contributed by the fictitious r^{-1} singularity. This can be investigated semi-quantitatively in the following way.

Let us consider the hypothetical problem of a line dipole embedded in a metal, such that the potential near the axis is given by Eq. (1). Then the Thomas-Fermi equation tells us that the potential in the lattice is

$$V(\mathbf{r})=\frac{aE}{3\pi\epsilon}\left(\frac{1-2\nu}{1-\nu}\right)K_1(r/r_0)\frac{\sin\theta}{r_0}, \tag{5}$$

where $K_1(z)$ is the modified Bessel function of the second kind, varying as $1/z$ for small z and as $(\pi/2z)^{\frac{1}{2}}\exp(-z)$ for large z; the value of r_0 will not concern us for the moment. This potential gives rise to an average change in resistivity, by the same method as above, just equal to that in Eq. (3) multiplied by a function

$$f(c)=1-(3/2c)\tan^{-1}c+[2(1+c^2)]^{-1}, \tag{6}$$

where $c=2k_0r_0$. The function f is a monotonically increasing function of r_0, and varies from 0 to 1 as r_0 varies from 0 to ∞. That is, as $r_0\to\infty$, the potential and the resistivity change are just those of the unshielded line dipole given in Eqs. (1) and (3). However, we can now cut off the potential at any desired length by making use of the exponential dependence in K_1. Cutting off the potential at about a lattice spacing by letting $c=2.7$, corresponding to setting $k_0=1.37\times10^8$ cm^{-1} for copper, and $r_0\sim10^{-8}$ cm, we find f to be 0.39. Thus the fictitious contribution to the resistivity arising from within the nearest neighbor distance is about half of the value calculated in Eq. (3), and hence, the calculation can probably be trusted to about that accuracy. It should be emphasized that this entire calculation has been performed for a simple cubic lattice, and hence, is not directly applicable to more complex crystals, particularly since the variation of elastic constants with direction has not been included.

Finally, the anisotropy in the resistivity should be mentioned. This calculation gives a change in resistivity in the x-(slip) direction 1/3 that in the y-direction, whereas K and MS found ratios of about 8 and 2, respectively. This difference is a result of their approximations for taking account of the discontinuity in displacement across the plane connecting the dislocation axes. A later publication will discuss the anisotropy in more detail; it will also show that properly performed calculations using these two types of potential give closely related results for the magnitude of the resistivity change, as well as the same anisotropy, namely the ratio 1/3.

The writer would like to express his warmest thanks to Professors J. Bardeen and J. S. Koehler for enlightening conversations, and to Mr. Paul Leurgans for checking some of the calculations.

* Research supported by the ONR.

[1] J. S. Koehler, Phys. Rev. **75**, 106 (1949), to be referred to as K.

[2] J. K. Mackenzie and E. H. Sondheimer, Phys. Rev. **77**, 264 (1950), to be referred to as MS.

[3] Rolf Landauer, Phys. Rev. **82**, 520 (1951), to be referred to as L.

[4] Dr. Landauer has been kind enough to compare our treatments, and now agrees that Eq. (3) in this note is correct.

[5] D. L. Dexter (to be published).

[5a] Equation (4) for the collision operator in reference 2 and all resulting expressions should be multiplied by the factor $\frac{1}{2}$.

Long-Range Proton-Proton Tensor Force*

NORMAN F. RAMSEY
Harvard University, Cambridge, Massachusetts
and
Brookhaven National Laboratory, Upton, Long Island, New York

(Received January 18, 1952)

THE molecular beam magnetic resonance experiments with molecular hydrogen[1,2] provide an accurate measurement of the tensor interaction between two protons three-quarters of an angstrom apart. The magnetic part of this interaction depends only upon the magnetic moment of the proton and the mean inverse cube of the internuclear spacing. The first of these quantities is accurately known from nuclear resonance experiments,[1,2] while the second can be inferred from spectroscopic data[4] on H_2. Therefore, a comparison of the value computed in this way with the experimental value will either detect or set an upper limit to the long-range nonmagnetic tensor interaction between two protons.

To account for the observed radiofrequency spectrum of H_2 one assumes,[1] among other things, a proton-proton interaction of the form $K(r)S_{12}$, where S_{12} is the usual tensor operator.[5] The expectation value of $K(r)$ in the first rotational and zeroth vibrational state of the molecule is then the quantity that is experimentally determined. If this experimental quantity is called $\langle K(r)\rangle_{0,1}^{\text{expt}}$, it is related to the usual parameters of the molecular hydrogen theory[1,2] by

$$\langle K(r)\rangle_{0,1}^{\text{expt}}=(5/4)hd=\mu_H H''=(4.7750\pm0.0010)\times10^{-23}\text{ erg} \tag{1}$$

if the value[2,6] for d is taken to be 57,671±11 cps. The quantity $\langle K(r)\rangle_{0,1}^{\text{expt}}$ can be assumed to consist of a magnetic part $\langle K(r)\rangle_{0,1}^{\text{mag}}$ and a nonmagnetic or nuclear part $\langle K(r)\rangle_{0,1}^{\text{nuc}}$, and

the magnetic part can be calculated theoretically from the experimental data of Herzberg[4] on the rotation-vibration spectrum of H_2.

In the calculation of $\langle K(r)\rangle_{0,1}{}^{\text{mag}}$ care must be taken in that this quantity depends on $\langle 1/r^3\rangle_{0,1}$, whereas the spectroscopic data determines $\langle 1/r^2\rangle_{0,1}$, and the relation between these two quantities is complicated by the zero-point vibration of the molecule, by the asymmetry of the nuclear potential within the molecule, and by centrifugal stretching. If, however, one approximates the nuclear potential well by a Morse potential, he can show that

$$\langle K(r)\rangle_{0,1}{}^{\text{mag}}=\mu_H{}^2\langle 1/r^3\rangle_{0,1}$$
$$=\mu_H{}^2\left(\frac{8\pi^2 c\mu}{h}B_0\right)^2\left\{1+\frac{3}{2}\frac{B_e}{\omega_e}+\left(\frac{B_e}{\omega_e}\right)^2\left[-\frac{13}{4}(ar_e)^2+\frac{153}{8}(ar_e)^2\right.\right.$$
$$\left.\left.-\frac{83}{2}(ar_e)+\frac{87}{8}\right]-\frac{3}{8}\frac{\gamma_e}{B_e}\right\}, \quad (2)$$

where the notation is that of Herzberg,[4] except for the Morse parameter a. It should be noted that only in the third order is the value affected by the anharmonicity of the potential. This feature is a consequence of Herzberg's[4] parameter B_0 being for the same molecular vibrational state as in the molecular beam experiments, and it makes possible a considerable increase in accuracy of the calculation since the anharmonicity in the ground state is not well known. When the present best values[4,6,7] of the experimental parameters are used and when ar_e is taken as 1.5, the value of $\langle K(r)\rangle_{0,1}{}^{\text{mag}}$ becomes $(4.7732\pm0.0040)\times10^{-22}$ erg.

Within the estimated error $\langle K(r)\rangle_{0,1}{}^{\text{mag}}$ agrees with $\langle K(r)\rangle_{0,1}{}^{\text{exp}}$[6]. Consequently, $\langle K(r)\rangle_{0,1}{}^{\text{nuc}}$ must be less than 5×10^{-22} erg or 3×10^{-10} Mev. This result means, for example, that if there is a Yukawa type field giving rise to a tensor force and with a field particle weighing less than a tenth electron mass, the coupling $g^2/\hbar c$, of the nucleons to the field must be less than 3×10^{-8}, and the potential from this field of two protons 2.8×10^{-13} cm apart must be less than 2×10^{-6} Mev.

The author wishes to thank Mr. Vaughn Culler and Mr. N. J. Harrick for checking the present calculations.

* This work was partially supported by the joint program of the ONR and AEC.

[1] Kellogg, Rabi, Ramsey, and Zacharias, Phys. Rev. **56**, 728 (1939).
[2] Kolsky, Phipps, Ramsey, and Silsbee, Phys. Rev. **79**, 883 (1950); **80**, 483 (1950); and **81**, 1061 (1951).
[3] Thomas, Driscoll, and Hipple, Phys. Rev. **78**, 787 (1950).
[4] G. Herzberg, Can. J. Research, **A28**, 144 (1950).
[5] W. Rarita and J. Schwinger, Phys. Rev. **59**, 436 (1951).
[6] Barnes, Bray, Harrick, and Ramsey (unpublished results).
[7] J. W. DuMond and E. R. Cohen, Phys. Rev. **82**, 556 (1951).

The Gyromagnetic Ratios of Li^7, Na^{23}, Al^{27}, and P^{31}

T. Kanda,* Y. Masuda,* R. Kusaka, Y. Yamagata, and J. Itoh
Department of Physics, Osaka University, Osaka, Japan
(Received October 23, 1951)

THE gyromagnetic ratios of Li^7, Na^{23}, Al^{27}, and P^{31} were measured with respect to that of the proton using the magnetic resonance method. The method of measurment is as follows: Two sets of coils, each containing a sample of a similar solution of the salt composed of the nucleus whose gyromagnetic ratio is to be measured were placed between pole pieces of an electromagnet. These coils consist of the oscillation circuits of two autodyne detectors. Each of these detectors was connected to a 200 cps (modulation frequency of magnetic field) resonance amplifier, a lock-in amplifier, and a recording milliammeter. First, keeping the magnetic field constant, the nuclear magnetic resonance frequency for the nucleus whose moment is to be measured was determined with one setting of the detector and the proton resonance frequency was measured with the other. Let the ratio of these frequencies be ν_{s1}/ν_{p1}. Then, without changing the apparatus, the ratio of the magnetic resonance frequencies was measured by interchanging only the frequencies of the two detectors. Let it be ν_{s2}/ν_{p1}. Then by a simple calculation, it can be shown that the true ratio of the gyromagnetic ratios of these nuclei to that of the proton (without diamagnetic correction) is given by

$$\{(\nu_{s1}/\nu_{p2})\cdot(\nu_{s2}/\nu_{p1})\}^{\frac{1}{2}}.$$

By this procedure, an inhomogeneity of the magnetic field at the position of the two samples can be wholly eliminated. The frequency was determined by measuring the audio beat frequency with some harmonics of a 100-kc/sec crystal oscillator calibrated by an 8-Mc/sec standard wave (*JJY*). An appropriate value of magnetic field strength (*ca.* 2000 oersted) was selected so that the beat with 100-kc/sec harmonics fell in the range of audio frequencies. Each measurement was repeated five times.

The results are shown in Table I, which lists the nucleus whose moment was measured, the salt used, the added paramagnetic catalyst, the approximate resonant frequency for the nucleus measured that for the proton, and the mean value of ratios of gyromagnetic ratios without diamagnetic correction. The errors indicated in the last column of the table are maximum errors, being about three times the usual probable errors.

For comparison, the ratio of gyromagnetic ratios of the nuclei in question measured by other authors in the same substances that we used are listed in Table II.

TABLE I. Experimental results.

Nucleus	Salt	Paramag. catalyst	Approximate value of ν_s	Approximate value of ν_p	Mean value of ratios of gyromag. ratios
Li^7	LiCl	$0.1N$ $MnSO_4$	3.3 Mc/sec	8.5 Mc/sec	0.388637 ± 0.000010
Na^{23}	NaI	$0.1N$ $MnSO_4$	2.2	8.3	0.264514 ± 0.000009
Al^{27}	$AlCl_3$	...	2.0	7.7	0.260579 ± 0.000008
P^{31}	P_2O_5	$0.1N$ $Fe(NO_3)_3$	3.2	7.9	0.404804 ± 0.000010

TABLE II. Results of other investigators.

Nucleus	Ratio of gyromagnetic ratios
Li^7	0.388625 ± 0.00004[a] 0.38862 ± 0.00002[b] 0.388611 ± 0.000017[c]
Na^{23}	0.26450 ± 0.00003[a]
Al^{27}	0.26056 ± 0.00003[a] 0.26062 ± 0.00011[b] 0.260579 ± 0.000013[d]
P^{31}	0.40496 ± 0.00009[a] 0.40481 ± 0.00004[a]

[a] F. Bitter, Phys. Rev. **75**, 1326 (1949).
[b] J. R. Zimmerman and D. Williams, Phys. Rev. **76**, 350 (1949).
[c] K. Siegbahn and G. Lindström, Arkiv. Fysik **1**, 6, 193 (1949).
[d] R. E. Sheriff and D. Williams, Phys. Rev. **82**, 651 (1951).
* R. V. Pound, Phys. Rev. **73**, 1112 (1948).
* Now at Department of Physics, University of Kobe, Kobe, Japan.

Experiments with Audiofrequencies on Superconductors*

B. Serin and C. A. Reynolds
Physics Department, Rutgers University, New Brunswick, New Jersey
(Received January 9, 1952)

IN connection with our recent paper[1] with the above title, we recently have learned[2] of an earlier paper of Galkin and Bezuglyi[3] which is critical of our conclusions as reported in abstract form.[4] We therefore take this opportunity to discuss certain points about our work in more detail than we have done previously.

Briefly, we superimposed direct and alternating currents on tin wires, and measured the average potential difference, V_{dc}, as a function of the amplitude of the ac, I_{ac}. We found that the experimental curves agreed with the calculated curves for low frequency ac (<50 cycles/sec). However, as the frequency was increased, the curves changed in character; the maxima increased

TABLE I. The observed values of P are tabulated as a function of frequency for a sample without a glass envelope. The ac amplitude for each value of P is given, as well as the calculated value of P.

Frequency (cycles/sec)	I_{ac} (ma)	P (observed)	P (calculated)
50	156	1.15	1.41
200	156	1.18	1.41
2000	165	1.21	1.42
20,000	175	1.68	1.47

markedly in height and occurred at slightly larger values of the ac. We attributed this anomalous behavior to the large values of the ratio (r/d) of radius to skin depth of the wires, and obtained experimental support for this conclusion by making measurements on samples of various conductivities and sizes and correlating the observed deviations with the values of r/d. On the other hand, Galkin and Bezuglyi suggest that the anomalies can be traced to the fact that, at high frequencies, the wires become adiabatically isolated from the liquid bath. The wires could then be cooled by the magnetocaloric effect, during part of the cycle of the ac, thereby increasing the critical current necessary to restore the sample to the normal state. The increased critical current would necessitate a larger I_{ac} at the maximum, thereby producing a larger maximum. To support this mechanism, Galkin and Bezuglyi describe an experiment in which a tin specimen of diameter 0.15 mm was drawn in a glass capillary tube, and then cut into two pieces. The glass was removed from one of the pieces with hydrofluoric acid, but the other specimen was left in the glass envelope. Runs were then made on both samples. For the sample without glass envelope the character of the curves $V_{dc}(I_{ac})$ was independent of frequency up to 20,000 cycles/sec. At the same temperature the curves $V_{dc}(I_{ac})$ for the sample in the glass envelope was independent of frequency up to 2000 cycles/sec, but at larger frequencies the maxima increased in size up to 10,000 cycles/sec. Further increase in frequency did not affect the size of the maxima.

The above experimental result is in disagreement with all of our data. In our first investigations, it was standard procedure to remove the glass from the samples with hydrofluoric acid. Contrary to the result of Galkin and Bezuglyi, we always observed a monotonic increase with frequency of the values of the maxima of the curves $V_{dc}(I_{ac})$ in the range 50 cycles/sec to 20,000 cycles/sec. A typical set of values of $P=[(V_{dc})_{max}/I_{dc}R_n]$ for various frequencies is given in Table I, where R_n is the resistance of the sample in the normal state and I_{dc} is the value of the dc. The values of the ac amplitudes at the maxima are also tabulated. This sample was about 7 cm long, had a diameter of about 0.13 mm and was prepared from spectrographically pure tin supplied by the Johnson, Mathey Company. The data were taken at 3.71°K, with $I_{dc}=40$ ma and the critical current, $I_c\simeq 120$ ma. The bases of the calculated values of P are given below.

Data of the general type shown in Table I were obtained in seven different samples of high purity tin from which the glass had been removed; at least two runs were made on each sample. However, for these samples the curves of restoration of resistance with direct current (Silsbee effect) were quite broad. We felt that the broadening was the result of the strains unavoidably introduced into the samples by handling. To reduce the possibility of straining the samples, the expedient was then adopted of leaving the samples in the glass envelope, except at the ends where the glass was removed, so that the sample could be mounted in clamps which served as current and potential leads. The thickness of the glass never exceeded 0.1 mm. The samples with glass envelopes exhibited quite sharp curves of Silsbee effect. A set of values of the pertinent quantities for a glass covered sample is given in Table II. This sample, prepared from pure tin, had a diameter of 0.164 mm and was 4.0 cm long. The data were taken at $T=3.70$°K, with $I_{dc}=145$ ma and $I_c\simeq 240$ ma. Similar data were obtained with five different samples of pure tin.

TABLE II. The observed values of P are tabulated as a function of frequency for a sample with a glass envelope. The ac amplitude for each value of P is given, as well as the calculated value of P.

Frequency (cycles/sec)	I_{ac} (ma)	P (observed)	P (calculated)
30	382	1.07	1.24
300	382	1.15	1.24
3000	382	1.23	1.24
5000	406	1.30	1.25
8000	425	1.36	1.28
10,000	440	1.39	1.30
15,000	453	1.42	1.31

The values of P can be calculated for an ideal case. We assume that the resistance of the sample is zero when the total current is less than the critical value. At the critical value, I_c, the resistance jumps discontinuously to its value in the normal state and remains constant for all larger values of the current. A straight forward calculation gives

$$P=0.5+\frac{2\sqrt{x-\sin^{-1}[(x-1)/(x+1)]}}{\pi}, \quad x>1,$$

where $x=I_c/I_{dc}$. Since at the maximum value of V_{dc}, $I_{ac}=I_{dc}+I_c$, it is then possible from the measured values of I_{ac} and I_{dc} to calculate P. The calculated values of P given in Tables I and II have been determined in this way. It is to be noted that at low frequencies the observed values of P are smaller than the calculated values of P. This is to be expected, since the resistance of an actual sample does not exhibit a discontinuous increase in resistance, but rather a sharp increase to about 0.8 R_n at the critical current followed by a very slow increase of resistance up to R_n. We would not consider it inappropriate to multiply all the calculated values of P by the factor necessary to obtain agreement between the calculated and observed values at the lowest frequency. However, we have not made this correction, since it is then clear that the calculated values of P are the largest possible values for the measured values of I_{dc} and I_{ac}, if it is assumed that the effective resistance of the samples is unchanged.

It is clear from Tables I and II that at sufficiently high frequencies the observed values of P appreciably exceed these largest possible values. This behavior was exhibited by each of our twelve pure samples. Thus it is clear that deviations exist which are greater than any that can be explained by the increase in I_{ac} due to cooling. We must conclude that at sufficiently high frequencies the effective resistance of our samples is increased above the normal value. In view of the experimental results and the analysis given above, the interpretation of Galkin and Bezuglyi is inadequate. The data is more in keeping with the skin effect interpretation given in our paper.[1]

* This work has been supported by the joint program of the ONR and AEC, the Rutgers University Research Council, and the Radio Corporation of America.
[1] Serin, Reynolds, Feldmeier, and Garfunkel, Phys. Rev. **84**, 802 (1951).
[2] We are very grateful to Dr. D. Shoenberg for calling our attention to this paper, and for his great kindness in providing us with an English translation.
[3] Galkin and Bezuglyi, J. Exp. Theoret. Phys. (USSR) **20**, 1145 (1950).
[4] Serin, Feldmeier, and Garfunkel, Phys. Rev. **76**, 167 (1949); Serin, Reynolds, and Garfunkel, Phys. Rev. **79**, 211 (1950).

Variational Calculation of Scattering Cross Sections*

E. GERJUOY†
New York University, New York, New York
AND
DAVID S. SAXON
National Bureau of Standards, Los Angeles, California
(Received January 14, 1952)

WE report the results of calculations attempting to assess the utility of Schwinger's variational formulation[1] of the scattering problem, when ka is so large that a phase-shift analysis, i.e., an expansion in a series of spherical harmonics, is a slowly

converging procedure. With a stationary expression[1] we compute $A(\mathbf{n}, \mathbf{n}_0)$, the scattering amplitude of waves proceeding to infinity along the direction $\mathbf{n}$ as a result of a wave $\exp(ik\mathbf{n}_0\cdot\mathbf{r})$ incident along the direction $\mathbf{n}_0$. The differential cross section is $|A(\mathbf{n}, \mathbf{n}_0)|^2$ and the total cross section is[2] $\sigma=(4\pi/k)\,\mathrm{Im}A(\mathbf{n}_0, \mathbf{n}_0)$. This formulation has been used previously with good results to estimate scattering by two-dimensional scatterers, e.g., plane slits.[3] The use of variational expressions for the individual phase shifts has also been reported.[4]

For square well potentials $V(r)$ we have evaluated in closed form the integral

$$\int\int d\mathbf{r}d\mathbf{r}'\psi(\mathbf{r}, -\mathbf{n})V(r)\cdot G(\mathbf{r}, \mathbf{r}')V(r')\psi(\mathbf{r}', \mathbf{n}_0), \qquad (1)$$

for $\mathbf{n}=\mathbf{n}_0$, with $\psi(\mathbf{r}, \mathbf{n})=\exp(iK\mathbf{r}\cdot\mathbf{n})\cdot G(\mathbf{r}, \mathbf{r}')$ is the free space Green's function $\exp(ik|\mathbf{r}-\mathbf{r}'|)/4\pi|\mathbf{r}-\mathbf{r}'|$. We thereby obtain in closed form a variational estimate of σ. With K corresponding to the wave number inside the well, the variational formulation appears to yield significantly better results than the customary Born approximation for a square well of depth 21.3 Mev, with range $R=2.8\times10^{-13}$ cm, corresponding to triplet $n-p$ scattering by central forces with no exchange (Fig. 1).[5] There is also a signifi-

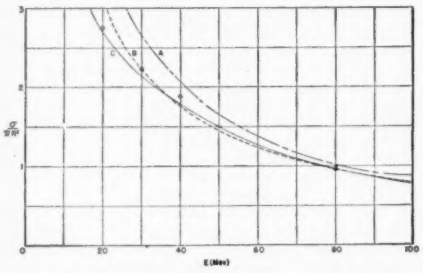

FIG. 1. Total cross sections against energy. Curve A is the Born approximation, curve B the variational result, and curve C the improved variational result. The exact points indicated by the circles are from Bethe and Camac (see reference 5).

cant improvement over the Born approximation for the case of acoustic scattering by a refractive sphere, with index of refraction 1.25. In part this improvement is ascribable to the inclusion of the integral (1), which integral appears also in second Born approximation, in part to the choice of a better trial function inside the well than the Born $\psi(\mathbf{r}, \mathbf{n})=\exp(ik\mathbf{r}\cdot\mathbf{n})$.

A further improvement can be obtained using a still better trial function inside the well, namely, a linear combination of forward and backward traveling plane waves, $\psi(\mathbf{r}, \mathbf{n})=\exp(iK\mathbf{r}\cdot\mathbf{n})+\alpha\exp(-iK\mathbf{r}\cdot\mathbf{n})$ as suggested by the results of Latter.[6] It is unnecessary to make specific assumptions concerning the magnitude of α, since parity conservation enables us to obtain independent integral equations and thence independent variational expressions for the even and odd parts of the solution, remembering that the variational expression[2] for $A(\mathbf{n}, \mathbf{n}_0)$ is independent of normalizing factors in the trial function. This improved variational result is also plotted in Fig. 1.

With the use of the combination $\exp(iK\mathbf{r}\cdot\mathbf{n})+\alpha\exp(-iK\mathbf{r}\cdot\mathbf{n})$, exchange can be included with little additional complication. For the square well we have been unable to evaluate (1) in closed form except for $\mathbf{n}=\mathbf{n}_0$, with $\psi(\mathbf{r}, \mathbf{n})=\exp(iK\mathbf{r}\cdot\mathbf{n})$. However, (1) can be evaluated in closed form for the ψ for arbitrary $\mathbf{n}$, with $V(r)$ a Yukawa well, which means that in this case closed forms can be obtained for the estimated differential and total cross sections including exchange using a trial function which is a combination of forward and backward traveling waves. Jost and Pais[7] have evaluated (1) in the Yukawa case, when $K=k$. Their method can also be used for $K\neq k$, but we have found it possible and equally convenient to evaluate (1) with $K\neq k$ by standard contour integral techniques, after transforming to momentum space.

Further details will be forthcoming soon.

* In part this work was performed at the Mathematics Research Group at Washington Square College of Arts and Science, New York University, and was supported by the U. S. Air Force through sponsorship of the Air Force Cambridge Research Laboratories. The preparation of this report was sponsored in part by the ONR.

† On leave from the University of Southern California, Los Angeles, California.

[1] W. Kohn, Phys. Rev. **74**, 1763 (1948).
[2] B. A. Lippman and Julian Schwinger, Phys. Rev. **79**, 469 (1950).
[3] Harold Levine and Julian Schwinger, Phys. Rev. **74**, 958 (1948).
[4] F. Rohrlich and J. Eisenstein, Phys. Rev. **75**, 705 (1949).
[5] M. Camac and H. A. Bethe, Phys. Rev. **73**, 191 (1948).
[6] A. Latter, Phys. Rev. **83**, 1056 (1951).
[7] R. Jost and A. Pais, Phys. Rev. **82**, 840 (1951).

Critical Domain Size in Ferroelectrics

W. KÄNZIG AND M. PETER
Swiss Federal Institute of Technology, Zürich, Switzerland
(Received January 2, 1952)

IT is well known that small ferromagnetic particles with linear dimensions of the order of magnitude of the domain wall thickness behave as single domains.[1] The surface energy of the Bloch wall presents a splitting up of such a small particle into several domains. Similar effects have now been observed in ferroelectrics.

Colloidal KH_2PO_4 was prepared by grinding single crystals in a colloid grinding mill using a suitable protecting colloid. By means of a centrifuge different samples with homogeneous particle size ranging from 650A up to 5000A were obtained. Crystal size and shape were determined with the electron microscope. The crystals are approximately spherical. Debye-Scherrer patterns show that the lattice is not distorted by the grinding procedure.

The state of polarization below the Curie point ($\theta=123°$K) was investigated by observing the spontaneous strain with x-ray diffraction. For unstressed crystals the spontaneous strain was shown to be proportional to the spontaneous polarization.[2] The volume conductivity of the colloid is probably less than 10^{-16} ohm^{-1} cm^{-1} in the neighborhood of the Curie temperature and below.

The main results may be stated as follows: Colloidal particles with a mean diameter $D\leqq1500$A show no measurable spontaneous strain from the Curie point down to the temperature of liquid nitrogen, whereas particles with $D\geqq4000$A undergo about the same spontaneous strain as macroscopic domains do. The dielectric constant of the colloids has a peak value at a temperature coinciding (within the limits of error, $\pm0.5°$C) with the Curie temperature of the macroscopic crystal, indicating that the spontaneous strain is not prevented by mechanical clamping (frozen protecting colloid).[3] Hence particles with no measurable strain have only a small spontaneous polarization. This result is confirmed by the fact that the decrease of the dielectric constant below the Curie point is less pronounced for colloids showing no spontaneous strain.

The influence of the electrical conductivity on the polarization effects was investigated by repeating the same experiments with a conducting colloid: Macroscopic KD_2PO_4-crystals behave like macroscopic KH_2PO_4-crystals, the only essential difference is that the Curie temperature of KD_2PO_4 is much higher ($\theta=213°$K).[4,5] At this temperature the colloid is not frozen and shows a conductivity of about 10^{-9} ohm^{-1} cm^{-1}. The KD_2PO_4-particles were imbedded in a protecting colloid, in which the exchangeable hydrogens were replaced by deuterium.

Debye-Scherrer photographs taken at various temperatures revealed that in contrast to the nonconducting case (KH_2PO_4) even the smallest particles ($D\approx750$A) in the conducting colloid

undergo the same spontaneous strain and, therefore, the same spontaneous polarization as macroscopic domains do.

These effects can be accounted for by the assumption of a critical domain size between 1500A and 4000A (probably nearer to the lower limit). If a crystal of these linear dimensions is cooled below the Curie point, it could only polarize as a single domain.

If it is nonconducting and imbedded in a nonconducting medium of not too high permittivity, the depolarization factor is larger than the Lorentz correction. Therefore, no spontaneous polarization can take place. (This result is in contrast to the behavior of small ferromagnetic particles, where the depolarizing field is less effective, since the magnetic dipoles are aligned by interactions which are about 10^4 times larger than the ordinary dipole-dipole interaction.)

If, however, the ferroelectric crystal or the imbedding medium is a conductor (KD_2PO_4-colloid), the depolarizing field breaks down and the normal spontaneous polarization results.

Large crystals ($D \geqq 4000$A) can split up in two or more domains with a consequent reduction of the depolarizing field. Hence also in the nonconducting case spontaneous polarization is observed.

A full account of the present investigations will appear in the *Helvetica Physica Acta*. Similar experiments with ferroelectrics of $BaTiO_3$-type are in progress.

The authors are indebted to Dr. P. Scherrer for illuminating discussions. They wish to thank all those who have generously offered help and advice: Dr. Frey-Wyssling, Dr. K. Mühlethaler, Mr. A. Vogel (electron microscope work), Dr. K. Clusius, Dr. P. Jordan, Mr. H. Gränicher (deuterium-substituted colloid), and members of the Institute of Applied Physics.

[1] W. C. Elmore, Phys. Rev. **54**, 1092 (1938).
[2] M. de Quervain, Helv. Phys. Acta **17**, 509 (1944).
[3] H. Baumgartner, Helv. Phys. Acta **24**, 326 (1951).
[4] W. Bantle, Helv. Phys. Acta **15**, 373 (1942).
[5] B. Zwicker and P. Scherrer, Helv. Phys. Acta **17**, 346 (1944).

Search for Natural Radioactivity of Calcium 48*

JOHN W. JONES AND TRUMAN P. KOHMAN
Department of Chemistry, Carnegie Institute of Technology, Pittsburgh, Pennsylvania
(Received January 7, 1952)

IT has been noted on several occasions[1,2] that Ca^{48}, which occurs to the extent of 0.18 percent in natural calcium,[3] has an exceptionally low proton-neutron ratio in comparison with stable nuclides in this region and accordingly, might be unstable. If this is the case, the absence of readily detectable natural radioactivity in calcium[4] would indicate a very long lifetime. On the other hand, empirical and theoretical indications that 20 protons and 28 neutrons both form closed-shell configurations would make the stability of $_{20}Ca_{28}^{48}$ plausible.

One of us[2] has pointed out that if Ca^{48} is beta-labile, it would transform to the well-known 44-hour Sc^{48} and that chemical extraction of the daughter from a large quantity of calcium would provide a sensitive method of detecting the activity of the parent. Negative results of such a test indicated that the half-life for decay of Ca^{48} to Sc^{48} must be at least 5×10^{15} years.[5]

Collins, Nier, and Johnson[6] have recently determined the mass of Ca^{48} as 47.96778±10. There have been several measurements of the Ti^{48} mass[7-9] the latest[8] giving 47.96313±6. Sc^{48} is reported to emit a simple beta-spectrum of 0.64-Mev maximum energy[9] and gamma-rays of 0.98 and 1.33 Mev in series.[10] Although there is a possibility of other gamma-radiation of lower energy,[10] this has not been reported by others,[11] and it is unlikely that its intensity could be sufficient for it to be assigned to the main mode of disintegration. Thus we take the $Sc^{48}\rightarrow Ti^{48}$ disintegration energy to be 2.95±0.05 Mev. The $Ca^{48}-Sc^{48}$ mass difference is then +0.00148±13, whence the $Ca^{48}\rightarrow Sc^{48}$ transition is exoergic by 1.38±0.12 Mev. Other Ti^{48} mass values[7] give energies between −1.8 and +1.2 Mev for this transition but with larger uncertainties. Both of the masses used above were obtained with the same instrument and the same reference ion, $C^{13}(H^1)_4^+$. A direct comparison of Ca^{48} and Ti^{48} would be desirable; since the packing fraction separation is nearly 0.9×10^{-4}, this should be feasible.

With this new indication of the instability of Ca^{48}, we have undertaken a more intensive search for the $Ca^{48}\rightarrow Sc^{48}$ transition. One hundred pounds of calcium nitrate, containing 9 kg of Ca, was dissolved to make a 45 percent aqueous solution. A small amount of $CaCO_3$ was precipitated with $(NH_4)_2CO_3$, filtered out, and dissolved in HNO_3. After refiltering, the solution was made alkaline with NH_4OH, which formed a visible precipitate, presumably because of small amounts of silicates leached from the glass vessels and carried down by the $CaCO_3$. This precipitate was separated on a sintered glass filter and dissolved in HNO_3. Barium was added and removed as the sulfate, and finally a small amount of calcium was added and precipitated as the oxalate. In separate experiments using Sc^{48} as a tracer, 80–90 percent recovery of Sc was obtained in the CaC_2O_4 precipitate.

The activities were measured by filtering the precipitates onto filter paper disks and mounting beneath the mica window of a conventional lead-shielded counter having a background of 25 counts per minute. Alternate sample and background counts were made for a week following separation. In several experiments no detectable amount of 44-hour activity was found. Small and variable amounts of shorter-lived activity were found in both the $BaSO_4$ and CaC_2O_4 fractions, but this could easily be accounted for by entrainment of natural radio-elements from the air during filtration of the large volume of initial solution.

We calculate a minimum half-life of 2×10^{16} years for the decay of Ca^{48} to 44-hour Sc^{48}. Accordingly,[12] if the energy available for this transition is 1 Mev or more, the logarithm of the comparative lifetime ft in seconds must be at least 24.8. This is greater than that for any observed beta-ransition, the largest known value being that of In^{115}, 22.6. The $Ca^{48}\rightarrow Sc^{48}$ transition is quite similar in both atomic number and energy to the $K^{40}\rightarrow Ca^{40}$ transition, for which the spin change is 4, but the lifetimes differ by a factor of at least 10^7. Thus the spin of Sc^{48} must be at least 5 and possibly greater; this is in agreement with the absence[9] of observable transitions from Sc^{48} to the ground state of Ti^{48}. Nordheim[13] has indicated that odd-odd nuclides commonly have large nuclear spins, as is the case for Lu^{176}, whose spin has been measured as $\geqslant 7$. A possible configuration for $_{21}Sc_{27}^{48}$ according to Nordheim's scheme involves a $f_{7/2}$ orbital for each odd nucleon, coupled so as to give a net spin equal or close to the maximum possible value of 7.

We plan to continue these experiments with larger amounts of calcium and more sensitive counters. We are also investigating the possibility that Ca^{48} might decay to Ti^{48} via a metastable excited state of Sc^{48}, by-passing the ground state of the latter. Unless this occurs with a half-life much shorter than the ground-state transition, it would appear that Ca^{48} possesses no geochronological value.[5]

* This work has been supported by the AEC. Sc^{48} was obtained from the Isotopes Division of the AEC.

[1] I. Joliot-Curie, J. phys. radium (8) **6**, 209 (1945); M. N. Saha and A. K. Saha, Trans. Natl. Inst. Sci. India **2**, 193 (1946); Nature **158**, 6 (1946); S. Meyer and A. Koss-Rosenqvist, Acta Phys. Austriaca **2**, 114, 245 (1949).
[2] T. P. Kohman, Phys. Rev. **73**, 16 (1948).
[3] A. O. Nier, Phys. Rev. **53**, 282 (1938); J. R. White and A. E. Cameron, Phys. Rev. **74**, 991 (1948).
[4] M. Curie, thesis, Paris, 1903, Chem. News **88**, 99 (1903); Hevesy, Pahl, and Hosemann, Nature **134**, 377 (1934); R. Overstreet and L. Jacobson, Phys. Rev. **72**, 349 (1947).
[5] T. P. Kohman, Phys. Rev. **73**, 1223 (1948).
[6] Collins, Nier, and Johnson, Phys. Rev. **84**, 717 (1951); A. O. Nier, private communication.
[7] A. J. Dempster, Phys. Rev. **53**, 64 (1938); F. W. Aston, Nature **141**, 1096 (1938); T. Okuda and K. Ogata, Phys. Rev. **60**, 690 (1941); H. E. Duckworth, Phys. Rev. **62**, 19 (1942); H. E. Duckworth and R. S. Preston, Phys. Rev. **82**, 468 (1951).
[8] Collins, Nier, and Johnson, Bull. Am. Phys. Soc. **26**, No. 6, 30 (1951); A. O. Nier, private communication.
[9] G. P. Smith, Phys. Rev. **61**, 578 (1942).
[10] W. C. Peacock and M. Deutsch, Phys. Rev. **69**, 306 (1946).
[11] H. Walke, Phys. Rev. **57**, 163 (1940); C. E. Mandeville, Phys. Rev. **64**, 147 (1943); C. T. Hibdon and M. L. Pool, Phys. Rev. **67**, 313 (1945).
[12] E. Feenberg and G. Trigg, Revs. Modern Phys. **22**, 399 (1950).
[13] L. W. Nordheim, Phys. Rev. **78**, 294 (1950); Argonne National Laboratory Report 4626, Part II (1951); Revs. Modern Phys. **23**, 322 (1952).

The Half-Life of the 1.3-Mev Excited State in K^{41}

L. G. Elliott
Atomic Energy Project, National Research Council of Canada, Chalk River, Ontario, Canada
(Received January 21, 1952)

THE ground state of K^{41} is classified as a $d_{3/2}$ level,[1] while the first excited state of the 19th proton would be expected to be an $f_{7/2}$ level. A gamma-ray transition between these levels would then be magnetic quadrupole ($M2$).

About 99.3 percent of A^{41} beta-disintegrations lead to a 1.3-Mev excited state in K^{41}, and 0.7 perent lead to the ground state.[2] An assignment of $f_{7/2}$ to this excited state is consistent with these observed beta-transition probabilities. The theoretical half-life given by Weisskopf's formula[3] for such a 1.3-Mev $M2$ transition is 0.45×10^{-9} second.

The half-life of this 1.3-Mev excited state in K^{41} has been measured by the following delayed coincidence experiment. A source of the 109-minute A^{41} activity was prepared by thermal neutron irradiation of a sample of 99.6 percent tank argon sealed in a thin quartz bulb. After a 20-minute neutron irradiation, the source was placed between two *trans*-stilbene scintillation counters using *IP21* photomultipliers. One counter was sensitive to beta-rays, while the other was covered with sufficient absorber to stop the beta-radiation and leave the counter sensitive to gamma-radiation. The counter pulses were led to a coincidence apparatus consisting of four coincidence mixers arranged with beta-pulse delays of 4×10^{-9} second inserted between successive mixers. The individual mixers are similar in principle to that described by Bell and Petch[4] and were adjusted to have a resolving time of about $2\tau_0=4\times10^{-9}$ second. Coincidence counts were then recorded in the four mixing channels for a series of delays in either the beta- or the gamma-counter lines leading to the coincidence apparatus. In this way four independent sets of data were obtained in each run. The set of data obtained in one of the mixing channels during one run and corrected for A^{41} decay is shown in Fig. 1. Prompt coincidence curves were obtained by replacing the source of A^{41} by a source of Au^{198}. One such curve is also shown in Fig. 1 for comparison.

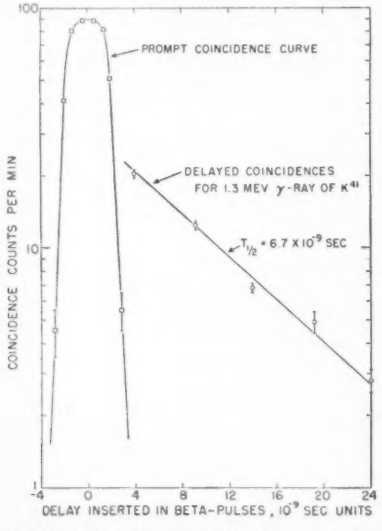

FIG. 1. The delayed coincidence curve taken in one mixing channel and showing the half-life of the 1.3-Mev gamma-transition in K^{41} with a prompt coincidence curve for comparison. The measured background of random coincidences was small and has been subtracted at each point.

The mean value of the half-life of the 1.3-Mev excited state in K^{41} obtained from two runs using different sources is $(6.7\pm0.5)\times10^{-9}$ second. This is seen to be appreciably longer than the theoretical half-life given by Weisskopf's formula.

The author is indebted to G. J. R. MacLusky of the Electronics Branch for the design and construction of the coincidence apparatus.

[1] M. G. Mayer, Phys. Rev. **78**, 18 (1950).
[2] Bleuler, Boltmann, and Zünti, Helv. Phys. Acta **19**, 419 (1946).
[3] V. F. Weisskopf, Phys. Rev. **83**, 1073 (1951).
[4] R. E. Bell and H. E. Petch, Phys. Rev. **76**, 1409 (1949).

The Tetraneutron*

K.-H. Sun and F. A. Pecjak
Westinghouse Research Laboratories, East Pittsburgh, Pennsylvania
and
A. J. Allen
University of Pittsburgh, Pittsburgh, Pennsylvania
(Received January 16, 1952)

IT is known that a system of two protons and two neutrons has an unusually high binding energy. If one considers that the filling of neutrons and protons in a nucleus is, in general, independent of each other, one might infer that a certain amount of binding energy may be obtained if two neutrons are substituted for the two protons in the above case; thus forming a tetraneutron.

Assuming the tetraneutron is unstable with respect to a helium nucleus but stable with respect to free neutrons, one could set up an upper limit for the binding energy of the tetraneutron as follows:

$$4n \rightarrow n^4 + Q_1 \tag{1}$$

$$n^4 \xrightarrow{\beta^-} H^4 + Q_2 \tag{2}$$

$$H^4 \xrightarrow{\beta^-} He^4 + Q_3. \tag{3}$$

Combining these equations and using Breit and McIntosh's limiting values for Q_3,[1] one obtains

$$Q_1 = [(9.4 \text{ to } 13.8) - Q_2] \text{ Mev}. \tag{4}$$

If reaction (2) occurs, Q_2 is positive; then the maximum value of Q_1, the binding energy of the tetraneutron, will be about 14 Mev.

If one considers the following two exothermic reactions and combines them with reaction (1)

$$X^A + n \rightarrow Y^{A-3} + 4n - |Q_5| \tag{5}$$

$$X^A + n \rightarrow Y^{A-3} + n^4 - |Q_6| \tag{6}$$

one obtains

$$|Q_5| - |Q_6| = Q_1 \tag{7}$$

It is obvious that if reaction (6) can be carried out before reaction (5) by using energies of impinging neutrons lower than that of the threshold for reaction (5), it should indicate the existence of the tetraneutron. This method of detection is particularly convenient if the binding energy of the tetraneutron is larger than, say, 3 Mev.

The maximum energy of neutrons produced by the 16-Mev deuterons from the University of Pittsburgh cyclotron on Be is about 18 Mev at a convenient angle where high intensity fast neutrons are available. These neutrons were used to bombard Rh^{103} and Bi^{209}. The thresholds for the reactions $Rh^{103}(n, 4n)Rh^{100}$ and $Bi^{209}(n, 4n)Bi^{206}$ are, respectively, 27.8 and 20.8 Mev (from the calculated mass data by Metropolis and Reitwiesner[2]). Many experiments were tried to search for the Rh^{100} and Bi^{206} activities; none were found. Some 20-hr activities were noted in the bombarded Rh-samples, but were attributed to the Pt impurities present in the Rh-samples. This indicates either that the tetra-

neutron does not exist, or that if it exists, its binding energy is below 3 Mev or the yield is extremely small. The upper limit of yield may be set as a few microbarns from the present experiment with bismuth.

Another method to detect the existence of a tetraneutron, which is applicable especially if its binding energy is less than 3 Mev, is to look for a monoenergetic recoil group from a reaction of the type,

$$Bi^{209}+H^1\rightarrow Po^{206}+n^4+Q_8 \qquad (8)$$

where Q_8 is about -21.5 Mev if the binding energy of n^4 is taken near zero. Using a 32-Mev proton beam, such as the one from the linear accelerator of the University of California, the Po^{206} recoils from a very thin target may assume an energy in the neighborhood of 540 kev at a 30° angle from the proton beam. Because of the high momentum of the recoils, they may be separated from other particles by a magnetic field. The presence of monoenergetic Po^{206} group will be a direct proof of the existence of the tetraneutron.

If the tetraneutron or other polyneutrons are shown to be nonexisting, then the simultaneous presence of both proton(s) and neutron(s) must be a necessary condition in the formation of any nucleus with mass number greater than one.

* Assisted by the joint program of the ONR and AEC.

[1] G. Breit and J. S. McIntosh, Phys. Rev. **83**, 1245 (1951).
[2] N. Metropolis and G. Reitwiesner, *Tables of Atomic Masses* (Argonne National Laboratories, Chicago, 1950).

Radiative $\pi-\mu$ Decay

TETSUO EGUCHI*
Institute for Atomic Research and Department of Physics, Iowa State College, Ames, Iowa
(Received January 18, 1952)

SINCE the discovery by Lattes, Occhialini, and Powell[1] of the decay of a π-meson into a μ-meson, it has been believed that the μ-meson produced by the decay had a definite kinetic energy 4.1 Mev, the decay energy 33 Mev being shared by the μ-meson and a neutral particle of small mass. However, recently a number of decays of positive π-mesons into μ-mesons having anomalously short range have been found by Fry[2] and others.[3] According to the observations by Fry, 8 tracks of μ-mesons with energy less than 3.5 Mev have been found among about 6000 ordinary $\pi-\mu$ decays. Of these, four events might possibly be interpreted as decays in flight. Furthermore, μ-mesons of ordinary range have a higher probability of getting out of the emulsion than the short-range particles. Considering these effects, the probability of the anomalous $\pi-\mu$ decay is estimated to be about 3×10^{-4} that of the ordinary decay.[3]

Because a charged μ-meson is accelerated to a high velocity by the decay, we can expect the decay process to be accompanied by a continuous γ-ray spectrum. This effect has been considered in the case of nuclear β-decay by Knipp and Uhlenbeck,[4] Bloch,[5] and Chang and Falkoff;[6] nuclear K-capture by Møller[7] and Morrison and Schiff;[8] meson production by Schiff;[9] and mesonic β-decay by Feer.[10] The problem of radiative $\pi-\mu$ decay has been considered nonrelativistically by Primakoff,[11] using the Bloch and Nordsieck method. The present calculation, which was initiated independently, is a relativistic second-order perturbation analysis. As will be seen, the two calculations give roughly the same probability for the anomalous decay.

We assume that the π-meson is described by a scalar or a pseudoscalar field Ψ, which satisfies the Klein-Gordon equation, and that the μ-meson and neutral particle are described by spinor fields ψ and φ, respectively, both of which satisfy Dirac equations. The Hamiltonian density of the interaction of these three fields is assumed to be proportional to

$$(\psi^*\eta\varphi)\Psi, \qquad (1)$$

where η is given either by $\eta=\beta$ if Ψ is scalar, or by $\eta=\beta\alpha_1\alpha_2\alpha_3$ if Ψ is pseudoscalar, β and α's being conventional Dirac operators.

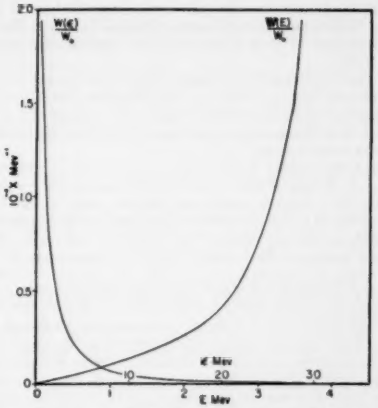

FIG. 1. The probability distributions of the μ-meson and the photon in the radiative $\pi-\mu$ decay (per normal decay). The curve rising to the right gives the probability per Mev interval of a μ-meson of kinetic energy E. The curve rising to the left gives the probability per Mev interval of a photon of energy ϵ.

The probabilities of radiationless and radiative $\pi-\mu$ decay are calculated relativistically by ordinary perturbation methods, assuming the π-meson to be at rest before the decay and neglecting the mass of the neutral particle. The probability per unit time for the decay of the π-meson into a μ-meson of kinetic energy between E and $E+dE$, a photon of energy between ϵ and $\epsilon+d\epsilon$, and a neutral particle with the remaining energy, is given by

$$W(E,\epsilon)dEd\epsilon=\frac{4}{\pi}\cdot\frac{e^2}{\hbar c}\cdot W_0\cdot\left(\frac{1+E_0}{2E_0+E_0^2}\right)^2 \cdot\frac{(E_0-E-\epsilon)(1+E)}{[2(1+E_0)(E+\epsilon)-E_0^2]^2}\cdot\left[(2+2E_0+E_0^2)-(2E_0+E_0^2)\cdot\frac{(2E+E^2)\cos^2\theta+\epsilon(2E+E^2)^{\frac{1}{2}}\cos\theta}{(E_0-E-\epsilon)(1+E)}-\frac{2(1+E_0)}{1+E}\right]dEd\epsilon, \qquad (2)$$

for both scalar and pseudoscalar assumptions. In the expression (2), W_0 is the probability per unit time of the radiationless decay; $E_0=0.33$ is the decay energy, all energy quantities being measured in the unit of mass energy of the μ-meson (about 100 Mev); and θ is the angle between the emitted μ-meson and the photon, which is given by

$$\cos\theta=\frac{(E_0-E-\epsilon)^2-(2E+E^2)-\epsilon^2}{2\epsilon(2E+E^2)^{\frac{1}{2}}} \qquad (3)$$

from the conservation of energy and momentum.

By integrating (2) over ϵ for a given value of E or over E for a given value of ϵ, we get the energy distribution of the μ-meson $\mathbf{W}(E)dE$ or the photon $W(\epsilon)d\epsilon$, respectively. The ranges of these integrations are given by $-1\leq\cos\theta\leq1$ with (3). The energy distributions thus obtained are shown in Fig. 1; they have an "infrared catastrophe" at 4.1 and 0 Mev, respectively. Although Primakoff[11] gives 17 Mev as the upper limit of the photon energy, our formula gives 28.9 Mev for this value. In the former case the decay energy is shared by the neutral particle and the photon, but in the latter it is shared by the μ-meson and the photon, the third particle being at rest in both cases. On integrating the distribution of the μ-meson graphically from 0 to 3.5 Mev, we get the value 1.3×10^{-4} for the probability of radiative decay relative to the radiationless decay. The corresponding value obtained by Primakoff[11] is 2×10^{-4}. These values are not inconsistent with the value found by Fry,[2] if one considers the small number of events which have actually been observed. The probability for getting

a photon with energy more than 1 Mev is 3×10^{-4} per ordinary decay. The average photon energy per decay is 12 kev. It would be of interest to have an experimental determination of these quantities.

In the interaction (1) we have assumed that a π-meson interacts directly with a μ-meson. Of the alternative assumptions concerning the mechanism of the decay, that in which the mesons interact only through nucleons[12] might be of special interest and is under consideration.

The author wishes to express his hearty thanks to the Departments of Physics of both Iowa State College and Kyushu University for making it possible for him to study in the former institution. He is also indebted to Professor J. K. Knipp for his valuable advice and constant encouragement and to Dr. W. F. Fry for making available his latest data on this problem.[13]

* On leave from Kyushu University, Fukuoka, Japan.
[1] Lattes, Occhialini, and Powell, Nature **160**, 453, 486 (1947).
[2] W. F. Fry, Nuovo cimento **8**, 590 (1951); Phys. Rev. **83**, 1268 (1951); and also private communication.
[3] F. M. Smith, reported by W. H. Barkas at Washington meeting, Phys. Rev. **83**, 236 (1951); C. F. Powell, *Cosmic Radiation, Colston Papers* (Butterworth Scientific Publications, London, 1949); Bramson, Seifert, and Havens, Bull. Am. Phys. Soc. **26**, No. 6, 23 (1951); R. Sagane and E. Gross, private comunication.
[4] J. K. Knipp and G. E. Uhlenbeck, Physica **3**, 425 (1936).
[5] F. Bloch, Phys. Rev. **50**, 272 (1936).
[6] C. S. W. Chang and D. Falkoff, Phys. Rev. **76**, 365 (1949).
[7] C. Møller, Physik Z. Sowjetunion **11**, 9 (1937).
[8] P. Morrison and L. I. Schiff, Phys. Rev. **58**, 24 (1940).
[9] L. I. Schiff, Phys. Rev. **76**, 89 (1949).
[10] D. B. Feer, Phys. Rev. **75**, 731 (1949).
[11] H. Primakoff, Phys. Rev. **84**, 1255 (1951); and private communication.
[12] J. Tiomno and J. A. Wheeler, Revs. Modern Phys. **21**, 153 (1949).
[13] Dr. Fry has recently informed the author that considerations similar to the above have been made by Y. Yamaguchi *et al.*, private communication.

Internal Conversion in the *L*-Shell*

H. GELLMAN, B. A. GRIFFITH, AND J. P. STANLEY
Computation Centre McLennan Laboratory, University of Toronto, Toronto, Ontario, Canada
(Received January 11, 1952)

IN a previous paper,[1] the authors have given the results of calculations for the internal conversion of γ-radiation in the L_I-shell. The present communication contains a summary of these results together with the corresponding results for the L_{II}- and L_{III}-shells. The calculations reported here complete a program undertaken with the object of providing a table of internal conversion coefficients for the *L*-shell covering the range of γ-ray energies and atomic numbers employed by Reitz.[2]

All values given for the internal conversion coefficient are based on formulas derived from those obtained by Goertzel and Rose.[3] The method of derivation of those formulas has been reported earlier, together with a summary of the actual formulas for: the L_I-shell—electric dipole, electric quadrupole, and magnetic dipole; the L_{II}-shell—electric dipole; and the L_{III}-shell—electric dipole.

The additional modified formulas required for the present calculations are quite similar and we hope to publish them at a later date. It should be noted that these formulas take account of relativistic terms but not the effects of screening. It is expected that numerical values for internal conversion coefficients for the *L*-shell will be computed by a method which, like that of Reitz, allows for screening effects; at that time the present results should furnish a good estimate of the importance of screening effects for internal conversion in the *L*-shell.

TABLE I. Internal conversion coefficients for electric dipole radiation (observed L_N-electrons/observed photons of energy k).

Atomic number Z	Gamma-ray energy k (mc^2 units)	L_I shell	L_{II} shell	L_{III} shell	L shell
92	0.09273	0.2372	0.2567	0.2856	0.7795
	0.2927	0.02097	0.009763	0.007779	0.03851
	0.6427	0.003916	0.001076	0.0006813	0.005673
84	0.0833	0.2910	0.2606	0.3544	0.9060
	0.2333	0.03011	0.01241	0.01185	0.05437
	0.5333	0.004569	0.001080	0.0008520	0.006501
49	0.0283	2.202	1.347	2.531	6.080
	0.2083	0.01520	0.001819	0.0002605	0.01962
	0.4083	0.002440	0.0001763	0.0002468	0.002863

TABLE II. Internal conversion coefficients for electric quadrupole radiation (observed L_N-electrons/observed photons of energy k).

Atomic number Z	Gamma-ray energy k (mc^2 units)	L_I shell	L_{II} shell	L_{III} shell	L shell
92	0.09273	9.199	235.2	202.9	447.3
	0.2927	0.1548	1.239	0.7025	2.096
	0.6427	0.01694	0.04557	0.01660	0.07911
84	0.0833	5.300	195.4	195.9	396.6
	0.2333	0.1103	1.617	1.184	2.911
	0.5333	0.01546	0.04494	0.02219	0.08259
49	0.0283	5.787	1792.	3260.	5058.
	0.2083	0.1026	0.1059	0.1188	0.3273
	0.4083	0.01176	0.004734	0.005271	0.02176

TABLE III. Internal conversion coefficients for magnetic dipole radiation (observed L_N-electrons/observed photons of energy k).

Atomic number Z	Gamma-ray energy k (mc^2 units)	L_I shell	L_{II} shell	L_{III} shell	L shell
92	0.09273	43.98	4.244	0.06309	48.29
	0.2927	1.896	0.1758	0.002150	2.074
	0.6427	0.2079	0.02046	0.0003458	0.2287
84	0.0833	27.85	2.397	0.02979	30.28
	0.2333	1.381	0.1123	0.002303	1.496
	0.5333	0.1313	0.01071	0.0003588	0.1424
49	0.0283	19.22	1.299	0.05643	20.58
	0.2083	0.05396	0.001244	0.0004160	0.05562
	0.4083	0.007751	0.0001476	0.00007558	0.007974

Tables I, II, and III give values for the internal conversion coefficient in the electric dipole, the electric quadrupole, and the magnetic dipole cases, respectively. Values are shown for each of three atomic numbers and for three γ-ray energies. Except for the use of IBM machines in the calculation of the hypergeometric functions, all numerical work was done on Marchant and Friden desk calculating machines.

* This project has been carried out in the Computation Center, University of Toronto, with the aid of funds provided by the National Research Council and the Defence Research Board of Canada.
[1] Gellman, Griffith, and Stanley, Phys. Rev. **80**, 866 (1950).
[2] J. R. Reitz, Phys. Rev. **77**, 10 (1950).
[3] Rose, Goertzel, Spinrad, Harr, and Strong, Phys. Rev. **83**, 79 (1951).

Fine Structure and Angular Correlation in Po^{210}*

S. DE BENEDETTI AND G. H. MINTON
Carnegie Institute of Technology, Pittsburgh, Pennsylvania
(Received January 18, 1952)

POLONIUM^{210} is usually considered as a pure α-emitter, although the presence of a weak γ-radiation (energy 803 kev, intensity about 10^{-5} per α) is definitely established.[1,2] The low energy α-particles preceding these γ-rays have escaped observation despite repeated attempts to study the fine structure of Po.

By using a coincidence method we were able to detect the low energy α-group and to study its angular correlation relative to the γ-rays following it.

For the first part of our experiments a source of Po was immersed in a scintillating solution (terphenyl phenylcyclohexane) and the height of the scintillation pulses was studied with a differential pulse-height selector (Fig. 1, curve I). Then, a thick piece of stilbene was located near the α-source and used to detect the γ-rays in coincidence with the α-particles. A fast coincidence circuit[3] (3×10^{-9} sec resolving time) was used in order to minimize the random counting rate. The pulse-height distribution produced by α-particles in coincidence with γ-rays is shown in Fig. 1, curve II. The shift between the two curves of Fig. 1 is, within experimental error, in agreement with an energy difference of 0.8 Mev.

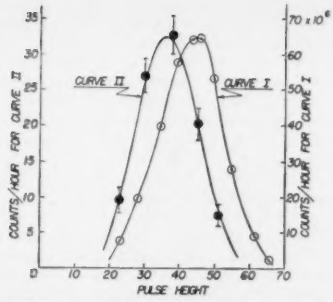

FIG. 1. Scintillation pulse-height distributions for Po-α-particles. Curve II is the distribution produced by α-particles in coincidence with γ-rays.

The number of coincidences was also studied as a function of artificial delays introduced in the coincidences selector. The result indicated that the half-life of the γ-emitting state of Pb^{206} is less than 10^{-9} sec.

In the second part of the experiment a stronger Po source was used. The α-particles were collimated by means of an aperture defining the direction of their emission within $\pm 10°$, and detected by a stilbene crystal after having traveled 1 cm in air. The γ-detector defined the angle of emission of the γ-rays within $\approx \pm 15°$, and the coincidences were counted as a function of the angle between α- and γ-rays. From the raw data was subtracted the background due to random coincidences (measured by interposing a sufficiently long delay) and that caused by spurious immediate coincidences (measured as a function of angle, with the α-detector covered by a thin absorber).

The results are plotted in Fig. 2 together with the curve $\sin^2 2\vartheta$. The total background amounted to about 30 percent of the net counting rate on the maxima.

If one assumes that both Po^{210} and Pb^{206} have 0 spins in their ground states, they must have the same parity (probably even) since they are connected by α-decay. Thus the γ-rays cannot be of magnetic polarity, having to carry the same angular momentum and parity as the short range α-particle. The agreement of the experimental curve with the $\sin^2 2\vartheta$ distribution indicates that the γ-rays are electric quadrupole ($E2$) and that the short-range α-particles have angular momentum 2. The fact that the 0.8-Mev excited state of Pb^{206} has spin 2 and the same parity as the ground state is in agreement with the behavior of most other even-even nuclei.[4] The $E2$ assignment is also consistent with the short half-life of the γ-emitting state.

However, this assignment seems difficult to reconcile with measurements of conversion coefficients of the γ-rays from Pb^{206}.[1,2] One might look for an explanation of this disagreement in the incompleteness in the theory of K/L ratios for high Z, and in the experimental difficulties of an absolute measurement of K conversion coefficients.

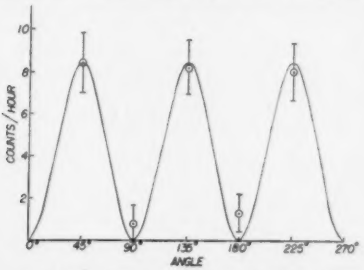

FIG. 2. Angular distribution of γ-rays from Po. The background has been subtracted. The curve is a plot of $\sin^2 2\vartheta$.

* Supported in part by the AEC.

[1] D. E. Alburger and S. Friedlander, Phys. Rev. **81**, 523 (1951).

[2] Grace, Allen, West, and Halban, Proc. Phys. Soc. (London) **A64**, 493 (1951). (See this paper for a more extensive list of references.)

[3] S. De Benedetti and H. Richings, Phys. Rev. **82**, 771 (1951); Rev. Sci. Instr. (to be published).

[4] M. Goldhaber and A. W. Sunyar, Phys. Rev. **83**, 906 (1951).

Zinc as an Acceptor in Germanium

W. C. DUNLAP, JR.
General Electric Research Laboratory, Schenectady, New York
(Received January 8, 1952)

IT has long been known that some third and fifth column elements can act as donor (electron) or acceptor (hole) impurities for germanium and silicon. In particular, arsenic, antimony, and phosphorus are donors; indium, aluminum, gallium, and boron are acceptors. Numerous other elements (notably tin) have been taken to be effective as impurities.[1] In most, if not all, such cases, it has not been established that traces of impurity in the added element were not responsible for the observed effects.

In the present note, I wish to report what seems to be convincing evidence that zinc can act as an acceptor element in germanium. The evidence is based upon two sorts of experiments.

In the first experiments, several samples of single crystal germanium were prepared by adding small amounts of highest purity zinc (Johnson-Mathey 99.99 percent material) to the melt. In all such melts, the germanium crystals were p-type. The resistivity of the single crystals was measured in the temperature range of liquid hydrogen to room temperature. A curve of log conductivity *versus* $1/T$ for a single crystal of zinc-doped germanium is shown in Fig. 1. The activation energy for excitation of carriers from the impurity state can be obtained from the slope of the $\log\sigma$ *versus* $1/T$ curve. This value for the zinc single crystals is 0.031 ev. The significant point for this discussion is that this value is greater by a factor of five or ten than values obtained for such acceptors as indium. A high activation energy might be expected for zinc in a substitutional site because of its position in the second column of the periodic table.

A striking fact is that the activation energy for zinc-doped samples is the same, within experimental error, as the activation energy previously found for heat-treated germanium.[3] This may

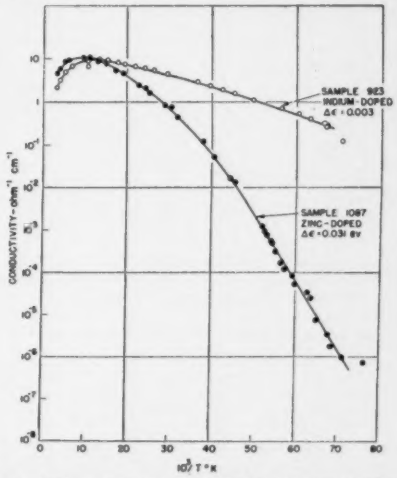

FIG. 1. Conductivity *vs* $1/T$ plots for indium-doped and zinc-doped single crystals of germanium in the temperature range 12–300°K.

point to a similarity between the acceptor centers in zinc-doped germanium and the lattice defects found in heat-treated material.

In the second set of experiments, zinc has been deposited on single crystals of n-type germanium by heating the germanium with a small amount of radioactive zinc (of the order 1–3 micrograms). The diffusion rate has been measured from the location of the $p-n$ junction formed by the penetration of the zinc.[3] These results show that zinc diffuses much more rapidly than indium, gallium, or aluminum. The diffusion coefficient at 900°C is about 1×10^{-11} cm²/sec, the activation energy for diffusion about 2.5 ev.

Additional evidence for the electrical activity of zinc can be obtained by determining the amount of diffusing impurity required to effect the formation of the $p-n$ junction at the depths observed. This amount is orders of magnitude greater than the impurity present and is roughly equal to the amount of zinc actually used.

I wish to thank F. C. Kelley and R. N. Hall for furnishing samples of zinc-doped germanium, and W. DeSorbo for help in the low temperature measurements.

[1] H. C. Torrey and C. A. Whitmer, *Crystal Rectifiers* (McGraw-Hill Book Company, Inc., New York, 1948), p. 364.
[2] W. DeSorbo and W. C. Dunlap, Jr., Phys. Rev. **83**, 879 (1951). (See also erratum on p. 869.)
[3] The diffusion experiments referred to are being reported in detail elsewhere.

Proton Bombardment of Lithium

J. K. Bair, H. B. Willard, C. W. Snyder, T. M. Hahn,* J. D. Kington, and F. P. Green
Oak Ridge National Laboratory, Oak Ridge, Tennessee
(Received January 16, 1952)

LITHIUM of normal isotopic ratio has been bombarded with monoenergetic protons of energies between 1.8 and 5.3 Mev. The yield of neutrons in the forward direction was measured using a conventional "long" counter at a distance of one meter from the rotating target. Gamma-rays of energy greater than roughly 10 Mev were detected using a large sodium iodide crystal as a scintillation detector.

Protons beams, of from one to three microamperes, from the electrostatic generator were obtained after 105° deflection in the analyzer magnet. The beam energy was controlled by varying the corona current in accord with the error signal obtained from slits placed at the 105° beam exit port. The energy calibration was made by correlating magnet current with beam energy by observing the known[1] gamma-ray resonances of fluorine below 1.5 Mev with mass-one, mass-two, and mass-three beams. With careful magnet recycling, repeated runs indicate that the energy determination is accurate to ±0.2 percent relative to the 1.882 $Li^7(p,n)Be^7$ threshold. The fluorine measurements indicate a spread in beam energy of 0.1 percent or less.[2]

The curve of Fig. 1 shows a typical neutron yield in the forward direction for proton energies between 1.8 and 5.3 Mev. Background was negligible. Target thickness was approximately 18 kev at the threshold. In addition to the geometrical peak and the well-known[3] peak at 2.30 Mev, another maximum in the yield occurs at a bombarding energy of about 4.89 Mev corresponding to an excited state in Be^8 in the vicinity of 21.5 Mev. Full width at half-maximum of the resonance at 4.89 Mev is approximately 0.4 Mev.

The lower curve of Fig. 1 shows a typical yield of gamma-rays with energy greater than about 10 Mev. Operation of the counter was checked by observing the 440-kev resonance with the mass-three beam. Target thickness was 15 kev. Background was negligible. The intensity is essentially constant over the region studied. A level with 3 percent of the intensity of the 440-kev resonance would have been easily observed.

The high radiative capture cross section of iodine together with the copious yield of neutrons gave sufficient "background" count in the NaI crystal to effectively prevent the obtaining of a low energy gamma-ray yield curve with the techniques immediately available.

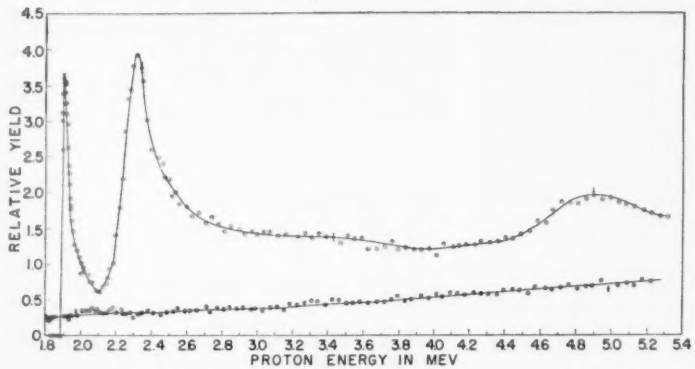

FIG. 1. Yields from the proton bombardment of lithium. Upper curve: neutrons in the forward direction. Lower curve: gamma-rays of energy greater than approximately 10 Mev.

* Summer research participant on leave from the University of Kentucky.
[1] Chao, Tollestrup, Fowler, and Lauritsen, Phys. Rev. **79**, 108 (1950); T. W. Bonner and J. E. Evans, Phys. Rev. **73**, 666 (1948); Bennett, Bonner, Mandeville, and Watt, Phys. Rev. **70**, 882 (1946).
[2] Willard, Bair, Kington, Hahn, Snyder, and Green (to be published).
[3] C. S. Hill and W. E. Shoupp, Phys. Rev. **73**, 931 (1948); R. F. Taschek and P. Hemmendinger, Phys. Rev. **74**, 373 (1948).

THE AMERICAN INSTITUTE OF PHYSICS

INCORPORATED 1931

57 East 55 Street [illegible] 22, N.Y.

MEMBER SOCIETIES:

American Physical Society
Karl K. Darrow, Secretary, Columbia University, New York 27, New York.

Optical Society of America
Arthur C. [illegible], Secretary, Massachusetts Institute of Technology, Cambridge 39, Massachusetts.

Acoustical Society of America
Wallace Waterfall, Secretary, 57 East 55th Street, New York 22, New York.

Society of Rheology
G. J. Dienes, Secretary, Brookhaven National Laboratory, Upton, Long Island, New York.

American Association of Physics Teachers
R. F. Paton, Secretary, University of Illinois, Urbana, Illinois.

AFFILIATED SOCIETIES:

American Crystallographic Association
Electron Microscopy Society of America
Physical Society of Cincinnati
Physics Club of Chicago
Physics Club of New Jersey
Cleveland Physics Society
Physics Club of the Lehigh Valley
Sigma Pi Sigma

ASSOCIATES:

Over seventy [illegible] industrial corporations and [illegible] associations which contribute to the support of the Institute.

JOURNALS:

The Physical Review
S. A. Goudsmit, Editor, Brookhaven National Laboratory, Upton, Long Island, New York.

Reviews of Modern Physics
J. W. Buchta, Editor, University of Minnesota, Minneapolis, Minnesota.

Journal of the Optical Society of America
Wallace [illegible], Editor, National Bureau of Standards, Washington 25, D. C.

The Journal of the Acoustical Society of America
Harry A. Wheeler, Editor, 57 East 55th Street, New York 22, New York.

American Journal of Physics
Thomas [illegible], Editor, Michigan State College, East Lansing, Michigan.

The Review of Scientific Instruments
Gaylord [illegible], Editor, Randal Morgan Laboratory of Physics, University of Pennsylvania, Philadelphia, Pennsylvania.

The Journal of Chemical Physics
Joseph E. Mayer, Editor, Institute for Nuclear Studies, University of Chicago, Chicago 37, Illinois.

Journal of Applied Physics
Elmer Hutchisson, Editor, Case Institute of Technology, Cleveland 6, Ohio.

Physics Today
Gaylord P. Harnwell, Editorial Director; Beatrice Scott Hunter, Managing Editor; American Institute of Physics, [illegible] 55th Street, New York 22, New York.

OFFICERS

Gaylord P. Harnwell, Chairman
Massachusetts Institute of Technology

George B. Pegram, Treasurer
Columbia University

GOVERNING BOARD

Karl K. Darrow
G. J. Dienes
S. A. Goudsmit
G. P. Harnwell
George B. Pegram
F. V. Hunt
Rudolph Kingslake
Hugh S. Knowles
C. C. Lauritsen
F. W. Loomis
William F. Meggers
George B. Pegram
I. I. Rabi
Duane Roller
Frederick Seitz
Francis G. Slack
John C. Slater
Richard M. Sutton
Mark W. Zemansky

Committee on Finance
Merritt Low

ADMINISTRATIVE STAFF

Henry A. Barton, Director
Wallace Waterfall
Executive Secretary
Theodora Vonderlehr
Advertising Manager
Ruth P. Bryant
Publication Manager
Betty H. Goodwin
Assistant Secretary
Elaine B. Nystrom
Circulation Manager
Katherine Smith
Assistant Treasurer

THE American Institute of Physics was founded in 1931 as a federation of leading societies in the field of Physics. It combines into one corporation various functions on behalf of physics which can best be done by the societies jointly. Its purpose is the advancement and diffusion of the science and its applications to human welfare. To this end it [illegible] the Journals listed on the [illegible] fosters unity and efficiency of effort among all who are interested in physics; renders various direct services to physicists, to the public, and to [illegible] government agencies, trade associations, educational institutions, and the technical industries, and serves in such manner as to promote all opportunities and fulfill the responsibilities of physics to society by [illegible] and constructive [illegible]